

5.1 WINGS IN SIDESLIP

5.1.1 WING SIDESLIP DERIVATIVE C_{Y_β}

5.1.1.1 WING SIDESLIP DERIVATIVE C_{Y_β} IN THE LINEAR ANGLE-OF-ATTACK RANGE

The wing contribution to the derivative C_{Y_β} is small, of the order α^2 , and its accurate estimation is not vital.

Methods are presented in this section for estimation of wing side force due to sideslip in the subsonic and supersonic speed regimes. Methods for the estimation of this derivative in the transonic speed regime are not available.

A. SUBSONIC

In Reference 1 a simplified theory consisting of an application of strip theory and lifting-line theory is applied to constant-chord swept wings in sideslip to determine approximate relations for the low-speed sideslip derivatives. The method presented in this section for estimating the wing side force due to sideslip at low subsonic speeds is taken from Reference 1. It is valid in the linear-lift region.

DATCOM METHOD

The wing sideslip derivative C_{Y_β} at low speeds neglecting the effect of dihedral is given in Reference 1 as

$$C_{Y_\beta} = C_L^2 \left[\frac{6 \tan \Lambda_{c/4} \sin \Lambda_{c/4}}{\pi A (A + 4 \cos \Lambda_{c/4})} \right] \frac{1}{57.3} \text{ (per deg)} \quad 5.1.1.1-a$$

The increment in side force due to dihedral at low subsonic speeds can be approximated by

$$\frac{\Delta C_{Y_\beta}}{|\Gamma|} = -0.0001 \text{ (\beta and \Gamma in degrees)} \quad 5.1.1.1-b$$

For subcritical speeds, the low-speed derivative can be modified by the Prandtl-Glauert rule to yield approximate corrections for the first-order three-dimensional effects of compressibility. The resulting expression from Reference 2 is

$$\left(\frac{C_{Y_\beta}}{C_L} \right)_M = \frac{A + 4 \cos \Lambda_{c/4}}{AB + 4 \cos \Lambda_{c/4}} \left(\frac{C_{Y_\beta}}{C_L} \right)_{\text{low speed}} \quad 5.1.1.1-c$$

where

$$B = \sqrt{1 - M^2 \cos^2 \Lambda_{c/4}}$$

Calculated values for the wing side force due to sideslip obtained by the Datcom method for the wing configurations of References 3, 4, and 5 are compared with experimental data in Figure 5.1.1.1-5. The comparison indicates that the calculated values are fairly reliable over a range of lift coefficient (starting from zero) that decreases as wing sweep increases. Large discrepancies are noted for highly swept wings at lift coefficients for which the flow is believed to be partially separated.

Sample Problem

Given: The wing of Reference 5

$$A = 4.0 \quad \Lambda_{c/4} = 60^\circ \quad \lambda = 0.6 \quad \Gamma = 0.6 \quad M = 0.13$$

Compute:

$$\sin \Lambda_{c/4} = 0.866$$

$$\cos \Lambda_{c/4} = 0.500$$

$$\tan \Lambda_{c/4} = 1.732$$

Solution:

$$\begin{aligned} \frac{C_{Y\beta}}{C_L^2} &= \left[\frac{6 \tan \Lambda_{c/4} \sin \Lambda_{c/4}}{\pi A (A + 4 \cos \Lambda_{c/4})} \right] \frac{1}{57.3} \text{ (per deg)} \quad (\text{Equation 5.1.1.1-a}) \\ &= \frac{(6)(1.732)(0.866)}{\pi(4)[4 + 4(0.500)]} \frac{1}{57.3} \\ &= \frac{9}{24\pi} \frac{1}{57.3} \\ &= 0.00208 \text{ per deg} \end{aligned}$$

C_L	C_L^2	$C_{Y\beta} \times 10^3$ (per deg)
0.05	0.0025	0.0052
0.10	0.010	0.0208
0.20	0.040	0.0832
0.30	0.090	0.1872
0.40	0.160	0.3328
0.50	0.250	0.5200
0.60	0.360	0.7488

These results are compared with experimental values in Figure 5.1.1.1-5.

B. TRANSONIC

No method is available in the literature for estimation of the wing contribution to the derivative C_{Y_β} in the transonic speed regime and none is presented in the Datcom. Furthermore, no experimental data are available in this speed regime.

C. SUPERSONIC

No general method has been developed for estimating the wing side force due to sideslip at supersonic speeds. However, theoretical methods are available for discrete planforms over certain speed ranges. A comprehensive summary of the available theoretical methods for calculating the wing side force due to sideslip is presented in Reference 6. The expressions for the derivatives for each planform have been obtained from application of the linearized theory for compressible flow as applied to thin airfoils. The linearized theory is directly applicable for the lateral motion of sideslip and the results are limited only by the complexity of the calculations required to determine the load distributions for certain planforms under certain conditions. Calculation complexities arise as a result of the existence of regions of interacting or mutually subsonic edges (a subsonic edge lying within the region of influence of another). Consequently, the theoretical calculations available are limited primarily to combinations of planforms and Mach lines that do not have interacting or mutually subsonic edges.

No experimental data are available in the supersonic speed regime; consequently, the quantitative accuracy of the estimation methods cannot readily be assessed. However, a review of the application of linearized theory for the prediction of wing lift-curve slope at supersonic speeds can at least lead to a qualitative conclusion of the theory's accuracy when applied to lateral derivatives. Comparison has shown that the agreement between experiment and linear compressible-flow theory with regard to wing lift-curve slope is satisfactory for most practical purposes. To conclude that linearized theory is therefore adequate for lateral derivative prediction seems somewhat questionable in that the lift-curve slope is dependent on the integrated pressure; whereas the lateral derivatives are dependent on pressure distribution. However, when coupled with the fact that the lateral derivatives are relatively insensitive to small shifts in spanwise center of pressure, the indication is that application of the linearized compressible-flow theory should give fairly good results at least insofar as general trends and orders of magnitude are concerned.

DATCOM METHODS

The Datcom methods are taken from References 7, 8, and 9 and present the wing side force due to sideslip over limited Mach number ranges for rectangular planforms, triangular planforms, and fully tapered sweptback planforms with swept forward or sweptback trailing edges. The results are mainly functions of planform geometry and Mach number.

Rectangular Planform: $A\beta \geq 1.0$

The wing side force due to sideslip for rectangular planforms (neglecting the effect of dihedral) is derived in Reference 7 as

$$\frac{C_{Y_\beta}}{\alpha^2} = - \frac{8M^2}{\pi A\beta^2} \frac{1}{57.3} \text{ (per deg)} \quad 5.1.1.1-d$$

where α is in radians and $\beta = \sqrt{M^2 - 1}$.

Equation 5.1.1.1-d is valid for Mach number and aspect ratio greater than that for which the Mach line from the leading edge of the tip section intersects the trailing edge of the opposite tip section ($A\beta \geq 1.0$).

Sweptback Planform ($\lambda = 0$): $\beta \cot \Lambda_{LE} \leq 1.0$

The wing side force due to sideslip for fully tapered sweptback planforms (neglecting the effect of dihedral) is derived in Reference 8 for triangular planforms and in Reference 9 for planforms with sweptforward or sweptback trailing edges as

$$\frac{C_{Y\beta}}{\alpha^2} = - \frac{\pi}{4} AM^2 Q(\beta C) \frac{1}{57.3} \text{ (per deg)} \quad 5.1.1.1-e$$

where α is in radians and $Q(\beta C)$ is obtained from figure 5.1.1.1-6.

Equation 5.1.1.1-e is valid for Mach number and aspect ratio for which the wing is contained within the Mach cones springing from the apex and the trailing edge at the center of the wing.

The increment in side force due to dihedral given by Equation 5.1.1.1-b is also applicable at supersonic speeds.

REFERENCES

1. Toll, T. A., and Queijo, M. J.: Approximate Relations and Charts for Low-Speed Stability Derivatives of Swept Wings. NACA TN 1581, 1948. (U)
2. Fisher, L.: Approximate Corrections for the Effects of Compressibility on the Subsonic Stability Derivatives of Swept Wings. NACA TN 1854, 1949. (U)
3. Wolhart, W. D., and Thomas, D. F., Jr.: Static Longitudinal and Lateral Stability Characteristics at Low Speed of Unswept-Midwing Models Having Wings with an Aspect Ratio of 2, 4, or 6. NACA TN 3649, 1956. (U)
4. Thomas, D. F., Jr., and Wolhart, W. D.: Static Longitudinal and Lateral Stability Characteristics at Low Speed of 45° Sweptback-Midwing Models Having Wings with an Aspect Ratio of 2, 4, or 6. NACA TN 4077, 1957. (U)
5. Wolhart, W. D., and Thomas, D. F., Jr.: Static Longitudinal and Lateral Stability Characteristics at Low Speed of 60° Sweptback-Midwing Models Having Wings with an Aspect Ratio of 2, 4, or 6. NACA TN 4397, 1958. (U)
6. Jones, A. L., and Alksne, A.: A Summary of Lateral-Stability Derivatives Calculated for Wing Planforms in Supersonic Flow. NACA TR 1062, 1951. (U)
7. Harmon, S. M.: Stability Derivatives at Supersonic Speeds of Thin Rectangular Wings with Diagonals Ahead of Tip Mach Lines. NACA TR 926, 1949. (U)
8. Ribner, H. S., and Malvestuto, F. S., Jr.: Stability Derivatives of Triangular Wings at Supersonic Speeds. NACA TR 908, 1948. (U)
9. Malvestuto, F. S., Jr., and Margolis, K.: Theoretical Stability Derivatives of Thin Sweptback Wings Tapered to a Point with Sweptback or Sweptforward Trailing Edges for a Limited Range of Supersonic Speeds. NACA TR 971, 1950. (U)

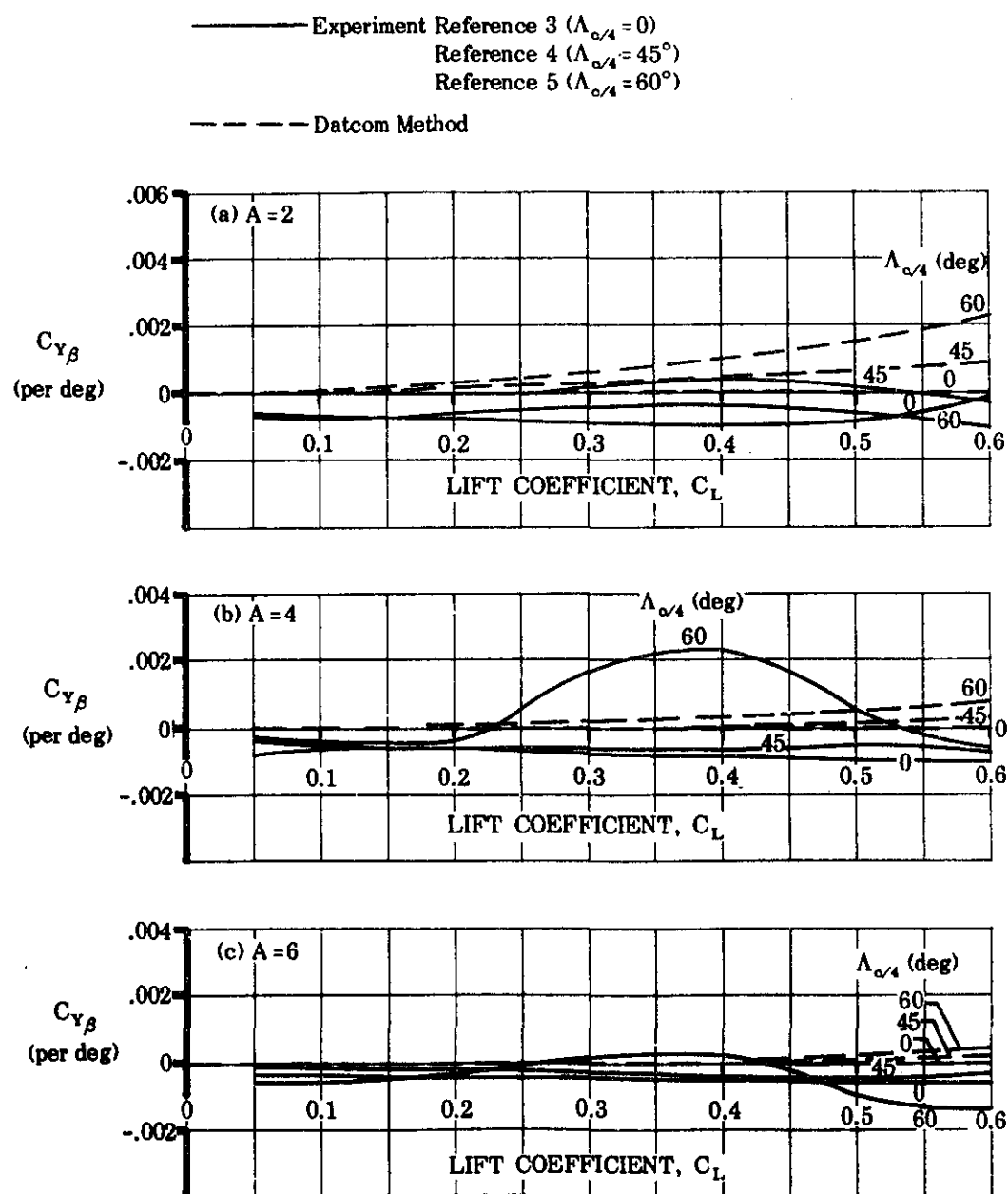


FIGURE 5.1.1.1-5 COMPARISON OF CALCULATED AND EXPERIMENTAL VALUES OF WING SIDE FORCE DUE TO SIDESLIP FOR THE WING CONFIGURATIONS OF REFERENCES 3, 4, AND 5

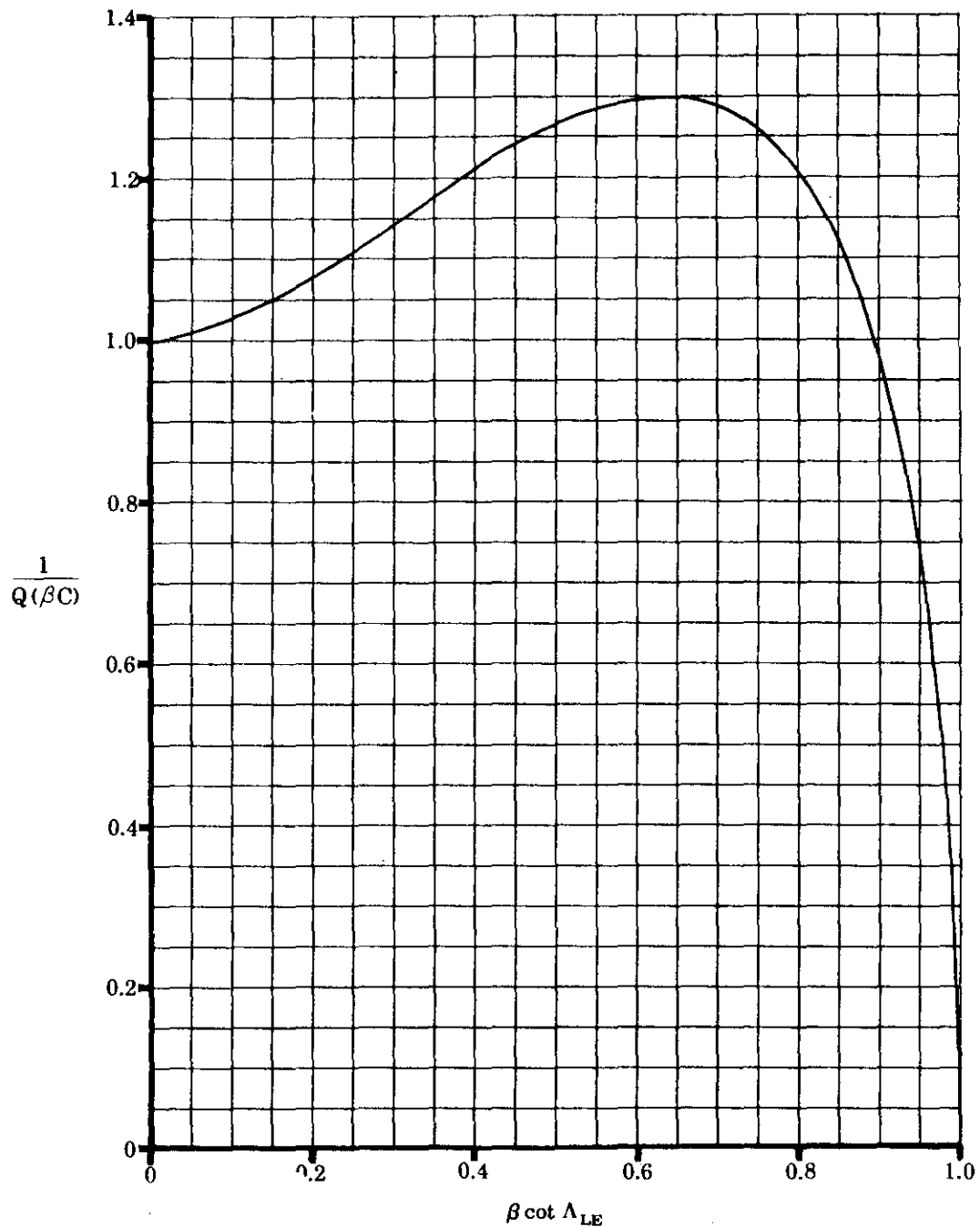


FIGURE 5.1.1.1-6 ELLIPTIC INTEGRAL FACTOR OF THE STABILITY DERIVATIVE

5.1.2 WING SIDESLIP DERIVATIVE $C_{l\beta}$

5.1.2.1 WING SIDESLIP DERIVATIVE $C_{l\beta}$ IN THE LINEAR ANGLE-OF-ATTACK RANGE

A. SUBSONIC

For wings at low angles of attack and subsonic speeds, the rolling moment due to sideslip is principally a function of wing aspect ratio, taper ratio, dihedral angle, and sweep.

The effect of aspect ratio on the rolling moment of unswept wings is treated theoretically in reference 1. In this reference, a wing in sideslip is represented by a suitably restricted system of vortices. The span loading is calculated and then integrated to obtain the rolling moment. The results show that $C_{l\beta}$ for three-dimensional unswept wings increases approximately linearly with $1/A$ and decreases slightly with taper ratio.

The vortex representation used in reference 1 for unswept wings is applied to swept straight-tapered planforms in reference 2. Here, the rolling moment is found to be a strong function of sweep, but the increment provided by sweep is relatively insensitive to variations of aspect ratio and taper ratio.

A rather different approach to the straight-tapered-wing rolling-moment problem is taken in reference 3. Here, the effects of sweep on $C_{l\beta}$ are calculated as the difference between the effective lift-curve slopes for the upwind and downwind wing panels. Panel lift-curve slope is assumed to be a function of effective sweep angle ($\Lambda \pm \beta$) and effective geometric aspect ratio. Aspect-ratio effects are then taken to be the difference between the experimental and the calculated values for swept wings.

In spite of their widely differing approaches, references 2 and 3 give similar results. For very low aspect ratios, slender-body theory, as applied in reference 4, shows that $C_{l\beta} = -2/3 A$ (per radian). This value compares well with experimental data for low-aspect-ratio delta wings.

Neither reference 2 nor reference 3 defines a lower aspect-ratio limit, below which the respective theories are invalid. However, since neither theory converges to the slender-body value at low aspect ratios, there must be a transition region between the high-aspect-ratio values of references 2 and 3 and the slender-body value of reference 4.

At subsonic speeds methods are presented for determining the rolling moment due to sideslip for the following classes of wing planforms:

Straight-Tapered Wings (conventional, trapezoidal wings)

Non-Straight-Tapered Wings

Double-delta wings
Cranked wings

These two general categories of non-straight-tapered wings are illustrated in sketch (a) of Section 4.1.3.2. Their wing-geometry parameters are presented in Section 2.2.2.

The Datcom method for straight-tapered wings is a combination of the methods of references 1, 2, 3, and 4. Reference 4 is used for low-aspect-ratio wings. References 1, 2, and 3 are used for high aspect ratios, with experimental data serving as a guide as to which theory is most applicable. For intermediate aspect ratios the experimental data of references 8 through 13 are used as a guide in constructing a faired curve between the slender-body values of reference 4 and the high-aspect-ratio values of references 1, 2, and 3. Mach number effects are calculated by the method of reference 3. The effect of uniform geometric dihedral is accounted for by the method of references 5 and 6, that of nonuniform geometric dihedral by the method of reference 6, and that of wing twist by the method of reference 7.

The Datcom method for double-delta and cranked wings is taken from reference 14. In addition to wing aspect ratio, taper ratio, dihedral angle, and sweep, the location of the leading-edge or trailing-edge sweep break is an important factor in determining the rolling moment due to sideslip of these non-straight-tapered wings. The method is based on the results presented for straight-tapered wings. The composite wing is divided into two individual panels and a "weighted-lift" relationship is applied to the rolling moment due to sideslip of each panel calculated using the straight-tapered wing method.

The subsonic methods presented in this section are valid for sideslip angles between -5° and $+5^{\circ}$ at speeds up to $M = 0.60$ and low angles of attack.

No provision is made for the effective-dihedral contribution of the wing tip shape. This contribution is important only for thick wings and taper ratios near 1.0.

DATCOM METHODS

Straight-Tapered Wings

The subsonic rolling moment due to sideslip of a straight-tapered wing with uniform geometric dihedral at low angles of attack is given by the following equations:

For $A \geq 1.0$:

$$C_{l\beta} = C_L \left[\left(\frac{C_{l\beta}}{C_L} \right)_{\Lambda_{c/2}} K_{M\Lambda} + \left(\frac{C_{l\beta}}{C_L} \right)_A \right] + \Gamma \left(\frac{C_{l\beta}}{\Gamma} K_{M\Gamma} \right) + \theta \tan \Lambda_{c/4} \frac{\Delta C_{l\beta}}{\theta \tan \Lambda_{c/4}} \text{ (per degree)}$$

5.1.2.1-a

For $A < 1.0$:

$$C_{l\beta} = C_L \left[-\frac{1}{57.3} \frac{2}{3} \frac{1}{A} \right] \cdot \Gamma \left(\frac{A}{6} \right) \text{ (per degree)} \quad 5.1.2.1-a'$$

where

$$\left(\frac{C_{l\beta}}{C_L} \right)_{\Lambda_{c/2}}$$

is the wing-sweep contribution obtained from figure 5.1.2.1-27.

$$K_{M\Lambda}$$

is the compressibility correction to the sweep contribution, obtained from figure 5.1.2.1-28a.

$$\left(\frac{C_{l\beta}}{C_L} \right)_A$$

is the aspect-ratio contribution, including taper-ratio effects, obtained from figure 5.1.2.1-28b.

$$\frac{C_{l\beta}}{\Gamma}$$

is the dihedral effect for uniform geometric dihedral, obtained from figure 5.1.2.1-29.

$$\Gamma$$

is the dihedral angle in degrees.

$$K_M \Gamma$$

is the compressibility correction factor to the uniform-geometric-dihedral effect, obtained from figure 5.1.2.1-30a.

$$\frac{\Delta C_{l\beta}}{\theta \tan \Lambda_{c/4}}$$

is the wing-twist correction factor, obtained from figure 5.1.2.1-30b.

$$\theta$$

is the wing-twist between the root and tip stations, negative for washout (see figure 5.1.2.1-30b).

For wings with nonuniform dihedral, the dihedral term of equation 5.1.2.1-a; i.e., $\Gamma \left(\frac{C_{l\beta}}{\Gamma} K_M \Gamma \right)$, is replaced by $\left(\frac{\beta C_{l\beta}}{\kappa \Gamma} \right) \left(\frac{\kappa \Gamma}{\beta} \right)$ (per degree).

where

$$\frac{\beta C_{l\beta}}{\kappa \Gamma}$$

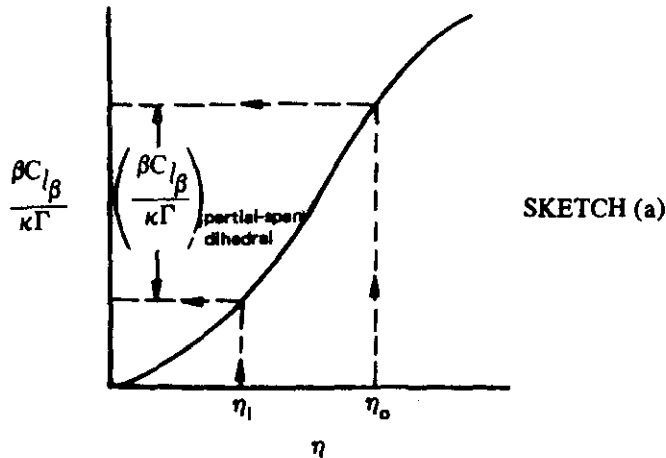
is the rolling-moment-due-to-sideslip parameter for any symmetric, spanwise distribution of dihedral angle, obtained from figure 5.1.2.1-31 as a function of Λ_β and $\beta A/\kappa$.

The parameter κ is the ratio of the two-dimensional lift-curve slope at the appropriate Mach number to 2π ; i.e., $(c_{l\alpha})_M / 2\pi$. The two-dimensional lift-curve slope is obtained from Section 4.1.1.2. For wings with airfoil sections varying in a reasonably linear manner with span, the average value of the lift-curve slopes of the root and tip sections is adequate.

The parameter Λ_β is the compressible sweep parameter given as $\Lambda_\beta = \tan^{-1} (\tan \Lambda_{c/4} / \beta)$.

$$\Gamma$$
 is the geometric dihedral in degrees.

Figure 5.1.2.1-31 applies directly to a gull-wing arrangement with the dihedral starting at the wing root and extending outboard to some spanwise station. For partial-span dihedral starting at some spanwise station η_i and extending outboard to some spanwise station η_o , the value of $\frac{\beta C_{l\beta}}{\kappa \Gamma}$ is obtained as illustrated in sketch (a).



SKETCH (a)

Lifting-surface theory has been used in reference 6 to obtain the rolling moment due to sideslip for any symmetric, spanwise distribution of dihedral. The theory is applicable only to wings for which $\beta A \geq 2$ and $\Lambda_\beta \leq 60^\circ$.

It should be noted that at $\eta = 1.0$ figure 5.1.2.1-31 gives the dihedral effect due to uniform dihedral. However, the uniform-dihedral term of equation 5.1.2.1-a has been retained because of the ease with which figure 5.1.2.1-29 can be applied.

Sample problem 1 at the conclusion of this paragraph (page 5.1.2.1-5) illustrates the use of this method applied to a straight-tapered, untwisted wing with no dihedral. A sample problem including the effect of uniform dihedral is presented in paragraph A of Section 5.2.2.1.

A comparison of low-speed test values with results calculated by using this method for straight-tapered wings is presented as table 5.1.2.1-A. The ranges of geometric parameters of the test data are:

$$0.25 \leq A \leq 6.93$$

$$-7.1^\circ \leq \Lambda_{c/2} \leq 75.3^\circ$$

$$0 \leq \lambda \leq 1.0$$

$$\Gamma = 0$$

$$\theta = 0$$

Test data are not available to permit substantiation of the effects of either wing-twist or dihedral on the wing rolling moment due to sideslip.

Non-Straight-Tapered Wings

The method for determining the rolling moment due to sideslip of double-delta and cranked wings is taken from reference 14. The non-straight-tapered wing is divided into two panels, with each panel having conventional straight-tapered geometry. Then for each of the constructed panels, the individual rolling moment due to sideslip is estimated by the method presented above for straight-tapered wings. The individual rolling-moment coefficients derived for each constructed panel are then weighted according to the proportion of the total lift that those panels produce. In order to maintain the proper span reference, the rolling-moment coefficient of the constructed inboard set of panels is further modified by multiplying its contribution by the ratio of the inboard span to the reference span (total wing span).

The method is applicable only to untwisted wings with zero degrees dihedral at low angles of attack.

The rolling moment due to sideslip of double-delta and cranked wings is obtained from the procedure outlined in the following steps:

- Step 1. Divide the composite wing into constructed inboard and outboard panels as discussed in paragraph A of Section 4.1.4.2 (see pages 4.1.4.2-5, -6), and determine their pertinent geometric parameters.
- Step 2. Determine the lift-curve slopes of the constructed inboard and outboard panels from figure 4.1.3.2-49, based on their respective areas S_i and S_o' .
- Step 3. Determine the rolling moment due to sideslip, based on the total wing area and span, by

$$\frac{C_{l\beta}}{C_L} = \frac{1}{(C_{L\alpha})_{\text{total}}} \left\{ (C_{L\alpha})_i \frac{S_i}{S_w} \left[\left(\frac{C_{l\beta}}{C_L} \right)_{A_{c/2,i}} K_M \Lambda_i + \left(\frac{C_{l\beta}}{C_L} \right)_{A_{i'}} \frac{b_i}{b_w} \right] + (C_{L\alpha})'_o \frac{S_o'}{S_w} \left[\left(\frac{C_{l\beta}}{C_L} \right)_{A_{c/2,o'}} K_M \Lambda_o' + \left(\frac{C_{l\beta}}{C_L} \right)_{A_o'} \right] \right\} \text{ (per degree)} \quad 5.1.2.1-b$$

where the subscript i and the prime and subscript o denote the constructed inboard and outboard panels, respectively.

The parameters $(C_{l\beta}/C_L)_{A_{c/2}}$, $K_M \Lambda$, and $(C_{l\beta}/C_L)_A$ are obtained from figures 5.1.2.1-27, 5.1.2.1-28a, and 5.1.2.1-28b, respectively, by using the geometry of the constructed inboard and outboard panels.

$$(C_{L\alpha})_{\text{total}} = (C_{L\alpha})_i \frac{S_i}{S_w} + (C_{L\alpha})'_o \frac{S_o'}{S_w}$$

If the aspect ratio of an individual set of constructed wing panels is less than one, $C_{l\beta}/C_L$ for that set of panels is calculated by equation 5.1.2.1-a'. For example, if the aspect ratio of the constructed inboard panel is less than one, then equation 5.1.2.1-b would be expressed as

$$\frac{C_{l\beta}}{C_L} = \left(\frac{1}{C_{L\alpha}} \right)_{\text{total}} \left\{ (C_{L\alpha})_i \frac{S_i}{S_w} \left[-\frac{1}{57.3} \frac{2}{3} \frac{1}{A_i} \right] \frac{b_i}{b_w} + (C_{L\alpha})'_o \frac{S_o'}{S_w} \left[\left(\frac{C_{l\beta}}{C_L} \right)_{A_{c/2,o'}} K_M \Lambda_o' + \left(\frac{C_{l\beta}}{C_L} \right)_{A_o'} \right] \right\}$$

Sample problem 2 on page 5.1.2.1-6 illustrates the use of this method.

A comparison of low-speed test values with results calculated by this method is presented as table 5.1.2.1-B (taken from reference 14). The limited availability of experimental data precludes substantiation of this method.

1. Straight-Tapered Wing

Sample Problems

Given: A sweptback wing of reference 29.

$$A = 4.0 \quad \lambda = 0.60 \quad \Lambda_{c/2} = 59.2^\circ \quad \Gamma = 0 \quad \theta = 0 \quad M = 0.13$$

Compute:

$$\left(\frac{C_l \beta}{C_L} \right)_{\Lambda_{c/2}} = -0.0072 \text{ per deg (figure 5.1.2.1-27, interpolated)}$$

$$\frac{A}{\cos \Lambda_{c/2}} = \frac{4.0}{\cos 59.2^\circ} = 7.81$$

$$M \cos \Lambda_{c/2} = 0.13 \cos \Lambda_{c/2} = 0.067$$

$$K_{MA} = 1.00 \text{ (figure 5.1.2.1-28a)}$$

$$\left(\frac{C_l \beta}{C_L} \right)_A = -0.0016 \text{ per deg (figure 5.1.2.1-28b)}$$

Solution:

$$\begin{aligned} \frac{C_l \beta}{C_L} &= \left[\left(\frac{C_l \beta}{C_L} \right)_{\Lambda_{c/2}} K_{MA} + \left(\frac{C_l \beta}{C_L} \right)_A \right] \text{ (equation 5.1.2.1-a with } \Gamma = 0, \theta = 0) \\ &= [(-0.0072)(1.0) + (-0.0016)] \\ &= -0.0088 \text{ per deg (based on } S_w b_w) \end{aligned}$$

This result compares with a test value of -0.0094 from reference 29.

2. Non-Straight-Tapered Wing

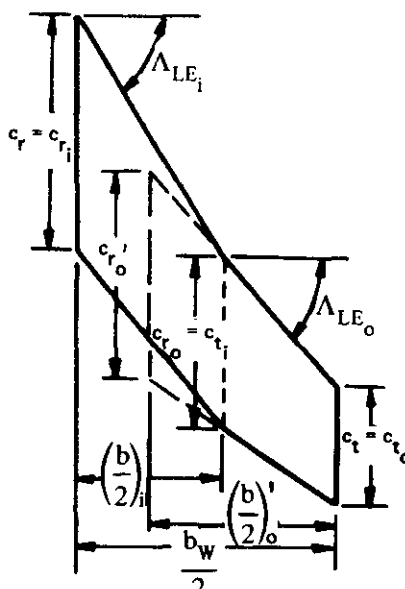
Given: A cranked wing of reference 30.

Total-Wing Characteristics:

$$\begin{aligned} S_w &= 12.10 \text{ sq ft} \quad \frac{b_w}{2} = 3.0 \text{ ft} \quad \lambda_w = 0.470 \\ \eta_B &= 0.583 \quad c_{r_w} = 2.75 \text{ ft} \quad A_w = 2.975 \\ \Lambda_{LE_i} &= 59.0^\circ \quad \Lambda_{LE_o} = 48.5^\circ \quad \Lambda_{c/2_i} = 55.0^\circ \\ \Lambda_{c/2_o} &= 41.0^\circ \quad \Gamma = 0 \quad \theta = 0 \end{aligned}$$

Constructed-Inboard-Panel Characteristics:

$$\begin{aligned} S_i &= 8.18 \text{ sq ft} \quad A_i = 1.50 \quad \lambda_i = 0.70 \\ \left(\frac{b}{2} \right)_i &= 1.75 \text{ ft} \quad \Lambda_{c/2_i} = 55.0^\circ \quad \Lambda_{LE_i} = 59.0^\circ \end{aligned}$$



$$\frac{S_i}{S_w} = 0.676$$

Constructed-Outboard-Panel Characteristics:

$$S'_o = 7.72 \text{ sq ft} \quad A'_o = 2.34 \quad \lambda'_o = 0.55 \quad \left(\frac{b}{2}\right)'_o = 2.125 \text{ ft}$$

$$\left(\Lambda_{LE}\right)'_o = \Lambda_{LE_o} = 48.5^\circ \quad \left(\Lambda_{c/2}\right)'_o = \Lambda_{c/2_o} = 41.0^\circ \quad \frac{S'_o}{S_w} = 0.638$$

Additional Characteristics:

$$M = 0.18; \quad \beta = 0.984 \quad \kappa = 1.0 \text{ (assumed)}$$

Compute

$$\left(C_{L\alpha}\right)_i \text{ and } \left(C_{L\alpha}\right)'_o \text{ (Section 4.1.3.2)}$$

$$\frac{A_i}{\kappa} \left[\beta^2 + \tan^2 \Lambda_{c/2_i} \right]^{1/2} = \frac{1.50}{1.0} \left[0.9676 + (1.4281)^2 \right]^{1/2} = 2.60$$

$$\left(\frac{C_{L\alpha}}{A}\right)_i = 1.19 \text{ per rad (figure 4.1.3.2-49)}$$

$$\left(C_{L\alpha}\right)_i = \left(\frac{C_{L\alpha}}{A}\right)_i A_i = (1.19)(1.5) = 1.785 \text{ per rad}$$

$$\frac{A'_o}{\kappa} \left[\beta^2 + \tan^2 \Lambda_{c/2'_o} \right]^{1/2} = \frac{2.34}{1.0} \left[0.9676 + (0.8693)^2 \right]^{1/2} = 3.07$$

$$\left(\frac{C_{L\alpha}}{A}\right)'_o = 1.11 \text{ per rad (figure 4.1.3.2-49)}$$

$$\left(C_{L\alpha}\right)'_o = \left(\frac{C_{L\alpha}}{A}\right)'_o A'_o = (1.11)(2.34) = 2.60 \text{ per rad}$$

$$\begin{aligned} \left(C_{L\dot{\alpha}}\right)_{\text{total}} &= \left(C_{L\alpha}\right)_i \frac{S_i}{S_w} + \left(C_{L\alpha}\right)'_o \frac{S'_o}{S_w} \\ &= 1.785(0.676) + 2.60(0.638) = 2.865 \end{aligned}$$

$$\left(\frac{C_{l\beta}}{C_L} \right)_{\Lambda_{c/2_i}} \quad \text{and} \quad \left(\frac{C_{l\beta}}{C_L} \right)_{\Lambda_{c/2_o}},$$

$$\left(\frac{C_{l\beta}}{C_L} \right)_{\Lambda_{c/2_i}} = -0.0045 \text{ per deg (figure 5.1.2.1-27, interpolated for } A_i, \lambda_i, \text{ and } \Lambda_{c/2_i})$$

$$\left(\frac{C_{l\beta}}{C_L} \right)_{\Lambda_{c/2_o}} = -0.0032 \text{ per deg (figure 5.1.2.1-27, interpolated for } A'_o, \lambda'_o, \text{ and } \Lambda_{c/2_o})$$

$K_M \Lambda_i$ and $K_M \Lambda'_o$

$$\frac{A_i}{\cos \Lambda_{c/2_i}} = \frac{1.50}{0.5736} = 2.615$$

$$M \cos \Lambda_{c/2_i} = (0.18)(0.5736) = 0.103$$

$$K_M \Lambda_i = 1.0 \text{ (figure 5.1.2.1-28a)}$$

$$\frac{A'_o}{\cos \Lambda_{c/2_o}} = \frac{2.34}{0.7547} = 3.10$$

$$M \cos \Lambda_{c/2_o} = (0.18)(0.7547) = 0.136$$

$$K_M \Lambda'_o = 1.0 \text{ (figure 5.1.2.1-28a)}$$

$$\left(\frac{C_{l\beta}}{C_L} \right)_{A_i} \quad \text{and} \quad \left(\frac{C_{l\beta}}{C_L} \right)_{A'_o}$$

$$\left(\frac{C_{l\beta}}{C_L} \right)_{A_i} = -0.0065 \text{ per deg (figure 5.1.2.1-28b at } A_i \text{ and } \lambda_i)$$

$$\left(\frac{C_{l\beta}}{C_L} \right)_{A'_o} = -0.0034 \text{ per deg (figure 5.1.2.1-28b at } A'_o \text{ and } \lambda'_o)$$

Solution:

$$\begin{aligned}
 \frac{C_{l\beta}}{C_L} &= \frac{1}{(C_{L\alpha})_{\text{total}}} \left\{ \left(C_{L\alpha} \right)_i \frac{S_i}{S_w} \left[\left(\frac{C_{l\beta}}{C_L} \right)_{A_{c/2_i}} K_M \Lambda_i + \left(\frac{C_{l\beta}}{C_L} \right)_{A_i} \right] \frac{b_i}{b_w} \right. \\
 &\quad \left. + \left(C_{L\alpha} \right)_o \frac{S'_o}{S_w} \left[\left(\frac{C_{l\beta}}{C_L} \right)_{A_{c/2_o}} K_M \Lambda'_o + \left(\frac{C_{l\beta}}{C_L} \right)_{A'_o} \right] \right\} \text{ (equation 5.1.2.1-b)} \\
 &= \frac{1}{2.865} \left\{ 1.785 (0.676) \left[-0.0045 (1.0) + (-0.0065) \frac{3.5}{6.0} + 2.60 (0.638) \left[-0.0032 (1.0) + (-0.0034) \right] \right] \right\} \\
 &= \frac{1}{2.865} \left\{ -0.00774 - 0.01095 \right\} = -0.00652 \text{ per deg (based on } S_w b_w)
 \end{aligned}$$

This result compares with a test value of -0.00628 from reference 30.

B. TRANSONIC

As the Mach number increases above $M = 0.6$, the rolling-moment derivative $C_{l\beta}$ of straight-tapered wings also increases, up to the force-break Mach number. The increase is nonlinear, with the largest gradient occurring just below the force-break Mach number. Beyond the force-break Mach number the value of the rolling-moment derivative falls off abruptly.

This variation with Mach number is quite similar to that of the wing lift-curve slope, as discussed in paragraph B of Section 4.1.3.2. This correspondence should perhaps be expected, since $C_{l\beta}$ has been successfully treated by using the effective lift-curve slopes of the upwind and downwind panels (reference 3).

The similarity in Mach number characteristics between rolling moment and lift-curve slope suggests a transonic interpolation method based on lift-curve slope, for calculating rolling moment. An interpolation equation is presented that is based on the square of the lift-curve slope values at $M = 0.6$ and at $M = 1.4$.

Although this interpolation method gives good results in most cases, it must be recognized that it is an interpolation technique and should be replaced by more accurate methods or data if they are available.

The Datcom method is limited to straight-tapered wings and is valid for sideslip angles between -5° and $+5^\circ$ and low angles of attack.

DATCOM METHOD

The wing rolling moment due to sideslip of straight-tapered wings may be approximated through the transonic region by means of the interpolation formula

$$\frac{C_{l\beta}}{C_L} = \left\{ \left[\frac{\left(\frac{C_{l\beta}}{C_N} \right)_{M=1.4} - \left(\frac{C_{l\beta}}{C_L} \right)_{M=0.6}}{\left(C_{N\alpha}^2 \right)_{M=1.4} - \left(C_{L\alpha}^2 \right)_{M=0.6}} \right] \left(\frac{M-0.6}{0.8} \right) + \left(\frac{C_{l\beta}}{C_L} \right)_{M=0.6} \right\} \left(C_{L\alpha}^2 \right)^{-1} \text{ (per degree)} \quad 5.1.2.1-c$$

where

$$\left(\frac{C_{l\beta}}{C_L} \right)_{M=0.6}$$

is the sideslip derivative at $M = 0.6$ from the straight-tapered wing method of paragraph A.

$$\left(\frac{C_{l\beta}}{C_N} \right)_{M=1.4}$$

is the sideslip derivative at $M = 1.4$ from the straight-tapered-wing method of paragraph C.

$$\left(C_{L\alpha}^2 \right)_{M=0.6}$$

is the square of the lift-curve slope at $M = 0.6$ from the straight-tapered-wing method of paragraph A of Section 4.1.3.2 (figure 4.1.3.2-49).

$$\left(C_{N\alpha}^2 \right)_{M=1.4}$$

is the square of the normal-force-curve slope at $M = 1.4$ from the straight-tapered-wing method of paragraph C of Section 4.1.3.2.

The transonic interpolation procedure is the same for wing-alone and wing-body configurations. Since the only available experimental data are for wing-body configurations, the sample problem of paragraph B of Section 5.2.2.1 can be taken as an example of the application of this method.

C. SUPERSONIC

The rolling moment due to sideslip for a wing at supersonic speeds is mainly a function of planform, Mach number, and dihedral angle.

A comprehensive summary of theoretical methods for calculating the effect of planform on rolling moment is given in reference 15. The information presented in this reference is not generalized, but is presented for discrete straight-tapered planforms over certain speed ranges. This is done because the theoretical calculations available are limited primarily to combinations of planforms and Mach lines that do not have mutually interacting subsonic edges. Techniques for handling mutually interacting subsonic edges are lengthy and involved. Consequently, numerical results are available for only a relatively few planforms that require such methods. Even when the boundary conditions can be specified and a linear-theory analysis carried out, the rolling moment cannot be generally expressed as a linear function of sideslip angle (see reference 16). To obtain the derivative $C_{l\beta}$, it is necessary to plot C_l against β and measure the slope.

For planforms having streamwise tips there are additional questions concerning whether or not the Kutta condition applies at the trailing tip. In reference 6 it is assumed that it does. In reference 8 it is assumed that it does not, and values of opposite (negative) sign are obtained. In very few cases should any significant contribution be expected from the trailing tip. Nevertheless, most experimental measurements made to date give negative values of $C_{l\beta}$.

Reference 17 indicates that agreement between experiment and theory for straight-tapered swept wings with streamwise tips may be obtained by integrating the span loading at combined angles of attack and sideslip; references 7 and 18 show calculations for such span loadings. However, there is no simple analytic expression for calculating $C_{l\beta}/\alpha$, and general digital computer solutions are not yet available.

For delta wings, the theory of reference 16 predicts a discontinuity and change in sign for $C_{l\beta}$ at the Mach number at which the leading edge is sonic. Since discontinuities of this type do not occur physically, there is some question as to what shape the $C_{l\beta}$ curve should have in the sonic-leading-edge region.

The above discussions indicate the present uncertain status of supersonic rolling-moment theory.

None of the previously mentioned theoretical methods are used in the Datcom. However, the discussion is included because no method yet developed is entirely satisfactory for all configurations over the entire speed range. It is felt that the Datcom does give best results for the widest range of configurations and speeds, but it must be recognized that there may be regions where one of the references mentioned gives better results.

Methods are presented for determining the rolling moment due to sideslip for the following classes of wing planforms:

Straight-Tapered Wings (conventional, trapezoidal wings)

Non-Straight-Tapered Wings

Double-delta wings

Cranked wings

These two general categories of non-straight-tapered wings are illustrated in sketch (a) of Section 4.1.3.2. Their wing-geometry parameters are presented in Section 2.2.2.

The straight-tapered-wing method is essentially that of reference 19, with the nomograph of page J.2-1.10 represented by an equation. This is done because of the inaccuracy of the nomograph at the higher Mach numbers, where the rolling moments are small. The nomograph of reference 19 was derived by writing the effective lift-curve slope for each wing panel as a function of sweepback and sideslip, multiplying this effective lift-curve slope by the spanwise center-of-pressure location, and taking the derivative of this product with respect to sideslip angle. One characteristic of this method is that it does not give positive rolling moments with positive sideslip angles (negative dihedral effect) for any speed range or planform. This is in direct opposition to certain other theories (reference 16) but is in qualitative agreement with experimental data. (References 20 through 27).

Another characteristic of the straight-tapered-wing method is that it predicts a linear variation of $C_{l\beta}$ with C_L . This, however, is not in agreement with the experimental data of references 20 through 27. In these tests, $C_{l\beta}$ is nonlinear with both angle of attack and sideslip. Since all these experimental tests are on wing-body combinations, it is not known to what extent the experimental nonlinearities may be caused by the body or by wing-body interference effects.

Geometric-dihedral effects are accounted for by the method of reference 28. This reference bases the dihedral parameter $C_{l\beta}/\Gamma$ on the damping-in-roll parameter C_{l_p} , by means of the following equation:

$$\frac{C_{l\beta}}{\Gamma} = \frac{2}{(57.3)^2} \left(\frac{1+2\lambda}{1+3\lambda} \right) C_{l_p} \quad (\text{per degree}^2) \quad 5.1.2.1-d$$

Although this equation is strictly an approximation, comparison of experimental data with values calculated from it shows that it gives good results. This success is largely due to the use of C_{l_p} as a base, since this latter derivative is one for which supersonic theory has given best results.

The Datcom method for double-delta and cranked wings is taken from reference 14. The supersonic prediction method has resulted from an analysis based on the same guide lines as the subsonic analysis. The straight-tapered-wing method is used as a base and a wing-lift prediction technique is used to weight the rolling-moment contributions of the various portions of the wing.

The nonlinearities of $C_{l\beta}$ with both angle of attack and sideslip, discussed above in connection with straight-tapered wings, also exist for the double-delta and cranked wings investigated during the course of the study conducted in connection with reference 14.

DATCOM METHODS

Straight-Tapered Wings

The rolling moment at Mach numbers above 1.4 for conventional, untwisted wings with uniform geometric dihedral in the linear angle-of-attack and sideslip ranges is given by

$$C_{l\beta} = -0.061 C_N \frac{C_{N\alpha}}{57.3} \left[1 + \lambda (1 + \Lambda_{LE}) \right] \left(1 + \frac{\Lambda_{LE}}{2} \right) \frac{\tan \Lambda_{LE}}{\beta} \left[\frac{M^2 \cos^2 \Lambda_{LE}}{A} + \left(\frac{\tan \Lambda_{LE}}{4} \right)^{4/3} \right] + \Gamma \left(\frac{C_{l\beta}}{\Gamma} \right) \quad (\text{per degree}) \quad 5.1.2.1-e$$

where

Λ_{LE} is the wing leading-edge sweep in radians.

$C_{N\alpha}$ is the wing normal-force-curve slope per radian, obtained from the straight-tapered-wing method of paragraph C of Section 4.1.3.2.

$\frac{C_{l\beta}}{\Gamma}$ is the dihedral parameter calculated by using equation 5.1.2.1-d with C_{l_p} (per radian) obtained from paragraph C of Section 7.1.2.2.

Γ is the dihedral angle in degrees (uniform dihedral).

Sample problem 1 on page 5.1.2.1-16 illustrates the use of this method applied to a straight-tapered wing with zero degrees dihedral.

A sample problem including the effect of uniform dihedral is presented in paragraph C of Section 5.2.2.1.

A comparison of test values of supersonic wing rolling moments due to sideslip with results calculated by using this method is presented as table 5.1.2.1-C. The ranges of Mach number and geometric parameters of the data are:

$$3.0 \leq A \leq 4.0$$

$$20.9^\circ \leq \Lambda_{LE} \leq 62.9^\circ$$

$$0.140 \leq \lambda \leq 0.250$$

$$\Gamma = 0$$

$$1.62 \leq M \leq 4.65$$

A data summary of calculated versus test values of the dihedral parameter $(\Delta C_{l\beta})_r$ (including fuselage effects) is presented for wing-body configurations at supersonic speeds in Section 5.2.2.1 (table 5.2.2.1-E).

Non-Straight-Tapered Wings

The method for determining the rolling moment due to sideslip of double-delta and cranked wings is taken from reference 14. The composite wing is divided into two panels with each panel having conventional straight-tapered geometry. Then the lift-curve slopes and geometric characteristics of the two panels are substituted into the straight-tapered-wing method (equation 5.1.2.1-e). In order to maintain the proper span reference the rolling-moment contribution of the innermost panel is further modified by multiplying its contribution by the ratio of its span to the reference span (total wing span).

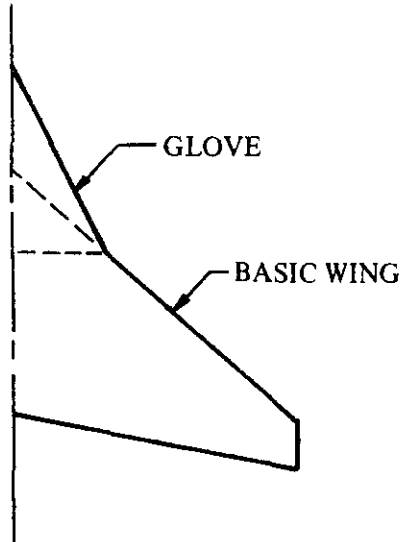
The method is applicable only to untwisted wings with zero degrees dihedral at low angles of attack and sideslip. A further restriction is that the composite-wing trailing edge must be unbroken (straight trailing edge from root to tip).

The rolling-moment derivative $C_{l\beta}$ of double-delta and cranked wings is obtained from the procedure outlined in the following steps:

- Step 1. Divide the composite wing into two panels as follows (see sketch (b)), and determine their pertinent geometric characteristics.

Basic Wing — the outboard leading and trailing edges extended to the center line.
This constructed panel is denoted by the subscript bw.

Glove — a delta wing superimposed over the basic wing. The glove leading edge is that of the inboard panel. This zero-taper wing is denoted by the subscript g.



SKETCH (b)

- Step 2. Determine the normal-force-curve slopes of the glove and basic wing (per radian) by using the supersonic design charts of Section 4.1.3.2. $(C_{N\alpha})_{bw}$ is obtained from figure 4.1.3.2-56 and $(C_{N\alpha})_g$ from figure 4.1.3.2-63.

Step 3. Determine the "lift-interference factor" K_L from figure 4.1.3.2-6] as a function of the glove normal-force-curve slope.

Step 4. Determine the rolling moment due to sideslip, based on the total wing area and span, by

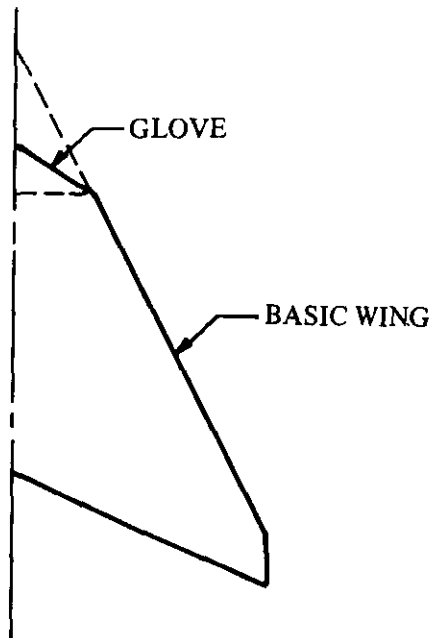
$$\frac{C_{l\beta}}{C_N} = -0.061 \left[\frac{K_L (C_{N\alpha})_g \frac{S_g}{S_w}}{57.3} \right] \left(1 + \frac{\Lambda_{LEg}}{2} \right) \left(\frac{\tan \Lambda_{LEg}}{\beta} \right) \left[\frac{M^2 \cos^2 \Lambda_{LEg}}{A_g} + \left(\frac{\tan \Lambda_{LEg}}{4} \right)^{4/3} \right] \frac{b_g}{b_w}$$

$$-0.061 \left[\frac{K_L (C_{N\alpha})_{bw} \frac{S_{bw}}{S_w}}{57.3} \right] \left[1 + \lambda_{bw} \left(1 + \Lambda_{LE_{bw}} \right) \right] \left(1 + \frac{\Lambda_{LE_{bw}}}{2} \right) \cdot$$

$$\left(\frac{\tan \Lambda_{LE_{bw}}}{\beta} \right) \left[\frac{M^2 \cos^2 \Lambda_{LE_{bw}}}{A_{bw}} + \left(\frac{\tan \Lambda_{LE_{bw}}}{4} \right)^{4/3} \right] \text{ (per degree)} \quad 5.1.2.1-f$$

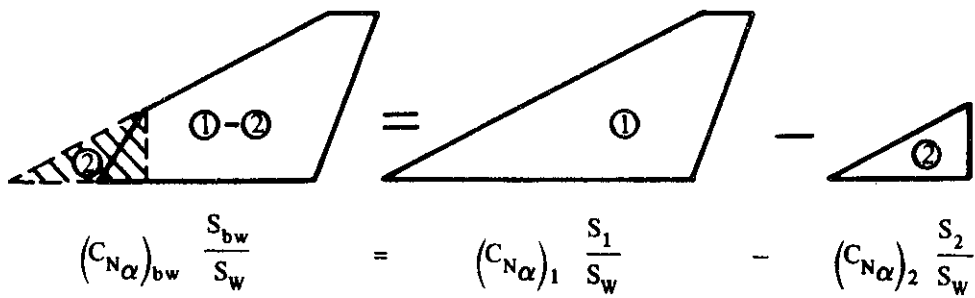
where the subscripts g and bw denote the glove and basic wing, respectively. The leading-edge sweep of the panels, Λ_{LE_g} and $\Lambda_{LE_{bw}}$, are in radians.

Another class of composite wings of practical interest are those with the outboard wing sweep greater than the inboard wing sweep. In treating such wings, if the basic wing breakdown is defined as in sketch (b), some additional wing area is created forward of the wing sweep break as illustrated in sketch (c).



SKETCH (c)

For this class of composite wings the normal-force-curve slope of the basic wing $(C_{N\alpha})_{bw}$ is determined by extending the basic-wing leading edge to the center line, calculating the normal-force-curve slope of the extended basic wing panel, and calculating and subtracting the normal-force-curve slope of the section of the basic-wing panel forward of the wing sweep break. This is shown schematically in sketch (d).



SKETCH (d)

During the course of study conducted in connection with reference 14, the normal-force-curve slopes of the basic wing and glove were correlated with test data for configurations with the outboard wing sweep greater than the inboard wing sweep through the use of an empirical correlation factor K , which corresponds to the "lift-interference factor" K_L . A complete analysis was not accomplished; however, based on a limited amount of rolling-moment data, K appears to be approximately one.

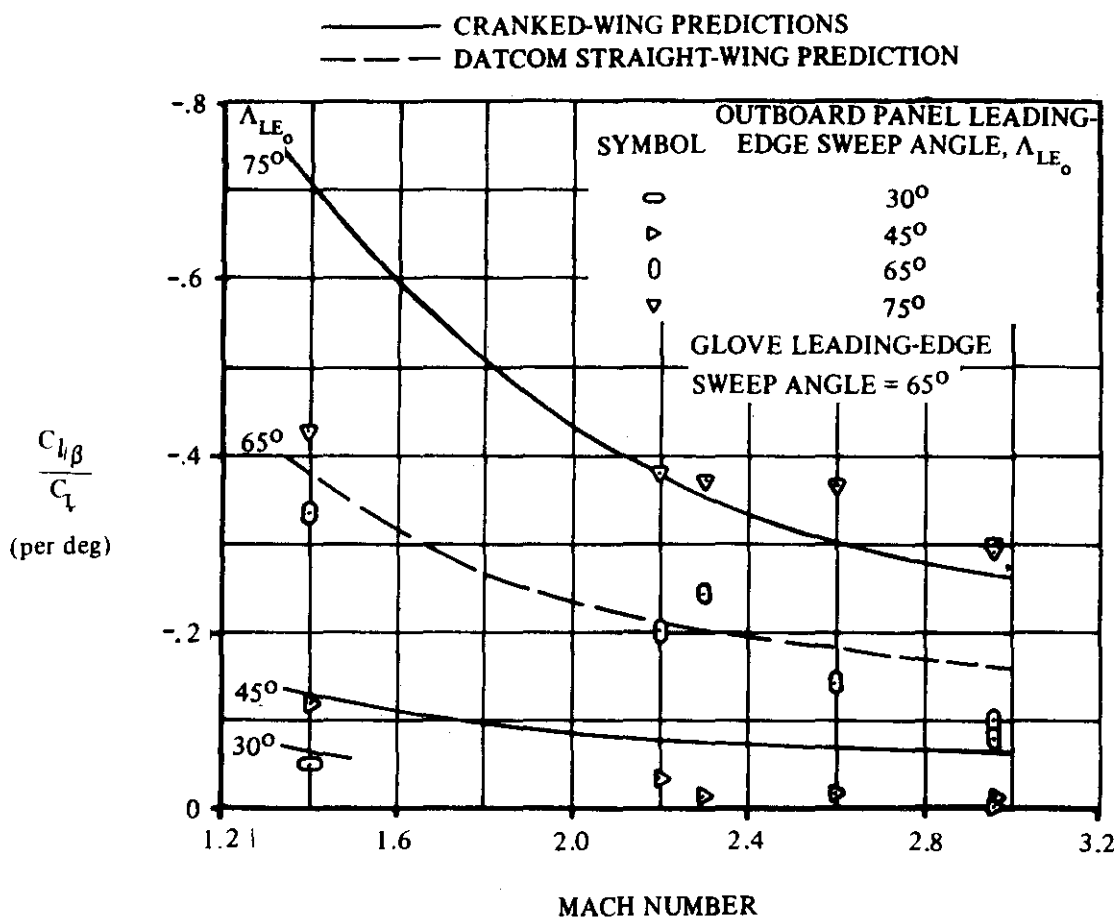
The rolling moment due to sideslip for this class of composite wings is obtained using equation 5.1.2.1-f in the following manner:

1. The term K_L is replaced by the term K , where $K = 1.0$.
2. The product of the normal-force-curve slope and the ratio of basic-wing area to total-wing area is replaced by the expression shown in sketch (d).
3. The aspect ratio, taper ratio, and sweepback of the basic wing are considered to be those of the extended basic wing, which corresponds to panel ① in sketch (d).
4. The glove has the same geometry as in cases where the glove sweep is greater than the outboard wing sweep.

Sample problem 2 on page 5.1.2.1-18 illustrates the use of the non-straight-tapered-wing method.

A comparison of test values of supersonic wing rolling moments due to sideslip with results calculated by using this method is presented as table 5.1.2.1-D (taken from reference 14). A specific comparison of test values with calculated results for a cranked wing is shown in sketch (e). Also shown is a comparison of test values and results calculated by using the straight-tapered-wing method for the case where the basic-wing and the glove sweep angles are the same.

It is suggested that this method be restricted to Mach numbers above 1.4 and to glove leading-edge sweep angles less than 80° . At high leading-edge sweep angles the terms $\tan \Lambda_{LEg} / \beta$ and $(\tan \Lambda_{LEg} / 4)^{4/3}$ become excessively large and equation 5.1.2.1-f overpredicts $C_l \beta$.



COMPARISON OF CRANKED-WING ROLLING-MOMENT-COEFFICIENT PREDICTIONS WITH TEST DATA

SKETCH (e)

Sample Problems

1. Straight-Tapered Wing

Given: A wing-body configuration with a midwing location from reference 25.

$$A = 3.0$$

$$\lambda = 0.250$$

$$\Lambda_{LE} = 30.97^\circ = 0.540 \text{ rad}$$

$$\Gamma = 0$$

$$M = 2.01; \beta = 1.744$$

Airfoil section: 4-percent circular arc

Compute:

$$\Delta y = 0.47 \text{ (figure 2.2.1-8)}$$

$$\Delta y_{\perp} = \frac{\Delta y}{\cos \Lambda_{LE}} = \frac{0.47}{0.8575} = 0.548 \quad (\text{Section 4.1.3.2})$$

$$\delta_{\perp} = \tan^{-1} \frac{\Delta y_{\perp}}{5.85} = \tan^{-1} 0.09368 = 5.35^0$$

$$\frac{\tan \Lambda_{LE}}{\beta} = \frac{0.6002}{1.744} = 0.3442$$

$$\frac{M^2 \cos^2 \Lambda_{LE}}{A} = \frac{(2.01)^2 (0.8575)^2}{3.0} = 0.990$$

$$\left(\frac{\tan \Lambda_{LE}}{4} \right)^{4/3} = \left(\frac{0.6002}{4.0} \right)^{4/3} = 0.0797$$

$C_{N\alpha}$ (Section 4.1.3.2)

$$A \tan \Lambda_{LE} = (3.0) (0.6002) = 1.80$$

$$\beta (C_{N\alpha})_{\text{theory}} = 3.83 \text{ per rad (figure 4.1.3.2-56c)}$$

$$(C_{N\alpha})_{\text{theory}} = 2.20 \text{ per rad}$$

$$\frac{C_{N\alpha}}{(C_{N\alpha})_{\text{theory}}} = 1.0 \quad (\text{figure 4.1.3.2-60})$$

$$C_{N\alpha} = \frac{C_{N\alpha}}{(C_{N\alpha})_{\text{theory}}} (C_{N\alpha})_{\text{theory}} = (1.0) (2.20) = 2.20 \text{ per rad}$$

Solution:

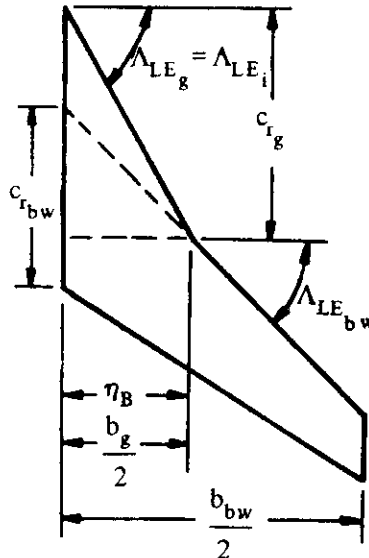
$$\begin{aligned} \frac{C_{I\beta}}{C_N} &= -0.061 \frac{C_{N\alpha}}{57.3} \left[1 + \lambda (1 + \Lambda_{LE}) \right] \left(1 + \frac{\Lambda_{LE}}{2} \right) \frac{\tan \Lambda_{LE}}{\beta} \left[\frac{M^2 \cos^2 \Lambda_{LE}}{A} + \left(\frac{\tan \Lambda_{LE}}{4} \right)^{4/3} \right] \\ &\quad (\text{equation 5.1.2.1-e with } \Gamma = 0) \\ &= -0.061 \frac{2.20}{57.3} \left[1 + 0.25 (1 + 0.540) \right] \left(1 + \frac{0.540}{2} \right) (0.3442) [0.990 + 0.0797] \\ &= -0.00152 \text{ per deg (based on } S_w b_w) \end{aligned}$$

This result compares with a test value of -0.00143 from reference 25.

2. Non-Straight-Tapered Wing

Given: A hypothetical cranked wing

Total Wing Characteristics:



$$S_w = 7.05 \text{ sq ft} \quad \frac{b_w}{2} = 2.50 \text{ ft}$$

$$c_{t_w} = 0.608 \text{ ft} \quad \eta_B = 0.400 \quad \Lambda_{LE_i} = 60^\circ$$

$$\Lambda_{LE_o} = 45^\circ$$

Glove Characteristics:

$$A_g = 2.31 \quad \lambda_g = 0 \quad S_g = 1.732 \text{ sq ft}$$

$$\frac{S_g}{S_w} = 0.246 \quad \frac{b_g}{2} = 1.0 \text{ ft}$$

$$\Lambda_{LE_g} = \Lambda_{LE_i} = 60^\circ = 1.047 \text{ rad}$$

Basic Wing Characteristics:

$$A_{bw} = 3.97 \quad \lambda_{bw} = 0.407 \quad S_{bw} = 6.30 \text{ sq ft} \quad \frac{b_{bw}}{2} = \frac{b_w}{2} = 2.50 \text{ ft}$$

$$\Lambda_{LE_{bw}} = \Lambda_{LE_o} = 45^\circ = 0.785 \text{ rad} \quad \frac{S_{bw}}{S_w} = 0.894$$

Additional Characteristics:

$$M = 2.96; \beta = 2.79$$

Compute:

$$1 + \frac{\Lambda_{LE_g}}{2} = 1.524$$

$$\frac{\tan \Lambda_{LE_g}}{\beta} = \frac{1.732}{2.79} = 0.621$$

$$\frac{M^2 \cos^2 \Lambda_{LE_g}}{A_g} = \frac{(2.96)^2 (0.50)^2}{2.31} = 0.948$$

$$\left(\frac{\tan \Lambda_{LE_g}}{4}\right)^{4/3} = \left(\frac{1.732}{4}\right)^{4/3} = 0.3276$$

$$\left(C_{N\alpha}\right)_g \quad (\text{Section 4.1.3.2})$$

$$\frac{\beta}{\tan \Lambda_{LE_g}} = \frac{2.79}{1.732} = 1.611$$

$$\frac{\left(C_{N\alpha}\right)_g}{A_g} = 0.624 \text{ per rad (figure 4.1.3.2-63)}$$

$$\left(C_{N\alpha}\right)_g = 1.44 \text{ per rad}$$

K_L (Section 4.1.3.2)

$$\frac{1}{\beta} \left(C_{N\alpha}\right)_g \frac{S_g}{S_w} = \frac{1}{2.79} (1.44) (0.246) = 0.127 \text{ per rad}$$

$$K_L = 0.873 \text{ (figure 4.1.3.2-61)}$$

$$1 + \lambda_{LE_{bw}} = 1.785; 1 + \frac{\Lambda_{LE_{bw}}}{2} = 1.393$$

$$\frac{\tan \Lambda_{LE_{bw}}}{\beta} = \frac{1.00}{2.79} = 0.358$$

$$\frac{M^2 \cos^2 \Lambda_{bw}}{A_{bw}} = \frac{(2.96)^2 (0.7071)^2}{3.97} = 1.103$$

$$\left(\frac{\tan \Lambda_{LE_{bw}}}{4}\right)^{4/3} = \left(\frac{1.00}{4.0}\right)^{4/3} = 0.1575$$

$\left(C_{N\alpha}\right)_{bw}$ (Section 4.1.3.2)

$$\frac{\tan \Lambda_{LE_{bw}}}{\beta} = 0.358; A \tan \Lambda_{LE_{bw}} = 3.97$$

$$\beta C_{N\alpha} = 4.07 \text{ per rad (figures 4.1.3.2-56c through -56e, interpolated)}$$

$$\left(C_{N\alpha}\right)_{bw} = 1.46 \text{ per rad}$$

Solution:

$$\begin{aligned}
 \frac{C_l \beta}{C_L} &= -0.061 \left[\frac{K_L \left(C_{N\alpha} \right)_g \frac{S_g}{S_w}}{57.3} \right] \left(1 + \frac{\Lambda_{LEg}}{2} \right) \left(\frac{\tan \Lambda_{LEg}}{\beta} \right) \left[\frac{M^2 \cos^2 \Lambda_{LEg}}{A_g} + \left(\frac{\tan \Lambda_{LEg}}{4} \right)^{4/3} \right] \frac{b_g}{b_w} \\
 &\quad -0.061 \left[\frac{K_L \left(C_{N\alpha} \right)_{bw} \frac{S_{bw}}{S_w}}{57.3} \right] \left[1 + \lambda_{bw} (1 + \Lambda_{LEbw}) \right] \left(1 + \frac{\Lambda_{LEbw}}{2} \right) \\
 &\quad \left(\frac{\tan \Lambda_{LEbw}}{\beta} \right) \left[\frac{M^2 \cos^2 \Lambda_{LEbw}}{A_{bw}} + \left(\frac{\tan \Lambda_{LEbw}}{4} \right)^{4/3} \right] \tag{equation 5.1.2.1-f} \\
 &= -0.061 \left[\frac{0.873 (1.44) (0.246)}{57.3} \right] (1.524) (0.621) [0.948 + 0.3276] \frac{2.0}{5.0} \\
 &\quad -0.061 \left[\frac{0.873 (1.46) (0.894)}{57.3} \right] [1 + 0.407 (1.785)] (1.393) (0.358) [1.103 + 0.1575] \\
 &= -0.061 [0.00261] - 0.061 [0.0216] \\
 &= -0.00148 \text{ per deg}
 \end{aligned}$$

REFERENCES

1. Weissinger, J.: Der schiebende Tragflügel bei gesunder Stromung. Bericht S 2 der Lilienthal-Gesellschaft für Luftfahrtforschung, 1938-39. (U)
2. Queijo, M.: Theoretical Span Load Distributions and Rolling Moments for Sideslipping Wings of Arbitrary Planform in Incompressible Flow. NACA TR 1269, 1956. (U)
3. Polhamus, E., and Sleeman, W., Jr.: The Rolling Moment Due to Sideslip of Swept Wings at Subsonic and Transonic Speeds. NASA TN D-209, 1960. (U)
4. Ribner, H.: The Stability Derivatives of Low-Aspect Ratio Triangular Wings at Subsonic and Supersonic Speeds. NACA TN 1423, 1947. (U)
5. Bird, J.: Some Theoretical Low-Speed Span Loading Characteristics of Swept Wings in Roll and Sideslip. NACA TR 969, 1950. (U)
6. DaYoung, J.: Theoretical Antisymmetric Span Loading for Wings of Arbitrary Plan Form at Subsonic Speeds. NACA TR 1056, 1951. (U)
7. Sherman, W., and Margolis, K.: Theoretical Calculations of the Effects of Finite Sideslip at Supersonic Speeds on the Span Loading and Rolling Moment for Families of Thin Sweptback Tapered Wings at Angle of Attack. NACA TN 3046, 1953. (U)
8. Goodman, A., and Brewer, J.: Investigation at Low Speeds of the Effect of Aspect Ratio and Sweep on Static and Yawing Stability Derivatives of Untapered Wings. NACA TN 1669, 1948. (U)
9. McCormack, G., and Walling, W.: Aerodynamic Study of a Wing-Fuselage Combination Employing a Wing Swept Back 63°—Investigation of a Large-Scale Model at Low Speed. NACA RM A8D02, 1949. (U)
10. Goodman, A., and Thomas, D.: Effects of Wing Position and Fuselage Size on the Low-Speed Static and Rolling Stability Characteristics of a Delta-Wing Model. NACA TR 1224, 1955. (U)

11. Wolhart, W., and Thomas, D.: Static Longitudinal and Lateral Stability Characteristics at Low Speeds of Unswept-Midwing Models Having Wings with an Aspect Ratio of 2, 4, or 6. NACA TN 3649, 1956. (U)
12. Thomas, D., and Wolhart, W.: Static Longitudinal and Lateral Stability Characteristics at Low Speed of 45° Sweptback-Midwing Models Having Wings with an Aspect Ratio of 2, 4, or 6. NACA TN 4077, 1957. (U)
13. Letko, W.: Experimental Determination at Subsonic Speeds of the Oscillatory and Static Lateral Stability Derivatives of a Series of Delta Wings with Leading-Edge Sweep from 30° to 86.5°. NACA RM L57A30, 1957. (U)
14. Benepe, D.B., Kouri, B.G., Webb, J.B., et al: Aerodynamic Characteristics of Non-Straight-Taper Wings. AFFDL-TR-66-73, 1966. (U)
15. Jones, A., and Aiksne, A.: A Summary of Lateral-Stability Derivatives Calculated for Wing Plan Forms in Supersonic Flow. NACA TN 1052, 1951. (U)
16. Jones, A., and Spreiter, J.: The Rolling Moment Due to Sideslip of Triangular, Trapezoidal, and Related Plan Forms in Supersonic Flow. NACA TN 1700, 1948. (U)
17. Harmon, S.: Stability Derivatives at Supersonic Speeds of Thin Rectangular Wings with Diagonals Ahead of Tip Mach Lines. NACA TR 925, 1949. (U)
18. Margolis, K., Sherman, W., and Hennah, M.: Theoretical Calculation of the Pressure Distribution, Span Loading, and Rolling Moment due to Sideslip at Supersonic Speeds for Thin Sweptback Tapered Wings with Supersonic Trailing Edges and Wing Tips Parallel to the Axis of Wing Symmetry. NACA TN 2898, 1953. (U)
19. Decker, J., et al: USAF Stability and Control Handbook, M-03671, 1956. (C) Title Unclassified
20. Lessing, H.: Aerodynamic Study of a Wing-Fuselage Combination Employing a Wing Swept Back 63°—Effect of Sideslip on Aerodynamic Characteristics at a Mach Number of 1.4 with the Wing Twisted and Cambered. NACA RM A50F09, 1950. (U)
21. Hamilton, C.: Aerodynamic Characteristics at Supersonic Speeds of a Series of Wing-Body Combinations Having Cambered Wings With an Aspect Ratio of 3.5 and a Taper Ratio of 0.2. Effects of Sweep Angle and Thickness Ratio on the Static Lateral Stability Characteristics at $M = 2.01$. NACA RM L52E23, 1952. (U)
22. Christensen, F.: An Experimental Investigation of Four Triangular-Wing—Body Combinations in Sideslip at Mach Numbers 0.6, 0.9, 1.4, and 1.7. NACA RM A53L22, 1954. (U)
23. Dunning, R., and Ulman, E.: Static Longitudinal and Lateral Stability Data From an Exploratory Investigation at Mach Number 4.06 of an Airplane Configuration Having a Wing of Trapezoidal Plan Form. NACA RM L55A21, 1956. (U)
24. Spearman, M.: Investigation of the Aerodynamic Characteristics in Pitch and Sideslip of a 45° Sweptback-Wing Airplane Model With Various Vertical Locations of the Wing and Horizontal Tail. NACA RM L55B18, 1955. (U)
25. Robinson, R.: Effects of Vertical Location of the Wing and Horizontal Tail on the Static Lateral and Directional Stability of a Trapezoidal-Wing Airplane Model at Mach Numbers of 1.41 and 2.01. NACA RM L58C18, 1958. (U)
26. Jaquet, B.M., and Fournier, R.: Effects of Wing Sweep, Horizontal-Tail Configuration, and a Ventral Fin on Static Stability Characteristics of a Model with Wing of Aspect Ratio 3 at Mach Numbers from 2.29 to 4.65. NACA RM L58E06, 1958. (U)
27. Boatright, W.: Experimental Investigation of Effects of Wing Plan Form and Dihedral Angle on Sideslip Derivatives of Sweptback-Wing—Body Combinations at Supersonic Speeds. NACA RM L58E08, 1958. (U)
28. Purser, P.: An Approximation to the Effect of Geometric Dihedral on the Rolling Moment due to Sideslip for Wings at Transonic and Supersonic Speeds. NACA RM L52B01, 1952. (U)
29. Wolhart, W., and Thomas, D.: Static Longitudinal and Lateral Stability Characteristics at Low Speed of 60° Sweptback-Midwing Models Having Wings With an Aspect Ratio of 2, 4, or 6. NACA TN 4397, 1958. (U)
30. Mansell, C.J.: Low-Speed Wind-Tunnel Tests on Two Thin Cranked Wings with 60-Degree Sweepback Inboard. ARC R&M 2995, 1957. (U)
31. Kruger, W.: Six-Component Measurements on a Cranked Swept-Back Wing. Great Britain Ministry of Supply Translation 816, 1947. (U)
32. Lange, R.H., and McLemore, H.C.: Low-Speed Lateral Stability and Aileron Effectiveness Characteristics at a Reynolds Number of 3.5×10^6 of a Wing With Leading Edge Sweepback Decreasing From 45° at the Root to 20° at the Tip. NACA RM L50D14, 1950. (U)

33. Jernell, L.S.: Aerodynamic Characteristics at Mach Numbers from 2.50 to 4.63 of a Variable-Sweep Model at Sweep Angles from 55° to 75°. NASA TM X-959, 1964. (C) Title Unclassified
34. Landrum, E.J.: Effect of Skewed Wing-Tip Controls on a Variable-Sweep Wing-Fuselage Configuration at Mach Numbers of 1.41 and 2.20. NASA TM X-951, 1964. (C) Title Unclassified
35. Landrum, E.J., and Babb, C.D.: Effect of Skewed Wing-Tip Controls on a Variable-Sweep Wing-Fuselage Configuration at Mach Numbers from 2.60 to 4.62. NASA TM X-1031, 1964. (C) Title Unclassified
36. Spearman, M.L., and Foster, G.V.: Static Longitudinal and Lateral Aerodynamic Characteristics at Mach Number of 2.01 of a Tailless Delta V/STOL Configuration Having Variable-Sweep Wing Panels. NASA TM X-634, 1961. (C) Title Unclassified
37. Spearman, M.L.: Static Longitudinal and Lateral Aerodynamic Characteristics at Mach Numbers of 1.41 and 2.20 of a Model of a Low Aspect Ratio 83.5° Delta-Wing Airplane Having Auxiliary Variable-Sweep Wing Panels. NASA TM X-708, 1963. (C) Title Unclassified
38. Campbell, J.P., and McKinney, M.O.: Summary of Methods for Calculating Dynamic Lateral Stability and Response and for Estimating Lateral Stability Derivatives. NACA TR 1088, 1952. (U)

TABLE 5.1.2.1-A
LOW-SPEED ROLLING MOMENT DUE TO SIDESLIP
DATA SUMMARY AND SUBSTANTIATION

Ref.	A	$\Lambda_{c/2}$ (deg)	λ	M	$R_I \times 10^{-6}$	$\left(\frac{C_I}{C_L} \beta\right) \times 10^3$ calc (per deg)	$\left(\frac{C_I}{C_L} \beta\right) \times 10^3$ test (per deg)	$\Delta C_I \beta \times 10^3$ (per deg) (Calc—Test)
8	1.34	0	1.0	0.13	1.6	- 8.8	- 8.0	- 0.8
		45				+11.8	-11.6	-0.2
		60				-13.5	-14.6	1.1
	2.61	0			1.1	- 4.3	- 4.4	0.1
		45				- 8.0	- 8.0	0
		60				-11.0	-11.3	0.3
	5.16	0			0.8	- 1.8	- 1.2	- 0.6
		45				- 6.3	- 5.6	- 0.7
		60				-10.2	-10.0	- 0.2
9	3.5	58.3	0.25	0.13	8.0	- 7.8	- 8.2	0.4
10	2.31	40.9	0	0.17	2.1	- 5.0	- 4.5	- 0.5
11	2	-7.1	0.6	0.13	1.0	- 4.0	- 4.2	0.2
	4	-3.6			0.7	- 1.4	- 1.4	0
	6	-2.4			0.6	- 0.5	- 0.7	0.2
12	2	41.2	0.6	0.13	1.0	- 7.5	- 7.5	0
	4	43.0			0.7	- 5.5	- 5.5	0
	6	43.8			0.6	- 5.0	- 4.5	- 0.5
13	0.25	83.2	0	0.13	1.0	-46.5	-40.0	-6.5
	0.53	75.3				-22.0	-20.0	-2.0
	1.07	61.7				- 9.9	-11.6	1.7
	2.31	40.9				- 5.0	- 4.1	- 0.9
	4.0	26.6				- 2.3	- 2.0	- 0.3
	6.93	16.1				- 1.0	- 1.0	0
29	2	58.0	0.6	0.13	1.0	-10.1	-10.6	0.5
	4	59.2			0.7	- 8.8	- 9.4	0.6
	6	59.4			0.6	- 8.7	- 9.4	0.7

$$\text{Average Error} = \frac{\sum |\Delta C_I \beta \times 10^3|}{n} = 0.7 \times 10^{-3} \text{ per deg}$$

TABLE 5.1.2.1-B
 LOW-SPEED ROLLING MOMENT DUE TO SIDESLIP
 OF NON-STRAIGHT-TAPERED WINGS
 DATA SUMMARY

Ref.	Config.	Planform	Λ_{LE_i} (deg)	Λ_{LE_o} (deg)	M	R_l _{MAC} $\times 10^{-6}$	$\left(\frac{c_l \beta}{c_L}\right)$ _{calc} $\times 10^3$ (per deg)	$\left(\frac{c_l \beta}{c_L}\right)$ _{test} $\times 10^3$ (per deg)	$\Delta \frac{c_l \beta}{c_L} \times 10^3$ (per deg)
30	WB	Cranked TE	60	60	0.18	1.26	-5.68	-5.03	-0.65
31	W	Cranked LE	59	48.5	0.18	↓ 0.84	-6.52	-6.28	-0.24
32	W	Cranked ^(a)	45	30.25	0.132	0.48	-2.45	-2.97	0.52
		Cranked ^(a)	45	30.20	0.07		-2.97	-2.20	-0.77
(a) Two breaks in leading-edge sweep									
$\text{Average Error} = \frac{\sum \left \Delta \frac{c_l \beta}{c_L} \times 10^3 \right }{n} = 0.65 \times 10^{-3} \text{ per deg}$									

TABLE 5.1.2.1-C
SUPersonic WING ROLLING MOMENT DUE TO SIDESLIP
DATA SUMMARY AND SUBSTANTIATION

Ref.	A	Λ_{LE} (deg)	λ	M	$R_f \times 10^{-6}$	$\left(\frac{C_l \beta}{C_N} \right)_{calc} \times 10^3$ (per deg)	$\left(\frac{C_l \beta}{C_N} \right)_{test} \times 10^3$ (per deg)	$\Delta C_l \beta \times 10^3$ (per deg) (Calc.-Test)	
21	3.5	20.9	0.200	2.01	2.20	-0.85	-0.80	-0.05	
		41.7				-1.78	-1.00	-0.78	
		51.6				-2.34	-1.80	-0.54	
23	3.0	38.3	0.140	4.06	2.7	-1.50	-1.00	-0.50	
24	4.0	49.4	0.200	2.01	1.84	-1.84	-2.02	0.18	
25	3.0	31.0	0.250	2.01	1.84	-1.66	-1.43	-0.23	
26	3.0	38.7	0.143	2.29	2.10	-1.75	-1.33	-0.42	
				2.98		-1.66	-1.66	0	
				3.96		-1.57	-1.77	0.20	
				4.65		-1.73	-1.86	0.13	
27	3.0	50.7	0.200	1.62	0.64	-3.05	-1.49	-1.56	
				2.62	0.72	-2.20	-1.56	-0.64	
				1.62	0.64	-2.43	-1.27	-1.16	
				2.62	0.72	-1.70	-1.87	0.17	
				1.62	0.64	-4.90	-3.10	-1.80	
		62.9			2.62	0.72	-2.70	-2.41	-0.29

Note: In calculating $C_l \beta / C_N$ for this table, experimental values of $C_{N\alpha}$ were used.

$$\text{Average Error} = \frac{\sum |\Delta C_l \beta \times 10^3|}{n} = 0.54 \times 10^{-3} \text{ per deg}$$

TABLE 5.1.2.1-D
SUPERSONIC ROLLING MOMENT DUE TO SIDESLIP OF
NON-STRAIGHT-TAPERED WINGS

DATA SUMMARY

Ref.	Config.	Planform	Λ_{LE_i} (deg)	Λ_{LE_o} (deg)		R_Q/ft $\times 10^{-6}$	$\left(\frac{C_l\beta}{C_L}\right)_{calc} \times 10^3$ (per deg)	$\left(\frac{C_l\beta}{C_L}\right)_{test} \times 10^3$ (per deg)	$\Delta \frac{C_l\beta}{C_L} \times 10^3$ (per deg)
33	WB	Cranked	60	75	2.50 2.96 3.95	3.0	-5.38 -4.40 -3.37		
34	WB	Cranked	65	30 45	1.41 2.20 2.60 2.96 3.95	3.0	-1.19 -2.27 -1.31 -1.14 -1.08 -0.99		
35									(a)
34				75	1.41 2.20		-12.60 -6.61		
35					2.60 2.96 3.95		-5.41 -4.79 -3.68		
36	WBN	Double Delta	81 73	50 50	2.01 2.01	1.10	-8.74 -3.68		
37	WBN		83.5 ↓	50 ↓	1.41 2.20	1.45 2.26	-17.90 -10.30		

(a) This information is classified CONFIDENTIAL.

$$\text{Average Error} = \frac{\sum \left| \Delta \frac{C_l\beta}{C_L} \times 10^3 \right|}{n} = 1.61 \times 10^{-3} \text{ per deg}$$

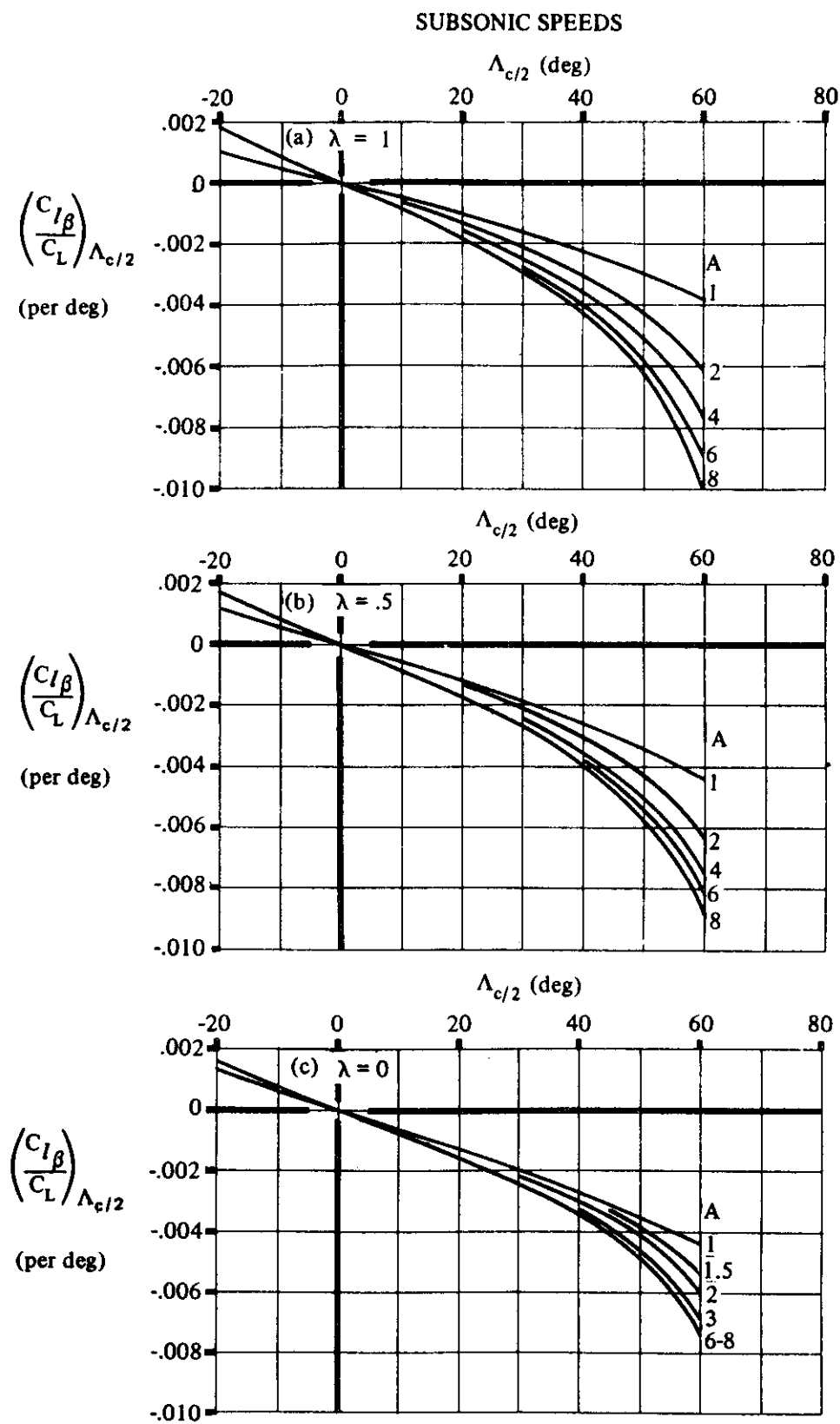


FIGURE 5.1.2.1-27 WING SWEEP CONTRIBUTION TO $C_{I\beta}$

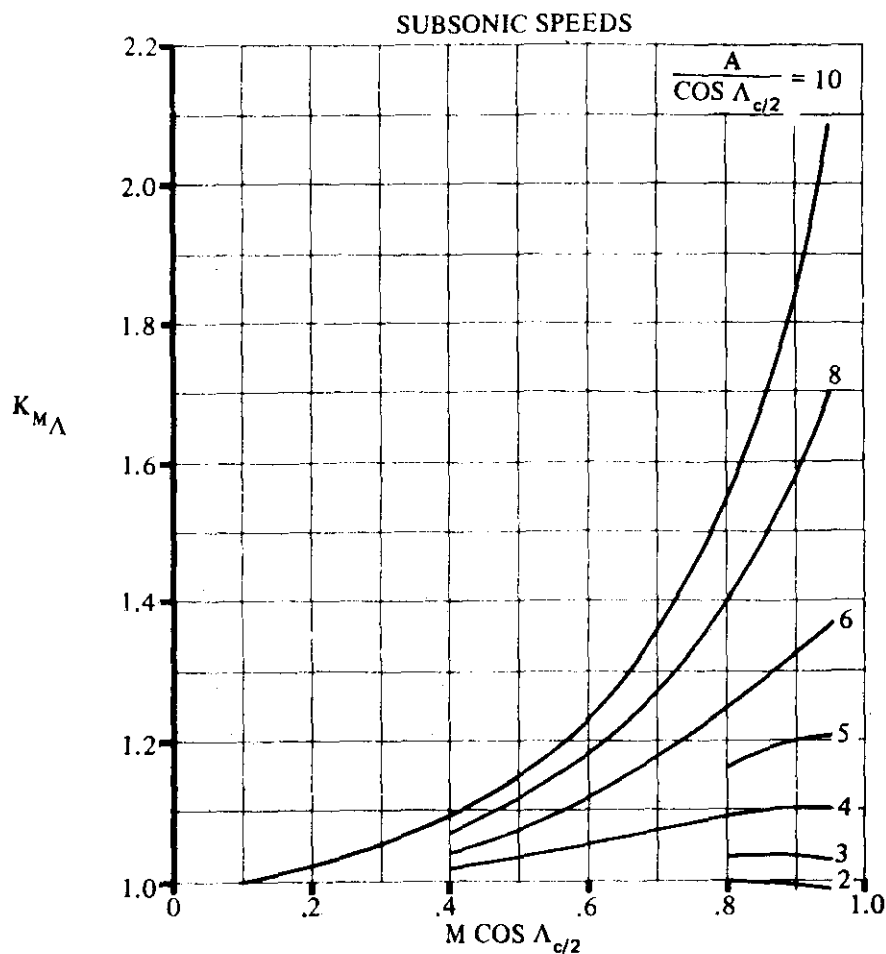


FIGURE 5.1.2.1-28a COMPRESSIBILITY CORRECTION FACTOR TO SWEEP CONTRIBUTION TO WING $C_{l\beta}$

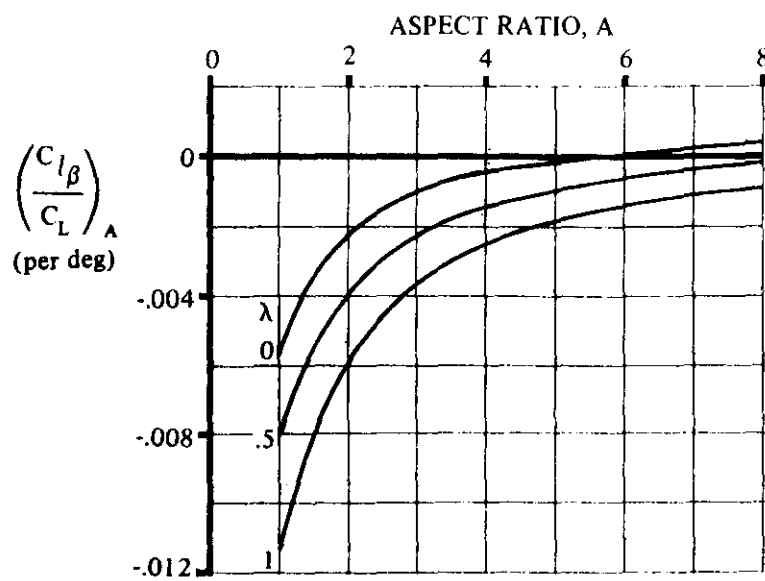


FIGURE 5.1.2.1-28b ASPECT RATIO CONTRIBUTION TO WING $C_{l\beta}$

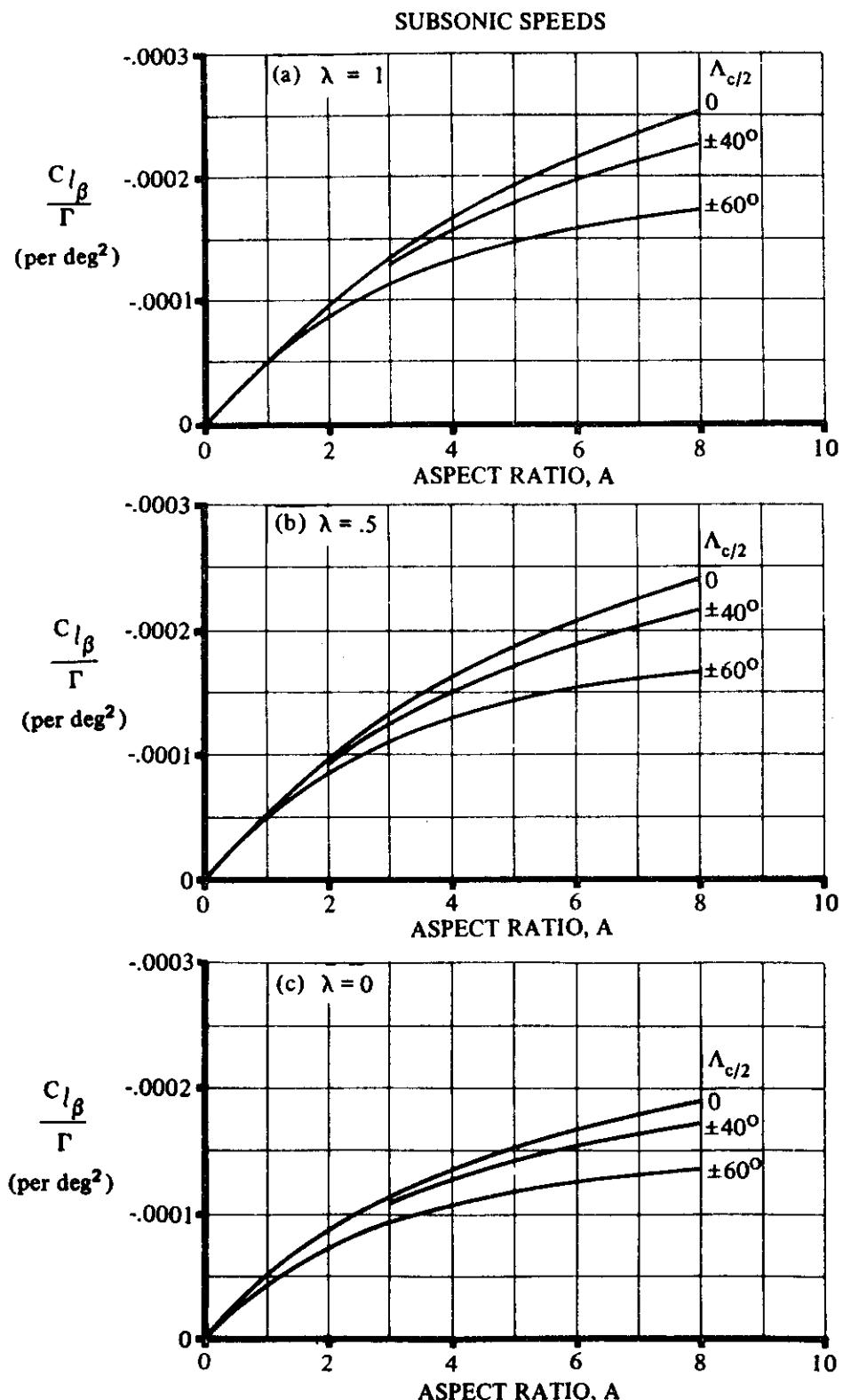


FIGURE 5.1.2.1-29 EFFECT OF UNIFORM GEOMETRIC DIHEDRAL ON WING $C_{l\beta}$

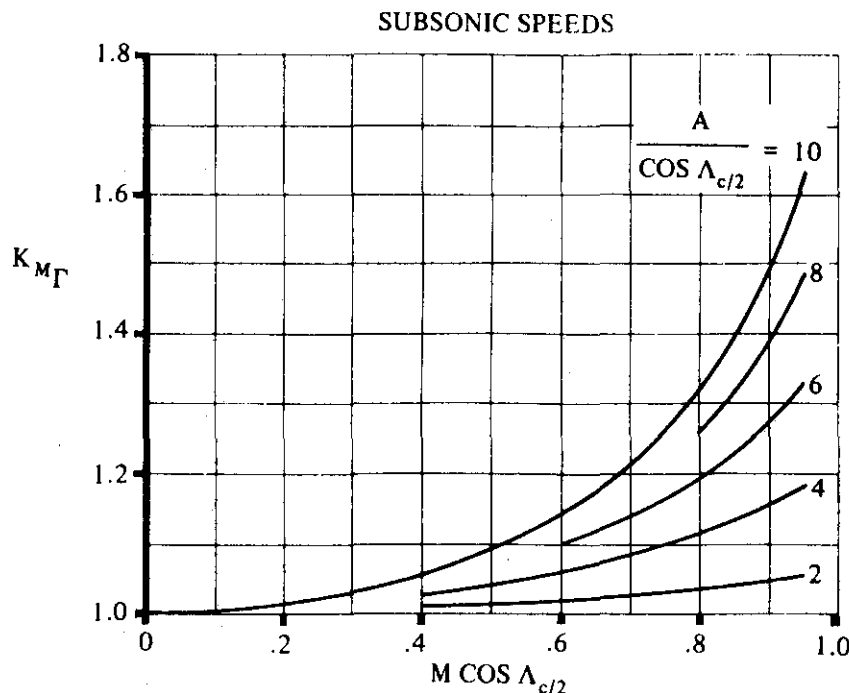


FIGURE 5.1.2.1-30a COMPRESSIBILITY CORRECTION TO DIHEDRAL EFFECT ON WING $C_{l\beta}$

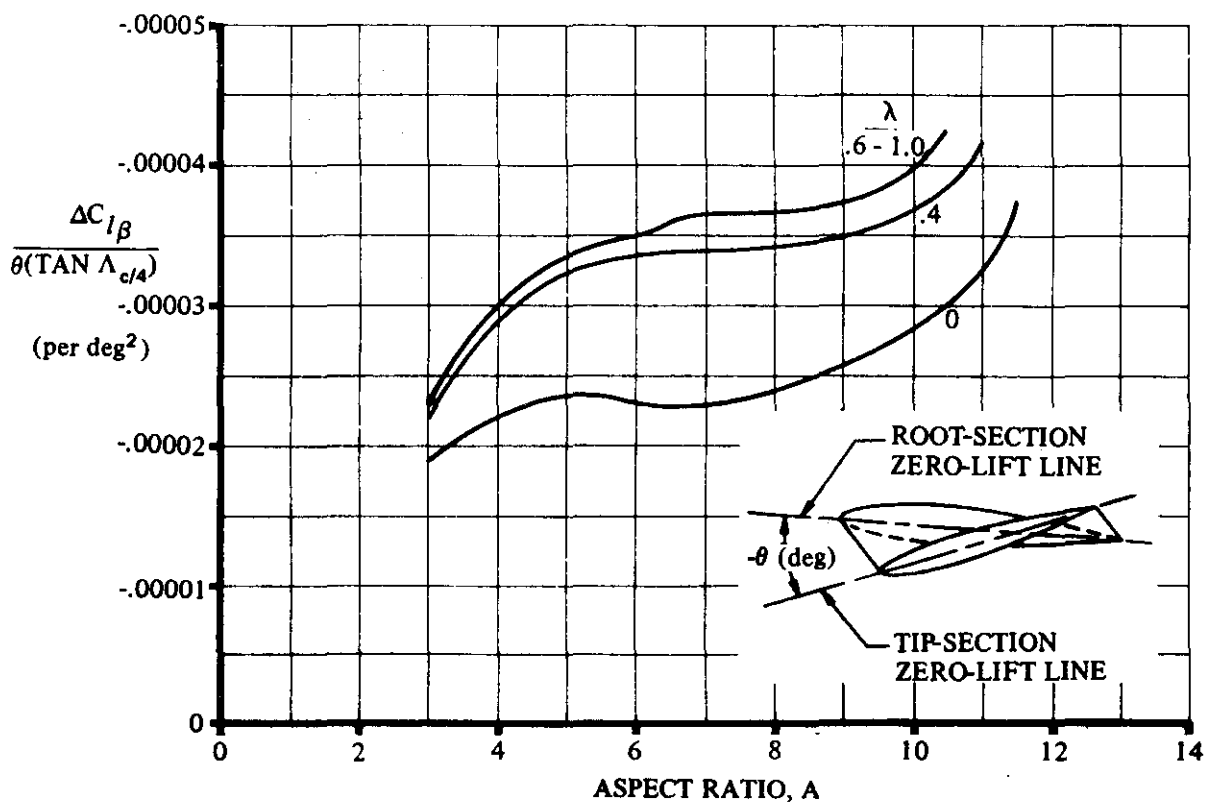


FIGURE 5.1.2.1-30b EFFECT OF WING TWIST ON WING $C_{l\beta}$

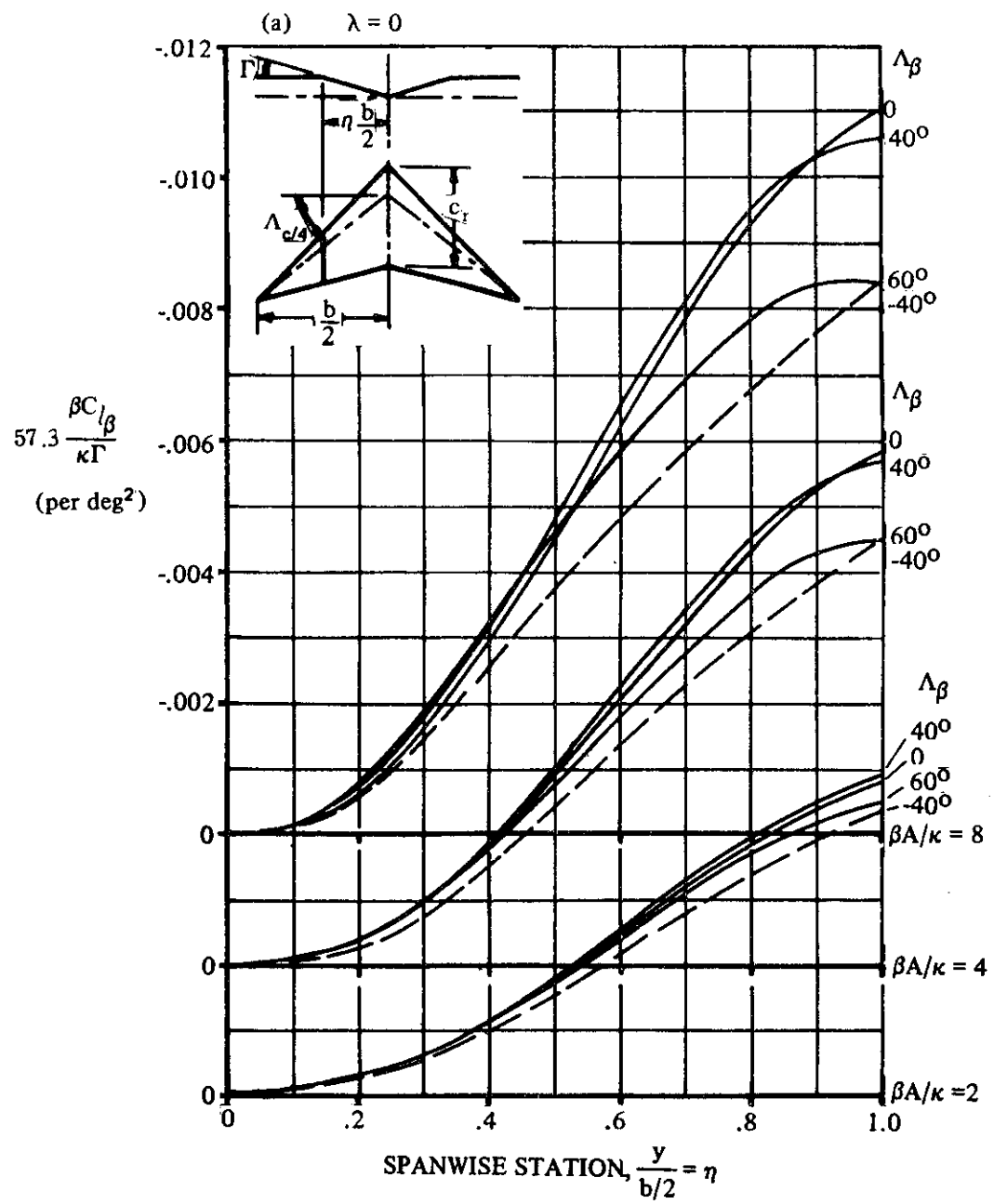


FIGURE 5.1.2.1-31 ROLLING MOMENT DUE TO SIDESLIP FOR SYMMETRIC SPANWISE DISTRIBUTION OF DIHEDRAL ANGLE

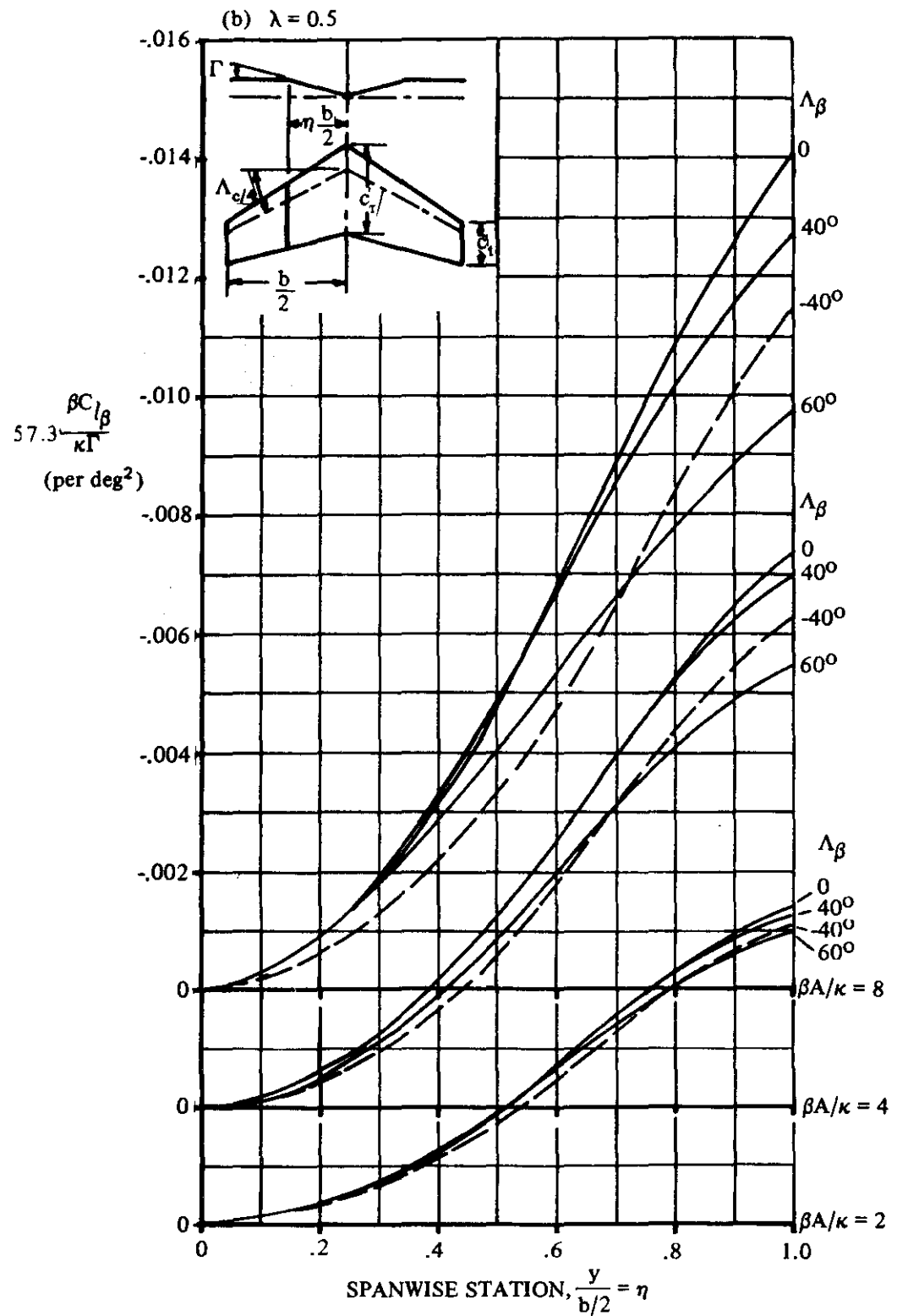


FIGURE 5.1.2.1-31 (CONTD)

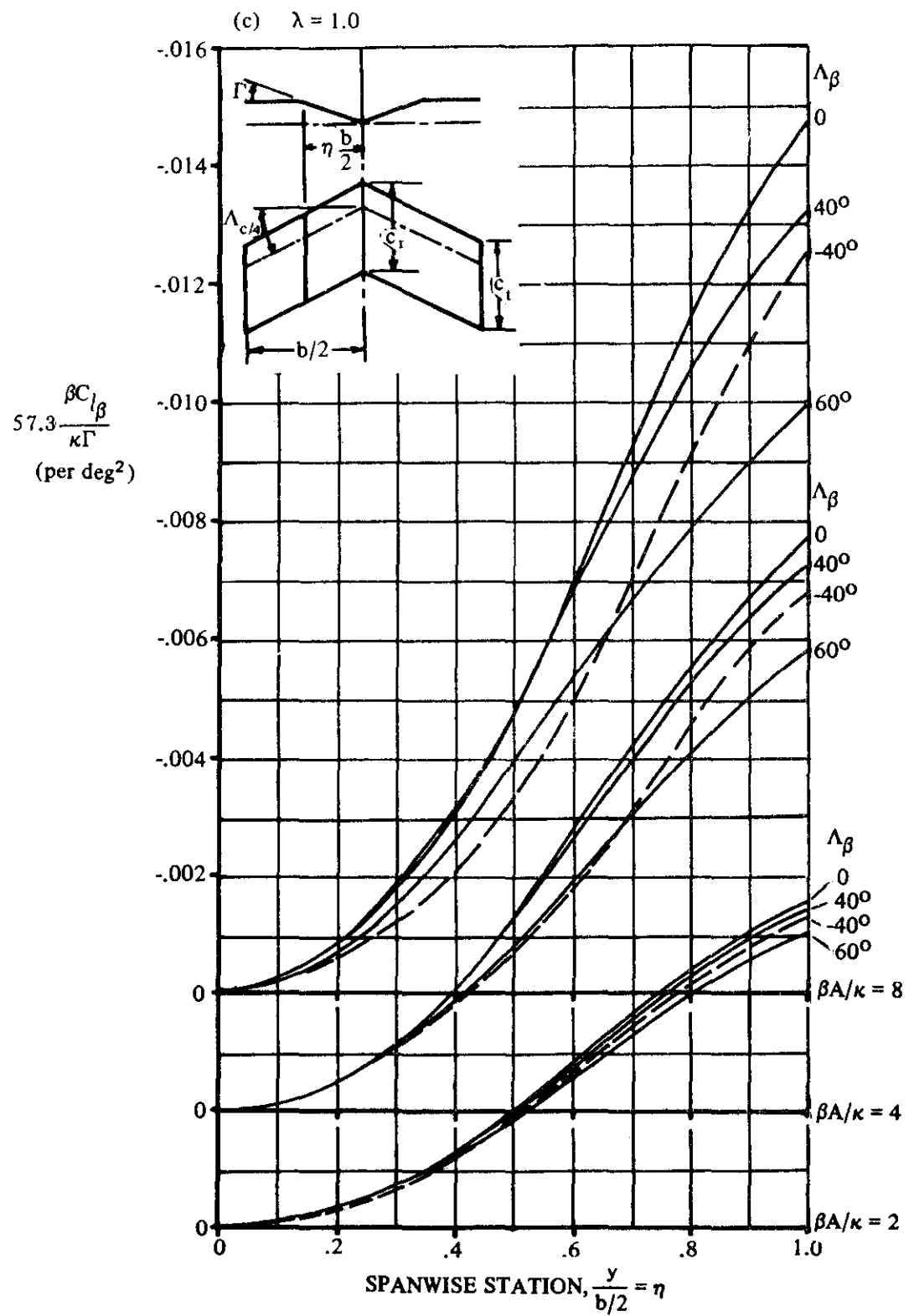


FIGURE 5.1.2.1-31 (CONTD)

5.1.2.2 WING ROLLING-MOMENT COEFFICIENT C_l AT ANGLE OF ATTACK

A. SUBSONIC

In Section 5.1.2.1, the wing rolling moments due to sideslip were discussed in terms of the parameters $\frac{C_{l\beta}}{C_L}$ and $\frac{C_{l\beta}}{\Gamma}$. These parameters imply that the rolling moment is a linear function of both lift coefficient and dihedral angle.

This linearity holds true only if the flow is everywhere attached. Once separation takes place, the rolling-moment derivatives may vary considerably from the linear-range value, even changing sign in certain cases.

Because of the nonlinear nature of the separation effects governing $C_{l\beta}$, no theoretical analysis of this parameter at the higher angles of attack has been successful. An empirical approach along the lines of Section 4.1.3.4 appears to be feasible. However, until a systematic method is developed, the presentation of this Handbook will be limited to a qualitative discussion of the important parameters governing $C_{l\beta}$ at high angles of attack, including certain representative examples.

Effect of Planform

As was mentioned in Section 4.1.3.4, planform shape plays an important part in determining the place at which separation first appears on a wing and how it subsequently progresses with increasing angle of attack. The manner in which the various separation patterns influence the rolling-moment characteristics is illustrated in figure 5.1.2.2-4.

For the unswept wing of figure 5.1.2.2-4, separation occurs first at the wing trailing edge and then progresses forward with increasing angle of attack. When this wing is yawed, the separated area is displaced toward the downwind wing tip (presumably the result of spanwise boundary-layer flow). The size of the separated area on the downwind panel also increases with increasing angle of attack. The resulting lift differential between the upwind and downwind panels then gives rise to a powerful negative rolling moment (positive dihedral effect).

For swept and delta wings, separation occurs first at the wing leading edge. The separated flow rolls into two strong vortices lying along the wing leading edges. Changes in magnitude and distribution of the lift force on the wing are associated with these vortices. When these wings are yawed, the decrease in sweep angle of the upwind wing panel causes the leading-edge vortex on this panel to lose strength and to turn away from the leading edge farther inboard than the corresponding vortex on the downwind panel (see figure 5.1.2.2-4). This asymmetry results in a relative loss in lift on the upwind wing panel, even though there is a partially compensating effective increase in angle of attack due to the geometry of combined sweep and yaw. At angles of attack beyond the stall, flow over the wing is completely separated and all wing planforms have basically similar rolling-moment characteristics.

The trends presented in figure 5.1.2.2-4 are valid only for small sideslip angles ($\pm 5^\circ$). At larger angles of sideslip, the curves of C_l as a function of β for the swept and delta wings reverse, and these wings then show positive-dihedral characteristics, as shown in figure 5.1.2.2-5.

Effect of Leading-Edge Shape

Since leading-edge shape is shown to have an important effect on the strength of the wing leading-edge vortex, and hence on the wing lift (Section 4.1.3.4), it is to be expected that wing rolling moments that also depend on vortex characteristics are influenced by wing leading-edge shape.

The effect of wing airfoil section (leading-edge shape) on $C_{l\beta}$ is illustrated in figure 5.1.2.2-6.

Briefly summarized, this figure shows that the sharper the wing leading edge, the lower the lift coefficient at which $C_{l\beta}$ deviates from the linear-theory value (figures 5.1.2.2-6a and 5.1.2.2-6b). Reducing the Reynolds number tends to promote leading-edge separation and thus produces the same effects as sharpening the leading edge (figure 5.1.2.2-6c).

Under certain circumstances, introduction of leading-edge roughness also triggers leading-edge separation and therefore causes the rolling-moment characteristics to deviate from linear values.

Very Low Aspect Ratios

For very low-aspect-ratio wings, $C_{l\beta}$ at high angles of attack is not only highly nonlinear but may also be non-symmetrical with respect to sideslip. Experimental data showing this effect for low-aspect-ratio triangular wings is given in reference 3. This unusual characteristic may be related to the formation of unsymmetrical leading-edge vortices similar to those observed for bodies of revolution at high angles of attack in references 4 and 5. In these two references it is shown that as the angle of attack is increased for bodies of revolution, the vortex system changes from a steady symmetric pair to a steady asymmetric configuration of two or more vortices and, finally, at large angles of attack, to an unsteady asymmetric arrangement. Experimental tests with free flying low-aspect-ratio-wing models have shown that undesirable lateral characteristics are present for aspect ratios considerably larger than those at which static asymmetric rolling moments cease to be apparent (reference 6). However, in this test the static rolling-moment characteristics may be obscured by the dynamic coupling effects of free flight.

Geometric Dihedral

The effects of geometric dihedral on wings at high angles of attack are directly related to the lift-curve slope at the same angle of attack. This relationship is

$$\left(\frac{C_{l\beta}}{\Gamma}\right)_{c_L} = \left(\frac{C_{l\beta}}{\Gamma}\right)_{c_L=0} \frac{(C_{L_s})_{c_L}}{(C_{L_s})_{c_L=0}}. \quad 5.1.2.2-a$$

It is evident that near maximum lift, where the lift-curve slope is small, a variation in geometric dihedral is not an effective way to change the wing rolling-moment characteristics.

B. TRANSONIC

The transonic rolling-moment characteristics of wings at high angles of attack generally show considerable variation with Mach number. (reference 2).

The changes in rolling-moment characteristics are roughly related to changes in panel lift characteristics. At transonic Mach numbers ($M > .9$) the wing lift-curve slope and maximum-lift characteristics undergo marked changes (see Sections 4.1.3.2 and 4.1.3.4), which are reflected in changes in the wing rolling moments.

For swept wings, the negative-dihedral effects at high angles of attack are reduced or eliminated with increasing Mach number. This is due to changes in the leading-edge vortex characteristics with Mach number that permit the leading wing panel to carry more lift.

For unswept wings, the increased compressibility effects on the force-break characteristics of the more highly loaded leading wing tend to reduce or even reverse the positive-dihedral characteristics in evidence at lower speeds. Mach number effects on the rolling moment due to geometric dihedral of any wing at high angles of attack are small.

C. SUPERSONIC

Experimental data on wing rolling moments due to sideslip at supersonic speeds and high angles of attack are relatively scarce, but the following general trends are observed.

Effect of Planform

For swept wings, the positive-dihedral effects that are in evidence at low angles of attack increase in magnitude with increasing angle of attack. This characteristic is relatively insensitive to Mach number variations (reference 7).

For unswept wings at Mach numbers below 2 the value of $C_{l\beta}$ tends toward zero with increasing angle of attack. This is true for the high-wing, midwing, and low-wing configurations tested in reference 8. At Mach numbers above 2 the same configurations show a trend toward increasingly positive dihedral effects with increasing angle of attack. At the higher Mach numbers the unswept-wing characteristics are similar to the swept-wing characteristics.

Geometric Dihedral

The experimental data of reference 7 show that up to 12° angle of attack the rolling-moment increment due to dihedral is essentially the same as at zero angle of attack. This result is somewhat unexpected, since a calculation of the local angles of attack of the left and right wing panels individually would predict a variation in dihedral effect (see reference 7). Possibly the discrepancy is due to sweep and/or wing-body interference effects.

If the geometric dihedral effects are assumed to be independent of angle of attack for all configurations at supersonic speeds, then the methods of Section 5.1.2.1 intended for low angles of attack are also applicable at the higher angles of attack.

REFERENCES

1. Johnson, J., Jr.: Low-Speed Measurements of Static Stability, Damping in Yaw, and Damping in Roll of a Delta, a Swept, and an Unswept Wing for Angles of Attack from 0° to 90°. NACA RM L56B01, 1956. (U)
2. Poitamus, E., and Sleiman, W., Jr.: The Rolling Moment Due to Sideslip of Swept Wings at Subsonic and Transonic Speeds. NASA TN D-208, 1960. (U)
3. Letko, W.: Experimental Determination at Subsonic Speeds of the Oscillatory and Static Lateral Stability Derivatives of a Series of Delta Wings with Leading-Edge Sweep from 30° to 86.5°. NACA RM L57A01, 1957. (U)
4. Allen, R. J., and Perkins, E.: Characterization of Flow Over Inclined Bodies of Revolution. NACA RM A50L07, 1951. (U)
5. Gowen, F., and Perkins, E.: A Study of the Effects of Body Shape on the Vortex Wakes of Inclined Bodies at a Mach Number of 2. NACA RM A58I17, 1958. (U)
6. Tost, L.: Low-Speed Static Stability and Damping-in-Roll Characteristics of Some Swept and Unswept Low-Aspect-Ratio Wings. NASA TN 1468, 1947. (U)
7. Boatright, W.: Experimental Investigation of Effects of Wing Plan Form and Dihedral Angle on Sideslip Derivatives of Sweptback-Wing-Body Combinations at Supersonic Speeds. NACA RM L58E08, 1958. (C) Title Unclassified
8. Robinson, R.: Effects of Vertical Location of the Wing and Horizontal Tail on the Static Lateral and Directional Stability of a Trapezoidal-Wing Airplane Model at Mach Numbers of 1.41 and 2.01. NACA RM L58C18, 1958. (U)
9. Jaquet, B., and Fournier, B.: Effects of Wing Sweep, Horizontal-Tail Configuration, and a Ventral Fin on Static Stability Characteristics of a Model with a Wing of Aspect Ratio 2 at Mach Numbers From 2.20 to 4.65. NACA RM L58E06, 1958. (C) Title Unclassified

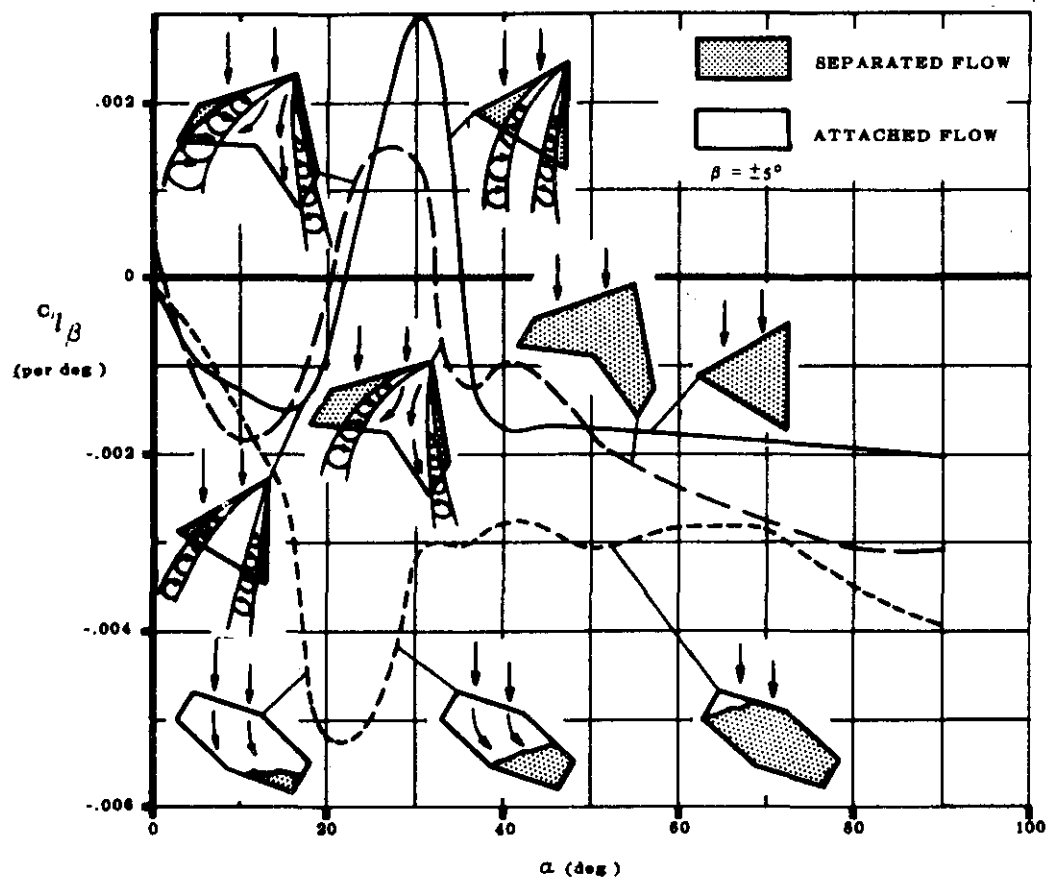


FIGURE 5.1.2.2-4 EFFECT OF PLANFORM ON THE VARIATION OF C_l/β WITH ANGLE OF ATTACK, ZERO DIHEDRAL, LOW SPEEDS (FROM REF. 1).

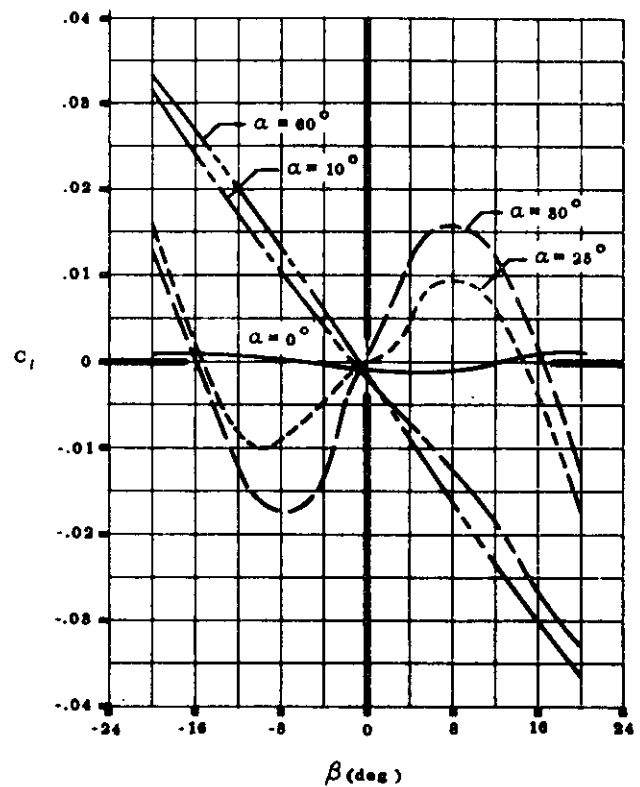


FIGURE 5.1.2.2-5 VARIATIONS OF ROLLING MOMENT WITH SIDESLIP FOR A DELTA WING AT LOW SPEEDS, ZERO DIHEDRAL. (REF. 1).

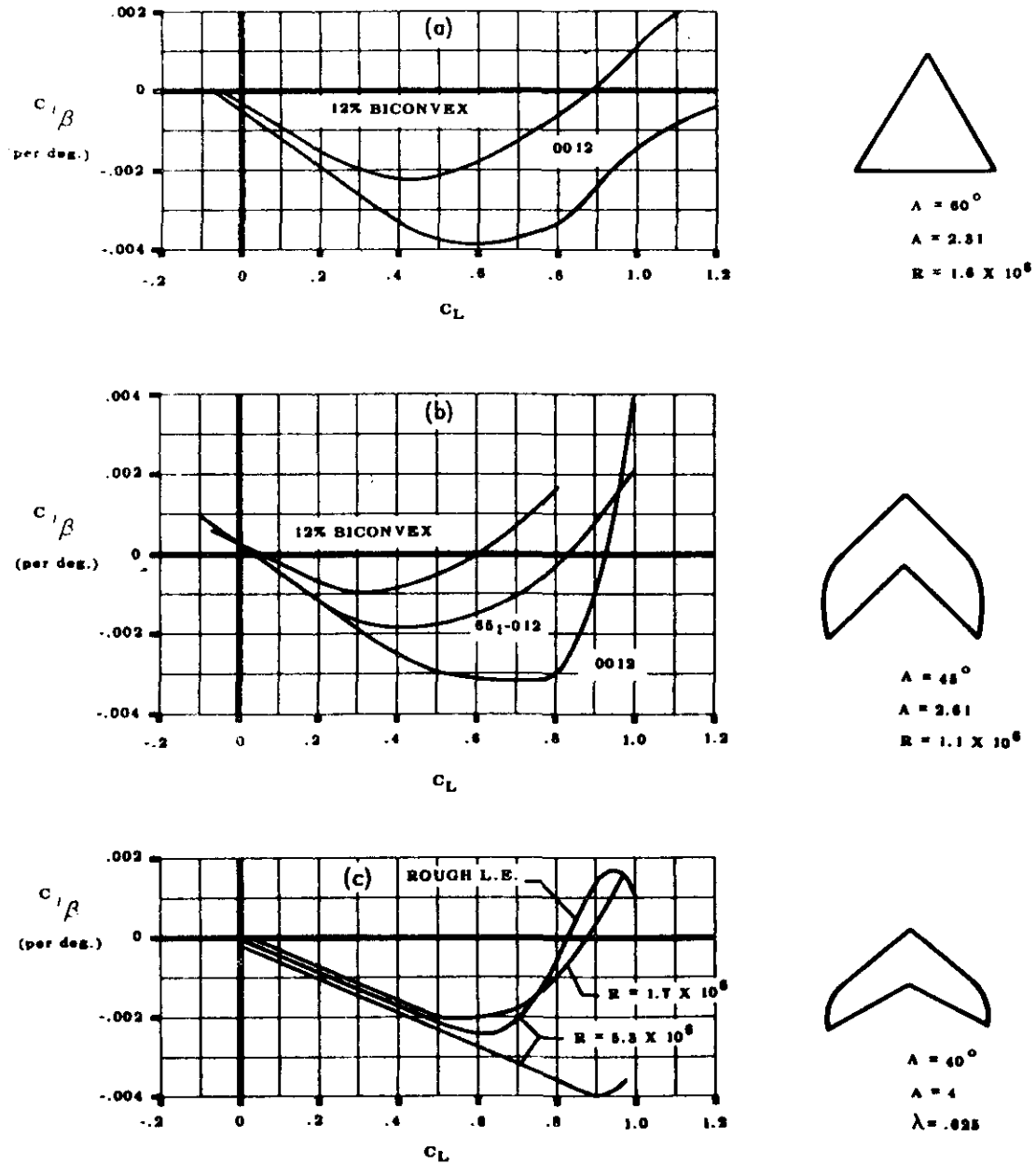


FIGURE 5.1.2.2-6 EFFECT OF ANGLE OF ATTACK ON $C_{l/\beta}$ AT LOW SPEEDS

5.1.3 WING SIDESLIP DERIVATIVE C_{n_β}

5.1.3.1 WING SIDESLIP DERIVATIVE C_{n_β} IN THE LINEAR ANGLE-OF-ATTACK RANGE

The yawing moment of a wing in sideslip is primarily caused by the asymmetrical induced-drag distribution associated with the asymmetrical lift distribution. The wing contribution to the derivative C_{n_β} is important only at large incidences.

Methods are presented in this section for estimating the wing yawing moment due to sideslip in the subsonic and supersonic speed regimes. Methods for estimating this derivative in the transonic speed regime are not available.

A. SUBSONIC

The Datcom method presented herein is based on the same theory as that used to determine wing side force due to sideslip, and the general discussion of Paragraph A of Section 5.1.1.1 is directly applicable here. The method is valid in the linear angle-of-attack region.

DATCOM METHOD

The yawing moment derivative at low speeds is given in Reference 1 as

$$\frac{C_{n_\beta}}{C_L^2} = \frac{1}{57.3} \left[\frac{1}{4\pi A} - \frac{\tan \Lambda_{c/4}}{\pi A(A + 4 \cos \Lambda_{c/4})} \left(\cos \Lambda_{c/4} - \frac{A}{2} - \frac{A^2}{8 \cos \Lambda_{c/4}} + 6 \frac{\bar{x}}{c} \frac{\sin \Lambda_{c/4}}{A} \right) \right]$$

(per deg) 5.1.3.1-a

where \bar{x} is the longitudinal distance (positive rearward) from the coordinate origin (usually the center of gravity) to the wing aerodynamic center.

The wing contribution to the yawing moment due to sideslip at low speeds is shown to be independent of both taper ratio and dihedral in References 2 and 3, respectively.

For subcritical speeds, the low-speed derivative can be modified by the Prandtl-Glauert rule to yield approximate corrections for the first-order three-dimensional effects of compressibility. The resulting expression from Reference 4 is

$$\left(\frac{C_{n_\beta}}{C_L^2} \right)_M = \left(\frac{A + 4 \cos \Lambda_{c/4}}{AB + 4 \cos \Lambda_{c/4}} \right) \left(\frac{A^2 B^2 + 4AB \cos \Lambda_{c/4} - 8 \cos^2 \Lambda_{c/4}}{A^2 + 4A \cos \Lambda_{c/4} - 8 \cos^2 \Lambda_{c/4}} \right) \left(\frac{C_{n_\beta}}{C_L^2} \right)_{\substack{\text{low} \\ \text{speed}}} \quad 5.1.3.1-b$$

where

$$B = \sqrt{1 - M^2 \cos^2 \Lambda_{c/4}}.$$

Calculated values for the wing yawing moment due to sideslip at low subsonic speeds obtained by the Datcom method for the wing configurations of References 5, 6, and 7 are compared with experimental data in Figure 5.1.3.1-5. The comparison indicates that the calculated values are fairly reliable over a range of lift coefficient (starting from zero) that decreases as wing sweep increases. Large discrepancies are noted for highly swept wings at lift coefficients for which the flow is believed to be partially separated.

Sample Problem

Given: The wing of Reference 5

$$A = 4.0 \quad \Lambda_{c/4} = 60^\circ \quad \frac{x}{c} = 0.037 \quad M = 0.13$$

Compute:

$$\sin \Lambda_{c/4} = 0.866$$

$$\cos \Lambda_{c/4} = 0.500$$

$$\tan \Lambda_{c/4} = 1.732$$

Solution:

$$\frac{C_{n\beta}}{C_L^2} = \frac{1}{57.3} \left[\frac{1}{4\pi A} - \frac{\tan \Lambda_{c/4}}{\pi A(A + 4 \cos \Lambda_{c/4})} \left(\cos \Lambda_{c/4} - \frac{A}{2} - \frac{A^2}{8 \cos \Lambda_{c/4}} + 6 \frac{x}{c} \frac{\sin \Lambda_{c/4}}{A} \right) \right]$$

(per deg) (equation 5.1.3.1-a)

$$= \frac{1}{57.3} \left[\frac{1}{16\pi} - \frac{1.732}{4\pi [4 + (4)(0.50)]} \left(0.50 - \frac{4}{2} - \frac{(4)^2}{(8)(0.50)} + (6)(0.037) \frac{0.866}{4} \right) \right]$$

$$= \frac{1}{57.3} [(0.01989) - (0.02297)(-5.452)]$$

$$= \frac{1}{57.3} [(0.01989) + (0.1252)]$$

$$= 0.00253 \text{ per deg}$$

C_L	C_L^2	$C_{n\beta} \times 10^3$ (per deg)
0.05	0.0025	0.00633
0.10	0.010	0.0253
0.20	0.040	0.1012
0.30	0.090	0.2277
0.40	0.160	0.4048
0.50	0.250	0.6325
0.60	0.360	0.9108

These results are compared with experimental values in Figure 5.1.3.1-5.

B. TRANSONIC

There are no methods available for estimating the wing yawing moment due to sideslip in the transonic regime and none are presented in the Datcom. Furthermore, there are no experimental data available in the transonic speed regime.

C. SUPERSONIC

No general method has been developed for estimating the wing yawing moment due to sideslip at supersonic speeds. However, theoretical methods are available for discrete planforms over certain speed ranges. A comprehensive summary of the available theoretical methods for calculating the wing yawing moment due to sideslip is presented in Reference 9. Datcom methods are based on the same theory as that used to determine wing side force due to sideslip, and the general discussion of Paragraph C of Section 5.1.1.1 is directly applicable here.

DATCOM METHODS

The Datcom methods are taken from References 10, 11, and 12 and present the wing yawing moment due to sideslip for rectangular planforms, triangular planforms, and fully tapered sweptback planforms with sweptforward or sweptback trailing edges. The results are mainly functions of planform geometry and Mach number. The general trend of the variation of $C_{n\beta}$ with Mach number and aspect ratio is a reduction in the magnitude of the derivative with an increase in these parameters.

Rectangular Planform: $A\beta \geq 1.0$

The wing yawing moment due to sideslip for rectangular planforms referred to an arbitrary moment center is given in Reference 10 as

$$\frac{C_{n\beta}}{\alpha^2} = \frac{1}{\pi A^2 \beta^2} \left[\frac{4M^2}{3} + 8M^2 \frac{x}{c} - \pi \left\{ \frac{A(1-\beta^2)}{\beta} \frac{3+\beta^2}{3\beta^2} \right\} \right] \frac{1}{57.3} \text{ (per deg)} \quad 5.1.3.1-c$$

where α is in radians, $\beta = \sqrt{M^2 - 1}$ and x is the distance of the origin of moments from the midchord point, measured along the longitudinal axis, positive ahead of midchord point.

Equation 5.1.3.1-c is valid for Mach number and aspect ratio greater than that for which the Mach line from the leading edge of the tip section intersects the trailing edge of the opposite tip section ($A\beta \geq 1.0$).

Sweptback Planform ($\lambda = 0$): $\beta \cot \Lambda_{LE} \leq 1.0$

The wing yawing moment due to sideslip for fully tapered sweptback planforms is derived in Reference 11 for triangular planforms and in Reference 12 for planforms with sweptforward or sweptback trailing edges as

$$\frac{C_{n\beta}}{\alpha^2} = \frac{\pi}{3} \left[E''(\beta C) F_9(N) + \left(\frac{A^2}{16} F_{11}(N) + \frac{x}{c} \right) M^2 Q(\beta C) \right] \frac{1}{57.3} \text{ (per deg)} \quad 5.1.3.1-d$$

where α is in radians and

$Q(\beta C)$ is obtained from Figure 5.1.1.1-6

$E''(\beta C)$ is obtained from Figure 7.1.1.1-8

$F_{11}(N)$ is obtained from Figure 7.1.1.2-8

$F_9(N)$ is obtained from Figure 5.1.3.1-6

x is the distance of the origin of moments from the $2/3 c_{rB}$ point of the basic triangular wing, measured along the longitudinal axis, positive ahead of the $2/3 c_{rB}$ point. (See Sketch(a) of Section 7.1.1.1 for definition of basic triangular wing.)

For a triangular planform the factors $F_9(N)$ and $F_{11}(N)$ are equal to 1.0.

Equation 5.1.3.1-d is valid for Mach number and aspect ratio for which the wing is contained within the Mach cones springing from the apex and the trailing edge at the center of the wing.

REFERENCES

1. Toll, T.A., and Queijo, M. J.: Approximate Relations and Charts for Low-Speed Stability Derivatives of Swept Wings. NACA TN 1581, 1948. (U)
2. Letko, W., and Cowan, J. W.: Effect of Taper Ratio on Low-Speed Static and Yawing Stability Derivatives of 45° Sweptback Wings with Aspect Ratio of 2.61. NACA TN 1671, 1948. (U)
3. Queijo, M. J., and Jaquet, B.: Investigation of Effects of Geometric Dihedral on Low-Speed Static Stability and Yawing Characteristics of an Untapered 45° Sweptback-Wing Model of Aspect Ratio 2.61. NACA TN 1668, 1948. (U)
4. Fisher, L.: Approximate Corrections for the Effects of Compressibility on the Subsonic Stability Derivatives of Swept Wings. NACA TN 1854, 1949. (U)
5. Wolhart, W. D., and Thomas, D. F., Jr.: Static Longitudinal and Lateral Stability Characteristics at Low Speed of Unswept-Midwing Models Having Wings with an Aspect Ratio of 2, 4, or 6. NACA TN 3649, 1956. (U)
6. Thomas, D. F., Jr., and Wolhart, W.D.: Static Longitudinal and Lateral Stability Characteristics at Low Speed of 45° Sweptback-Midwing Models Having Wings with an Aspect Ratio of 2, 4, or 6. NACA TN 4077, 1957. (U)
7. Wolhart, W. D., and Thomas, D. F., Jr.: Static Longitudinal and Lateral Stability Characteristics at Low Speed of 60° Sweptback-Midwing Models Having Wings with an Aspect Ratio of 2, 4, or 6. NACA TN 4397, 1958. (U)
8. Jones, A.L.: The Theoretical Lateral-Stability Derivatives for Wings at Supersonic Speeds. Jour. Aero. Sci., Vol. 17, No. 1, January 1950. (U)
9. Jones, A. L., and Alksne, A.: A Summary of Lateral-Stability Derivatives Calculated for Wing Planforms in Supersonic Flow. NACA TR 1052, 1951. (U)
10. Harmon, S. M.: Stability Derivatives at Supersonic Speeds of Thin Rectangular Wings with Diagonals Ahead of Tip Mach Lines. NACA TR 925, 1949. (U)
11. Ribner, H.S., and Malvestuto, F.S., Jr.: Stability Derivatives of Triangular Wings at Supersonic Speeds. NACA TR 908, 1948. (U)
12. Malvestuto, F. S., Jr., and Mergolis, K.: Theoretical Stability Derivatives of Thin Sweptback Wings Tapered to a Point with Sweptback or Sweptforward Trailing Edges for a Limited Range of Supersonic Speeds. NACA TR 971, 1950. (U)

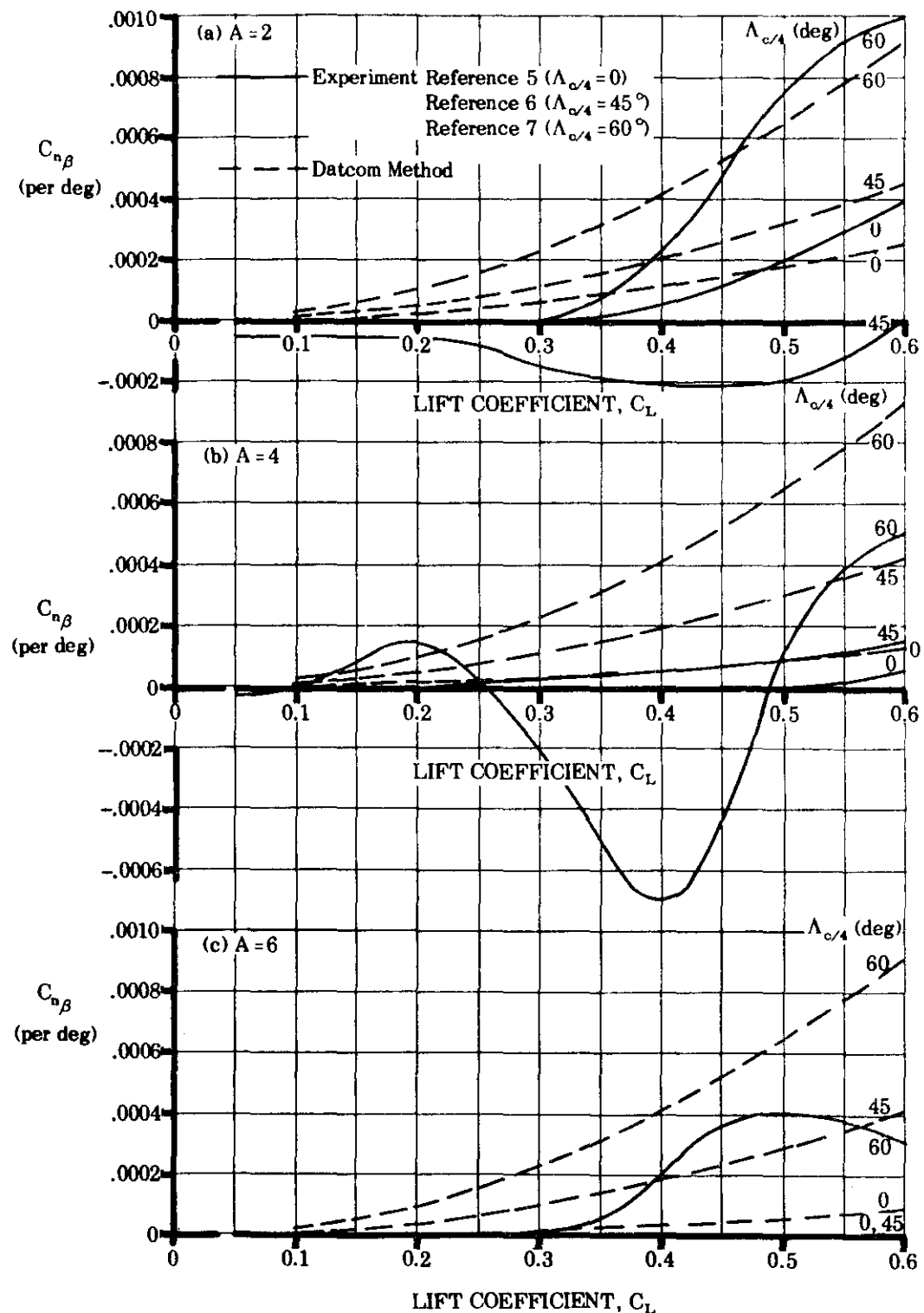


FIGURE 5.1.3.1-5 COMPARISON OF CALCULATED AND EXPERIMENTAL VALUES OF WING YAWING MOMENT DUE TO SIDESLIP FOR THE WING CONFIGURATIONS OF REFERENCES 5, 6, AND 7.

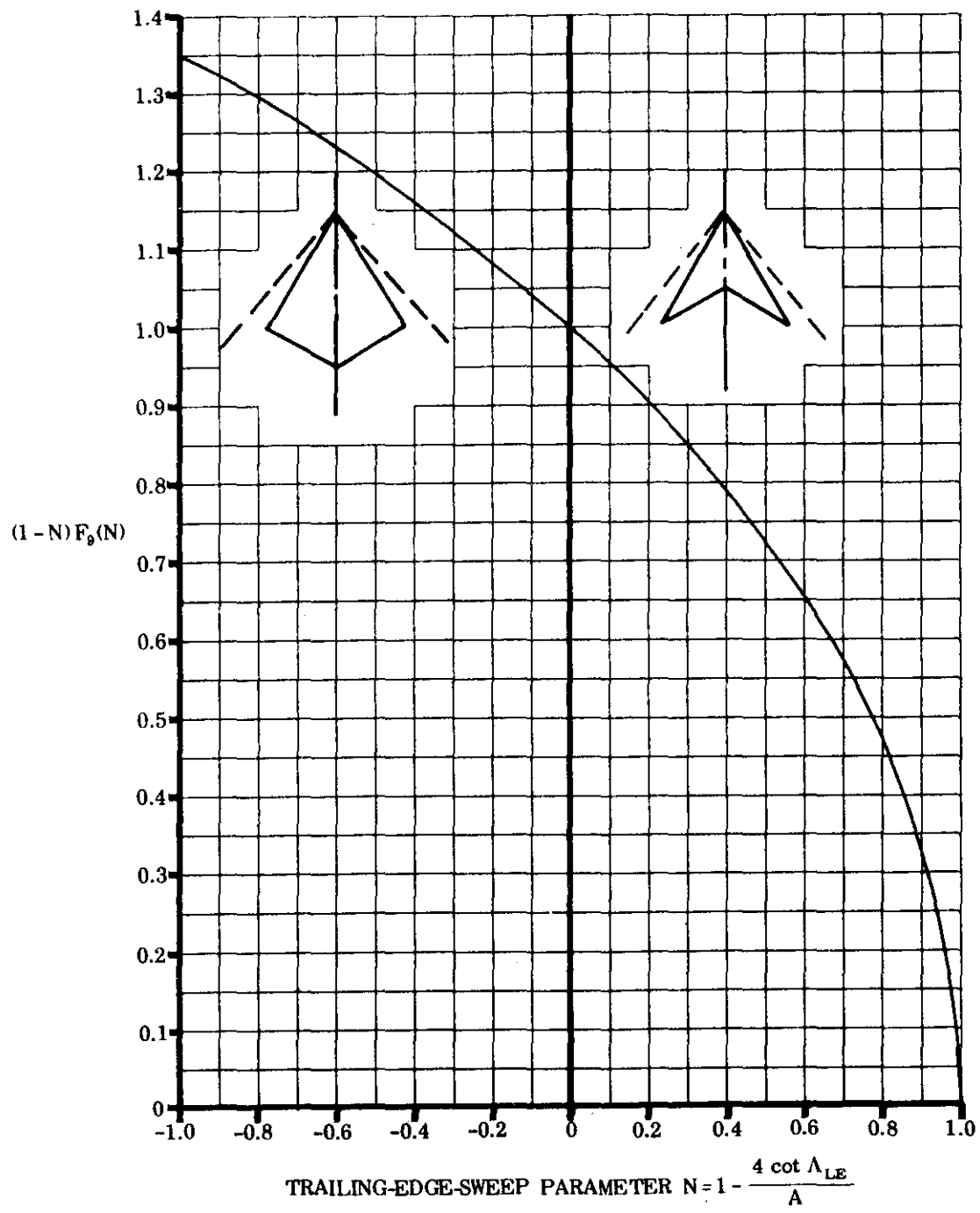


FIGURE 5.1.3.1-6 $F_g(N)$ FACTOR OF THE STABILITY DERIVATIVE

5.2 WING-BODY COMBINATIONS IN SIDESLIP

5.2.1 WING-BODY SIDESLIP DERIVATIVE $C_{Y\beta}$

5.2.1.1 WING-BODY SIDESLIP DERIVATIVE $C_{Y\beta}$ IN THE LINEAR ANGLE-OF-ATTACK RANGE

The wing-body side force due to sideslip can be considered as the sum of the side forces of the body, the wing, the wing-body interference, and the wing dihedral effect. The wing side force due to sideslip at low lift coefficient is small in comparison to that due to the body and is neglected in the Datcom methods of this Section.

Wing-body interference, which is primarily a function of wing vertical position on the body, is presented as a fraction of the body contribution. Experimental investigations show that the contribution of wing-body interference to the sideslip derivative $C_{Y\beta}$ is essentially independent of sweep, wing planform, taper ratio, and Mach number.

The body is the chief contributor to the side force of a wing-body combination. Experimental results for the body alone show a negative lateral force which increases as the body fineness ratio is decreased.

The range of applicability of the method is limited to the linear angle-of-attack range.

A. SUBSONIC

The wing-body side force due to sideslip is estimated by the following method.

DATCOM METHOD

The wing-body side force due to sideslip, based on wing area, is given by

$$(C_{Y\beta})_{WB} = K_i (C_{Y\beta})_B \left(\frac{\text{Body Reference Area}}{S_w} \right) + (\Delta C_{Y\beta})_\Gamma \quad 5.2.1.1-a$$

where

K_i is the wing-body interference factor obtained from figure 5.2.1.1-7

$(C_{Y\beta})_B$ is the body side force due to sideslip obtained from paragraph A of Section 4.2.1.1 as

$$(C_{Y\beta})_B = - (C_{L\alpha})_B$$

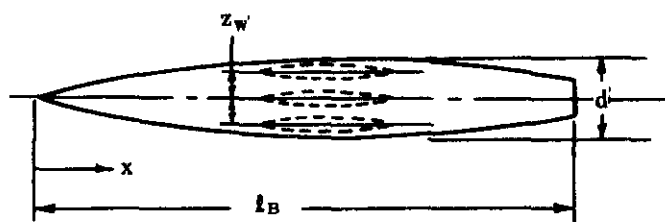
$(\Delta C_{Y\beta})_\Gamma$ is the increment in side force due to wing dihedral and is approximated by $(\Delta C_{Y\beta})_\Gamma = -0.0001 |\Gamma|$ (Γ and β in degrees) (equation 5.1.1.1-b)

For a rapid but approximate estimation of the body side force due to sideslip, slender-body theory can be used, which gives $(C_{Y\beta})_B = -2$ (per rad), where $(C_{Y\beta})_B$ is based on the body cross-sectional area at x_0 (see page 4.2.1.1-1 for definition of x_0).

A comparison of experimental data and values of wing-body side force due to sideslip at subsonic speeds calculated by equation 5.2.1.1-a is presented as table 5.2.1.1-A.

Sample Problem

Given: The wing body configuration of reference 3.



$$l_B = 3.45 \text{ ft} \quad d = 0.5 \text{ ft} \quad f = 6.90 \quad z_w = 0, \pm 0.1667 \text{ ft} \quad S_w = 2.25 \text{ sq ft}$$

$$\frac{x_1}{l_B} = 0.50 \quad V_B^{2/3} = 0.542 \text{ sq ft} \quad \Gamma = 0$$

$$S_0 = 0.175 \text{ sq ft} \text{ (area distribution curve at } \frac{x_0}{l_B})$$

Compute:

$$z_w / \frac{d}{2} = 0, \pm 0.667$$

$$\left. \begin{array}{l} K_i \text{ High} = 1.57 \\ K_i \text{ Mid} = 1.0 \\ K_i \text{ Low} = 1.33 \end{array} \right\} \text{ (figure 5.2.1.1-7)}$$

$$(k_2 - k_1) = 0.890 \text{ (figure 4.2.1.1-20a)}$$

$$\frac{x_0}{l_B} = 0.640 \text{ (figure 4.2.1.1-20b)}$$

$$\begin{aligned} (C_{Y\beta})_B &= - \left[\frac{2(k_2 - k_1) S_0}{V_B^{2/3}} \right] \text{ (per rad)} \quad \text{(equation 4.2.1.1-a)} \\ &= - \frac{(2)(0.89)(0.175)}{0.542} = -0.575 \text{ per rad (based on } V_B^{2/3}) \end{aligned}$$

Solution:

$$\begin{aligned} (C_{Y\beta})_{WB} &= K_i (C_{Y\beta})_B \left(\frac{\text{Body Reference Area}}{S_w} \right) + (\Delta C_{Y\beta}) \Gamma \quad \text{(equation 5.2.1.1-a)} \\ &= K_i (-0.575) \left(\frac{0.542}{2.25} \right) + 0 \\ &= -0.1385 K_i \text{ per rad} \\ &= -0.00242 K_i \text{ per deg} \end{aligned}$$

Wing Position	K_i	$(C_{Y\beta})_{WB}$ (per deg)
High	1.57	-0.00380
Mid	1.0	-0.00242
Low	1.33	-0.00322

These results compare with experimental values of -0.004 per deg, -0.0024 per deg, and -0.0034 per deg for the high-, mid-, and low-wing configurations, respectively, obtained from reference 3.

B. TRANSONIC

The contribution of wing-body interference to the side force derivative is essentially independent of Mach number. Furthermore, slender-body theory states that body force characteristics are not functions of Mach number.

DATCOM METHOD

The method presented in paragraph A is applicable throughout the transonic speed regime.

C. SUPERSONIC

The contribution of wing-body interference to the side force derivative is essentially independent of Mach number. Several of the theoretical methods that have been developed for estimating body force characteristics at supersonic speeds are discussed in paragraph C of Section 4.2.1.1.

The experimental results of reference 6 indicate a negative lateral force increment due to wing camber at supersonic speeds; however, no method is available to predict this effect.

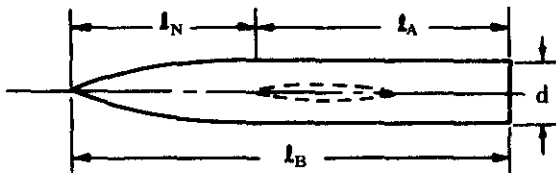
DATCOM METHOD

The method presented in paragraph A is applicable throughout the supersonic speed range. The body side force due to sideslip is obtained by conversion of the body lift-curve slope of paragraph C of Section 4.2.1.1.

A comparison of experimental data and values of wing-body side force due to sideslip at supersonic speeds calculated by the Datcom method is presented as table 5.2.1.1-B.

Sample Problem

Given: The midwing-ogive-cylinder body configuration of reference 12.



$$d = 0.0625 \text{ ft} \quad l_N = 0.2188 \text{ ft} \quad l_A = 0.4062 \text{ ft} \quad S_w = 0.0506 \text{ sq ft} \quad S_b = 0.00307 \text{ sq ft}$$

$$\Gamma = 10^\circ \quad M = 1.62, 2.62$$

Compute:

$$f_N = \frac{l_N}{d} = 3.5$$

$$f_A = \frac{l_A}{d} = 6.5$$

$$\frac{f_A}{f_N} = \frac{6.5}{3.5} = 1.857$$

$$\beta_M = 1.62 = \sqrt{M^2 - 1} = 1.275$$

$$\beta_M = 2.62 = \sqrt{M^2 - 1} = 2.42$$

$$(\beta/f_N)_{M=1.62} = \frac{1.275}{3.5} = 0.364$$

$$(\beta/f_N)_{M=2.62} = \frac{2.42}{3.5} = 0.691$$

$$\left. \begin{aligned} [(C_{Y\beta})_B]_{M=1.62} &= -2.78 \text{ per rad (based on } S_b) \\ [(C_{Y\beta})_B]_{M=2.62} &= -3.06 \text{ per rad (based on } S_b) \end{aligned} \right\} \text{ (figure 4.2.1.1-21a; } (C_{Y\beta})_B = -(C_{N\alpha})_B)$$

$$K_1 = 1.0 \text{ (figure 5.2.1.1-7; mid-wing configuration)}$$

$$(\Delta C_{Y\beta})\Gamma = (-0.0001)(10) = -0.0010 \text{ per deg (equation 5.1.1.1-b)}$$

Solution:

$$\begin{aligned}
 (C_{Y\beta})_{WB} &= K_1 (C_{Y\beta})_B \left(\frac{\text{Body Reference Area}}{S_w} \right) + (\Delta C_{Y\beta}) \Gamma \\
 &= 1.0 (C_{Y\beta})_B \left(\frac{0.00307}{0.0506} \right) + (-0.0010) \\
 &= 0.0607 (C_{Y\beta})_B - 0.0010
 \end{aligned} \tag{equation 5.2.1.1-a}$$

M	$(C_{Y\beta})_B$ (per rad)	$(C_{Y\beta})_B$ (per deg)	$0.0607 (C_{Y\beta})_B$ (per deg)	$(C_{Y\beta})_{WB}$ (per deg)
1.62	-2.78	-0.0485	-0.00294	-0.00394
2.62	-3.06	-0.0534	-0.00324	-0.00424

These results compare with experimental values of -0.0038 per degree and -0.0042 per degree at Mach numbers 1.62 and 2.62, respectively, obtained from reference 12.

REFERENCES

- Queijo, M., and Wolhart, W.: Experimental Investigation of the Effect of Vertical-Tail Size and Length and of Fuselage Shape and Length on the Static Lateral Stability Characteristics of a Model with 45° Sweptback Wing and Tail Surfaces. NACA TR 1049, 1951. (U)
- Goodman, A., and Thomas, D., Jr.: Effects of Wing Position and Fuselage Size on the Low-Speed Static and Rolling Stability Characteristics of a Delta-Wing Model. NACA TR 1224, 1955. (U)
- Goodman, A.: Effects of Wing Position and Horizontal-Tail Position on the Static Stability Characteristics of Model with Unswept and 45° Sweptback Surfaces with some Reference to Mutual Interference. NACA TN 2504, 1951. (U)
- Savage, H. F., and Tinling, B. E.: The Subsonic Static Aerodynamic Characteristics of an Airplane Model having a Triangular Wing of Aspect Ratio 3. II- Lateral and Directional Characteristics. NACA TN 4042, 1957. (U)
- Kuhn, R. E., and Draper, J. W.: Wind-Tunnel Investigation of the Effects of Geometric Dihedral on the Aerodynamic Characteristics in Pitch and Sideslip of an Unswept- and a 45° Sweptback-Wing-Fuselage Combination at High Subsonic Speeds. NACA RM L53F09, 1953. (U)
- Christensen, F. B.: An Experimental Investigation of Four Triangular-Wing-Body Combinations in Sideslip at Mach Numbers 0.6, 0.9, 1.4 and 1.7. NACA RM A53L22, 1954. (U)
- Jacquet, B. J., and Williams, J. L.: Wind-Tunnel Investigation at Low Speeds of Effect of Size and Position of Closed Air Ducts on Static Longitudinal and Static Lateral Stability Characteristics of Unswept-Midwing Models having Wings of Aspect Ratio 2, 4, and 6. NACA TN 3481, 1955. (U)
- Kuhn, R. E., and Fournier, P. G.: Wind-Tunnel Investigation of the Static Lateral Stability Characteristics of Wing-Fuselage Combinations at High Subsonic Speeds. NACA RM L52G11a, 1952. (U)
- Wiggins, J. W., Kuhn, R. E., and Fournier, P. G.: Wind-Tunnel Investigation to Determine the Horizontal- and Vertical-Tail Contributions to the Static Lateral Stability Characteristics of a Complete-Model Swept-Wing Configuration at High Subsonic Speeds. NACA TN 3818, 1956. (U)
- Letko, W., and Williams, J. L.: Experimental Investigation at Low Speed of Effects of Fuselage Cross Section on Static Longitudinal and Lateral Stability Characteristics of Model Having 0° and 45° Sweptback Surfaces. NACA TN 3551, 1955. (U)
- Robinson, R. B.: Effects of Vertical Location of the Wing and Horizontal Tail on the Static Lateral and Directional Stability of a Trapezoidal-Wing Airplane Model at Mach Numbers of 1.41 and 2.01. NACA RM L58C18, 1958. (U)
- Boatright, W. B.: Experimental Investigation of Effects of Wing Planform and Dihedral Angle on Sideslip Derivatives of Sweptback-Wing-Body Combinations at Supersonic Speeds. NACA RM L58E06, 1958. (U)
- Spearman, M. L., Driver, C., and Hughes, W. C.: Investigation of Aerodynamic Characteristics in Pitch and Sideslip of a 45° Sweptback-Wing Airplane Model with Various Vertical Locations of Wing and Horizontal Tail. Basic-Data Presentation, M = 2.01. NACA RM L54L06, 1955. (U)

TABLE 5.2.1.1-A
LOW SPEED WING-BODY SIDE FORCE DUE TO SIDESLIP
DATA SUMMARY

Ref	M	f	Wing Position	Γ (deg)	x_1	x_0	$(k_2 - k_1)$	S_0 sq ft	V_B^{23} sq ft	S_w sq ft	K _t	$C_{Y\beta} \times 10^3$ per deg	* $C_{Y\beta} \times 10^3$ per deg	$\Delta C_{Y\beta} \times 10^3$ per deg (Calc - Test)	
1	0.13	5.00	Mid	0	0.50	0.64	0.825	0.163	0.415	2.25	1.00	-2.090	-2.20	0.11	
		6.67					0.880	0.162	0.496			-2.200	-2.21	0.01	
		10.00					0.940	0.166	0.652			-2.240	-2.25	0.01	
		6.67					0.880	0.162	0.586			-2.210	-2.28	0.07	
		6.67					0.880	0.181	0.530			-2.470	-2.28	-0.19	
2	0.17	12.0	High	0	0.40	0.595	0.955	0.110	0.464	4.00	1.57	-1.445	-2.00	0.555	
											1.00	-0.920	-1.20	0.28	
											1.33	-1.220	-1.60	0.38	
			Low				0.925	0.198	0.690			1.57	-2.510	-3.00	0.49
											1.00	-1.600	-2.00	0.40	
											1.33	-2.125	-2.00	-0.125	
			9.00				0.860	0.440	1.174			1.57	-5.180	-5.60	0.42
											1.00	-3.300	-2.40	-0.90	
											1.33	-4.390	-4.60	0.21	
3	0.17	6.90	High	0	0.50	0.64	0.888	0.175	0.542	2.25	1.57	-3.760	-4.00	0.24	
											1.00	-2.400	-2.40	0	
											1.33	-3.190	-3.40	0.21	
4	0.25	12.0	High	0	0.75	0.765	0.955	0.195	0.924	4.00	1.58	-2.560	-2.60	0.04	
											1.00	-2.980	-3.100	0.12	
							0.937	0.136	0.522	2.25		1.58	-2.480	-2.000	-0.48
													-2.480	-2.000	-0.48
													-2.980	-3.000	0.02
6	0.60	9.87	Mid	0	0.50	0.645	0.94	0.180	0.798	4.014	1.0	-1.470	-1.40	-0.07	
													-1.40	-1.40	-0.07
							0.95	0.090	0.410	2.007			-1.490	-1.40	-0.09
													-1.40	-1.40	-0.09
9	0.40	9.84	Mid	0	0.61	0.70	0.937	0.136	0.522	2.25	1.0	-1.980	-1.90	-0.08	
10	0.13	7.50	Mid	0	0.40	0.59	0.900	0.196	0.609	2.25	1.0	-2.254	-2.20	-0.054	

*Test result at $\alpha = 0$

$$\text{Average Error} = \frac{\sum |\Delta C_{Y\beta}|}{n} = 0.217 \times 10^{-3} \text{ (per deg)}$$

TABLE 5.2.1.1-B
SUPersonic WING-BODY SIDE FORCE DUE TO SIDESLIP
DATA SUMMARY

Ref	M	Wing Position	K ₁	Γ (deg)	f _N	f _A	S _b sq ft	S _w sq ft	$C_{Y\beta \text{ calc}} \times 10^3$ per deg	* $C_{Y\beta \text{ test}} \times 10^3$ per deg	$\Delta C_{Y\beta} \times 10^3$ per deg (Calc-Test)
11	1.41	High	1.72	0	7.00	15.00	.0605	1.33	-3.54	-3.00	-0.54
		Mid	1.00						-2.06	-1.60	-0.46
		Low	1.42						-2.93	-3.50	0.57
	2.01	High	1.72						-3.68	-3.50	-0.18
		Mid	1.00						-2.14	-1.80	-0.34
		Low	1.42						-3.04	-3.50	0.46
12	1.72	Mid	1.00	0	3.50	6.50	.00307	0.0506	-2.94	-2.80	-0.14
				-5					-3.44	-3.20	-0.24
				-10					-3.94	-3.80	-0.14
	2.02			0					-3.24	-3.20	-0.04
				-5					-3.70	-3.70	0
				-10					-4.20	-4.20	0
13	2.01	High	1.73	0	4.30	6.67	.0605	1.00	-4.90	-4.60	-0.30
		Mid	1.00						-2.85	-2.90	0.05
		Low	1.43						-4.08	-5.00	0.92
		Mid	1.00	3					-3.15	-3.00	-0.15
				3					-3.15	-3.00	-0.15

*Test result at $\alpha = 0$.

$$\text{Average Error} = \frac{\sum |\Delta C_{Y\beta}|}{n} = 0.275 \times 10^{-3} \text{ (per deg)}$$

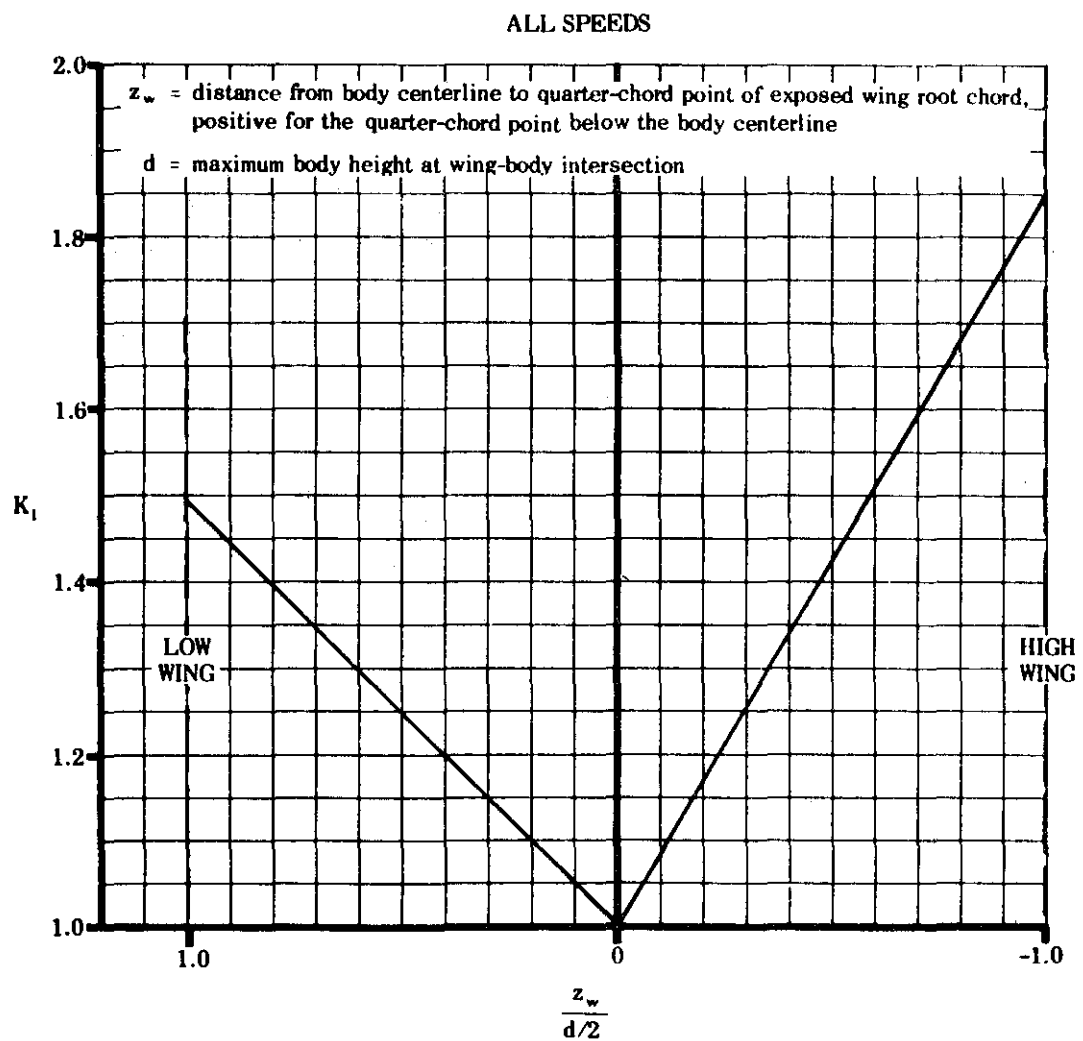


FIGURE 5.2.1.1-7 WING-BODY INTERFERENCE FACTOR FOR WING-BODY SIDESLIP DERIVATIVE $C_{Y\beta}$

5.2.1.2 WING-BODY SIDE-FORCE COEFFICIENT C_y AT ANGLE OF ATTACK

The wing-body side force developed at combined angles is nonlinear with respect to both sideslip and angle of attack due to viscous cross-flow effects and cross-coupling of upwash and sidewash velocities. To obtain the sideslip derivative $C_{Y\beta_{WB}}$ it is recommended that $C_{Y_{WB}}$ be calculated at several angles of attack for a small sideslip angle ($\beta \leq 4^\circ$). Then at each angle of attack the side force is assumed linear with sideslip for small values of β so that

$$C_{Y\beta_{WB}} = \frac{C_{Y_{WB}}}{\beta}.$$

A. SUBSONIC

No method is presently available for determining the viscous cross-flow effects and cross-coupling of upwash and sidewash velocities at angles of attack and subsonic speeds.

The method presented herein is restricted to first-order approximations at relatively low angles of attack.

DATCOM METHOD

It is recommended that the method of paragraph A of Section 5.2.1.1 be used in the linear-lift angle-of-attack region.

B. TRANSONIC

The comments of paragraph A for the subsonic case also apply to wing-body combinations at combined angles and transonic speeds.

DATCOM METHOD

It is recommended that the method of paragraph B of Section 5.2.1.1 be used in the linear-lift angle-of-attack region.

C. SUPERSONIC

Although higher order slender-body solutions which account for cross-coupling of upwash and sidewash velocities at supersonic speeds are presently unavailable, an approximate method is developed in reference 1 which accounts for the effects of angle of attack on wing-body interference.

Two types of interference forces are considered significant at combined sideslip and angle of attack. One effect is due to the influence of the forebody on cross flow. The resulting asymmetric wing loading causes interference pressures on the sides of the body that increase the body side force. The other effect is produced by the wing inhibiting the viscous cross flow occurring along the body at large angles of attack. This phenomenon is termed "viscous cross-flow suppression" in that it reduces the body side force. No attempt is made to estimate the magnitude of wing sweepback effects on wing-body interference and the effect of body vortices on wing-body interference is considered negligible.

DATCOM METHOD

The method presented in this Section for estimating the wing-body side-force coefficient is that of reference 1. The determination of the body-alone contribution is adapted from the method of reference 2 which is discussed in Section 4.2.1.2. For combined angles the method is valid only for circular bodies. In addition reference 1 specifies that the wing leading edge be supersonic. But fair accuracy is obtained for configurations with subsonic leading edges when the aspect ratio is not too low. The wing-alone contribution to side force is usually very small and is therefore neglected.

Reference 1 gives two expressions for wing-body interference effects, one for midwing and one for tangent-wing configurations. The forebody cross-flow effect is zero for the midwing case since the wing plane then coincides with a body-alone cross-flow streamline and no change in cross flow takes place. Therefore, the midwing case is based on the premise that the sole effect of the wing is to inhibit the nonlinear effects of the viscous body cross flow.

The wing-body contribution to the side-force coefficient at combined sideslip and angle of attack is given by

$$C_{Y_{WB}} = C_{Y_B} + C_{Y_{W(B)}} \quad 5.2.1.2-a$$

where C_{Y_B} is the body-alone side-force contribution given by

$$C_{Y_B} = -\frac{S_B}{S_w} 2 \beta - c_{d_c} \frac{S_{BS}}{S_w} \beta \alpha' \quad 5.2.1.2-b$$

where

$\frac{S_B}{S_w}$ is the ratio of the body frontal area to the total wing area

β is the sideslip angle in radians

c_{d_c} is the cross-flow drag coefficient, obtained from figure 4.2.1.2-23b), with $M_c = M_\infty \sin \alpha'$

$\frac{S_{BS}}{S_w}$ is the ratio of the body side area to the total wing area

α' is the angle of inclination, $\alpha' = \sqrt{\alpha^2 + \beta^2}$, in radians

$C_{Y_{W(B)}}$ is the side-force contribution of the wing due to the presence of the body, given by

$$C_{Y_{W(B)}} = -2\eta_B K_{W(B)} k(\alpha) \frac{S_B}{S_w} \beta - \frac{c_{d_c} c_{r_e} d}{S_w} \beta (\beta - \alpha') \quad 5.2.1.2-c$$

where the first term on the right-hand side is the forebody cross-flow effect and is taken as zero for the midwing case, and the second term on the right-hand side is an approximate effect of the wing inhibiting the viscous cross flow occurring along the body at large angles of attack.

η_B is the Mach number correction to the wing-body interference coefficient, from figure 5.2.1.2-7

$K_{W(B)}$ is the wing-body interference coefficient, or apparent-mass ratio, from figure 5.3.1.1-25oo. For wing positions other than midwing ($K_{W(B)} = 0$) or tangent, a nonlinear interpolation is described in Method 3, paragraph A, Section 5.3.1.1.

$k(\alpha)$ is the angle-of-attack correction to the wing-body interference coefficient. Values of this parameter for high- and low-tangent wings are presented in figure 5.2.1.2-8. For wing positions other than midwing ($k(\alpha) = 0$) or tangent, a nonlinear interpolation is described in Method 3, paragraph A, Section 5.3.1.1.

d is the average body diameter at the exposed wing root

c_{r_e} is the exposed root chord of the wing

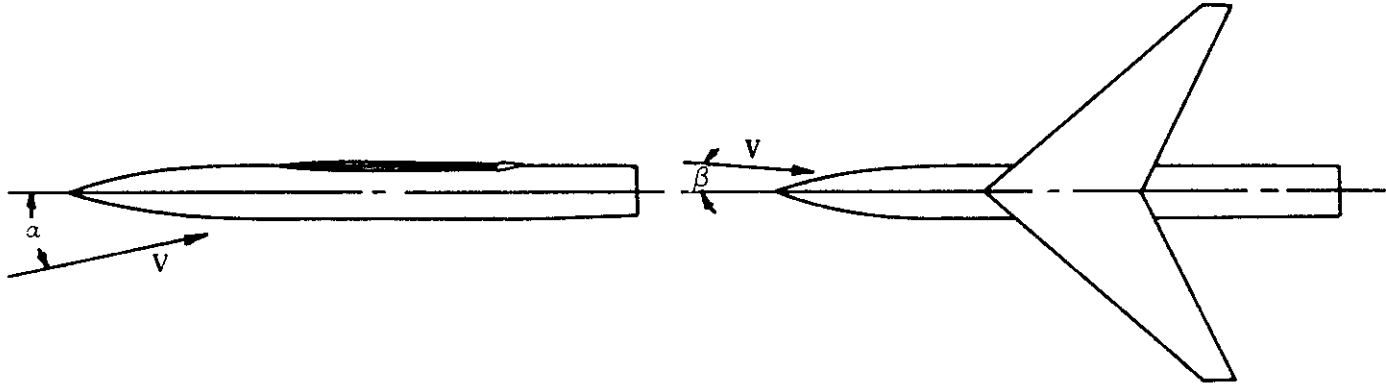
Values for the incremental coefficient resulting from the addition of wings in the mid- and high- and low-tangent positions on circular bodies, calculated using equation 5.2.1.2-c, are compared with experimental results in figure 5.2.1.2-5.

The incremental coefficient resulting from the addition of a wing in the midbody position is presented in figure 5.2.1.2-5a. The Datcom method does not account for additional differential load on the body resulting from unequal panel loading occurring with yawed sweptback wings. This neglected effect, in conjunction with the approximate account of viscous cross-flow suppression may account for the lack of better agreement between experimental and calculated results at higher angles of attack.

The incremental coefficient resulting from the addition of sweptback wings in the high- and low-tangent positions on a body are presented in figure 5.2.1.2-5b through -5d. The agreement between experimental and calculated values is surprisingly good in view of the fact that the angle-of-attack correction to the wing-body interference coefficient, $k(\alpha)$, applies strictly to unswept two-dimensional wings. The additional differential load on the body occurring with yawed sweptback wings tends to compensate for the reduction in $k(\alpha)$ resulting from wing sweepback.

Sample Problem

Given: The wing-body configuration of reference 3. Find the side-force coefficient developed by the wing-body combination at $\alpha = 12^\circ$ and $\beta = 4^\circ$.



Wing Characteristics

High-tangent wing

$$S_w = 144.0 \text{ sq in.}$$

$$b_w = 24.0 \text{ sq in.}$$

$$c_{re} = 8.90 \text{ in.}$$

Body Characteristics

Ogive-cylinder body

$$d = 3.33 \text{ in.}$$

$$S_B = 8.70 \text{ sq in.}$$

$$S_{BS} = 110.0 \text{ sq in.}$$

Additional Characteristics

$$M_\infty = 2.01$$

$$\alpha = 12^\circ = 0.209 \text{ rad}$$

$$\beta = 4^\circ = 0.070 \text{ rad}$$

$$\alpha' = \sqrt{\alpha^2 + \beta^2} = 12.65 \text{ deg} = 0.221 \text{ rad}$$

Compute:

Body-along contribution

$$M_c = M_\infty \sin \alpha' = 2.01 \sin 12.56^\circ = 0.440$$

$$c_{dc} = 1.30 \text{ (figure 4.2.1.2-23b)}$$

$$C_{Y_B} = -\frac{S_B}{S_w} 2\beta - c_{dc} \frac{S_{BS}}{S_w} \beta \alpha' \quad (\text{equation 5.2.1.2-b})$$

$$= -\frac{8.70}{144.0} (2)(0.070) - (1.30) \frac{110.0}{144.0} (0.070)(0.221)$$

$$= -0.0238 \text{ (based on } S_w)$$

Wing interference contribution

$$\sqrt{M^2 - 1} \frac{d}{c_{re}} = \sqrt{(2.01)^2 - 1} \left(\frac{3.33}{8.90} \right) = 0.651$$

$$\eta_B = 0.81 \text{ (figure 5.2.1.2-7)}$$

$$\frac{d}{b_w} = \frac{3.33}{24.0} = 0.139$$

$$K_{WB} = 1.22 \text{ (figure 5.3.1.1-2500)}$$

$$\frac{c_{re}}{d} = \frac{8.90}{3.33} = 2.67$$

$$k(\alpha) = 2.27 \text{ (figures 5.2.1.2-8d, 5.2.1.2-8e, and 5.2.1.2-8f by interpolation)}$$

$$C_{Y_{WB}} = -2\eta_B K_{WB} k(\alpha) \frac{S_B}{S_w} \beta - \frac{c_{de} c_{re} d}{S_w} \beta (\beta - \alpha') \quad \text{(equation 5.2.1.2-c)}$$

$$= -2(0.81)(1.22)(2.27) \frac{8.70}{144.0} (0.070) - \frac{(1.30)(8.90)(3.33)(0.70)(0.070 - 0.221)}{144.0}$$

$$= -0.0162 \text{ (based on } S_w)$$

Solution:

$$\begin{aligned} C_{Y_{WB}} &= C_{Y_B} + C_{Y_{WB}} \quad \text{(equation 5.2.1.2-a)} \\ &= -0.0238 - 0.0162 \\ &= -0.0400 \text{ (based on } S_w) \end{aligned}$$

This compares with an experimental value (based on S_w) of $C_{Y_{WB}} = -0.0480$ from reference 3.

A comparison between calculated and experimental results for this configuration at sideslip angles of 2, 4, and 8 degrees and over an angle-of-attack range to 16 degrees is presented in figure 5.2.1.2-6.

REFERENCES

1. Kaattari, G. E.: Estimation of Directional Stability Derivatives at Moderate Angles and Supersonic Speeds. NASA Memo 12-1-58A, 1959. (U)
2. Allen, H., and Perkins, E. W.: Characteristics of Flow Over Inclined Bodies of Revolution. NACA RM A50L07, 1951. (U)
3. Spearman, M. L.: Effect of Wing Location and Geometric Dihedral for the Wing-Body Combination, $M = 2.01$. NACA RM L55B18, 1955. (U)
4. Spearman, M. L., Driver, C., and Hughes, W. C.: Investigation of Aerodynamic Characteristics in Pitch and Sideslip of a 45° Sweptback-Wing Airplane Model with Various Vertical Locations of Wing and Horizontal Tail -- Basic-Data Presentation, $M = 2.01$. NACA RM L54L06, 1955. (U)

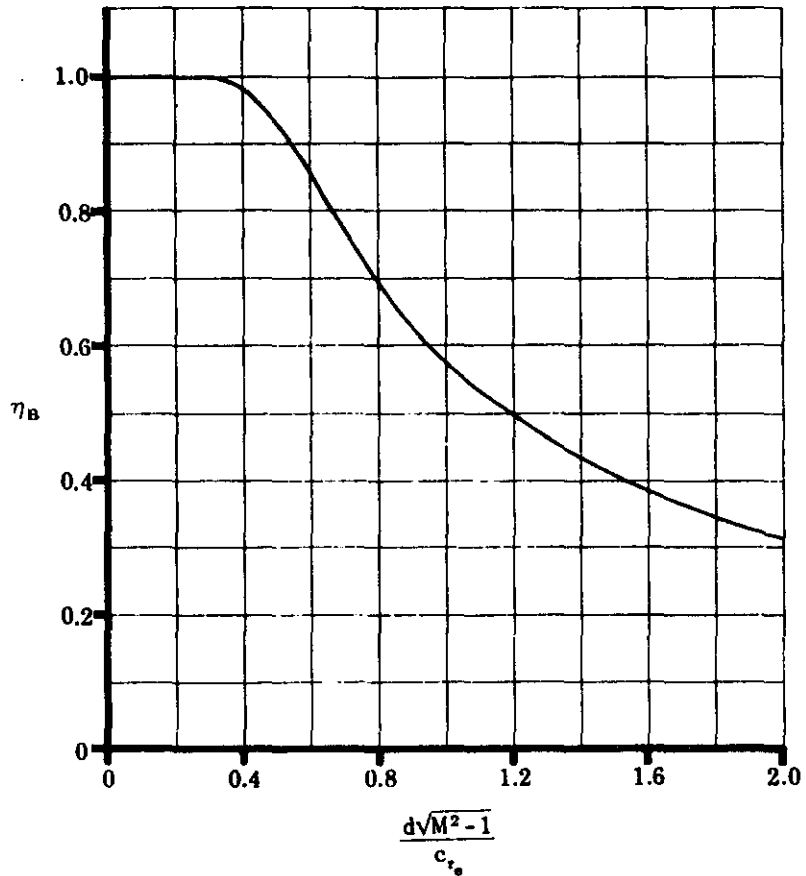


FIGURE 5.2.1.2-7 MACH NUMBER CORRECTION TO WING-BODY INTERFERENCE COEFFICIENT

LOW WING

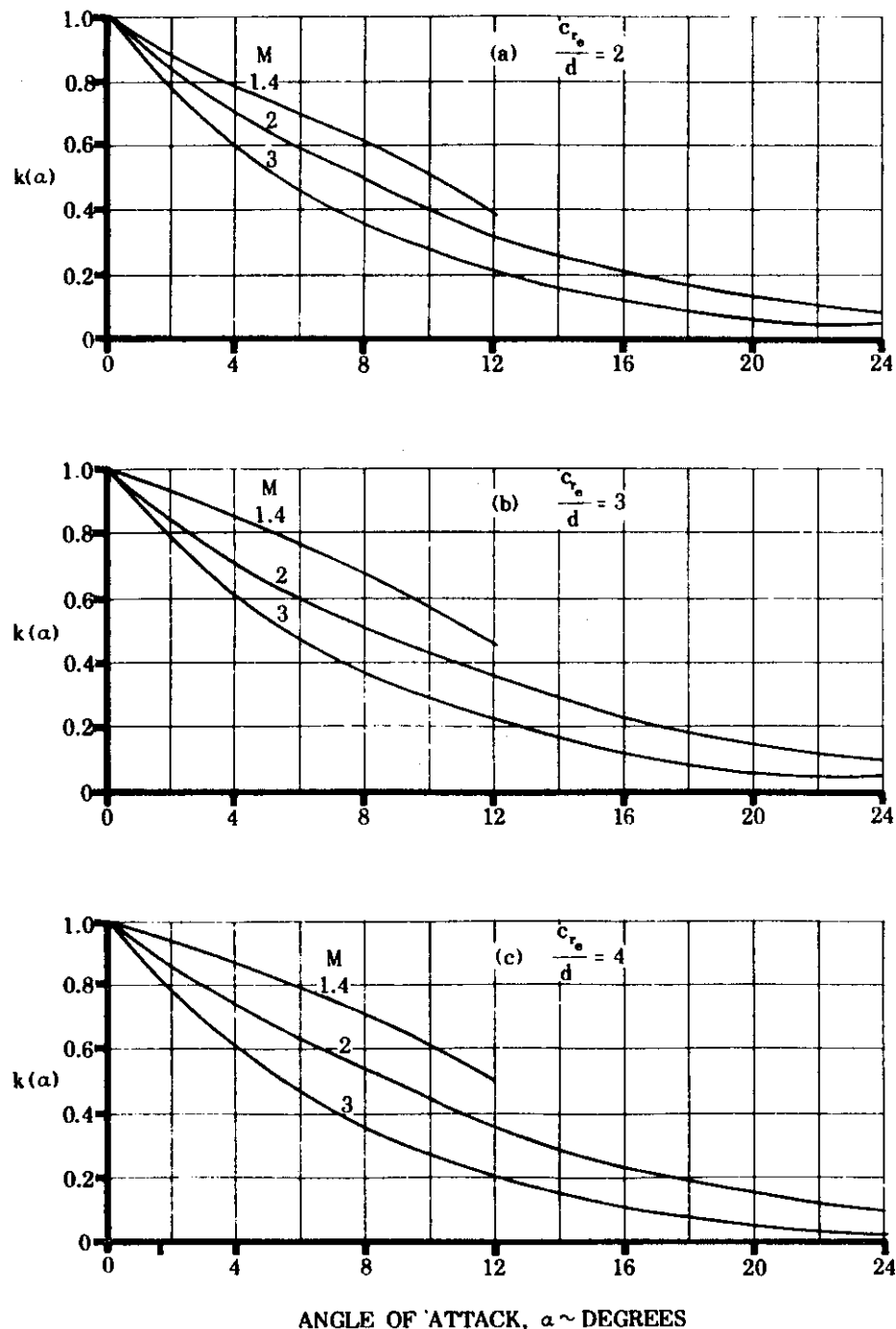


FIGURE 5.2.1.2-8 ANGLE-OF-ATTACK CORRECTION TO WING-BODY INTERFERENCE COEFFICIENT

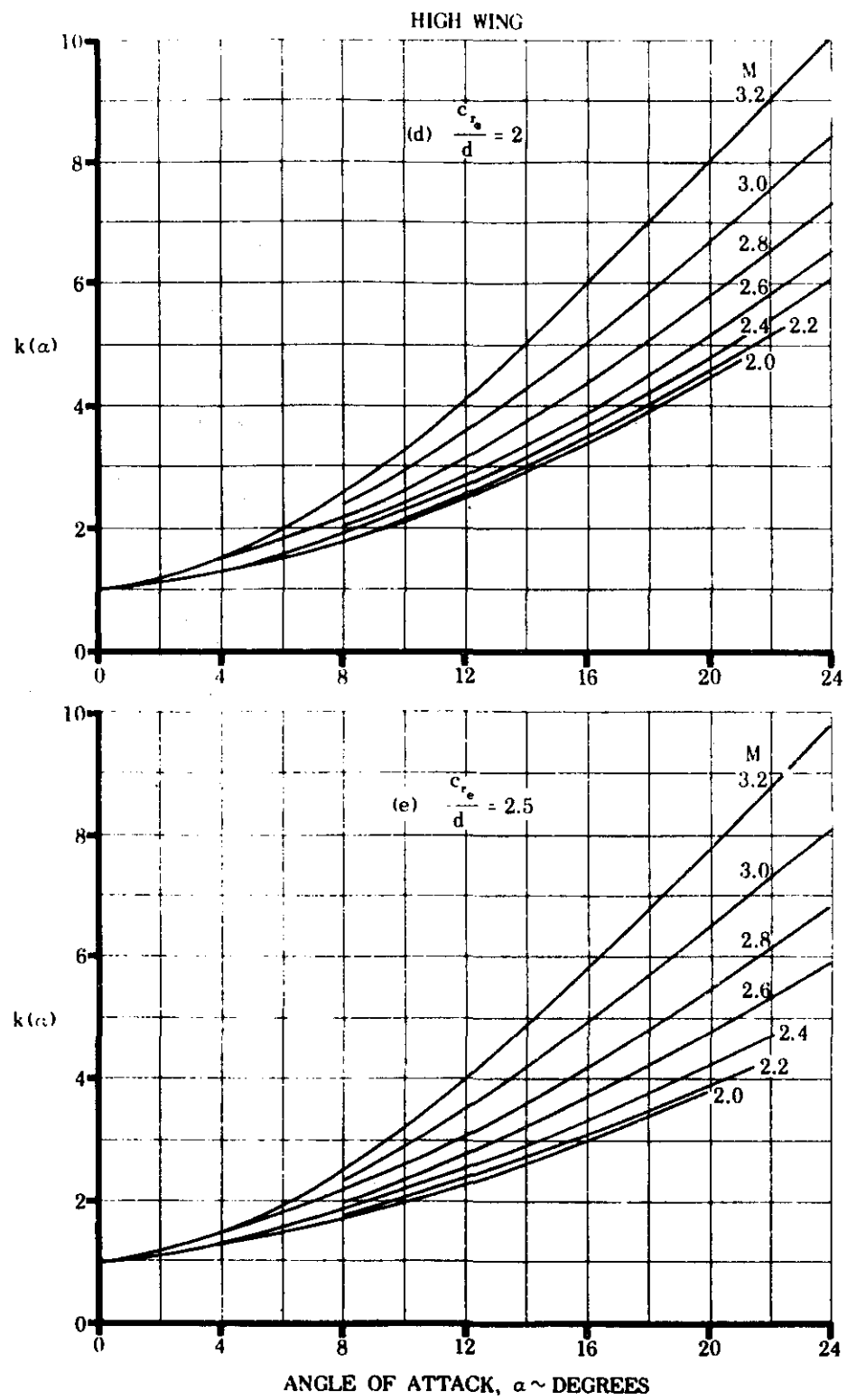


FIGURE 5.2.1.2-8 ANGLE-OF-ATTACK CORRECTION TO WING-BODY INTERFERENCE COEFFICIENT (contd)

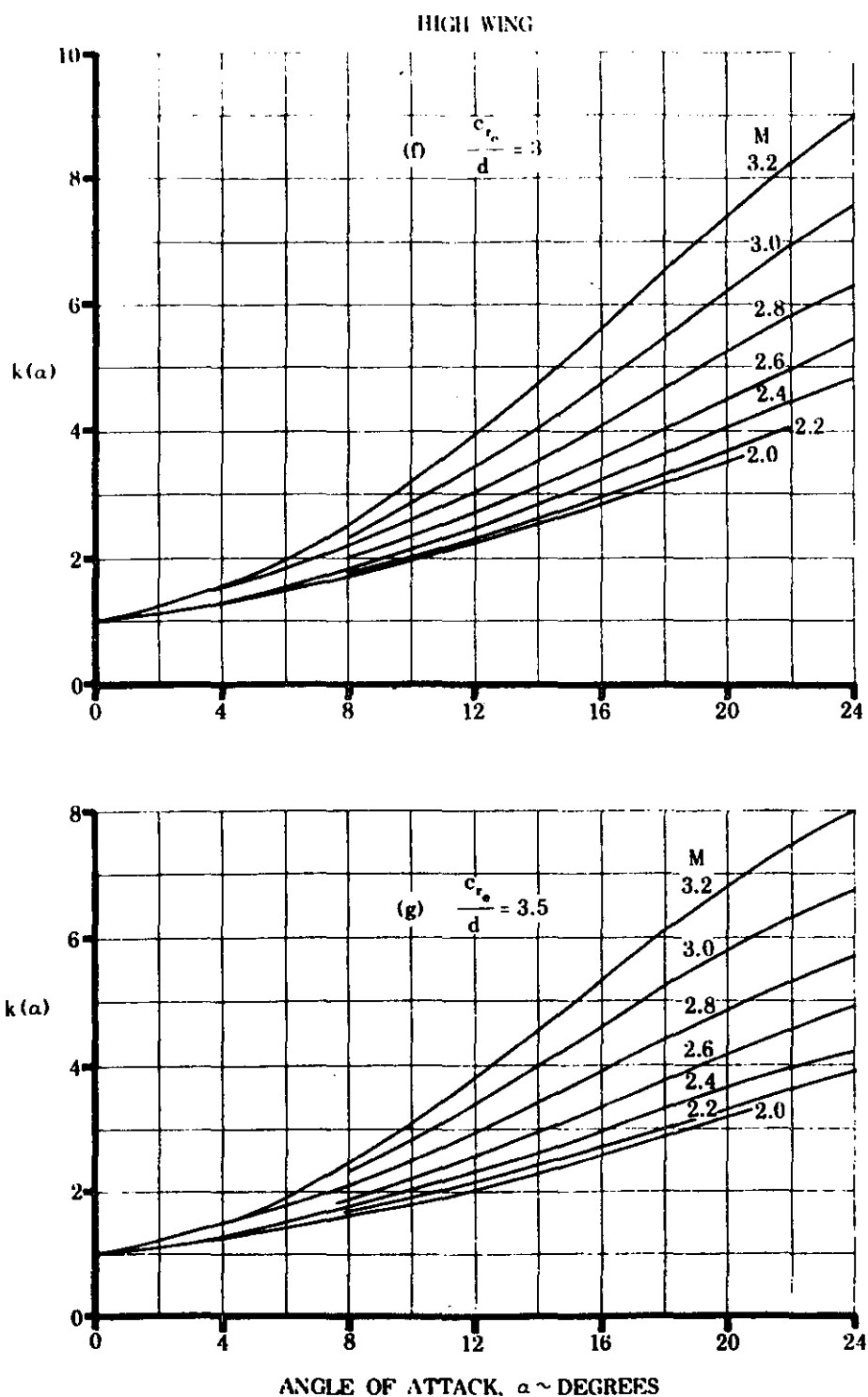


FIGURE 5.2.1.2-8 ANGLE-OF-ATTACK CORRECTION TO WING-BODY INTERFERENCE COEFFICIENT (contd)

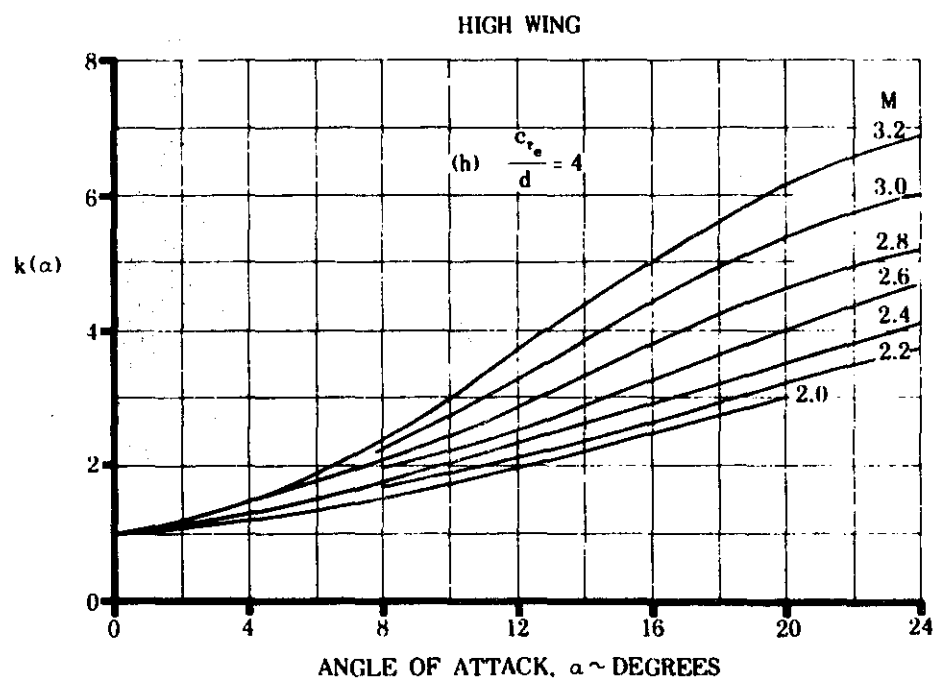


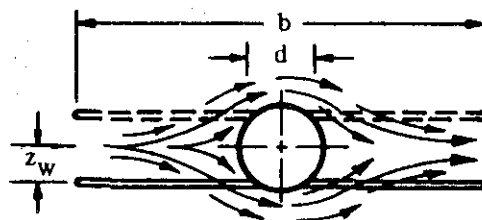
FIGURE 5.2.1.2-8 ANGLE-OF-ATTACK CORRECTION TO WING-BODY INTERFERENCE COEFFICIENT (contd)

5.2.2 WING-BODY SIDESLIP DERIVATIVE C_{I_β}

5.2.2.1 WING-BODY SIDESLIP DERIVATIVE C_{I_β} IN THE LINEAR ANGLE-OF-ATTACK RANGE

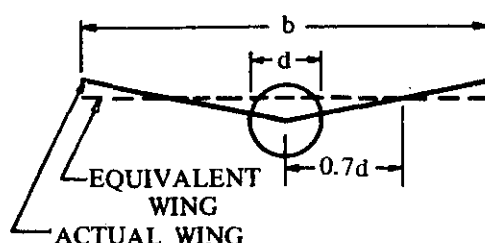
A. SUBSONIC

The addition of a body to a wing in sideslip is shown experimentally to change the wing rolling moment in two ways. First, there is the well known change in effective dihedral as a function of wing height on the body. This occurs because the cross flow around the body induces changes in the local angle of attack of the wing (see sketch (a)). The resulting change in lift distribution has a significant influence on C_{I_β} . The simplified expression presented in the Datcom for determining the body-induced effect on wing height is based on a fuselage of circular cross section, and is presented in such sources as references 1 and 2. The sign of the value of this effect is dependent upon whether the wing is located above or below the center line of the fuselage. A high location of the wing results in more positive effective dihedral and a low location results in less positive effective dihedral than a midwing location.



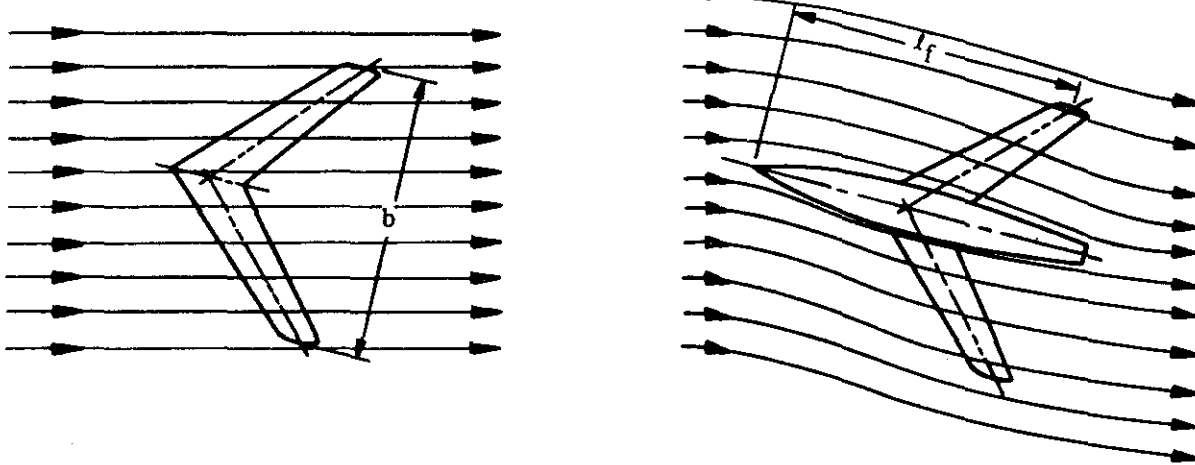
SKETCH (a)

For wings with geometric dihedral, the body-induced effect on wing height must be modified, since the vertical position of the wing relative to the fuselage varies along the span (see sketch (b)). The method presented in the Datcom to account for this modification is taken from reference 3. The method is applicable only for wings with dihedral that intersect the vertical plane of symmetry of a body of circular cross section at or near the midfuselage height. In reference 3 the wing with dihedral is replaced with a wing without dihedral at some effective height relative to the fuselage, and the fuselage flow effect for the equivalent wing is then evaluated. The vertical position of the equivalent wing was taken to coincide with the wing with dihedral at the spanwise position equal to 0.7d.



SKETCH (b)

The second fuselage effect on rolling moment is a decrease in wing-body positive effective dihedral with increasing fuselage length. This effect is discussed in reference 3, where it is suggested that this may be the result of the fuselage reducing the wing effective sideslip angle (see sketch (c)).



SKETCH (c)

In reference 3 an empirical study of limited scope shows that the fuselage effects may be correlated as a function of the ratio of fuselage length ahead of the wing-tip half-chord point and the wing span $\frac{l_f}{b}$

More extensive studies indicate that the parameter $\frac{A}{\cos \Lambda_{c/2}}$ is also important. There may be additional parameters, such as the ratio of the body diameter to wing span and fuselage cross-sectional shape that also exert an influence. The design chart presented herein is limited to the parameters $\frac{l_f}{b}$ and $\frac{A}{\cos \Lambda_{c/2}}$, and is based on experimental data from configurations employing fuselages of circular cross section.

The increments in $C_{l\beta}$ due to the body-induced effects on wing height and the effect of fuselage length have been derived for configurations with fuselages of circular cross section. Not enough test data exist to determine any effect the fuselage cross-sectional shape may have on the fuselage-length parameter. On the other hand, both theory and experiment indicate that the body-induced effects on wing height are strongly influenced by the cross-sectional shape of the fuselage.

It is suggested that for non-body-of-revolution configurations the equivalent diameter be used in determining the increments in $C_{l\beta}$ due to the body-induced effects on wing height.

The subsonic method is valid for configurations with straight-tapered wings for sideslip angles between -50° and $+50^\circ$ at speeds up to the force-break Mach number and at low angles of attack. The

fuselage-effect parameters do not include the effect of either nonuniform geometric dihedral or non-straight-tapered planforms.

DATCOM METHOD

The rolling moment due to sideslip, based on the product of the wing area and span S_b , for straight-tapered wing-body combinations at low angles of attack is given by

$$C_{l_\beta} = C_L \left[\left(\frac{C_{l_\beta}}{C_L} \right)_{\Lambda_{c/2}} K_{M_\Lambda} K_f + \left(\frac{C_{l_\beta}}{C_L} \right)_A \right] + \Gamma \left[\frac{C_{l_\beta}}{\Gamma} K_{M_\Gamma} + \frac{\Delta C_{l_\beta}}{\Gamma} \right] + (\Delta C_{l_\beta})_{z_w} + \theta \tan \Lambda_{c/4} \left(\frac{\Delta C_{l_\beta}}{\theta \tan \Lambda_{c/4}} \right) \text{ (per degree)} \quad 5.2.2.1-a$$

where

C_L is the wing-body lift coefficient.

$\left(\frac{C_{l_\beta}}{C_L} \right)_{\Lambda_{c/2}}$ is the wing-sweep contribution obtained from paragraph A of Section 5.1.2.1 (figure 5.1.2.1-27)

K_{M_Λ} is the compressibility correction to the sweep contribution obtained from paragraph A of Section 5.1.2.1 (figure 5.1.2.1-28a)

K_f is the empirical fuselage-length-effect correction factor obtained from figure 5.2.2.1-26.

$\left(\frac{C_{l_\beta}}{C_L} \right)_A$ is the aspect ratio contribution obtained from paragraph A of Section 5.1.2.1 (figure 5.1.2.1-28b)

Γ is the geometric dihedral angle in degrees, positive for the wing tip above the plane of the root chord.

$\frac{C_{l_\beta}}{\Gamma}$ is the wing dihedral effect for uniform geometric dihedral obtained from paragraph A of Section 5.1.2.1 (figure 5.1.2.1-29).

K_{M_Γ} is the compressibility correction factor to the dihedral effect obtained from paragraph A of Section 5.1.2.1 (figure 5.1.2.1-30a).

$$\frac{\Delta C_{I_\beta}}{\Gamma}$$

is the body-induced effect on wing height due to uniform geometric dihedral given by*

$$\frac{\Delta C_{I_\beta}}{\Gamma} = -0.0005 \sqrt{A} \left(\frac{d}{b}\right)^2 \quad (\text{per degree}^2) \quad 5.2.2.1-b$$

where d/b is the average fuselage diameter at the wing root divided by the wing span. For non-body-of-revolution configurations, the average equivalent diameter at the wing root should be used, where $(d_{\text{equiv}})_{av} = \sqrt{\frac{\text{average cross-sectional area}}{0.7854}}$

$(\Delta C_{I_\beta})_{z_w}$ is the increment in C_{I_β} due to the body-induced effect on wing height for configurations with wings located above or below the midfuselage height. This increment is given by

$$(\Delta C_{I_\beta})_{z_w} = \frac{1.2 \sqrt{A}}{57.3} \left(\frac{z_w}{b}\right) \left(\frac{2d}{b}\right) \quad (\text{per degree}) \quad 5.2.2.1-c$$

where

$\frac{z_w}{b}$ is the vertical distance from the center line of the fuselage to the quarter-chord point of the root chord divided by the wing span, positive for the wing located below the center line of the fuselage.

$\frac{d}{b}$ is defined under equation 5.2.2.1-b

$$\frac{\Delta C_{I_\beta}}{\theta \tan \Lambda_{c/4}}$$

is the wing-twist correction factor obtained from paragraph A of Section 5.1.2.1 (figure 5.1.2.1-30b).

θ is the wing twist between the root and tip sections in degrees, negative for washout (see figure 5.1.2.1-30b).

For the case of a wing with dihedral mounted on a body at a location other than at or near the midfuselage height, both the modification of the body-induced effect on wing height due to dihedral (equation 5.2.2.1-b) and the body-induced effect on wing height (equation 5.2.2.1-c) should be considered.

A comparison of test values with results calculated by using the Datcom method for wing-body configurations without dihedral and with the wings mounted at the midfuselage location is presented as table 5.2.2.1-A. Comparisons of test values with results calculated by using the Datcom method for the effects of dihedral and wing height are presented in tables 5.2.2.1-B and 5.2.2.1-C, respectively.

*Equation 5.2.2.1-b is derived by replacing z_w in equation 5.2.2.1-c with the expression for the height above the fuselage center line of an equivalent wing at a height corresponding to the height of the .07d spanwise station of a wing with dihedral (see sketch (b)).

Test data are not available to permit substantiation of the effect of wing twist on the wing-body rolling moment due to sideslip.

Sample Problem

1. Midwing, no dihedral, no twist

Given: The wing-body configuration of reference 8 designated 60-4-0.6-006.

$$A = 4.0 \quad \lambda = 0.6 \quad \Lambda_{c/2} = 59.08^\circ \quad b = 36.0 \text{ in.} \quad l_f = 49.58 \text{ in.}$$

$$z_w = 0 \text{ (midwing)} \quad \Gamma = 0 \quad \theta = 0 \quad M = 0.60$$

Body of revolution

Compute:

$$\left(\frac{C_{I_\beta}}{C_L} \right)_{\Lambda_{c/2}} = -0.00723 \text{ per deg} \quad (\text{figure 5.1.2.1-27})$$

$$\left(\frac{C_{I_\beta}}{C_L} \right)_A = -0.00180 \text{ per deg} \quad (\text{figure 5.1.2.1-28b})$$

$$M \cos \Lambda_{c/2} = (0.60) \cos 59.08^\circ = 0.308$$

$$A/\cos \Lambda_{c/2} = 4.0/\cos 59.08^\circ = 7.785$$

$$K_{M_A} = 1.02 \quad (\text{figure 5.1.2.1-28a})$$

$$l_f/b = 49.58/36.0 = 1.377$$

$$K_f = 0.685 \quad (\text{figure 5.2.2.1-26})$$

Solution:

$$C_{I_\beta} = C_L \left[\left(\frac{C_{I_\beta}}{C_L} \right)_{\Lambda_{c/2}} K_{M_A} K_f + \left(\frac{C_{I_\beta}}{C_L} \right)_A \right] \quad (\text{equation 5.2.2.1-a})$$

$$= C_L [(-0.00723)(1.02)(0.685) + (-0.00180)]$$

$$= C_L [-0.00505 - 0.00180]$$

$$\frac{C_{I_\beta}}{C_L} = -0.00685 \text{ per deg}$$

This result compares with a test value of -0.0074 per degree from reference 8.

2. High wing, dihedral, no twist

Given: A wing-body configuration of reference 16.

$$A = 6.383 \quad \lambda = 1.0 \quad \Lambda_{c/2} = 0 \quad b = 60.0 \text{ in.} \quad l_f = 15.7 \text{ in.}$$

$$d = 6.70 \text{ in. (average over root chord)} \quad z_w = -2.66 \text{ in. (high wing)}$$

$$\Gamma = 5^0 \quad \theta = 0 \quad M = 0.105 \quad \text{Body of revolution}$$

Compute:

$$\left(\frac{C_{I_\beta}}{C_L} \right)_{\Lambda_{c/2}} = 0 \quad (\text{figure 5.1.2.1-27})$$

$$\left(\frac{C_{I_\beta}}{C_L} \right)_A = -0.0013 \text{ per deg} \quad (\text{figure 5.1.2.1-28b})$$

$$M \cos \Lambda_{c/2} = (0.105) (\cos 0) = 0.105$$

$$A/\cos \Lambda_{c/2} = 6.383/(\cos 0) = 6.383$$

$$K_{M_A} = 1.0 \quad (\text{figure 5.1.2.1-28a})$$

$$l_f/b = 15.7/60.0 = 0.262$$

$$K_f = 1.0 \quad (\text{figure 5.2.2.1-26})$$

Determine dihedral-effect parameters

Geometric dihedral

$$\frac{C_{I_\beta}}{\Gamma} = -0.000224 \text{ per deg}^2 \quad (\text{figure 5.1.2.1-29})$$

$$K_{M_\Gamma} = 1.0 \quad (\text{figure 5.1.2.1-30a})$$

Body-induced effect on wing height due to dihedral

$$\frac{\Delta C_{I_\beta}}{\Gamma} = -0.0005 \sqrt{A} \left(\frac{d}{b}\right)^2 \quad (\text{equation 5.2.2.1-b})$$

$$= -0.0005 \sqrt{6.383} \left(\frac{6.7}{60}\right)^2$$

$$= -0.000016 \text{ per deg}^2$$

Determine the effect of wing height

$$z_w/b = -2.66/60.0 = -0.0443$$

$$2d/b = 2(6.70)/60.0 = 0.223$$

$$\Delta C_{I_\beta z_w} = \frac{1.2 \sqrt{A}}{57.3} \left(\frac{z_w}{b}\right) \left(\frac{2d}{b}\right) \quad (\text{equation 5.2.2.1-c})$$

$$= \frac{1.2 \sqrt{6.383}}{57.3} (-0.0443) (0.223)$$

$$= -0.000547 \text{ per deg}$$

Solution:

$$C_{I_\beta} = C_L \left[\left(\frac{C_{I_\beta}}{C_L} \right)_{\Lambda_{c/2}} K_{M_\Lambda} K_f + \left(\frac{C_{I_\beta}}{C_L} \right)_\Lambda \right] + \Gamma \left[\frac{C_{I_\beta}}{\Gamma} K_{M_\Gamma} + \frac{\Delta C_{I_\beta}}{\Gamma} \right]$$

$$+ \Delta C_{I_\beta z_w} \quad (\text{equation 5.2.2.1-a})$$

Midwing, no dihedral

$$\frac{C_{I_\beta}}{C_L} = \left[\left(\frac{C_{I_\beta}}{C_L} \right)_{\Lambda_{c/2}} K_{M_\Lambda} K_f + \left(\frac{C_{I_\beta}}{C_L} \right)_\Lambda \right]$$

$$= [(0) (1.0) (1.0) + (-0.0013)]$$

$$= -0.0013 \text{ per deg}$$

Dihedral effect

$$\Gamma \left[\frac{C_{l_\beta}}{\Gamma} K_{M_f} + \frac{\Delta C_{l_\beta}}{\Gamma} \right] = (5.0) [(-0.000224)(1.0) + (-0.000016)] = -0.0012 \text{ per deg}$$

This compares with a test value of -0.00115 per degree from reference 16.

Wing-height effect

$$(\Delta C_{l_\beta})_{z_w} = -0.000547 \text{ per deg}$$

This compares with a test value of -0.00053 per degree from reference 16.

B. TRANSONIC

Test data show that the variation of wing-body rolling moment due to sideslip is similar to that of the lift-curve slope. This correspondence should be expected, since C_{l_β} has been treated by using effective lift-curve slopes in reference 3.

The similarity in Mach number characteristics between rolling moment and lift-curve slope suggests a transonic interpolation method, based on lift-curve slope, for calculating rolling moment. An interpolation equation is presented that is based on the square of the lift-curve-slope values at the force-break Mach number M_{fb} and at $M = 1.4$.

Since no reliable method exists for predicting the variation of the wing-body lift-curve slope with Mach number over the transonic speed range, wing-alone lift-curve slopes are used in the Datcom method. For slender wing-body configurations, the aerodynamic interference effects are relatively insensitive to Mach number, and the use of the wing-alone lift-curve-slope values in the interpolation method should give satisfactory results. However, for nonslender configurations transonic interference effects can become quite large and sensitive to minor changes in local contour. For these configurations the interpolation method cannot be expected to provide satisfactory results unless wing-body test values of the lift-curve slope are used.

The method is limited to configurations with straight-tapered wings and is applicable over the sideslip-angle range of $\beta = \pm 50^\circ$.

DATCOM METHOD

The wing-body rolling moment due to sideslip of straight-tapered wing-body configurations, based on the product of the wing area and span S_b , may be approximated through the transonic region from M_{fb} to $M = 1.4$ by means of the interpolation formula

$$\frac{C_{I_\beta}}{C_L} = \left\{ \left[\frac{\left(\frac{C_{I_\beta}}{C_N} \right)_{M=1.4} - \left(\frac{C_{I_\beta}}{C_L} \right)_{M_{fb}}}{\left(C_{N_\alpha}^2 \right)_{M=1.4} \left(C_{L_\alpha}^2 \right)_{M_{fb}}} \right] \left(\frac{M - M_{fb}}{1.4 - M_{fb}} \right) + \frac{\left(\frac{C_{I_\beta}}{C_L} \right)_{M_{fb}}}{\left(C_{L_\alpha}^2 \right)_{M_{fb}}} \right\} \left(C_{L_\alpha}^2 \right)_M \quad (\text{per degree}) \quad 5.2.2.1-d$$

where

$$\left(\frac{C_{I_\beta}}{C_L} \right)_{M_{fb}}$$

is the wing-body sideslip-derivative slope at the force-break Mach number M_{fb} , obtained by using the method of paragraph A. The force-break Mach number is defined in paragraph B of Section 4.1.3.2.

$$\left(\frac{C_{I_\beta}}{C_N} \right)_{M=1.4}$$

is the wing-body sideslip-derivative slope $M = 1.4$, obtained by using the method of paragraph C.

$$\left(C_{L_\alpha}^2 \right)_{M_{fb}}$$

is the square of the wing-alone lift-curve slope at M_{fb} , obtained by using the method of paragraph B of Section 4.1.3.2.

$$\left(C_{N_\alpha}^2 \right)_{M=1.4}$$

is the square of the wing-alone normal-force-curve slope at $M = 1.4$, obtained by using the straight-tapered-wing method of paragraph C of Section 4.1.3.2.

$$\left(C_{L_\alpha}^2 \right)_M$$

is the square of the wing-alone lift-curve slope at pre-determined Mach numbers, obtained by using the methods of paragraphs B and C of Section 4.1.3.2. The pre-determined Mach numbers consist of those at the end points of the method ($M = M_{fb}$ and $M = 1.4$) and two intermediate Mach numbers defined in paragraph B of Section 4.1.3.2 as $M_a = M_{fb} + 0.007$ and $M_b = M_{fb} + 0.14$.

The increments in C_{I_β} due to fuselage transverse flow and wing height may be approximated by equations 5.2.2.1-b and 5.2.2.1-c, respectively.

Equation 5.1.2.1-d for determining the effect of geometric dihedral at supersonic speeds is also applicable at transonic speeds. However, no known method exists for determining transonic values of C_{I_p} required for this method. It is suggested that reference be made to table 7-A for transonic C_{I_p} test data.

If test data are not available the supersonic method of paragraph C of Section 7.1.2.2 should be used to approximate C_{I_p} .

Sample Problem

Given: A wing-body configuration of reference 6.

Wing Characteristics:

$$A = 2.0 \quad \lambda = 0 \quad \Lambda_{LE} = 63.4^\circ \quad \Lambda_{TE} = 0 \quad \Lambda_{c/2} = 45^\circ$$

$$b = 34.0 \text{ in.} \quad S_w = 578.0 \text{ sq in.} \quad z_w = 0 \text{ (midwing)}$$

$$\text{NACA 0005-63 airfoil} \quad \theta = 0 \quad \Gamma = 0 \quad t/c = 0.05$$

Body of revolution

Body Characteristics:

$$d = 6.12 \text{ in.} \quad l_f = 55.12 \text{ in.}$$

Additional Characteristics:

$$\kappa = 1.0 \text{ (assumed)} \quad M_{fb} \leq M \leq 1.4$$

Compute:

Determine M_{fb} , M_a , M_b , $(C_{L\alpha})_{M_{fb}}$, $(C_{L\alpha})_{M_a}$, and $(C_{L\alpha})_{M_b}$ (paragraph B, Section 4.1.3.2).

$$(M_{fb})_{\Lambda=0} = 1.0 \quad (\text{figure 4.1.3.2-53a})$$

$$(M_{fb})_\Lambda = 1.0 \quad (\text{figure 4.1.3.2-53b})$$

$$(C_{L\alpha})_{fb}$$

$$\beta_{fb} = \sqrt{M_{fb}^2 - 1} = 0$$

$$\frac{A}{\kappa} \left[(\beta_{fb})^2 + \tan^2 \Lambda_{c/2} \right]^{1/2} = \frac{2.0}{1.0} [(0) + (1)]^{1/2} = 2.0$$

$$\frac{\left[(C_{L\alpha})_{M_{fb}} \right]_{\text{theory}}}{A} = 1.30 \text{ per rad} \quad (\text{figure 4.1.3.2-49})$$

$$\left[(C_{L\alpha})_{M_{fb}} \right]_{\text{theory}} = (1.30)(2) = 2.60 \text{ per rad}$$

$$\frac{(C_{L\alpha})_{M_{fb}}}{[(C_{L\alpha})_{M_{fb}}]_{\text{theory}}} = 1.08 \quad (\text{figure 4.1.3.2-54a})$$

$$(C_{L\alpha})_{M_{fb}} = (2.60)(1.08) = 2.81 \text{ per rad} = 0.049 \text{ per deg}$$

$$M_a = M_{fb} + 0.07 = 1.07$$

$$(C_{L\alpha})_{M_a}$$

$$\frac{a}{c} = -0.07 \quad (\text{figure 4.1.3.2-54b})$$

$$(C_{L\alpha})_{M_a} = \left(1 - \frac{a}{c}\right)(C_{L\alpha})_{M_{fb}}$$

$$= [1 - (-0.07)] (2.81) = 3.00 \text{ per rad} = 0.0524 \text{ per deg}$$

$$M_b = M_{fb} + 0.14 = 1.14$$

$$(C_{L\alpha})_{M_b}$$

$$\frac{b}{c} = 0.11 \quad (\text{figure 4.1.3.2-54c})$$

$$(C_{L\alpha})_{M_b} = \left(1 - \frac{b}{c}\right)(C_{L\alpha})_{M_{fb}}$$

$$= [1 - (0.11)] (2.86) = 2.55 \text{ per rad} = 0.0444 \text{ per deg}$$

Determine $(C_{N\alpha})_{M=1.4}$ (paragraph C, Section 4.1.3.2)

$$\beta = \sqrt{M^2 - 1} = 0.98$$

$$\beta/\tan \Lambda_{LE} = 0.98/\tan 63.4^\circ = 0.491$$

$$\tan \Lambda_{TE}/\tan \Lambda_{LE} = 0$$

$$\frac{(C_{N\alpha})_{\text{theory}}}{A} = 1.31 \text{ per rad} \quad (\text{figure 4.1.3.2-63})$$

$$(C_{N\alpha})_{\text{theory}} = (1.31)(2) = 2.62 \text{ per rad}$$

$$\Delta y_1 = 1.37 \quad (\text{figure 2.2.1-8})$$

$$\frac{C_{N\alpha}}{(C_{N\alpha})_{\text{theory}}} = 1.0 \quad (\text{figure 4.1.3.2-60})$$

$$(C_{N\alpha})_{M=1.4} = (1.0)(2.62) = 2.62 \text{ per rad} = 0.0457 \text{ per deg}$$

Determine $\left(\frac{C_{I\beta}}{C_L}\right)_{M_{fb}}$ and $\left(\frac{C_{I\beta}}{C_L}\right)_{M=1.4}$

$$\left(\frac{C_{I\beta}}{C_L}\right)_{M_{fb}}$$

$$\left(\frac{C_{I\beta}}{C_L}\right)_{\Lambda_{c/2}} = -0.0035 \text{ per deg} \quad (\text{figure 5.1.2.1-27})$$

$$\left(\frac{C_{I\beta}}{C_L}\right)_A = -0.0022 \text{ per deg} \quad (\text{figure 5.1.2.1-28b})$$

$$M_{fb} \cos \Lambda_{c/2} = (1.0) (\cos 45^\circ) = 0.7071$$

$$\frac{A}{\cos \Lambda_{c/4}} = \frac{2}{0.7071} = 2.83$$

$$K_{M_A} = 1.015 \quad (\text{figure 5.1.2.1-28a})$$

$$l_f/b = 55.12/34.0 = 1.62$$

$$K_f = 1.0 \quad (\text{figure 5.2.2.1-26})$$

$$\left(\frac{C_{I\beta}}{C_L}\right)_{M_{fb}} = \left[\left(\frac{C_{I\beta}}{C_L}\right)_{\Lambda_{c/2}} K_{M_A} K_f + \left(\frac{C_{I\beta}}{C_L}\right)_A \right] \quad (\text{equation 5.2.2.1-a})$$

$$\begin{aligned}
&= [(-0.0035)(1.015)(1.0) + (-0.0022)] \\
&= -0.00575 \text{ per deg}
\end{aligned}$$

$$\left(\frac{C_{I_\beta}}{C_N} \right)_{M=1.4}$$

$$\left(\frac{C_{I_\beta}}{C_N} \right)_{M=1.4} = -0.061 \frac{C_{N_\alpha}}{57.3} \left[1 + \lambda(1 + \Lambda_{LE}) \right] \left(1 + \frac{\Lambda_{LE}}{2} \right) \left(\frac{\tan \Lambda_{LE}}{\beta} \right) .$$

$$\left[\frac{M^2 \cos^2 \Lambda_{LE}}{A} + \left(\frac{\tan \Lambda_{LE}}{4} \right)^{4/3} \right] \quad (\text{equation 5.2.2.1-e})$$

$$= -0.061 \frac{2.62}{57.3} [1 + 0] \left(1 + \frac{63.4/57.3}{2} \right) \left(\frac{\tan 63.4^\circ}{0.98} \right).$$

$$\left[\frac{(1.4)^2 \cos^2 63.4^\circ}{2.0} + \left(\frac{\tan 63.4^\circ}{4} \right)^{4/3} \right]$$

$$= -0.061 (0.0457)[1](1 + 0.5532)(2.038)[0.1965 + (0.3965)]$$

$$= -0.00523 \text{ per deg}$$

Solution:

$$\begin{aligned}
\frac{C_{I_\beta}}{C_L} &= \left\{ \left[\frac{\left(\frac{C_{I_\beta}}{C_N} \right)_{M=1.4} - \left(\frac{C_{I_\beta}}{C_L} \right)_{M_{fb}}}{\left(C_{L_\alpha^2} \right)_{M=1.4}} \right] \left(\frac{M - M_{fb}}{1.4 - M_{fb}} \right) + \frac{\left(\frac{C_{I_\beta}}{C_L} \right)_{M_{fb}}}{\left(C_{L_\alpha^2} \right)_{M_{fb}}} \right\} \left(C_{L_\alpha^2} \right)_M \\
&\quad (\text{equation 5.2.2.1-d})
\end{aligned}$$

$$= \left\{ \left[\frac{(-0.00523)}{(0.0457)^2} - \frac{(-0.00575)}{(0.049)^2} \right] \left(\frac{M - 1.0}{1.4 - 1.0} \right) + \frac{(-0.00575)}{(0.049)^2} \right\} \left(C_{L_\alpha^2} \right)_M$$

$$= \left\{ [-0.10] \left(\frac{M - 1.0}{0.4} \right) - 2.309 \right\} \left(C_{L_\alpha^2} \right)_M$$

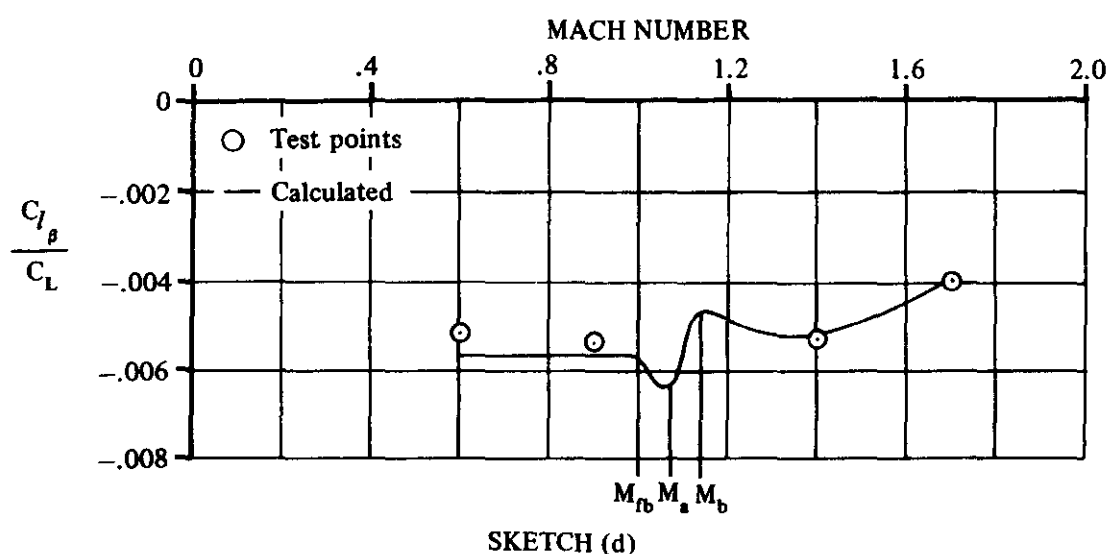
$$\left(\frac{C_{I_\beta}}{C_L} \right)_{M_a = 1.07}$$

$$\begin{aligned}\left(\frac{C_{I_\beta}}{C_L} \right)_{M_a = 1.07} &= \left\{ [-0.100] \left(\frac{1.07 - 1.0}{0.4} \right) - 2.309 \right\} (0.0524)^2 \\ &= \left\{ [-0.100] (0.175) - 2.309 \right\} (0.002745) \\ &= -0.00639 \text{ per deg}\end{aligned}$$

$$\left(\frac{C_{I_\beta}}{C_L} \right)_{M_b = 1.14}$$

$$\begin{aligned}\left(\frac{C_{I_\beta}}{C_L} \right)_{M_b = 1.14} &= \left\{ [-0.100] \left(\frac{1.14 - 1.0}{0.4} \right) - 2.309 \right\} (0.0444)^2 \\ &= \left\{ [-0.100] (0.350) - 2.309 \right\} (0.00197) \\ &= -0.00462 \text{ per deg}\end{aligned}$$

The calculated results are compared with test values in sketch (d). Additional points have been calculated at $M = 0.6, 0.9$, and 1.7 .



C. SUPERSONIC

The present status of supersonic rolling-moment theory is discussed in paragraph C of Section 5.1.2.1. As indicated therein, insufficient experimental data exist at the present time to distinguish between the supersonic rolling moments for wing-alone and for wing-body configurations where the wing is mounted on the fuselage center line. Therefore, for configurations with the wing mounted on the fuselage center line the supersonic wing-alone method of paragraph C is employed.

Experimental data indicate that for wings located at positions other than on the fuselage center line there is a considerable variation in effective dihedral with wing height on the body. Furthermore, the effect of geometric dihedral on the body-induced effect due to wing height, discussed in paragraph A, must also be considered at supersonic speeds. No methods have been developed to account for the body-induced effects on wing height at supersonic speeds. The subsonic methods of paragraph A (equations 5.2.2.1-b and 5.2.2.1-c) are applied at supersonic speeds.

DATCOM METHOD

The supersonic rolling moment due to sideslip for wing-body configurations with straight-tapered wings at low angles of attack and at $M = 1.4$ and higher speeds is approximated by

$$C_{I_\beta} = -0.061 C_N \frac{C_{N\alpha}}{57.3} \left[1 + \lambda(1 + \Lambda_{LE}) \right] \left(1 + \frac{\Lambda_{LE}}{2} \right) \left(\frac{\tan \Lambda_{LE}}{\beta} \right) \left[\frac{M^2 \cos^2 \Lambda_{LE}}{A} + \left(\frac{\tan \Lambda_{LE}}{4} \right)^{4/3} \right] \\ + \Gamma \left[\frac{C_{I_\beta}}{\Gamma} + \frac{\Delta C_{I_\beta}}{\Gamma} \right] + \Delta C_{I_\beta}_{z_w} \quad (\text{per degree}) \quad 5.2.2.1-e$$

where

Λ_{LE} is the wing leading-edge sweep in radians.

$C_{N\alpha}$ is the wing normal-force-curve slope per radian, obtained by using the straight-tapered-wing method of paragraph C of Section 4.1.3.2.

$\frac{C_{I_\beta}}{\Gamma}$ is the wing dihedral effect for uniform geometric dihedral, calculated by using equation 5.1.2.1-d with C_{I_β} (per radian) obtained by using the method of paragraph C of Section 7.1.2.2.

$\frac{\Delta C_{I_\beta}}{\Gamma}$ is the body-induced effect on wing height due to uniform geometric dihedral obtained by using equation 5.2.2.1-b.

$(\Delta C_{I_\beta})_{z_w}$ is the increment in C_{I_β} due to the body-induced effect on wing height for configurations with wings located above or below the fuselage center line, obtained by using equation 5.2.2.1-c.

A comparison of test values with results calculated by using the Datcom method for wing-body configurations without dihedral and with wings mounted at the midfuselage location is presented as table 5.2.2.1-D. A comparison of test values with results calculated by using the Datcom method for the effects of dihedral is presented as table 5.2.2.1-E.

It is difficult to assess the validity of the Datcom method for establishing the value of $C_{l\beta}/C_L$, even at small lift coefficients. Test data show that for many configurations the variation of $C_{l\beta}$ with C_L at supersonic speeds is nonlinear throughout the lift-coefficient range. Some of the test values listed in table 5.2.2.1-D are questionable, and those configurations for which no test values are listed exhibit nonlinear rolling moment due to sideslip throughout the lift-coefficient range.

Although the data of table 5.2.2.1-E are limited, it appears that the method provides relatively good results for the effect of dihedral on $C_{l\beta}$ at supersonic speeds.

Not enough experimental data are available to assess the validity of equation 5.2.2.1-c applied at supersonic speeds for determining the effect of wing vertical location. Equation 5.2.2.1-c has been applied to the configurations of references 19 and 20; the results of these calculations are compared with test values in table 5.2.2.1-F. The calculated values are somewhat less than the test values in all cases.

Sample Problem

Given: The wing-body configuration of reference 19.

Wing Characteristics:

$$A = 4.0 \quad \lambda = 0.2 \quad \Lambda_{LE} = 49.4^\circ \quad \Lambda_{c/2} = 42.5^\circ$$

$$b = 24.0 \text{ in.} \quad \Gamma = 3^\circ \quad z_w = 0 \text{ (midwing)} \quad \text{NASA 65A004 airfoil}$$

Body Characteristics:

$$d = 3.33 \text{ in.} \quad d/b = 0.139 \quad \text{Body of revolution}$$

Additional Characteristics:

$$M = 2.01; \beta = 1.74 \quad C_{N\alpha} = 2.235 \text{ per rad (test value)}$$

Midwing, no dihedral

Compute:

$$\left(1 + \Lambda_{LE}\right) = 1 + \frac{49.4}{57.3} = 1.862$$

$$[1 + \lambda(1 + \Lambda_{LE})] = [1 + 0.2(1.862)] = 1.372$$

$$\left(1 + \frac{\Lambda_{LE}}{2}\right) = \left[1 + \frac{49.4}{2(57.3)}\right] = 1.431$$

$$(\tan \Lambda_{LE}/\beta) = \tan 49.4^\circ / 1.74 = 0.6705$$

$$\left[\frac{M^2 \cos^2 \Lambda_{LE}}{A} + \left(\frac{\tan \Lambda_{LE}}{4} \right)^{4/3} \right] = \left[\frac{(2.01)^2 \cos^2 49.4^\circ}{4.0} + \left(\frac{\tan 49.4^\circ}{4} \right)^{4/3} \right] = 0.621$$

Solution:

$$\begin{aligned} \frac{C_{I_p}}{C_N} &= -0.061 \frac{C_N \alpha}{57.3} [1 + \lambda(1 + \Lambda_{LE})] \left(1 + \frac{\Lambda_{LE}}{2}\right) \left(\frac{\tan \Lambda_{LE}}{\beta}\right) \left[\frac{M^2 \cos^2 \Lambda_{LE}}{A} + \left(\frac{\tan \Lambda_{LE}}{4} \right)^{4/3} \right] \\ &\quad (\text{equation 5.2.2.1-e with } \Gamma = 0, z_w = 0) \\ &= -0.061 \frac{2.235}{57.3} [1.372](1.431)(0.6705)[0.621] \\ &= -0.00195 \text{ per deg} \end{aligned}$$

This compares with a test value of -0.0019 per degree from reference 19.

Dihedral effect

Compute:

$$\beta A = (1.74)(4.0) = 6.96$$

$$A \tan \Lambda_{c/2} = (4.0) (\tan 42.5^\circ) = 3.67$$

$$\frac{C_{I_p} \text{ theory}}{A} = -0.0665 \text{ per rad} \quad (\text{figure 7.1.2.2-38, interpolated})$$

$$\Delta y_\perp = 0.80 \quad (\text{figure 2.2.1-8})$$

$$\delta_\perp = \tan^{-1} \frac{\Delta y_\perp}{5.85} = \tan^{-1} \frac{0.80}{5.85} = 7.8^\circ$$

$$\frac{C_{I_p}}{(C_{I_p})_{\text{theory}}} = 0.918 \quad (\text{figure 7.1.2.2-40})$$

$$C_{I_p} = \left[\frac{(C_{I_p})_{\text{theory}}}{A} \right] A \frac{C_{I_p}}{(C_{I_p})_{\text{theory}}} \quad (\text{equation 7.1.2.2-d})$$

$$= [-0.0665] (4.0) (0.918) = -0.244 \text{ per rad}$$

$$\frac{C_{I_\beta}}{\Gamma} = \frac{2}{(57.3)^2} \left(\frac{1+2\lambda}{1+3\lambda} \right) C_{I_p} \quad (\text{equation 5.1.2.1-d})$$

$$= \frac{2}{(57.3)^2} \left(\frac{1.4}{1.6} \right) (-0.244) = -0.000130 \text{ per deg}^2$$

$$\frac{\Delta C_{I_\beta}}{\Gamma} = -0.0005 \sqrt{A} \left(\frac{d}{b} \right)^2 \quad (\text{equation 5.2.2.1-b})$$

$$= -0.0010 \sqrt{4.0} \left(\frac{3.33}{24} \right)^2$$

$$= -0.0000193 \text{ per deg}^2$$

Solution:

$$\Gamma \left(\frac{C_{I_\beta}}{\Gamma} + \frac{\Delta C_{I_\beta}}{\Gamma} \right) \quad (\text{dihedral effect term of equation 5.2.2.1-e})$$

$$3.0 [-0.000130 + (-0.0000193)] = -0.000448 \text{ per.deg}$$

This compares with a test value of -0.00046 per degree from reference 19.

REFERENCES

1. Campbell, J. P., and McKinney, M. O.: Summary of Methods for Calculating Dynamic Lateral Stability and Response and for Estimating Lateral Stability Derivatives. NACA TR 1098, 1952. (U)
2. Levacic, I.: Rolling Moment Due to Sideslip. Part III. RAE Aero Rep. No. 2139, 1946. (U)
3. Polhamus, E. C., and Steeman, W. C., Jr.: The Rolling Moment Due to Sideslip of Swept Wings at Subsonic Speeds. NASA TN D-209, 1960. (U)
4. Wolhart, W. D., and Thomas, D. F., Jr.: Static Longitudinal and Lateral Stability Characteristics at Low Speed of 60° Sweptback-Midwing Models Having Wings With an Aspect Ratio of 2, 4, or 6. NACA TN 4397, 1958. (U)
5. Kuhn, R. E., and Draper, J. W.: Wind-Tunnel Investigation of the Effects of Geometric Dihedral on the Aerodynamic Characteristics in Pitch and in Sideslip of an Unswept- and a 45° Sweptback-Wing-Fuselage Combination at High Subsonic Speeds. NACA RM L53F09, 1953. (U)
6. Christensen, F. B.: An Experimental Investigation of Four Triangular-Wing-Body Combinations in Sideslip at Mach Numbers 0.6, 0.9, 1.4, and 1.7. NACA RM A53L22, 1954. (U)
7. Letko, W., and Williams, J. L.: Experimental Investigation at Low Speed of Effects of Fuselage Cross Section on Static Longitudinal and Lateral Stability Characteristics of Models Having 0° and 45° Sweptback Surfaces. NACA TN 3551, 1955. (U)
8. Kuhn, R. E., and Fournier, P. G.: Wind-Tunnel Investigation of the Static Lateral Stability Characteristics of Wing-Fuselage Combinations at High Subsonic Speeds – Sweep Series. NACA RM L52G11a, 1952. (U)
9. Steeman, W. C., Jr.: An Experimental Study at High Subsonic Speeds of Several Tail Configurations on a Model Having a 45° Sweptback Wing. NACA RM L57C08, 1957. (U)

10. Goodson, K. W., and Becht, R. E.: Wind-Tunnel Investigation at High Subsonic Speeds of the Stability Characteristics of a Complete Model Having Sweptback-, M-, W-, and Cranked-Wing Plan Forms and Several Horizontal-Tail Locations. NACA RM L54C29, 1954. (U)
11. Brewer, J. D., and Lichtenstein, J. H.: Effect of Horizontal Tail on Low-Speed Static Lateral Stability Characteristics of a Model Having 45° Sweptback Wing and Tail Surfaces. NACA TN 2010, 1950. (U)
12. Fournier, P. G.: Wind-Tunnel Investigation of the Aerodynamic Characteristics in Pitch and Sideslip at High Subsonic Speeds of a Wing-Fuselage Combination Having a Triangular Wing of Aspect Ratio 4. NACA RM L53G14a, 1953. (U)
13. Wiggins, J. W.: Wind-Tunnel Investigation at High Subsonic Speeds of the Static Longitudinal and Static Lateral Stability Characteristics of a Wing-Fuselage Combination Having a Triangular Wing of Aspect Ratio 2.31 and an NACA 65A003 Airfoil. NACA RM L53G09a, 1953. (U)
14. Fournier, P. G., and Byrnes, A. L., Jr.: Wind-Tunnel Investigation of the Static Lateral Stability Characteristics of Wing-Fuselage Combinations at High Subsonic Speeds. NACA RM L52L18, 1953. (U)
15. Wiggins, J. W., and Fournier, P. G.: Wind-Tunnel Investigation of the Static Lateral Stability Characteristics of Wing-Fuselage Combinations at High Subsonic Speeds – Taper Ratio Series. NACA TN 4174, 1957. (U)
16. House, R. O., and Wallace, A. R.: Wind-Tunnel Investigation of Effect of Interference on Lateral-Stability Characteristics of Four NACA 23012 Wings, an Elliptical and a Circular Fuselage, and Vertical Fins. NACA TR 705, 1941. (U)
17. Savage, H. F., and Tinling, B. E.: The Subsonic Static Aerodynamic Characteristics of an Airplane Model Having a Triangular Wing of Aspect Ratio 3. II—Lateral and Directional Characteristics. NACA TN 4042, 1957. (U)
18. Goodman, A., and Thomas, D. F., Jr.: Effects of Wing Position and Fuselage Size on the Low-Speed Static and Rolling Stability Characteristics of a Delta-Wing Model. NACA TR 1224, 1955. (U)
19. Spearman, M. L.: Investigation of the Aerodynamic Characteristics in Pitch and Sideslip of a 45° Sweptback-Wing Airplane Model With Various Vertical Locations of the Wing and Horizontal Tail. – Effect of Wing Location and Geometric Dihedral for the Wing-Body Combination, $M = 2.01$. NACA RM L55B18, 1955. (U)
20. Robinson, R. B.: Effects of Vertical Location of the Wing and Horizontal Tail on the Static Lateral and Directional Stability of a Trapezoidal-Wing Airplane Model at Mach Numbers of 1.41 and 2.01. NACA RM L58C18, 1958. (U)
21. Boatright, W. B.: Experimental Investigation of Effects of Wing Plan Form and Dihedral Angle on Sideslip Derivatives of Sweptback-Wing-Body Combinations at Supersonic Speeds. NACA RM L58E08, 1958. (U)
22. Faryn, M. O., and Campbell, J. F.: Effects of Wing Dihedral and Planform on Stability Characteristics of a Research Model at Mach Numbers From 1.80 to 4.63. NASA TN D-2914, 1965. (U)
23. Jernell, L. S.: Effects of Wing Planform on the Aerodynamic Characteristics of a Wing-Body-Tail Model at Mach Number From 1.70 to 4.63. NASA TN D-3105, 1965. (U)

TABLE 5.2.2.1-A
SUBSONIC WING-BODY ROLLING MOMENT DUE TO SIDESLIP

Midwing Configurations
No Dihedral

DATA SUMMARY

Ref.	A	λ	$\Lambda_c/2$ (deg)	$\frac{l_f}{b}$	M	C_l/\bar{C}_L Calc. (per deg)	C_l/\bar{C}_L Test (per deg)	$\Delta\left(\frac{C_l}{C_L}\right)$ Calc.-Test (per deg)	% Percent Error
4	2.0	0.6	58.1	0.962	0.13	-0.0102	-0.0092	-0.0010	10.9
	4.0		59.1	0.680		-0.0083	-0.0089	0.0006	-6.7
	6.0		59.4	0.555		-0.0079	-0.0083	0.0004	-4.8

TABLE 5.2.2.1-A (CONTD)

Ref.	A	λ	$\Delta_c/2$ (deg)	$\frac{l_f}{b}$	M	C_l/C_L Calc. (per deg)	C_l/C_L Test (per deg)	$\Delta \left(\frac{C_l}{C_L} \right)$ Calc.-Test (per deg)	% Percent Error	
5	4.0	0.6	0	0.833	0.50	-0.0018	-0.0016	-0.0002	12.5	
					0.80	-0.0018	-0.0020	0.0002	-10.0	
			43.2		0.93	-0.0018	-0.0020	0.0002	-10.0	
					0.50	-0.0056	-0.0053	-0.0003	5.7	
					0.80	-0.0059	-0.0057	-0.0002	3.5	
					0.93	-0.0061	-0.0060	-0.0001	1.7	
6	2.0	0	45.0	1.62	0.60	-0.0057	-0.0052	-0.0005	9.6	
					0.90	-0.0057	-0.0054	-0.0003	5.6	
7	4.0	0.6	-3.58	0.713	0.13	-0.00155	-0.0020	0.00045	-22.5	
						-0.0054	-0.0052	-0.0002	3.8	
8	4.0	0.6	0	0.897	0.60	-0.0018	-0.0014	-0.0004	28.6	
					0.93	-0.0018	-0.00188	0.00008	-4.3	
			30.0	1.05	0.60	-0.0043	-0.0039	-0.0004	10.3	
					0.93	-0.0045	-0.0042	-0.0003	7.1	
			59.1	1.38	0.60	-0.0069	-0.0074	0.0005	-6.8	
					0.93	-0.0072	-0.0078	0.0006	-7.7	
9	4.0	0.3	40.9	1.19	0.60	-0.00457	-0.00344	-0.00113	32.8	
10	4.0	0.3	40.9	1.19	0.80	-0.00467	-0.00506	0.00039	-7.7	
11	4.0	0.6	43.15	0.873	0.13	-0.00555	-0.00508	-0.00047	9.3	
12	4.0	0	26.6	1.08	0.40	-0.0024	-0.0029	0.00050	-17.2	
13	2.31	0	40.9	1.53	0.40	-0.0049	-0.0049	0	0	
14	2.0	0.6	41.2	1.38	0.60	-0.0076	-0.0079	0.0003	-3.8	
					0.93	-0.0076	-0.0080	0.0004	-5.0	
			6.0	0.6	43.8	1.02	0.60	-0.0046	-0.00504	
						0.93	-0.0052	-0.0064	0.00044	-8.7
						0.93	-0.0064	0.0012	-18.8	
15	4.0	0.3	40.9	1.157	0.40	-0.0044	-0.0047	0.0003	-6.4	
					0.80	-0.0047	-0.0052	0.0005	-9.6	
					0.95	-0.0048	-0.0046	-0.0002	4.3	
					0.95	-0.0067	-0.0068	0.0001	-1.5	
					0.95	-0.0067	-0.0068	0.0001	-1.5	
$\text{Average Error} = \frac{\sum e }{n} = 8.9\%$										

TABLE 5.2.2.1-B
 EFFECT OF DIHEDRAL ON SUBSONIC ROLLING
 MOMENT DUE TO SIDESLIP
 $\alpha = 0$

DATA SUMMARY

Ref.	A	λ	$\Delta c/2$ (deg)	$\frac{d}{b}$	Γ (deg)	M	$(\Delta C_{I_\beta})_\Gamma$ Calc. (per deg)	$(\Delta C_{I_\beta})_\Gamma$ Test (per deg)	$\Delta [(\Delta C_{I_\beta})_\Gamma]$ Calc.-Test (per deg)	e Percent Error
5	4.0	0.6	0	0.139	5.0 - 5.0 10.0 - 10.0 10.0 - 10.0 10.0 - 10.0 5.0 - 5.0 10.0 - 10.0 10.0 - 10.0 10.0 - 10.0	0.13 0.0095 0.0019 0.0019 -0.0020 0.0020 -0.0021 0.0021 -0.00086 0.00086 -0.00173 0.00173 -0.0018 0.0018 -0.0019 0.0019	-0.00095 0.00095 -0.0019 0.0019 -0.0020 0.0020 -0.0021 0.0021 -0.00086 0.00086 -0.00173 0.00173 -0.0018 0.0018 -0.0019 0.0019	-0.00117 0.00104 -0.0022 0.0022 -0.0025 0.0023 -0.0028 0.0026 -0.00087 0.00087 -0.00195 0.00187 -0.00214 0.0019 -0.00236 0.00204	0.00022 -0.00009 0.0003 -0.0003 0.0006 -0.0003 0.0007 -0.0005 0.00011 -0.00011 0.00022 -0.00014 0.00034 -0.0001 0.00046 -0.00014	-18.8 - 8.7 -13.6 -13.6 -20.0 -13.0 -25.0 -19.2 -11.3 -11.3 -11.3 -11.3 -15.9 - 5.3 -19.1 - 6.9 - 4.3
16	6.38	1.0	0	0.112	5.0 - 5.0 10.0 - 10.0 10.0 - 10.0	0.106 0.0012 -0.0015 -0.00005	-0.0012 0.0019 -0.00204 -0.00014			
$\text{Average Error} = \frac{\sum e }{n} = 13.2\%$										

TABLE 5.2.2.1-C

EFFECT OF WING HEIGHT ON SUBSONIC
ROLLING MOMENT DUE TO SIDESLIP
 $\alpha = 0$

DATA SUMMARY

Ref.	A	λ	$\Lambda_{c/2}$ (deg)	$\frac{d}{b}$	$\frac{z_w}{b}$	M	$(\Delta C_l)_\beta z_w$ Calc. (per deg)	$(\Delta C_l)_\beta z_w$ Test (per deg)	$\Delta [(\Delta C_l)_\beta z_w]$ Calc.-Test (per deg)	e Percent Error
17	3.0	0	33.6	0.144	-0.0501	0.25	-0.00052	-0.0005	-0.00002	4.0
						0.80	-0.00052	-0.0006	0.00008	-13.3
						0.90	-0.00052	-0.00066	0.00014	-21.2
18	2.31	0	56.6	0.115	-0.0411	0.17	-0.0003	-0.00035	0.00005	-14.3
				0.229	-0.0822		-0.0012	-0.0011	-0.0001	9.1
					0.0822		0.0012	0.00095	0.00025	26.3
				0.153	-0.0548		-0.00053	-0.00045	-0.00008	17.8
					0.0548		0.00053	0.00065	-0.00012	-18.5
16	6.10	0.333	0	0.112*	-0.0559	0.105	-0.000645	-0.00070	0.000055	-7.9
					0.0622		0.00072	0.00073	-0.00001	-1.4
	6.38	1.0		0.112*	-0.0628		-0.00074	-0.00108	0.00034	-31.5
					0.0664		0.00078	0.00070	0.00008	11.4
				0.112	-0.0443		-0.000547	-0.00053	-0.000017	3.2
					0.0496		0.00059	0.00064	-0.00005	-7.8
	6.10	0.333			-0.0375		-0.00044	-0.00062	0.00018	-29.0
					0.0447		0.00052	0.00055	-0.00003	-5.5
					-0.0382		-0.00044	-0.00055	0.00011	-20.0
					0.0443		0.00051	0.00040	0.00011	27.5

*Elliptical cross section, $d = d_{equiv}$

$$\text{Average Error} = \frac{\sum |e|}{n} = 15.0\%$$

TABLE 5.2.2.1-O
SUPersonic WING-BODY ROLLING MOMENT DUE TO SIDESLIP

Midwing Configurations
No Dihedral

DATA SUMMARY

Ref.	A	λ	Δ_{LE} (deg)	M	* C_I/\bar{C}_L Calc. (per deg)	C_I/\bar{C}_L Test (per deg)	$\Delta(C_I/\bar{C}_L)$ Calc.-Test (per deg)	e Percent Error
19	4.0	0.2	49.4	2.01	-0.00161	-0.0019	0.00029	-15.3
20	3.0	0.25	30.97	1.41	-0.00231	-0.0023	-0.00001	0.4
↓	↓	↓	↓	2.01	-0.0017	-0.0019	0.0002	-10.5
16	4.0	0	45.0	1.40	-0.00246	—	—	—
↓	2.0	0	63.43	↓	-0.00524	-0.00530	0.00006	-1.1
↓	↓	↓	↓	1.70	-0.00394	-0.0040	0.00006	-1.5
21	3.0	0.2	50.71	1.62	-0.0030	-0.0030	0	0
↓	↓	↓	↓	2.62	-0.0022	—	—	—
↓	4.0	0.2	49.4	1.62	-0.0024	—	—	—
↓	↓	↓	↓	2.62	-0.0017	—	—	—
↓	3.0	0.2	62.9	1.62	-0.00495	—	—	—
↓	↓	↓	↓	2.62	-0.00270	-0.00207	-0.00063	30.4
22	3.0	0.25	31.0	2.50	-0.00179	-0.0012	-0.00059	49.2
↓	↓	↓	↓	2.86	-0.0017	-0.00122	-0.00048	39.3
↓	↓	↓	↓	3.96	-0.00164	-0.0014	-0.00024	17.1
↓	1.313	0.15	73.0	4.83	-0.00163	-0.00144	-0.00019	13.2
↓	↓	↓	↓	2.16	-0.00883	-0.00831	-0.00052	6.3
↓	↓	↓	↓	2.50	-0.00709	-0.00690	-0.00019	2.8
↓	↓	↓	↓	2.86	-0.00676	-0.00662	-0.00014	2.5
↓	↓	↓	↓	2.86	-0.00494	-0.00464	-0.00030	6.5

* Test values of $C_{N\alpha}$ were used in calculating C_I/\bar{C}_L .

$$\text{Average Error} = \frac{\sum |e|}{n} = 12.7\%$$

TABLE 5.2.2.1-E
EFFECT OF DIHEDRAL ON SUPERSONIC ROLLING
MOMENT DUE TO SIDESLIP

Midwing Configurations
 $\alpha = 0$

DATA SUMMARY

Ref.	A	λ	Δ_{LE} (deg)	$\frac{d}{b}$	Γ (deg)	M	$(\Delta C I_\beta)_\Gamma$ Calc. (per deg)	$(\Delta C I_\beta)_\Gamma$ Test (per deg)	$\Delta [(\Delta C I_\beta)_\Gamma]$ Calc.-Test (per deg)	ϵ Percent Error
19	4.0	0.2	49.4	0.139	3.0 - 3.0	2.01 1	-0.00045 0.00045	-0.00046 0.00046	0.00001 -0.00001	- 2.2 - 2.2
21	3.0	0.2	50.71	0.160	- 5.0 - 10.0 - 5.0 - 10.0	1.62 2.62 1.62 2.62	0.00086 0.00173 0.00059 0.00119	0.00091 0.0015 0.0006 0.00116	-0.00005 0.00023 -0.00001 0.00003	- 5.5 15.3 - 1.7 2.6
	4.0	0.2	49.4	0.139	- 5.0 - 10.0 - 5.0 - 10.0	1.62 2.62 1.62 2.62	0.00092 0.00185 0.00060 0.00120	0.0009 0.0016 0.00055 0.00105	0.00002 0.00025 0.00005 0.00015	2.2 15.6 9.1 14.3
	3.0	0.2	62.9	0.160	- 5.0 - 10.0 - 5.0 - 10.0	1.62 2.62 1.62 2.62	0.00071 0.00143 0.00061 0.00123	0.00085 0.0018 0.0006 0.0011	-0.00014 -0.00037 0.00001 0.00013	-16.5 -20.6 1.7 11.8
22	3.0	0.25	31.0	0.146	3.0 3.0 3.0 - 3.0	2.50 2.86 4.63 1.80	-0.00035 -0.000327 -0.00018 -0.00027	-0.00041 -0.00036 -0.00019 -0.00025	0.00006 0.000033 0.00001 -0.00002	-14.6 - 9.2 - 5.3 8.0
	1.313	0.15	73.0	0.233	3.0 3.0 3.0 - 3.0	2.16 2.50 2.86 1	-0.000282 -0.000273 -0.00024 0.00021	-0.00026 -0.00022 -0.00019 0.00024	-0.000022 -0.000018 -0.00006 -0.00003	8.5 24.1 - 6.0 -12.5

$$\text{Average Error} = \frac{\sum |\epsilon|}{n} = 10.5\%$$

TABLE 5.2.2.1-F
EFFECT OF WING HEIGHT ON SUPERSONIC ROLLING
MOMENT DUE TO SIDESLIP

$\alpha = 0$

DATA SUMMARY

Ref.	A	λ	Δ_{LE} (deg)	$\frac{d}{b}$	$\frac{z_w}{b}$	M	$(\Delta C_I)_\beta z_w$ Calc. (per deg)	$(\Delta C_I)_\beta z_w$ Test (per deg)
19	4.0	0.2	49.4	0.139	-0.588 0.588 -0.588 0.588	2.01 1.41 2.01 1.41	-0.00068 0.00068 -0.00069 0.00069	-0.00103 0.00103 -0.00110 0.00120
20	3.0	0.26	30.97	0.139	-0.588 0.588 -0.588 0.588	2.01 1.41 2.01 1.41	-0.00069 0.00069 -0.00069 0.00069	-0.00085 0.00080

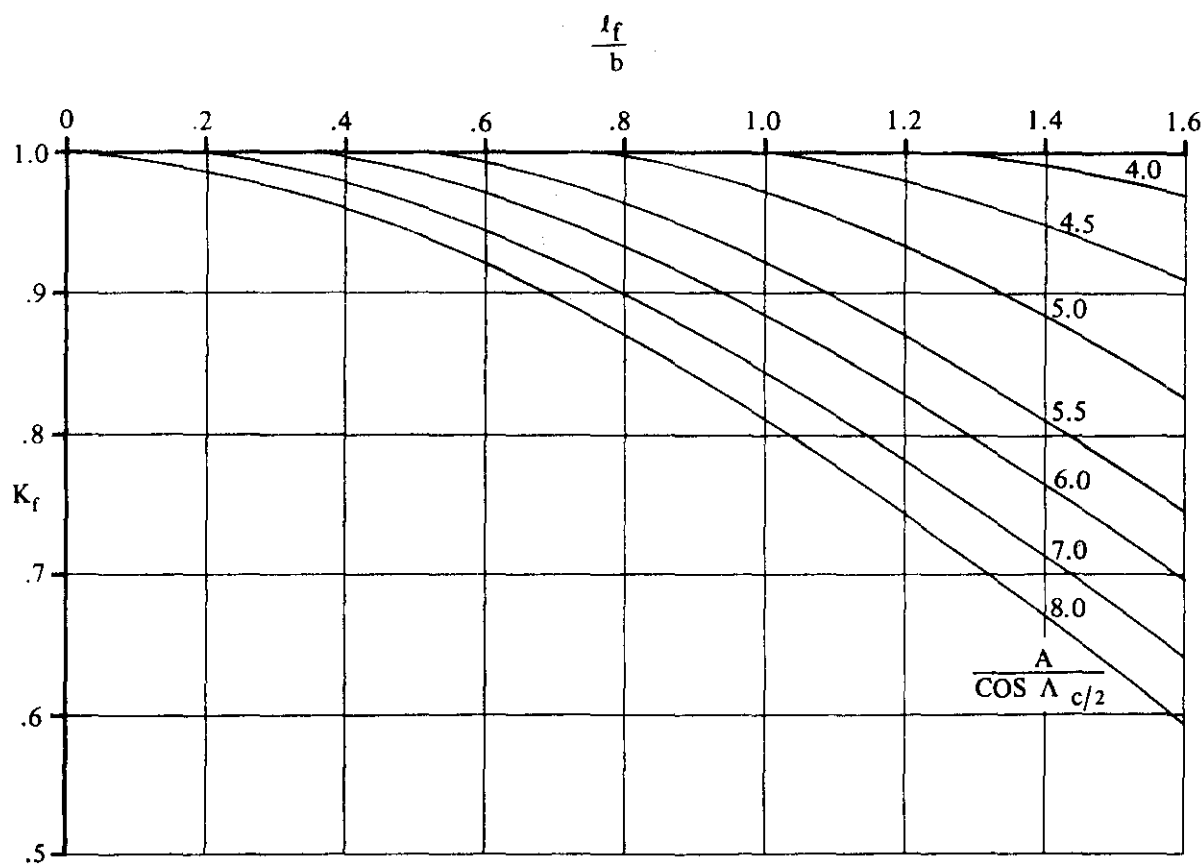
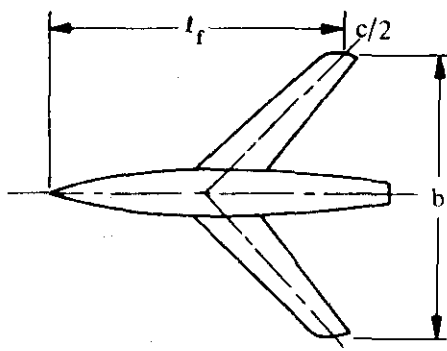


FIGURE 5.2.2.1-26 FUSELAGE CORRECTION FACTOR

5.2.3 WING-BODY SIDESLIP DERIVATIVE C_{n_B}

5.2.3.1 WING-BODY SIDESLIP DERIVATIVE C_{n_B} IN THE LINEAR ANGLE-OF-ATTACK RANGE

The wing-body yawing moment due to sideslip can be considered as the sum of the yawing moments of the body, the wing, and the wing-body interference. The wing contribution is important only at large incidences and is deleted from the solution of wing-body yawing moment due to sideslip. The method provided herein gives the total wing-body sideslip derivative C_{n_B} as the sum of the body and wing-body interference contributions.

The unstable directional stability contribution of the fuselage is dominant in this analysis, and since slender-body theory predicts the body contribution to be essentially independent of Mach number, the method presented is considered to be valid for all speeds.

Experimental investigations have shown that the wing-body interference contribution to the yawing-moment derivative is essentially independent of sweep, taper ratio, and Mach number. Furthermore, the evidence of references 1, 2, and 3 is that the effect of wing vertical position on wing-body yawing moment is small.

The maximum angle of applicability is limited to the linear-lift region. Above this angle-of-attack limitation, separation occurs and both the wing and wing-fuselage interference have an appreciable effect on the wing-body sideslip derivative C_{n_B} as a result of the changes in the magnitude and orientation of the resultant force on the two wing semispans.

DATCOM METHOD

All Speeds

The total wing-body sideslip derivative C_{n_B} , based on the product of total wing area and wing span S_B , and referred to an arbitrary moment center, is given by

$$(C_{n_B})_{WB} = -K_N K_{R_f} \frac{S_{B_S}}{S_W} \frac{l_B}{b} \quad (\text{per degree}) \quad 5.2.3.1-3$$

where

K_N is an empirical factor related to the sideslip derivative for body plus wing-body interference, obtained from figure 5.2.3.1-8 as a function of the body geometry.

K_{R_f} is an empirical Reynolds-number factor obtained from figure 5.2.3.1-9 as a function of the fuselage Reynolds number.

S_{B_S} is the projected side area of the body.

l_B is the length of the body.

A comparison of results calculated by using this method with test data is presented as table 5.2.3.1-A.

It should be noted that the upper limit of the fuselage Reynolds number of the test data is 49.2 million. For configurations at higher full-scale Reynolds numbers the method is expected to give results that are satisfactory for preliminary design.

Sample Problem

- Given: The wing-body configuration of reference 12.

Body Characteristics:

$$l_B = 4.1 \text{ ft} \quad S_{B_S} = 1.35 \text{ sq ft} \quad x_m = 2.5 \text{ ft} \quad h = 0.416 \text{ ft}$$

$$w = 0.416 \text{ ft} \quad h_1 = 0.315 \text{ ft} \quad h_2 = 0.388 \text{ ft}$$

Wing Characteristics:

$$S_W = 2.25 \text{ sq ft} \quad b = 3.0 \text{ ft}$$

Additional Characteristics:

$$M = 0.91 \quad R_f = 3.87 \times 10^6 \text{ per ft}$$

Compute:

$$\frac{x_m}{l_B} = \frac{2.5}{4.1} = 0.610$$

$$\frac{l_B^2}{S_{B_S}} = \frac{(4.1)^2}{1.35} = 12.45$$

$$\sqrt{\frac{h_1}{h_2}} = \sqrt{\frac{0.315}{0.388}} = 0.902$$

$$\frac{h}{w} = \frac{0.416}{0.416} = 1.00$$

$$K_N = 0.00105 \text{ per deg} \quad (\text{figure 5.2.3.1-8})$$

$$R_I_{\text{fuselage}} = (3.87 \times 10^6) l_B = (3.87 \times 10^6)(4.1) = 15.87 \times 10^6$$

$$K_{R_I} = 1.567 \quad (\text{figure 5.2.3.1-9})$$

Solution:

$$(C_{n_\beta})_{WB} = -K_N K_{R_I} \frac{S_{B_S}}{S_W} \frac{l_B}{b} \quad (\text{equation 5.3.2.1-a})$$

$$= -(0.00105)(1.567) \frac{1.35}{2.25} \frac{4.1}{3.0}$$

$$= -0.00135 \text{ per deg} \quad (\text{based on } S_W b)$$

This compares with a test value of -0.00130 per degree from reference 12.

REFERENCES

1. Goodman, A., and Thomas, D. F., Jr.: Effects of Wing Position and Fuselage Size on the Low-Speed Static and Rolling Stability Characteristics of a Delta-Wing Model. NACA TR 1224, 1955. (U)
2. Goodman, A.: Effects of Wing Position and Horizontal-Tail Position on the Static Stability Characteristics of Models With Unswept and 45° Sweptback Surfaces With Some Reference to Mutual Interference. NACA TN 2504, 1951. (U)
3. Spearman, M. L., Driver, C., and Hughes, W. C.: Investigation of Aerodynamic Characteristics in Pitch and Sideslip of a 45° Sweptback-Wing Airplane Model With Various Vertical Locations of Wing and Horizontal Tail. Basic-Data Presentation, M = 2.01. NACA RM L54L06, 1955. (U)
4. Jaquet, B. M., and Brewer, J. D.: Effects of Various Outboard and Central Fins on Low-Speed Static-Stability and Rolling Characteristics of a Triangular-Wing Model. NACA RM L9E18, 1949. (U)
5. Queijo, M. J., and Wolhart, W. D.: Experimental Investigation of the Effect of Vertical-Tail Size and Length and of Fuselage Shape and Length on the Static Lateral Stability Characteristics of a Model with 45° Sweptback Wing and Tail Surfaces. NACA TR 1049, 1951. (U)
6. Brewer, J. D., and Lichtenstein, J. H.: Effect of Horizontal Tail on Low-Speed Static Lateral Stability Characteristics of a Model Having 45° Sweptback Wing and Tail Surfaces. NACA TN 2010, 1950. (U)
7. Letko, W., and Williams, J. L.: Experimental Investigation at Low Speed of Effects of Fuselage Cross Section on Static Longitudinal and Lateral Stability Characteristics of Models Having 0° and 45° Sweptback Surfaces. NACA TN 3651, 1955. (U)
8. Graham, D., and Koenig, D. G.: Tests in the Ames 40- by 80-Foot Wind Tunnel of an Airplane Configuration With an Aspect Ratio 2 Triangular Wing and an All-Movable Horizontal Tail - Lateral Characteristics. NACA RM A51L03, 1952. (U)
9. Bird, J. D., Lichtenstein, J. H., and Jaquet, B. M.: Investigation of the Influence of Fuselage and Tail Surfaces on Low-Speed Static Stability and Rolling Characteristics of a Swept-Wing Model. NACA TN 2741, 1952. (U)

10. Fournier, P. G.: Low-Speed Static Stability Characteristics of a Complete Model With an M-Wing in Mid and High Positions and With Three Horizontal-Tail Heights. NACA RM L55J06, 1956. (U)
11. Anon. Unpublished preliminary wind-tunnel tests of the Model DC-10. McDonnell Douglas Company, 1968. (U)
12. Merritt, F. D., Roensch, R. L., and Weiner, A. H.: Results of a DC-8-AWACS Test in the Galcit 10-Foot Low-Speed Wind Tunnel. McDonnell Douglas Company Report DAC 67253, 1967. (U)
13. Savage, H. F., and Tinling, B. E.: The Subsonic Static Aerodynamic Characteristics of an Airplane Model Having a Triangular Wing of Aspect Ratio 3. II – Lateral and Directional Characteristics. NACA TN 4042, 1957. (U)
14. Wiggins, J. W., Kuhn, R. E., and Fournier, P. G.: Wind-Tunnel Investigation to Determine the Horizontal- and Vertical-Tail Contributions to the Static Lateral Stability Characteristics of a Complete-Model Swept-Wing Configuration at High Subsonic Speeds. NACA TN 3818, 1956. (U)
15. Kuhn, R. E., and Draper, J. W.: Wind-Tunnel Investigation of the Effects of Geometric Dihedral on the Aerodynamic Characteristics in Pitch and Sideslip of an Unswept- and a 45° Sweptback-Wing-Fuselage Combination at High Subsonic Speeds. NACA RM L53F09, 1953. (U)
16. Christensen, F. B.: An Experimental Investigation of Four Triangular-Wing-Body Combinations in Sideslip at Mach Numbers 0.6, 0.9, 1.4, and 1.7. NACA RM A53L22, 1954. (U)
17. Steeman, W. C., Jr.: An Experimental Study at High Subsonic Speeds of Several Tail Configurations on a Model Having a 45° Sweptback Wing. NACA RM L57C08, 1957. (U)
18. Goodson, K. W., and Becht, R. E.: Wind-Tunnel Investigation at High Subsonic Speeds of the Stability Characteristics of a Complete Model Having Sweptback, M-, W-, and Cranked-Wing Plan Forms and Several Horizontal-Tail Locations. NACA RM L54C29, 1954. (U)
19. Spearman, M. L., and Robinson, R. B.: Static Lateral Stability and Control Characteristics of a Model of a 45° Swept-Wing Fighter Airplane With Various Vertical Tails at Mach Numbers of 1.41, 1.61, and 2.01. NACA RM L56D05, 1956. (U)
20. Spearman, M. L., and Robinson, R. B.: Investigation of the Aerodynamic Characteristics in Pitch and Sideslip of a 45° Swept-Wing Airplane Configuration With Various Vertical Locations of the Wing and Horizontal Tail. Static Lateral and Directional Stability; Mach Numbers of 1.41 and 2.01. NACA RM L57J25a, 1957. (U)
21. Spearman, M. L.: Static Lateral and Directional Stability and Effective Sidewash Characteristics of a Model of a 35° Swept-Wing Airplane at a Mach Number of 1.61. NACA RM L56E23, 1956. (U)
22. Boatright, W. B.: Experimental Investigation of Effects of Wing Plan Form and Dihedral Angle on Sideslip Derivatives of Sweptback-Wing-Body Combinations at Supersonic Speeds. NACA RM L58E08, 1958. (U)
23. Robinson, R. B.: Effects of Canopy, Revised Vertical Tail, and a Yaw-Damper Vane on the Aerodynamic Characteristics of a 1/16-Scale Model of the Douglas D-558-II Research Airplane at a Mach Number of 2.01. NACA RM L54F25, 1954. (U)
24. Spearman, M. L., Robinson, R. B., and Driver, C.: The Effects of the Addition of Small Fuselage-Mounted Fins on the Static Directional Stability Characteristics of a Model of a 45° Swept-Wing Airplane at Angles of Attack up to 15.3° at a Mach Number of 2.01. NACA RM L56D16a, 1956. (U)
25. Spearman, M. L.: Investigation of the Aerodynamic Characteristics in Pitch and Sideslip of a 45° Sweptback-Wing Airplane Model With Various Vertical Locations of the Wing and Horizontal Tail. Effect of Wing Location and Geometric Dihedral for the Wing-Body Combination, $M = 2.01$. NACA RM L55B18, 1955. (U)
26. Hamilton, C. V.: Aerodynamic Characteristics at Supersonic Speeds of a Series of Wing-Body Combinations Having Cambered Wings With an Aspect Ratio of 3.5 and a Taper Ratio of 0.2. Effects of Sweep Angle and Thickness Ratio on the Static Lateral Stability Characteristics at $M = 2.01$. NACA RM L52E23, 1952. (U)
27. Jaquet, B. M., and Fournier, R. H.: Effects of Wing Sweep, Horizontal-Tail Configuration, and a Ventral Fin on Static Stability Characteristics of a Model With a Wing of Aspect Ratio 3 at Mach Numbers From 2.29 to 4.65. NACA RM L58E06, 1958. (U)

TABLE 5.2.3.1-A
WING-BODY YAWING MOMENT DUE TO SIDESLIP
DATA SUMMARY – ALL SPEEDS

Ref	M	$R_f \times 10^{-6}$	x_m (ft)	l_B (ft)	S_{BS} (sq ft)	$\sqrt{\frac{h_1}{h_2}}$	$\frac{h}{w}$	K_N (per deg)	$S_w b$ (cu ft)	K_{R_f}	$(C_{n\beta})_{WB}$ Calc. (per deg)	$(C_{n\beta})_{WB}$ Test (per deg)	Percent Error
4	0.13	3.69	1.93	4.0	1.76	1.008	1.0	0.0012	12.18	1.27	-0.00088	-0.00090	- 2.2
						1.77	1.01			1.27	-0.00090	-0.00090	0
5	0.13	2.32	1.26	2.5	0.833	1.0	1.0	0.00155	6.75	1.172	-0.00056	-0.00053	5.7
		3.10	1.67	3.34	1.11			0.00145		1.232	-0.00099	-0.00090	10.0
		4.64	2.5	5.0	1.67			0.00080		1.316	-0.00130	-0.00170	-23.5
		3.10	1.67	3.34	1.30	1.147		0.0016		1.232	-0.00127	-0.00140	- 9.3
					1.25	0.93		0.00113		1.232	-0.0010	-0.0010	0
6	0.13	3.09	1.67	3.33	1.117	1.0	1.0	0.00120	6.75	1.232	-0.00081	-0.00090	-10.0
7	0.13	3.48	2.00	3.75	1.43	1.02	1.0	0.00130	6.75	1.257	-0.00129	-0.00133	- 3.0
			2.12					0.00138		1.257	-0.00138	-0.00150	- 8.0
			2.00		1.29			0.00115		1.257	-0.00104	-0.00150	-30.7
			2.12					0.00130		1.257	-0.00117	-0.00145	-19.3
			2.00		1.736		2.213	0.00190		1.257	-0.00230	-0.00260	-11.5
			2.12					0.00210		1.257	-0.00255	-0.00270	- 5.6
8	0.13	49.2	23.91	56.16	181.33	1.0	1.0	0.00045	7812.5	1.80	-0.00106	-0.00120	-11.7
1	0.17	5.27	2.25	4.5	1.29	1.02	1.0	0.00095	12.18	1.343	-0.00060	-0.00060	0
					1.76			0.00110		1.343	-0.00085	-0.00095	0
					2.57			0.00140		1.343	-0.00179	-0.00200	-10.5
2	0.17	3.96	1.67	3.45	1.25	0.96	1.0	0.00105	6.75	1.283	-0.00086	-0.00090	- 4.4
9	0.17	5.35	2.25	4.5	1.63	1.0	1.0	0.00100	10.94	1.345	-0.00090	-0.00100	-10.0
10	0.17	9.20	3.97	7.39	3.75	0.946	1.0	0.00073	36.00	1.456	-0.00082	-0.00100	-18.0
11	0.20	10.8	72.0	152.9	1730.0	1.05	1.10	0.00085	434.337	1.49	-0.00071	-0.00085	- 9.4
12	0.20	21.2	83.08	163.0	2800.0	1.03	1.0	0.00137	547.866	1.625	-0.00185	-0.00190	- 2.6
			32.0							1.71	-0.00195	-0.00170	14.7
			46.0							1.79	-0.00204	-0.00187	9.1
13	0.25	9.74	3.30	6.0	2.44	0.86	1.0	0.00092	13.85	1.468	-0.00142	-0.00120	18.3
				5.42	2.17	0.83		0.00090		1.447	-0.00110	-0.00100	10.0
14	0.40	9.66	2.5	4.1	1.36	0.89	1.0	0.00105	6.75	1.464	-0.00126	-0.00130	- 3.1

TABLE 5.2.3.1-A (CONT'D)

Ref	M	$R_f \text{ fus} \times 10^{-6}$	x_m (ft)	l_B (ft)	$S_{B,S}$ (sq ft)	$\sqrt{\frac{h_1}{h_2}}$	$\frac{h}{w}$	K_N (per deg)	$S_w b$ (cu ft)	K_{R_f}	$(C_{n\beta})_{WB}$ Calc. (per deg)	$(C_{n\beta})_{WB}$ Test (per deg)	% Percent Error
15	0.50	11.4	2.5	4.1	1.35	0.89	1.0	0.00105	6.75	1.488	-0.00129	-0.00130	- 0.8
	0.70	14.42						0.00105		1.548	-0.00133	-0.00130	2.3
	0.80	15.38						0.00105		1.558	-0.00134	-0.00130	3.1
	0.91	15.87						0.00105		1.567	-0.00135	-0.00130	3.8
	0.93	16.92	↓	↓	↓	↓	↓	0.00105	↓	1.567	-0.00135	-0.00130	3.8
16	0.60	8.0	3.18	5.04	2.03	0.85	1.0	0.00110	11.36	1.427	-0.00140	-0.00130	7.7
	0.90	10.6	↓	↓	↓	↓	↓	0.00110	↓	1.483	-0.00147	-0.00135	8.9
17	0.60	5.11	0.87	1.52	0.189	0.95	1.0	0.00110	0.25	1.336	-0.00168	-0.00110	52.7
	0.94	6.38						0.00110		1.380	-0.00174	-0.00160	8.7
	0.60	5.11			0.181			0.00098		1.336	-0.00144	-0.00150	- 4.0
	0.94	6.38	↓	↓	↓	↓	↓	0.0009	↓	1.380	-0.00149	-0.00180	-17.2
18	0.80	13.86	2.60	4.56	1.64	0.98	1.0	0.00110	6.76	1.537	-0.00188	-0.00170	10.6
	0.92	16.63	↓	↓	↓	↓	↓	0.00110	↓	1.576	-0.00192	-0.00180	6.7
16	1.4	7.61	2.265	3.78	1.07	0.87	1.0	0.00095	5.69	1.417	-0.00096	-0.00097	- 1.0
	1.4	16.50	3.18	5.04	2.03	0.85	1.0	0.00110	11.36	1.573	-0.00156	-0.00130	20.0
	1.7	20.00	↓	↓	↓	↓	↓	0.00110	↓	1.62	-0.00160	-0.00140	14.3
20	1.41	9.12	1.56	3.05	0.74	0.98	1.0	0.001	2.67	1.462	-0.00123	-0.00115	6.9
	2.01	7.52	↓	↓	↓	↓	↓	0.001	↓	1.413	-0.00120	-0.00094	27.7
19	1.41	6.04	2.08	3.37	1.118	0.98	1.08	0.0015	6.10	1.37	-0.00152	-0.00150	1.3
	1.61	5.76						0.0015		1.36	-0.00151	-0.00165	- 8.5
	2.01	5.00	↓	↓	↓	↓	↓	0.0015	↓	1.331	-0.00148	-0.00160	- 7.5
20	1.41	9.11	1.73	3.04	0.738	0.97	1.0	0.00115	2.0	1.462	-0.00189	-0.00150	26.0
	2.01	8.79	↓	↓	↓	↓	↓	0.00115	↓	1.447	-0.00188	-0.00170	10.6
21	1.61	7.64	1.59	2.69	0.820	1.04	1.0	0.00170	2.35	1.416	-0.00227	-0.00253	-10.3
22	1.62	2.69	0.39	0.625	0.032	0.97	1.0	0.00122	0.023	1.204	-0.00130	-0.00095	36.8
	2.62	3.015						0.00122	0.020	1.228	-0.00152	-0.00145	4.8
			↓	↓	↓	↓	↓	0.00122	↓	1.228	-0.00152	-0.00152	0
			↓	↓	↓	↓	↓	0.00122	0.023	1.228	-0.00132	-0.00127	3.9
3	2.01	9.747	1.734	3.04	0.717	0.95	1.0	0.00106	2.0	1.468	-0.00170	-0.00170	0
23	2.01	8.42	1.357	2.625	0.65	1.07	1.0	0.00130	1.07	1.437	-0.00297	-0.00345	-13.9
24	2.01	3.38	1.50	2.74	0.71	1.06	1.34	0.00150	1.26	1.25	-0.00298	-0.00296	2.4
25	2.01	9.75	1.73	3.04	0.736	0.98	1.0	0.00115	2.0	1.468	-0.00189	-0.00175	8.0

TABLE 5.2.3.1-A (CONTD)

Ref	M	$R_f \text{ fus} \times 10^{-6}$	x_m (ft)	I_B (ft)	S_{BS} (sq ft)	$\sqrt{\frac{h_1}{h_2}}$	$\frac{h}{w}$	K_N (per deg)	$S_w b$ (cu ft)	K_{R_f}	$(C_{n_p})_{WB}$ Calc. (per deg)	$(C_{n_p})_{WB}$ Test (per deg)	Percent Error	
26	2.01	7.02	1.385	2.00	0.358	0.99	1.0	0.00150	3.43	1.40	-0.00686	-0.00626	9.8	
27	2.29	10.6	1.958	3.43	0.962	0.965	1.0	0.00115	1.68	1.485	-0.00255	-0.00273	-6.6	
	2.98											-0.00280	-8.9	
	3.96											-0.00262	-2.7	
↓	4.65	↓	↓	↓	↓	↓	↓	↓	↓	↓	↓	↓	-0.00275	-7.3

$\text{Average Error} = \frac{\sum e }{n} = 9.7\%$

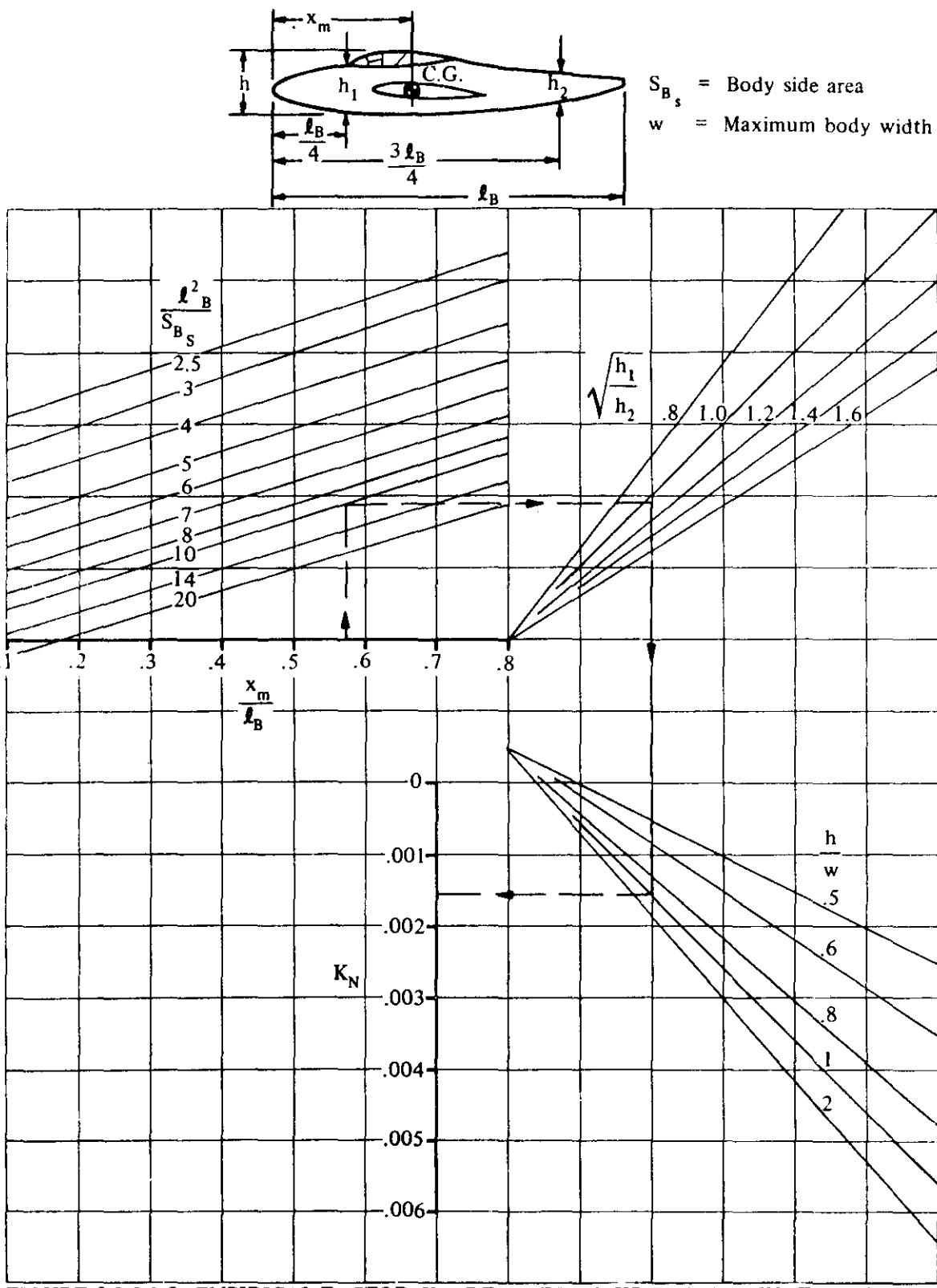


FIGURE 5.2.3.1-8 EMPIRICAL FACTOR K_N RELATED TO SIDESLIP DERIVATIVE $C_{n\beta}$ FOR BODY + WING-BODY INTERFERENCE

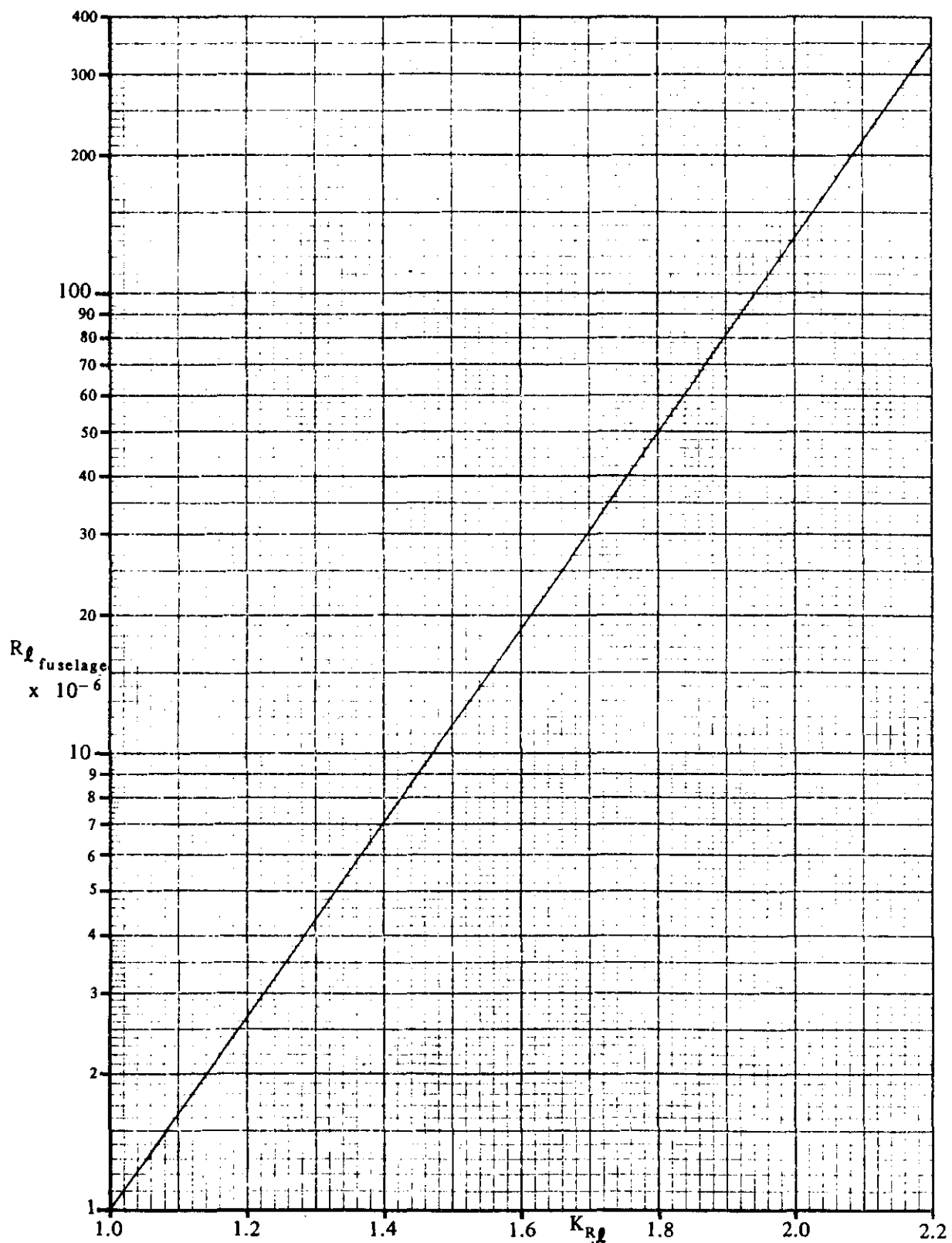


FIGURE 5.2.3.1-9 EFFECT OF FUSELAGE REYNOLDS NUMBER ON WING-BODY $C_{n\beta}$

5.2.3.2 WING-BODY YAWING-MOMENT COEFFICIENT C_n AT ANGLE OF ATTACK

The wing-body yawing moment developed at combined angles is nonlinear with respect to both sideslip and angle of attack because of viscous cross-flow effects and cross-coupling of upwash and sidewash velocities. To obtain the sideslip derivative $C_{n\beta_{WB}}$ it is recommended that $C_{n_{WB}}$ be calculated at several angles of attack for a small sideslip angle ($\beta \leq 4^\circ$). Then at each angle of attack the yawing moment is assumed linear with sideslip for small values of β so that

$$C_{n\beta_{WB}} \approx \frac{C_{n_{WB}}}{\beta}.$$

A. SUBSONIC

No method is presently available for determining the wing-body yawing moment at large angles of attack and subsonic speeds. The method presented herein is restricted to first-order approximations at relatively low angles of attack.

DATCOM METHOD

It is recommended that the method of Section 5.2.3.1 be used in the linear-lift angle-of-attack range.

B. TRANSONIC

No method is presently available for determining the wing-body yawing moment at large angles of attack and transonic speeds. The method presented herein is restricted to first-order approximations at relatively low angles of attack.

DATCOM METHOD

It is recommended that the method of Section 5.2.3.1 be used in the linear-lift angle-of-attack range.

C. SUPERSONIC

The method for estimating the wing-body yawing-moment coefficient $C_{n_{WB}}$ is based on the theory involved in estimating $C_{Y_{WB}}$ presented in Section 5.2.1.2. Therefore, the comments in that Section applying to the aerodynamics of wing-body interference also apply to this Section but are not repeated here.

To obtain the wing-body yawing-moment coefficient it is necessary to apply the appropriate moment arm to the side-force coefficient of Section 5.2.1.2. The center of pressure of the aerodynamic forces on the body at angle of attack establishes one moment arm. No simple method is available for estimating the body-alone center of pressure. The method suggested herein is necessarily tentative and will be updated as information becomes available. Of course, test values at the appropriate angle of attack are to be preferred. The position at which the wing-body interference side force acts on the body establishes a second moment arm. In the method that follows, this position is expressed as a function of the vertical location of the wing on the body and is based on the assumption that both the pressure and viscous force components of interference act at the same location.

The same limitations apply to the estimation of the yawing moments as to the estimation of the side force: although the wing leading edge should be supersonic, fair results are obtained for subsonic leading edges if the aspect ratio is not too low. Furthermore, correlation of experimental and estimated values of the wing-body interference moment indicates that the Datcom method is in actuality only warranted for cases in which the mid-point of the wing root chord is substantially displaced from the moment reference point.

DATCOM METHOD

The yawing-moment coefficient for wing-body combinations at supersonic speeds is given by the equation

$$C_{n_{WB}} = C_{n_B} + \left[\frac{x_m - \bar{l}_{WB}}{b_w} \right] C_{Y_{WB}} \quad 5.2.3.2-a$$

where

C_{n_B} is the body-alone contribution given by

$$C_{n_B} = \left[\frac{x_m}{l_B} - x_{c.p.} \right] \frac{l_B}{b_w} C_{Y_B} \quad 5.2.3.2-b$$

where

x_m is the distance from the body nose to the moment center

l_B is the body length

$x_{c.p.}$ is the distance from the body nose to the body center of pressure, measured in body lengths.

This parameter is approximated by $x_{c.p.} = \frac{C_m}{C_L}$

where C_m and C_L are obtained from paragraph C of Sections 4.2.2.2 and 4.2.1.2, respectively, at $\alpha = \alpha'$. The pitching-moment coefficient from Section 4.2.2.2 is referred to the body nose ($x_m = 0$).

b_w is the wing span

C_{Y_B} is the body-alone side-force coefficient obtained from Section 5.2.1.2

\bar{l}_{WB} is the distance from the body nose to the center of pressure of the wing-induced body side force

For midwing configurations

$$\bar{l}_{WB} = l_n + \frac{1}{2} c_r \quad 5.2.3.2-c$$

where

l_n is the distance from the body nose to the juncture of the wing leading edge and body

For tangent wing configurations

$$\bar{l}_{WB} = l_n + c_r \left[\frac{x_{l(a)}}{x_{l(a=0)}} \right] \left[\frac{x_{l(a=0)}}{c_r} \right] \quad 5.2.3.2-d$$

where

$x_{l(a)}$ is the distance to the center of pressure of the wing-induced body side force from the juncture of the wing leading edge and the body at the proper angle of attack

$x_{l(a=0)}$ is the distance to the center of pressure of the wing-induced body side force from the juncture of the wing leading edge and the body at zero angle of attack

$\frac{x_{l(a)}}{x_{l(a=0)}}$ is obtained from figure 5.2.3.2-6

$\frac{x_{l(a=0)}}{c_r}$ is obtained from figure 5.2.3.2-8

Values for the incremental coefficient resulting from the addition of wings in the mid and high- and low-tangent positions on circular bodies, calculated using the second term on the right-hand side of equation 5.2.3.2-a, are compared with experimental results in figure 5.2.3.2-5. This correlation is somewhat inconclusive in that for the conventional wing locations considered the centers of pressure of the wing-body interference side forces are close to the moment reference point. The resulting small yawing moments are likely no larger than the yawing moments of the wing alone which are neglected in the method. Furthermore, exact knowledge of the wing effects on the body cross-flow load distribution is precluded since the center of pressure of the body cross-flow loading is not accurately known.

Sample Problem

Given: Configuration of the sample problem, paragraph C, Section 5.2.1.2. This configuration is also tested in reference 1 of this Section. Some of the characteristics are repeated. Find the yawing-moment coefficient developed by the wing-body combination at $\alpha = 12^\circ$ and $\beta = 4^\circ$.

Characteristics

$$\begin{aligned} l_B &= 36.5 \text{ in.} & l_n &= 15.62 \text{ in.} & x_m &= 20.81 \text{ in.} & c_{r_e} &= 8.90 \text{ in.} & c_{r_e}/d &= 2.67 \\ b_w &= 24.0 \text{ in.} & x_{c.p.} &= 0.36 \text{ at } \alpha' = 12.65^\circ \text{ (test results)} & M &= 2.01 & \alpha' &= 12.65^\circ \end{aligned}$$

Compute:

Body-alone yawing-moment coefficient C_{Y_B}

$$C_{Y_B} = -0.0238 \text{ (based on } S_w \text{) (sample problem, paragraph C, Section 5.2.1.2)}$$

$$C_{n_B} = \left[\frac{x_m}{l_B} - x_{c.p.} \right] \frac{l_B}{b_w} C_{Y_B} \quad (\text{equation 5.2.3.2-b})$$

$$= (0.57 - 0.36) \frac{36.5}{24.0} (-0.0238)$$

$$= -0.0076 \text{ (based on } S_w b_w \text{)}$$

Wing interference yawing-moment coefficient

$$\frac{x_{l(\alpha)}}{x_{l(\alpha=0)}} = 0.77 \text{ (figure 5.2.3.2-6)}$$

$$\sqrt{M^2 - 1} \left[\frac{d}{c_{r_e}} \right] = \sqrt{(2.01)^2 - 1} \left[\frac{3.33}{8.90} \right] = 0.651$$

$$\frac{x_{l(\alpha=0)}}{c_{r_e}} = 0.90 \text{ (figure 5.2.3.2-8)}$$

$$\begin{aligned} \bar{l}_{w(B)} &= l_n + c_{r_e} \left[\frac{x_{l(\alpha)}}{x_{l(\alpha=0)}} \right] \left[\frac{x_{l(\alpha=0)}}{c_{r_e}} \right] & (\text{equation 5.2.3.2-d}) \\ &= 15.62 + 8.90 (0.77) (0.90) \\ &= 21.78 \end{aligned}$$

$$C_{Y_{w(B)}} = -0.0162 \text{ (based on } S_w \text{) (sample problem, paragraph C, Section 5.2.1.2)}$$

Solution:

$$C_{nWB} = C_{nB} + \left[\frac{x_m - \bar{x}_{W(B)}}{b_w} \right] C_{Y_{W(B)}} \quad (\text{equation 5.2.3.2-a})$$

$$= -0.0076 + \frac{20.81 - 21.78}{24.0} (-0.0162)$$

$$= -0.00695 \text{ (based on } S_{wbw})$$

This compares with an experimental value (based on S_{wbw}) of $C_{nWB} = -0.0070$ from reference 1.

A comparison between calculated and experimental results for this configuration at sideslip angles of 2, 4, and 8 degrees and over an angle-of-attack range to 16 degrees is presented in figure 5.2.3.2-4.

REFERENCES

1. Spearman, M. L., Driver, C., and Hughes, W. C.: Investigation of Aerodynamic Characteristics in Pitch and Sideslip of a 45° Sweptback-Wing Airplane Model with Various Vertical Locations of Wing and Horizontal Tail - Basic-Data Presentation, $M = 2.01$. NACA RM L54L06, 1955. (U)
2. Keastari, G. E.: Estimation of Directional Stability Derivatives at Moderate Angles and Supersonic Speeds. NASA Memo 12-1-58A, 1959. (U)

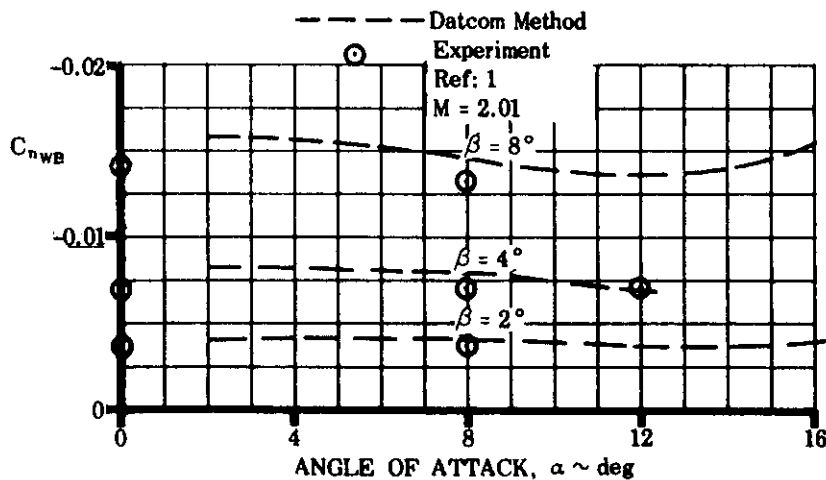


FIGURE 5.2.3.2-4 COMPARISON OF EXPERIMENTAL AND CALCULATED VALUES OF WING-BODY YAWING-MOMENT COEFFICIENT FOR THE SAMPLE PROBLEM CONFIGURATION

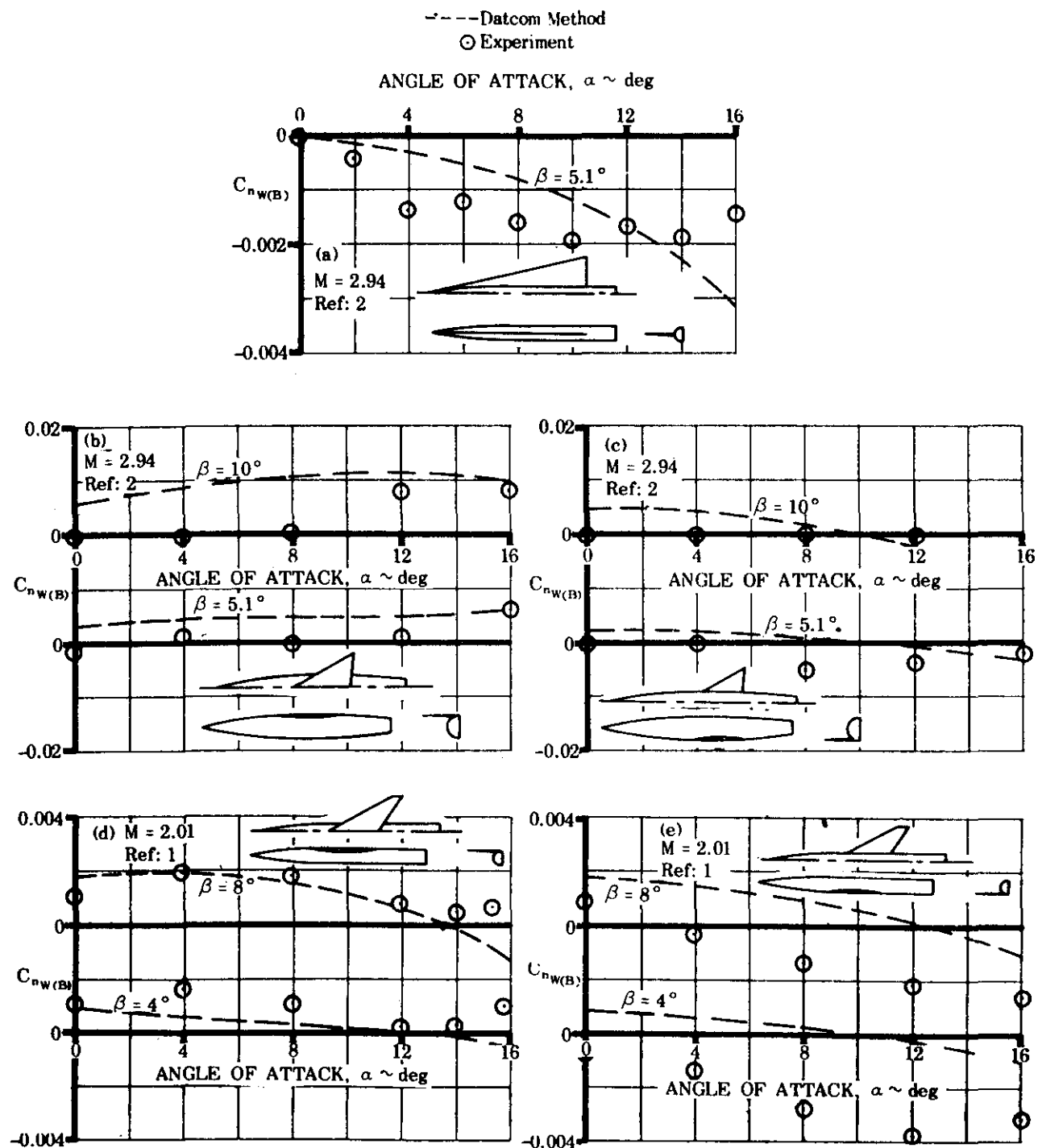


FIGURE 5.2.3.2-5 COMPARISON OF EXPERIMENTAL AND CALCULATED YAWING-MOMENT COEFFICIENT INCREMENTS DUE TO ADDING A WING TO A BODY

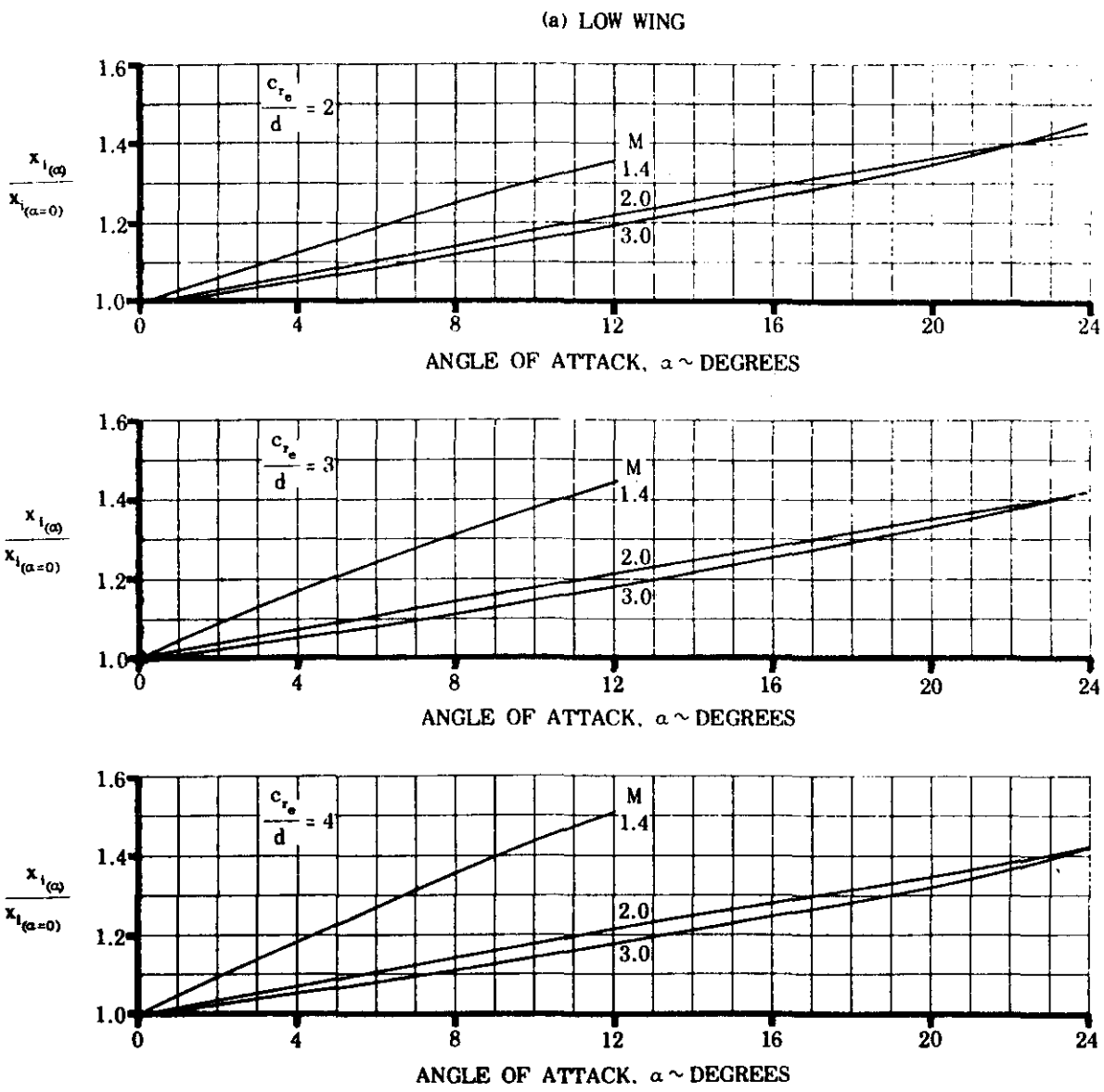


FIGURE 5.2.3.2-6 EFFECT OF ANGLE OF ATTACK ON CENTER-OF-PRESSURE LOCATION OF WING-INDUCED BODY SIDE FORCE

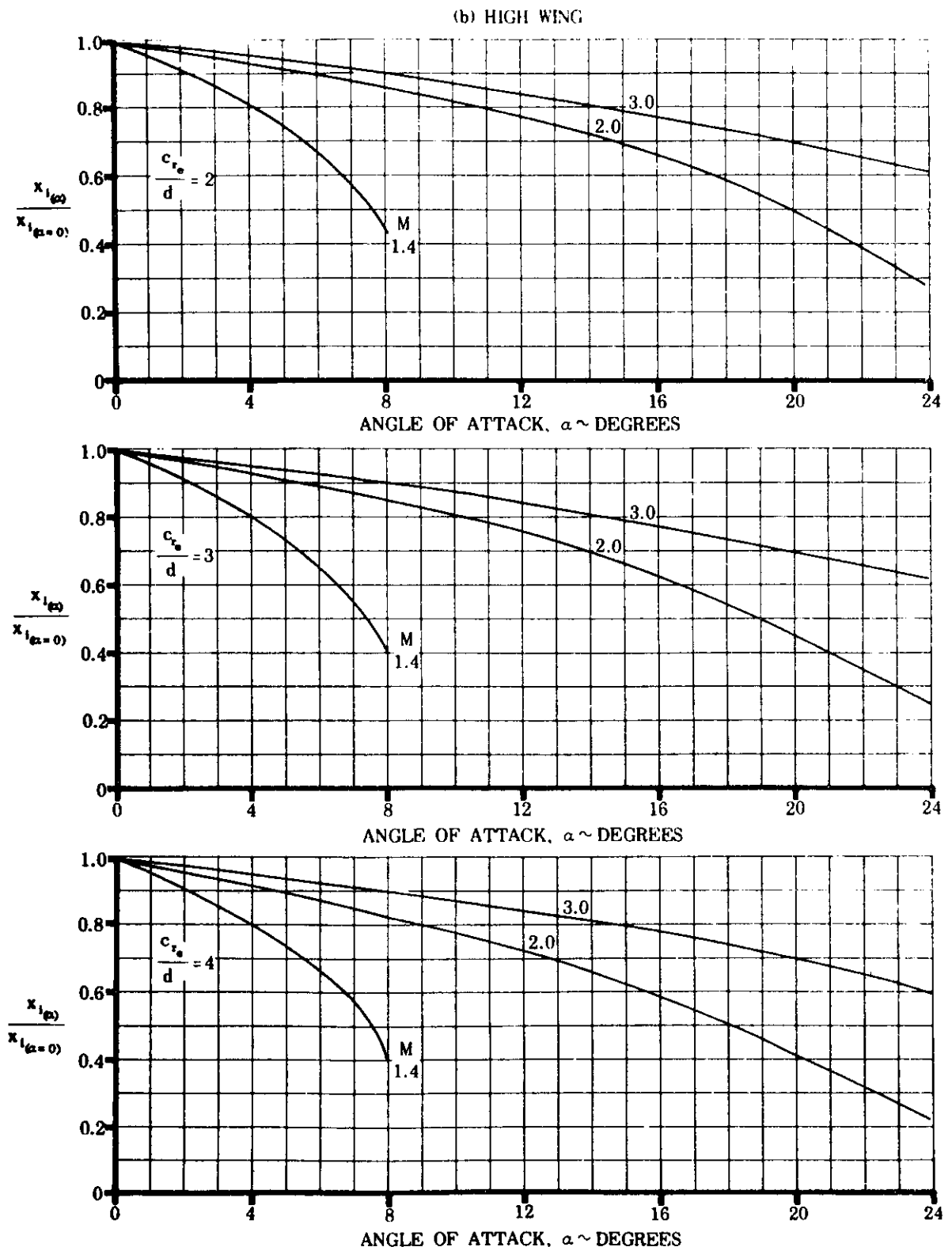


FIGURE 5.2.3.2-6 EFFECT OF ANGLE OF ATTACK ON CENTER-OF-PRESSURE LOCATION OF WING-INDUCED BODY SIDE FORCE (contd)

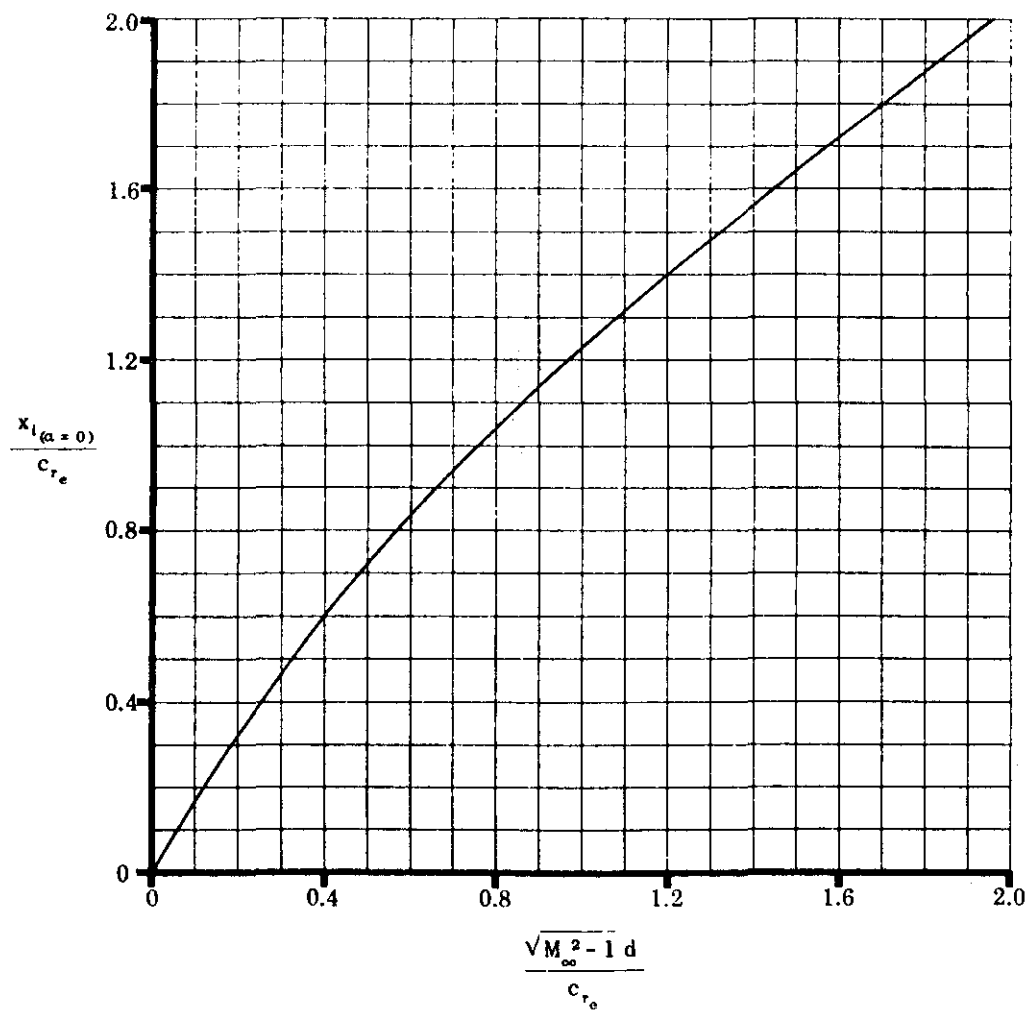


FIGURE 5.2.3.2-8 CENTER-OF-PRESSURE LOCATION OF WING-INDUCED BODY SIDE FORCE AT ZERO ANGLE OF ATTACK

5.3 TAIL-BODY COMBINATIONS IN SIDESLIP

5.3.1 TAIL-BODY SIDESLIP DERIVATIVE $C_{Y\beta}$

5.3.1.1 TAIL-BODY SIDESLIP DERIVATIVE $C_{Y\beta}$ IN THE LINEAR ANGLE-OF-ATTACK RANGE

The contributions of panels present in the empennage to the vehicle sideslip derivative $C_{Y\beta}$ are presented in this section for speeds ranging from low subsonic to hypersonic. The methods presented include the mutual interference effects of the wing, body, and the horizontal panels.

A. SUBSONIC

At subsonic speeds the vehicle body and horizontal tail affect the flow on the vertical tail in such a way as to increase the effectiveness of the vertical tail. This phenomenon, known as the "end-plate effect," is frequently represented by an effective change in panel aspect ratio required to give the same lift effectiveness as the actual panel in the presence of the other vehicle components. Interferences also exist between the vertical tail, the body, and any forward lifting surface.

In the literature, these mutual interference effects are treated in various ways. In some cases, the wing-body wake and sidewash effects are treated independently of the body and horizontal-tail end-plate effects. The British are notable for this approach. In other cases, all the interference effects are lumped into a single vertical-tail effectiveness parameter. One of the methods presented herein uses this latter approach.

The effect of each of the vehicle components on the subsonic vertical-tail effectiveness is discussed in the following paragraphs.

Effect of Body Cross Flow

A body in sideslip exhibits a flow characteristic similar to a cylinder in cross flow. For potential flow the peak local velocity occurs at the top of the cylinder and is equal to twice the free-stream cross-flow velocity. Actually, separation exists on the leeward side, reducing the peak velocity from the potential-flow value. In either case, the velocity decays to the free-stream cross-flow value with distance from the body surface. Thus, it is to be expected that tail-body combinations with large bodies and small tails have a greater effectiveness per unit area than combinations with large tails and small bodies. This trend is exhibited by test data. The vertical panel itself causes a load carry-over from the panel onto the body. This carry-over increases the effectiveness of the vertical panel and is included in the methods presented.

Effect of Horizontal Surface

The presence of a horizontal panel in the vicinity of a vertical panel causes a change in the pressure loading of the latter if the horizontal panel is at a height where the vertical panel has an appreciable gradient, i.e., at a relatively high or low position. Test data substantiate the greater effectiveness of horizontal panels in these positions and the relative ineffectiveness of a horizontal panel at the midspan position on the vertical panel.

Effect of Wing-Body Wake and Sidewash

The effect of wing-body wake and sidewash on the effectiveness of the vertical panel is discussed in detail in Section 5.4.1. This effect is implicitly included in only one of the methods presented herein (Method 3).

Several approaches to this problem have been taken in the literature. Reference 1 presents a method accounting for the effects of body size relative to vertical-panel size, and dealing with horizontal-tail height ranging from positions on the body to the top of the vertical. This method appears to be the most accurate one available. It is presented in this Section as Method 1.

Reference 2 contains a method which is also widely used. Included in this method is a chart for twin tails that is presented in this section. The charts give the average lift-curve slope of the two panels. (The interferences and hence the individual lift-curve slope of the panels differ somewhat.)

A different approach is given in reference 3. This method is based on the assumption that the ratio of the increment in side force due to the addition of a vertical panel to the side force developed by the panel alone is the same as the ratio of the increment in apparent mass of the cross section at the base of the empennage with panel added to the apparent mass of the panel alone. The development of the apparent-mass concept is

given in many places in the literature, e.g., reference 4. The panel alone is taken to be the actual panel reflected about a reflection plane. This assumption implies two-dimensional flow and a slender configuration with all surfaces of the empennage lying in the base plane of the configuration. It is shown in reference 3, however, that good accuracy is obtained for nonslender configurations where the longitudinal locations of the separate surfaces are not in the base plane. This method is limited to configurations in which the horizontal surfaces are mounted on the body or configurations with no horizontal surface. The charts for this method are also used for the supersonic method.

There are some additional effects that are not accounted for by these methods. For instance, dorsal fins may cause a considerable error in the values obtained, although the effect of dorsal fins is more pronounced at the higher angles of sideslip. The use of lift-curve slopes for double-delta wings may decrease this error. A method for calculating the lift-curve slope of double-delta wings is presented in Section 4.1.3.2 under the nonstraight-tapered-wing methods. Dihedral in the horizontal surfaces is known to change the pressure loading on the vertical panel and hence its effectiveness. For rapidly converging bodies, flow separation frequently exists at the juncture of the vertical panel with the body. This effect generally decreases the effectiveness of the vertical tail and is not accounted for by the methods included herein. Similar effects can result when the maximum thickness of two orthogonal panels are made to coincide.

DATCOM METHODS

Method 1

Vertical Panels on Plane of Symmetry

The contribution of the vertical panel to the sideslip derivative $C_{Y\beta}$ is determined by the following steps (reference 1).

Step 1. The effective aspect ratio of the vertical panel is determined by means of the equation

$$A_{\text{eff}} = \frac{(A)_{V(B)}}{(A)_V} (A)_V \left\{ 1 + K_H \left[\frac{(A)_{V(HB)}}{(A)_{V(B)}} - 1 \right] \right\} \quad 5.3.1.1-a$$

where

$\frac{(A)_{V(B)}}{(A)_V}$ is the ratio of the aspect ratio of the vertical panel in the presence of the body to that of the isolated panel. This ratio is given in figure 5.3.1.1-22a as a function of span-to-body-diameter ratio and tail taper ratio.

$(A)_V$ is the geometric aspect ratio of the isolated panel with the span and area of the panel measured to the body center line.

$\frac{(A)_{V(HB)}}{(A)_{V(B)}} = \frac{(A)_{V(HB)}}{\frac{(A)_{V(B)}}{(A)_V} (A)_V}$ is the ratio of the vertical-panel aspect ratio in the presence of the horizontal tail and body to that of the panel in the presence of the body alone. This ratio is given in figure 5.3.1.1-22b as a function of the horizontal and vertical position of the horizontal tail on the vertical panel.

K_H is a factor accounting for the relative size of the horizontal and vertical tails, obtained from figure 5.3.1.1-22c.

Step 2. The lift-curve slope of the vertical panel is determined from paragraph A of Section 4.1.3.2, with the effective aspect ratio of the vertical panel determined from equation 5.3.1.1-a.

Step 3. The wake and sidewash effects as represented by the parameter $\left(1 + \frac{\partial \sigma}{\partial \beta}\right) \frac{q_V}{q_\infty}$ are presented in Section 5.4.1 for the appropriate Mach number and vehicle geometry.

Step 4. The increment in $C_{Y\beta}$ due to the vertical panel is given by the equation (based on wing area)

$$(\Delta C_{Y\beta})_{VWBD} = -k(C_{L_a})_v \left(1 + \frac{\partial \sigma}{\partial \beta}\right) \frac{q_v}{q_\infty} \frac{S_v}{S_w} \quad 5.3.1.1-b$$

where $(C_{L_a})_v$ is obtained from Step 2

$\left(1 + \frac{\partial \sigma}{\partial \beta}\right) \frac{q_v}{q_\infty}$ is obtained from Step 3

k is an empirical factor obtained from figure 5.3.1.1-22d

$\frac{S_v}{S_w}$ is the ratio of the vertical panel area (measured to the body centerline) to the total wing area

This method is substantiated by test data in table 5.3.1.1-B.

Method 2

Twin Vertical Panels

The contribution of twin vertical panels mounted on the tips of a horizontal tail or wing is given by the following steps. This method (from reference 2) includes the effects of the wing-body wake and sidewash.

Step 1. Determine the ratio of the effective to actual aspect ratio, $\frac{A_{eff}}{A}$, from figure 5.3.1.1-24a as a function of the geometric variable shown.

Step 2. Determine the lift-curve slope of the equivalent rectangular vertical panel $(C_{Y\beta})_{V_{eff}}$ from figure 5.3.1.1-24b; use the effective aspect ratio found in Step 1 and the total trailing-edge angle of the airfoil section.

Step 3. The increment in vehicle sideslip derivative $C_{Y\beta}$ due to the twin panels (based on total wing area) is given by the equation

$$(\Delta C_{Y\beta})_{VWBD} = -\frac{(C_{Y\beta})_{VWBD}}{(C_{Y\beta})_{V_{eff}}} (C_{Y\beta})_{V_{eff}} \frac{2S_v}{S_w} \quad 5.3.1.1-c$$

where $\frac{(C_{Y\beta})_{VWBD}}{(C_{Y\beta})_{V_{eff}}}$ is obtained from figure 5.3.1.1-24c for the appropriate geometry shown

$(C_{Y\beta})_{V_{eff}}$ is obtained from Step 2 above

S_v is the area of a single vertical panel

There are not sufficient data existing to substantiate the accuracy of this method, although reference 2 indicates that the method is accurate to within ± 10 percent.

Method 3

A third general method is based on the work in reference 3. This method is limited to configurations in which the horizontal tail is mounted on the body or configurations with no horizontal tail. It is discussed in the introduction to this Section. The charts of this method are also used in the supersonic method of paragraph C.

The method as presented for the vertical panel estimates the increment in $C_{Y\beta}$ due to the addition of one panel in the empennage and includes the effects of all existing panels on the added panel. An extension of the method to determine the total empennage side force due to sideslip at subsonic speeds which results from the addition of all panels present in the empennage is presented in paragraph A of Section 5.6.1.1.

Contribution of Vertical Panel

The side force-curve slope (based on total wing area) of a vertical panel added to an empennage is given by the equation

$$(\Delta C_{Y\beta})_p = -K(C_{L\alpha})_p \frac{S_p}{S_w} \quad 5.3.1.1-d$$

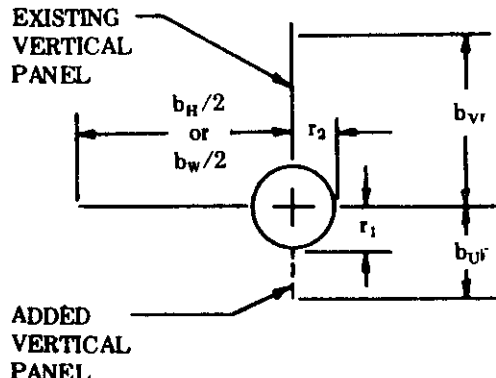
where the subscript p refers to the added vertical panel (either an upper vertical stabilizing surface V or a lower vertical stabilizing surface U)

$(C_{L\alpha})_p$ is the lift-curve slope of the isolated vertical panel mounted on a reflection plane from paragraph A of Section 4.1.3.2. For this calculation the aspect ratio must be taken as twice the aspect ratio defined by the average exposed span and exposed area.

S_p is the area of the exposed vertical panel

K is the apparent mass factor from figures 5.3.1.1-25a through 5.3.1.1-25nn. When using these figures the vertical panel for which the contribution to $C_{Y\beta}$ is desired is termed the "added panel" and other panels existing in the empennage are termed the "existing panels" as shown schematically in sketch (a).

The body radii dimensions r_1 and r_2 are defined in the region of the tail panels. If these dimensions change in this region the average values should be used. In general interpolation procedures must be used since the geometry rarely coincides with that of a specific figure. Since the variation of parameters between figures is generally non-linear, graphical interpolation using at least three points is recommended. An index of the K charts and the range of variables covered by each is presented as table 5.3.1.1-A.



SKETCH (a)

Although the sketches on the figures show only the upper vertical panel as the added panel, the added panel can be either the upper or lower vertical panel. Special mention is made of figures 5.3.1.1-25g through 5.3.1.1-25p. Figures 5.3.1.1-25g through 5.3.1.1-25k are used to estimate the K value due to adding an upper vertical stabilizing surface to a body with the horizontal surface in the high tangent position. These figures also apply in estimating the K value due to adding a lower vertical stabilizing surface to a body with a horizontal surface located in the low tangent position. Figures 5.3.1.1-25l through 5.3.1.1-25p are used in the same manner as figures 5.3.1.1-25g through 5.3.1.1-25k except that the horizontal surface is tangent to the body on the side opposite to which the panel is added.

Apparent mass factor solutions for bodies other than circular or elliptic cross sections are not available. In treating bodies of other cross-sectional shapes the assumption is made that the ratio of height to width, r_1/r_2 , is the important parameter and that details of the body contour are of secondary importance. This assumption has been used in reference 3, where the body was other than circular or elliptic, and the resulting correlation with experiment was as good as for the cases to which the figures apply directly.

The case of a vertical tail added to an empennage consisting of a horizontal panel located at other than the mid-position on the elliptical body is not covered by the K charts (see table 5.3.1.1-A). To handle such a case, either the body must be considered circular and an interpolation made for horizontal panel height, or the horizontal panel must be assumed located at the mid-position and an interpolation performed between r_1/r_2 ratios. A comparison of the effect of both horizontal panel location and body shape on the K factor should be made in determining the proper approach to the K factor solution.

Contribution of Horizontal Tail

In determining the total empennage side force due to sideslip which results from the addition of all panels present in the empennage the horizontal tail must be added first (see method 3, paragraph A, Section 5.6.1.1). Although the horizontal tail contribution to $C_{Y\beta}$ is usually small and for most calculations can be neglected; it can provide a significant contribution to the sideslip derivative $C_{n\beta}$.

The contribution to the sideslip derivative $C_{Y\beta}$ (based on total wing area) of a horizontal tail added to a body is given by

$$(\Delta C_{Y\beta})_{H(B)} = K_{H(B)} (C_{Y\beta})_B \frac{S_{B_{Ref}}}{S_w} \quad 5.3.1.1-e$$

where

$(C_{Y\beta})_B$ is the side force due to sideslip (based on body reference area, $S_{B_{Ref}}$) obtained from Section 4.2.1.1 by conversion of the body lift-curve slope i.e.; $(C_{Y\beta})_B = -(C_{L\alpha})_B$

$K_{H(B)}$ is the apparent mass factor due to the addition of a horizontal tail in the presence of a body for the appropriate tail span and vertical position from figure 5.3.1.1-2500.

For a horizontal tail mounted at an intermediate position on the body (between mid- and high- or low-tangent position), the following second order interpolation using the equation of an ellipse should be applied

$$K_{H(B)} = K_{\text{High or Low}} \left\{ 1 - \left[1 - \left(\frac{Z_H}{r_1} \right)^2 \right]^{\frac{1}{2}} \right\}$$

A substantiation table comparing experimental data with results calculated by this method is shown in table 5.3.1.1-B. A comparison is made in this table of the relative accuracy of Method 1 and Method 3.

Sample Problems

1. Method 1

Given: The configuration of reference 6 consisting of wing, body, horizontal tail, and vertical tail. Find the effect of adding the vertical tail to the wing-body-horizontal tail combination.

Wing Characteristics

$$A_w = 3.0 \quad S_w = 576.0 \text{ sq in.} \quad b_w = 41.56 \text{ in.} \quad z_w = 0 \quad \Lambda_{o/w} = 45^\circ$$

Horizontal Tail Characteristics

$$A_H = 4.0 \quad S_H = 121.6 \text{ sq in.} \quad b_H = 22.42 \text{ in.} \quad z_H = 0$$

Vertical Tail Characteristics

$$A_V = 1.50 \quad S_V = 153.7 \text{ sq in.} \quad b_V = 15.23 \text{ in.} \quad c_{rv} = 17.40 \text{ in.} \quad \lambda_V = 0.160$$

$\Lambda_{c/2V} = 41.9^\circ$ Airfoil: NACA 0003.5-64

Additional Characteristics

$$M = 0.25 \quad r_1 = 2.8 \text{ in.} \quad d = 6.0 \text{ in.} \quad x/c_V = 0.55$$

Compute:

$$(c I_a)_V = 6.18 \text{ per rad (Section 4.1.1.2)}$$

$$K = \frac{c I_a}{2\pi} = 0.984$$

$$b_V/2r_1 = 2.72$$

$$\frac{(A)_{V(B)}}{(A)_V} = 1.47 \text{ (figure 5.3.1.1-22a)}$$

$$(A)_{V(B)} = \frac{(A)_{V(B)}}{(A)_V} (A)_V = 2.20$$

$$S_H/S_V = 0.820$$

$$K_H = 0.83 \text{ (figure 5.3.1.1-22c)}$$

$$z_H/b_V = 0$$

$$\frac{(A)_{V(HB)}}{(A)_{V(B)}} = 1.10 \text{ (figure 5.3.1.1-22b)}$$

$$S_V/S_W = 0.267$$

$$z_W/d = 0$$

$$A_{eff} = (A)_{V(B)} \left[1 + K_H \left[\frac{(A)_{V(HB)}}{(A)_{V(B)}} - 1 \right] \right] = 2.38 \text{ (equation 5.3.1.1-a)}$$

$$\frac{A_{eff}}{K} [\beta^2 + \tan^2 \Lambda_{c/2V}]^{1/2} = 3.193$$

$$\frac{C_{L_a}}{A_{eff}} = 1.08 \text{ (figure 4.1.3.2-49)}$$

$$(C_{L_a})_{V(HB)} = \left(\frac{C_{L_a}}{A_{eff}} \right) A_{eff} = 2.57 \text{ per rad}$$

$$\left(1 + \frac{\partial \sigma}{\partial \beta} \right) \frac{q_V}{q_\infty} = 0.724 + 3.06 \frac{S_V/S_W}{1 + \cos \Lambda_{c/2W}} + 0.4 \frac{z_W}{d} + 0.009 A_W = 1.230 \text{ (equation 5.4.1-a)}$$

$$k = 0.87 \text{ (figure 5.3.1.1-22d)}$$

Solution:

$$(\Delta C_{Y\beta})_{V(WBH)} = -k(C_{L\alpha})_{V(BH)} \left(1 + \frac{\partial \sigma}{\partial \beta}\right) \frac{q_v}{q_\infty} \frac{S_v}{S_w} \quad (\text{equation 5.3.1.1-b})$$

$$= -0.734 \text{ per rad}$$

This compares with an experimental value of -0.76 per radian obtained from reference 6.

2. Method 2

Given: A configuration consisting of wing, body, and twin vertical panels mounted on the tips of a horizontal tail.
Find the effect of adding the twin vertical panels to the configuration.

Twin Vertical Tail Characteristics

$$A_V = 1.39 \quad b_V = 5.0 \text{ ft} \quad b'_V = 4.0 \text{ ft} \quad S_V = 18.0 \text{ ft} \quad \phi_{TE_V} = 10^\circ$$

Additional Characteristics

$$S_w = 144.0 \text{ sq ft} \quad l_B = 55.0 \text{ ft} \quad b_H = 12.0 \text{ ft} \quad r_1 = 1.50 \text{ ft}$$

Compute:

$$b'_V/b_V = 0.80$$

$$\frac{A_{eff}}{A} = 1.20 \quad (\text{figure 5.3.1.1-24a})$$

$$A_{eff} = 1.67$$

$$(C_{Y\beta})_{V_{eff}} = 2.40 \quad (\text{figure 5.3.1.1-24b})$$

$$2r_1/b_V = 0.6$$

$$b_H/l_B = 0.22$$

$$\frac{(C_{Y\beta})_{V(WBH)}}{(C_{Y\beta})_{V_{eff}}} = 0.61 \quad (\text{figure 5.3.1.1-24c})$$

Solution:

$$(\Delta C_{Y\beta})_{V(WBH)} = -\frac{(C_{Y\beta})_{V(WBH)}}{(C_{Y\beta})_{V_{eff}}} \frac{2S_V}{S_w} \quad (\text{equation 5.3.1.1-c})$$

$$= -0.366 \text{ per rad}$$

3. Method 3

Given: A configuration of reference 10 consisting of wing, body, horizontal tail, and vertical tail. Find the effect of adding the vertical tail to the wing-body-horizontal tail configuration.

Vertical Tail Characteristics

$$A_V = 1.40 \quad A_{V_e} = 1.37 \quad S_V = 48.6 \text{ sq in.} \quad S_{V_e} = 36.2 \text{ sq in.} \quad \Lambda_{c/2V} = 39.4^\circ$$

$$\lambda_V = 0.645 \quad \lambda_{V_e} = 0.60 \quad b_V = 8.25 \text{ in.} \quad \text{NACA 65008 airfoil}$$

Additional Characteristics

$$M = 0.13 \quad r_1 = 1.20 \quad r_2 = 2.65 \quad \frac{b_H}{2} = 6.70 \text{ in.} \quad S_w = 324 \text{ sq in.}$$

Compute:

$$(c_{L_a})_v = 6.67 \text{ per rad (Section 4.1.1.2)}$$

$$K = \frac{(c_{L_a})_v}{2\pi} = 1.06 \quad (\text{ratio of section lift-curve slope to } 2\pi)$$

$$2A_{V_e} = 2.74$$

$$\frac{2A_{V_e}}{K} [\beta^2 + \tan^2 \Lambda_{c/2_v}]^{1/2} = 3.26$$

$$\frac{(C_{L_a})_v}{2A_{V_e}} = 1.08 \text{ per rad (figure 4.1.3.2-49)}$$

$$(C_{L_a})_v = (1.08) (2A_{V_e}) = 2.96 \text{ per rad (based on } S_{V_e})$$

Determine the apparent-mass factor due to adding the upper vertical stabilizer to the wing-body-horizontal tail configuration. In this case the empennage consists of the body, horizontal tail, and upper vertical stabilizer. The apparent-mass factor to be found is that due to adding the upper vertical stabilizer to the combination of body and horizontal tail, $K_{V(HB)}$

$$\left(\frac{r_1}{r_2}\right) = 0.451, \left(r_2 / \frac{b}{2}\right)_H = 0.396, \left(\frac{r_1}{b}\right)_U^{\text{existing panel}} = 1.000, \left(\frac{r_1}{b}\right)_V^{\text{added panel}} = 0.1455$$

Using the above parameters and table 5.3.1.1-A it is seen that $K_{V(HB)}$ is obtained by interpolation from figures 5.3.1.1-25s, -25t, -25u for $r_1/r_2 = 0.333$, 5.3.1.1-25y, -25z, -25aa for $r_1/r_2 = 0.667$; 5.3.1.1-25c, -25d, -25e for $r_1/r_2 = 1.000$. An interpolation between those values of $K_{V(HB)}$ gives, for $r_1/r_2 = 0.451$

$$K_{V(HB)} = 1.135.$$

Solution

$$(\Delta C_{Y_\beta})_p = -K (C_{L_a})_p \frac{S_{p_e}}{S_w} \quad (\text{equation 5.3.1.1-d})$$

$$(\Delta C_{Y_\beta})_{V(HB)} = -K_{V(HB)} (C_{L_a})_V \frac{S_{V_e}}{S_w}$$

$$= (-1.135) (2.96) \left(\frac{36.2}{324}\right)$$

$$= -0.375 \text{ per rad (based on } S_w)$$

This corresponds to an experimental value of $-0.367 \text{ per radian}$ obtained from reference 10.

B. TRANSONIC

The side force on a vertical panel depends on three general factors. These are the lift characteristics of the panel itself, the effect of the wing-body wake and sidewash, and the interference effects of the body and horizontal surface.

The lift characteristics of the isolated panel at transonic speeds can be estimated by methods such as that described in paragraph B of Section 4.1.3.2. The wake and sidewash, on the other hand, are affected by the detailed geometry of the flow field, which can be radically changed by relatively minor variations in the vehicle geometry. This is true because of the sensitivity of transonic flow to local contour and area distribution changes and because of shock-induced boundary-layer separation. In addition, the vertical panel is usually contained in a small segment of the flow field so that local variations in the field can have pronounced effects upon the resultant forces on the tail. The interference effects of the body and horizontal tail at transonic speeds are likewise sensitive to local configuration geometry and cannot be eliminated.

Because of the above reasons, the vertical tail contribution to the sideslip derivative $C_{Y\beta}$ is difficult to estimate reliably, and its value is usually obtained by wind-tunnel testing or estimated from comparison with similar configurations.

DATCOM METHOD

No method is available in the literature for estimating this derivative and none is presented in the Datcom. However, some data in this speed regime can be found in references 11, 12, and 13.

C. SUPERSONIC

The problem of estimating the effectiveness of panels in the empennage in generating side forces due to sideslip at supersonic speeds is complicated by the presence of shock waves. These shock waves cause marked regions of differentiation on the surfaces of an added panel (see sketch b). Each region is characterized by different Mach numbers, pressures, and velocity directions. In addition, vortices from the body and the wake from the forward lifting surfaces can have important effects on the forces generated. The method presented herein, taken from reference 3, does not account for the effects of vortices and wakes. However, these effects are small at low angles of attack.

DATCOM METHOD

The method of this Section is for estimating the increment in $C_{Y\beta}$ due to the addition of a panel (either a vertical stabilizer or a horizontal tail) in the empennage. The vertical panel contribution includes the effects of all existing panels on the added panel. An extension of the method to determine the total empennage side force due to sideslip at supersonic speeds which results from the addition of all panels present in the empennage is presented in paragraph C of Section 5.6.1.1.

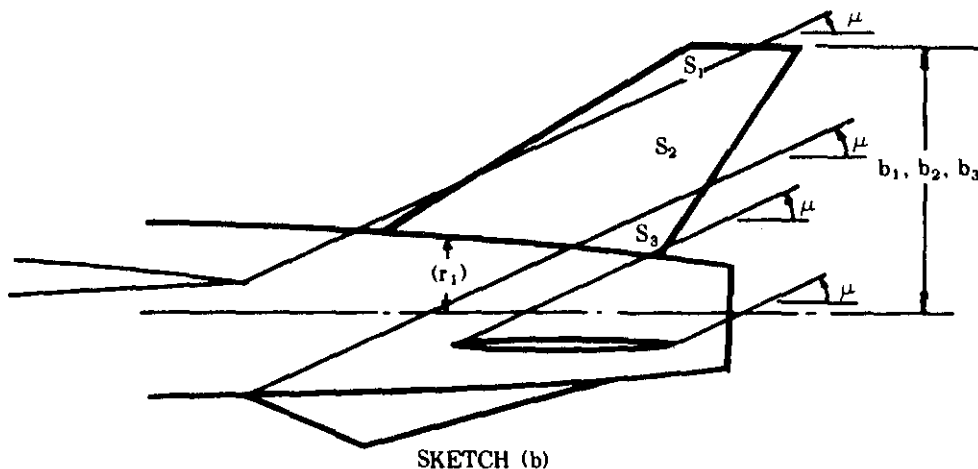
The method is based on the same apparent mass concept as used in Method 3 of paragraph A. A weighted apparent mass factor is obtained for each region defined by a system of Mach lines characteristic of the configuration. The total effective apparent mass K' is then determined and used to obtain the desired force contribution of the added panel.

This method is limited to configurations in which the horizontal tail is mounted on the body or configurations with no horizontal tail.

Contribution of Vertical Panel

When adding a vertical panel to a configuration, the following general procedure is used. However, a more thorough understanding will be gained by studying the sample problems.

Step 1. Construct the Mach lines ($\mu = \sin^{-1} \frac{1}{M}$) emanating from the exposed root chord leading and trailing edges of all panels other than that to be added, as shown in sketch (b). (This is an approximation to the horizontal panel flow field boundaries strictly applicable to a flat plate airfoil at zero angle of attack and does not account for the effects of vortices and wakes.)



SKETCH (b)

- Step 2. Determine the areas or regions on the added panel affected by each vehicle component, S_1 , S_2 , S_3 , etc.
- Step 3. Determine the body-radius-to-semi-span ratios for each region for both the horizontal and vertical surfaces. The vertical span of a given region is taken as the total span of the added panel measured to the body centerline, as shown in sketch (b). The semi-span of horizontal surfaces (wings and horizontal tails) is the maximum semi-span of these surfaces. The radius of the body for a given region is taken to be the average radius for that region.
- Step 4. The apparent mass factors K for each region are determined from figures 5.3.1.1-25a through 5.3.1.1-25m using the geometry of each region as determined in Step 3. In determining the K factors for each region any point lying forward of the Mach line from the leading-edge body juncture of a panel does not feel the presence of the panel, and any point lying behind the shock wave drawn from the trailing-edge body juncture of a panel does not feel the presence of the panel. For example, referring to sketch (b), the upper vertical panel is divided into three regions of influence. Region S_1 senses the presence of the body and the wing; region S_2 only the body; and region S_3 the body and the lower vertical stabilizer. Interpolation for the appropriate geometry must frequently be made when using these charts. It is recommended that at least three points be used in these interpolations because of the nonlinearities of the characteristics involved. (See Method 3 of paragraph A for a general discussion on the use of the K charts.)
- Step 5. Each apparent mass factor is reduced by the ratio of the area of its region on the added panel (Step 2) to the total exposed panel area.
- Step 6. The total effective apparent-mass factor for the added panel K' is then the sum of those calculated for each region (Step 5). For example in the case illustrated in sketch (b), K' of the upper vertical panel in the presence of wing, body, horizontal tail, and ventral is given as

$$K' = K_{V(WB)} \frac{S_1}{S_{V_e}} + K_{V(B)} \frac{S_2}{S_{V_e}} + K_{V(BU)} \frac{S_3}{S_{V_e}}$$

- Step 7. The side-force curve slope (based on total wing area) of a vertical panel added to an empennage is given by

$$(\Delta C_{V\beta})_p = -K' (C_{N_a})_p \frac{S_{p_a}}{S_w} \quad 5.3.1.1-1$$

where the subscript p and S_{p_a} are as defined in Method 3 of paragraph A, and $(C_{N_a})_p$ is the normal-force-curve slope of the isolated vertical panel mounted on a reflection plane, from paragraph C of Section 4.1.3.2, based on twice the aspect ratio defined by the average exposed span and exposed area.

Contribution of Horizontal Tail

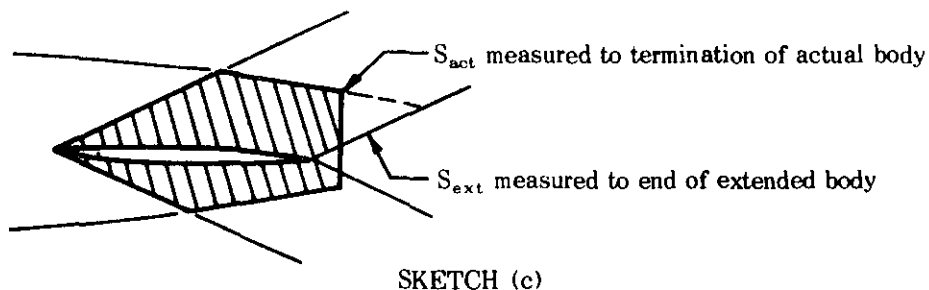
In determining the total empennage side force due to sideslip which results from the addition of all panels present in the empennage the horizontal tail must be added first (see paragraph C, Section 5.6.1.1). Although the horizontal tail contribution to $C_{Y\beta}$ is usually small and for most calculations can be neglected; it can provide a significant contribution to the sideslip derivative $C_{n\beta}$.

The contribution to the sideslip derivative $C_{Y\beta}$ (based on total wing area) of a horizontal tail added to a body is given by

$$(\Delta C_{Y\beta})_{H(B)} = K_{H(B)} (C_{Y\beta})_B \frac{S_{act}}{S_{ext}} \frac{S_{B_{Ref}}}{S_w} \quad 5.3.1.1-g$$

where $K_{H(B)}$, $(C_{Y\beta})_B$, and $S_{B_{Ref}}$, are as defined in Method 3 of paragraph A

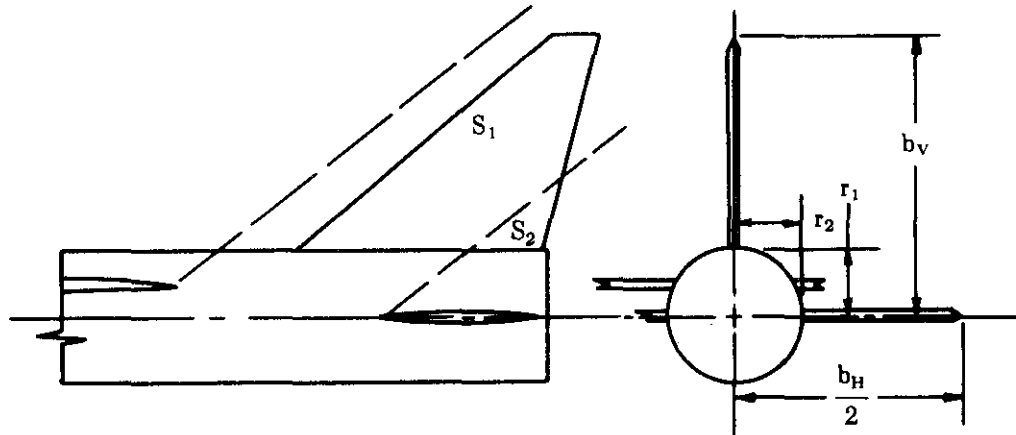
$\frac{S_{act}}{S_{ext}}$ is the ratio of the actual projected side area of the fuselage to that of the extended fuselage as determined by Mach lines ($\mu = \sin^{-1} \frac{1}{M}$) originating from the leading and trailing edge of the exposed root chord (see sketch (c))



This method is substantiated in table 5.3.1.1-C (from reference 3).

Sample Problems

- Given: The configuration of reference 16 consisting of wing, body, horizontal tail, and upper vertical stabilize. Find the effect of adding the vertical tail to the wing-body-horizontal tail combination.



Vertical Tail Characteristics

$A_V = 1.59$	$A_{V_e} = 1.48$	$S_V = 35.3 \text{ sq in.}$	$S_{V_e} = 21.9 \text{ sq in.}$	$\Lambda_{LE_V} = 50.4^\circ$
$\lambda_V = 0.153$	$\lambda_{V_e} = 0.192$	$b_V = 7.48 \text{ in.}$	NACA 65A005 airfoil	

Additional Characteristics

$$\begin{array}{lll} M = 1.61 & \mu = \sin^{-1} \frac{1}{M} = 38.5^\circ & r_1 = 1.78 \text{ in.} \\ \frac{b_H}{2} = 6.06 \text{ in.} & S_w = 160.4 \text{ sq in.} & r_2 = 1.78 \text{ in.} \\ \end{array}$$

$z_H = 0$ (horizontal tail on body centerline)

Compute:

$$2A_{V_e} \tan \Lambda_{LEV} = 3.575$$

$$\beta = \sqrt{M^2 - 1} = 1.265$$

$$\frac{\tan \Lambda_{LEV}}{\beta} = 0.955$$

$\beta(C_{N_a})_v = 3.90$ per rad (figures 4.1.3.2-56a, -56b, -56c interpolated for $\lambda_{V_e} = 0.192$)

$(C_{N_a})_v = 3.08$ per rad (based on S_{V_e})

Determine the effective apparent mass ratio due to adding the vertical stabilizer to the wing-body-horizontal stabilizer combination. The empennage in this case consists of body, horizontal stabilizer and vertical stabilizer. The effective apparent mass ratio to be found is that due to adding the vertical stabilizer to the body and horizontal tail, $K'_{V(HB)}$.

Referring to the configuration sketch, the region S_1 senses only the body, while S_2 senses both the body and the horizontal stabilizer. Therefore, the effective apparent mass ratio is given by

$$K'_{V(HB)} = K_{V(B)} \frac{S_1}{S_{V_e}} + K_{V(HB)} \frac{S_2}{S_{V_e}}$$

Determine $K_{V(B)}$

$$\left(\frac{r_1}{r_2} \right) = 1.000; \left(\frac{r_1}{b} \right)_v \underset{\substack{\text{added} \\ \text{panel}}}{=} 0.238; \left(\frac{r_1}{b} \right)_U \underset{\substack{\text{existing} \\ \text{panel}}}{=} 1.000$$

using the above parameters and table 5.3.1.1-A it is seen that $K_{V(B)}$ is obtained from figure 5.3.1.1-25a

$$K_{V(B)} = 1.25$$

Determine $K_{V(HB)}$

$$\left(\frac{r_1}{r_2} \right) = 1.000; \left(\frac{r_2}{b_H/2} \right) = 0.293; \left(\frac{r_1}{b} \right)_v \underset{\substack{\text{added} \\ \text{panel}}}{=} 0.238; \left(\frac{r_1}{b} \right)_U \underset{\substack{\text{existing} \\ \text{panel}}}{=} 1.000$$

Using the above parameters and table 5.3.1.1-A it is seen that $K_{V(HB)}$ is obtained from figures 5.3.1.1-25b, -25c, and -25d interpolated for $(r_2/b_H/2) = 0.293$

$$K_{V(HB)} = 1.375$$

$$K'_{V(HB)} = (1.25) \left(\frac{19.9}{21.9} \right) + (1.375) \left(\frac{2.0}{21.9} \right) = 1.26$$

Solution:

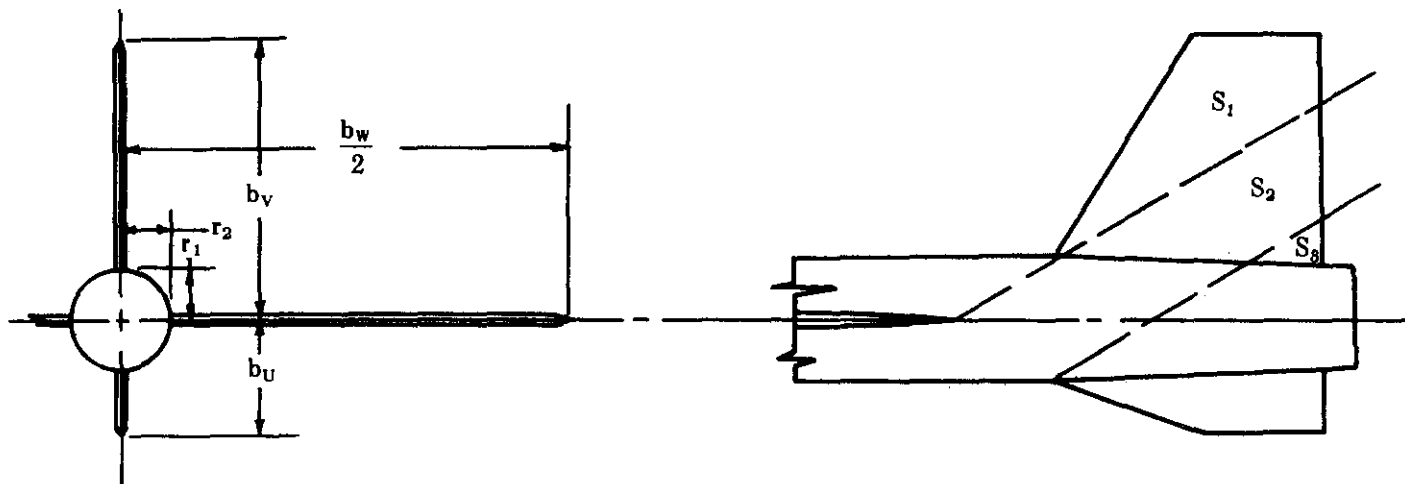
$$(\Delta C_{Y\beta}) = -K' (C_{N\alpha})_p \frac{S_{pe}}{S_w} \quad (\text{equation 5.3.1.1-f})$$

$$\begin{aligned} (\Delta C_{Y\beta})_{VWBH} &= -K'_{VWBH} (C_{N\alpha})_v \frac{S_{ve}}{S_w} \\ &= (-1.26) (3.08) \left(\frac{21.90}{160.4} \right) \end{aligned}$$

= -0.529 per rad (based on S_w)

This compares with an experimental value of -0.486 per radian from reference 16.

2. Given: The configuration of reference 18 consisting of wing, body, upper vertical stabilizer and lower vertical stabilizer. Find the effect of adding the upper vertical stabilizing surface to the wing-body-lower vertical stabilizer combination.



Upper Vertical Tail Characteristics

$A_v = 1.29$	$A_{ve} = 1.12$	$S_v = 43.5 \text{ sq in.}$	$S_{ve} = 31.6 \text{ sq in.}$	$\Lambda_{LEv} = 32.5^\circ$
$\lambda_v = 0.42$	$\lambda_{ve} = 0.482$	$b_v = 7.48 \text{ in.}$	airfoil: wedge nose, slab sides (constant thickness)	

Additional Characteristics

$M = 2.01$	$\mu = \sin^{-1} \frac{1}{M} = 29.8^\circ$	$r_1 = 1.50 \text{ in.}$	$r_2 = 1.50 \text{ in.}$
$S_w = 144 \text{ sq in.}$	$\frac{b_w}{2} = 12.0 \text{ in.}$	$S_1 = 16.35 \text{ sq in.}$	$S_2 = 14.10 \text{ sq in.}$
$z_w = 0$ (wing on body centerline)		$b_U = 3.05 \text{ in.}$	$S_3 = 1.15 \text{ sq in.}$

Compute:

$$2 A_{V_e} \tan \Lambda_{LEV} = 1.425$$

$$\beta = \sqrt{M^2 - 1} = 1.744$$

$$\frac{\tan \Lambda_{LEV}}{\beta} = 0.365$$

$$\beta(C_{N_a})_V = 3.68 \text{ per rad (figures 4.1.3.2-56c, -56d, -56e interpolated for } \lambda_{V_e} = 0.482)$$

$$(C_{N_a})_V = 2.12 \text{ per rad (based on } S_{V_e})$$

Determine the effective apparent mass ratio due to adding the upper vertical stabilizer to the wing-body-lower vertical stabilizer combination. The empennage in this case consists of body, upper vertical stabilizer and lower vertical stabilizer (ventral). The effective apparent mass ratio to be found is that due to adding the upper vertical stabilizer to the body and ventral, $K'_{V(BU)}$.

Referring to the configuration sketch, the region S_1 senses the wing and the body, S_2 senses only the body and S_3 senses both the body and the ventral. Therefore, the effective apparent mass ratio is given by

$$K'_{V(BU)} = K_{V(WB)} \frac{S_1}{S_{V_e}} + K_{V(B)} \frac{S_2}{S_{V_e}} + K_{V(BU)} \frac{S_3}{S_{V_e}}$$

Determine $K_{V(WB)}$

$$\left(\frac{r_1}{r_2} \right) = 1.000; \left(\frac{r_2}{b_w/2} \right) = 0.125; \left(\frac{r_1}{b} \right)_v = 0.200$$

v
added
panel

The ventral surface is not felt in region S_1 , therefore

$$\left(\frac{r_1}{b} \right)_U = 1.000$$

U
existing
panel

Using the above parameters and table 5.3.1.1-A it is seen that $K_{V(WB)}$ is obtained from figures 5.3.1.1-25b, -25c, -25d interpolated for $(r_2/b_w/2) = 0.125$

$$K_{V(WB)} = 1.36$$

Determine $K_{V(B)}$

$$\left(\frac{r_1}{r_2} \right) = 1.000; \left(\frac{r_1}{b} \right)_v = 0.200; \left(\frac{r_1}{b} \right)_U = 1.000 \text{ (region } S_2 \text{ does not sense the ventral)}$$

v
added
panel

Using the above parameters table 5.3.1.1-A it is seen that $K_{V(B)}$ is obtained from figure 5.3.1.1-25a

$$K_{V(B)} = 1.13$$

Determine K_{VBU} .

$$\left(\frac{r_1}{r_2}\right) = 1.000; \left(\frac{r_1}{b}\right)_V^{\text{added panel}} = 0.200; \left(\frac{r_1}{b}\right)_V^{\text{existing panel}} = 0.492$$

Using the above parameters and table 5.3.1.1-A it is seen that K_{VBU} is obtained from figure 5.3.1.1-25a interpolated for $(r_1/b)_V = 0.492$

$$K_{VBU} = 1.24$$

$$K'_{VBU} = (1.36) \left(\frac{16.35}{31.60} \right) + (1.13) \left(\frac{14.10}{31.60} \right) + (1.24) \left(\frac{1.15}{31.60} \right)$$

$$= 1.253$$

Solution:

$$(\Delta C_{Y\beta})_V = -K' (C_{Na})_p \frac{S_{V_e}}{S_w} \quad (\text{equation 5.3.1.1-f})$$

$$(\Delta C_{Y\beta})_{VBU} = -K'_{VBU} (C_{Na})_V \frac{S_{V_e}}{S_w}$$

$$= (-1.253) (2.12) \left(\frac{31.60}{144.0} \right)$$

$$= -0.583 \text{ per rad (based on } S_w)$$

This compares with an experimental value of -0.601 per radian from reference 18.

D. HYPERSONIC

A general discussion of hypersonic flow is given in paragraph D of Section 4.1.3.3 and in the references cited therein. The application of theories to tail components is complicated by the flow disturbances of forward components (body and wings) in the form of vortices, shock waves, and wakes. In general, these effects have not been generalized and specific configurations must either be compared to similar configurations for which data exist or be submitted to a test program. The recommendations of the Datcom for this speed regime are necessarily tentative and will be updated as information becomes available.

DATCOM METHOD

For configurations in which the tail panels are mounted on the body, it is recommended that the supersonic method described in paragraph C be applied at the higher Mach numbers. However, this method has not been substantiated beyond a Mach number of 6.86 (see table 5.3.1.1-C).

Alternatively, the vertical-panel contribution to $C_{Y\beta}$ may be estimated by the hypersonic small-disturbance theory, which gives a local pressure coefficient of

$$C_p = (\beta \pm \delta)^2 \left(\frac{\gamma + 1}{2} \pm \sqrt{\frac{(\gamma + 1)^2}{4} + \frac{4}{(M^2 - 1)(\beta \pm \delta)^2}} \right) \quad 5.3.1.1-h$$

where δ is the local slope of the surface of the vertical panel with respect to the vertical plane of symmetry in radians

γ is the ratio of specific heats

β is the sideslip angle in radians

The sign of $(\beta \pm \delta)$ should be chosen to give the correct local angle of sideslip.

The plus sign before the radical in equation 5.3.1.1-h applies to the compression side of the surface and the minus sign to the expansion side. The equation is strictly valid only for sharp-edged sections and for $\delta \ll 1$. For a slab-sided section the pressure coefficient becomes the side-force coefficient directly (based on exposed panel area).

For very high Mach numbers, Newtonian flow can be assumed. The pressure coefficient for this case is

$$C_p = 2 \sin^2 (\beta \pm \delta) \quad 5.3.1.1-i$$

Care must be taken to assure that portions of the panels that are "blanketed" by forward components, i.e., are not "seen" from the free-stream direction, are not included in the calculation. In these regions the pressure coefficient is assumed to be zero. The pressure coefficient is also assumed to be zero on the leeward side of the panel when the sideslip angle β is greater than the local panel slope δ .

These methods have not been substantiated, since not enough test data are available.

Sample Problem

Given:

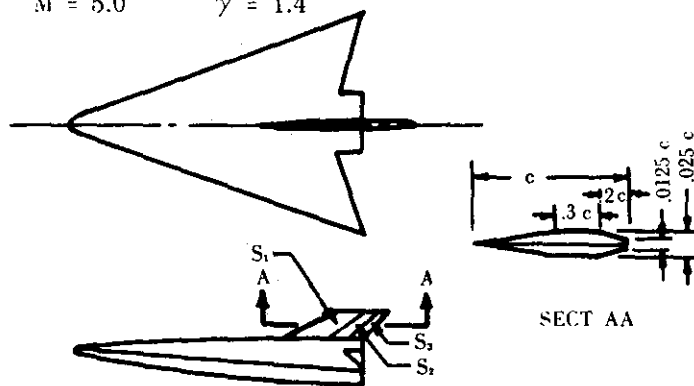
$$\frac{S_1}{S_v} = .5 \quad \frac{S_3}{S_v} = .2 \quad \frac{S_2}{S_v} = .3 \quad M = 5.0 \quad \gamma = 1.4$$

Compute (for $\beta = 1^\circ$):

$$\frac{\gamma + 1}{2} = 1.20$$

$$\frac{(\gamma + 1)^2}{4} = 1.44$$

$$M^2 - 1 = 24$$



Region	$\beta \pm \delta$ (rad)	
	Compression Side*	Expansion Side*
1	.04240	+.00750
2	.01745	-.01745
3	-.01396	-.04886

Values of pressure coefficient, C_p , calculated for each region by means of equation 5.3.1.1-h are listed in the following table (plus signs are used for flow compressions and minus signs for flow expansions in both tables).

Region	C_p	
	Compression Side	Expansion Side
1	.01960	+.00300
2	.00748	-.00674
3	-.00546	-.01728

*For a similar slab-sided surface. In actuality, both sides of region 1 are in compression and both sides of region 3 are in an expansion field.

Solution:

The sum of the pressure coefficients acting on the two sides of a given region is given by the difference of the two pressure coefficients

$$(C_p)_{\text{side compression}} - (C_p)_{\text{side extension}} = \Delta C_p$$

Thus, combining the pressure coefficients for each region and converting to side force coefficient gives

$$\begin{aligned}\Delta C_Y &= \Delta C_{p1} \frac{S_1}{S_V} + \Delta C_{p2} \frac{S_2}{S_V} + \Delta C_{p3} \frac{S_3}{S_V} \\ &= .0166 \times .5 + .01422 \times .3 + .01182 \times .2 \\ &= .015\end{aligned}$$

Therefore

$$(\Delta C_{Y_\beta})_V = -.015 \text{ per degree or } -.86 \text{ per radian}$$

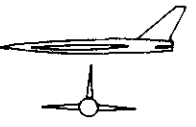
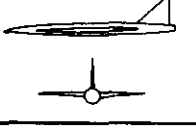
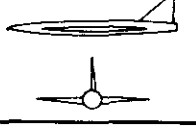
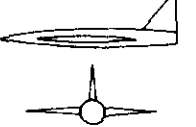
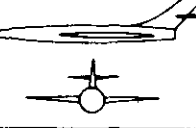
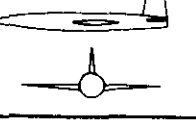
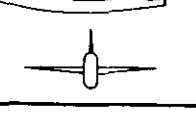
This is essentially the configuration of reference 19.

TABLE 5.3.1.1-A
APPARENT MASS FACTOR INDEX

Figure 5.3.1.1-25()	$\frac{r_1}{r_2}$	Horizontal Surface Position	$\left(\frac{r_2}{b/2}\right)_H$	$\left(\frac{r_1}{b}\right)$ added vertical panel	$\left(\frac{r_1}{b}\right)$ existing vertical panel
			$\left(\frac{r_2}{b/2}\right)_W$		
a	1.000	—	—	0 to 1.0	0.1 to 1.0
b			0		0 to 1.0
c			0.2		0.1 to 1.0
d	1.000	Mid	0.4	0 to 1.0	0.1 to 1.0
e			0.6		0.1 to 1.0
f			0.8		0.1 to 1.0
g		Tangent to body on same side	0		0 to 1.0
h			0.2		0.1 to 1.0
i	1.000		0.4	0 to 1.0	0.1 to 1.0
j			0.6		0.1 to 1.0
k			0.8		0.1 to 1.0
l		Tangent to body on side opposite	0		0 to 1.0
m			0.2		0.1 to 1.0
n	1.000		0.4	0 to 1.0	0.1 to 1.0
o			0.6		0.1 to 1.0
p			0.8		0.1 to 1.0
q	0.333	—	—	0 to 1.0	0.1 to 1.0
r			0		0 to 1.0
s			0.2		0.1 to 1.0
t	0.333	Mid	0.4	0 to 1.0	0.1 to 1.0
u			0.6		0.1 to 1.0
v			0.8		0.1 to 1.0
w	0.667	—	—	0 to 1.0	0.1 to 1.0
x			0		0 to 1.0
y			0.2		0.1 to 1.0
z	0.667	Mid	0.4	0 to 1.0	0.1 to 1.0
aa			0.6		0.1 to 1.0
bb			0.8		0.1 to 1.0
cc	1.500	—	—	0 to 1.0	0.1 to 1.0
dd			0		0 to 1.0
ee			0.2		0.1 to 1.0
ff	1.500	Mid	0.4	0 to 1.0	0.1 to 1.0
gg			0.6		0.1 to 1.0
hh			0.8		0.1 to 1.0
ii	3.000	—	—	0 to 1.0	0.1 to 1.0
jj			0		0 to 1.0
kk			0.2		0.1 to 1.0
ll	3.000	Mid	0.4	0 to 1.0	0.1 to 1.0
mm			0.6		0.1 to 1.0
nn			0.8		0.1 to 1.0
oo	1.000	Mid or tangent position	0 to ∞	1.0	1.0

TABLE 5.3.1.1-B*

SURSONIC CONTRIBUTION OF VERTICAL PANELS TO C_{Y_B}
DATA SUMMARY AND SUBSTANTIATION

Ref.	Configuration Sketch	Surface	A	b (in.)	λ_V	λ_{V_e}	Λ_{LE} (deg)	Airfoil	r_1/r_2	x/c_v	Panel Added	M	Method 1			Method 3			$(\Delta C_{Y_B})_{Test}$ (per rad)	Percent Error					
													$k(C_{L_\alpha})_{V(BH)}$ (per rad)	$\left(1 + \frac{\partial \sigma}{\partial \beta}\right) \frac{q_v}{q_\infty}$	$(\Delta C_{Y_B})_{Calc.}$ (per rad)	$(C_{L_\alpha})_v$ (per rad)	K	$(\Delta C_{Y_B})_{Calc.}$ (per rad)	Method 1	Method 3					
6		W	3.0	41.56	—	—	53.1	—	1.000	.50	BWHV _S -BW	.25	.431	1.115	-.481	—	—	—	—	-.54	10.9	—			
										.55	BWHV _L -BW	.25	.597	1.230	-.734	—	—	—	—	-.76	3.4	—			
		H	4.0	22.42	—	—	—	—		—	BV _S -B	.25	.428	1.0	-.428	.370	1.16	-.429	—	-.44	2.7	2.5			
		V _S	1.50	13.28	.160	.195	54.0	NACA 0003.5-64		—	BV _L -B	.25	.578	1.0	-.578	.514	1.07	-.550	—	-.56	3.2	1.8			
		V _L	1.50	15.23	.160	.189	54.0	NACA 0003.5-64		.55	BHV _L -B	.25	.597	1.0	-.597	.514	1.25	-.642	—	-.63	5.2	1.9			
		—	—	—	—	—	—	—		.50	BHV _S -B	.25	.431	1.0	-.431	.370	1.34	-.496	—	-.47	8.3	5.5			
8		W	2.31	36.50	—	—	—	—	1.000	—	BV-B	.17	.254	1.0	-.254	.239	.94	-.225	—	-.25	1.6	10.0			
										—	—	—	—	—	—	—	—	—	—	—	—				
		W	2.31	36.50	—	—	—	—	1.000	—	BV-B	.17	.317	1.0	-.317	.293	1.01	-.296	—	-.30	5.7	1.3			
										—	—	—	—	—	—	—	—	—	—	—	—				
		W ₁	2.31	36.50	—	—	60.0	—	1.000	—	BW ₁ V-BW ₁	.17	.446	1.050	-.468	—	—	—	—	—	-.43	8.8	—		
										—	BW ₂ V-BW ₂	.17	.446	.918	-.409	—	—	—	—	—	-.34	20.3	—		
		W ₃	2.31	36.50	—	—	60.0	—		—	BW ₃ V-BW ₃	.17	.446	1.184	-.528	—	—	—	—	—	-.49	7.8	—		
										—	BV-B	.17	.446	1.0	-.446	.401	1.15	-.461	—	-.42	6.2	9.8	—		
9		W	4.0	36.00	—	—	46.7	—	1.000	1.00	BWHV-BW	.6	.461	1.247	-.575	—	—	—	—	—	-.46	25.0	—		
										—	BV-B	.6	—	—	—	—	.460	1.07	-.492	—	-.49	—	0.4	—	
		V	1.18	10.19	.500	.61	57.5	NACA 63(10)A009		—	—	—	—	—	—	—	—	—	—	—	—	—	—		
10		W	4.0	36.00	—	—	3.6	—	1.000	.25	BWHV-BW	.13	.430	.990	-.426	—	—	—	—	—	-.51	16.5	—		
										.25	BHV-BH	.13	—	—	—	—	.400	1.26	-.504	—	-.53	—	4.9	—	
		H	4.0	16.10	—	—	—	—		—	—	—	—	—	—	—	.331	1.53	-.506	—	-.53	—	4.5	—	
		W	4.0	36.00	—	—	—	—	2.210	.25	BHV-BH	.13	—	—	—	—	.448	1.11	-.497	—	-.49	—	—	1.4	—
										—	—	—	—	—	—	—	.448	1.11	-.497	—	-.49	—	—	—	
		H	4.0	16.10	—	—	—	—		.451	.25	BHV-BH	.13	—	—	—	.448	1.11	-.497	—	-.49	—	—	—	
		V	2.02	9.90	.600	.678	3.5	NACA 65A008		—	—	—	—	—	—	—	—	—	—	—	—	—	—		

*This table is a condensed form of that appearing in reference 3. Additional substantiation can be obtained from this reference.

TABLE 5.3.1.1-C*
SUPERSONIC CONTRIBUTION OF VERTICAL PANELS TO $C_{Y\beta}$
DATA SUMMARY AND SUBSTANTIATION

Ref.	Configuration Sketch	r_1/r_2	Surface	A	b (in.)	λ_{V_e}	ΔL_E (deg)	Panel Added	M	$(C_{L\alpha})_V$ (per rad)	K'	$(\Delta C_{V\beta})$ Calc. (per rad)	$(\Delta C_{V\beta})$ Test (per rad)	Percent Error e
15		1.000	W	2.45	10.48	.427	27.1	BWV-BW	1.82	-.418	1.41	-.589	-.56	5.2
			V	1.32	3.80	.378	44.0							
16		1.000	W	4.0	25.32	.538	38.1	BV-B	1.61	-.420	1.25	-.525	-.52	0.96
			H	3.5	12.12	.541	38.5							
			V	3.0	7.48	.192	50.4	BWHV-BWH	1.61	-.420	1.26	-.529	-.487	8.6
17		1.170	W	3.18	19.08	.483	48.0	BWHU-BWH	2.01	-.021	2.76	-.056	-.057	1.8
			H	3.06	9.12	.517	48.0							
			V	1.73	7.08	.392	49.2	BWHUV-BWHU	2.01	-.398	1.32	-.525	-.52	1.0
			U	---	2.56	.00	70.2							
17		.940	W	3.86	32.41	.313	49.7	BWV ₀ -BW	1.61	-.247	1.45	-.358	-.33	8.5
			H	3.54	15.74	.402	49.6	BWV ₀ -BW	2.01	-.195	1.72	-.335	-.30	11.7
			V ₀	1.10	7.20	.416	23.5	BWHV ₀ -BWH	1.61	-.247	1.49	-.368	-.37	.5
			V _{ext}	1.61	8.66	.260	23.5	BWHV ₀ -BWH	2.01	-.195	1.72	-.335	-.30	11.7
			V _{127%}	1.45	8.74	.290	23.5	BWHV _{ext} -BWH	1.61	-.321	1.32	-.424	-.41	3.4
18		1.000	W	4.	24.00	.225	49.4	BWV-BW	1.41	-.788	1.06	-.836	-.92	9.1
			V	1.29	8.59	.235	20.6	BWV-BW	2.01	-.470	1.16	-.545	-.65	16.2
18		1.000	W	4.	24.00	.225	49.4	BWV-BW	1.41	-.810	1.04	-.842	-.88	4.3
			V	1.29	8.59	.235	41.6	BWV-BW	2.01	-.482	1.12	-.540	-.60	10.0
18		1.000	W	4.	24.00	.225	49.4	BWV-BW	1.41	-.761	1.04	-.792	-.85	6.8
			V	1.29	8.59	.235	52.1	BWV-BW	2.01	-.512	1.06	-.542	-.53	2.3
18		1.000	W	4.	24.00	.225	49.4	BWV-BW	1.41	-.679	1.04	-.706	-.67	5.4
			V	1.29	8.59	.235	62.5	BWV-BW	2.01	-.554	1.04	-.586	-.50	17.2
20		1.0	W	3.00	4.33	.140	38.83	BWHUV-BWUV	6.86	.0670	1.79	-.120	---	---
			H	3.52	2.69	.261	22.63	BWHUV-BWH	6.86	.1110	1.758	-.195	---	---
			V = U	1.50	1.35	.333	22.63	BWHUV-BW	6.86	---	---	-.315**	-.321	1.9

*This table is a condensed form of that appearing in reference 3. Additional substantiation can be obtained from this reference.

**Sum of the two terms above.

REFERENCES

1. Decker, J., et al: USAF Stability and Control Handbook. M-03671, 1956. (C) Title Unclassified
2. Anon.: Royal Aeronautical Society Data Sheets—Aerodynamics, 1955. (U)
3. Goodwin, F. K., and Kaattari, G. E.: Estimation of Directional Stability Derivatives at Small Angles and Supersonic Speeds. NASA Memo 12-2-58A, 1958. (U)
4. Bryson, A. E., Jr.: Evaluation of the Inertia Coefficients of the Cross Section of a Slender Body. Jour. Aero. Sci., Vol. 21, No. 6, June 1954. (U)
5. Spencer, B., Jr.: A Simplified Method for Estimating Subsonic Lift-Curve Slope at Low Angles of Attack for Irregular Planform Wings. NASA TM X-525, 1961. (C) Title Unclassified
6. Savage, H. F., and Tinling, B. E.: The Subsonic Static Aerodynamic Characteristics of an Airplane Model Having a Triangular Wing of Aspect Ratio 3. II—Lateral and Directional Characteristics. NACA TN 4042, 1957. (U)
7. Paulson, J. W., and Boisseau, P. C.: Low-Speed Investigation of the Effect of Small Canard Surfaces on the Directional Stability of a Sweptback-Wing Fighter-Airplane Model. NACA RM L56F19a, 1956. (C) Title Unclassified
8. Goodman, A., and Thomas, D. F., Jr.: Effects of Wing Position and Fuselage Size on the Low-Speed Static and Rolling Stability Characteristics of a Delta-Wing Model. NACA TN 3063, 1954. (U)
9. Wiggins, J. W., Kuhn, R. E., and Fournier, P. G.: Wind-Tunnel Investigation to Determine the Horizontal- and Vertical-Tail Contributions to the Static Lateral Stability Characteristics of a Complete-Model Swept-Wing Configuration at High Subsonic Speeds. NACA TN 3818, 1956. (U)
10. Letko, W., and Williams, J. L.: Experimental Investigation at Low Speed of Effects of Fuselage Cross Section on Static Longitudinal and Lateral Stability Characteristics of Models Having 0° and 45° Sweptback Surfaces. NACA TN 3551, 1955. (U)
11. Hallissy, J. M., Jr.: Transonic Wind-Tunnel Measurements of Static Lateral and Directional Stability and Vertical-Tail Loads for a Model with a 45° Sweptback Wing. NACA RM L55L19, 1956. (U)
12. Arabian, D. D., and Schmeer, J. W.: Lateral Stability and Control Measurements of a Fighter-Type Airplane With Low-Aspect-Ratio Unswept Wing and a Tee-Tail. NACA RM L55F08, 1956. (U)
13. Osborne, R. S.: Aerodynamic Characteristics of a 0.0667-Scale Model of the North American X-15 Research Airplane at Transonic Speeds. NASA TM X-24, 1959. (U)
14. Spearman, M. L., Robinson, R. B., and Driver, C.: The Effects of the Addition of Small Fuselage-Mounted Fins on the Static Directional Stability Characteristics of a Model of a 45° Swept-Wing Airplane at Angles of Attack Up to 15.3° at a Mach Number of 2.01. NACA RM L56D16A, 1956. (C) Title Unclassified
15. Spearman, M. L., and Driver, C.: Longitudinal and Lateral Stability Characteristics of a Low-Aspect-Ratio Unswept-Wing Airplane Model at Mach Numbers of 1.82 and 2.01. NACA RM L56H06, 1957. (U)
16. Spearman, M. L.: Static Lateral and Directional Stability and Effective Sidewash Characteristics of a Model of a 35° Swept-Wing Airplane at a Mach Number of 1.61. NACA RM L56E23, 1956. (U)
17. Spearman, M. L., and Robinson, R. B.: Static Lateral Stability and Control Characteristics of a Model of a 45° Swept-Wing Fighter Airplane With Various Vertical Tails at Mach Numbers of 1.41, 1.61, and 2.01. NACA RM L56D05, 1956. (U)
18. Spearman, M. L., and Robinson, R. B.: Investigation of the Aerodynamic Characteristics in Pitch and Sideslip of a 45° Swept-Wing Airplane Configuration With Various Vertical Locations of the Wing and Horizontal Tail. Static Lateral and Directional Stability; Mach Numbers of 1.41 and 2.01. NACA RM L57J25a, 1957. (U)
19. Dennis, D. H., and Petersen, R. H.: Aerodynamic Performance and Static Stability at Mach Numbers Up to 5 of Two Airplane Configurations With Favorable Lift Interference. NASA Memo 1-8-59A, 1959. (U)
20. Ridyard, H. W., Fetterman, D. E., Jr., and Penland, J. A.: Static Lateral Stability Data From an Exploratory Investigation at a Mach Number of 6.86 of an Airplane Configuration Having a Wing of Trapezoidal Planform. NACA RM L55A21a, 1955. (U)

SUBSONIC
METHOD 1—SINGLE VERTICAL TAILS

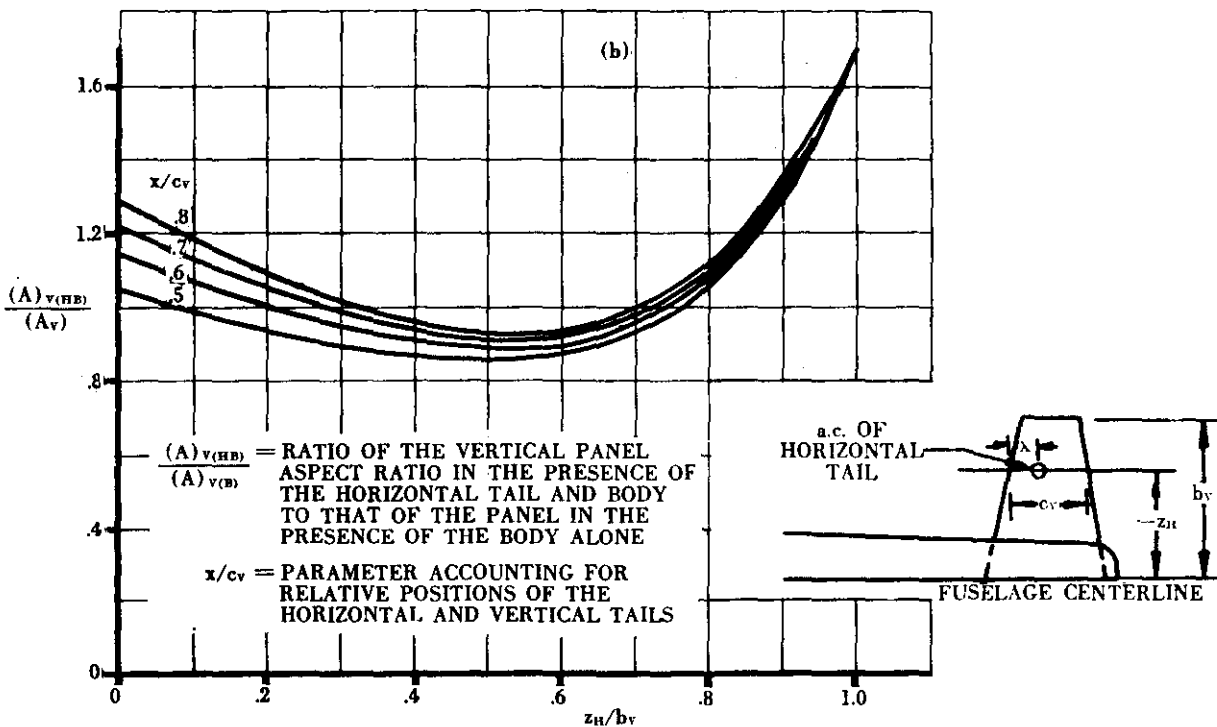
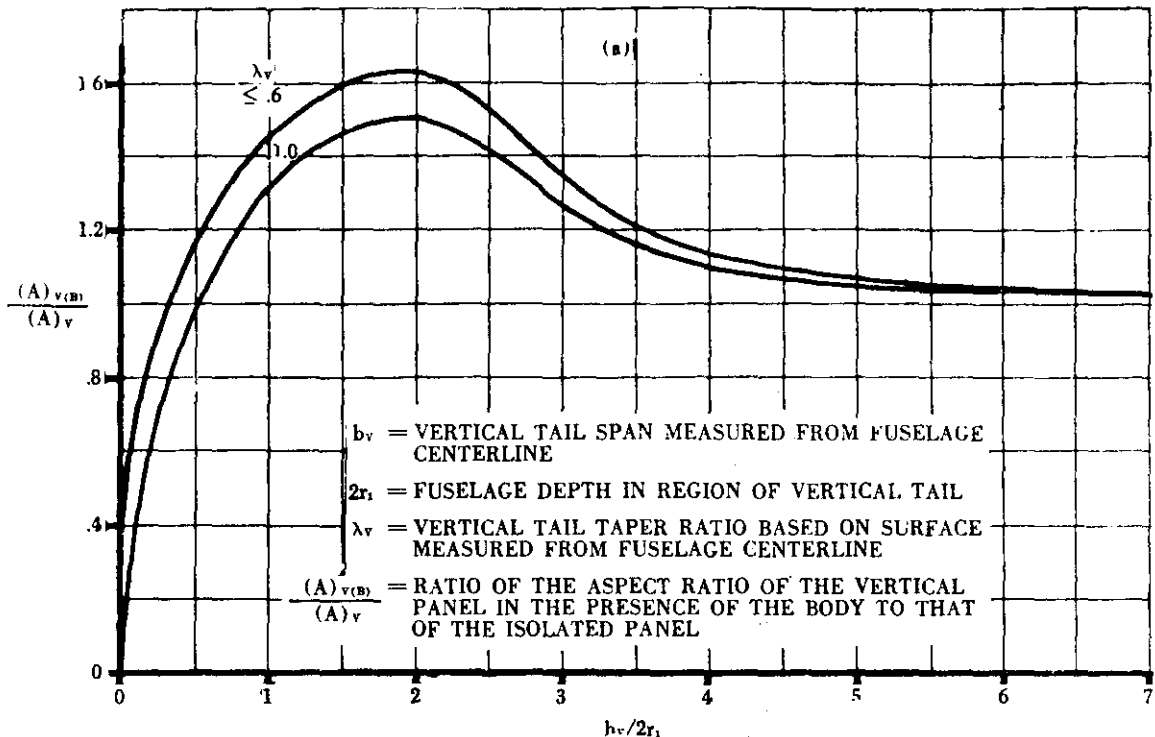


FIGURE 5.3.1.1-22 CHARTS FOR ESTIMATING THE SIDESLIP DERIVATIVE $(C_{r\beta})_{v(WBH)}$ FOR SINGLE VERTICAL TAILS

SUBSONIC
METHOD 1—SINGLE VERTICAL TAILS

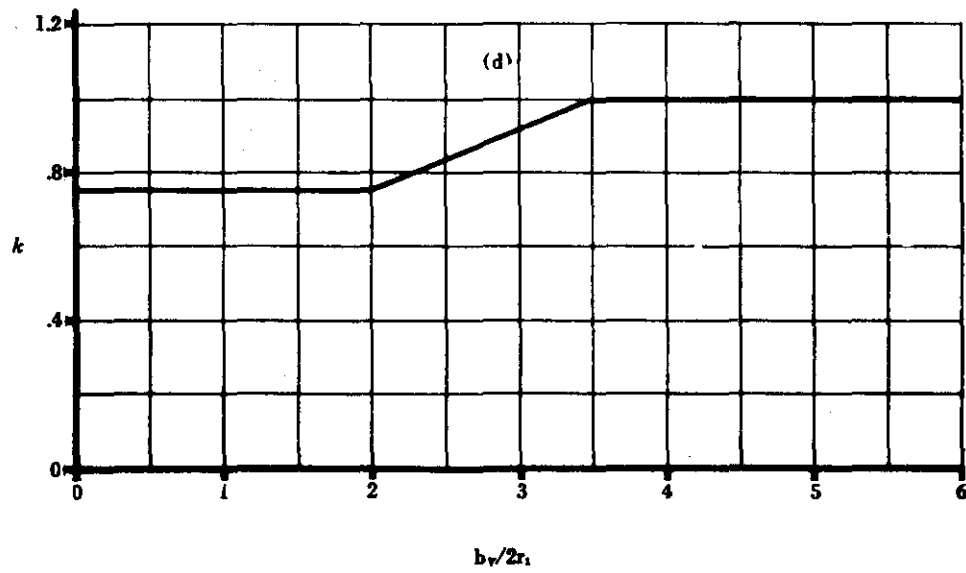
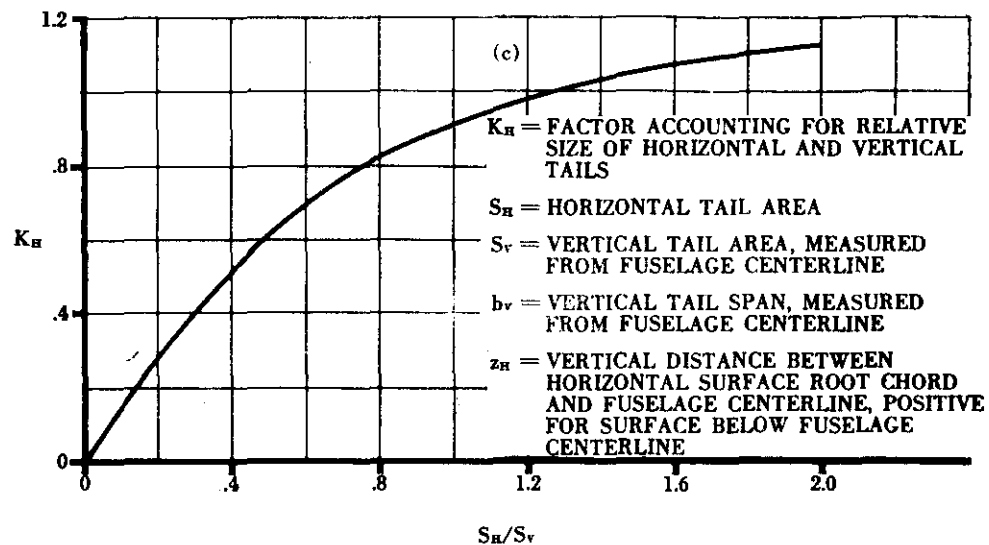


FIGURE 5.3.1.1-22(CONTD) CHARTS FOR ESTIMATING THE SIDESLIP DERIVATIVE $(C_{r\beta})_{V(WBH)}$ FOR SINGLE VERTICAL TAILS

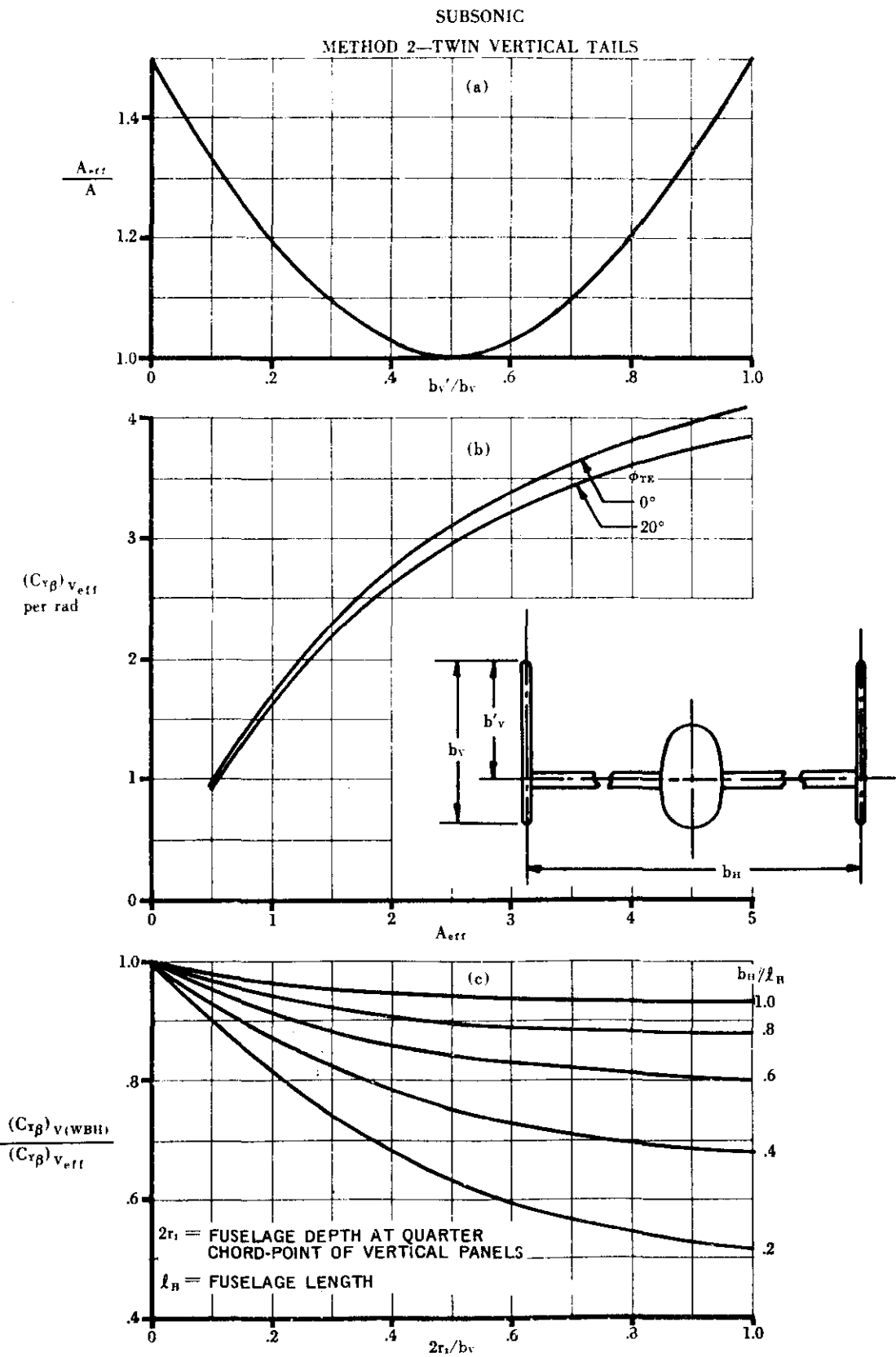


FIGURE 5.3.1.1-24 CHARTS FOR ESTIMATING THE SIDESLIP DERIVATIVE $(C_{r\beta})_{V(WBH)}$ FOR TWIN VERTICAL TAILS.

SUBSONIC AND SUPERSONIC

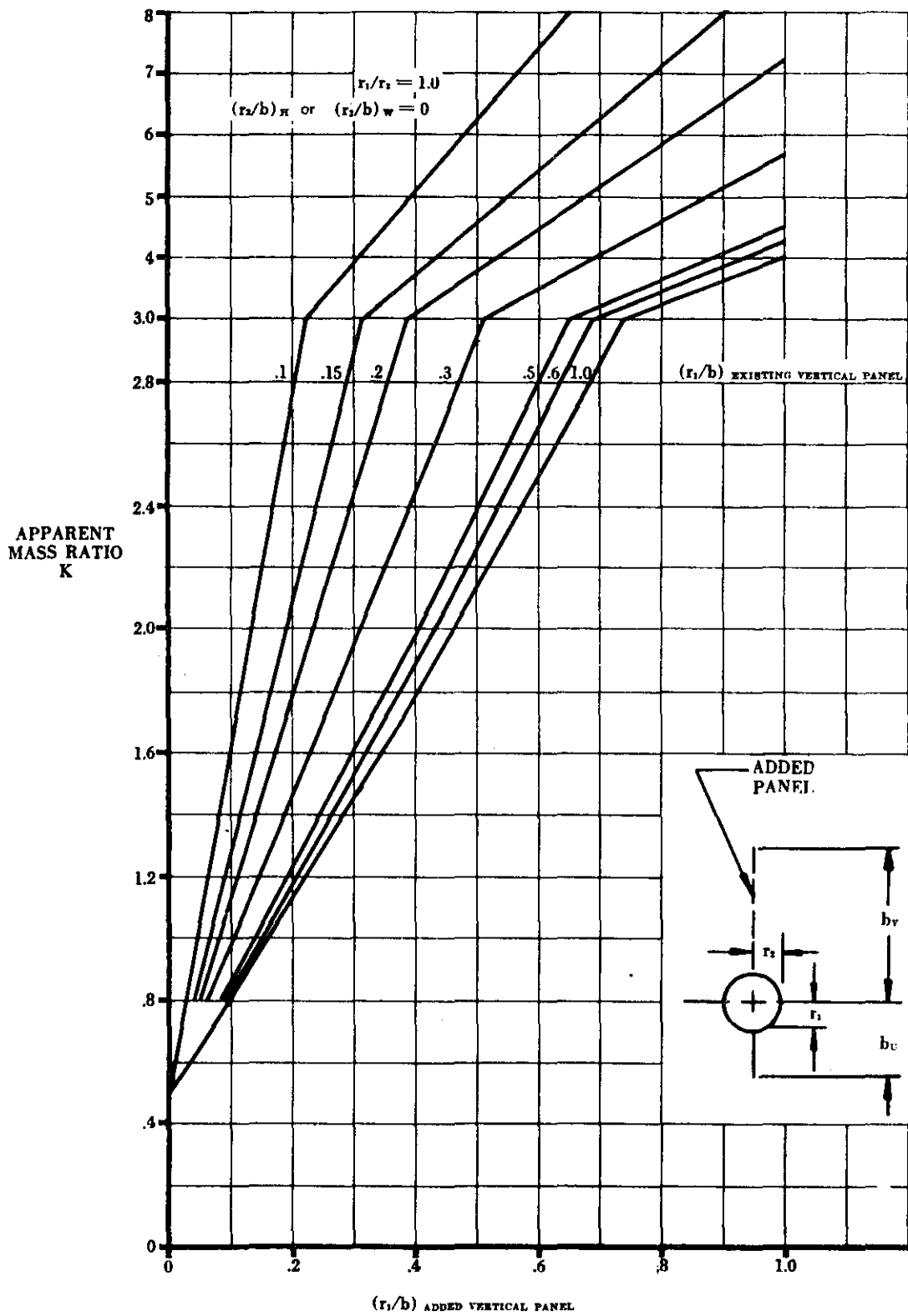


FIGURE 5.3.1.1-25a APPARENT MASS FACTORS

SUBSONIC AND SUPERSONIC

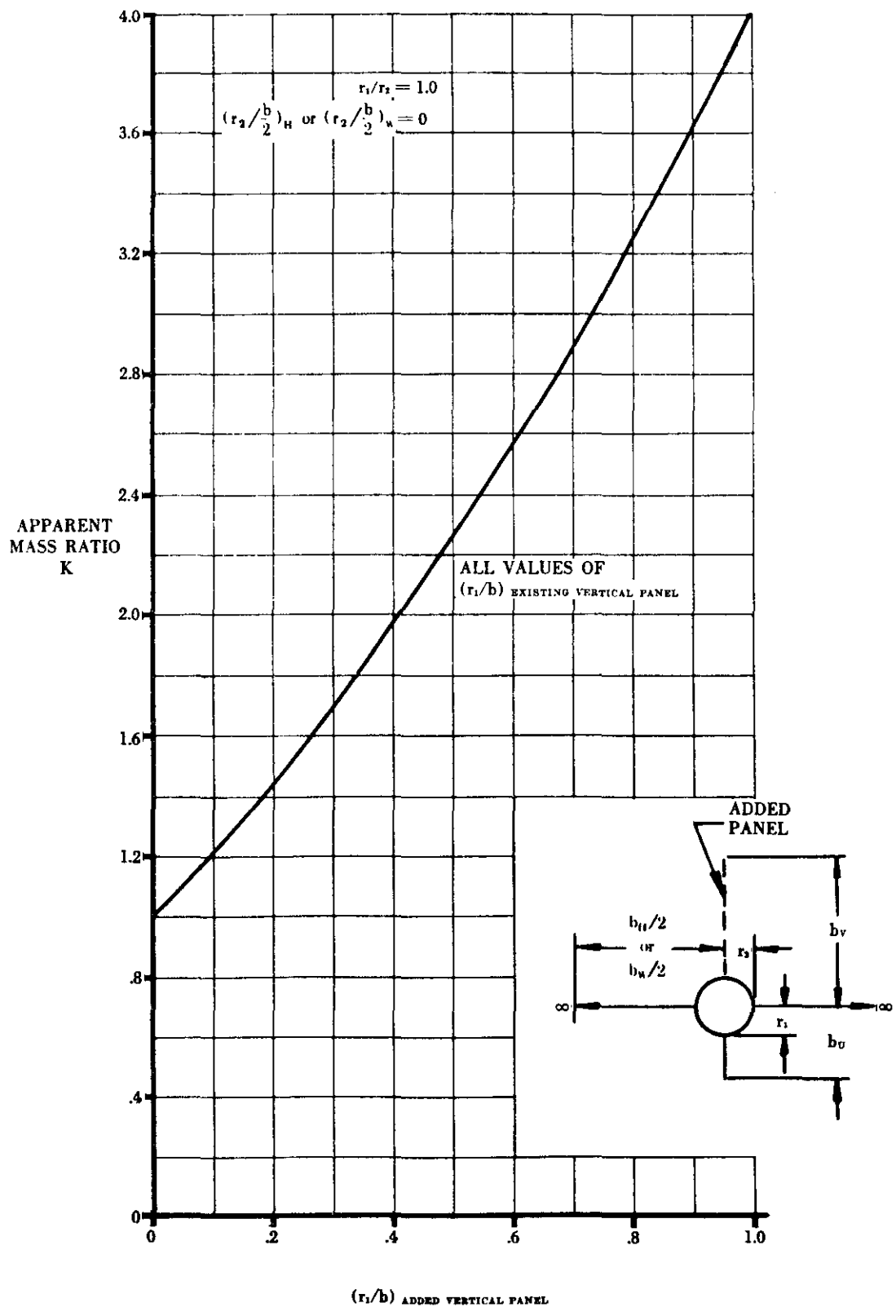


FIGURE 5.3.1.1-25b APPARENT MASS FACTORS (CONTD)

SUBSONIC AND SUPERSONIC

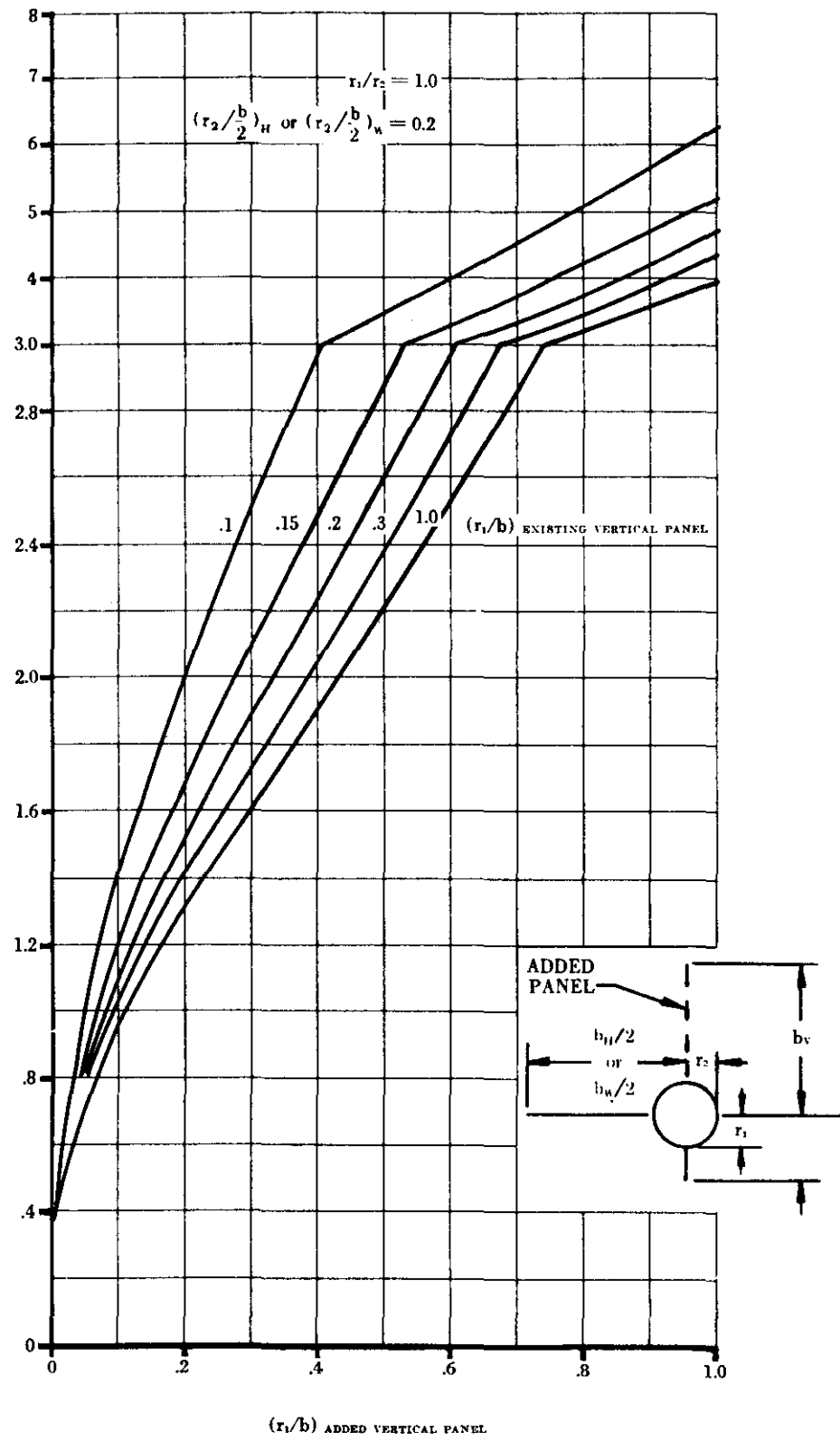


FIGURE 5.3.1.1-25c APPARENT MASS FACTORS (CONT'D)

SUBSONIC AND SUPERSONIC

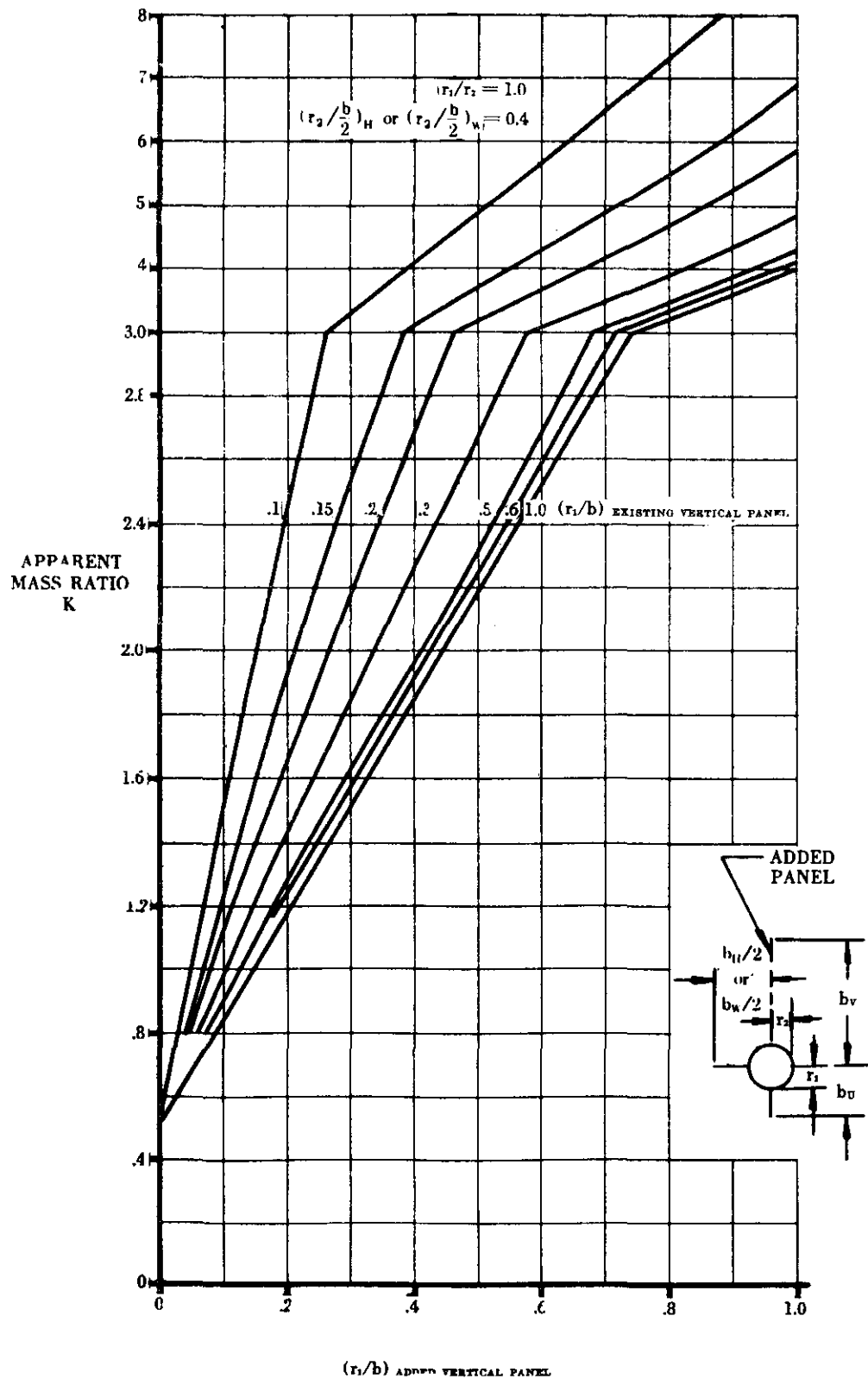


FIGURE 5.3.1.1-25d APPARENT MASS FACTORS (CONTD)

SUBSONIC AND SUPERSONIC

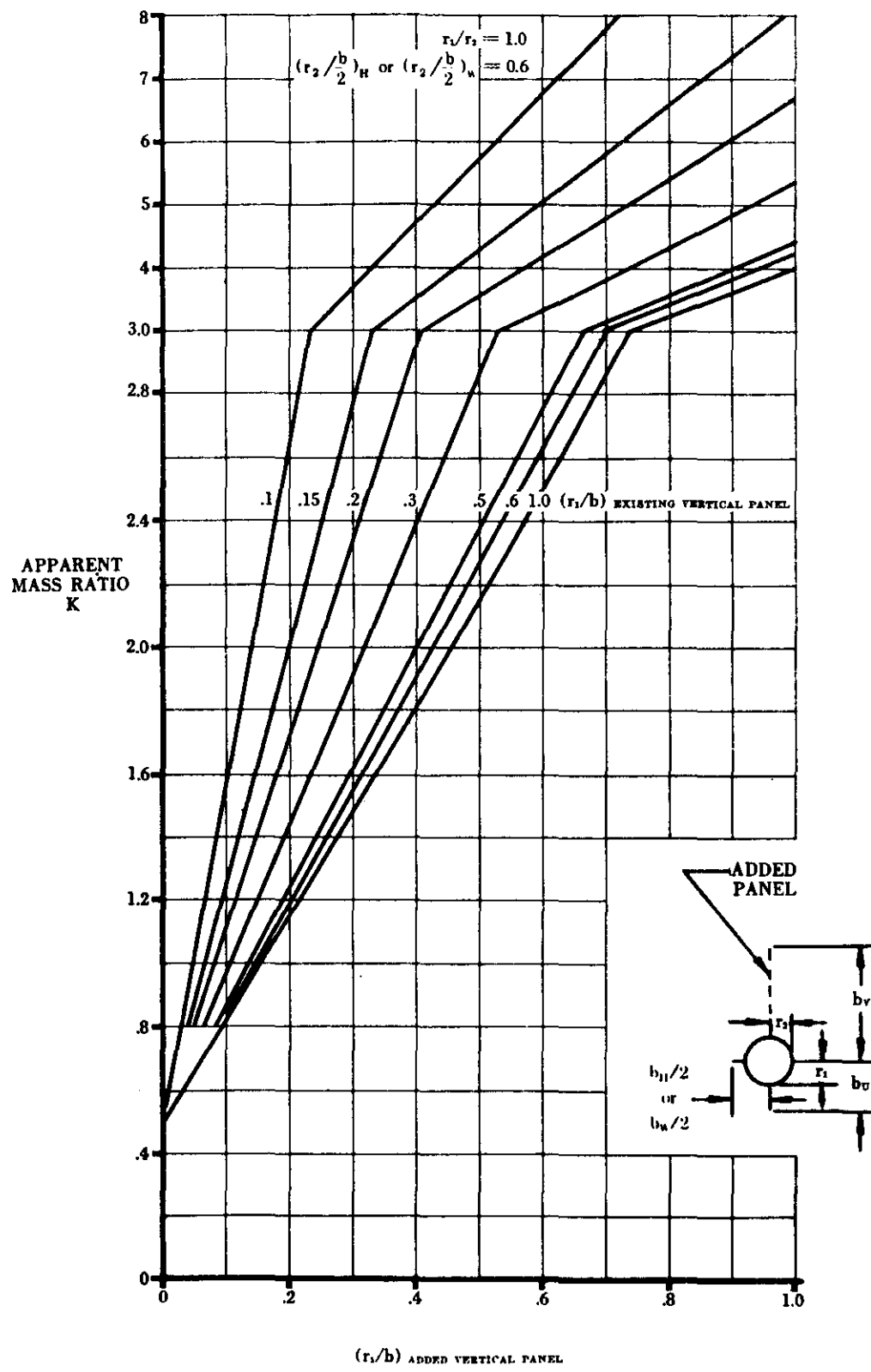


FIGURE 5.3.1.1-25e APPARENT MASS FACTORS (CONTD)

SUBSONIC AND SUPERSONIC

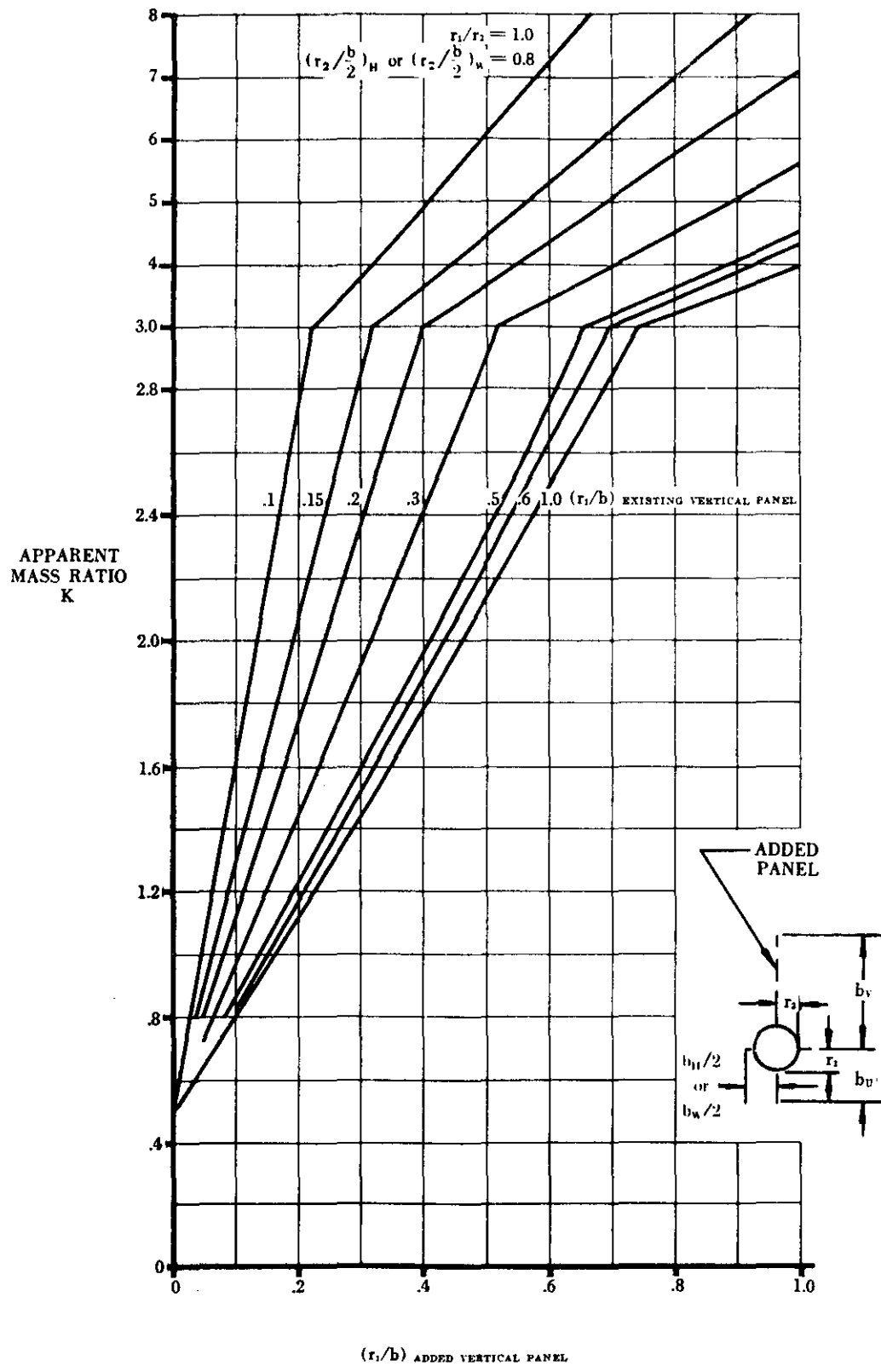


FIGURE 5.3.1.1-25f APPARENT MASS FACTORS (CONTD)

SUBSONIC AND SUPERSONIC

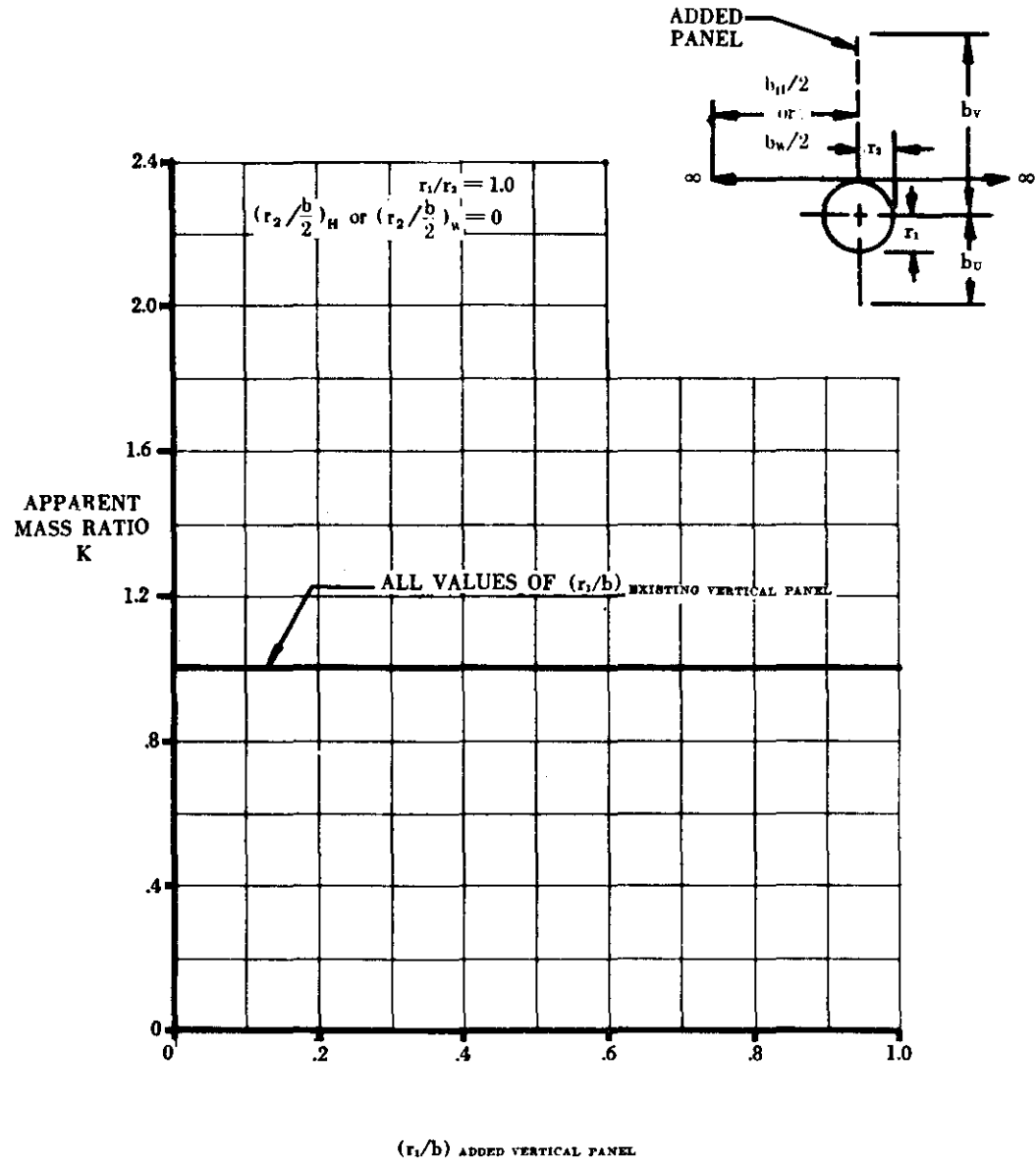


FIGURE 5.3.1.1-25g APPARENT MASS FACTORS (CONTD)

SUBSONIC AND SUPERSONIC

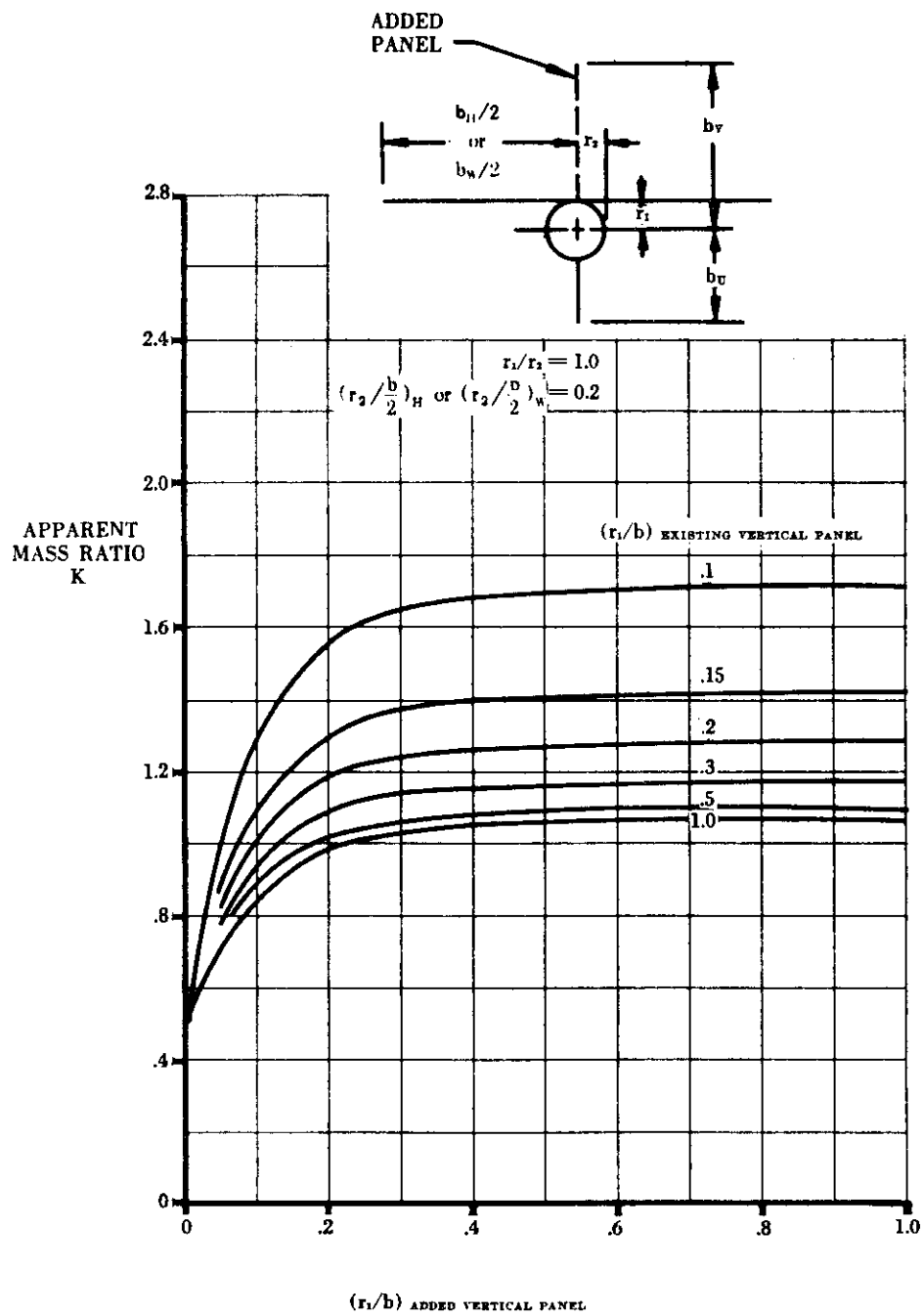


FIGURE 5.3.1.1-25h APPARENT MASS FACTORS (CONTD)

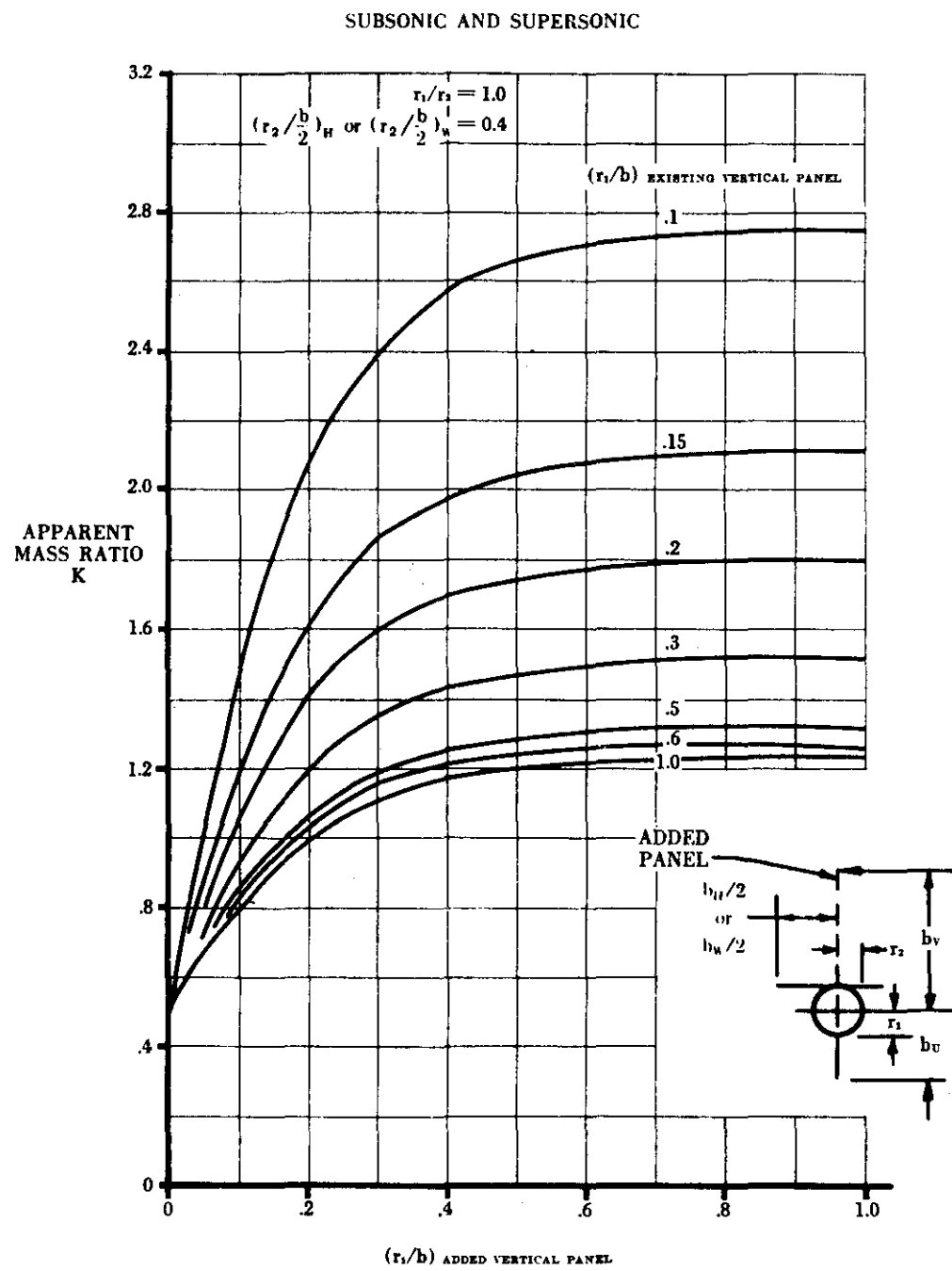


FIGURE 5.3.1.1-25i APPARENT MASS FACTORS (CONTD)

SUBSONIC AND SUPERSONIC

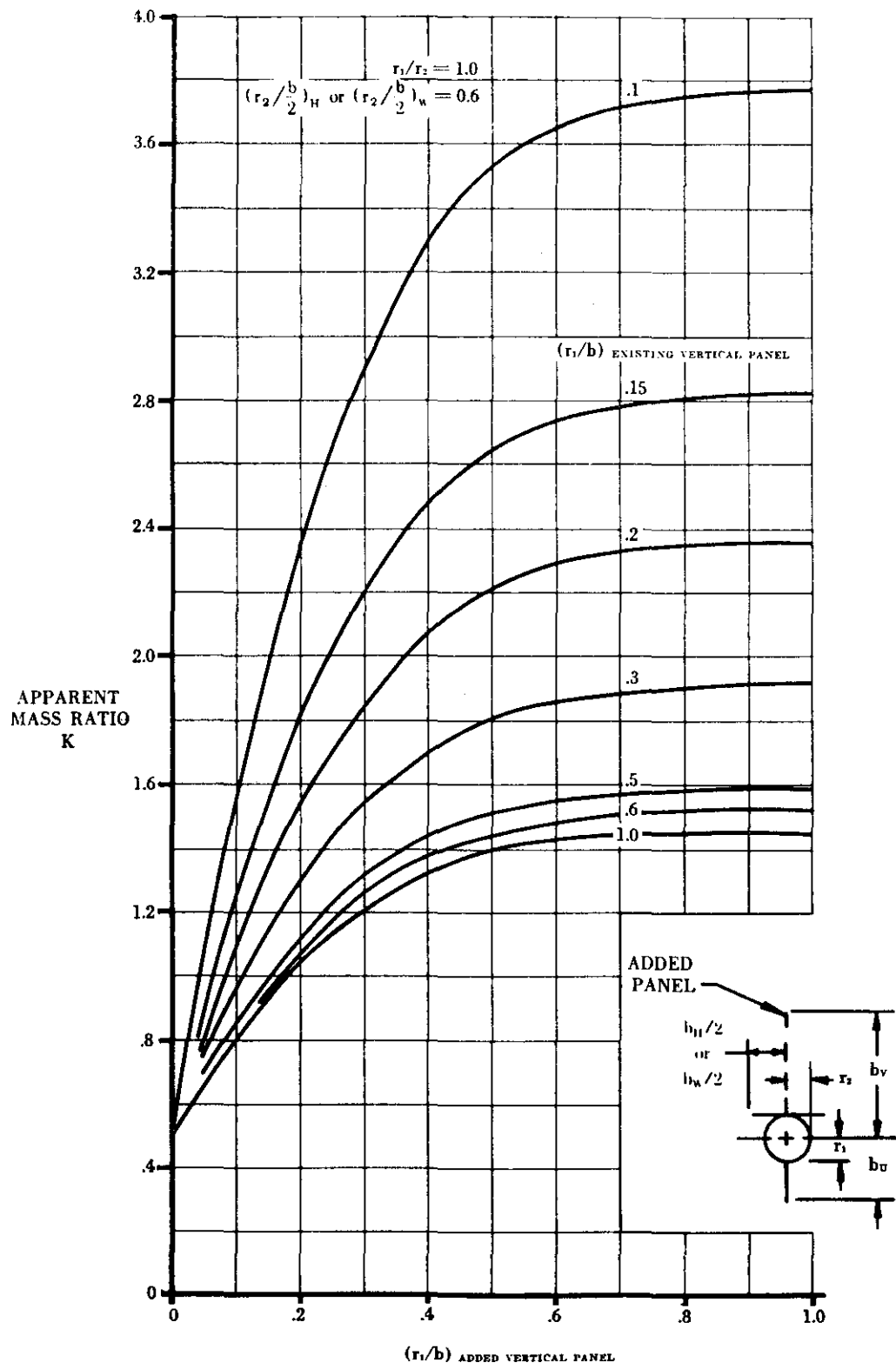


FIGURE 5.3.1.1-25j APPARENT MASS FACTORS (CONTD)

SUBSONIC AND SUPERSONIC

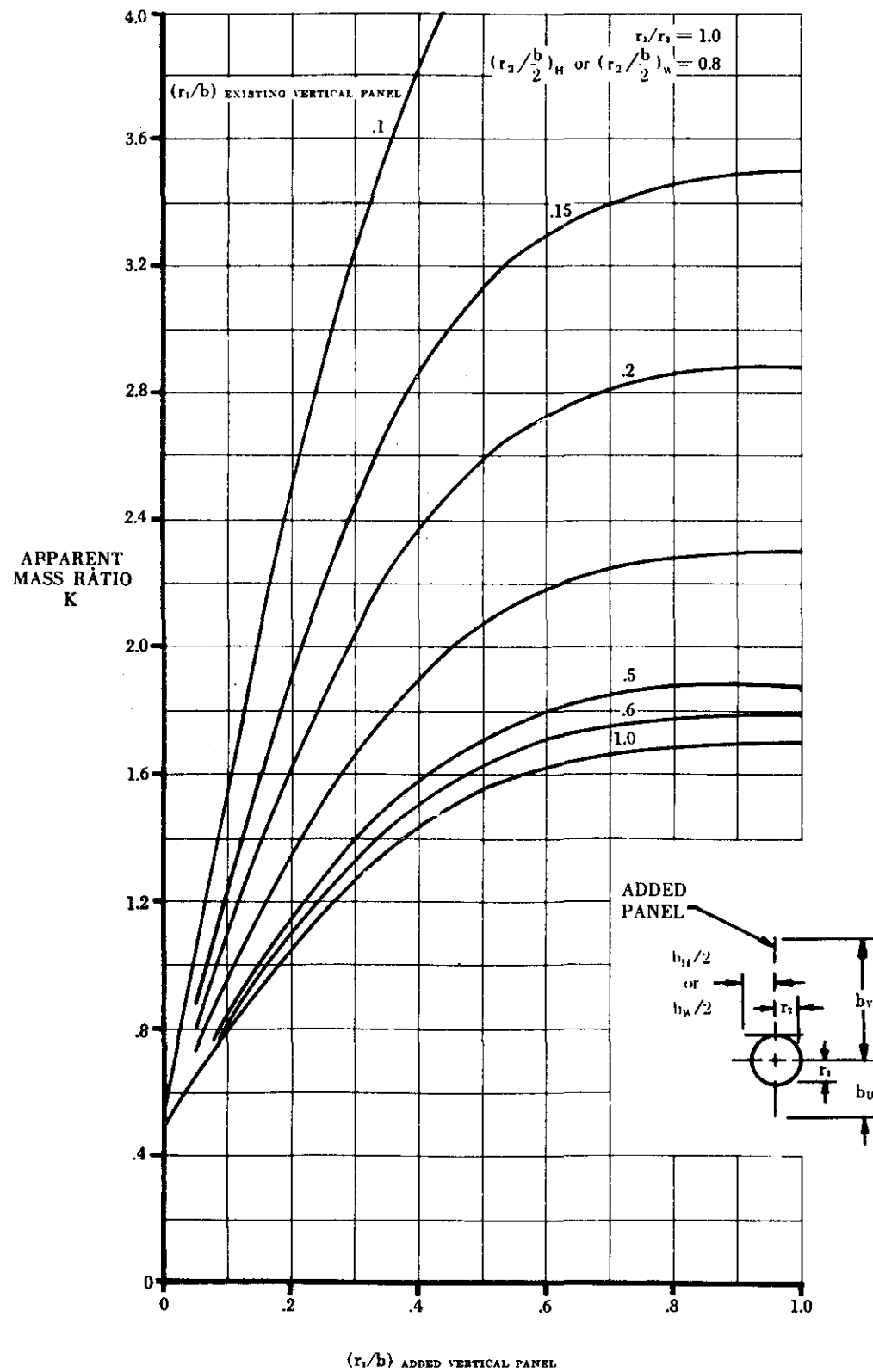


FIGURE 5.3.1.1-25k APPARENT MASS FACTORS (CONTD)

SUBSONIC AND SUPERSONIC

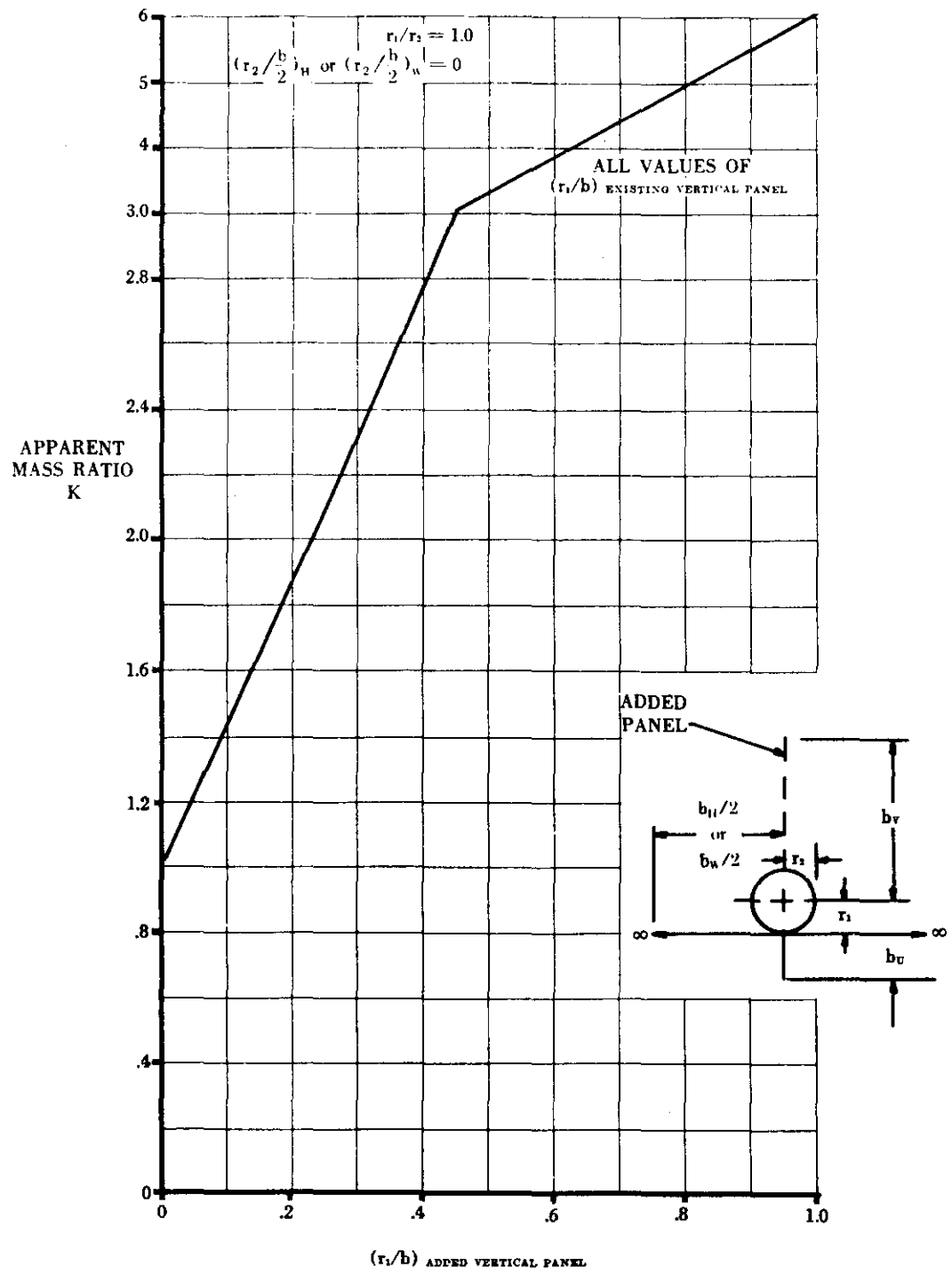


FIGURE 5.3.1.1-25I APPARENT MASS FACTORS· (CONTD)

SUBSONIC AND SUPERSONIC

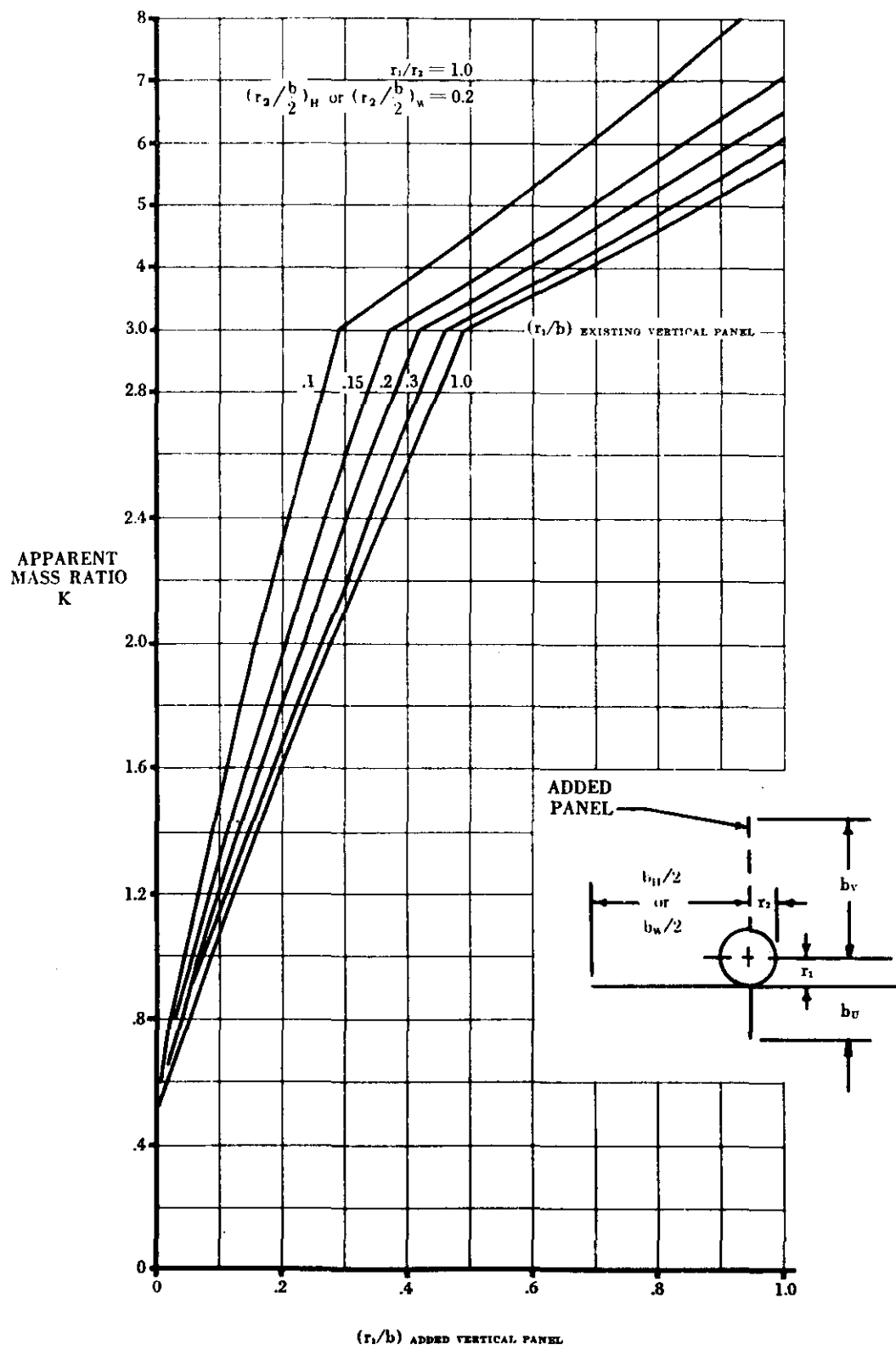


FIGURE 5.3.1.1-25m APPARENT MASS FACTORS (CONTD)

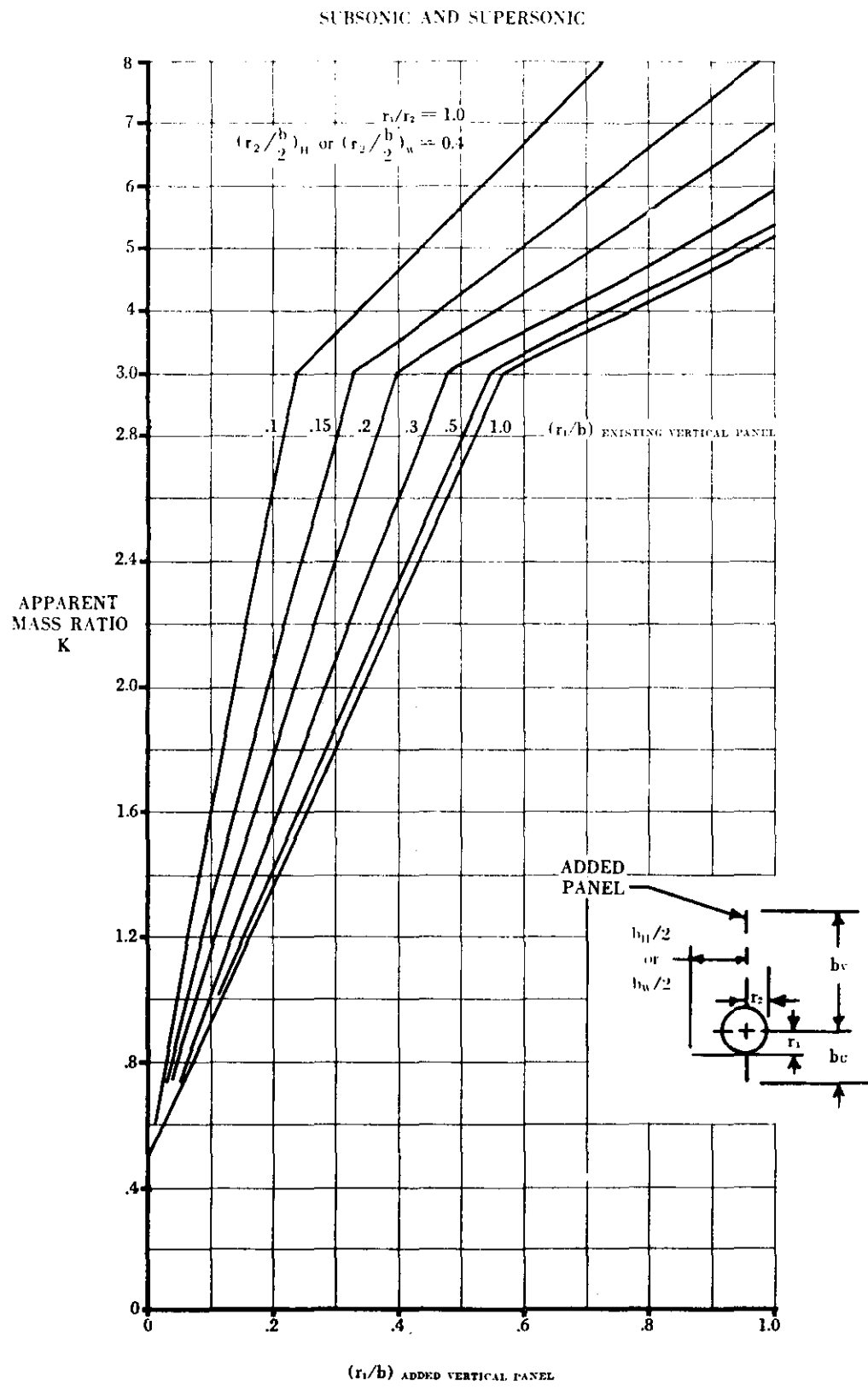


FIGURE 5.3.1.1-25n APPARENT MASS FACTORS (CONTD)

SUBSONIC AND SUPERSONIC

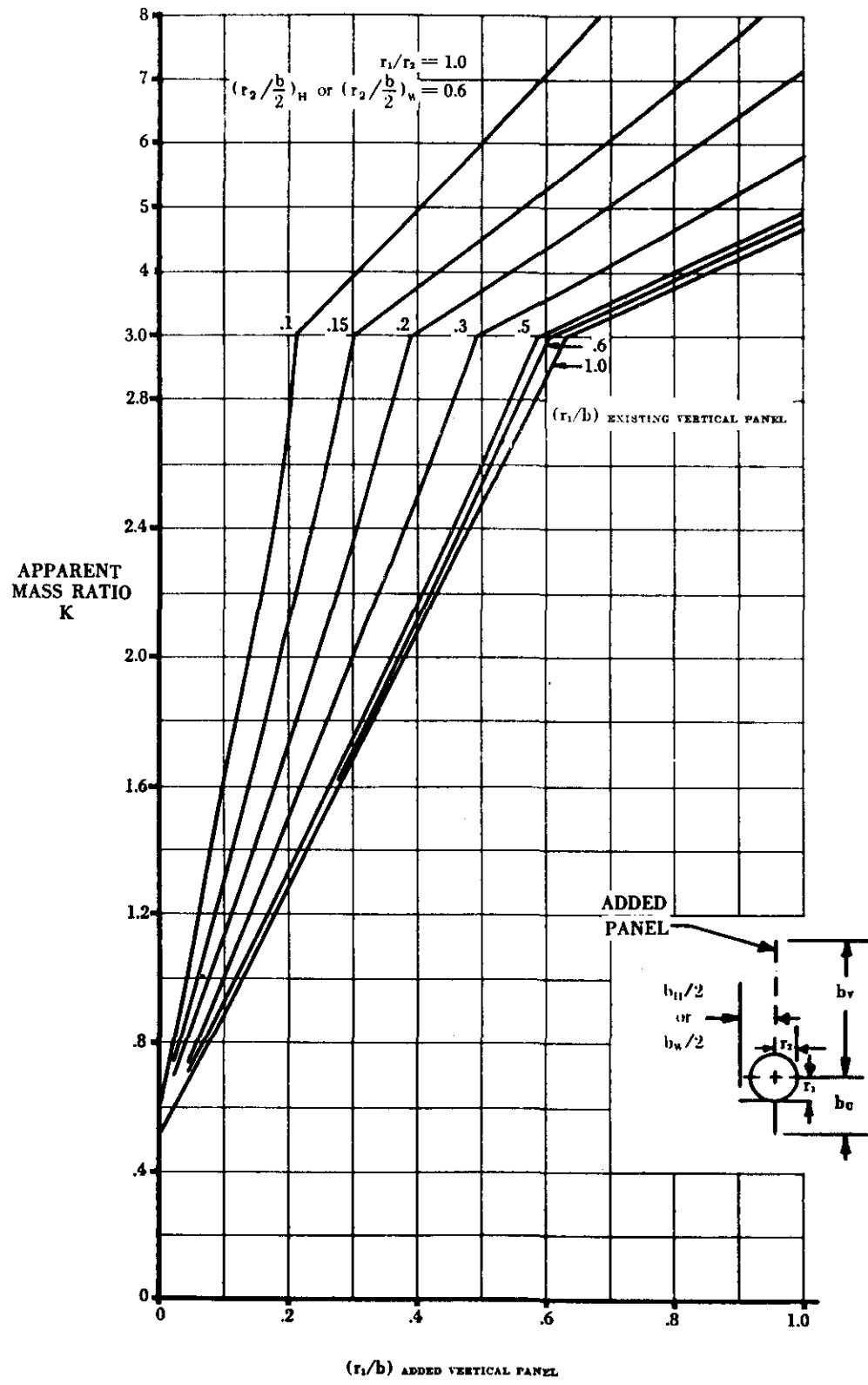


FIGURE 5.3.1.1-25o APPARENT MASS FACTORS (CONTD)

SUBSONIC AND SUPERSONIC

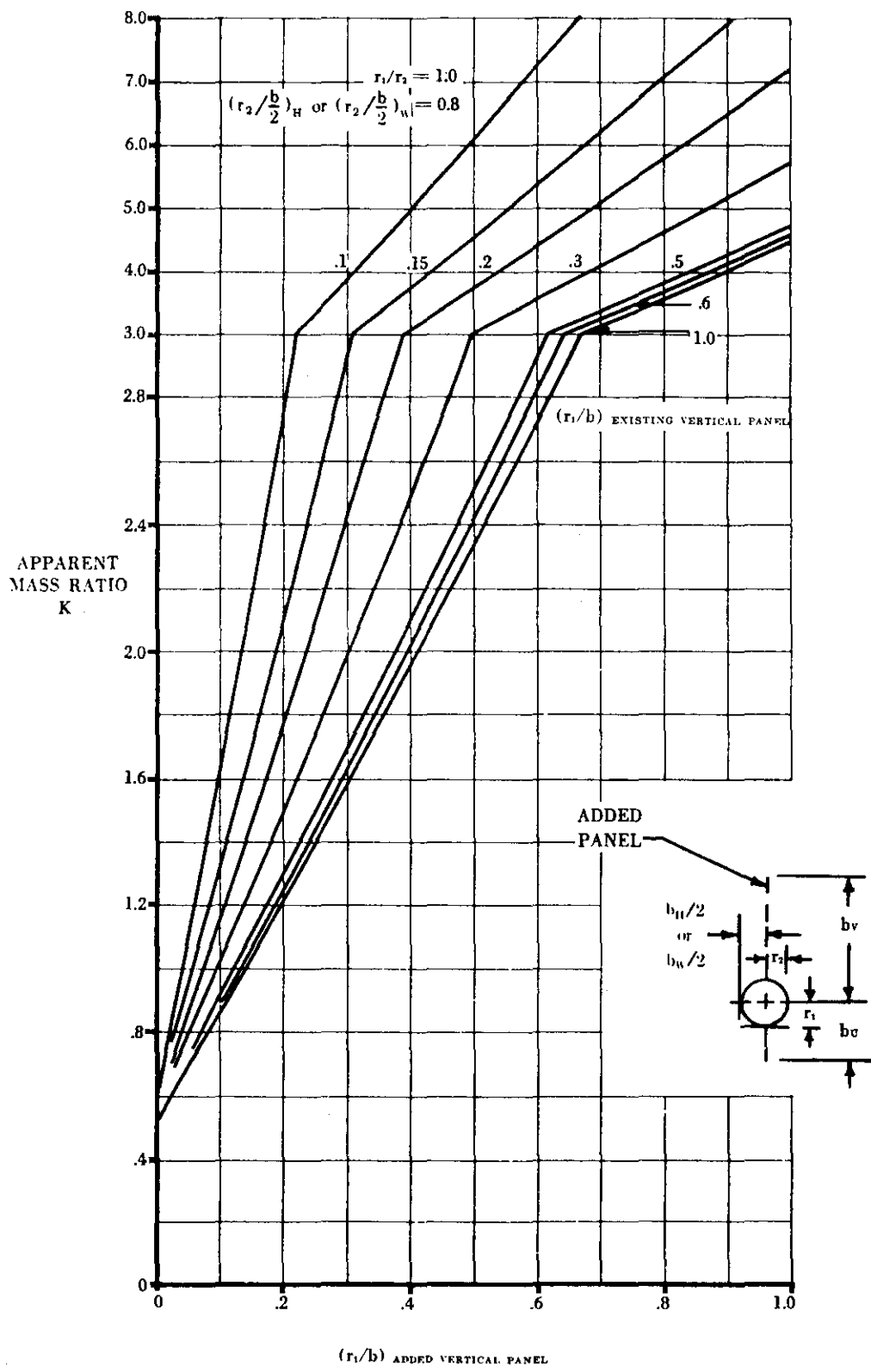


FIGURE 5.3.1.1-25p APPARENT MASS FACTORS (CONT'D)

SUBSONIC AND SUPERSONIC

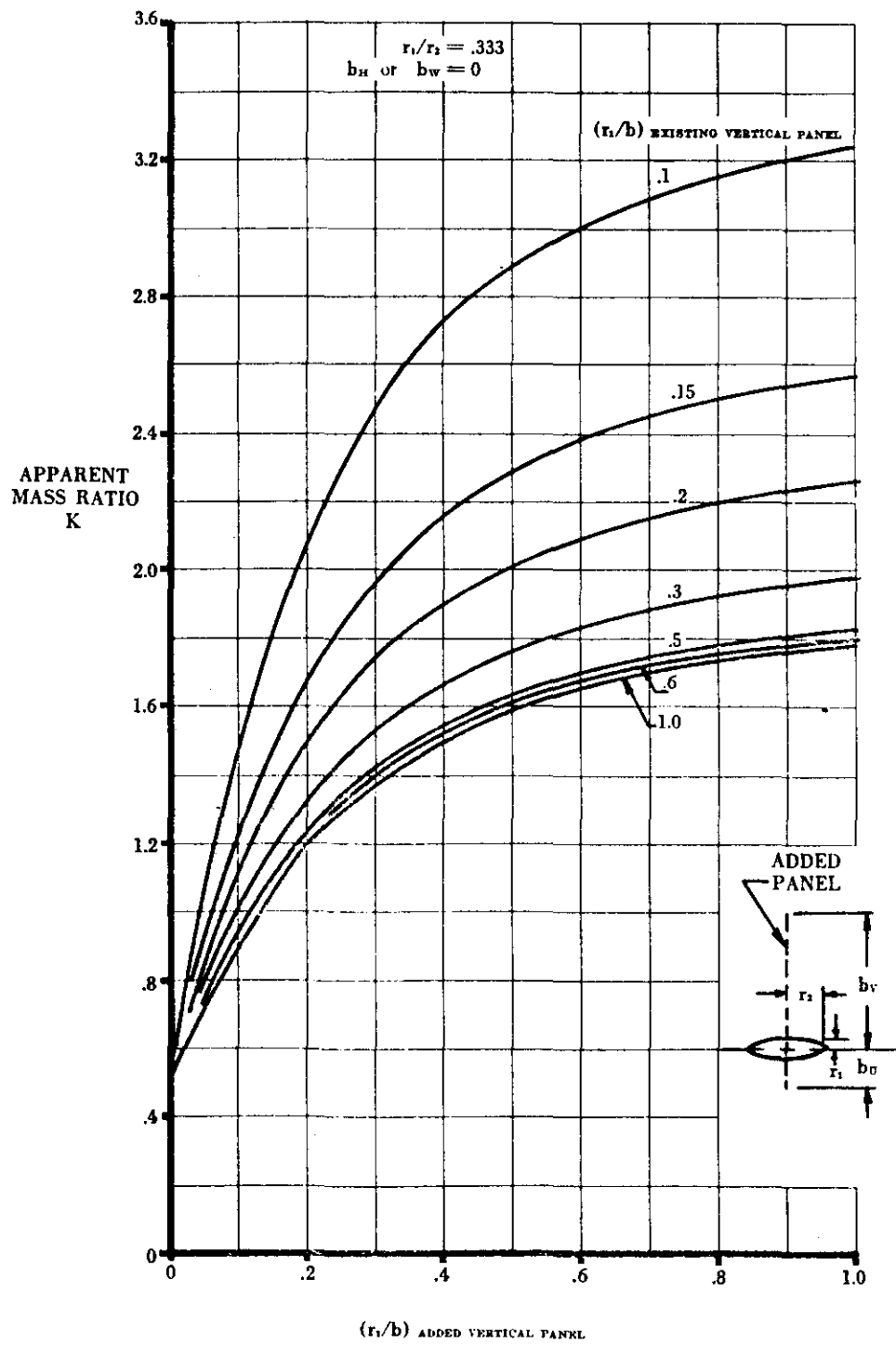


FIGURE 5.3.1.1-25q APPARENT MASS FACTORS (CONTD)

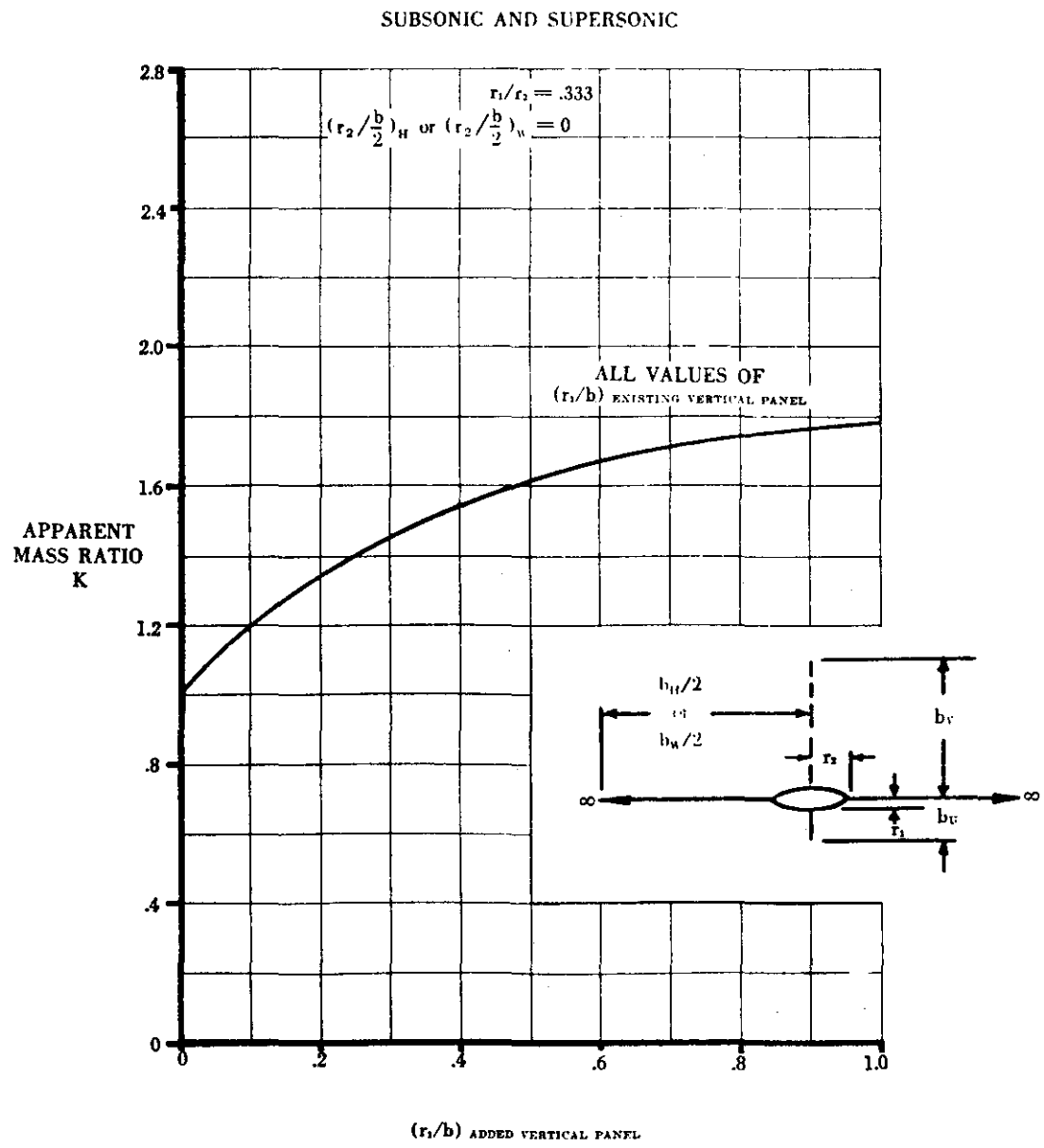


FIGURE 5.3.1.1-25f APPARENT MASS FACTORS (CONTD)

SUBSONIC AND SUPERSONIC

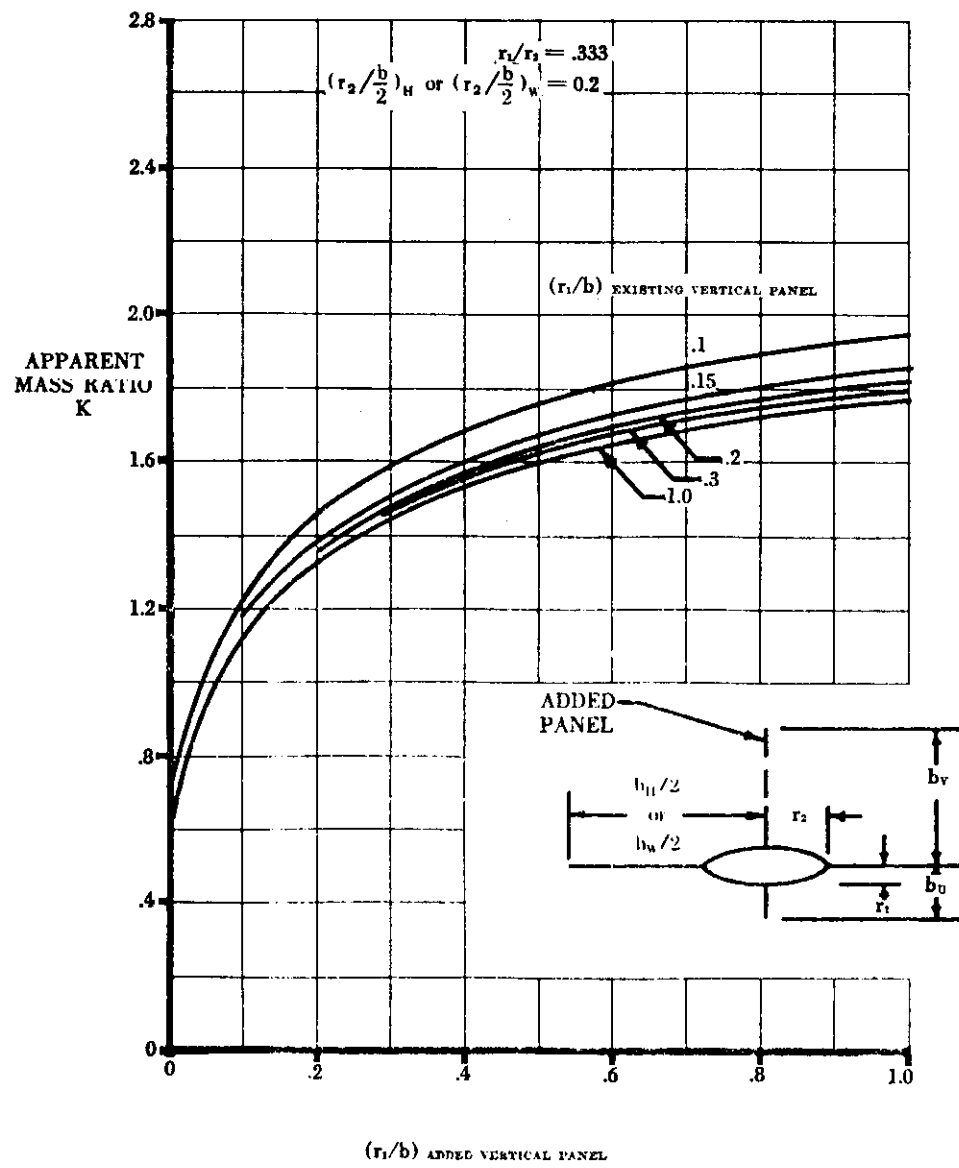


FIGURE 5 : 1.1-25: APPARENT MASS FACTORS (CONTD)

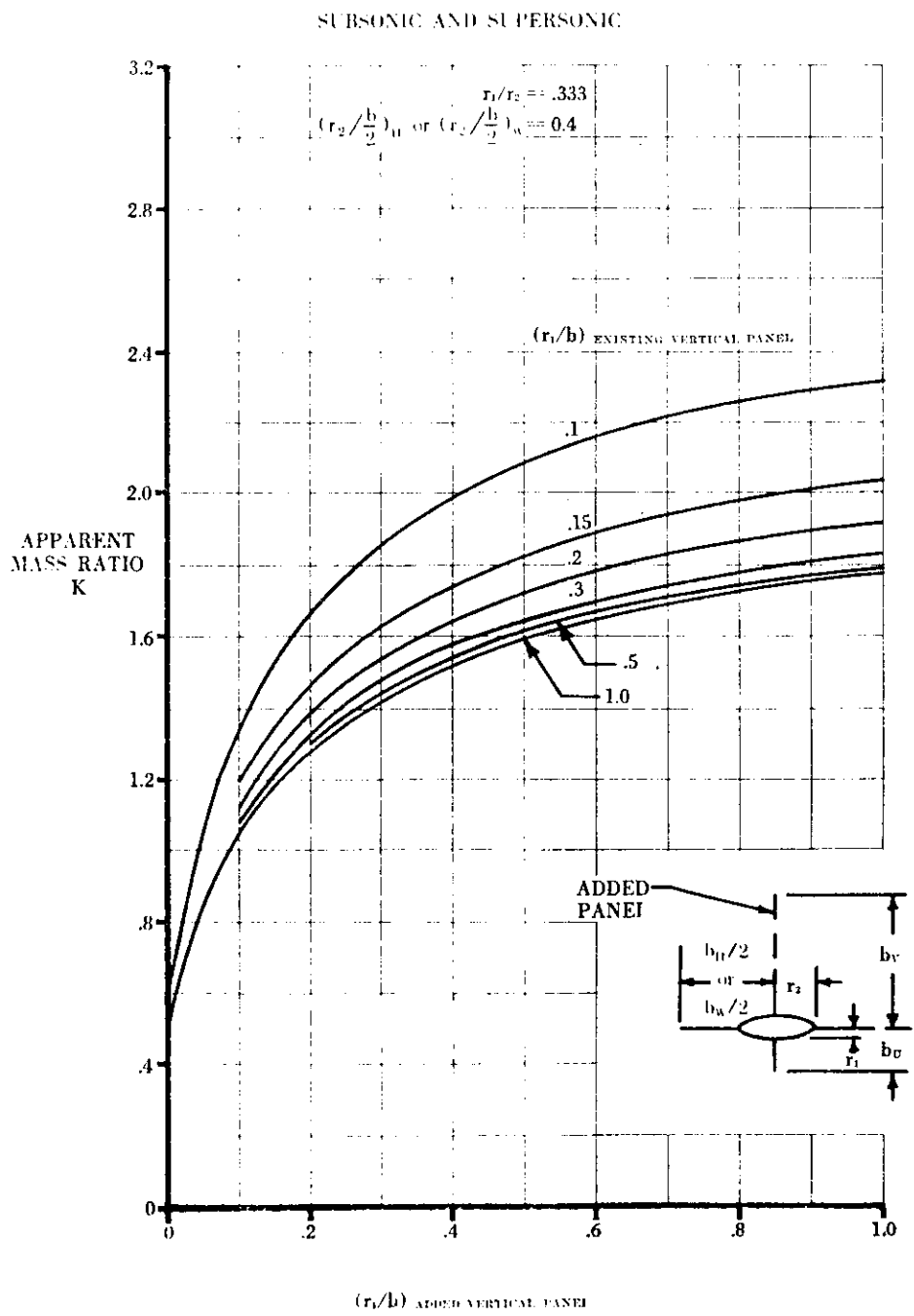


FIGURE 5.3.1.1-25t APPARENT MASS FACTORS (CONTD)

SUBSONIC AND SUPERSONIC

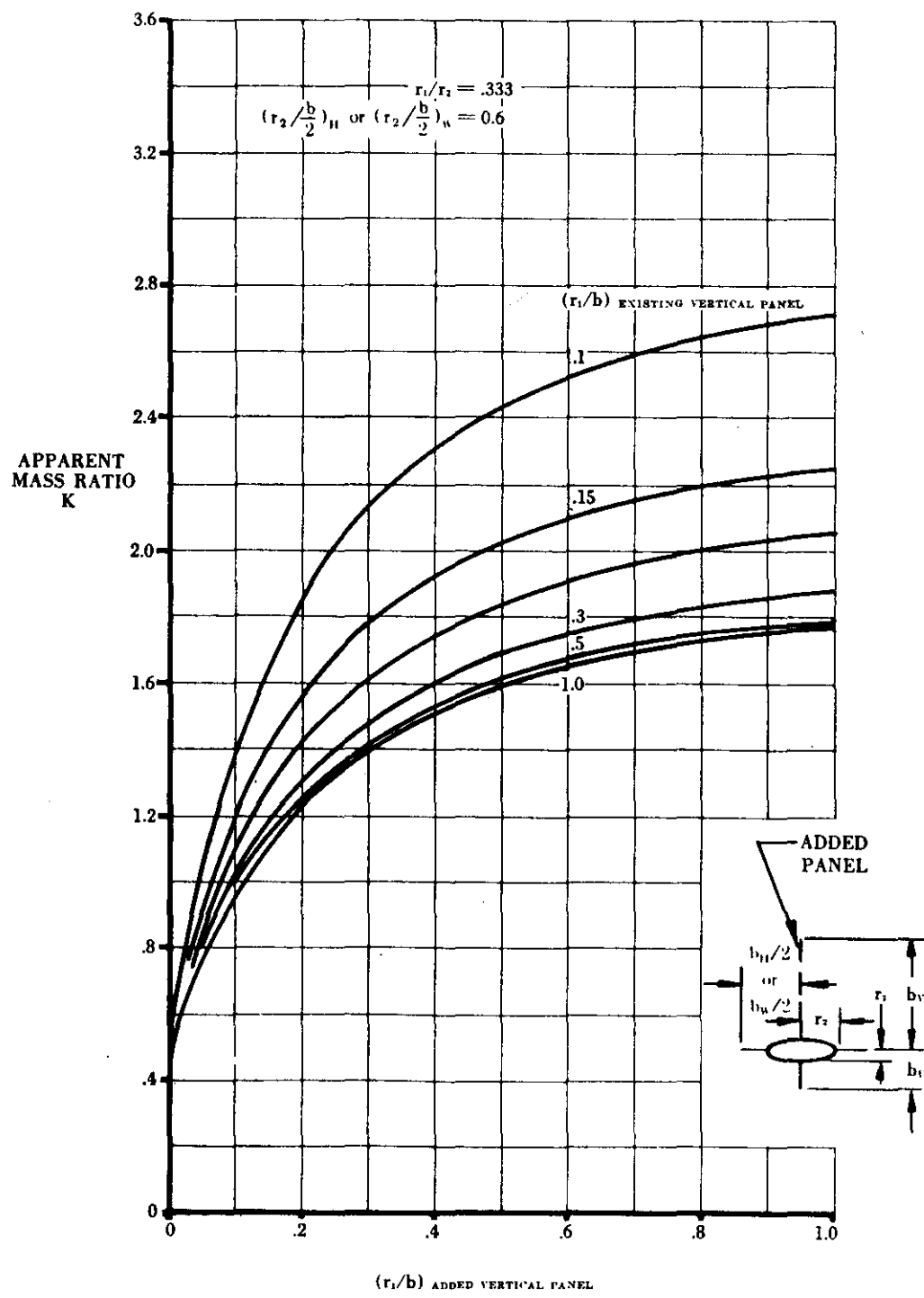


FIGURE 5.3.1.1-25u APPARENT MASS FACTORS (CONTD)

SUBSONIC AND SUPERSONIC

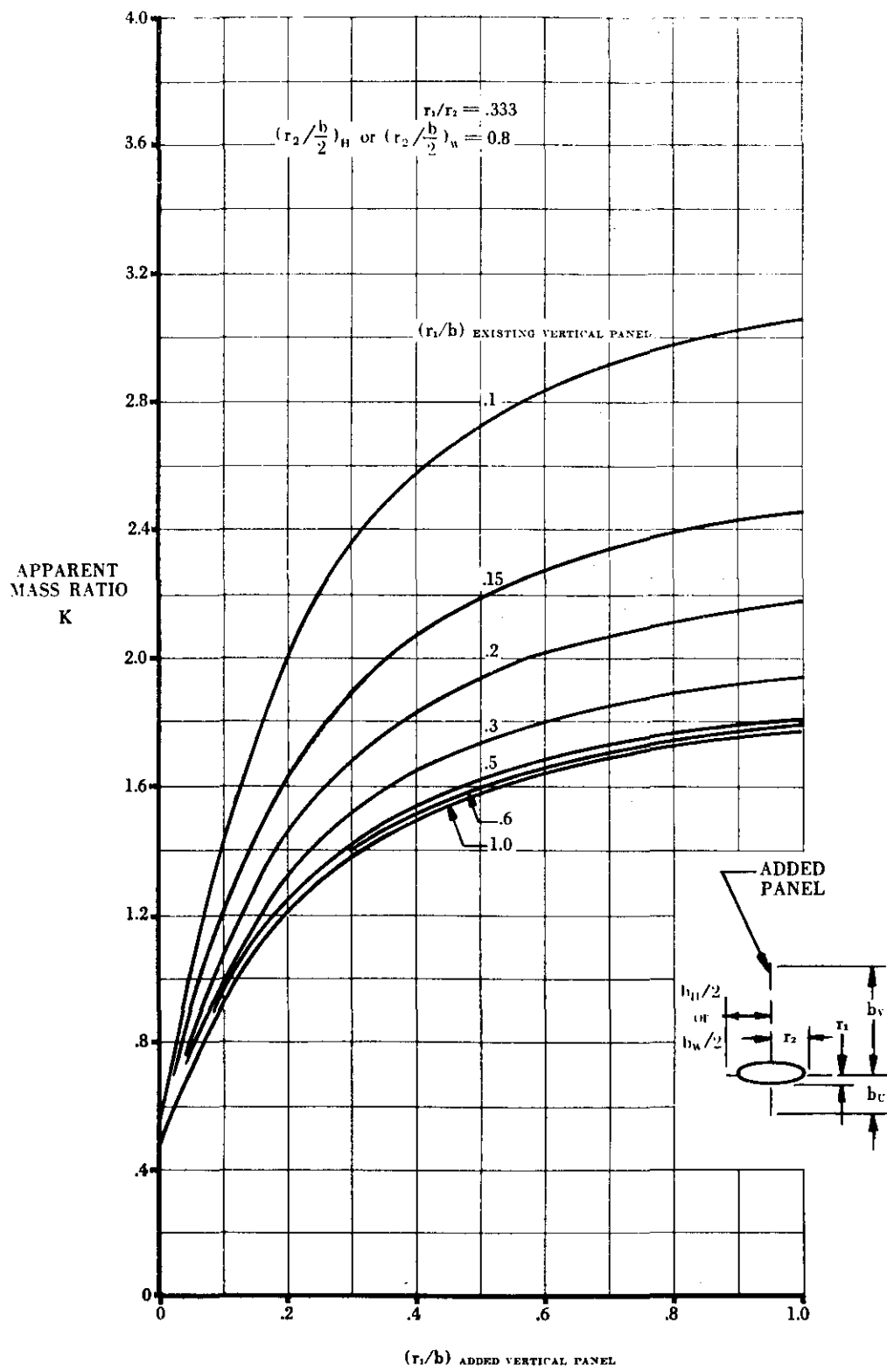


FIGURE 5.3.1.1-25v APPARENT MASS FACTORS (CONTD)

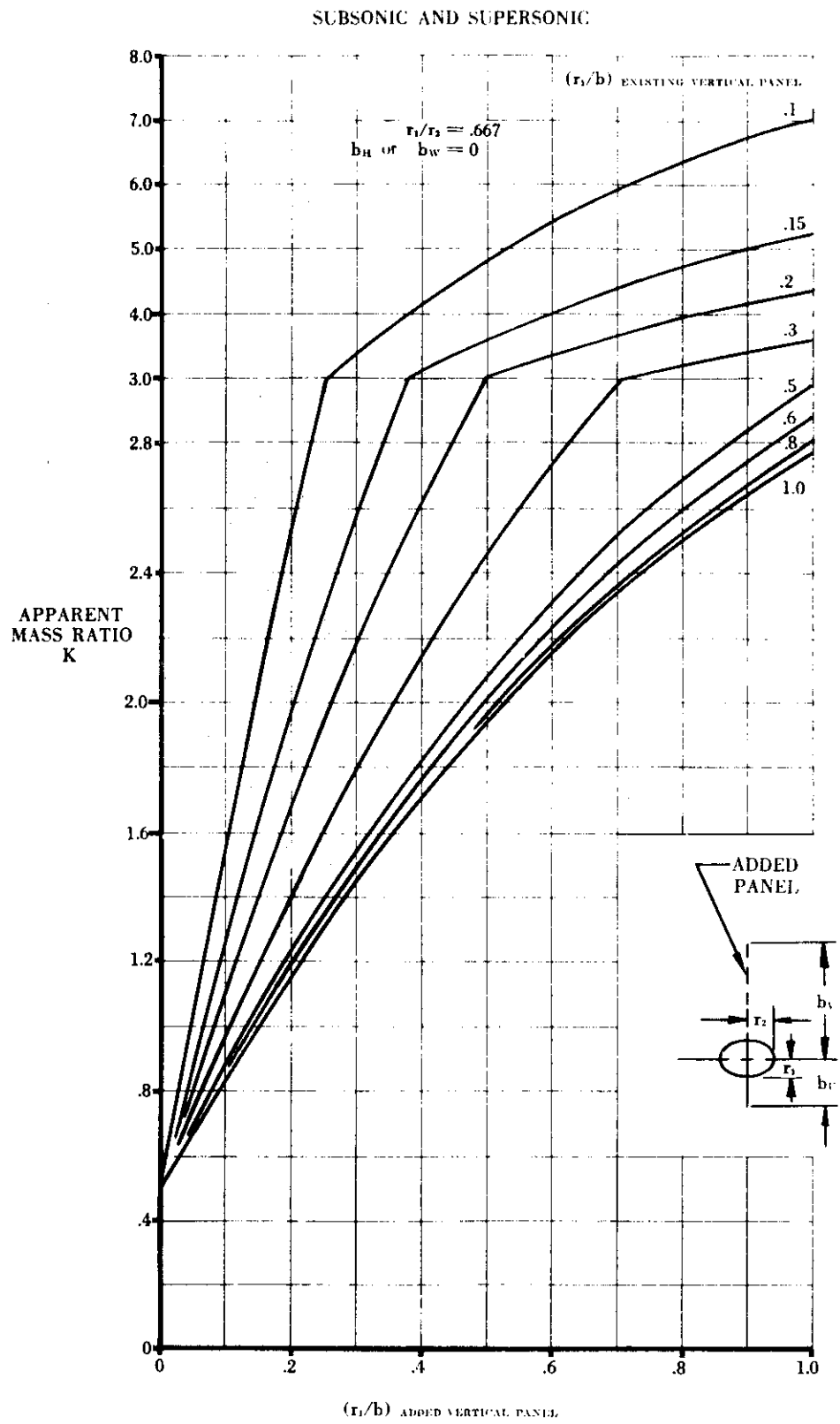


FIGURE 5.3.1.1-25w APPARENT MASS FACTORS (CONTD)

SUBSONIC AND SUPERSONIC

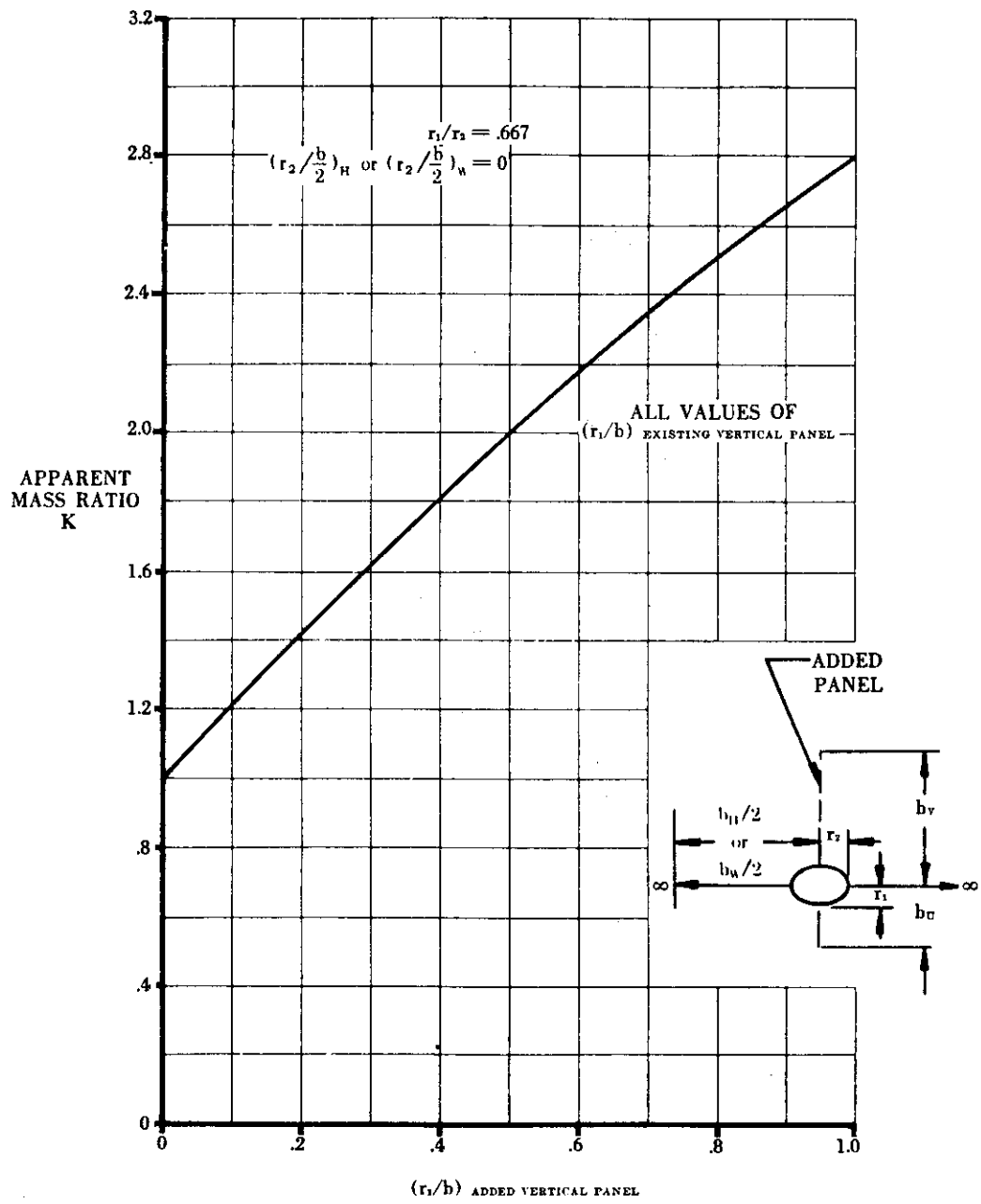


FIGURE 5.3.1.1-25X APPARENT MASS FACTORS (CONTD)

SUBSONIC AND SUPERSONIC

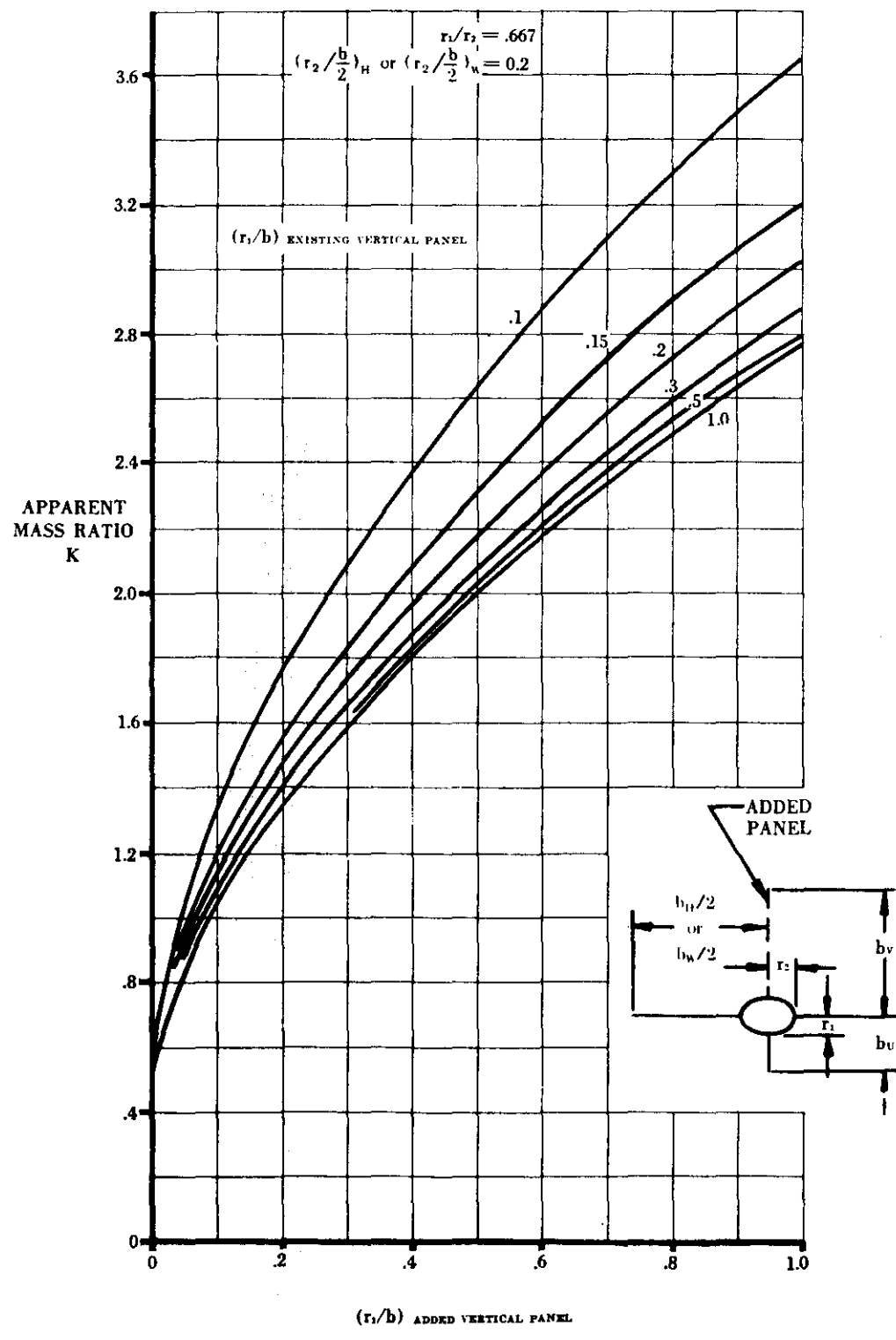


FIGURE 5.3.1.1-25y APPARENT MASS FACTORS (CONTD)

SUBSONIC AND SUPERSONIC

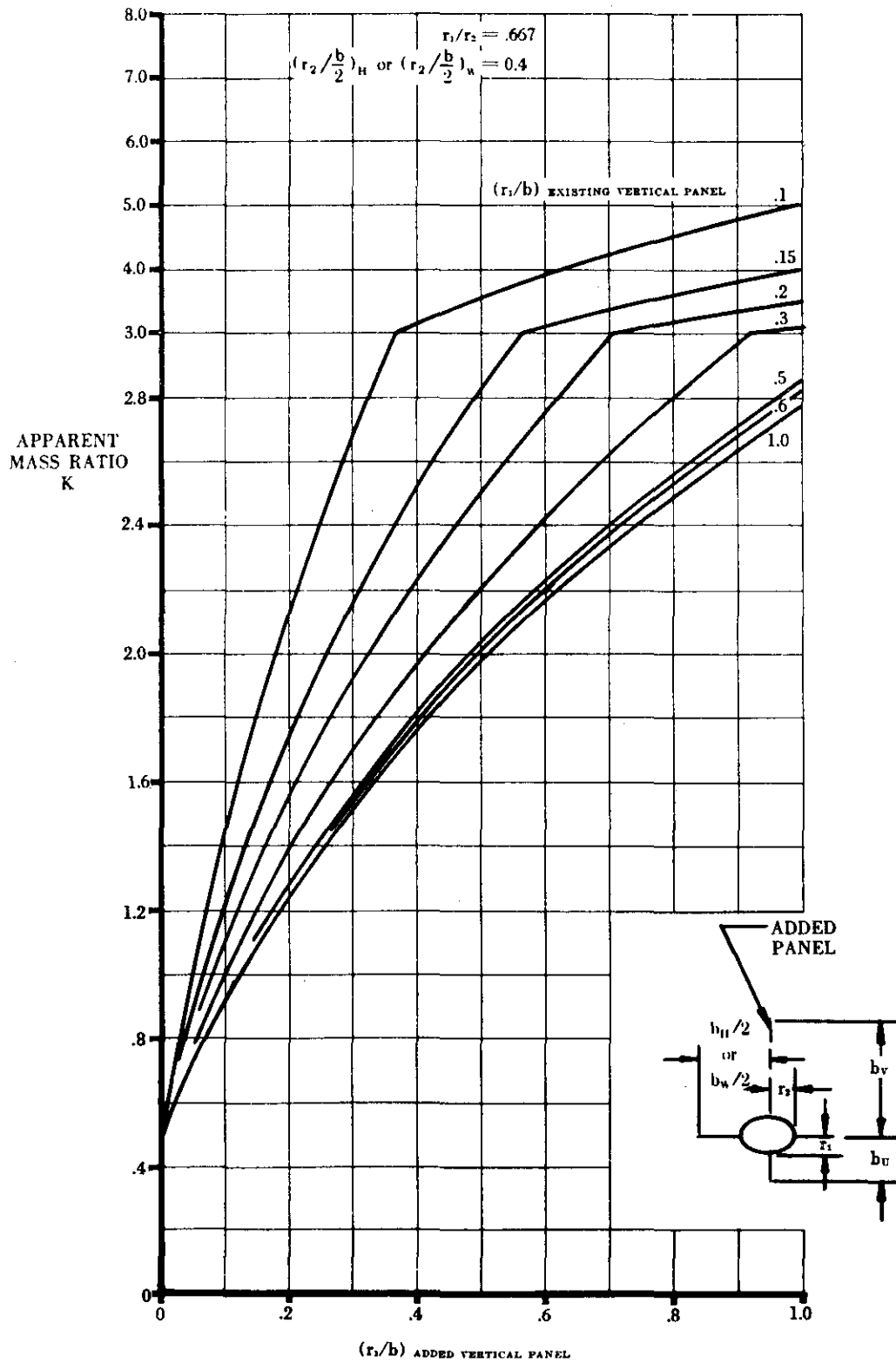


FIGURE 5.3.1.1-25Z APPARENT MASS FACTORS (CONTD)

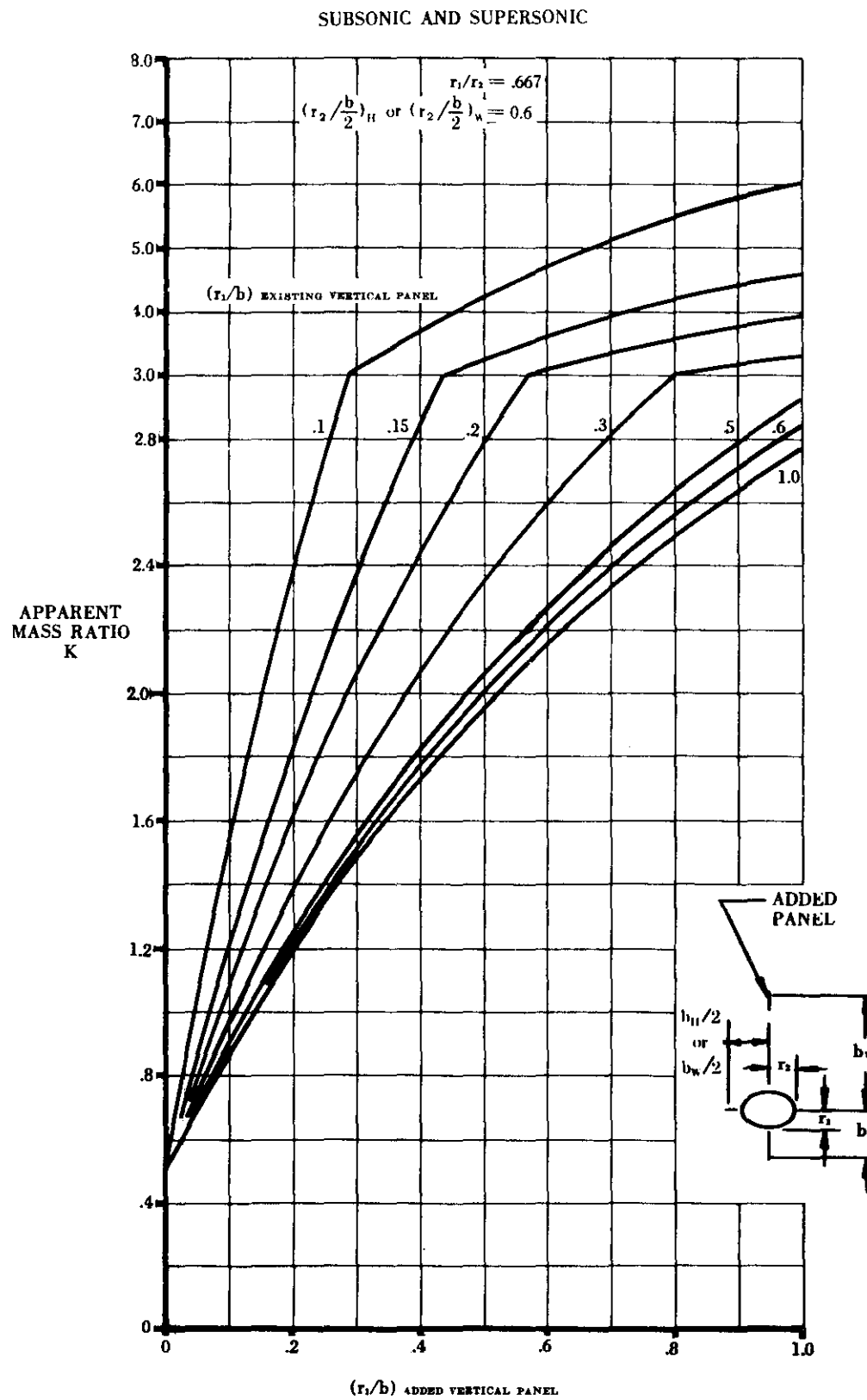


FIGURE 5.3.1.1-25aa APPARENT MASS FACTORS (CONTD)

SUBSONIC AND SUPERSONIC

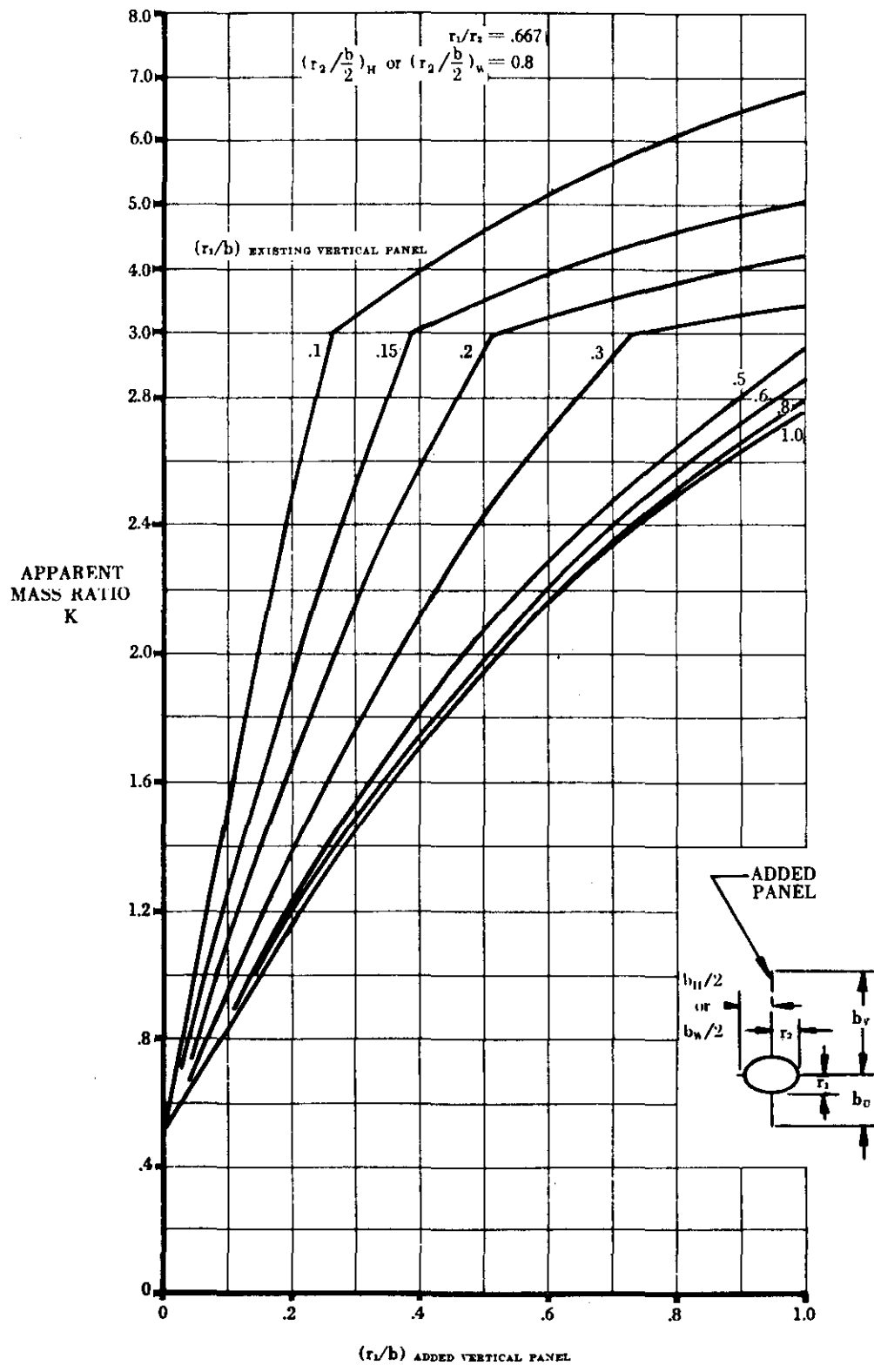


FIGURE 5.3.1.1-25bb APPARENT MASS FACTORS (CONT'D)

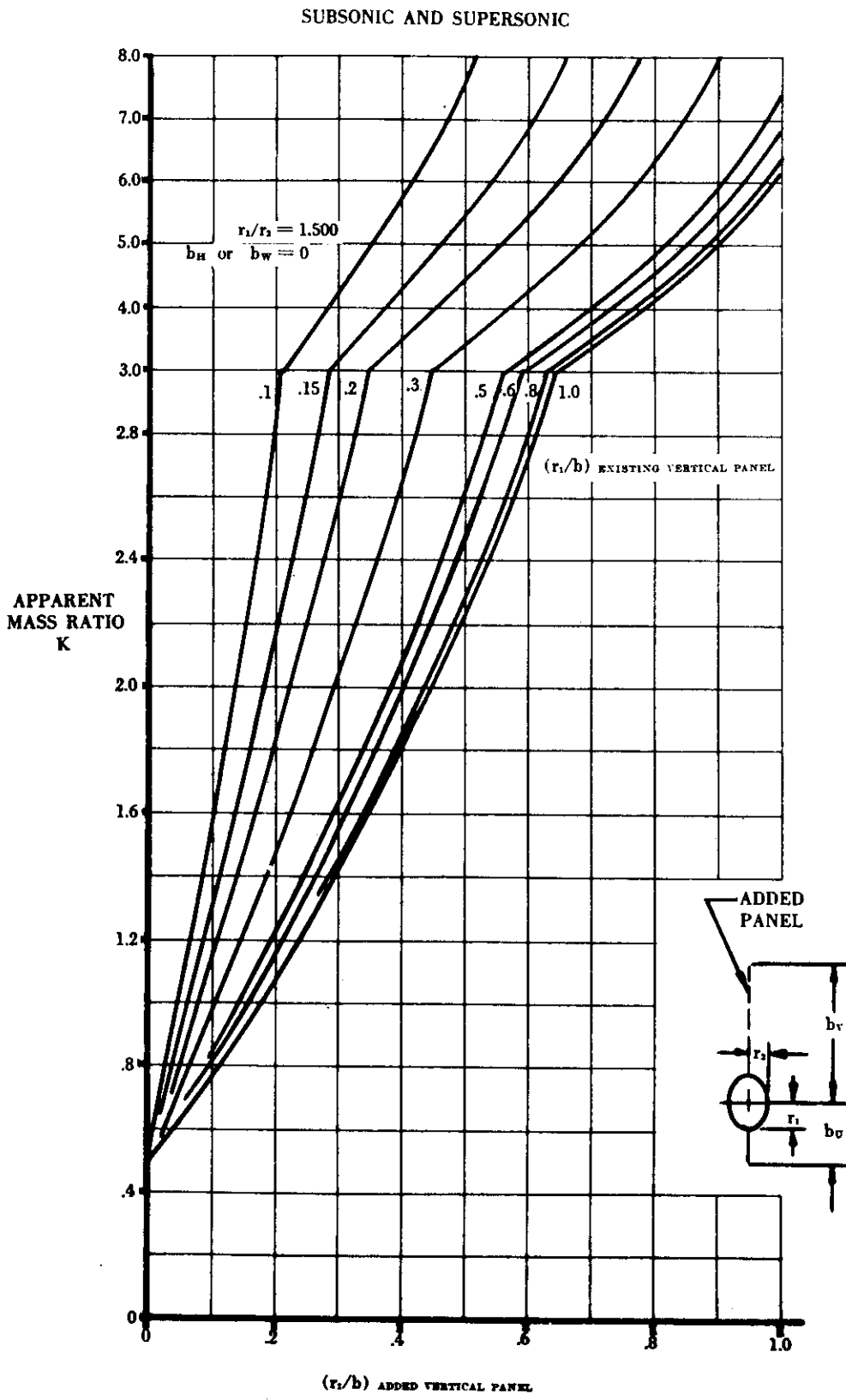


FIGURE 5.3.1.1-25cc APPARENT MASS FACTORS (CONTD)

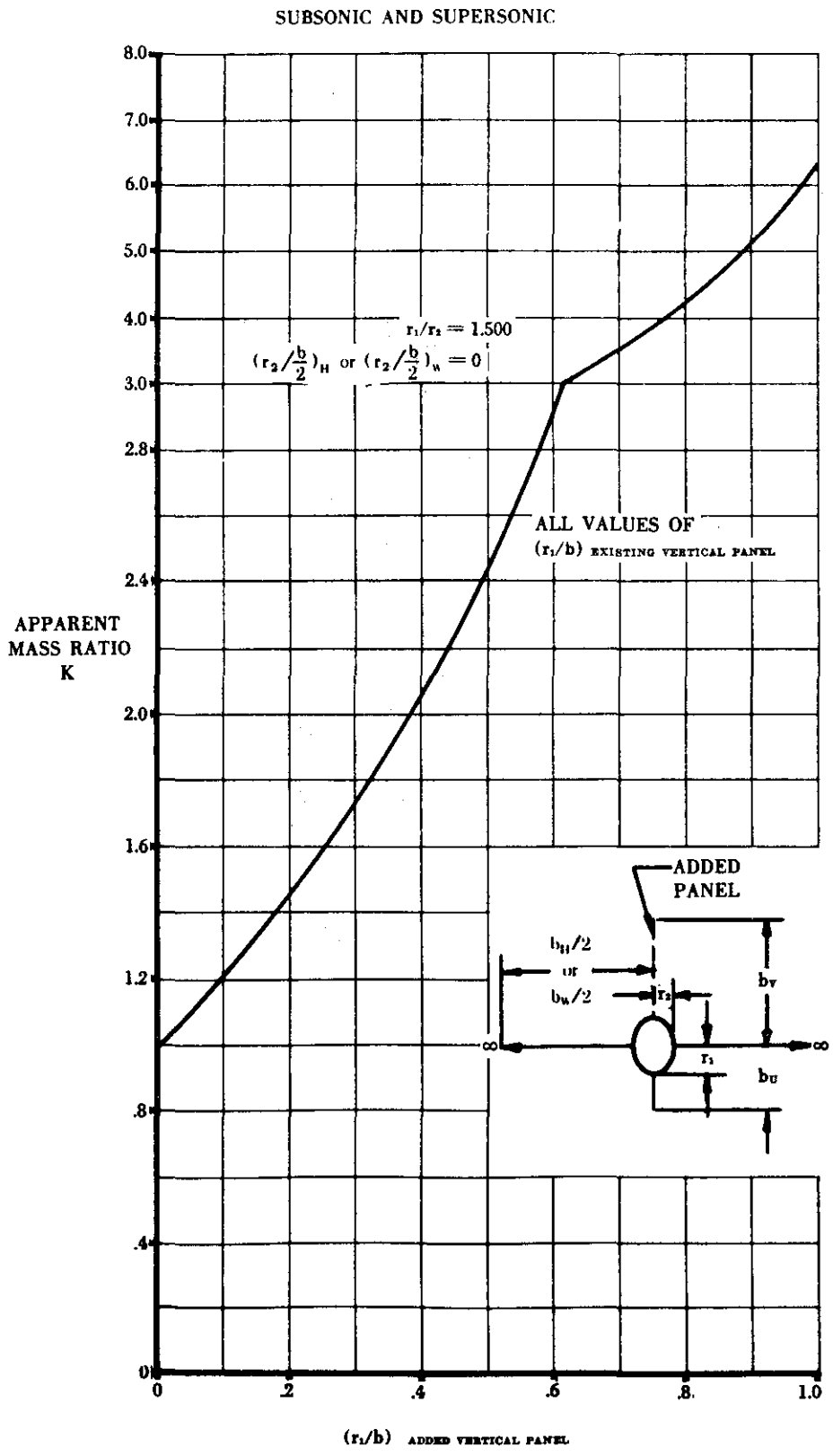


FIGURE 5.3.1.1-25dd APPARENT MASS FACTORS (CONTD)

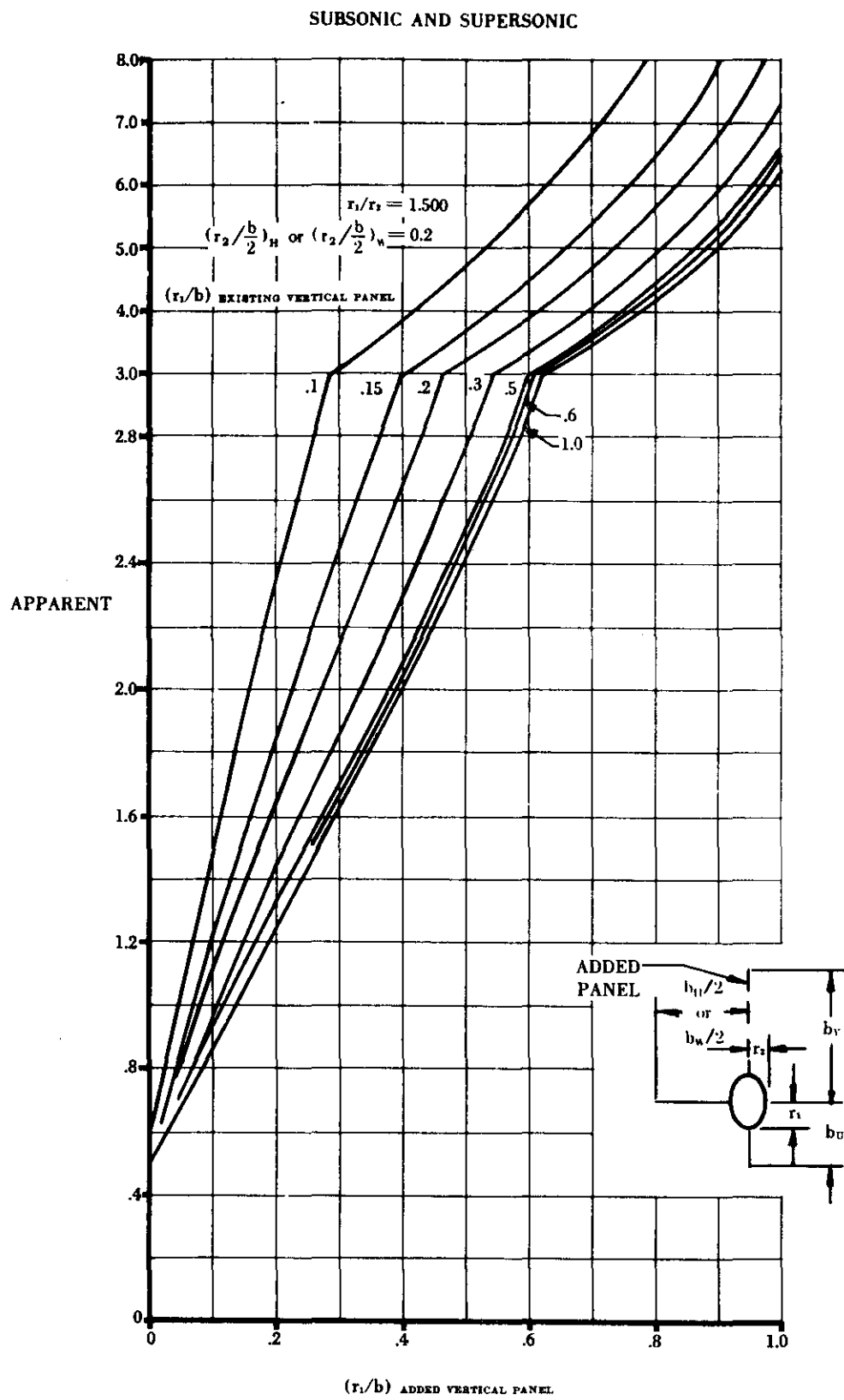


FIGURE 5.3.1.1-25ee APPARENT MASS FACTORS (CONTD)

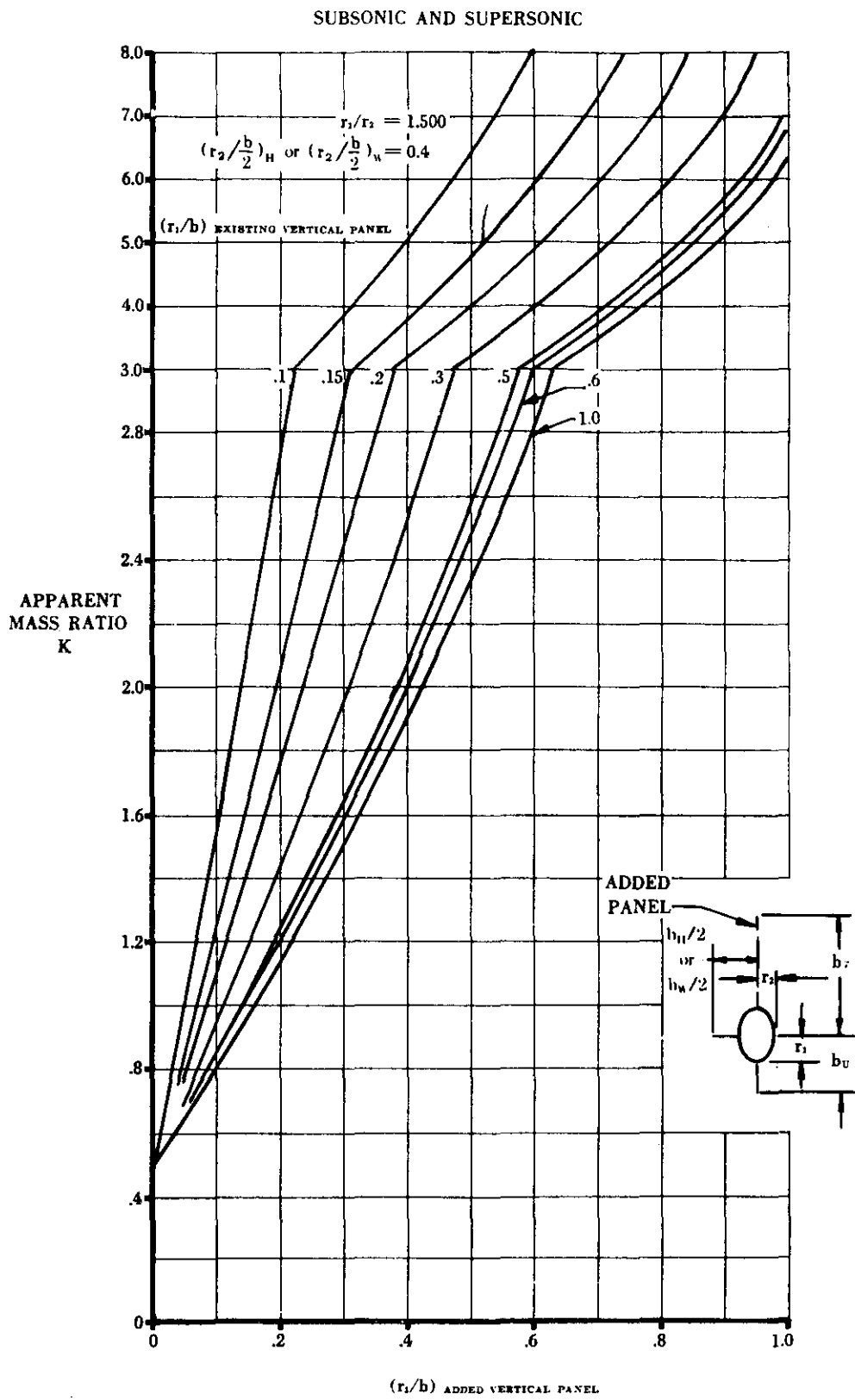


FIGURE 5.3.1.1-25ff APPARENT MASS FACTORS (CONTD)

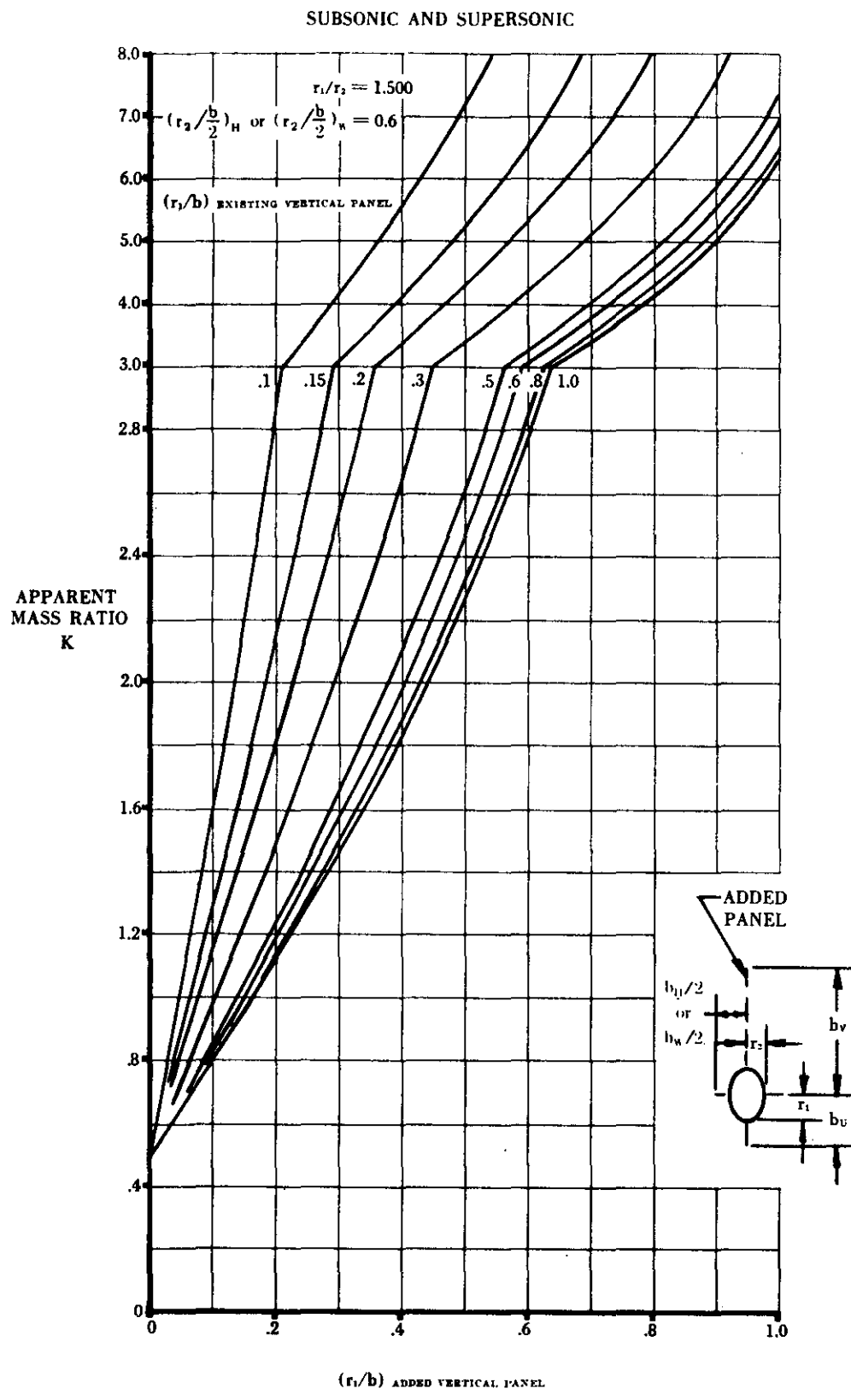


FIGURE 5.3.1.1-25gg APPARENT MASS FACTORS (CONTD)

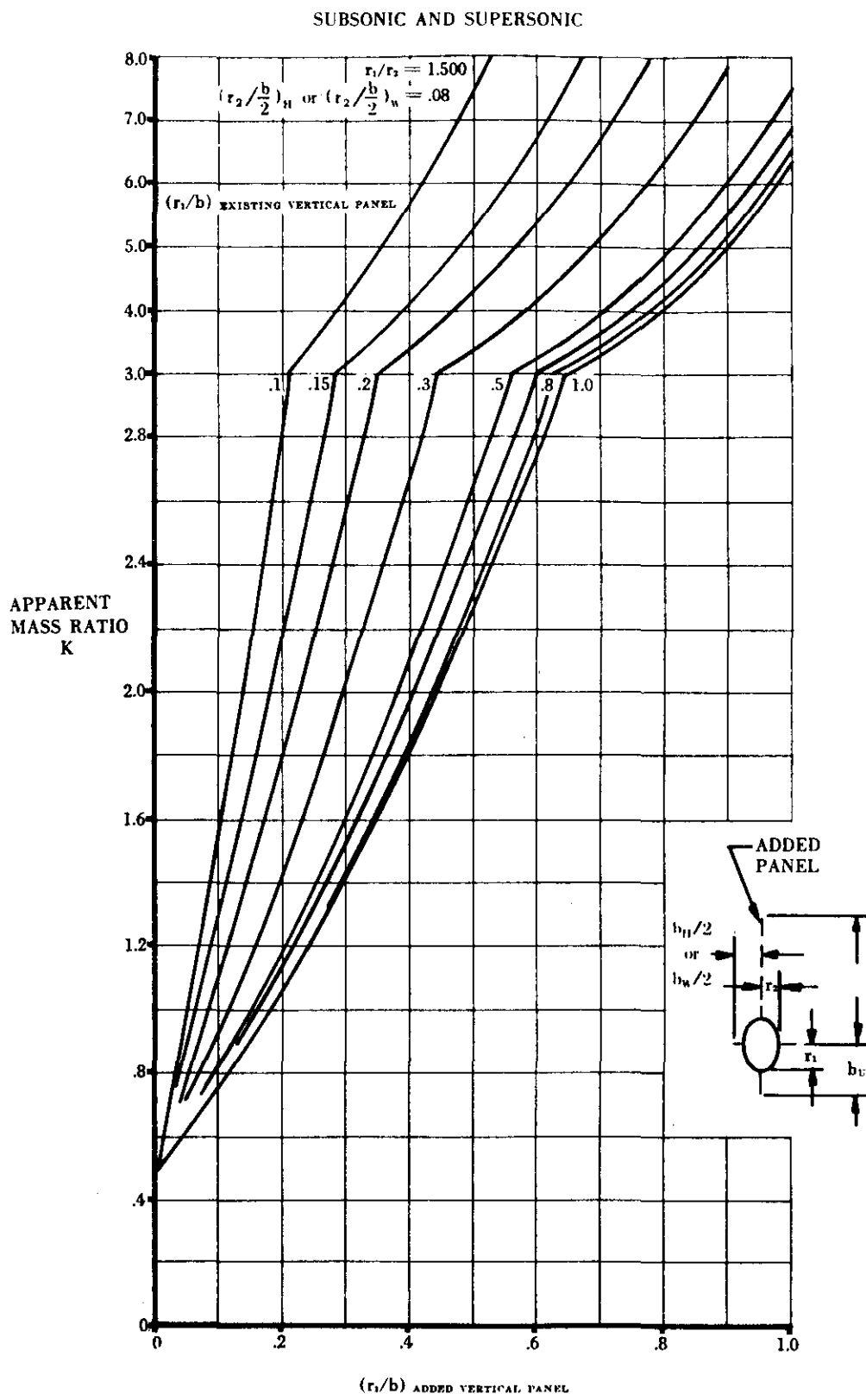
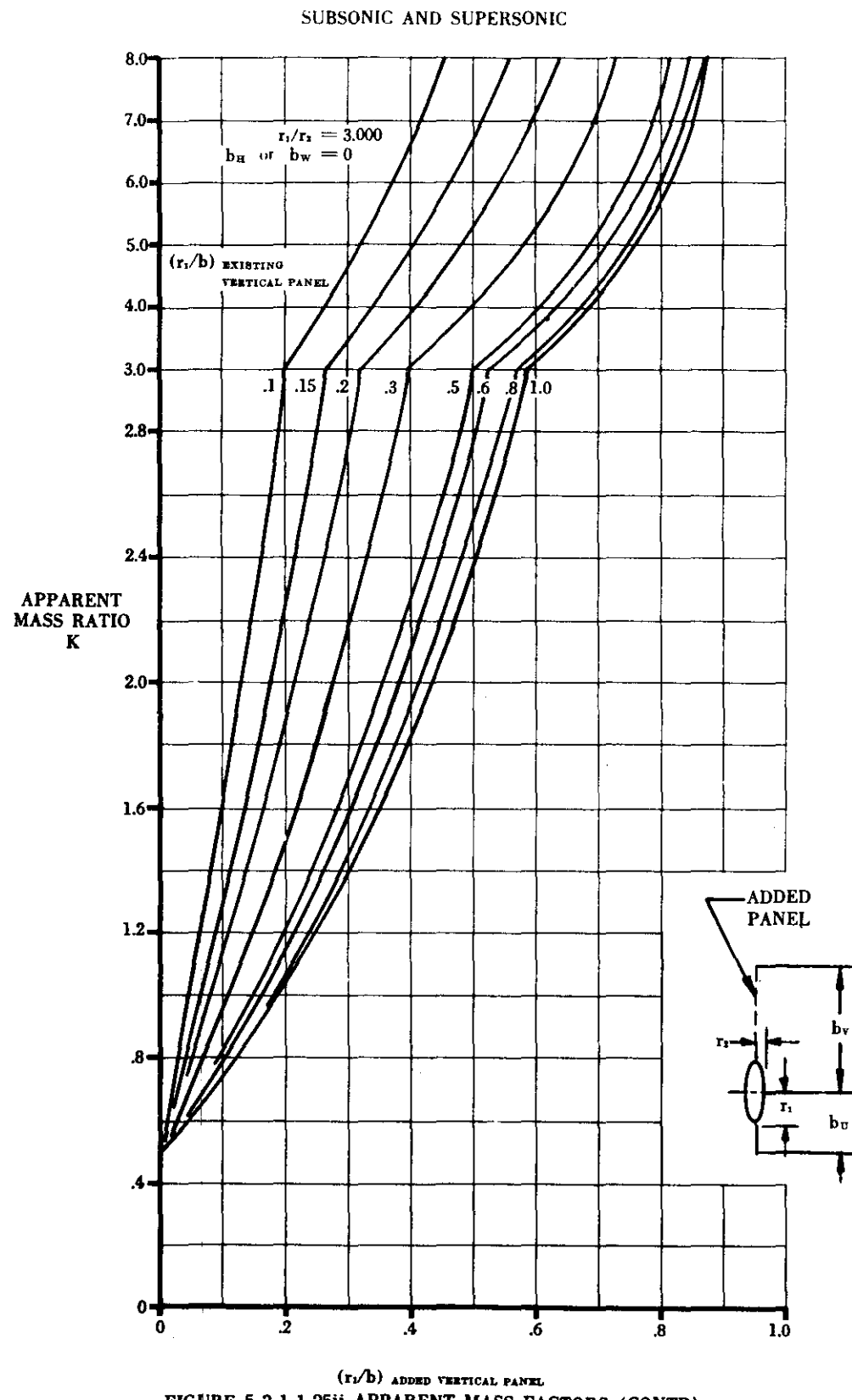


FIGURE 5.3.1.1-25hh APPARENT MASS FACTORS (CONTD)



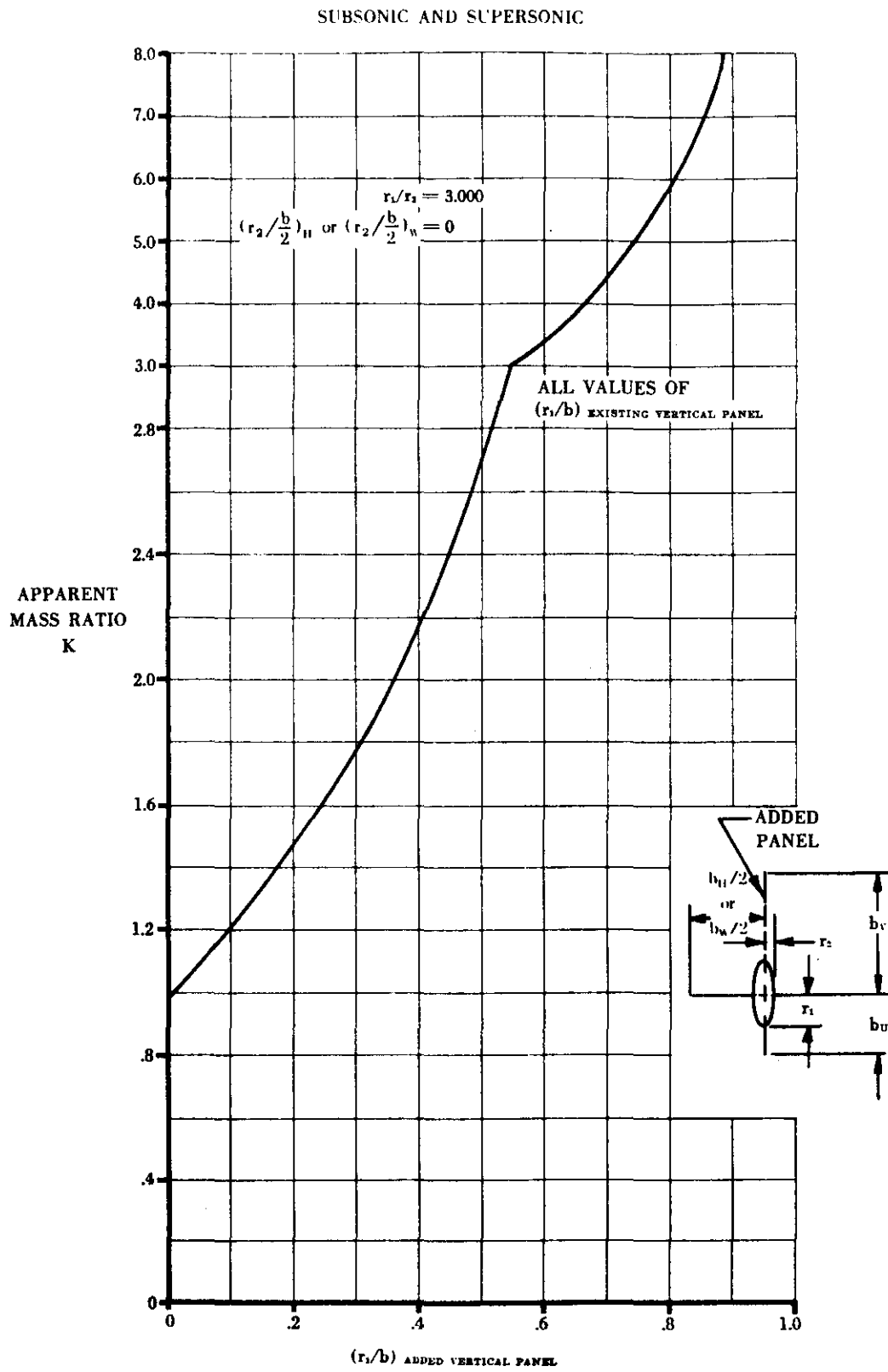


FIGURE 5.3.1.1-25jj APPARENT MASS FACTORS (CONTD)

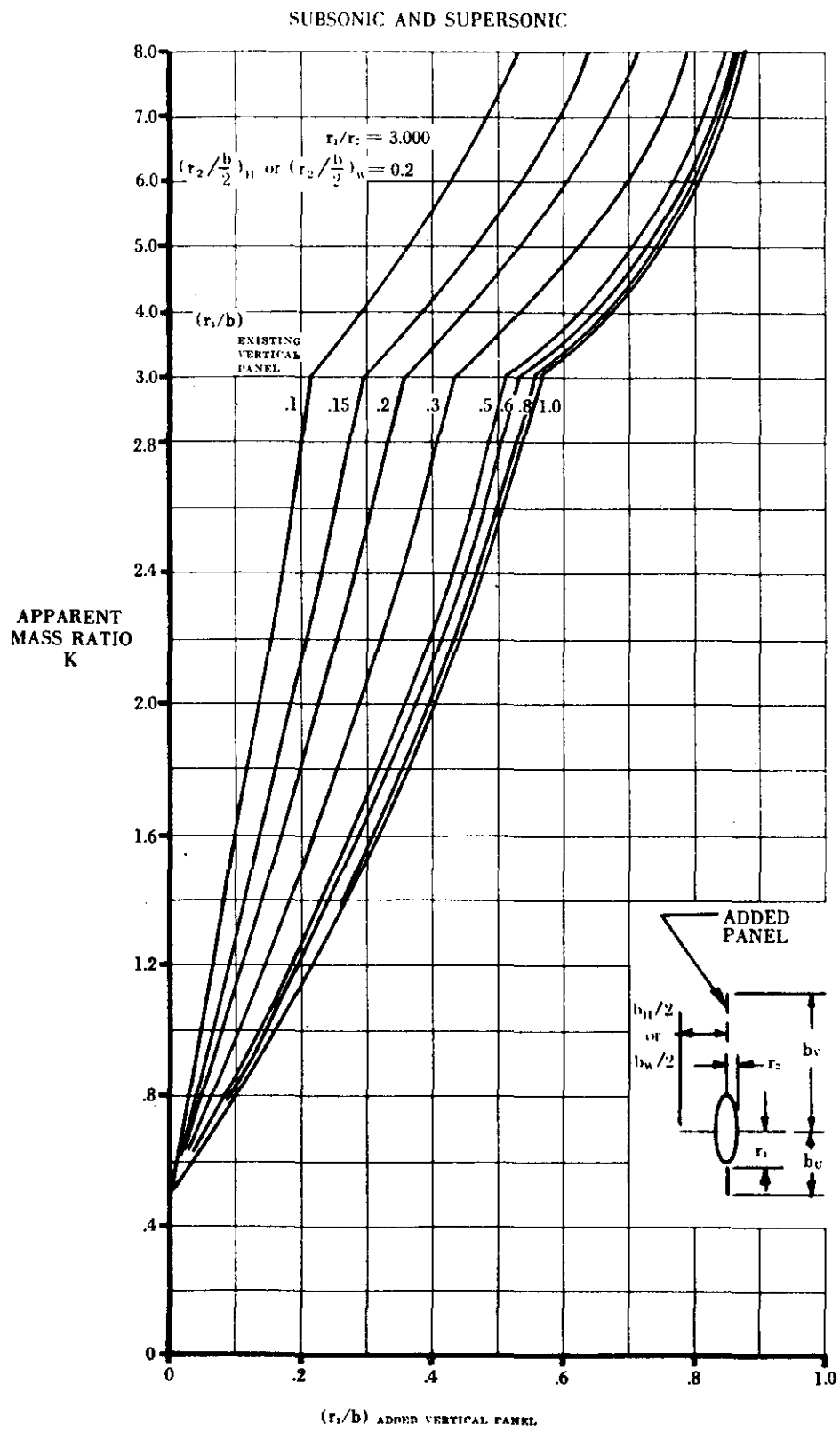


FIGURE 5.3.1.1-25kk APPARENT MASS FACTORS (CONTD)

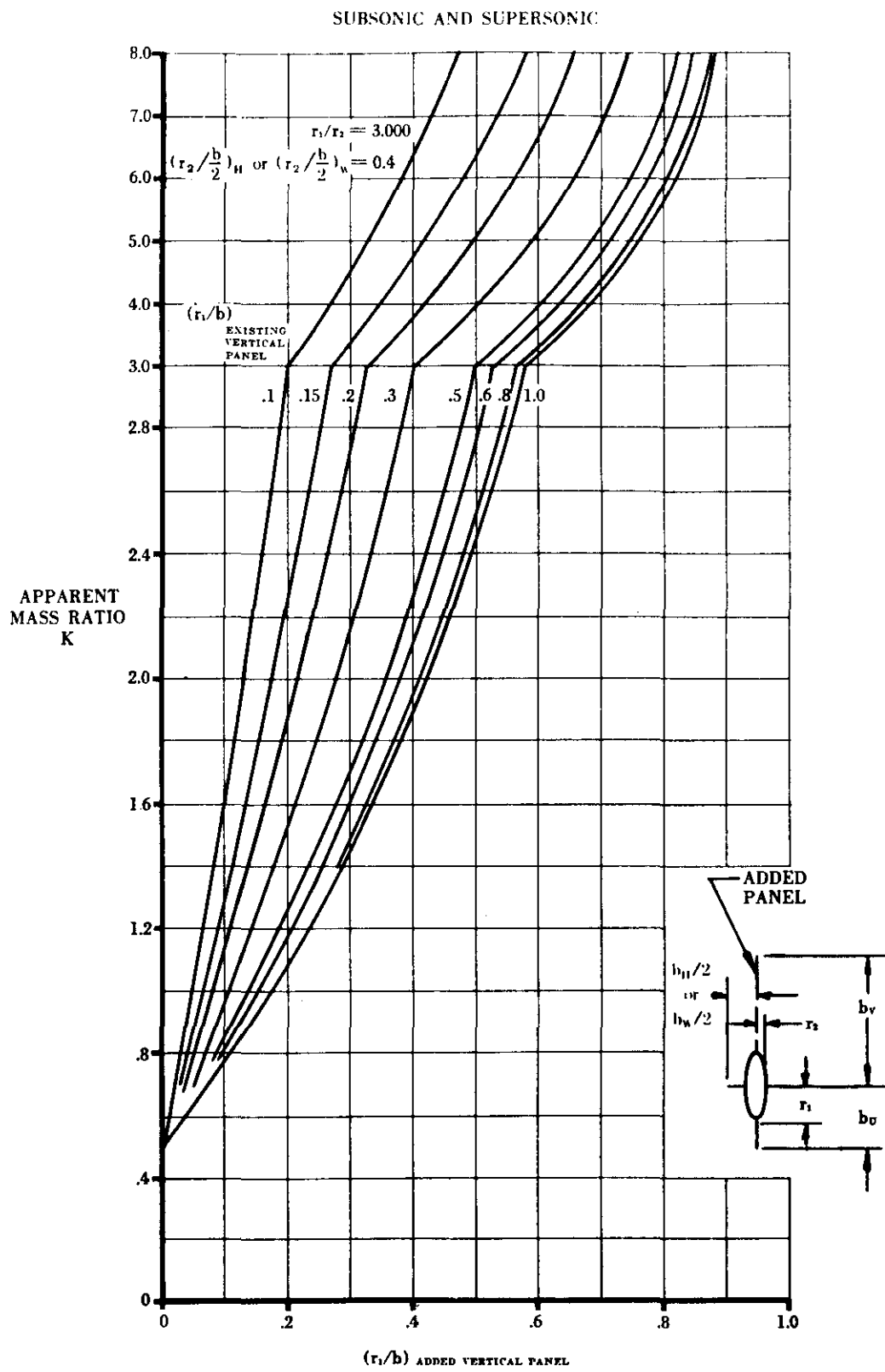


FIGURE 5.3.1.1-25ll APPARENT MASS FACTORS (CONTD)

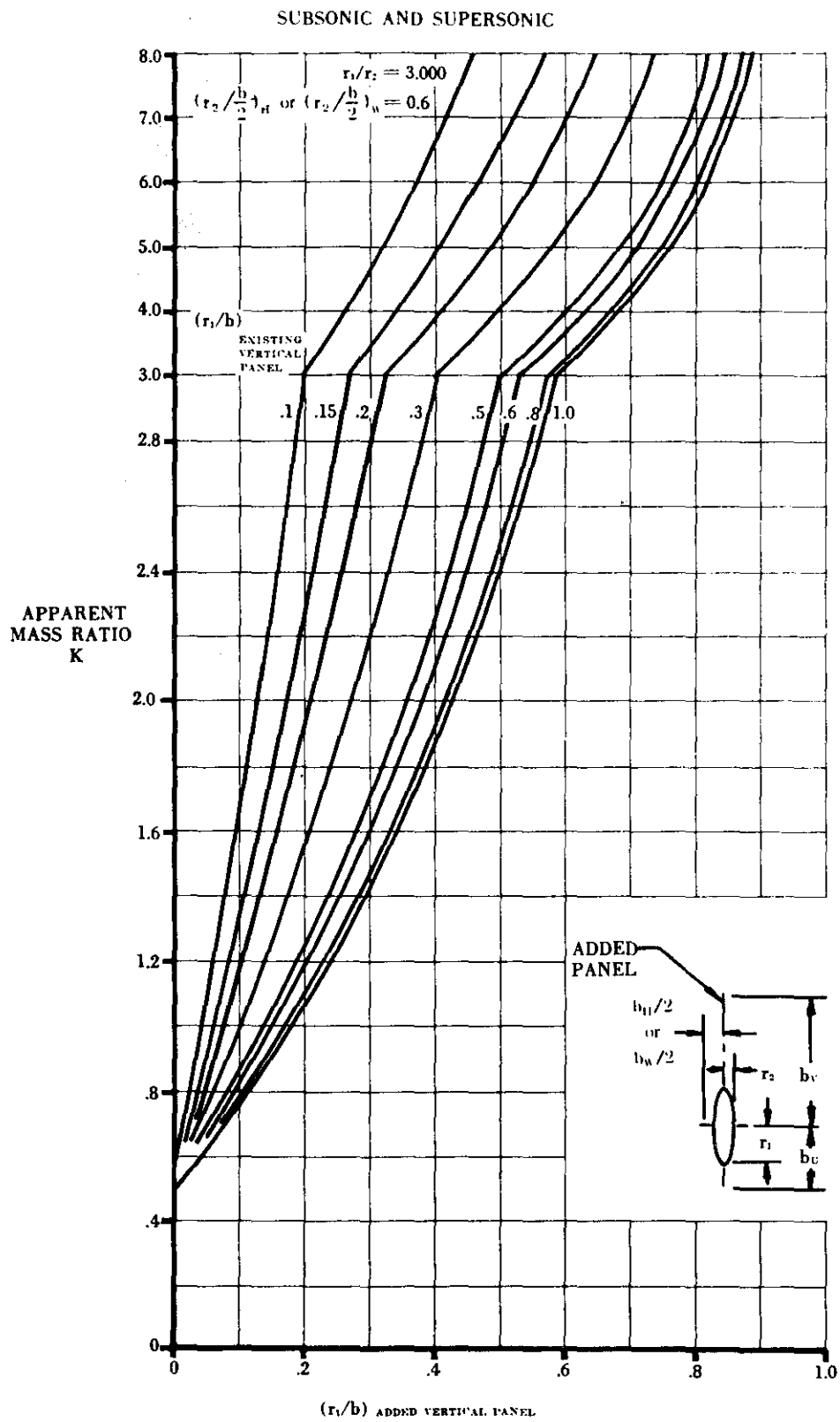


FIGURE 5.3.1.1-25mm APPARENT MASS FACTORS (CONTD)

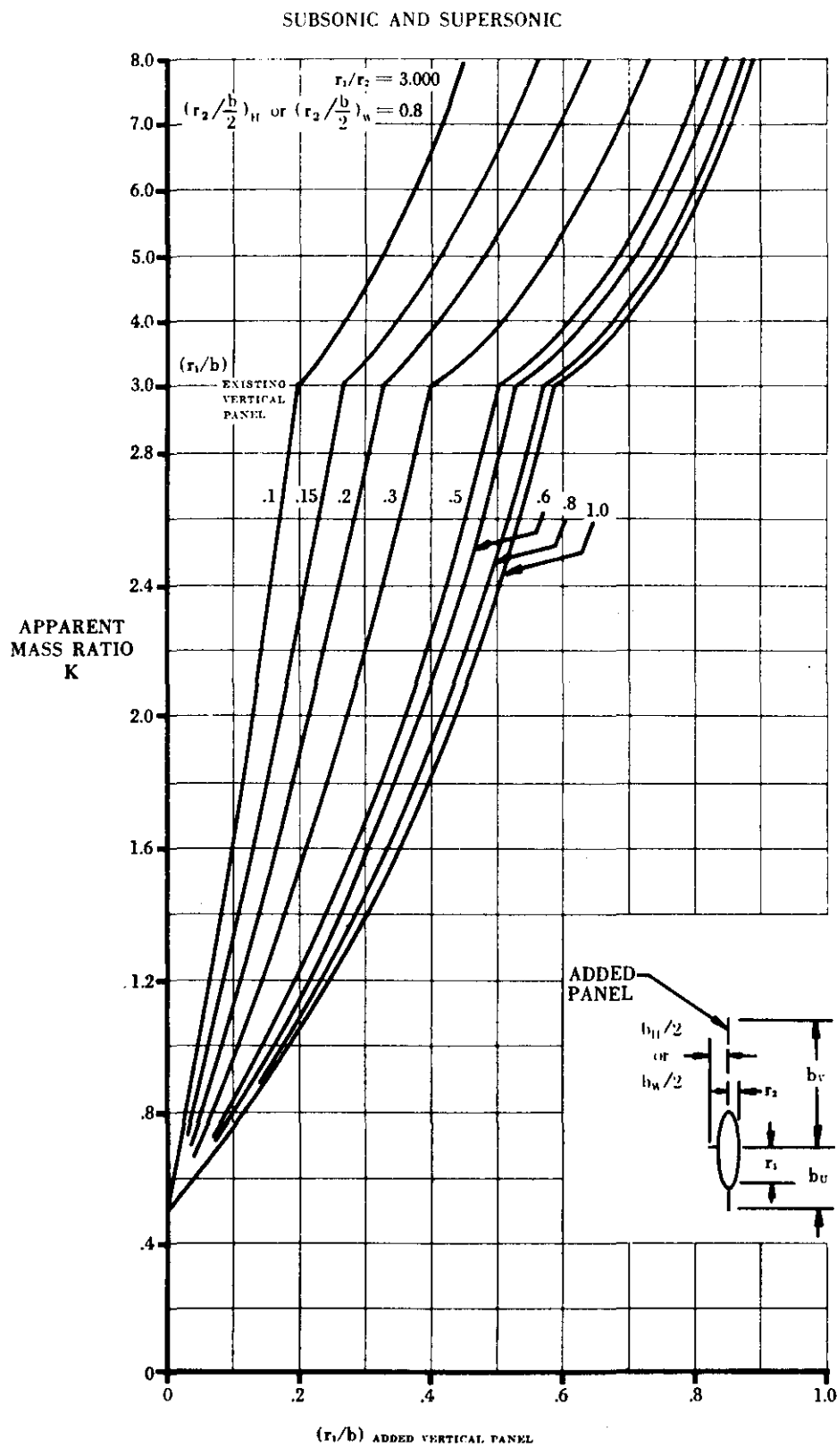


FIGURE 5.3.1.1-25nn APPARENT MASS FACTORS (CONT'D)

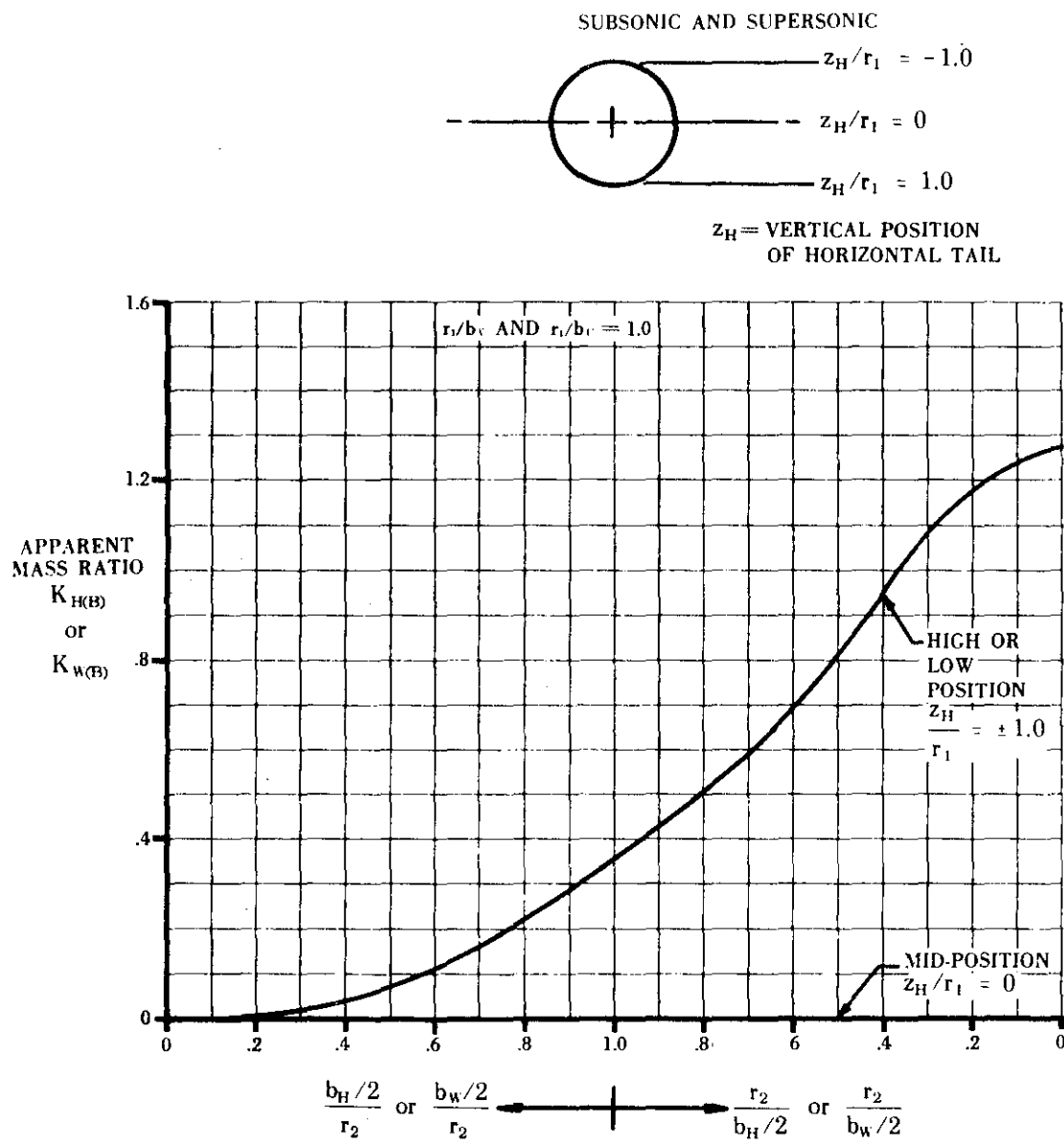


FIGURE 5.3.1.1-2500 APPARENT MASS FACTORS (CONT'D)

5.3.1.2 TAIL-BODY SIDE-FORCE COEFFICIENT C_Y AT ANGLE OF ATTACK

The tail-body side force developed at combined angles is nonlinear with respect to both sideslip and angle of attack because of the body-vortex induced sidewash on the upper vertical tail and the cross-coupling of upwash and sidewash velocities. To obtain the sideslip derivative $C_{Y\beta}$, it is recommended that C_Y be calculated at several angles of attack for a small sideslip angle ($\beta \leq 4^\circ$). Then at each angle of attack the side force is assumed linear with sideslip for small values of β so that

$$C_{Y\beta} \approx \frac{C_Y}{\beta}.$$

A. SUBSONIC

The analysis of tail-body combinations at subsonic speeds and zero angle of attack is described in paragraph A of Section 5.3.1.1. At combined sideslip and angle of attack, however, two other phenomena must be considered: the body-vortex interference, and the cross-coupling effect of sideslip and angle-of-attack induced cross-flow velocities. Unfortunately neither of these phenomena can be estimated at other than supersonic speeds.

The method presented herein is restricted to first-order approximations at relatively low angles of attack.

DATCOM METHOD

It is recommended that the methods of paragraph A of Section 5.3.1.1 be used in the linear-lift angle-of-attack region.

B. TRANSONIC

As stated for the subsonic case the body-vortex interference and cross-coupling of upwash and sidewash velocities due to combined angles cannot be estimated at other than supersonic speeds.

Furthermore, as stated in paragraph B of Section 5.3.1.1, no method is available for estimating the side force on a vertical panel at zero angle of attack.

DATCOM METHOD

No method is available for estimating this coefficient and none is presented in the Datcom.

C. SUPERSONIC

The method of this Section is an extension of that presented as Method 3 of paragraph A and in paragraph C of Section 5.3.1.1. The discussion appearing there also applies here and will not be repeated. At combined sideslip and angle of attack, however, two additional effects must be considered. The cross-coupling effect of sideslip and angle of attack induces cross-flow velocities at the tail panels, and at angle of attack the body sheds vortices which proceed downstream to cause interference at the tail.

The method presented herein does not account for interferences existing between a wing and tail surfaces. If a wing is present in the configuration three additional types of interference exist between the wing and tail panels at supersonic speeds. These interferences produce additional nonlinear effects which are accounted for in paragraph C of Section 5.6.1.2.

DATCOM METHOD

The method presented in this Section for estimating the tail contribution to the sideslip coefficient C_Y is from reference 1, and uses the apparent-mass concept described in Method 3 of paragraph A in Section 5.3.1.1. The method prescribes the order in which the tail panels should be added to the configuration for analysis purposes.

This order is:

The horizontal tail is always added first, but the method is valid only for configurations with a horizontal tail mounted on the body or for configurations with no horizontal tail.

The remaining tail panels are then added, starting with the most aft and working forward (the position is measured in a streamwise direction to the leading edge of the exposed root chord).

The proper weighting of the apparent-mass ratios, which accounts for partial-panel areas affected by existing panels, is outlined in paragraph C of Section 5.3.1.1. The result is an effective apparent-mass factor K' .

For tail-body configurations at angle of attack, the horizontal-tail pressure field is not delineated by Mach lines alone. The pressure field produced is bounded by shock waves at the upper trailing edge and the lower leading edge (at positive angles of attack). If the airfoil is assumed to be thin, it is an easy matter to define the expansion and compression fields by direct application of shock-expansion theory. We assume that the flow in the region of the tail is the two-dimensional shock-expansion field corresponding to the exposed root chord of the horizontal surface. Any effects of horizontal surface-body interference or horizontal surface section in distorting the shock-expansion field are neglected. This method is also used in Section 5.6.1.2 to define the pressure field produced by a wing. The method is described below:

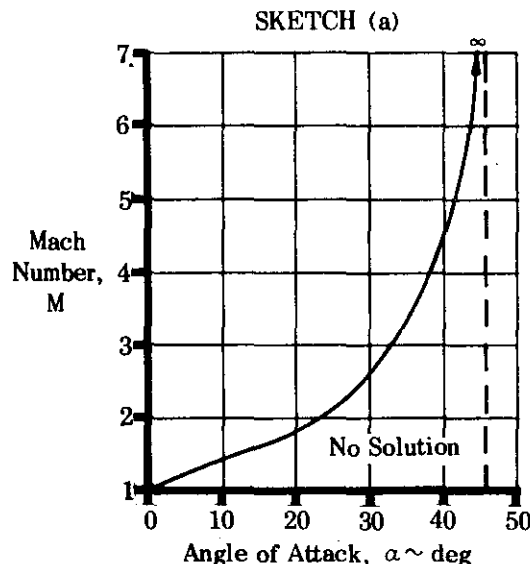
Upper surface of panel:

1. Find the leading-edge Mach line $\mu = \sin^{-1} \frac{1}{M_\infty}$ (measured relative to the free stream).
2. Find Mach number M_1 aft of expansion from figure 4.4.1-82. Read ν at M_∞ . Then read M_1 at $\nu + \alpha = \nu_1$.
3. Find trailing-edge shock angle. Enter figure 4.4.1-81 at $-\delta' = \alpha$ and read θ_1 at M_1 (measured relative to the chord plane of the horizontal surface).

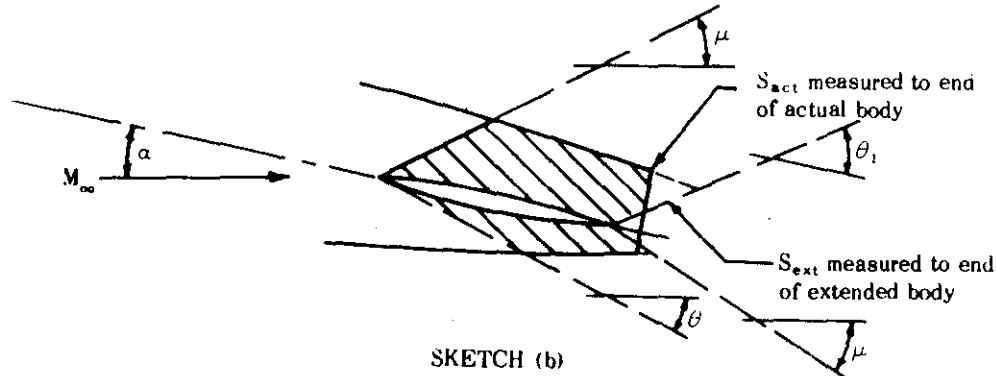
Lower surface of panel:

1. Find leading-edge shock angle. Enter figure 4.4.1-81 at $-\delta' = \alpha$ and read θ at M_∞ (measured relative to the free stream).
2. Find Mach number M_2 beneath wing from figure 4.4.1-82. Read ν at M_∞ . Then read M_2 at $\nu - \alpha = \nu_2$.
3. Find trailing-edge Mach line (end of expansion), $\mu = \sin^{-1} \frac{1}{M_\infty}$ (measured relative to the free stream).

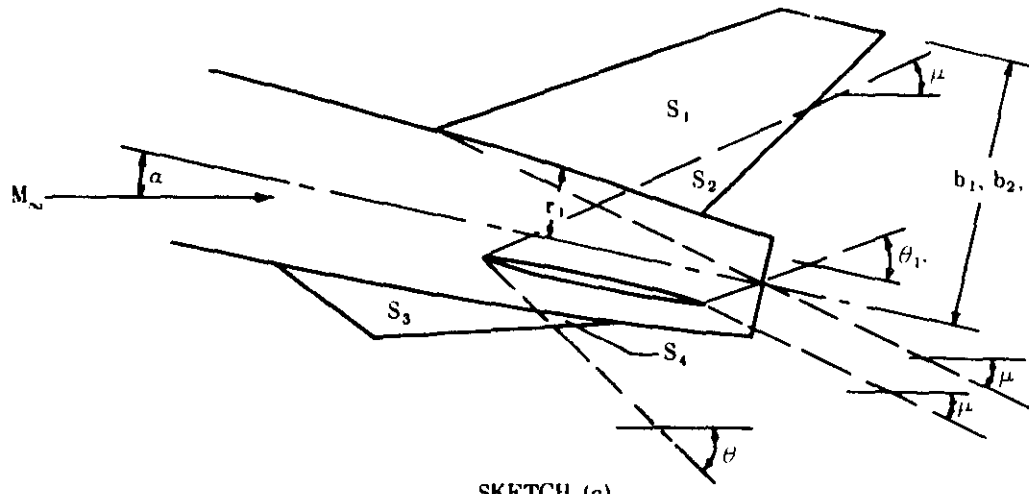
For a specified initial Mach number there is a maximum value of the angle of attack for which there exists an oblique shock solution. Or, conversely, for a specified angle of attack there is a minimum initial Mach number for which there is an oblique shock solution. The relation between Mach number and angle of attack below which no oblique shock solutions may be obtained is indicated in sketch (a).



The pressure-field boundaries produced by a horizontal tail are defined in sketch (b) which shows the body area influenced by the horizontal tail. Compare this with sketch (c) of Section 5.3.1.1.

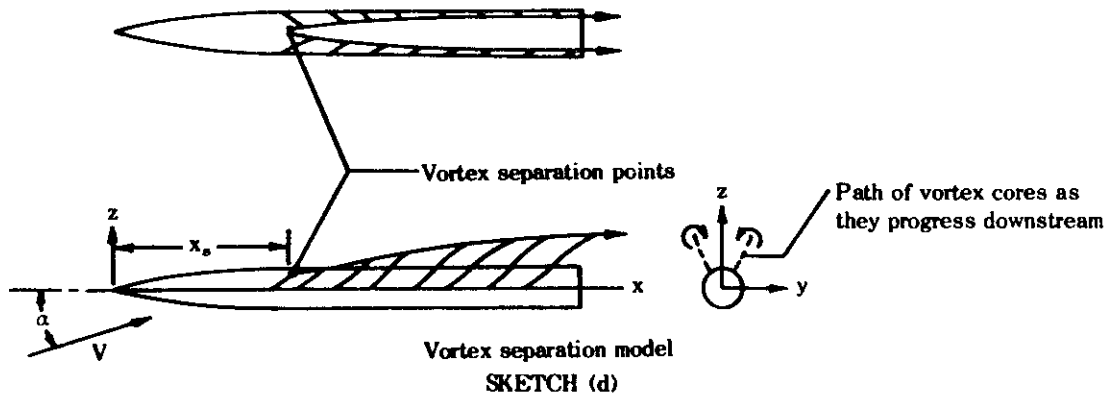


The pressure-field boundaries of a typical tail-body configuration are illustrated in sketch (c). For this example the vertical tail exposed root-chord leading edge is aft of the ventral fin exposed root-chord leading edge; therefore, the ventral fin has no effect on the vertical tail since it is added later. At the angle of attack and Mach number represented the horizontal tail influences both the vertical tail and the ventral fin; however, the vertical tail does not influence the ventral fin.



The modifying effect of angle of attack on the tail contribution to the side-force coefficient is accounted for by the cross-coupling interference factor K_ϕ , developed from slender-body theory in reference 2.

The effect of body-vortex induced sidewash on the upper vertical tail side-force coefficient is calculated using interference factors from references 3 and 4, and vortex strengths and positions from Section 4.3.1.3. A simplified model of body-vortex separation is shown in sketch (d). At some distance x_s behind the body nose a pair of vortices separates from the body. As the vortices progress downstream, they increase in strength as a result of small vortex filaments originating on the body and feeding into the vortex cores. The positions and vortex strengths of a body of revolution are dependent upon angle of attack and the axial distance x behind the body nose. These vortex strengths and positions are presented in Section 4.3.1.3 as functions only of a single nondimensional parameter and the results are presented in the y - z coordinate system. In the method that follows these vortex strengths and positions are resolved into vertical tail reference coordinates for the configuration at combined angle of attack and sideslip. The estimation procedure for finding vortex positions and strengths is restricted to circular bodies; therefore, the Datcom method is not valid for other body shapes.



The contribution of the tail panels to the side-force coefficient is determined from the following equation

$$C_{Y_{HVB}} = C_{Y_{HB}} + C_{Y_V} + C_{Y_U} \quad 5.3.1.2-a$$

where

$C_{Y_{HB}}$ is the contribution of the horizontal tail in the presence of the body, calculated by equation 5.3.1.2-b

C_{Y_V} is the contribution of the vertical tail, including body and horizontal tail interference effects, effects of cross-coupling of α and β , and effects of body vortices, and may include ventral fin interference. Calculate by equation 5.3.1.2-c.

C_{Y_U} is the contribution of the ventral fin, including body and horizontal tail interference effects, and effects of cross-coupling of α and β , and may include vertical tail interference. Calculate by equation 5.3.1.2-g. (Ventral fins are not affected by body vortices.)

The following procedure is used in determining the contributions of the tail panels:

Step 1

Determine the contribution of the horizontal tail in the presence of the body. The procedure is completely analogous to that for determining the contribution of the wing in the presence of the body in Section 5.2.1.2. This is always calculated first but cannot be analyzed if the panel is not body-mounted. The equation is

$$C_{Y_{HB}} = 2 \eta_B K_{HB} k(\alpha) \frac{S_B}{S_w} \frac{S_{act}}{S_{ext}} \beta - \frac{c_{d,c} (c_r)_H d}{S_w} \beta (\beta - \alpha') \quad 5.3.1.2-b$$

where the first term on the right-hand side is the forebody cross-flow effect and is taken as zero for the midtail case, and the second term on the right-hand side is an approximate effect of the horizontal inhibiting the viscous cross-flow occurring along the body at large angles of attack.

η_B is the Mach number correction to the horizontal tail-body interference coefficient from figure 5.2.1.2-7 using the exposed root chord of the horizontal tail and the average body diameter at the horizontal tail

K_{HB} is the horizontal tail-body interference coefficient, or apparent-mass ratio, from figure 5.3.1.1-2500. For tail positions other than midtail ($K_{HB} = 0$) or tangent, a nonlinear interpolation is described in Method 3, paragraph A, Section 5.3.1.1.

$k(\alpha)$ is the angle-of-attack correction to the horizontal tail-body interference coefficient obtained from figure 5.2.1.2-8 using the exposed root chord of the horizontal tail and the average body diameter at the horizontal tail. For tail positions other than midtail ($k(\alpha) = 0$) or tangent, a nonlinear interpolation is described in Method 3, paragraph A, Section 5.3.1.1.

$\frac{S_{act}}{S_{ext}}$	is the ratio of the actual projected side area of the fuselage to that of the extended fuselage as illustrated in sketch (b). These areas are bounded by the shock waves and expansion fans of the horizontal tail.
c_{d_c}	is the cross-flow drag coefficient, obtained from figure 4.2.1.2-35b, with $M_c = M_\infty \sin \alpha'$
$(c_{r_e})_H$	is the exposed root chord of the horizontal tail
β	is the sideslip angle in radians
α'	is the angle of inclination, $\alpha' = \sqrt{\alpha^2 + \beta^2}$, in radians

Step 2

Determine the vertical tail contribution by

$$C_{Y_V} = C_{Y_{V(K,\phi)}} + C_{Y_{V(\Gamma_B)}}$$
 5.3.1.2-c

where

$C_{Y_{V(K,\phi)}}$ accounts for horizontal tail-body interference and cross-coupling of α and β acting on the vertical stabilizer, given by equation 5.3.1.2-d

$C_{Y_{V(\Gamma_B)}}$ accounts for the effect of body vortices on the vertical stabilizer, given by equation 5.3.1.2-e

Compute:

$$C_{Y_{V(K,\phi)}} = \left[K'_V - K_{\phi_V} \alpha \tan \Lambda_{LEV} \right] (-C_{N_\alpha})_V \beta \frac{S_{v_e}}{S_w}$$
 5.3.1.2-d

where

K'_V is the effective apparent-mass ratio of the vertical tail, as described in paragraph C of Section 5.3.1.1, but refers to sketch (c) of this Section. This factor includes the presence of the horizontal tail; but does not include the presence of the ventral fin if the ventral fin is farther forward than the vertical tail as measured from the leading edges of the exposed root chords.

K_{ϕ_V} is the cross-coupling interference factor of the vertical tail, from figure 5.3.1.2-12

α is the angle of attack in radians

Λ_{LEV} is the sweepback angle of the vertical tail leading edge

$(C_{N_\alpha})_V$ is the normal-force-curve slope of the vertical tail as defined in paragraph C of Section 5.3.1.1

Compute:

$$C_{Y_{V(\Gamma_B)}} = \Delta i_v \left[\frac{\Gamma_B}{2\pi \alpha' Vr} \right] \frac{(-C_{N_\alpha})_V \alpha' S_{v_e}}{\left(\frac{b_v}{r} - 1 \right) S_w}$$
 5.3.1.2-e

where

$\frac{\Gamma_B}{2\pi \alpha' Vr}$ is the nondimensional vortex strength obtained from figure 4.3.1.3-15 of Section 4.3.1.3 with α replaced by α' in all cases and x taken as the distance from the body nose to the midpoint of the MAC of the exposed panel.

α' is the angle of inclination in radians: $\alpha' = \sqrt{\alpha^2 + \beta^2}$

r is the average radius of the body along the vertical tail exposed root chord

Δi_v

is the vortex interference factor:

$\Delta i_v = i_{v_1} - i_{v_2}$. The values of i_{v_1} and i_{v_2} are given in figure 5.3.1.2-13, where they are presented as functions of the positions of the body vortices at the vertical tail

$\frac{z_{v_1}}{b_v}, \frac{y_{v_1}}{b_v}, \frac{z_{v_2}}{b_v}, \text{ and } \frac{y_{v_2}}{b_v}$ (see sketch (e)). These are given by

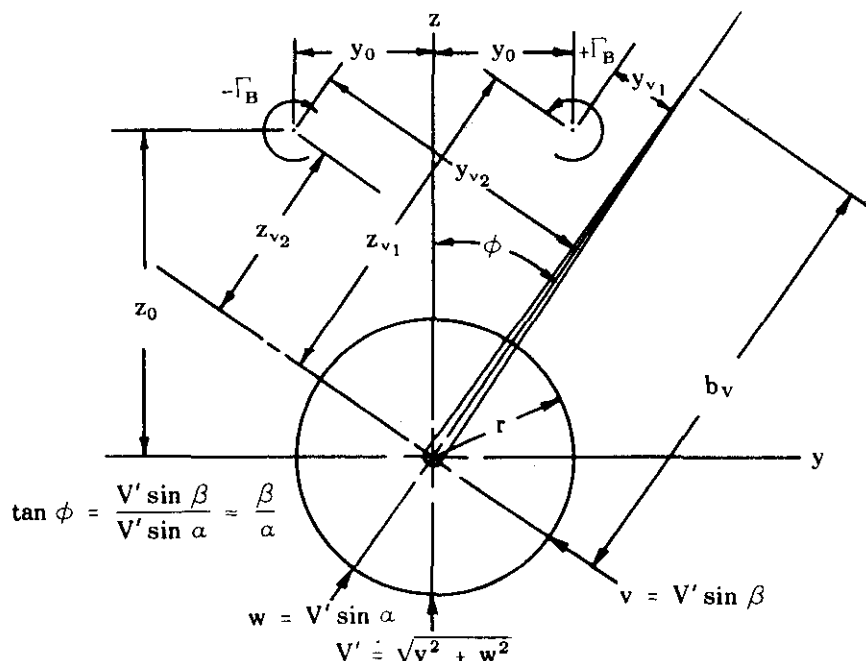
$$\left. \begin{aligned} \frac{z_{v_1}}{b_v} &= \frac{r}{b_v} \left[\frac{z_0}{r} \cos \phi + \frac{y_0}{r} \sin \phi \right] \\ \frac{y_{v_1}}{b_v} &= \frac{r}{b_v} \left[\frac{z_0}{r} \sin \phi - \frac{y_0}{r} \cos \phi \right] \\ \frac{z_{v_2}}{b_v} &= \frac{r}{b_v} \left[\frac{z_0}{r} \cos \phi - \frac{y_0}{r} \sin \phi \right] \\ \frac{y_{v_2}}{b_v} &= \frac{r}{b_v} \left[\frac{z_0}{r} \sin \phi + \frac{y_0}{r} \cos \phi \right] \end{aligned} \right\} \quad 5.3.1.2-f$$

where $\phi = \tan^{-1} \frac{\beta}{\alpha}$

$\frac{z_0}{r}$ is the vertical position of the body vortex in the y-z coordinate system from figure 4.3.1.3-13b

$\frac{y_0}{r}$ is the lateral position of the body vortex in the y-z coordinate system from figure 4.3.1.3-14

In reading these last two figures α must be replaced by α' in all cases and x is taken as the distance from the body nose to the midpoint of the MAC of the exposed panel.



TYPICAL ORIENTATION OF BODY VORTICES WITH RESPECT
TO TAIL PLANE FOR CONFIGURATION AT COMBINED ANGLES

SKETCH (e)

Step 3

Determine the ventral fin contribution by

$$C_{Y_U} = C_{Y_{VU(\alpha, \beta)}} = \left[K'_U + K_{\phi_U} \alpha \tan \Lambda_{LE_U} \right] (-C_{N_a})_U \beta \frac{S_{V_e}}{S_w} \quad 5.3.1.2-g$$

where

- K'_U is the effective apparent-mass ratio of the ventral fin, as described in paragraph C of Section 5.3.1.1, but refers to sketch (c) of this Section. This factor includes the presence of a horizontal tail; but does not include the presence of the vertical tail if the vertical tail is farther forward than the ventral fin, as measured from the leading edge of the exposed root chords.
- K_{ϕ_U} is the cross-coupling interference factor of the ventral fin from figure 5.3.1.2-12
- Λ_{LE_U} is the sweepback angle of the ventral fin leading edge
- $(C_{N_a})_U$ is the normal-force-curve slope of the ventral fin as defined in paragraph C of Section 5.3.1.1

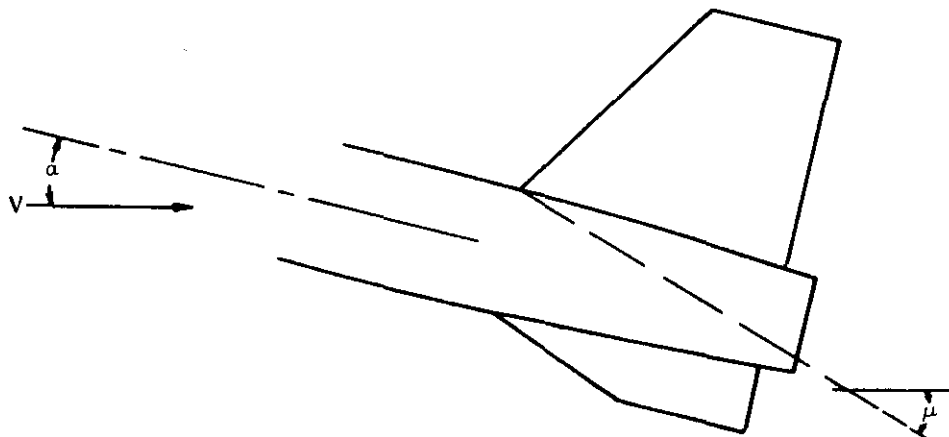
Step 4

All terms are now available for substitution into equation 5.3.1.2-a for finding $C_{Y_{HVU(\alpha, \beta)}}$.

Values for the incremental coefficient resulting from the addition of upper vertical tails to circular bodies, calculated using equation 5.3.1.2-c, are compared with experimental results in figure 5.3.1.2-11. It is evident from the experimental data that a strong destabilizing effect occurs with increasing angle of attack and that this effect is accurately predicted by the Datcom method over the angle-of-attack range of the tests.

Sample Problem

Given: The configuration of reference 5 consisting of body, vertical tail, and ventral tail. This is the same configuration as that of sample problem 2, paragraph C, Section 5.3.1.1. Find the side-force coefficient developed by the vertical and ventral tails in the presence of a body at $\alpha = 12^\circ$ and $\beta = 4^\circ$.



Body Characteristics

Ogive cylinder, with slight boattail

$d = 3.33$ in.

$r_1 = r_2 = 1.5$ in. (average values in region of tail panels)

Vertical Tail Characteristics

$S_{V_e} = 31.6$ sq in.

$b_V = 7.48$ in.

$\Lambda_{LE_V} = 32.5^\circ$

$A_{V_e} = 1.12$

$\lambda_{V_e} = 0.482$

Ventral Tail Characteristics

$$S_{U_e} = 8.54 \text{ sq in.} \quad b_U = 3.05 \text{ in.} \quad \Lambda_{LE_U} = 70^\circ \quad A_{U_e} = 0.35$$

$$\lambda_{U_e} = 0.428$$

Additional Characteristics

$$M = 2.01 \quad \alpha = 12^\circ = 0.209 \text{ rad} \quad \beta = 4^\circ = 0.070 \text{ rad}$$

$$\alpha' = \sqrt{\alpha^2 + \beta^2} = 12.65^\circ = 0.221 \text{ rad} \quad S_w = 144.0 \text{ sq in.}$$

$x/r = 21.87$ (x measured from nose to 50-percent-chord point of MAC of exposed vertical panel)

At positive angle of attack, vertical-tail exposed root-chord leading edge is aft of ventral-fin exposed root-chord leading edge.

Ventral fin is not influenced by presence of vertical tail at this angle of attack and Mach number.

Compute:

Step 1. Determine the horizontal-tail contribution $C_{Y_{HB}}$

$$C_{Y_{HB}} = 0 \text{ (horizontal tail off)}$$

Step 2. Determine the vertical tail contribution C_{Y_V}

Vertical tail interference and cross-coupling term $C_{Y_{V(\phi, \phi)}}$

Determine $K'_V = 1.13$ (figure 5.3.1.1-25a) at $(r_1/r_2) = 1.000$; $(r_1/b)_V^{\text{added panel}} = 0.200$; $(r_1/b)_U^{\text{existing panel}} = 1.000$;

Determine $K_{\phi_V} = 0.687$ (figure 5.3.1.2-12 at $(r_1/b)_V = 0.200$)

Determine $(C_{N_a})_V$ using $2A_{V_e}$

$(C_{N_a})_V = 2.12 \text{ per rad}$ (based on S_{V_e}) (sample problem 2, paragraph C, Section 5.3.1.1)

$$C_{Y_{V(\phi, \phi)}} = \left[K'_V - K_{\phi_V} \alpha \tan \Lambda_{LE_V} \right] (-C_{N_a})_V \beta \frac{S_{V_e}}{S_w} \quad (\text{equation 5.3.1.2-d})$$

$$= [1.13 - (0.687)(0.209) \tan 32.5^\circ] (-2.12)(0.070) \left(\frac{31.6}{144.0} \right)$$

$$= -0.0339 \text{ (based on } S_w)$$

Effect of body vortices on vertical tail contribution $C_{Y_V(\Gamma_B)}$

$$\frac{x_e}{r} = 10.6 \text{ (figure 4.3.1.3-13a at } \alpha' = 12.65^\circ)$$

$$\frac{\alpha'(x - x_e)}{r} = 0.221 (21.87 - 10.6) = 2.49$$

$$\frac{\Gamma_B}{2\pi \alpha' Vr} = 0.86 \text{ (figure 4.3.1.3-15 at } \alpha' = 12.65^\circ)$$

$$\frac{y_0}{r} = 0.71 \text{ (figure 4.3.1.3-14 at } \alpha' = 12.65^\circ)$$

$$\frac{z_0}{r} = 1.53 \text{ (figure 4.3.1.3-13b at } \alpha' = 12.65^\circ)$$

$$\phi = \tan^{-1} \frac{b_v^3}{a} = \tan^{-1} \frac{4}{12} = 18.4^\circ$$

Calculate position of vortices at vertical tail

$$\begin{aligned}\frac{z_{v1}}{b_v} &= \frac{r}{b_v} \left[\frac{z_0}{r} \cos \phi + \frac{y_0}{r} \sin \phi \right] && \text{(equation 5.3.1.2-f)} \\ &= \frac{1.50}{7.48} (1.53 \cos 18.4^\circ + 0.71 \sin 18.4^\circ) \\ &= 0.336\end{aligned}$$

$$\begin{aligned}\frac{y_{v1}}{b_v} &= \frac{r}{b_v} \left[\frac{z_0}{r} \sin \phi - \frac{y_0}{r} \cos \phi \right] && \text{(equation 5.3.1.2-f)} \\ &= \frac{1.50}{7.48} (1.53 \sin 18.4^\circ - 0.71 \cos 18.4^\circ) \\ &= -0.038\end{aligned}$$

$$\begin{aligned}\frac{z_{v2}}{b_v} &= \frac{r}{b_v} \left[\frac{z_0}{r} \cos \phi - \frac{y_0}{r} \sin \phi \right] && \text{(equation 5.3.1.2-f)} \\ &= \frac{1.50}{7.48} (1.53 \cos 18.4^\circ - 0.71 \sin 18.4^\circ) \\ &= 0.246\end{aligned}$$

$$\begin{aligned}\frac{y_{v2}}{b_v} &= \frac{r}{b_v} \left[\frac{z_0}{r} \sin \phi + \frac{y_0}{r} \cos \phi \right] && \text{(equation 5.3.1.2-f)} \\ &= \frac{1.50}{7.48} (1.53 \sin 18.4^\circ + 0.71 \cos 18.4^\circ) \\ &= 0.232\end{aligned}$$

Find vortex interference factor

$$\left. \begin{aligned}i_{v1} &= -1.4 \\ i_{v2} &= -0.9\end{aligned} \right\} \quad \text{(figure 5.3.1.2-13a)}$$

$$\Delta i_v = i_{v1} - i_{v2} = (-1.4) - (-0.9) = -0.5$$

$$\begin{aligned}C_{Y_W(\Gamma_B)} &= \Delta i_v \left[\frac{\Gamma_B}{2\pi \alpha' V_r} \right] \frac{(-C_{N_a})_v \alpha' S_{V_e}}{\left(\frac{b_v}{r} - 1 \right) S_w} && \text{(equation 5.3.1.2-e)} \\ &= (-0.5) (0.86) \frac{(-2.12) (0.221) (31.6)}{\left(\frac{7.48}{1.5} - 1 \right) (144.0)} \\ &= 0.01104 \text{ (based on } S_w)\end{aligned}$$

Total vertical tail contribution:

$$\begin{aligned} C_{Y_V} &= C_{Y_{V(B),\phi}} + C_{Y_V(T_B)} \quad (\text{equation 5.3.1.2-c}) \\ &= (-0.0339) + (0.01104) \\ &= -0.0229 \text{ (based on } S_w) \end{aligned}$$

Step 3 Determine the ventral tail contribution C_{Y_U}

Ventral fin interference and cross-coupling term $C_{Y_{U(B),\phi}}$

$$\text{Determine } K'_U = 2.11 \text{ (figure 5.3.1.1-25a) at } (r_1/r_2) = 1.000; (r_1/b)_U^{\text{added panel}} = 0.492; (r_1/b)_V^{\text{existing panel}} = 1.000$$

(no horizontal tail, and ventral fin is out of vertical tail influence).

$$\text{Determine } K_{\phi_U} = 0.535 \text{ (figure 5.3.1.2-12 at } (r_1/b)_U = 0.492)$$

$$\text{Determine } (C_{N_a})_U \text{ using } 2A_{U_e}$$

$$(C_{N_a})_U = 1.09 \text{ per rad (Section 4.1.3.2; based on } S_{U_e})$$

Total ventral fin contribution:

$$\begin{aligned} C_{Y_U} &= C_{Y_{U(B),\phi}} = [K'_U + K_{\phi_U} \alpha \tan \Lambda_{1,E_U}] (-C_{N_a})_U \beta \frac{S_{U_e}}{S_w} \quad (\text{equation 5.3.1.2-g}) \\ &= [2.11 + (0.535)(0.209) \tan 70^\circ] (-1.09)(0.070) \left(\frac{8.54}{144.0} \right) \\ &= -0.0109 \text{ (based on } S_w) \end{aligned}$$

Solution:

$$\begin{aligned} C_{Y_{HVU(B)}} &= C_{Y_{H(B)}} + C_{Y_V} + C_{Y_U} \quad (\text{equation 5.3.1.2-a}) \\ &= 0 + (-0.0229) + (-0.0109) \\ &= -0.0338 \text{ (based on } S_w) \end{aligned}$$

REFERENCES

1. Kaettler, G. E.: Estimation of Directional Stability Derivatives at Moderate Angles and Supersonic Speeds. NASA Memo 12-1-58A, 1958. (U)
2. Spahr, J. R.: Contribution of the Wing Panels to the Forces and Moments of Supersonic Wing-Body Combinations at Combined Angles. NACA TN 4146, 1958. (U)
3. Pitts, W. C., Nielsen, J. N., and Kaettler, G. E.: Lift and Center of Pressure of Wing-Body-Tail Combinations at Subsonic, Transonic, and Supersonic Speeds. NACA TR 1307, 1959. (U)
4. Spahr, J. R.: Theoretical Prediction of the Effects of Vortex Flows on the Loading, Forces, and Moments of Blended Aircraft. NASA TR R-10 1961. (U)
5. Spearman, M. L., Driver, C., and Hughes, W. C.: Investigation of Aerodynamic Characteristics in Pitch and Sideslip of a 45° Sweptback-Wing Airplane Model with Various Vertical Locations of Wing and Horizontal Tail - Basic-Data Presentation, $M = 2.01$. NACA RM L54L06, 1955. (U)

- - - DATCOM METHOD
 ○ EXPERIMENT

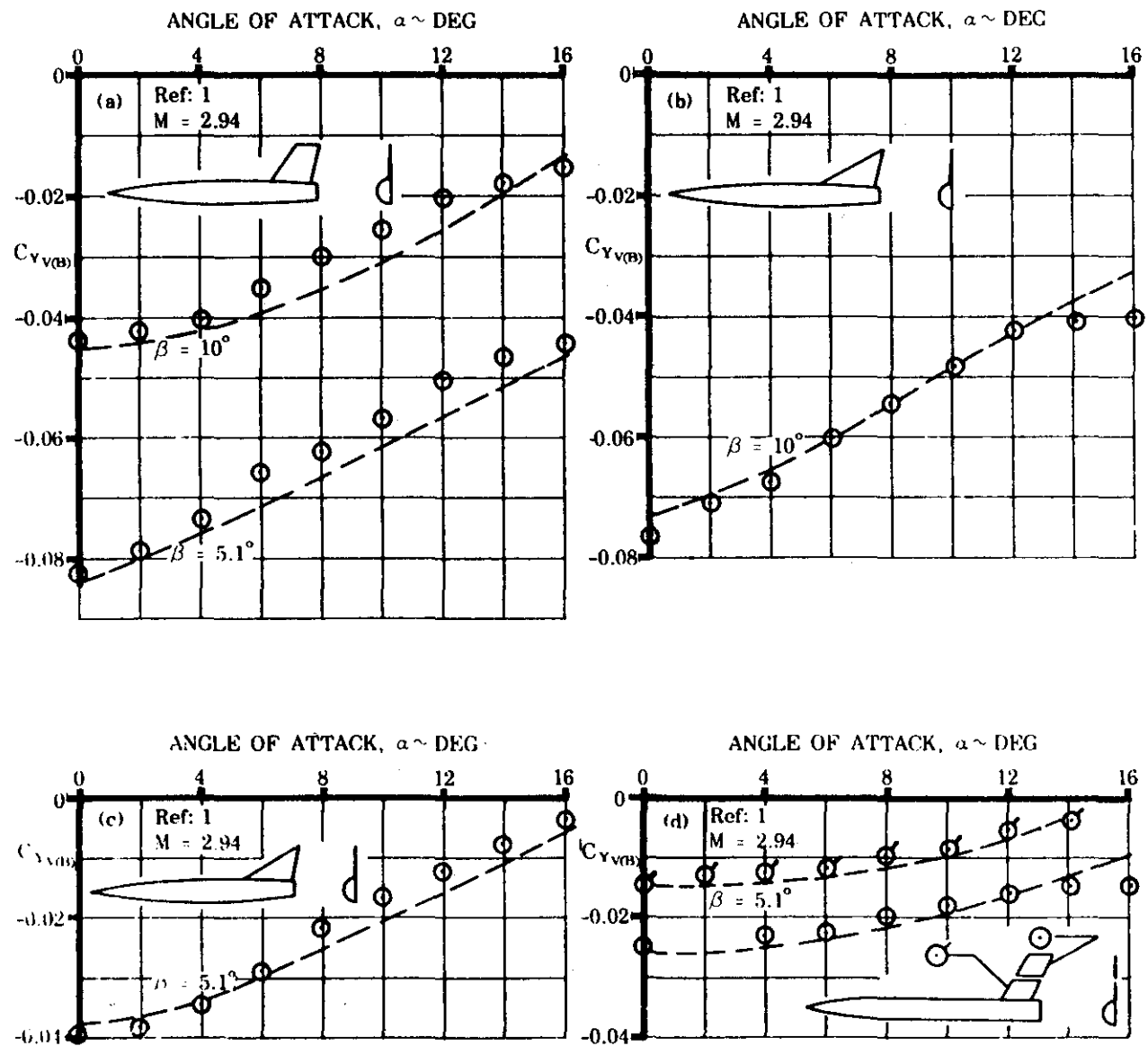


FIGURE 5.3.1.2-11 COMPARISON OF EXPERIMENTAL AND CALCULATED SIDE-FORCE COEFFICIENT INCREMENTS DUE TO ADDING A VERTICAL TAIL TO A BODY

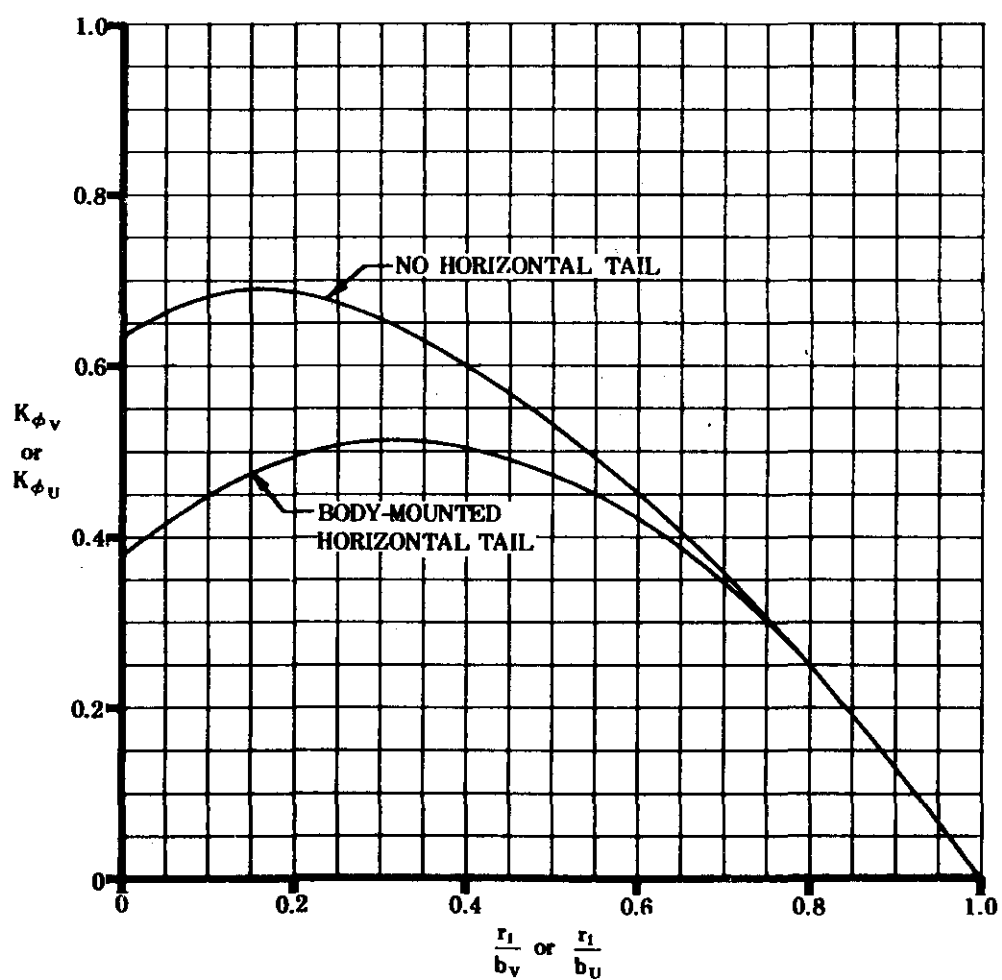


FIGURE 5.3.1.2-12 CROSS-COUPLING INTERFERENCE FACTOR

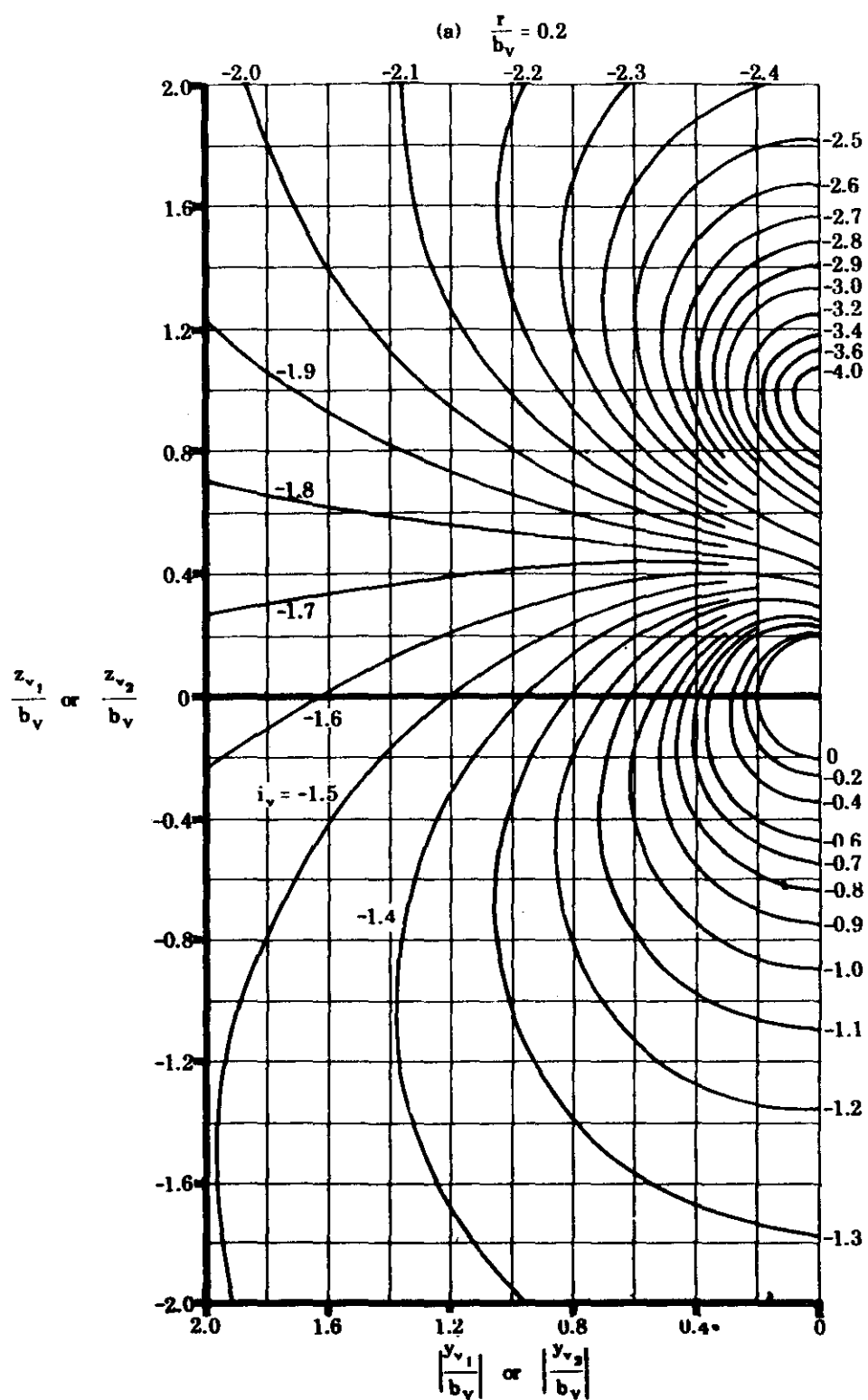


FIGURE 5.3.1.2-13 VORTEX INTERFERENCE FACTOR

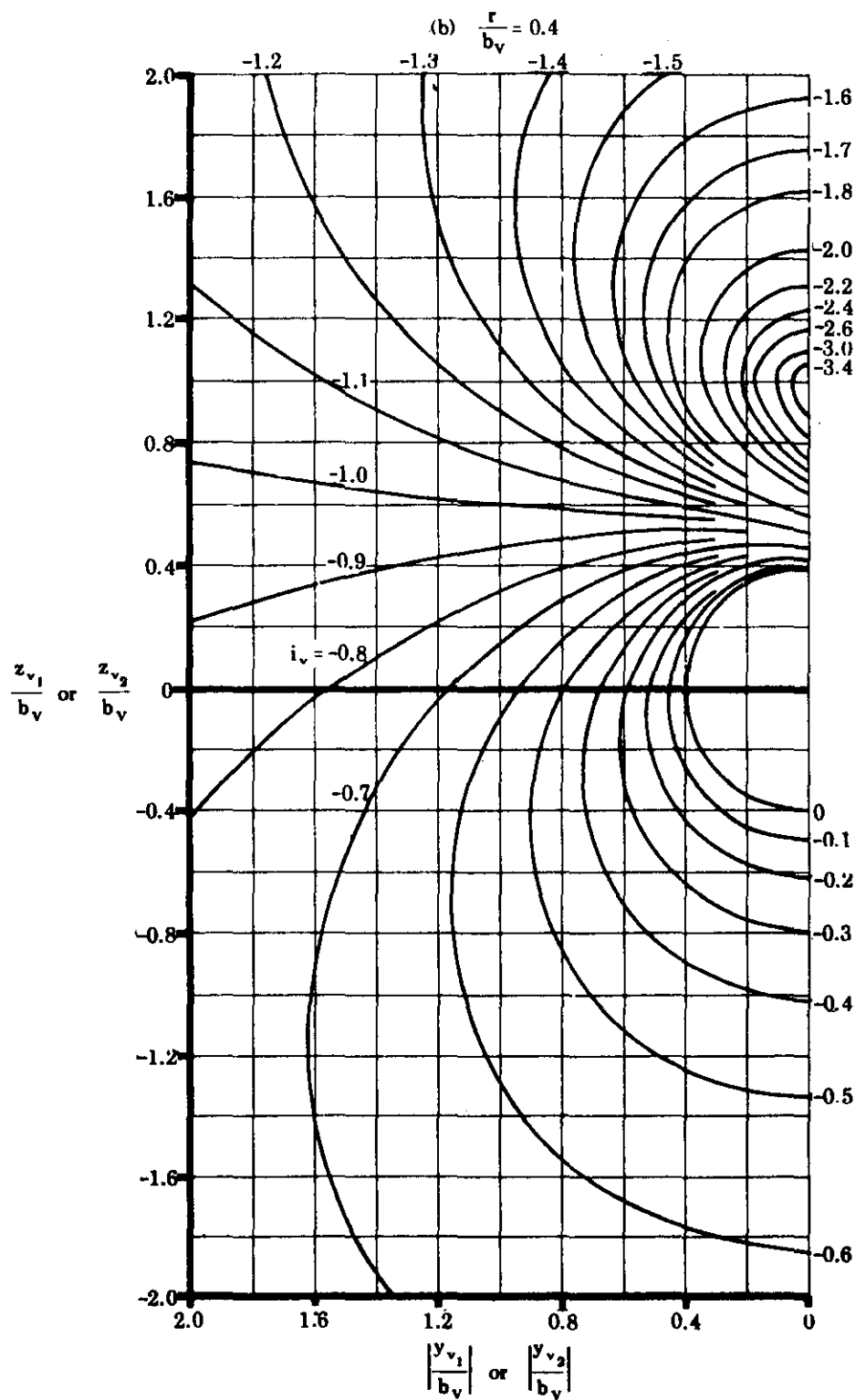


FIGURE 5.3.1.2-13 VORTEX INTERFERENCE FACTOR (contd)

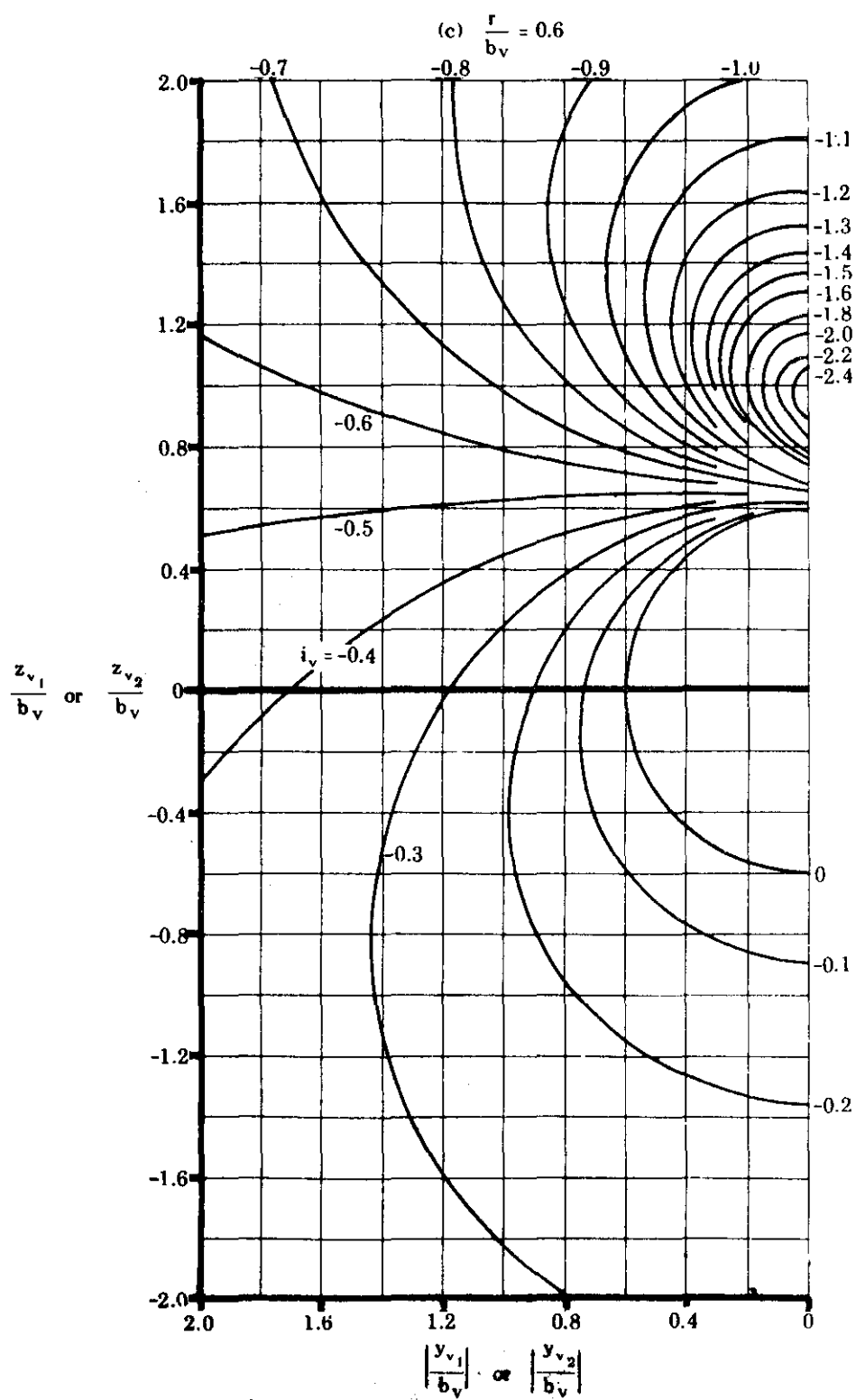


FIGURE 5.3.1.2-13 VORTEX INTERFERENCE FACTOR (contd)

5.3.2 TAIL-BODY SIDESLIP DERIVATIVE C_{l_β}

5.3.2.1 TAIL-BODY SIDESLIP DERIVATIVE C_{l_β} IN THE LINEAR ANGLE-OF-ATTACK RANGE

The method of estimating the contribution of panels in the empennage to the sideslip derivative C_{l_β} is similar to that for estimating the contribution of panels in the empennage to C_{n_β} . That is, the side force generated by an added panel is multiplied by an appropriate moment arm in order to obtain the rolling-moment contribution.

A refinement is required in the case of the contribution of a vertical panel (either an upper or lower vertical panel), since the pressure field that is generated by the vertical panel is reflected on the surface of the horizontal tail. These induced loads on the horizontal tail are perpendicular to this surface and therefore do not significantly affect the vehicle yawing moments or side forces. They do, however, contribute to the rolling moments and hence must not be neglected. The rolling-moment contribution of the horizontal tail is positive (opposes that due to the vertical panel) when the horizontal surface is in the low position with respect to the vertical panel. The rolling-moment contribution has no effect when the horizontal tail is mounted near the midspan of the vertical panel and is negative for the horizontal surface in the high position.

At subsonic speeds these contributions are usually small, and reasonable results are obtained when they are neglected. (Actually they would be quite difficult to estimate.) At transonic speeds they can be quite pronounced, because the pressure field of the entire horizontal surface is strongly influenced by the presence of the vertical panel. At supersonic speeds the interferences are restricted to regions on the horizontal surfaces within the boundaries defined by the shock-wave pattern of the vertical panel. As the Mach number increases, the region of influence decreases because the shock pattern becomes more swept. It is to be expected, therefore, that this horizontal-tail effect will become less significant as the supersonic Mach number increases.

Because of the complexity of the problem, no method for predicting the effects of panels in the empennage at transonic speeds is presented, and the method presented for supersonic speeds does not account for the horizontal-tail contribution. However, the effect of the presence of a horizontal tail is accounted for at supersonic speeds in computing the contribution of a vertical panel.

A. SUBSONIC

The contribution of panels in the empennage to the vehicle sideslip derivative C_{l_β} is based on the values of the panel contribution to C_{Y_β} estimated by the methods of Paragraph A of Section 5.3.1.1.

In addition to the pressure forces induced on the horizontal tail by the vertical tail, there can be other forces for a configuration having either significant twist and/or dihedral on the horizontal tail. If the horizontal tail is large relative to the wing, the effects of twist and/or dihedral may be worthy of consideration. To consider these effects on the horizontal tail, the method of Section 5.1.2.1 is used; i.e., treating the horizontal tail as an isolated wing. (Caution should be exercised to make certain that the horizontal-tail contribution to C_{l_β} is converted to the same reference area and

length $S_w b_w$ as the wing-body contribution, before adding them together.) However, since the horizontal-tail contribution is very small for most configurations in the subsonic speed regime, the method presented here neglects this contribution.

As mentioned above, reasonable results are obtained at subsonic speeds when the horizontal-tail contribution is neglected. However, in using Method 3 of Paragraph A, Section 5.3.1.1, if a horizontal tail is present in the empennage, its effect on the vertical-tail contribution must be accounted for by proper use of the apparent-mass factor (K) charts. If Method 1 or Method 2 of Paragraph A, Section 5.3.1.1 is used, the effect of a horizontal tail on the vertical-tail contribution is implicitly accounted for by the method.

DATCOM METHOD

The contribution of a vertical panel to the sideslip derivative $C_{l\beta}$ is estimated by

$$(\Delta C_{l\beta})_p = (\Delta C_{Y\beta})_p \frac{z_p \cos \alpha - \ell_p \sin \alpha}{b_w} \quad 5.3.2.1-a$$

where

p is the subscript referring to the added vertical panel (either an upper vertical stabilizing surface V or a lower vertical stabilizing surface U).

$(\Delta C_{Y\beta})_p$ is the side force due to sideslip of the added vertical panel determined as follows:

For configurations with horizontal panels mounted on the body or with no horizontal panels, use Method 1 or Method 3 of Paragraph A, Section 5.3.1.1.

For configurations with horizontal panels mounted on the vertical panel, use Method 1 of Paragraph A, Section 5.3.1.1.

For twin-vertical-panel configurations, use Method 2 of Paragraph A, Section 5.3.1.1.

z_p is the distance in the z-direction (normal to the longitudinal body axis) between the moment reference center (usually the vehicle center of gravity) and the MAC of the added panel, positive for the panel above the body.

ℓ_p is the distance parallel to the longitudinal body axis between the moment reference center (usually the vehicle center of gravity) and the quarter-chord point of the MAC of the added panel, positive for the added panel behind the moment reference center. The aerodynamic center of the vertical panel could be used, but the inaccuracies of the basic method do not warrant this degree of refinement.

b_w is the span of the wing.

All geometry used in determining the moment arms for the above method is based on the vertical panel extended to the body center line.

For a wingless configuration, b_w is replaced by the vehicle reference length and $(\Delta C_{Y_\beta})_p$ is based on the vehicle reference area.

Results calculated at zero angle of attack by this method are compared to experimental data in Table 5.3.2.1-A. The detailed geometry of the configurations used in this table is given in Table 5.3.1.1-B. It should be noted that the values of ΔC_{Y_β} used in Table 5.3.2.1-A are not test data, but are calculated by the method of Section 5.3.1.1. The errors inherent in estimating ΔC_{Y_β} are therefore implicitly included in Table 5.3.2.1-A. However, the errors due to ΔC_{Y_β} and those due to the moment arm can be separated by comparing the errors for a given configuration from Table 5.3.1.1-B (for ΔC_{Y_β}) with those of Table 5.3.2.1-A (for ΔC_{I_β}).

Sample Problems

- Given: The configuration of Reference 1 consisting of a wing, body, horizontal tail, and upper vertical tail. This is the same configuration as that of Sample Problem 1, Paragraph A, Section 5.3.1.1. Some of the characteristics are repeated.

Wing Characteristics:

$$S_w = 576.0 \text{ sq in.} \quad b_w = 41.56 \text{ in.} \quad z_w = 0$$

Additional Characteristics:

$$M = 0.25 \quad l_v = 24.89 \text{ in. (c.g. to } (\bar{c}/4)_v) \quad z_v = 5.78 \text{ in. (c.g. to } (MAC)_v)$$

$$\alpha = 0, 2^\circ, 4^\circ, 6^\circ$$

Compute:

$$(\Delta C_{Y_\beta})_{V(WBH)} = -0.734 \text{ per rad (based on } S_w) \text{ (Sample Problem 1, Paragraph A, Section 5.3.1.1)}$$

Solution:

$$(\Delta C_{I_\beta})_p = (\Delta C_{Y_\beta})_p \frac{z_p \cos \alpha - l_p \sin \alpha}{b_w} \quad (\text{Equation 5.3.2.1-a})$$

$$\begin{aligned} (\Delta C_{I_\beta})_{V(WBH)} &= (\Delta C_{Y_\beta})_{V(WBH)} \frac{z_v \cos \alpha - l_v \sin \alpha}{b_w} \\ &= -0.734 \left(\frac{5.78 \cos \alpha - 24.89 \sin \alpha}{41.56} \right) \text{ per rad (based on } S_w b_w) \end{aligned}$$

Test results from Reference 1 are listed in Column 6 of the calculation table.

(1) α (deg)	(2) $z_V \cos \alpha$ (in.)	(3) $l_V \sin \alpha$ (in.)	(4) $\frac{z_V \cos \alpha - l_V \sin \alpha}{b_W}$ $[(2) - (3)] / 41.56$	(5) $(\Delta C_{I_\beta})_{V(WBH)}$ -0.734 (4) (per rad)	(6) $(\Delta C_{I_\beta})_{V(WBH)}$ (test) (per rad)
0	6.780	0	0.1390	-0.1020	-0.0877
2	6.777	0.870	0.1180	-0.0865	-0.0802
4	6.766	1.740	0.0967	-0.0710	-0.0653
6	6.750	2.600	0.0758	-0.0566	-0.0464

2. Given: The configuration of Reference 2 consisting of a wing, body, horizontal tail, and vertical tail. This is the same configuration as that of Sample Problem 3, Paragraph A, Section 5.3.1.1. Some of the characteristics are repeated.

Wing Characteristics:

$$S_w = 324 \text{ sq in.} \quad b_w = 36.0 \text{ in.} \quad z_w = 0$$

Additional Characteristics:

$$M = 0.13 \quad l_v = 16.70 \text{ in. (c.g. to } (\bar{c}/4)_v \text{)} \quad z_v = 3.78 \text{ in. (c.g. to } (MAC)_v \text{)}$$

$$\alpha = 0, 2^\circ, 4^\circ, 6^\circ$$

Compute:

$$(\Delta C_{Y_\beta})_{V(WBH)} = -0.375 \text{ per rad (based on } S_w \text{)} \text{ (Sample Problem 3, Paragraph A, Section 5.3.1.1)}$$

Solution:

$$(\Delta C_{I_\beta})_p = (\Delta C_{Y_\beta})_p \frac{z_p \cos \alpha - l_p \sin \alpha}{b_w} \quad \text{(Equation 5.3.2.1-a)}$$

$$\begin{aligned} (\Delta C_{I_\beta})_{V(WBH)} &= (\Delta C_{Y_\beta})_{V(WBH)} \frac{z_v \cos \alpha - l_v \sin \alpha}{b_w} \\ &= -0.375 \left(\frac{3.78 \cos \alpha - 16.70 \sin \alpha}{36.0} \right) \text{ per rad (based on } S_w b_w \text{)} \end{aligned}$$

Test results from Reference 2 are listed in Column 6 of the calculation table.

(1) α (deg)	(2) $z_V \cos \alpha$ (in.)	(3) $l_V \sin \alpha$ (in.)	(4) $\frac{z_V \cos \alpha - l_V \sin \alpha}{b_W}$ $[(2) - (3)] / 36.0$	(5) $(\Delta C_l)_\beta V(WBH)$ -0.375 (4) (per rad)	(6) $(\Delta C_l)_\beta V(WBH)$ (test) (per rad)
0	3.780	0	0.105	-0.0394	-0.0401
2	3.778	0.582	0.0887	-0.0333	-0.0287
4	3.771	1.166	0.0723	-0.0271	-0.0115
6	3.759	1.745	0.0560	-0.0210	-0.0057

B. TRANSONIC

A brief discussion of the flow phenomena associated with a vertical panel at transonic speeds is given in Paragraph B of Section 5.3.1.1. The rolling moments due to the vertical panel are partly determined by the transonic lift-curve-slope characteristics of the isolated tail and partly by the wake and wash characteristics of the wing-body combination. In addition, the impingement on the horizontal-tail surface of the pressure field generated by the vertical panel can cause rolling moments. This latter effect can be large, since the pressure field at transonic speeds is frequently strong and is propagated to large distances from the source. The entire horizontal surface is therefore usually immersed in the field of the vertical panel.

DATCOM METHOD

Because of the complexity of the problem, no explicit method is available in the literature for estimating the contribution of a vertical panel to C_{l_β} at transonic speeds and none is presented in the Datcom. Some examples of the limited data available in the literature are shown in Figure 5.3.2.1-13.

C. SUPERSONIC

The procedure for estimating the rolling-moment contribution due to vertical panels at supersonic speeds is essentially the same as that at subsonic speeds. That is, the rolling-moment contribution of a vertical panel is based on the sideslip derivative ΔC_{Y_β} as obtained from Section 5.3.1.1. The problem of estimating the forces generated on vertical panels is complicated by the presence of shock waves. This effect is discussed in Paragraph C of Section 5.3.1.1.

As stated in the introduction to this section, no method is available for determining the horizontal-tail contribution to the derivative C_{l_β} . However, the effect of the horizontal tail on the vertical-tail contribution is accounted for by proper use of the apparent-mass factor (K) charts in determining the vertical-panel side force.

This method is limited to configurations in which the horizontal tail is mounted on the body or configurations with no horizontal tail.

DATCOM METHOD

The contribution of a vertical panel to the sideslip derivative $C_{I\beta}$ at supersonic speeds is given by Equation 5.3.2.1-a.

$$(\Delta C_{I\beta})_p = (\Delta C_{Y\beta})_p \frac{z_p \cos \alpha - l_p \sin \alpha}{b_w}$$

where the subscript p , z_p , and b_w are defined in Paragraph A, and

$(\Delta C_{Y\beta})_p$ is the side force due to sideslip of an added vertical panel obtained from Paragraph C of Section 5.3.1.1. (If a horizontal panel is present, its effect on the vertical panel must be included.)

l_p is the distance parallel to the longitudinal body axis between the moment reference center and the 50-percent-chord point of the MAC of the added vertical panel, positive for the panel aft of the moment reference center. The aerodynamic center of the vertical panel could be used, but the inaccuracies of the basic method do not warrant this degree of refinement.

All geometry used in determining the moment arms of the vertical panels is based on the exposed panel.

For a wingless configuration the remarks following the Datcom method of Paragraph A above are also applicable here.

Results calculated at zero angle of attack by this method are compared to experimental data in Table 5.3.2.1-B. The detailed geometry of the configurations used in this table is given in Table 5.3.1.1-C. It should be noted that the values of $\Delta C_{Y\beta}$ used in Table 5.3.2.1-B are calculated by the method of Paragraph C of Section 5.3.1.1.

Sample Problems

- Given: The configuration of Reference 3 consisting of a wing, body, horizontal tail, and upper vertical stabilizer. This is the same configuration as that of Sample Problem 1, Paragraph C, Section 5.3.1.1. Some of the characteristics are repeated.

Wing Characteristics:

$$S_w = 160.4 \text{ sq in.} \quad b_w = 25.31 \text{ in.} \quad z_w = 0$$

Additional Characteristics:

$$M = 1.61 \quad l_v = 11.40 \text{ in. (c.g. to } (\bar{c}/2)_{V_e} \text{)} \quad z_v = 4.0 \text{ in. (c.g. to } (MAC)_{V_e} \text{)}$$

$$\alpha = 0, 2^\circ, 4^\circ, 6^\circ$$

Compute:

$$(\Delta C_{Y\beta})_{V(WBH)} = -0.529 \text{ per rad (based on } S_w) \text{ (Sample Problem 1, Paragraph C, Section 5.3.1.1)}$$

Solution:

$$(\Delta C_{I\beta})_p = (\Delta C_{Y\beta})_p \frac{z_p \cos \alpha - l_p \sin \alpha}{b_w} \quad (\text{Equation 5.3.2.1-a})$$

$$\begin{aligned} (\Delta C_{I\beta})_{V(WBH)} &= (\Delta C_{Y\beta})_{V(WBH)} \frac{z_v \cos \alpha - l_v \sin \alpha}{b_w} \\ &= 0.529 \left(\frac{4.0 \cos \alpha - 11.40 \sin \alpha}{25.31} \right) \text{ per rad (based on } S_w b_w) \end{aligned}$$

Test values from Reference 3 are listed in Column 6 of the calculation table.

(1)	(2)	(3)	(4)	(5)	(6)
α (deg)	$z_v \cos \alpha$ (in.)	$l_v \sin \alpha$ (in.)	$\frac{z_v \cos \alpha - l_v \sin \alpha}{b_w}$ $[(2) - (3)] / 25.31$	$(\Delta C_{I\beta})_{V(WBH)}$ -0.529 (4) (per rad)	$(\Delta C_{I\beta})_{V(WBH)}$ (test) (per rad)
0	4.000	0	0.158	-0.0836	-0.1010
2	3.998	0.398	0.143	-0.0756	-0.0930
4	3.990	0.796	0.126	-0.0667	-0.0803
6	3.978	1.191	0.110	-0.0582	-0.0647

2. Given: The configuration of Reference 4 consisting of a wing, body, upper vertical stabilizer, and lower vertical stabilizer. This is the same configuration as that of Sample Problem 2, Paragraph C, Section 5.3.1.1. Some of the characteristics are repeated.

Wing Characteristics:

$$S_w = 144.0 \text{ sq in.} \quad b_w = 24.0 \text{ in.} \quad z_w = 0$$

Additional Characteristics:

$$M = 2.01 \quad l_v = 12.0 \text{ in. (c.g. to } (\bar{c}/2)_{V_e}) \quad z_v = 4.15 \text{ in. (c.g. to } (MAC)_{V_e})$$

$$\alpha = 0, 2^\circ, 4^\circ, 6^\circ$$

Compute:

$$(\Delta C_{Y\beta})_{V(WBU)} = -0.583 \text{ per rad (based on } S_w) \text{ (Sample Problem 2, Paragraph C, Section 5.3.1.1)}$$

Solution:

$$(\Delta C_{I\beta})_p = (\Delta C_{Y\beta})_p \frac{z_p \cos \alpha - l_p \sin \alpha}{b_w} \quad (\text{Equation 5.3.2.1-a})$$

$$\begin{aligned} (\Delta C_{I\beta})_{V(WBU)} &= (\Delta C_{Y\beta})_{V(WBU)} \frac{z_v \cos \alpha - l_v \sin \alpha}{b_w} \\ &= -0.583 \left(\frac{4.15 \cos \alpha - 12.0 \sin \alpha}{24.0} \right) \text{ per rad (based on } S_w b_w) \end{aligned}$$

Test values from Reference 4 are listed in Column 6 of the calculation table.

(1)	(2)	(3)	(4)	(5)	(6)
α (deg)	$z_v \cos \alpha$ (in.)	$l_v \sin \alpha$ (in.)	$\frac{z_v \cos \alpha - l_v \sin \alpha}{b_w}$ $[(2) - (3)] / 24.0$	$(\Delta C_{I\beta})_{V(WBU)}$ -0.583 (4) (per rad)	$(\Delta C_{I\beta})_{V(WBU)}$ (test) (per rad)
0	4.150	0	0.173	-0.1010	-0.0745
2	4.147	0.419	0.166	-0.0905	-0.0774
4	4.140	0.838	0.138	-0.0805	-0.0803
6	4.127	1.254	0.120	-0.0700	-0.0830

D. HYPERSONIC

A general discussion of hypersonic flows is given in the introduction to Paragraph D of Section 4.1.3.3 and in several standard texts. No explicit method exists for estimating the contribution of an added tail panel to the sideslip derivative $C_{I\beta}$ at hypersonic speeds.

The supersonic method for estimating the derivative $(\Delta C_{Y\beta})_p$ (Paragraph C, Section 5.3.1.1) has been substantiated to reasonably high Mach numbers (6.86) and can be used for estimating the contribution of an added vertical panel, as in Paragraph C above. However, the method should be applied with caution, since the basic assumptions are increasingly violated as the Mach number increases. The hypersonic small-disturbance theory and Newtonian theory can also be used to estimate the forces and therefore the moments on the vertical panel. Newtonian flow, however, is limited to the upper range of hypersonic Mach numbers.

DATCOM METHODS

Method 1

Extended Supersonic Method

The method described in Paragraph C of this section can be used up to Mach numbers of approximately 7.

Method 2

Hypersonic Small-Disturbance Theory

Equation 5.3.2.1-a can be used to estimate hypersonic values of the vertical-panel contribution $(\Delta C_{l_\beta})_V$, where $(\Delta C_{Y_\beta})_V$ in this equation is obtained from Equation 5.3.1.1-h, and ℓ_p is determined as in Paragraph C above.

Method 3

Newtonian Theory

Equation 5.3.2.1-a is again used, but the vertical-panel contribution $(\Delta C_{Y_\beta})_V$ in this equation is based upon the use of Equation 5.3.1.1-i for this case, and ℓ_p is determined as in Paragraph C above. This method is most successful in the upper range of hypersonic Mach numbers.

Because of the general lack of test data in this speed regime, no substantiation tables are presented.

Sample Problem

Method 2

Given: The configuration of Reference 5. This is the same configuration as that of the sample problem, Paragraph D, Section 5.3.1.1. Some of the characteristics are repeated.

Wing Characteristics:

$$S_w = 19.15 \text{ sq in.} \quad b_w = 5.60 \text{ in.} \quad z_w = 0$$

Additional Characteristics:

$$M = 5.0 \quad z_V = 0.795 \text{ in. (c.g. to } (MAC)_V)_e \quad \alpha = 0$$

Compute:

$$\frac{z_V}{b_w} = \frac{0.795}{5.60} = 0.142$$

$$(\Delta C_{Y_\beta})_V = -0.86 \text{ per rad (based on } S_w) \text{ (Sample Problem, Paragraph D, Section 5.3.1.1)}$$

Solution:

$$(\Delta C_{I_\beta})_V = (\Delta C_{Y_\beta})_p \frac{z_p \cos \alpha - l_p \sin \alpha}{b_w} \quad (\text{Equation 5.3.2.1-a})$$

$$(\Delta C_{I_\beta})_V = (\Delta C_{Y_\beta})_V \frac{z_V}{b_w} \quad (\alpha = 0)$$

$$= -0.86 (0.142)$$

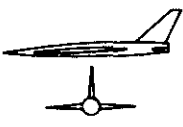
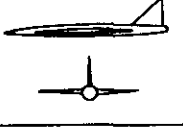
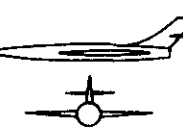
$$= -0.122 \text{ per rad (based on } S_w b_w)$$

This corresponds to an experimental value (based on $S_w b_w$) of -0.1146 per radian obtained from Reference 5.

REFERENCES

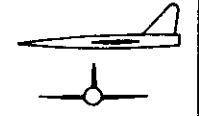
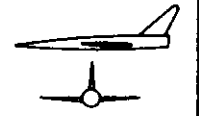
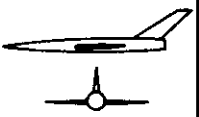
1. Savage, H. F., and Tinling, B. E.: The Subsonic Static Aerodynamic Characteristics of an Airplane Model Having a Triangular Wing of Aspect Ratio 3. II – Lateral and Directional Characteristics. NACA TN 4042, 1957. (U)
2. Letko, W., and Williams, J. L.: Experimental Investigation at Low Speed of Effects of Fuselage Cross Section on Static Longitudinal and Lateral Stability Characteristics of Models Having 0° and 45° Sweptback Surfaces. NACA TN 3551, 1955. (U)
3. Spearman, M. L.: Static Lateral and Directional Stability and Effective Sidewash Characteristics of a Model of a 35° Swept-Wing Airplane at a Mach Number of 1.61. NACA RM L56E23, 1956. (U)
4. Spearman, M. L., and Robinson, R. B.: Investigation of the Aerodynamic Characteristics in Pitch and Sideslip of a 45° Swept-Wing Configuration with Various Vertical Locations of the Wing and Horizontal Tail. Static Lateral and Directional Stability; Mach Numbers of 1.41 and 2.01. NACA RM L57J25a, 1957. (U)
5. Dennis, D. H., and Petersen, R. H.: Aerodynamic Performance and Static Stability at Mach Numbers Up to 5 of Two Airplane Configurations with Favorable Lift Interference. NASA Memo 1-8-59A, 1959. (U)

TABLE 5.3.2.1-A¹
SUBSONIC CONTRIBUTION OF VERTICAL PANELS TO $C_{l\beta}$
DATA SUMMARY AND SUBSTANTIATION

Ref. ²	Configuration Sketch	M	Panel Added	$(\Delta C_{Y\beta})_V$ Calc. (per rad)	$\frac{z_V}{b_W}$	$(\Delta C_{l\beta})_V$ Calc. (per rad)	$(\Delta C_{l\beta})_V$ Test (per rad)	Percent Error e
6		.25	BWHV _s -BW	-.481	.121	-.058	-.060	3.3
		.25	BWHV _L -BW	-.734	.139	-.102	-.091	12.1
		.25	BV _s -B	-.428	.121	-.052	-.065	20.0
		.25	BV _L -B	-.578	.139	-.080	-.102	21.6
		.25	BHV _L -BH	-.597	.139	-.083	-.095	12.6
		.25	BHV _s -BH	-.431	.121	-.052	-.058	10.3
8		.17	BV-B	-.254	.095	-.024	-.023	4.3
		.17	BV-B	-.317	.107	-.034	-.034	0
		.17	BV-B	-.446	.130	-.058	-.071	18.3
		.17	BW ₁ V-BW ₁	-.468	.130	-.061	-.069	11.6
9		.17	BW ₂ V-BW ₂	-.409	.130	-.053	-.052	1.9
		.17	BW ₃ V-BW ₃	-.528	.130	-.069	-.080	13.7
		.6	BWHV-BW	-.575	.125	-.072	-.069	4.3
		.13	BWHV-BW	-.426	.126	-.054	-.057	5.3

1. Refer to Table 5.3.1.1-B for configuration data
2. These references are found in Section 5.3.1.1

TABLE 5.3.2.1-B¹
 SUPERSONIC CONTRIBUTION OF VERTICAL PANELS TO $C_{l\beta}$
 DATA SUMMARY AND SUBSTANTIATION

Ref. ²	Configuration Sketch	M	Panel Added	$(\Delta C_{Y\beta})_V$ Calc. (per rad)	$\frac{z_V}{b_W}$	$(\Delta C_{l\beta})_V$ Calc. (per rad)	$(\Delta C_{l\beta})_V$ Test (per rad)	Percent Error e
16		1.61	BV-B	-.525	.158	-.083	-.083	0
		1.61	BWHV-BWH	-.529	.158	-.084	-.101	16.8
17		1.61	BWV _o -BW	-.358	.145	-.052	-.049	6.1
		2.01	BWV _o -BW	-.335	.145	-.048	-.034	41.2
		1.61	BWHV _o -BWH	-.368	.136	-.050	-.043	16.3
		2.01	BWHV _o -BWH	-.335	.145	-.048	-.034	41.2
		1.61	BWHV _{ext} -BWH	-.424	.151	-.064	-.054	18.5
		1.61	BWHV _{127\%} -BWH	-.471	.146	-.069	-.060	15.0
18		1.41	BWV-BW	-.836	.182	-.152	-.126	20.6
		2.01	BWV-BW	-.545	.182	-.099	-.103	3.9
18		1.41	BWV-BW	-.842	.182	-.153	-.126	21.4
		2.01	BWV-BW	-.540	.182	-.098	-.100	2.0
18		1.41	BWV-BW	-.792	.182	-.144	-.126	14.3
		2.01	BWV-BW	-.542	.182	-.099	-.092	7.6
18		1.41	BWV-BW	-.706	.182	-.128	-.097	32.0
		2.01	BWV-BW	-.586	.182	-.107	-.086	24.4
19		5.0	BWV-BW	-.860 ³	.142	-.122	-.123	.8

1. Refer to Table 5.3.1.1-C for configuration data
2. These references are found in Section 5.3.1.1
3. Refer to Sample Problem, Paragraph D, Section 5.3.1.1

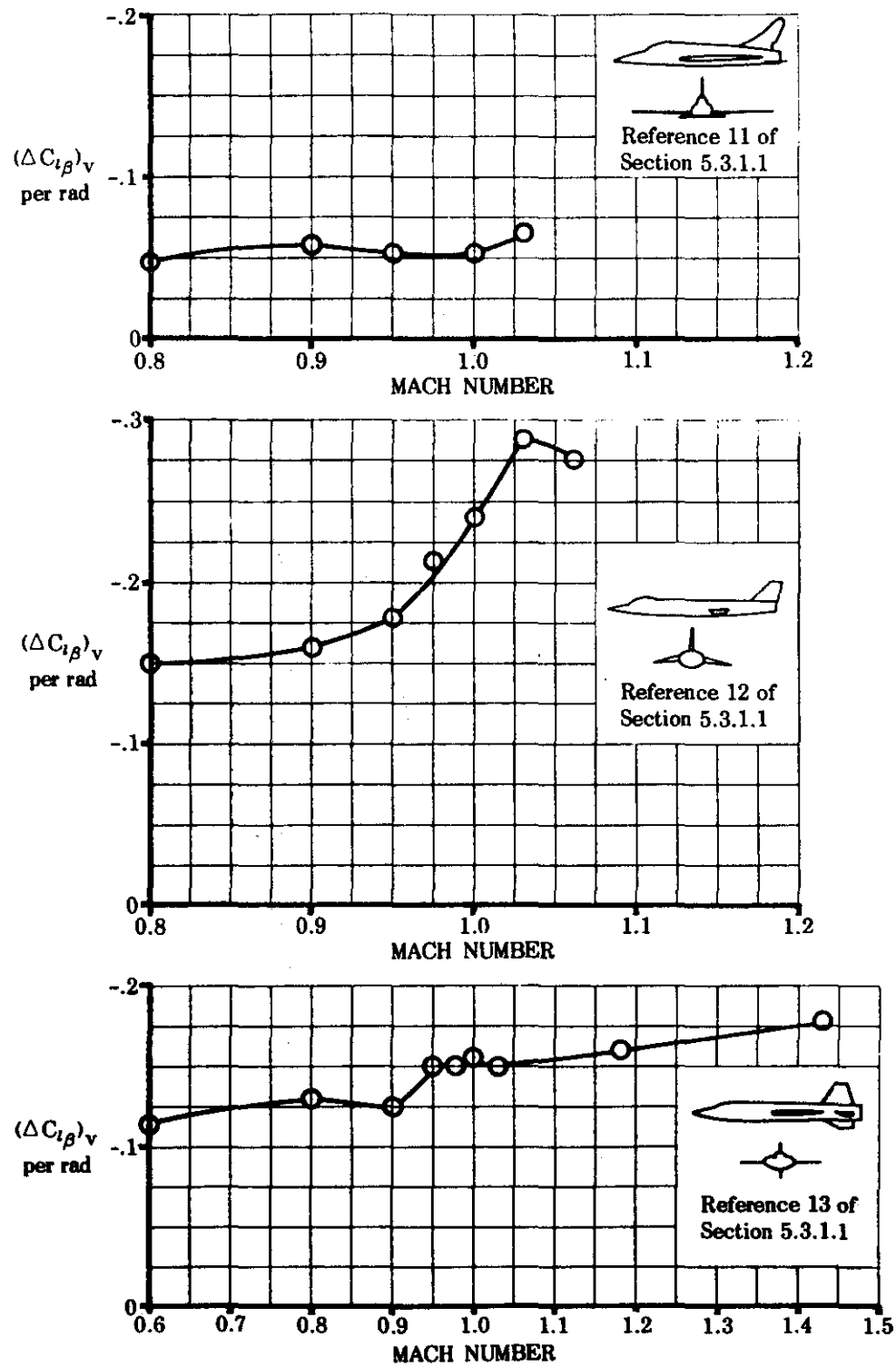


FIGURE 5.3.2.1-13 TYPICAL TRANSONIC DATA

5.3.3 TAIL-BODY SIDESLIP DERIVATIVE $C_{n\beta}$

5.3.3.1 TAIL-BODY SIDESLIP DERIVATIVE $C_{n\beta}$ IN THE LINEAR ANGLE-OF-ATTACK RANGE

The contribution of panels present in the empennage to the vehicle sideslip derivative $C_{n\beta}$ is estimated by the methods of this Section. The methods generally include the interference effects of other vehicle components.

Detailed discussion of the various aerodynamic aspects of adding tail panels to flight vehicles is given in Section 5.3.1.1 and is not repeated here.

A. SUBSONIC

The methods of estimating the contribution of panels present in the empennage to the sideslip derivative $C_{n\beta}$ are based on the methods for estimating the contribution of panels present in the empennage to the sideslip derivative $C_{Y\beta}$ in Section 5.3.1.1. The moment arm through which the panel side force acts can be taken as (a) the distance parallel to the longitudinal axis between the vehicle center of gravity and the quarter-chord point of the mean aerodynamic chord of the panel or (b) the distance parallel to the longitudinal axis between the vehicle center of gravity and the actual aerodynamic center of the panel. In most cases the former approximation is used, since the inaccuracies of estimating the side force of the panel do not warrant the refinements of (b). For short-coupled configurations, however, where the tail-length distance is relatively short and the size of the panel may be large, significant differences between results estimated by (a) and (b) may result; in such cases (b) is recommended.

DATCOM METHOD

Method 1

Simplified Method

The contribution of a panel to the sideslip derivative $C_{n\beta}$ at subsonic speeds is given by

$$(\Delta C_{n\beta})_p = -(\Delta C_{Y\beta})_p \frac{l_p}{b_w} \quad 5.3.3.1-a$$

where the subscript p refers to panels present in the empennage

$(\Delta C_{Y\beta})_p$ is the side force due to sideslip of the added panel determined as follows:

For configurations with the horizontal panel mounted on the body, or with no horizontal panel, use Method 1 or Method 3 of paragraph A, Section 5.3.1.1.

For configurations with the horizontal panel mounted on the vertical, use Method 1 of paragraph A, Section 5.3.1.1.

For twin-vertical panel configurations, use Method 2 of paragraph A, Section 5.3.1.1.

l_p is the distance parallel to the longitudinal axis between the moment reference center (usually the vehicle center of gravity) and the quarter-chord point of the MAC of the added panel, positive for the added panel behind the moment reference center.

b_w is the span of the wing

Method 2

Refined Method

In this case the contribution of a panel to the sideslip derivative $C_{n\beta}$ is given by

$$(\Delta C_{n\beta})_p = -(\Delta C_{Y\beta})_p \frac{[l_p + (x_{a.c.})_p]}{b_w} \quad 5.3.3.1-b$$

where $(\Delta C_{Y\beta})_p$, l_p , and b_w are defined in Method 1 above, and

$(x_{a.c.})_p$ is the distance between the quarter-chord point of the MAC of the added panel as determined from paragraph A of Section 4.1.4.2, positive for the a.c. behind the quarter-chord point. (In determining the vertical panel a.c. use the aspect ratio of the panel mounted on an infinite reflection plane.)

All geometry for the added panel of these methods is based on the panel extended to the body centerline.

Methods 1 and 2 of paragraph A, Section 5.3.1.1 lump the total empennage increment in $C_{Y\beta}$ into a single parameter. On the other hand, Method 3 gives the increment due to the addition of one panel (either a horizontal or vertical panel) including the mutual aerodynamic interference effects of all other panels present. An extension of Method 3 to determine the total empennage side force due to sideslip at subsonic speeds which results from the addition of all panels present in the empennage is presented in paragraph A of Section 5.6.1.1.

For a wingless configuration, b_w is replaced by the reference length for the vehicle, and $(\Delta C_{Y\beta})_p$ is based on the vehicle reference area.

Table 5.3.3.1-A compares results calculated by Method 1 with test data. The test cases for this table are the same as those used for table 5.3.1.1-B. Pertinent detailed information for table 5.3.3.1-A is therefore found in table 5.3.1.1-B and is not repeated.

Sample Problems

1. Method 1

Given: The configuration of reference 1, consisting of wing, body, horizontal tail, and upper vertical tail. This is the same configuration as that of sample problem 1, paragraph A, Section 5.3.1.1. Some of the characteristics are repeated. Find the effect of adding the vertical tail to the wing-body-horizontal tail configuration.

Wing Characteristics

$$S_w = 576.0 \text{ sq in.} \quad b_w = 41.56 \text{ in.} \quad z_w = 0$$

Additional Characteristics

$$M = 0.25 \quad l_v = 24.89 \text{ in. (c.g. to } (\bar{c}/4)_v \text{)}$$

Compute:

$$\frac{l_v}{b_w} = \frac{24.89}{41.56} = 0.599$$

$$(\Delta C_{Y\beta})_{VWBH} = -0.734 \text{ per rad (based on } S_w \text{)} \text{ (sample problem 1, paragraph A, Section 5.3.1.1)}$$

Solution:

$$(\Delta C_{n\beta})_p = -(\Delta C_{Y\beta})_p \frac{l_p}{b_w} \quad \text{(equation 5.3.3.1-a)}$$

$$\begin{aligned} (\Delta C_{n\beta})_{VWBH} &= -(\Delta C_{Y\beta})_{VWBH} \frac{l_v}{b_w} \\ &= -(-0.734)(0.599) \\ &= 0.440 \text{ per rad (based on } S_w b_w \text{)} \end{aligned}$$

This compares with an experimental value of 0.415 per radian obtained from reference 1.

2. Method 1

Given: The configuration of reference 2, consisting of wing, body, horizontal tail, and vertical tail. This is the same configuration as that of sample problem 3, paragraph A, Section 5.3.1.1. Some of the characteristics are repeated. Find the effect of adding the vertical tail to the wing-body-horizontal tail combination.

Wing Characteristics

$$S_w = 324 \text{ sq in.} \quad b_w = 36.0 \text{ in.} \quad z_w = 0$$

Additional Characteristics

$$M = 0.13 \quad l_v = 16.70 \text{ in. (c.g. to } (\bar{c}/4)_v)$$

Compute:

$$\frac{l_v}{b_w} = \frac{16.7}{36.0} = 0.464$$

$$(\Delta C_{Y\beta})_{V(WBHD)} = -0.375 \text{ per rad (based on } S_w) \text{ (sample problem 3, paragraph A, Section 5.3.1.1)}$$

Solution:

$$(\Delta C_{n\beta})_p = -(\Delta C_{Y\beta})_p \frac{l_p}{b_w} \quad \text{(equation 5.3.3.1-a)}$$

$$\begin{aligned} (\Delta C_{n\beta})_{V(WBHD)} &= -(\Delta C_{Y\beta})_{V(WBHD)} \frac{l_v}{b_w} \\ &= -(-0.375)(0.464) \\ &= 0.174 \text{ per rad (based on } S_w b_w) \end{aligned}$$

This compares with an experimental value of 0.178 per radian obtained from reference 2.

B. TRANSONIC

A brief discussion of the flow phenomena associated with forces generated on a vertical panel at transonic speeds is given in paragraph B of Section 5.3.1.1. As in the case for the vertical tail contribution to $C_{Y\beta}$, the transonic characteristics of the sideslip derivative $C_{n\beta}$ are closely associated with the transonic lift-curve-slope characteristics of the isolated panel (see introduction to paragraph B of Section 4.1.3.2).

DATCOM METHOD

No method is available for estimating the contribution of a tail panel to the sideslip derivative $C_{n\beta}$ and none is presented in the Datcom. Figure 5.3.3.1-11 presents some available information for this derivative.

C. SUPERSONIC

As in the subsonic case, the method of estimating supersonic values of $(\Delta C_{n\beta})_p$ is based on the values of $(\Delta C_{Y\beta})_p$ estimated by the method of Section 5.3.1.1. The problem of estimating the forces generated on vertical panels is complicated by the presence of shock waves. See paragraph C of Section 5.3.1.1 for a detailed description of this method. The moment arm through which the added vertical panel side force acts can be taken as (a) the distance parallel to the longitudinal axis between the vehicle center of gravity and the 50-percent-chord point of the mean aerodynamic center of the vertical panel, or (b) the distance parallel to the longitudinal axis between the vehicle center of gravity and the actual aerodynamic center of the vertical panel. For short-coupled configurations the latter approximation is, of course, more accurate. At supersonic speeds the centroid of area of the region of interference approximates the moment arm in the case of the increment gained by adding a horizontal surface.

This method is limited to configurations in which the horizontal tail is mounted on the body or configurations with no horizontal tail.

DATCOM METHODS

Method 1

Simplified Method

The contribution of an added panel (either a horizontal or vertical panel) to the sideslip derivative $C_{n\beta}$ at supersonic speeds is given by equation 5.3.3.1-a

$$(\Delta C_{n\beta})_p = -(\Delta C_{Y\beta})_p \frac{l_p}{b_w}$$

where the subscript p and b_w are defined in paragraph A, and

$(\Delta C_{Y\beta})_p$ is the side force due to sideslip of an added panel obtained from paragraph C of Section 5.3.1.1

l_p is the distance parallel to the longitudinal axis between the vehicle moment center and the 50-percent-chord point of the MAC of an added vertical panel, positive for the vertical panel aft of the vehicle moment center. In the case of the increment gained by adding a horizontal panel, l_p is the distance parallel to the longitudinal axis between the vehicle moment center and the centroid of area of the region of interference, positive for the horizontal panel aft of the vehicle moment center. (See sketch (c) of Section 5.3.1.1 for definition of area of region of interference.)

Method 2

Refined Method

For a more refined estimate of the contribution of an added panel to the sideslip derivative $C_{n\beta}$, equation 5.3.3.1-b is used

$$(\Delta C_{n\beta})_p = -(\Delta C_{Y\beta})_p \frac{[l_p + (x_{a.c.})_p]}{b_w}$$

where $(\Delta C_{Y\beta})_p$, l_p , and b_w are defined in Method 1 above, and

- $(x_{a.c.})_p$ is the distance parallel to the longitudinal axis between the 50-percent-chord point of the MAC of an added vertical panel and the aerodynamic center of the added panel obtained from paragraph C of Section 4.1.4.2, positive for the a.c. behind the 50-percent-chord point. (In determining the vertical panel a.c. use the aspect ratio of the isolated panel mounted on an infinite reflection plane.)

In the case of the increment gained by adding a horizontal panel, the moment arm is treated as in Method 1 above.

All geometry used in determining the moment arms of the vertical panels in the above methods is based on the exposed panel.

For a wingless configuration the remarks following the Datcom methods of paragraph A above are also applicable here.

Table 5.3.3.1-B compares results obtained by Method 1 with experimental data. The test configurations used in this table are the same as those used in Table 5.3.1.1-C. Detailed geometric variables are given in this latter table.

Sample Problems

1. Method 1

Given: The configuration of reference 3 consisting of wing, body, horizontal tail, and upper vertical stabilizer.

This is the same configuration as that of sample problem 1, paragraph C, Section 5.3.1.1. Some of the characteristics are repeated. Find the effect of adding the vertical tail to the wing-body-horizontal tail combination.

Wing Characteristics

$$S_w = 160.4 \text{ sq in.} \quad b_w = 25.31 \text{ in.} \quad z_w = 0$$

Additional Characteristics

$$M = 1.61 \quad l_v = 11.40 \text{ in. (c.g. to } (\bar{c}/2)_{v_e})$$

Compute:

$$\frac{l_v}{b_w} = \frac{11.40}{25.31} = 0.450$$

$$(\Delta C_{Y\beta})_{V(WBH)} = -0.529 \text{ per rad (based on } S_w) \text{ (sample problem 1, paragraph C, Section 5.3.1.1)}$$

Solution:

$$(\Delta C_{n\beta})_p = -(\Delta C_{Y\beta})_p \frac{l_p}{b_w} \quad (\text{equation 5.3.3.1-a})$$

$$\begin{aligned} (\Delta C_{n\beta})_{V(WBH)} &= -(\Delta C_{Y\beta})_{V(WBH)} \frac{l_v}{b_w} \\ &= -(-0.529)(0.450) \\ &= 0.238 \text{ per rad (based on } S_w b_w) \end{aligned}$$

This compares with an experimental value of 0.218 per radian obtained from reference 3.

2. Method 1

Given: The configuration of reference 4 consisting of wing, body, upper vertical stabilizer, and lower vertical stabilizer. This is the same configuration as that of sample problem 2, paragraph C, Section 5.3.1.1. Some of the characteristics are repeated. Find the effect of adding the upper vertical stabilizer to the wing-body-lower vertical stabilizer combination.

Wing Characteristics

$$S_w = 144.0 \text{ sq in.} \quad b_w = 24.0 \text{ in.} \quad z_w = 0$$

Additional Characteristics

$$M = 2.01 \quad l_v = 12.00 \text{ in. (c.g. to } (\bar{c}/2)_{v_e})$$

Compute:

$$\frac{l_v}{b_w} = \frac{12.00}{24.0} = 0.500$$

$$(\Delta C_{Y\beta})_{V(WBU)} = -0.583 \text{ per rad (based on } S_w) \text{ (sample problem 2, paragraph C, Section 5.3.1.1)}$$

Solution:

$$(\Delta C_{n\beta})_p = -(\Delta C_{Y\beta})_p \frac{l_p}{b_w} \quad (\text{equation 5.3.3.1-a})$$

$$\begin{aligned} (\Delta C_{n\beta})_{V(WBU)} &= -(\Delta C_{Y\beta})_{V(WBU)} \frac{l_v}{b_w} \\ &= -(-0.583)(0.500) \\ &= 0.2915 \text{ per rad (based on } S_w b_w) \end{aligned}$$

This compares with an experimental value of 0.277 per radian obtained from reference 4.

D. HYPERSONIC

A general discussion of hypersonic flows is given in the introduction to paragraph D of Section 4.1.3.3 and in several standard texts. No explicit method exists for estimating the contribution of an added tail panel to the sideslip derivative $C_{n\beta}$ at hypersonic speeds.

The supersonic method for estimating the derivative $(\Delta C_{Y\beta})_p$ (paragraph C, Section 5.3.1.1) has been substantiated to reasonably high Mach numbers (6.86) and can be used for estimating $(\Delta C_{n\beta})_p$ as in paragraph C above. However, the method should be applied with caution, since the basic assumptions are increasingly violated as the Mach number increases. The hypersonic small-disturbance theory and Newtonian Theory can also be used to estimate the forces and therefore the moments on the vertical panel. Newtonian flow, however, is limited to the upper range of hypersonic Mach numbers.

DATCOM METHODS

Method 1

Extended Supersonic Method

The method described in paragraph C can be used up to Mach numbers of approximately 7.

Method 2

Hypersonic Small-Disturbance Theory

Equation 5.3.3.1-a or 5.3.3.1-b can be used to estimate hypersonic values of $(\Delta C_{n\beta})_v$, where $(\Delta C_{Y\beta})_v$ is obtained from equation 5.3.1.1-h and l_p is as defined in paragraph C above. This method is generally limited to small angles of flow deflection.

Method 3

Newtonian Theory

Equation 5.3.3.1-a or 5.3.3.1-b can be used, but $(\Delta C_{Y\beta})_v$ is obtained by using equation 5.3.1.1-i to determine C_p in this case. l_p is as defined in paragraph C above. This method is most successful at the high hypersonic Mach numbers.

Because of the general lack of test data in this speed regime, no substantiation table is presented.

Sample Problem

Given: The configuration of reference 5. This is the same configuration as that of the sample problem, paragraph D, Section 5.3.1.1. Some of the characteristics are repeated. Find the effect of adding the vertical stabilizer to the wing-body configuration.

Wing Characteristics

$$S_w = 19.15 \text{ sq in.} \quad b_w = 5.60 \text{ in.}$$

Additional Characteristics

$$M = 5.0 \quad l_v = 2.79 \text{ in. (c.g. to } (\bar{c}/2)_{v_e})$$

Compute:

$$\frac{l_v}{b_w} = \frac{2.79}{5.60} = 0.499$$

$$(\Delta C_{Y\beta})_v = -0.86 \text{ per rad (based on } S_w) \text{ (sample problem, paragraph D, Section 5.3.1.1)}$$

Solution:

$$(\Delta C_{n\beta})_p = -(\Delta C_{Y\beta})_p \frac{l_p}{b_w} \quad (\text{equation 5.3.3.1-a})$$

$$(\Delta C_{n\beta})_v = -(\Delta C_{Y\beta})_v \frac{l_v}{b_w}$$

$-(-0.81)(0.499)$

0.430 per rad (based on S_{wbw})

This corresponds to an experimental value of 0.59 per radian obtained from reference 5.

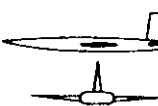
REFERENCES

1. Savage, H. F., and Tinling, B. E.: The Subsonic Static Aerodynamic Characteristics of an Airplane Model Having a Triangular Wing of Aspect Ratio 3. II - Lateral and Directional Characteristics. NACA TN 4042, 1957. (U)
2. Letko, W., and Williams, J. L.: Experimental Investigation at Low Speed of Effects of Fuselage Cross Section on Static Longitudinal and Lateral Stability Characteristics of Models Having 0° and 45° Sweptback Surfaces. NACA TN 3551, 1955. (U)
3. Spearman, M. L.: Static Lateral and Directional Stability and Effective Sidewash Characteristics of a Model of a 35° Swept-Wing Airplane at a Mach Number of 1.61. NACA RM L56E23, 1956. (U)
4. Spearman, M. L., and Robinson, R. B.: Investigation of the Aerodynamic Characteristics in Pitch and Sideslip of a 45° Swept-Wing Airplane Configuration with Various Vertical Locations of the Wing and Horizontal Tail. Static Lateral and Directional Stability; Mach Numbers of 1.41 and 2.01. NACA RM 1.57J25a, 1957. (U)
5. Dennis, D. H., and Peterson, R. H.: Aerodynamic Performance and Static Stability at Mach Numbers Up to 5 of Two Airplane Configuration with Favorable Lift Interference. NASA Memo 1-8-59A, 1959. (U)

TABLE 5.3.3.1-A^{1,2,3}
 SUBSONIC CONTRIBUTION OF VERTICAL PANELS TO $C_{n\beta}$
 DATA SUMMARY AND SUBSTANTIATION

Ref. ¹	Configuration Sketch	M	Panel Added	$(\Delta C_{Y\beta})_v$ Calc. (per rad)	$\frac{I_v}{b_w}$ Method 1	$(\Delta C_{n\beta})_v$ Calc. (per rad)	$(\Delta C_{n\beta})_v$ Test (per rad)	Percent Error e
6		.25	BWHV _s -BWH	-.481	.463	.223	.24	7.1
		.25	BWHV _L -BWH	-.734	.443	.325	.31	4.8
		.25	BV _s -B	-.428	.620	.265	.31	14.5
		.25	BV _L -B	-.578	.599	.346	.39	11.3
		.25	BHV _L -BH	-.597	.599	.358	.41	12.7
		.25	BHV _s -BH	-.431	.620	.267	.32	16.6
8		.17	BV-B	-.254	.58	.147	.14	5.0
		.17	BV-B	-.317	.57	.181	.18	.6
		.17	BV-B	-.446	.56	.250	.26	3.8
		.17	BW _s V-BW ₁	-.468	.56	.262	.25	4.8
		.17	BW _s V-BW ₂	-.409	.56	.229	.18	27.2
		.17	BW _s V-BW ₃	-.528	.56	.296	.30	1.3
9		.6	BWHV-BW	-.575	.425	.244	.23	6.1
		.6	BV-B	-.492	.425	.209	.24	12.9
10		.13	BWHV-BW	-.426	.464	.198	.21	5.7
		.13	BHV-BH	-.504	.464	.234	.22	6.4
		.13	BHV-BH	-.506	.464	.235	.21	11.9

TABLE 5.3.3.1-A^{1,2,3} (CONTD)

Ref. ³	Configuration Sketch	M	Panel Added	$(\Delta C_{Y\beta})_V$ Calc. (per rad)	$\frac{I_V}{b_w}$ Method 1	$(\Delta C_{n\beta})_V$ Calc. (per rad)	$(\Delta C_{n\beta})_V$ Test (per rad)	Percent Error e
10		.13	BHV-BH	-.497	.464	.230	.20	15.0

NOTES:

1. This table is a condensed form of that appearing in reference 2.
Additional substantiation can be obtained from this reference.
2. Refer to table 5.3.1.1-B for configuration data.
3. These references are found in Section 5.3.1.1.

TABLE 5.3.3.1-B^{1,2,3}
SUPersonic CONTRIBUTION OF VERTICAL PANELS TO $C_{n\beta}$
DATA SUMMARY AND SUBSTANTIATION

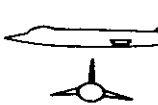
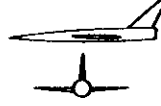
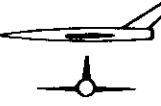
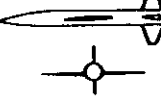
Ref. ³	Configuration Sketch	M	Panel Added	$(\Delta C_{Y\beta})_V$ Calc. (per rad)	$\frac{I_V}{b_w}$	$(\Delta C_{n\beta})_V$ Calc. (per rad)	$(\Delta C_{n\beta})_V$ Test (per rad)	Percent Error e
15		1.82	BWV-BW	-.589	.768	.453	.43	5.3
16		1.61	BV-B	-.525	.450	.236	.22	7.3
		1.61	BWHV-BWH	-.529	.450	.238	.218	9.2
14		2.01	BWHU-BWH	-.056	.439	.025	.034	26.5
		2.01	BWHUV-BWHU	-.525	.575	.302	.30	.7
17		1.61	BWV-BW	-.358	.403	.144	.14	2.9
		2.01	BWV-BW	-.335	.403	.135	.12	12.5
		1.61	BWHV-BWH	-.368	.403	.148	.15	1.3
		2.01	BWHV-BWH	-.335	.403	.135	.12	12.5
		1.61	BWHV _{ext} -BWH	-.424	.414	.176	.17	3.5
		1.61	BWHV _{large} -BWH	-.471	.410	.193	.17	13.5

TABLE 5.3.3.1-B^{1,2,3} (CONTD)

Ref. ¹	Configuration Sketch	M	Panel Added	$(\Delta C_{Y\beta})_V$ Calc. (per rad)	$\frac{t_v}{b_w}$	$(\Delta C_{n\beta})_V$ Calc. (per rad)	$(\Delta C_{n\beta})_V$ Test (per rad)	Percent Error <i>e</i>
18		1.41	BWV-BW	-.836	.465	.389	.37	5.1
		2.01	BWV-BW	-.545	.469	.256	.31	17.4
18		1.41	BWV-BW	-.842	.564	.475	.42	13.1
		2.01	BWV-BW	-.540	.564	.305	.30	1.7
18		1.41	BWV-BW	-.792	.630	.499	.45	10.9
		2.01	BWV-BW	-.542	.630	.342	.30	14.0
18		1.41	BWV-BW	-.706	.748	.528	.36	46.7
		2.01	BWV-BW	-.586	.748	.438	.32	36.9
20		6.86	BWHUV-BW	-.315	.645	.203	.18	12.8

NOTES:

1. This table is a condensed form of that appearing in reference 2. Additional substantiation can be obtained from this reference.
2. Refer to table 5.3.1.1-C for configuration data.
3. These references are found in Section 5.3.1.1.

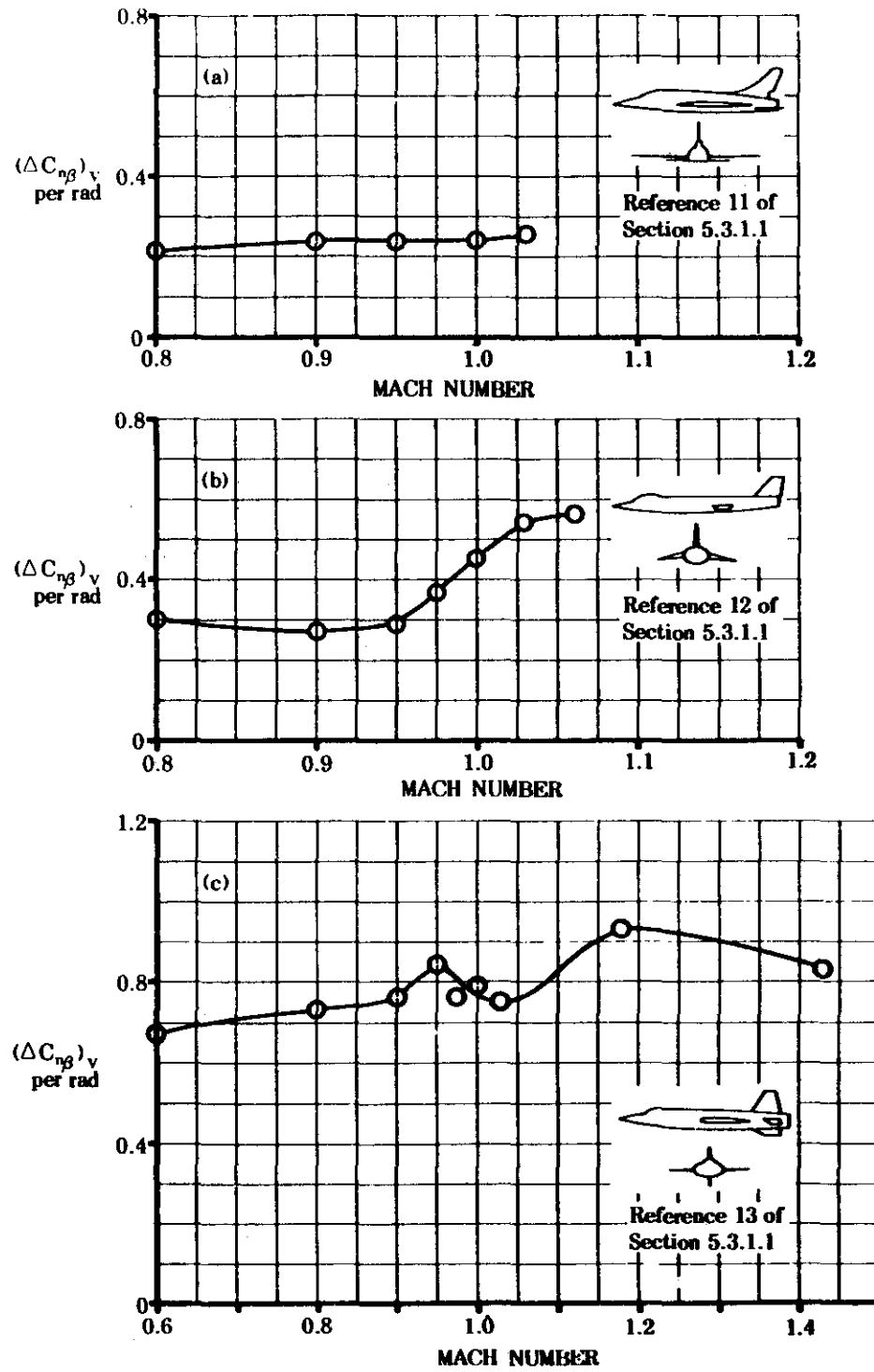


FIGURE 5.3.3.1-11. TYPICAL TRANSONIC DATA

5.3.3.2 TAIL-BODY YAWING-MOMENT COEFFICIENT C_n AT ANGLE OF ATTACK

The tail-body yawing moment developed at combined angles is nonlinear with respect to both sideslip and angle of attack because of the body-vortex induced sidewash on the upper vertical tail and the cross-coupling of upwash and sidewash velocities. To obtain the derivative $C_{n\beta}$, it is recommended that C_n be calculated at several angles of attack for a small sideslip angle ($\beta \leq 4^\circ$). Then, at each angle of attack, the yawing moment is assumed linear with sideslip for small values of β so that

$$C_{n\beta} \approx \frac{C_n}{\beta}$$

A. SUBSONIC

The comments appearing in Paragraph A of Section 5.3.1.2 apply here also. The method presented herein is restricted to first-order approximations at relatively low angles of attack.

DATCOM METHOD

It is recommended that the method of Paragraph A of Section 5.3.3.1 be used in the linear-lift angle-of-attack range.

B. TRANSONIC

The comments appearing in Paragraph B of Section 5.3.1.2 apply here also and will not be repeated.

DATCOM METHOD

No method is available for estimating this coefficient at angle of attack and none is presented in the Datcom.

C. SUPERSONIC

The comments in Paragraph C of Section 5.3.1.2 apply here also. As noted therein, the method for determining the side-force coefficient at angle of attack does not account for wing-tail interference effects. The yawing-moment coefficient at angle of attack for a configuration including a wing at supersonic speeds must be obtained from Paragraph C of Section 5.6.3.2.

DATCOM METHOD

The method for estimating the empennage contribution to the yawing moment at combined angles is essentially that of Section 5.3.1.2. The yawing-moment coefficient is obtained simply by applying the proper moment arms to the various side-force coefficients that comprise the total tail contribution. As noted in Section 5.3.1.2, the method is limited to circular bodies, and to the analysis of horizontal-tail effects only when the surface is body-mounted.

The contribution of the tail panels to the yawing-moment coefficient is given as

$$\begin{aligned}
 (C_n)_{HUV(B)} &= -\frac{\ell_H \cos \alpha + z_H \sin \alpha}{b_w} (C_Y)_{H(B)} - \frac{\ell_V \cos \alpha + z_V \sin \alpha}{b_w} (C_Y)_V \\
 &\quad - \frac{\ell_U \cos \alpha + z_U \sin \alpha}{b_w} (C_Y)_U
 \end{aligned} \tag{5.3.3.2-a}$$

where

$(C_Y)_{H(B)}$ is defined under Equation 5.3.1.2-a.

$(C_Y)_V$ is defined under Equation 5.3.1.2-a.

$(C_Y)_U$ is defined under Equation 5.3.1.2-a.

ℓ_H is the distance from the moment reference center to the center of pressure of the horizontal-tail interference side force, measured parallel to the longitudinal axis. The c.p. is taken at the centroid of the interference area, indicated by shading in Sketch (a) of Section 5.3.1.2.

z_H is the distance to the center of pressure of the horizontal-tail interference side force, measured from, and normal to, the longitudinal axis. z_H is positive when the c.p. is above the longitudinal axis. (The c.p. location is as assumed above.)

ℓ_V is the distance from the moment reference center to the center of pressure of the upper vertical tail, measured parallel to the longitudinal axis.

z_V is the distance to the center of pressure of the upper vertical tail, measured from, and normal to, the longitudinal axis. z_V is positive when the c.p. is above the longitudinal axis.

ℓ_U is the distance from the moment reference center to the center of pressure of the ventral fin, measured parallel to the longitudinal axis.

z_U is the distance to the center of pressure of the ventral fin, measured from, and normal to, the longitudinal axis. z_U is negative when the c.p. is below the longitudinal axis.

For the vertical panels the center of pressure is taken as the 50-percent-chord point of the mean aerodynamic chord of the exposed panel.

Values for the incremental coefficient resulting from the addition of upper vertical tails to circular bodies, calculated using the Datcom method, are compared with experimental results in Figure 5.3.3.2-4. It is evident from the experimental data that a strong destabilizing effect occurs with increasing angle of attack, and that this effect is fairly accurately predicted by the Datcom method over the angle-of-attack range of the tests.

Sample Problem

Given: Configuration of Sample Problem, Paragraph C, Section 5.3.1.2. No horizontal tail. Some characteristics are repeated. Find the yawing-moment coefficient developed by a vertical tail and a ventral fin.

Wing Characteristics:

$$\alpha = 12^\circ \quad S_W = 144.0 \text{ sq in.}$$

Additional Characteristics:

$$l_V = 12.0 \text{ in.} \quad l_U = 12.0 \text{ in.} \quad b_W = 24.0 \text{ in.} \quad z_V = 4.15 \text{ in.} \quad z_U = -2.15 \text{ in.}$$

$$\left. \begin{aligned} (C_{YV}) &= -0.0229 \\ (C_{YU}) &= -0.0109 \end{aligned} \right\} \text{ (based on } S_W \text{) (Sample Problem, Paragraph C, Section 5.3.1.2)}$$

$$M = 2.01$$

Solution:

$$\begin{aligned} (C_n)_{VU(B)} &= -\frac{l_V \cos \alpha + z_V \sin \alpha}{b_W} (C_Y)_V - \frac{l_U \cos \alpha + z_U \sin \alpha}{b_W} (C_Y)_U \quad (\text{Equation 5.3.3.2-a, horizontal tail off}) \\ &= -\frac{12.0 \cos 12^\circ + 4.15 \sin 12^\circ}{24.0} (-0.0229) - \frac{12.0 \cos 12^\circ - 2.15 \sin 12^\circ}{24.0} (-0.0109) \\ &= 0.0171 \text{ (based on } S_W b_W \text{)} \end{aligned}$$

REFERENCE

1. Kaattari, G. E.: Estimation of Directional Stability Derivatives at Moderate Angles and Supersonic Speeds. NASA Memo 12-1-58A, 1959. (U)

- - - DATCOM METHOD
 ○ EXPERIMENT

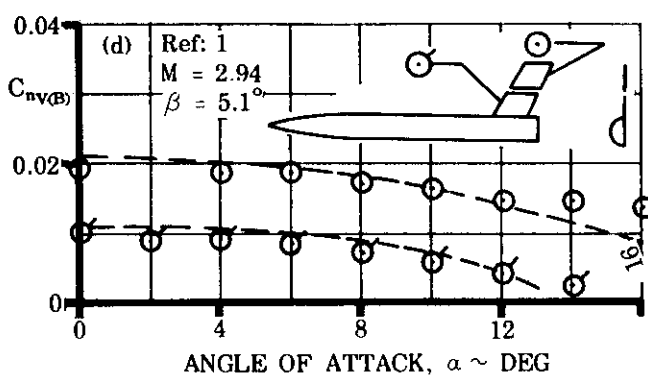
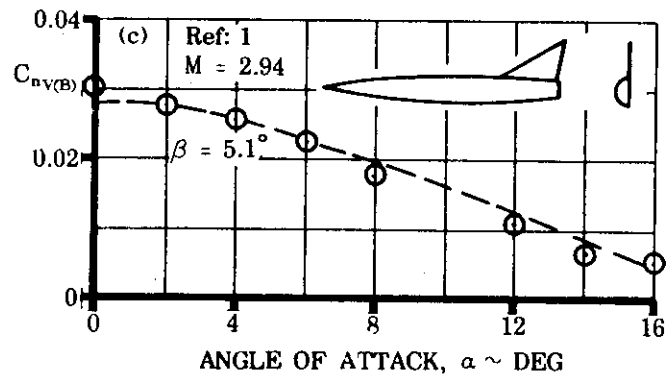
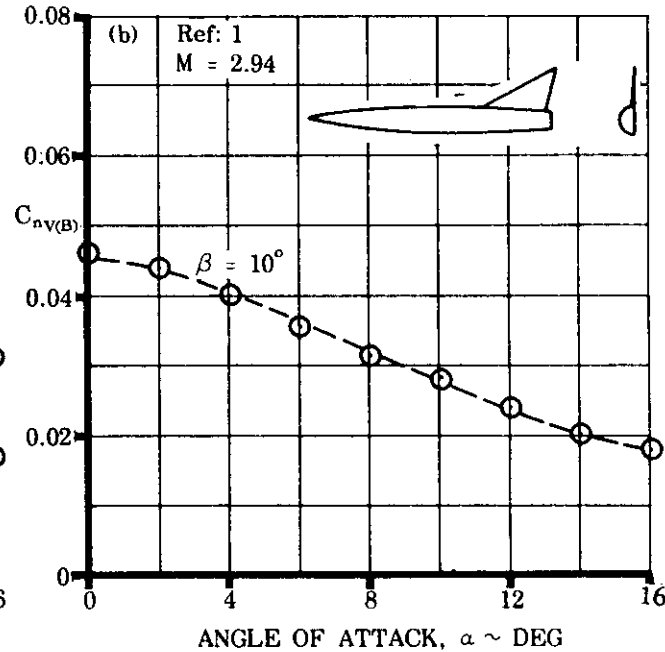
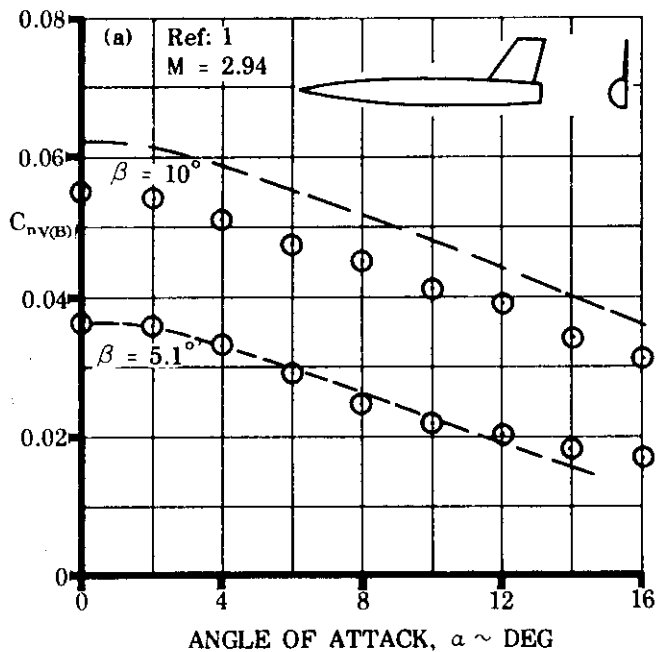


FIGURE 5.3.3.2-4 COMPARISON OF EXPERIMENTAL AND CALCULATED YAWING-MOMENT COEFFICIENT INCREMENTS DUE TO ADDING A VERTICAL TAIL TO A BODY

5.4 FLOW FIELDS IN SIDESLIP

5.4.1 WING-BODY WAKE AND SIDEWASH IN SIDESLIP

For a wing-body combination there are two contributions to the sidewash present at a vertical tail – that due to the body and that due to the wing.

The sidewash due to a body arises from the side force developed by a body in yaw. As a result of this side force a vortex system is produced, which in turn induces lateral-velocity components at the vertical tail. This sidewash from the body causes a destabilizing flow in the airstream beside the body. Above and below the fuselage, however, the flow is stabilizing.

The sidewash arising from a wing in yaw is small compared to that of a body. The flow above the wake center line moves inboard and the flow below the wake center line moves outboard.

For conventional aircraft the combination of the wing-body flow fields is such as to cause almost no sidewash effect below the wake center line.

At subsonic speeds an empirical equation is presented that gives the total sidewash effect directly, i.e., the combined sidewash angle and dynamic-pressure loss.

At supersonic speeds no generalized method is available.

DATCOM METHOD

A. SUBSONIC

A simple algebraic equation is presented that predicts the combined sidewash and dynamic-pressure parameter:

$$\left(1 + \frac{\partial\sigma}{\partial\beta}\right) \frac{q_V}{q_\infty}$$

This empirically derived expression is

$$\left(1 + \frac{\partial\sigma}{\partial\beta}\right) \frac{q_V}{q_\infty} = 0.724 + 3.06 \frac{\frac{S_V}{S_W}}{1 + \cos\Lambda_{c/4_W}} + .4 \frac{z_W}{d} + 0.009 A_W \quad 5.4.1-a$$

where

σ is the sidewash at the vertical tail, positive out the left wing

S_V is the vertical tail area, including the submerged area to the fuselage center line, square feet

z_W is the distance, parallel to the Z-axis, from wing root quarter-chord point to fuselage center line, feet. This value is positive for the quarter-chord point below the fuselage center line.

d is the maximum fuselage depth, feet

A comparison of test data with results calculated from Equation 5.4.1-a is shown in Table 5.4.1-A.

TABLE 5.4.1-A

Ref.	Λ_c/q_w (deg)	Λ	z_w/d	$\frac{S_v}{S_w}$	$\left(1 + \frac{\partial \alpha}{\partial \beta}\right)_{q_w}^q$ Test	$\left(1 + \frac{\partial \alpha}{\partial \beta}\right)_{q_w}^q$ Calc.	$ e $ Percent Error
1	45	4	0	.272	1.233	1.246	1.1
2	0	4	-.333	.150	.925	.889	3.9
	0	4	0	.150	1.004	.989	1.5
	0	4	.333	.150	1.090	1.089	0.1
	45	4	-.333	.150	.994	.929	6.5
	45	4	0	.150	1.067	1.029	3.3
	45	4	.333	.150	1.210	1.129	6.7
3	45	3	.390	.150	1.210	1.176	2.8
	45	3	-.390	.244	1.140	1.345	18.0
4	60	2	0	.150	1.068	1.048	1.9
	60	6	0	.150	1.10	1.084	1.3
5	45	2	0	.150	.998	1.021	2.3
	45	6	0	.150	1.023	1.057	3.3
6	0	2	0	.150	1.007	.971	3.6
	0	6	0	.150	.968	.989	2.2
7	0	4	0	.150	1.010	.989	2.1
	0	4	0	.150	.902	.989	9.6
	0	4	0	.150	.966	.989	2.4
	45	4	0	.150	1.040	1.029	1.1
	45	4	0	.150	.950	1.029	8.3
	45	4	0	.150	1.037	1.029	0.8
8	45	3	0	.203	1.170	1.124	3.9
	45	3	0	.203	1.13	1.124	5
	45	3	0	.267	1.20	1.237	3.1
	45	3	0	.267	1.252	1.237	1.2
	45	3	-.354	.203	1.030	.973	5.5
	45	3	-.354	.203	1.060	.973	8.2
	45	3	-.354	.267	1.152	1.086	5.7
	45	3	-.354	.267	1.082	1.086	0.4
9	52.5	2.31	-.333	.084	.743	.772	3.9
	52.5	2.31	-.333	.127	.792	.854	7.8
	52.5	2.31	-.333	.110	.740	.811	9.6
	52.5	2.31	-.333	.145	.792	.874	10.3
	52.5	2.31	-.333	.156	.729	.895	23.0
	52.5	2.31	.333	.084	1.155	1.038	10.1
	52.5	2.31	.333	.127	1.073	1.110	3.4
	52.5	2.31	.333	.110	1.060	1.077	1.6
	52.5	2.31	.333	.145	1.097	1.140	3.9
	52.5	2.31	.333	.156	1.147	1.161	1.2

Ref.	$A_c/4$ (deg)	A	z_w/d	$\frac{S_v}{S_w}$	$\left(1 + \frac{\partial\alpha}{\partial\beta}\right) \frac{q_v}{q_w}$ Test	$\left(1 + \frac{\partial\alpha}{\partial\beta}\right) \frac{q_v}{q_w}$ Calc.	$ \epsilon $ Percent Error
10	45	4	0	.150	1.09	1.029	5.6
	45	4	0	.150	.963	1.029	6.9
	45	4	0	.150	1.034	1.029	0.5
	45	4	0	.150	1.030	1.029	0.1
11	63	3.5	0	.168	1.130	1.207	6.8
12	56.5	2	0	.266	1.136	1.274	12.1
13	45	6	0	.151	1.053	1.049	3.4
	45	6	0	.151	1.062	1.049	6.8
14	0	5.9	.063	.160	1.030	1.047	1.7
15	40	2.5	.125	.165	1.070	1.063	1.2
16	35.92	6.95	—.387	.307	1.140	1.152	1.0
17	33.21	2.91	.417	.266	1.263	1.364	8.0
						Average Error = $\frac{\sum \epsilon }{n} = 4.7\%$	

REFERENCES

- Wiggins, J. W.; Kuhn, R. E.; and Fournier, P. G.: Wind-Tunnel Investigation to Determine the Horizontal- and Vertical-Tail Contributions to the Static Lateral Stability Characteristics of a Complete-Model Swept-Wing Configuration at High Subsonic Speeds. NACA TN 3818, November, 1956. (U)
- Letko, W.: Experimental Investigation at Low Speed of the Effects of Wing Position on the Static Stability of Models Having Fuselages of Various Cross Section and Unswept and 45° Sweptback Surfaces. NACA TN 3857, November, 1956. (U)
- Jaquet, B. M., and Fletcher, H. S.: Effect of Fuselage Nose Length and a Canopy on the Static Longitudinal and Lateral Stability Characteristics of 45° Sweptback Airplane Models Having Fuselages with Square Cross Sections. NACA TN 3961, April, 1957. (U)
- Wolhart, W. D., and Thomas, D. F., Jr.: Static Longitudinal and Lateral Stability Characteristics at Low Speed of 60° Sweptback-Midwing Models Having Wings With an Aspect Ratio of 2, 4, and 6. NACA TN 4397, September, 1958. (U)
- Thomas, D. F., Jr. and Wolhart, W. D.: Static Longitudinal and Lateral Stability Characteristics at Low Speed of 45° Sweptback-Midwing Models Having Wings With an Aspect Ratio of 2, 4, and 6. NACA TN 4077, September, 1957. (U)
- Wolhart, W. D., and Thomas, D. F., Jr.: Static Longitudinal and Lateral Stability Characteristics at Low Speeds of Unswept-Midwing Models Having Wings With an Aspect Ratio of 2, 4, and 6. NACA TN 3649, May, 1956. (U)
- Letko, W., and Williams, J. L.: Experimental Investigation at Low Speed of Effects of Fuselage Cross Section on Static Longitudinal and Lateral Stability Characteristics of Models Having 0° and 45° Sweptback Surface. NACA TN 3551, December, 1955. (U)
- Savage, H. F., and Tinling, B. E.: The Subsonic Static Aerodynamic Characteristics of an Airplane Model Having a Triangular Wing of Aspect Ratio 3. II-Lateral and Directional Characteristics. NACA TN 4042, August, 1957. (U)
- Goodman, A., and Thomas, D. F., Jr.: Effects of Wing Position and Fuselage Size on Low-Speed Static and Rolling Stability Characteristics of a Delta Wing Model. NACA TN 3063, February, 1954. (U)
- Brewer, J. D., and Lichtenstein, J. H.: Effect of Horizontal Tail on Low-Speed Static Lateral Stability Characteristics of a Model Having 45° Sweptback Wing and Tail Surfaces. NACA TN 2010, January, 1950. (U)
- McCormack, C. M.: Aerodynamic Study of a Wing-Fuselage Combination Employing a Wing Swept Back 63° — Aerodynamic Characteristics in Sideslip of a Large-Scale Model Having a 63° Swept-Back Vertical Tail. NACA RM A9F14, October 7, 1949. (U)

12. Graham, D., and Koenig, D. G.: Tests in the Ames 40- by 80-Foot Wind Tunnel of an Airplane Configuration With an Aspect Ratio 2 Triangular Wing and an All-Movable Horizontal Tail — Lateral Characteristics. NACA RM A51L03, February 11, 1952. (U)
13. Griner, R. F.: Static Lateral Stability Characteristics of an Airplane Model Having a 47.7° Sweptback Wing of Aspect Ratio 6 and the Contribution of Various Model Components at a Reynolds Number of 4.45×10^5 . NACA RM L53G09, September 1, 1953. (U)
14. Williams, J. L.: Measured and Estimated Lateral Static and Rotary Derivatives of a 1/12-Scale Model of a High Speed Fighter Airplane with Unswept Wings. NACA RM L53K09, January 11, 1954. (U)
15. Schudlenfrei, M., Comisarow, P., and Goodson, K. W.: Stability and Control Characteristics of an Airplane Model Having a 45.1° Swept-Back Wing With Aspect Ratio 3.87 and Taper Ratio 0.49. NACA RM L7B25, May 8, 1947. (U)
16. Hinds, W. E., and Graves, J. D.: Low-Speed Stability and Control Characteristics of the Model XA3D-1 Airplane. Douglas Aircraft Co. Report ES 15582, 1951. (U)
17. Cagle, B., and Kerhofer, W.: Report on Subsonic Wind Tunnel Tests of a 0.10-Scale Model of the Douglas (El Segundo) A4D-1 Airplane. CWT Rept. 732, 1955. (U)

5.5 LOW-ASPECT-RATIO WINGS AND WING-BODY COMBINATIONS IN SIDESLIP

During recent years much work has been done on problems associated with the design and operation of advanced flight vehicles. These vehicles include re-entry configurations and those designed for hypersonic cruise. The requirement that these vehicles operate within the atmosphere at hypersonic speeds necessitates the use of configurations that are not well suited for subsonic flight at low altitudes. For the most part, the configurations proposed for this type of mission feature extremely low aspect ratios of the order of two or less, and thick, generously rounded lifting surfaces. These configurations also often have large blunt bases.

The use of conventional subsonic theories and related test data does not result in adequate estimates of the aerodynamic characteristics for this type of vehicle. The methods presented in this section for estimating the aerodynamic characteristics of advanced flight vehicles at subsonic speeds are necessarily semiempirical in nature. The methods are based on test data, which have been correlated with the aid of the extension of available theory. A large portion of the material is related to delta or modified-delta configurations, since a major portion of the pertinent theory and test results relates to these planforms.

In the following group of sections (5.5.1, 5.5.2, and 5.5.3) methods are presented for estimating the side force, rolling moment, and yawing moment on specific types of advanced flight vehicles over the linear sideslip-angle range and at angles of attack up to 20°.

The pertinent aerodynamic forces and moments acting on the vehicle are illustrated on figure 5.5-6. These forces and moments are presented in a normal-force axis system that is introduced in Section 4.8. The reference axes are oriented with respect to the particular configuration under consideration such that the normal force is zero at zero angle of attack and also so that the rolling moment due to sideslip is zero for zero normal force.

The axis designated $X' - X'$ in figure 5.5-6 is the zero-normal-force reference axis defined in Section 4.8 as the axis passing through the centroid of the base area and the most forward point on the vehicle nose. If this axis is parallel to the free stream, the normal force acting on the body is zero by definition, and the zero-normal-force angle of attack α_{N_0} is specified (see Section 4.8.1.1).

Although the position of the axes such that the normal force is zero at zero angle of attack is readily determined, there is no accurate way of establishing the position of the axes for an arbitrary configuration such that the rolling moment due to sideslip is zero at zero normal force.

In the sections that follow, the position of the axis which results in zero rolling moment due to sideslip at zero normal force has been defined by using available test data. The required axis position, represented by axis $O - O$ of figure 5.5-6, is parallel to the $X' - X'$ axis and located at a distance Δ from $X' - X'$, where Δ is given by

$$\Delta = \left[\frac{K'_I \beta_{X'X'}}{K_Y \beta} \right]_{N_0} b$$

The data in the following sections are presented with respect to this "zero normal force - zero rolling moment" axis system. In this axis system the normal-force coefficient, angle of attack, side-force derivative with respect to sideslip, rolling-moment derivative with respect to sideslip, and yawing-moment derivative with respect to sideslip are designated by C_N' , α' , $K_Y \beta$, $K'_I \beta$, and $K'_{n\beta}$, respectively.

The lateral-directional characteristics for the defined body-axis system are related to the more familiar stability-axis system by

$$K_{Y\beta} = C_{Y\beta}$$

$$K'_{l\beta} = C_{l\beta} \cos \alpha' - C_{n\beta} \sin \alpha' - K_{Y\beta} \frac{\Delta}{b}$$

$$K'_{n\beta} = C_{n\beta} \cos \alpha' + C_{l\beta} \sin \alpha'$$

For symmetrical configurations (symmetry about the Z = 0 plane)

$$\alpha' = \alpha$$

$$K'_{l\beta} = K_{l\beta}$$

$$K'_{n\beta} = K_{n\beta}$$

A general notation list is included in this section for all sections included under Section 5.5.

Sketches showing planform geometry for nearly all configurations analyzed in Sections 5.5.1.1 through 5.5.3.2 are presented in table 4.8-A

NOTATION		
SYMBOL	DEFINITION	SECTION
A	aspect ratio of surface	Several
b	surface span	Several
c _r	surface root chord	5.5.3.1 5.5.3.2
h _b	maximum height of base	Several
l _B	total length of body	Several
N ₁	uniform distribution of normal force acting on a pure delta wing	5.5.2.1
N ₂	concentrated component of normal force acting on leading edge of a pure delta wing	5.5.2.1
N' _{2L}	left leading-edge component of concentrated normal force	5.5.2.1

SYMBOL	DEFINITION	SECTION
N'_{2R}	right leading-edge component of concentrated normal force	5.5.2.1
$R_{\frac{1}{3} LE}$	effective radius of round leading-edge wing, perpendicular to leading edge at $c_r/3$ from the nose (see figure 4.8.1.2-11b)	5.5.1.2 5.5.2.2 5.5.3.1 5.5.3.2
S	planform area	Several
S_{BS}	projected side area of configuration	Several
$(S_{BS})_{.2c_r}$	projected side area of configuration forward of $.2c_r$	5.5.3.1 5.5.3.2
V_∞	free-stream velocity	5.5.2.1
$(x_{c.p.})_p$	chordwise distance from the configuration nose to the center of pressure of the pressure component of the side force, positive for c.p. aft of nose	5.5.3.1 5.5.3.2
$x_{centroid S_{BS}}$	chordwise distance from the nose of the configuration to the centroid location of the projected side area, positive aft of the nose	5.5.3.1 5.5.3.2
$x_{centroid W}$	chordwise distance from the nose of the configuration to the centroid location of the wing planform, positive aft of the nose	5.5.3.1 5.5.3.2
α_{N_0}	angle of attack at zero normal force	5.5
α'	angle of attack ($\alpha - \alpha_{N_0}$), (see figure 4.8-12)	5.5 5.5.2.2
β	angle of sideslip, positive nose left	Several
Δ	<ol style="list-style-type: none"> perpendicular distance between zero-normal-force reference axis $X'-X'$ and "zero normal force – zero rolling moment" reference axis $0-0$, positive for $0-0$ below $X'-X'$ (see figure 5.5-6) distance of c.p. of leading-edge component of normal force on a pure delta wing, measured from and normal to the root chord (see sketch (b), Section 5.5.2.1) 	5.5 5.5.2.1
δ_L	total wedge angle of sharp-leading-edged wing, perpendicular to leading edge at $c_r/3$ from nose (see figure 4.8.1.2-11a)	5.5.1.2 5.5.2.2
δ_{eL}	effective wedge angle of sharp-leading-edged wing, perpendicular to leading edge at $c_r/3$ from nose (see figure 4.8.1.2-11a)	5.5.1.2 5.5.2.2

SYMBOL	DEFINITION	SECTION
δ_{L_1}	average lower-surface angle of sharp-leading-edged wing, perpendicular to wing leading edge at $c_r/3$ from nose (see figure 4.8.1.2-11a)	5.5.1.2 5.5.2.2
	wing semiapex angle	5.5.2.1 5.5.2.2
Λ_{LE}	sweepback angle of wing leading edge	Several
	taper ratio, $\frac{\text{tip chord}}{\text{root chord}}$	Several
C_f	skin-friction coefficient for incompressible flow	5.5.1.1 5.5.3.1
	rate of change of rolling-moment coefficient with sideslip angle, $\frac{\partial C_l}{\partial \beta}$ (stability axes)	5.5
$C_{N'}$	normal-force coefficient $\frac{N'}{qS}$ measured with respect to zero-normal-force reference plane	5.5.1.2 5.5.2.1 5.5.2.2 5.5.3.2
	value of coefficient at $\alpha' = 20^\circ$	5.5.1.2 5.5.2.2
	rate of change of yawing-moment coefficient with sideslip angle, $\frac{\partial C_n}{\partial \beta}$ (stability axis)	5.5
	rate of change of side-force coefficient with sideslip angle, $\frac{\partial C_Y}{\partial \beta}$ (stability axes)	5.5
$K'_{l\beta}$	rate of change of rolling-moment coefficient with sideslip angle, $\frac{\partial K_l}{\partial \beta}$, referred to the defined body axes	5.5 5.5.2.1 5.5.2.2
	value of parameter for a pointed-nose delta wing	5.5.2.2
	calculated value of parameter at $\alpha' = 20^\circ$	5.5.2.2
$K'_{l\beta_{XX'}}$	value of derivative referred to zero-normal-force axis	5.5

SYMBOL	DEFINITION	SECTION
$K'_{I\beta N_0}$	value of derivative near zero-normal-force	5.5.2.1 5.5.2.2
$\left[\frac{K'_{I\beta N_0}}{C_N'} \right]_\Delta$	value of parameter for pointed-nose delta wing	5.5.2.1 5.5.2.2
$\Delta \left[\frac{K'_{I\beta}}{C_N'} \right]_B$	increment in value of $\frac{K'_{I\beta}}{C_N'}$ of thin delta wing due to nose blunting	5.5.2.1 5.5.2.2
$\frac{(K'_{I\beta} / C_N')_{20}}{\left[(K'_{I\beta} / C_N')_{\text{calc}} \right]_{20}}$	sideslip-derivative correlation factor for $K'_{I\beta}$ at $\alpha' = 20^\circ$	5.5.2.2
$\Delta \frac{(K'_{I\beta} / C_N')_{20}}{\left[(K'_{I\beta} / C_N')_{\text{calc}} \right]_{20}}$	increment in correlation factor at $\alpha' = 20^\circ$ due to thickness effects	5.5.2.2
$K'_{n\beta}$	rate of change of yawing-moment coefficient with sideslip angle, $\frac{\partial K_n}{\partial \beta}$, referred to the defined body axes	5.5 5.5.3.1 5.5.3.2
$K'_{n\beta N_0}$	value of derivative at zero normal force	5.5.3.1
$K'_{Y\beta}$	rate of change of side-force coefficient with sideslip angle, $\frac{\partial K_Y}{\partial \beta}$, referred to the defined body axis	5.5 5.5.1.1 5.5.1.2 5.5.3.2
$K'_{Y\beta N_0}$	value of derivative at zero normal force	5.5.1.1 5.5.1.2 5.5.3.1
$(K'_{Y\beta})_{20}$	value of derivative at $\alpha' = 20^\circ$	5.5.1.2
$\Delta (K'_{Y\beta})_{20}$	increment in derivative accounting for change in α' from 0 to 20°	5.5.1.2
$\left[\frac{K'_{Y\beta}}{(C_N')^2} \right]_{20}$	sideslip-derivative correlation factor for $K'_{Y\beta}$ at $\alpha' = 20^\circ$	5.5.1.2

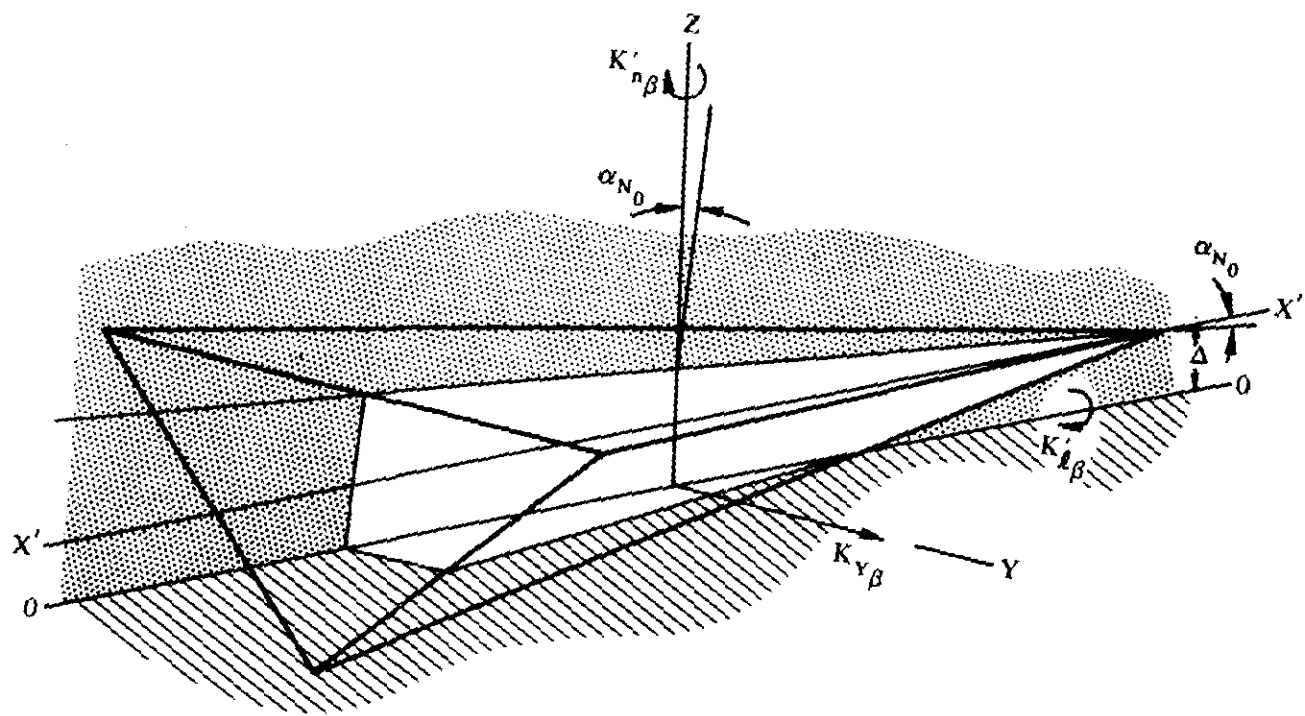


FIGURE 5.5-6 CONFIGURATION GEOMETRY - REFERENCE BODY AXES

5.5.1 WING, WING-BODY SIDESLIP DERIVATIVE K_{Y_β}

5.5.1.1 WING, WING-BODY SIDESLIP DERIVATIVE K_{Y_β} AT ZERO NORMAL FORCE

A. SUBSONIC

This section presents a method, taken from reference 1, for estimating the sideslip derivative K_{Y_β} at zero normal force for delta and modified-delta configurations at subsonic speeds.

The side force at zero normal force is assumed to be composed of two parts, side force due to skin friction and side force due to the pressures acting on the configuration. For thin configurations (essentially zero side area) the side force can be taken as equal to the skin-friction drag of the wing. As the thickness is increased, the influence of pressure distribution is introduced and the side force increases. However, this increase would be expected to be relatively small until the thickness becomes large enough so that the flow separates, causing the pressure drag to become appreciable. It is reported in reference 1 that many attempts were made to relate this phenomenon to existing theories, but without success. The available theories are usually appropriate only when the flow is attached or when the point of separation is known, as in the case of a thin, sharp-leading-edged delta wing. For the case of a moderately thick delta wing, the cross-flow components associated with sideslip tend to induce separation in an unpredictable manner. Therefore, the method presented is based on an empirical correlation of available test data.

The design chart presented was obtained by relating the sideslip derivative at zero normal force to the side area of the configuration. For zero side area, $K_{Y_{\beta N_0}}$ is taken to be equal to the incompressible skin-friction coefficient of the wing. For the purpose of the Datcom, the skin-friction coefficient of the wing is taken as $C_f = 0.006$. Therefore, for a wing with zero side area, $K_{Y_{\beta N_0}} = -0.006$ per radian.

Factors which might be expected to influence side force, but which are not isolated in the analysis, include planform geometry, aspect ratio, section thickness, and camber.

DATCOM METHOD

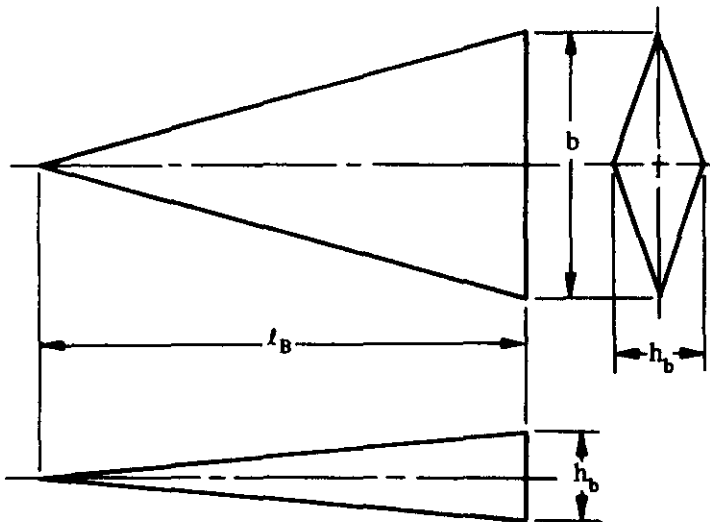
The zero-normal-force sideslip derivative $K_{Y_{\beta N_0}}$ of a delta or modified-delta configuration, based on planform area, is obtained from the procedure outlined in the following steps:

- Step 1. From the configuration geometry determine the projected side area of the configuration S_{B_S} and the planform area S .
- Step 2. Obtain $K_{Y_{\beta N_0}}$ as a function of S_{B_S}/S from figure 5.5.1.1-6 .

Values of the zero-normal-force sideslip derivative calculated by using this method are compared with test results in table 5.5.1.1-A. It should be noted that a considerable amount of scatter was involved in the data correlation used to define the design chart. A more accurate correlation was not obtainable because of the limited availability of test data and the uncertainties in the test results.

Sample Problem

Given: The delta-series configuration of reference 6 designated D-2. This is a sharp-edged delta model with a symmetrical diamond-shape cross section and a blunt trailing edge.



$$\begin{aligned}
 l_B &= 23.0 \text{ in.} \\
 b &= 12.374 \text{ in.} \\
 h_b &= 4.32 \text{ in.}
 \end{aligned}$$

Compute:

$$\begin{aligned}
 S &= \frac{1}{2} l_B b \\
 &= \frac{1}{2} (23.0)(12.374) = 142.3 \text{ sq in.}
 \end{aligned}$$

$$S_{BS} = \frac{1}{2} l_B h_b = \frac{1}{2} (23.0)(4.32) = 49.68 \text{ sq. in.}$$

$$\frac{S_{BS}}{S} = \frac{49.68}{142.3} = 0.349$$

Solution:

$$K_{Y\beta_{N_0}} = -0.110 \text{ per rad (based on } S) \quad (\text{figure 5.5.1.1-6})$$

This compares with a test value of -0.122 per radian from reference 6.

REFERENCES

1. Seager, D. B., and Ross, R.: Investigation of the Low-Speed Stability and Control Characteristics of Advanced Flight Vehicles. ASD-TDR-63-671, 1963. (C) Title Unclassified
2. Seager, D. B., and Meyer, J. E.: An Investigation of the Subsonic Aerodynamic Characteristics and the Landing Flare Maneuver for Hypersonic Re-entry Configurations. ASD-TDR-62-271, 1962. (C) Title Unclassified
3. Mantz, K., and Seager, D. B.: Tests to Determine the Subsonic Pressures, Forces and Moments Acting on a Hypersonic Re-entry Configuration. ASD-TDR-62-270, 1962. (C) Title Unclassified
4. Mantz, K., Seager, D. B., and Ross, R.: Tests to Determine Subsonic Pressures, Forces and Moments Acting on a Hypersonic Re-entry Configuration. ASD-TDR-62-270, Supplement 1, 1963. (U)

5. Sipe, O. E., and Seager, D. B.: Tests to Determine Subsonic Aerodynamic Characteristics of Hypersonic Re-entry Configurations. ASD-TR-61-485, 1961. (C) Title Unclassified
6. Mantz, D., Seager, D. B., and Ross, R.: Tests to Determine Subsonic Aerodynamic Characteristics of Hypersonic Re-entry Configurations. ASD-TR-61-485, Supplement 1, 1963. (U)
7. Graham, D., and Koenig, D. G.: Tests in the Ames 40- by 80-Foot Wind Tunnel of an Airplane Configuration With an Aspect Ratio 2 Triangular Wing and an All-Movable Horizontal Tail – Lateral Characteristics. NACA RM A51L03, 1952. (U)
8. Jaquet, B. M., and Brewer, J. D.: Low-Speed Static-Stability and Rolling Characteristics of Low-Aspect-Ratio Wings of Triangular and Modified Plan Forms. NACA RM L8L29, 1949. (U)
9. McKinney, M. O., Jr., and Drake, H. M.: Flight Characteristics at Low Speed of Delta-Wing Models. NACA RM L7K07, 1948. (U)
10. Keating, R. F. A.: Low-Speed Wind-Tunnel Tests on Sharp-Edged Gothic Wings of Aspect-Ratio 3/4. ARC CP 576, 1961. (U)
11. Goodman, A., and Thomas, D.: Effects of Wing Position and Fuselage Size on the Low-Speed Static and Rolling Stability Characteristics of a Delta-Wing Model. NACA TR 1224, 1955. (U)
12. Whittle, E. F., Jr., and Lovell, J. C.: Full-Scale Investigation of an Equilateral Triangular Wing Having 10-Percent Thick Biconvex Airfoil Sections. NACA RM L8G05, 1948. (U)
13. Olstad, W. B., Mugler, J. P., Jr., and Cahn, M. S.: Static Longitudinal and Lateral Stability Characteristics of a Right Triangular Pyramidal Lifting Re-entry Configuration at Transonic Speeds. NASA TN D-655, 1961. (U)
14. Ware, G. M.: Low-Subsonic-Speed Static Stability of Right-Triangular-Pyramid and Half-Cone Lifting Re-entry Configurations. NASA TN D-646, 1961. (U)
15. Paulson, J. W.: Low-Speed Static Stability and Control Characteristics of a Right Triangular Pyramid Re-entry Configuration. NASA Memo 4-11-59L, 1959. (U)
16. Ribner, H.: The Stability Derivatives of Low-Aspect-Ratio Triangular Wings at Subsonic and Supersonic Speeds. NACA TN 1423, 1947. (U)
17. Queijo, M.: Theoretical Span Load Distributions and Rolling Moments for Sideslipping Wings of Arbitrary Planform in Incompressible Flow. NACA TR 1269, 1956. (U)
18. Jones, R. T.: Properties of Low-Aspect-Ratio Pointed Wings at Speeds Below and Above the Speed of Sound. NACA TR 835, 1946. (U)
19. Edwards, G. G., and Savage, H. F.: The Subsonic Aerodynamic Characteristics of Some Blunt Delta Configurations with 75° Sweepback. NASA TM X-581, 1961. (C) Title Unclassified
20. McDevitt, J. B., and Rakich, J. V.: The Aerodynamic Characteristics of Several Thick Delta Wings at Mach Numbers to 6 and Angles of Attack to 50°. NASA TM X-162, 1960. (C) Title Unclassified
21. Hoerner, S. F.: Fluid Dynamic Drag. Published by author, 1958. (U)
22. Goodwin, F. K., and Kaattari, G. E.: Estimation of Directional Stability Derivatives at Small Angles and Subsonic and Supersonic Speeds. NASA Memo 12-2-58A, 1958. (U)
23. Harvey, J. K.: Some Measurements on a Yawed Slender Delta Wing with Leading Edge Separation. ARC 20451, R&M 3160, 1958. (U)
24. Nonweiler, T.: Theoretical Stability Derivatives of a Highly Swept Delta Wing and Slender Body Combination. College of Aeronautics, Cranfield, Report 50, 1958. (U)
25. Örnberg, T.: A Note on the Flow Around Delta Wings. Swedish Technical Note, K.T.H. Aero TN 38, 1954. (U)
26. Paulson, J. W.: Low-Speed Static Stability Characteristics of Two Configurations Suitable for Lifting Re-entry From Satellite Orbit. NASA Memo 10-22-58L, 1958. (C) Title Unclassified
27. Paulson, J. W., Shanks, R. E., and Johnson, J. L.: Low-Speed Flight Characteristics of Re-entry Vehicles of the Glide-Landing Type. NASA TM X-331, 1960. (C) Title Unclassified
28. Paulson, J. W., and Shanks, R. E.: Investigation of Low-Subsonic Flight Characteristics of a Model of a Hypersonic Boost-Glide Configuration Having a 78° Delta Wing. NASA TN D-894, 1961. (U)

29. Ware, G. M., and Shanks, R. E.: Investigation of the Low-Subsonic Flight Characteristics of a Model of a Re-entry Configuration Having a 75° Delta Wing. NASA TM X-684, 1962. (C) Title Unclassified
30. Weber, J.: Some Effects of Flow Separation on Slender Delta Wings. RAE Aero 2425, ARC 18073, 1955. (C) Title Unclassified
31. Campbell, J. P., and McKinney, M. O.: Summary of Methods for Calculating Dynamic Lateral Stability and Response and for Estimating Lateral Stability Derivatives. NACA TR 1098, 1952. (U)
32. Fink, P. T.: Some Low Speed Aerodynamic Properties of Cones. Experiments done in the Imperial College Aeronautical Laboratory. ARC 17,632, 1955. (C) Title Unclassified
33. Lee, G. H.: Note on the Flow Around Delta Wings with Sharp Leading Edges. ARC R&M 3070, 1958. (U)
34. Levacic, I.: Rolling Moment Due to Sideslip. Part II. The Effect of Sweepback and Planform. ARC 9278, 1945. (U)

TABLE 5.5.1.1-A
 SUBSONIC ZERO-NORMAL-FORCE SIDE-FORCE DERIVATIVE WITH RESPECT TO SIDESLIP
 DELTA PLANFORM CONFIGURATIONS

DATA SUMMARY

Ref.	Configuration	A	Λ_{LE} (deg)	$\frac{S_B}{S}$	$K_Y \beta_{N_0}$ Calc. (per rad)	$K_Y \beta_{N_0}$ Test (per rad)	$\Delta K_Y \beta_{N_0}$ Calc.-Test (per rad)
4	D-50	1.076	75	0.386	-0.150	-0.227	0.077
6	D-1	1.075	75	0.386	-0.150	-0.107	-0.043
	D-2	1.076	75	0.349	-0.110	-0.122	0.012
	D-5	1.076	75	0.386	-0.150	-0.219	0.069
	D-6	1.868	65	0.236	-0.030	-0.021	-0.009
	D-10	1.702	75	0.296	-0.060	-0.060	0
	WB-3	1.074	75	0.282	-0.051	-0.137	0.086
7	Wing Alone	2.00	63.4	0.050	-0.004	-0.010	0.006
8	2	2.31	60	0.115	-0.008	-0.015	0.007
9	1	3.00	53	0.045	-0.003	0	-0.003
	4	2.00	63	0.050	-0.004	0	-0.004
	6	1.00	76	0.050	-0.004	0	-0.004
	8	0.50	83	0.070	-0.005	0	-0.005
10	Wing Alone	0.75	Gothic	0.125	-0.009	0	-0.009
11	Wing Alone	2.31	60	0.045	-0.003	0	-0.003
12	Wing Alone	2.31	60	0.145	-0.011	-0.017	0.006
13	1	0.742	79.5	0.491	-0.325	-0.335	0.010
14	a	0.783	79.5	0.535	-0.412	-0.413	0.001
	b(basic)	0.783	79.5	0.491	-0.325	-0.344	0.019
	b($R = 1.5$ in.)	0.808	79.5	0.500	-0.337	-0.321	-0.016
	d	0.783	79.5	0.518	-0.375	-0.372	-0.003
15	1	0.780	79.4	0.528	-0.395	-0.401	0.006

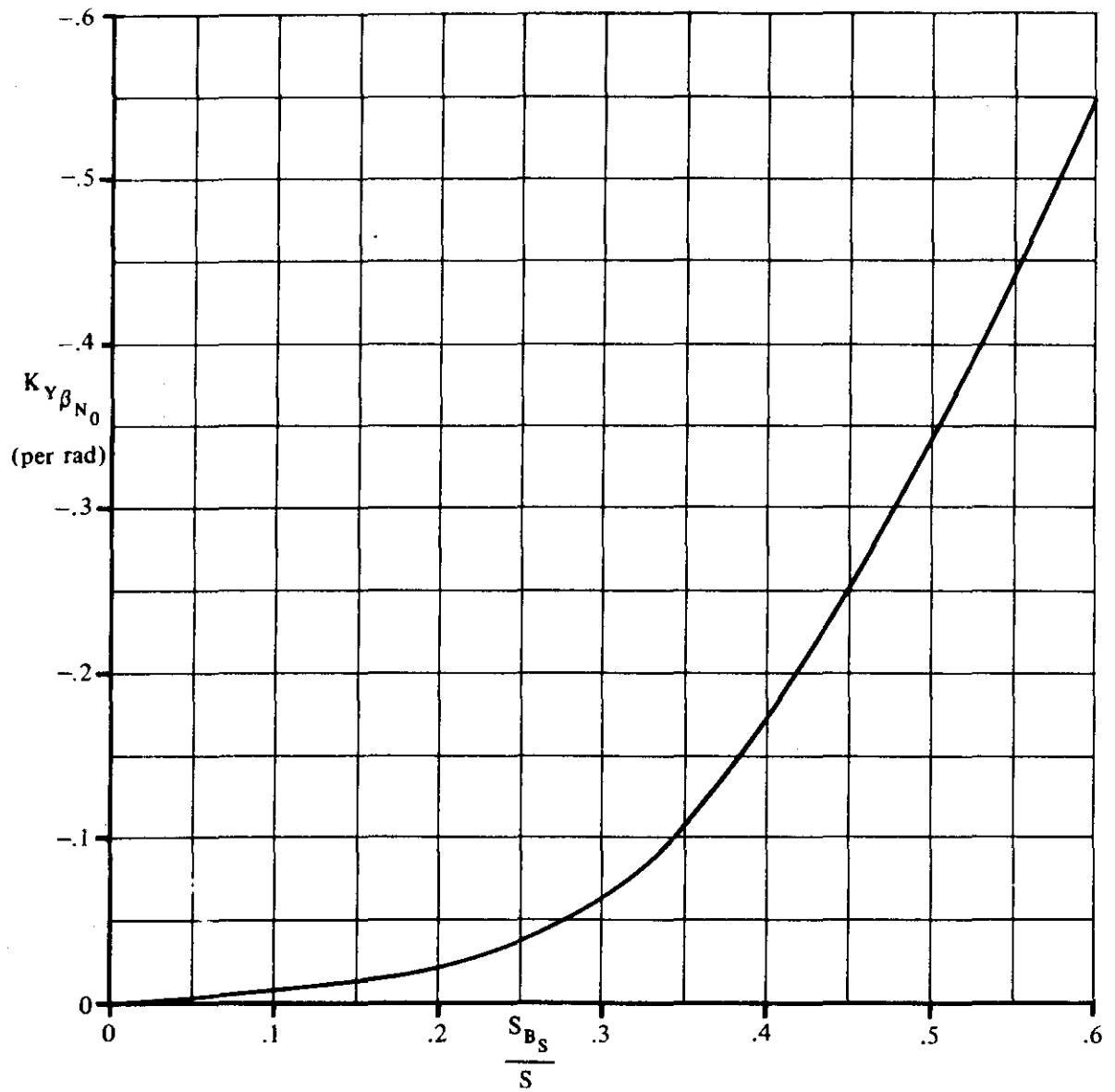


FIGURE 5.5.1.1-6 SIDE-FORCE DERIVATIVE WITH RESPECT TO SIDESLIP AT ZERO NORMAL FORCE – DELTA AND MODIFIED DELTA CONFIGURATIONS

5.5.1.2 WING, WING-BODY SIDESLIP-DERIVATIVE K_{Y_β} VARIATION WITH ANGLE OF ATTACK

A. SUBSONIC

This section presents a method for estimating the effects of angle of attack on the sideslip derivative K_{Y_β} of a delta or modified-delta planform re-entry configuration.

The Datcom method is taken from reference 1. An empirical correlation is presented for estimating K_{Y_β} at $\alpha' = 20^\circ$, and this correlation has been related to the normal-force coefficient to estimate K_{Y_β} at intermediate angles of attack.

Leading-edge shape was shown to have an important influence on the side force as well as on its variation with angle of attack. A lifting delta wing is characterized by two vortices that extend aft of the nose, at or somewhat inboard of the wing tips. These vortices move with respect to the wing as it is sideslipped, tending to remain fixed with respect to the free stream. Minimum pressures and, as a result, maximum local lifts, are observed in the area immediately below the cores of these vortices. It would, therefore, be expected that the side force produced by sideslipping a delta wing would depend to a significant degree upon the shape of the wing below the vortices. For example, if the minimum pressure acts on a region where the surface of the wing is sloped so that the contribution to side force is large, the value of K_{Y_β} would be expected to differ from that observed on a configuration with flat upper surfaces. During the study reported in reference 1 available test results were analyzed in an attempt to isolate this phenomenon; however, the results were not conclusive. Therefore, the influence of cross-sectional shape other than that related to leading-edge rounding or leading-edge angle is not included in the correlation curve presented in the Datcom method.

Test data show that K_{Y_β} tends to become more negative as angle of attack is increased for wings with small leading-edge radii, while the opposite is true for configurations with generously rounded leading edges. This phenomenon can be explained as follows: On a lifting delta wing the upper-surface pressures on the up-stream leading edge decrease as the sideslip angle is increased and the upper-surface pressures acting on the down-stream edge increase. If the leading-edge radius is large so that the flow does not separate readily, and so that these pressures are effective over a relatively large area, the change in K_{Y_β} due to increases in C_N' is positive. For sharper leading edges, the combination of the flow separating readily at the leading edges and the small side area in the vicinity of the minimum pressures at the up-stream leading edge results in a reduction in K_{Y_β} as C_N' is increased. This observation led to the development of the estimation procedure. Since the change in K_{Y_β} with C_N depends upon the pressure distribution produced by the lifting process, it was assumed that a correlation procedure could be developed that relates K_{Y_β} to the normal-force coefficient. The expression used in the correlation procedure is

$$K_{Y_\beta} = K_{Y_{\beta_{N_0}}} + \left(K_{Y_{\beta_{20}}} - K_{Y_{\beta_{N_0}}} \right) \left[\frac{C_N'}{C_{N_{20}'}} \right]^2$$

Semiempirical correlation curves based on the above expression and test values at $\alpha' = 20^\circ$ are presented in the Datcom method for delta and modified-delta wings with either round or sharp leading edges. These design charts are considered valid for sideslip angles between $\pm 5^\circ$ and angles of attack up to 20° .

DATCOM METHOD

The variation of the sideslip derivative $K_{Y\beta}$ with angle of attack for a delta or modified-delta configuration at low speeds, based on planform area, is obtained from the procedure outlined in the following steps:

- Step 1. Determine the effective leading-edge angle δ_{e1} for sharp leading edges or the effective leading-edge radius $R_{\frac{1}{3}LE}$ for round leading edges. These parameters are functions of the configuration geometry in a plane normal to the leading edge at $\frac{1}{3}c_r$ from the nose. The applicable configuration geometry is illustrated on figures 4.8.1.2-11a and 4.8.1.2-11b.
- Step 2. Determine the variation of sideslip derivative with angle of attack by

$$K_{Y\beta} = K_{Y\beta_{N_0}} + \left[\frac{\Delta K_{Y\beta}}{(C_N')^2} \right]_{20} (C_N')^2 \quad 5.5.1.2-a$$

where

$K_{Y\beta_{N_0}}$ is the side force due to sideslip at zero normal force obtained by using the method of Section 5.5.1.1.

C_N' is the normal-force coefficient at angle of attack obtained by using the method of Section 4.8.1.2.

$\left[\frac{K_{Y\beta}}{(C_N')^2} \right]_{20}$ is the semiempirical correlation factor for the sideslip derivative $K_{Y\beta}$ for delta and modified-delta configurations. It is presented as a function of effective leading-edge radius $R_{\frac{1}{3}LE}$ and S_{BS}/S for configurations with

round leading edges in figure 5.5.1.2-8, and as a function of effective leading-edge angle δ_{e1} and S_{BS}/S for configurations with sharp leading edges in figure 5.5.1.2-9.

S_{BS}/S is the ratio of the projected side area of the configuration to the planform area.

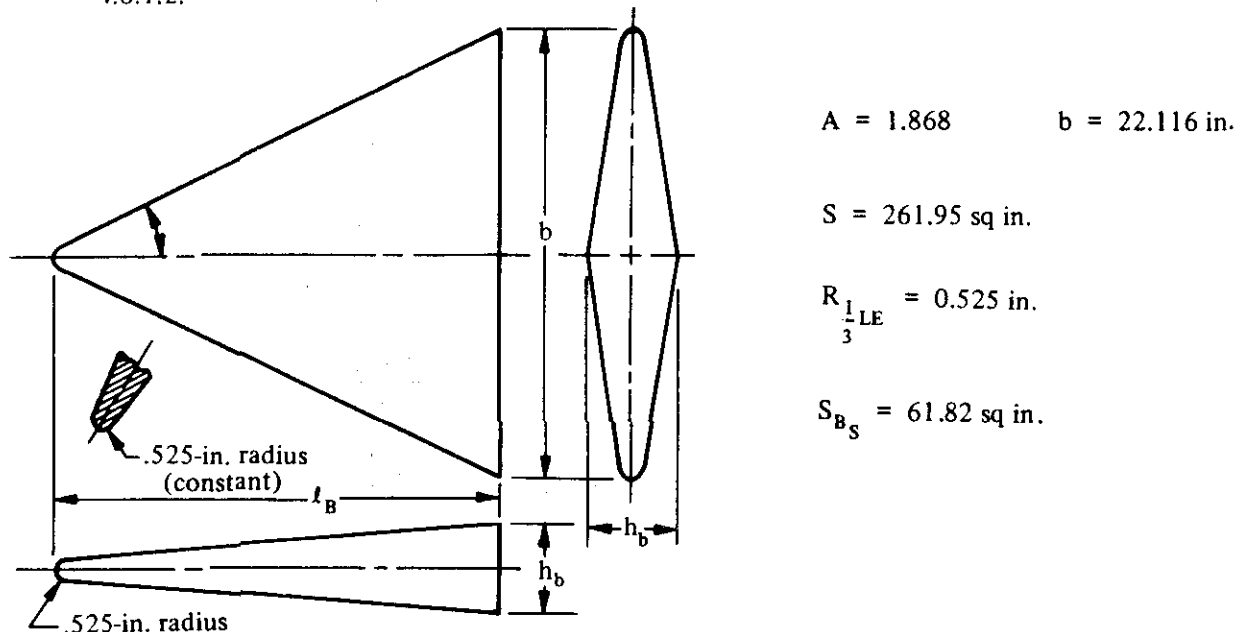
It should be noted that a considerable amount of scatter was involved in the data correlation used to define the design charts. In the case of sharp-leading-edged configurations it was necessary to estimate the nature of the effect of leading-edge angle on the basis of very few test data. Therefore, the accuracy of the design chart for sharp leading edges (figure 5.5.1.2-9) is questionable.

Nonlinearities in the variation of side force with sideslip may appear if the upper-surface slope is such that spanwise components of normal force, due to the negative pressures under the vortex, appear only for a limited range of sideslip angles. As indicated in the introduction, the available data are not sufficient to allow isolation of this effect. However, it should be realized that a constant value of $K_{Y\beta}$ valid for $\beta = \pm 5^\circ$ may not be a useful representation of the physical phenomena involved.

The variation of the sideslip derivative $K_{Y\beta}$ with normal force calculated by this method is compared with test data in table 5.5.1.2-A.

Sample Problem

Given: A delta model with a symmetrical diamond cross section, a blunt trailing edge, and round leading edges. This is model D-6 of reference 6. This is the configuration of sample problem 1 of Section 4.8.1.2.



The following variation of C_N' with α' from sample problem 1 of Section 4.8.1.2:

α'	0	5°	10°	15°	20°
C_N'	0	0.2017	0.4122	0.6323	0.8618

Compute:

$$S_{BS}/S = 61.82/261.95 = 0.236$$

$$K_{Y\beta_{N_0}} = -0.030 \text{ per rad} \quad (\text{figure 5.5.1.1-6})$$

$$R_{\frac{1}{3} \text{ LE}}/b = 0.525/22.116 = 0.0237$$

$$\left[\frac{\Delta K_{Y\beta}}{(C_N)^2} \right]_{20} = -0.095 \text{ per rad} \quad (\text{figure 5.5.1.2-8})$$

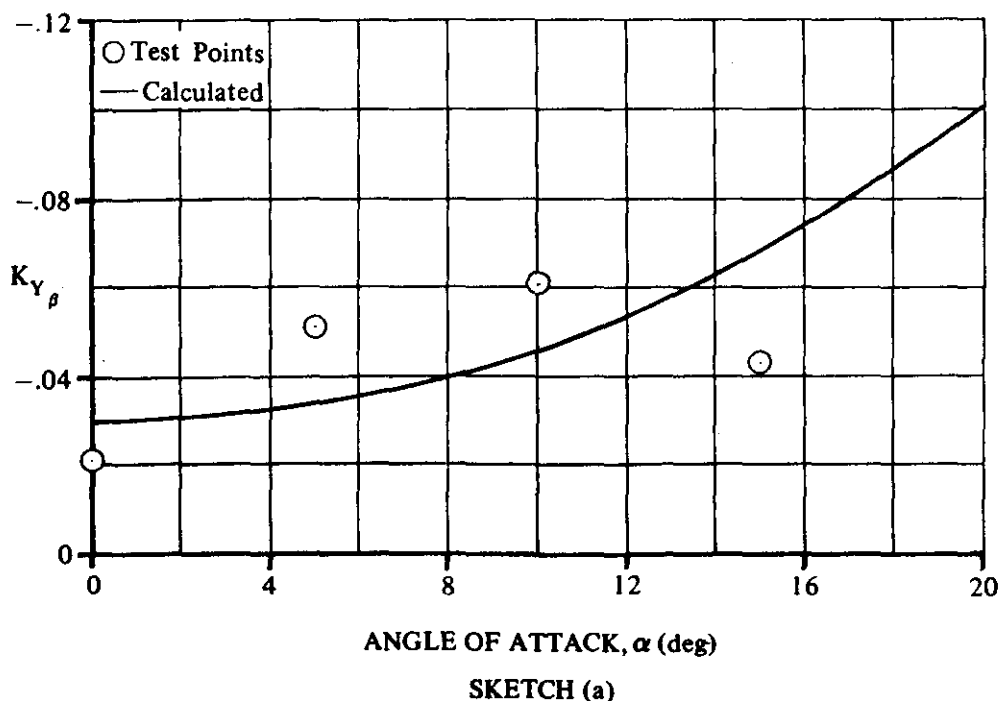
Solution:

$$K_{Y\beta} = K_{Y\beta_{N_0}} + \left[\frac{\Delta K_{Y\beta}}{(C_N)^2} \right]_{20} (C_N)^2 \quad (\text{equation 5.5.1.2-a})$$

$$= -0.030 + (-0.095) (C_N)^2$$

①	②	③	④	⑤
α (deg)	C_N (given)	$(C_N)^2$ ② ²	$-0.095(C_N)^2$ -0.095③	$K_{Y\beta}$ (based on S) (per rad) -0.030 + ④
0	0	0	0	-0.030
5	0.2017	0.041	-0.004	-0.034
10	0.4122	0.170	-0.016	-0.046
15	0.6323	0.400	-0.038	-0.068
20	0.8618	0.743	-0.071	-0.101

The calculated results are compared with test values in sketch (a) and in table 5.5.1.2-A.



REFERENCES

1. Seager, D. B., and Ross, R.: Investigation of the Low-Speed Stability and Control Characteristics of Advanced Flight Vehicles. ASD-TDR-63-671, 1963. (C) Title Unclassified
2. Seager, D. B., and Meyer, J. E.: An Investigation of the Subsonic Aerodynamic Characteristics and the Landing Flare Maneuver for Hypersonic Re-entry Configurations. ASD-TDR-62-271, 1962. (C) Title Unclassified
3. Mantz, K., and Seager, D. B.: Tests to Determine the Subsonic Pressures, Forces and Moments Acting on a Hypersonic Re-entry Configuration. ASD-TDR-62-270, 1962. (C) Title Unclassified
4. Mantz, K., Seager, D. B., and Ross, R.: Tests to Determine Subsonic Pressures, Forces and Moments Acting on a Hypersonic Re-entry Configuration. ASD-TDR-62-270, Supplement 1, 1963. (U)
5. Sipe, O. E., and Seager, D. B.: Tests to Determine Subsonic Aerodynamic Characteristics of Hypersonic Re-entry Configurations. ASD-TR-61-485, 1961. (C) Title Unclassified
6. Mantz, D., Seager, D. B., and Ross, R.: Tests to Determine Subsonic Aerodynamic Characteristics of Hypersonic Re-entry Configurations. ASD-TR-61-485, Supplement 1, 1963. (U)
7. Graham, D., and Koenig, D. G.: Tests in the Ames 40- by 80-Foot Wind Tunnel of an Airplane Configuration With an Aspect Ratio 2 Triangular Wing and an All-Movable Horizontal Tail — Lateral Characteristics. NACA RM A51L03, 1952. (U)
8. Jaquet, B. M., and Brewer, J. D.: Low-Speed Static-Stability and Rolling Characteristics of Low-Aspect-Ratio Wings of Triangular and Modified Plan Forms. NACA RM L8L29, 1949. (U)
9. McKinney, M. O., Jr., and Drake, H. M.: Flight Characteristics at Low Speed of Delta-Wing Models. NACA RM L7K07, 1948. (U)
10. Keating, R. F. A.: Low-Speed Wind-Tunnel Tests on Sharp-Edged Gothic Wings of Aspect-Ratio 3/4. ARC CP 576, 1961. (U)
11. Goodman, A., and Thomas, D.: Effects of Wing Position and Fuselage Size on the Low-Speed Static and Rolling Stability Characteristics of a Delta-Wing Model. NACA TR 1224, 1955. (U)
12. Whittle, E. F., Jr., and Lovell, J. C.: Full-Scale Investigation of an Equilateral Triangular Wing Having 10-Percent Thick Biconvex Airfoil Sections. NACA RM L8G05, 1948. (U)
13. Olstad, W. B., Mugler, J. P., Jr., and Cahn, M. S.: Static Longitudinal and Lateral Stability Characteristics of a Right Triangular Pyramidal Lifting Re-entry Configuration at Transonic Speeds. NASA TN D-655, 1961. (U)
14. Ware, G. M.: Low-Subsonic-Speed Static Stability of Right-Triangular-Pyramid and Half-Cone Lifting Re-entry Configurations. NASA TN D-646, 1961. (U)
15. Paulson, J. W.: Low-Speed Static Stability and Control Characteristics of a Right Triangular Pyramid Re-entry Configuration. NASA Memo 4-11-59L, 1959. (U)
16. Ribner, H.: The Stability Derivatives of Low-Aspect-Ratio Triangular Wings at Subsonic and Supersonic Speeds. NACA TN 1423, 1947. (U)
17. Queijo, M.: Theoretical Span Load Distributions and Rolling Moments for Sideslipping Wings of Arbitrary Planform in Incompressible Flow. NACA TR 1269, 1956. (U)
18. Jones, R. T.: Properties of Low-Aspect-Ratio Pointed Wings at Speeds Below and Above the Speed of Sound. NACA TR 835, 1946. (U)
19. Edwards, G. G., and Savage, H. F.: The Subsonic Aerodynamic Characteristics of Some Blunt Delta Configurations with 75° Sweepback. NASA TM X-581, 1961. (C) Title Unclassified
20. McDevitt, J. B., and Rakich, J. V.: The Aerodynamic Characteristics of Several Thick Delta Wings at Mach Numbers to 6 and Angles of Attack to 50°. NASA TM X-162, 1960. (C) Title Unclassified
21. Hoerner, S. F.: Fluid Dynamic Drag. Published by author, 1958. (U)
22. Goodwin, F. K., and Kaattari, G. E.: Estimation of Directional Stability Derivatives at Small Angles and Subsonic and Supersonic Speeds. NASA Memo 12-2-58A, 1958. (U)
23. Harvey, J. K.: Some Measurements on a Yawed Slender Delta Wing with Leading Edge Separation. AIAA 20451, RAM 3180, 1968. (U)

24. Nonweiler, T.: Theoretical Stability Derivatives of a Highly Swept Delta Wing and Slender Body Combination. College of Aeronautics, Cranfield, Report 50, 1958. (U)
25. Örnberg, T.: A Note on the Flow Around Delta Wings. Swedish Technical Note, K.T.H. Aero TN 38, 1954. (U)
26. Paulson, J. W.: Low-Speed Static Stability Characteristics of Two Configurations Suitable for Lifting Re-entry From Satellite Orbit. NASA Memo 10-22-58L, 1958. (C) Title Unclassified
27. Paulson, J. W., Shanks, R. E., and Johnson, J. L.: Low-Speed Flight Characteristics of Re-entry Vehicles of the Glide-Landing Type. NASA TM X-331, 1960. (C) Title Unclassified
28. Paulson, J. W., and Shanks, R. E.: Investigation of Low-Subsonic Flight Characteristics of a Model of a Hypersonic Boost-Glide Configuration Having a 78° Delta Wing. NASA TN D-894, 1961. (U)
29. Ware, G. M., and Shanks, R. E.: Investigation of the Low-Subsonic Flight Characteristics of a Model of a Re-entry Configuration Having a 75° Delta Wing. NASA TM X-684, 1962. (C) Title Unclassified
30. Weber, J.: Some Effects of Flow Separation on Slender Delta Wings. RAE Aero 2425, ARC 18073, 1955. (C) Title Unclassified
31. Campbell, J. P., and McKinney, M. O.: Summary of Methods for Calculating Dynamic Lateral Stability and Response and for Estimating Lateral Stability Derivatives. NACA TR 1098, 1952. (U)
32. Fink, P. T.: Some Low Speed Aerodynamic Properties of Cones. Experiments done in the Imperial College Aeronautical Laboratory. ARC 17,632, 1955. (C) Title Unclassified
33. Lee, G. H.: Note on the Flow Around Delta Wings with Sharp Leading Edges. ARC R&M 3070, 1958. (U)
34. Levecic, I.: Rolling Moment Due to Sideslip. Part II. The Effect of Sweepback and Planform. ARC 9278, 1945. (U)

TABLE 5.5.1.2-A

SUBSONIC SIDE-FORCE DERIVATIVE WITH RESPECT TO SIDESLIP -- VARIATION WITH NORMAL FORCE

DELTA PLANFORM CONFIGURATIONS

DATA SUMMARY

Ref.	Configuration	A	Δ_{LE} (deg)	$\frac{S_{BS}}{S}$	Leading Edge	C_N'	$K_Y \beta$ Calc. (per rad)	$K_Y \beta$ Test (per rad)	$\Delta K_Y \beta$ Calc.-Test (per rad)
4	D-50	1.076	75	0.386	Round $R_1 = 1.05$ in. —LE 3	0 .2 .4 .6	-0.150 -0.124 -0.044 0.088	-0.224 -0.215 -0.205 ---	0.074 0.091 -0.161 --
6	D-1	1.075	75	0.386	Round $R_1 = .525$ in. —LE 3	0 .2 .4 .6	-0.150 -0.150 -0.150 -0.150	-0.107 -0.100 -0.117 -0.157	-0.043 -0.050 -0.033 0.007

TABLE 5.5.1.2-A (CONTD)

Ref.	Configuration	A	Δ_{LE} (deg)	$\frac{S_B}{S}$	Leading Edge	C_N'	$K_Y \beta$ Calc. (per rad)	$K_Y \beta$ Test (per rad)	$\Delta K_Y \beta$ Calc.-Test (per rad)
6	D-2	1.076	75	0.349	Sharp $\delta_{e1} = 58^\circ$	0	-0.110	-0.122	0.012
						.2	-0.097	-0.070	-0.027
						.4	-0.056	-0.003	-0.053
						.6	0.012	0.057	-0.045
	D-5	1.076	75	0.386	Round $R_1 = 1.05$ in. —LE 3	0	-0.150	-0.219	0.069
						.2	-0.124	-0.208	0.084
						.4	-0.044	-0.196	0.152
						.6	0.088	--	--
	D-6	1.868	65	0.236	Round $R_1 = .525$ in. —LE 3	0	-0.030	-0.021	-0.009
						.2	-0.034	-0.051	0.017
						.41	-0.046	-0.061	0.015
						.63	-0.068	-0.043	-0.025
						.86	-0.101	--	--
	WB-3	1.074	75	0.282	Round $R_1 = .250$ in. —LE 3	0	-0.051	-0.137	0.086
						.2	-0.055	-0.184	0.129
						.4	-0.069	-0.231	0.162
						.6	-0.091	-0.277	0.186
14	b(basic)	0.783	79.5	0.491	Round $R_1 = .250$ in. —LE 3	0	-0.325	-0.344	0.019
						.2	-0.353	-0.482	0.129
						.4	-0.435	-0.521	0.086
						.6	-0.573	-0.539	-0.034
	b($R=1.5$ in.)	0.808	79.5	0.500	Round $R_1 = .250$ in. —LE 3	0	-0.337	-0.321	-0.016
						.2	-0.365	-0.475	0.110
						.4	-0.451	-0.548	0.097
						.6	-0.593	-0.557	-0.036
15	1	0.780	79.4	0.528	Round $R_1 = .50$ in. —LE 3	0	-0.395	-0.401	0.006
						.2	-0.416	-0.476	0.060
						.4	-0.480	-0.548	0.068
						.6	-0.586	-0.686	0

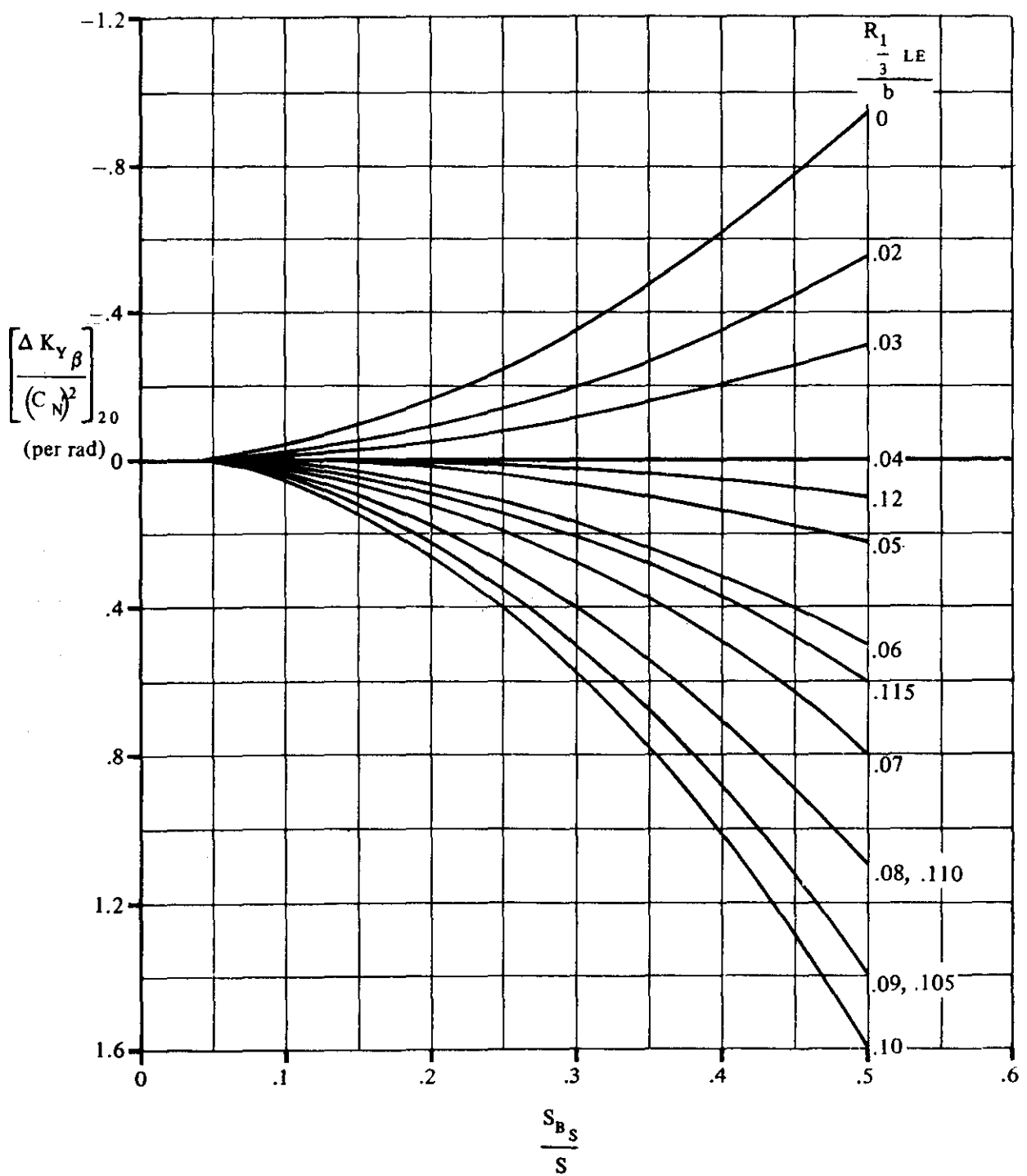


FIGURE 5.5.1.2-8 SIDE-FORCE-DERIVATIVE CORRELATION FACTOR FOR $K_{Y\beta}$ AT $\alpha' = 20^\circ$ – DELTA AND MODIFIED-DELTA CONFIGURATIONS WITH ROUND LEADING EDGES

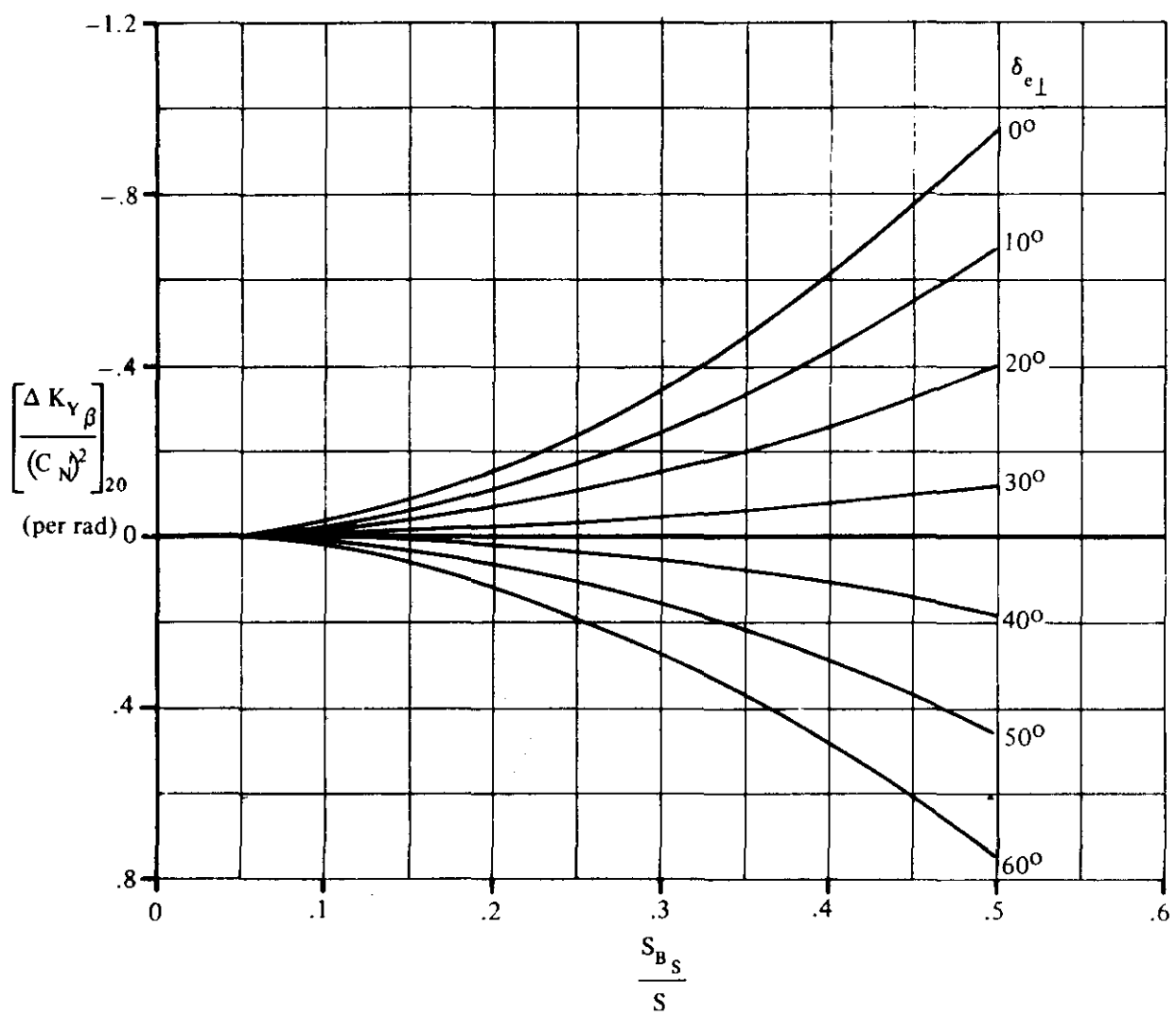


FIGURE 5.5.1.2-9 SIDE-FORCE-DERIVATIVE CORRELATION FACTOR FOR $K_{Y\beta}$ AT $\alpha' = 20^\circ$ – DELTA AND MODIFIED-DELTA CONFIGURATIONS WITH SHARP LEADING EDGES

5.5.2 WING, WING-BODY SIDESLIP DERIVATIVE $K'_{l\beta}$

5.5.2.1 WING, WING-BODY SIDESLIP DERIVATIVE $K'_{l\beta}$ NEAR ZERO NORMAL FORCE

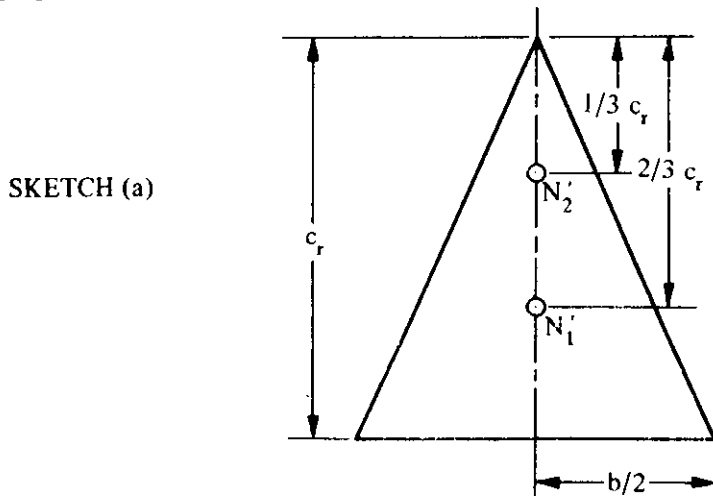
A. SUBSONIC

This section presents a method for estimating the sideslip derivative $K'_{l\beta}$ near zero normal force for delta and modified-delta configurations at subsonic speeds.

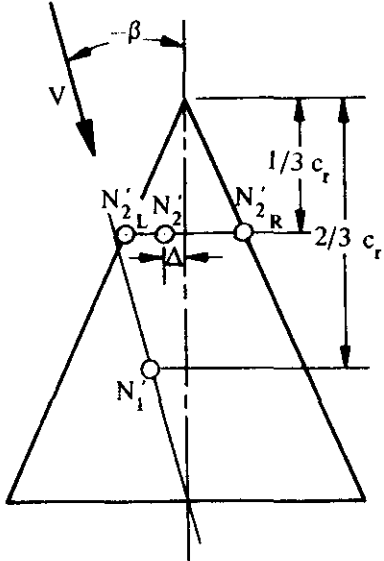
The subsonic rolling moment due to sideslip of a thin delta wing of vanishing aspect ratio ($A < 1$) with sharp leading edges and a pointed nose can be satisfactorily predicted at low lift coefficients by using the method presented in Section 5.1.2.1. However, this procedure is inadequate for proposed re-entry configurations. These configurations range in aspect ratio from low values of the order of $1/2$ up to 2 , and, for the most part, have thick, generously rounded lifting surfaces and blunt nose shapes.

The Datcom method is taken from reference 1. The method is semiempirical and was developed by first describing the pertinent aerodynamic phenomena in terms of a conceptual model and then using available experimental data to adjust the final theoretical results.

In determining the rolling moment due to sideslip of thin delta wings near zero normal force, it was necessary to define the spanwise variation of the normal-force loading due to sideslip, the longitudinal and lateral shifts in the configuration center of pressure due to sideslip, and the effect of sideslip on the total normal force. Briefly, the analysis proceeded as follows: From symmetry considerations and experimental results it was concluded that the total normal force is independent of sideslip angle near zero sideslip. Experimental data also show that the longitudinal position of the center of pressure does not change as the wing is sideslipped through small sideslip angles. Therefore, it was concluded that the change in $K'_{l\beta}$ results because of the spanwise shifts in normal force. It was then assumed that the normal force acting on a pure delta wing at zero sideslip can be divided into two components, one distributed uniformly over the planform and the other concentrated at the leading edge. The magnitude of the concentrated component at any spanwise station is proportional to the local chord. In accordance with this concept, the resultant of the uniform load acts at a point $2/3$ of the root chord aft of the wing apex, and the resultant of the leading-edge component acts at a point $1/3$ of the root chord aft of the wing apex (see sketch (a)). It was further assumed that when the wing is sideslipped, the center of



pressure of the uniform load moves normal to the root chord so as to maintain a line from the trailing edge of the root chord to the center of pressure in a plane parallel to the free stream. It was also assumed that the center of pressure of the leading-edge component moves normal to the root chord some distance Δ that is a function of the angle of sideslip (see sketch (b)). Any rolling-moment



GEOMETRY FOR DEFINING THE EFFECT OF SIDESLIP ON
CENTER-OF-PRESSURE POSITION – PURE DELTA WING
SKETCH (b)

contribution from the leading-edge component results from a normal-force differential between the right and left leading-edge components. The lateral position of their center of pressure is determined by balancing their rolling moments about the roll axis. By using the results given in reference 2 for the variation of the leading-edge component of normal force and the configuration geometry described by sketches (a) and (b), an expression was derived for the rolling moment due to sideslip of a thin delta wing near zero normal force. Finally, test data were used to refine the derived expression.

The final correlation is presented as figure 5.5.2.1-8a in the Datcom.

The effect of nose blunting was determined by analyzing a simplified model wherein a portion of the nose of a pure delta wing is removed by a straight cut normal to the root chord. The lateral center-of-pressure movement predicted by this technique is different from that observed, since actual nose blunting usually consists of rounding the forward part of the wing rather than cutting it off sharply. Therefore, an empirical factor was applied, based on the results of reference 3, to compensate for this difference.

It would be expected that thickness would influence rolling moment due to sideslip. The difference in the pressure distribution on the upper and lower surfaces of a lifting delta wing and the variation of the center-of-pressure locations due to thickness should result in an increment of rolling moment due to sideslip. However, during the study reported in reference 1, it was not possible to isolate the expected thickness effects with any degree of confidence. Therefore, the Datcom method does not include an increment showing the effect of thickness on rolling moment.

The Datcom method is considered valid for normal-force coefficients up to 0.3.

DATCOM METHOD

The rolling moment due to sideslip near zero normal force for delta and modified-delta configurations, based on the product of the planform area and span S_b , at low speeds is given by

$$K'_{l\beta_{N_0}} = C_{N'} \left\{ \left[\frac{K'_{l\beta_{N_0}}}{C_{N'}} \right]_{\Delta} + \Delta \left[\frac{K'_{l\beta}}{C_{N'}} \right]_B \right\} \quad (\text{per radian}) \quad 5.5.2.1-a$$

where

$C_{N'}$ is the normal-force coefficient.

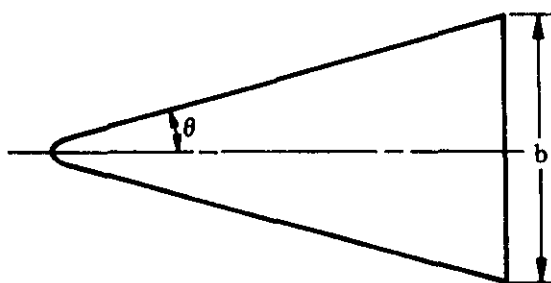
$\left[\frac{K'_{l\beta_{N_0}}}{C_{N'}} \right]_{\Delta}$ is the ratio of the sideslip derivative $K'_{l\beta}$ at zero normal force to the normal-force coefficient for a pointed-nose delta configuration. This parameter is obtained from figure 5.5.2.1-8a as a function of the wing semiapex angle θ .

$\Delta \left[\frac{K'_{l\beta}}{C_{N'}} \right]_B$ is the increment of the ratio of sideslip derivative $K'_{l\beta}$ to the normal-force coefficient, due to nose blunting. This parameter is obtained from figure 5.5.2.1-8b as a function of the configuration semiapex angle θ and the aspect ratio. The semiapex angle is measured as illustrated on figure 5.5.2.1-8b and the aspect ratio is that of the blunt-nose configuration.

A comparison of the rolling moment due to sideslip near zero normal force calculated by this method with test data is presented as table 5.5.2.1-A.

Sample Problem

Given: A blunt-nose delta-wing model with a symmetrical cross section and a blunt trailing edge. This is model D-5 of reference 7.



$$A = 1.076$$

$$\theta = 15^\circ$$

$$S = 160.19 \text{ sq in.}$$

$$b = 13.13 \text{ in.}$$

Compute:

$$\left[\frac{K'_{l\beta_{N_0}}}{C_{N'}} \right]_{\Delta} = -0.65 \text{ per rad} \quad (\text{figure 5.5.2.1-8a})$$

$$1 - \frac{4 \tan \theta}{A} = 1 - \frac{4 \tan 15^\circ}{1.076} = 0.0041$$

$$\Delta \left[\frac{K'_{l\beta}}{C_{N'}} \right]_{B} = 0.033 \text{ per rad} \quad (\text{figure 5.5.2.1-8b})$$

Solution:

$$\begin{aligned} \frac{K'_{l\beta}}{C_{N'}} &= \left\{ \left[\frac{K'_{l\beta_{N_0}}}{C_{N'}} \right]_{\Delta} + \Delta \left[\frac{K'_{l\beta}}{C_{N'}} \right]_{B} \right\} \quad (\text{equation 5.5.2.1-a}) \\ &= -0.65 + 0.033 \\ &= -0.617 \text{ per rad (based on Sb)} \end{aligned}$$

This compares with a test value of -0.556 per radian from reference 7.

REFERENCES

1. Seeger, D. B., and Ross, R.: Investigation of the Low-Speed Stability and Control Characteristics of Advanced Flight Vehicles. ASD-TDR-63-671, 1963. (C) Title Unclassified
2. Seeger, D. B., and Meyer, J. E.: An Investigation of the Subsonic Aerodynamic Characteristics and the Landing Flare Maneuver for Hypersonic Re-entry Configurations. ASD-TDR-62-271, 1962. (C) Title Unclassified
3. Edwards, G. G., and Savage, H. F.: The Subsonic Aerodynamic Characteristics of Some Blunt Delta Configurations with 75° Sweepback. NASA TM X-581, 1961. (C) Title Unclassified
4. Mantz, K., and Seeger, D. B.: Tests to Determine the Subsonic Pressures, Forces and Moments Acting on a Hypersonic Re-entry Configuration. ASD-TDR-62-270, 1962. (C) Title Unclassified
5. Mantz, K., Seeger, D. B., and Ross, R.: Tests to Determine Subsonic Pressures, Forces and Moments Acting on a Hypersonic Re-entry Configuration. ASD-TDR-62-270, Supplement 1, 1963. (U)
6. Sipe, O. E., and Seeger, D. B.: Tests to Determine Subsonic Aerodynamic Characteristics of Hypersonic Re-entry Configurations. ASD-TR-61-485, 1961. (C) Title Unclassified
7. Mantz, K., Seeger, D. B., and Ross, R.: Tests to Determine Subsonic Aerodynamic Characteristics of Hypersonic Re-entry Configurations. ASD-TR-61-485, Supplement 1, 1963. (U)
8. Graham, D., and Koenig, D. G.: Tests in the Ames 40- by 80-Foot Wind Tunnel of an Airplane Configuration with an Aspect Ratio 2 Triangular Wing and an All-Movable Horizontal Tail — Lateral Characteristics. NACA RM A51L03, 1952. (U)
9. Jaquet, B. M., and Brewer, J. D.: Low-Speed Static-Stability and Rolling Characteristics of Low-Aspect-Ratio Wings of Triangular and Modified Triangular Plan Forms. NACA RM L8L29, 1949. (U)

10. McKinney, M. O., Jr., and Drake, H. M.: Flight Characteristics at Low Speed of Delta-Wing Models. NACA RM L7K07, 1948. (U)
11. Jaquet, B. M., and Brewer, J. D.: Effects of Various Outboard and Central Fins on Low-Speed Static-Stability and Rolling Characteristics of a Triangular-Wing Model. NACA RM L9E18, 1949. (U)
12. Keeting, R. F. A.: Low-Speed Wind-Tunnel Tests on Sharp-Edged Gothic Wings of Aspect-Ratio 3/4. ARC CP 576, 1961. (U)
13. Goodman, A., and Thomas, D.: Effects of Wing Position and Fuselage Size on the Low-Speed Static and Rolling Stability Characteristics of a Delta-Wing Model. NACA TR 1224, 1955. (U)
14. Tosti, L. P.: Low Speed Static Stability and Damping-in-Roll Characteristics of Some Swept and Unswept Low-Aspect-Ratio Wings. NACA TN 1468, 1947. (U)
15. Lange/Wacke: Test Report on Three- and Six-Component Measurements on a Series of Tapered Wings of Small Aspect Ratio. (Partial Report: Triangular Wing.) NACA TM 1176, 1948. (U)
16. Whittle, E. F., Jr., and Lovell, J. C.: Full-Scale Investigation of an Equilateral Triangular Wing Having 10-Percent Thick Biconvex Airfoil Sections. NACA RM L8G05, 1948. (U)
17. Olstad, W. B., Mugler, J. P., Jr., and Cahn, M. S.: Static Longitudinal and Lateral Stability Characteristics of a Right Triangular Pyramidal Lifting Re-entry Configuration at Transonic Speeds. NASA TN D-655, 1961. (U)
18. Ware, G. M.: Low-Subsonic-Speed Static Stability of Right-Triangular-Pyramid and Half-Cone Lifting Re-entry Configurations. NASA TN D-646, 1961. (U)
19. Paulson, J. W., and Shanks, R. E.: Investigation of Low-Subsonic Flight Characteristics of a Model of a Hypersonic Boost-Glide Configuration Having a 78° Delta Wing. NASA TN D-894, 1961. (U)
20. Paulson, J. W.: Low-Speed Static Stability and Control Characteristics of a Right Triangular Pyramid Re-entry Configuration. NASA Memo 4-11-59L, 1959. (U)
21. Anderson, A. E.: An Investigation of a Large-Scale Triangular Wing of Aspect Ratio Two. — I. Characteristics of a Wing Having a Double-Wedge Airfoil Section with Maximum Thickness at 20-Percent Chord. NACA RM A7F06, 1947. (U)
22. McDevitt, J. B., and Rakich, J. V.: The Aerodynamic Characteristics of Several Thick Delta Wings at Mach Numbers to 6 and Angles of Attack to 50°. NASA TM X-162, 1960. (C) Title Unclassified
23. Shanks, R. E.: Investigation of the Low-Subsonic Flight Characteristics of a Model of an All-Wing Hypersonic Boost-Glide Configuration Having Very High Sweep. NASA TN D-369, 1960. (U)
24. Boisseau, P. C.: Investigation of the Low-Subsonic Flight Characteristics of a Model of a Re-entry Vehicle with a Thick Flat 75° Delta Wing and a Half-Cone Fuselage. NASA TN D-1007, 1962. (U)

TABLE 5.5.2.1-A
 SUBSONIC ROLLING MOMENT DUE TO SIDESLIP NEAR
 ZERO NORMAL FORCE
 DELTA PLANFORM CONFIGURATIONS
 DATA SUMMARY

Ref.	Configuration	A	θ (deg)	Nose Configuration	$\left[\frac{K_2 \beta N_0}{C'_N} \right]$ Calc. (per rad)	$\left[\frac{K_2 \beta N_0}{C'_N} \right]$ Test (per rad)	$\Delta \left[\frac{K_2 \beta N_0}{C'_N} \right]$ (Calc.-Test) (per rad)
6	D-60	1.076	15.0	blunt	-0.617	-0.586	-.031
7	D-1	1.076	15.0	blunt	-0.617	-0.544	-.073
	D-2	1.075		sharp	-0.617	-0.500	-.117
	D-5	1.076	↓	sharp	-0.617	-0.556	-.061
	D-6	1.868	25.0	blunt	-0.345	-0.368	.023
	WB-1	1.094	15.0	blunt	-0.557	-0.585	.028
	WB-3	1.074	↓	blunt	-0.600	-0.560	-.040
	WB-4	1.147	↓	blunt	-0.504	-0.456	-.048
8	Wing alone	2.00	26.17	sharp	-0.330	-0.320	-.010
9	1	2.31	30.0	sharp	-0.286	-0.636	.360
	2	↓	↓	sharp	-0.286	-0.585	.299
	3	↓	↓	sharp	-0.286	-0.585	.299
	4	1.07	15.0	sharp	-0.630	-0.970	.340
	7	4.00	45.0	sharp	-0.172	-0.320	.148
10	1	3.00	37.0	sharp	-0.218	-0.186	-.032
	4	2.00	27.0	sharp	-0.323	-0.246	-.077
	6	1.00	14.0	sharp	-0.675	-0.825	.150
	8	0.50	7.0	sharp	-1.370	-2.060	.690
11	Wing alone	2.31	30.0	sharp	-0.286	-0.370	.084
13	Wing alone	2.31	30.0	sharp	-0.286	-0.380	.094
14	11	3.00	37.0	sharp	-0.218	-0.225	.007
	12	2.00	26.2	sharp	-0.330	-0.262	-.068
	13	1.00	14.0	sharp	-0.675	-0.520	-.155
	14	0.50	7.1	sharp	-1.35	-0.936	-.414

TABLE 5.5.2.1-A (CONTD)

Ref.	Configuration	A	θ (deg)	Nose Configuration	$\left[\frac{K_i \beta_{N_0}}{C_{N'}} \right]$ Calc. (per rad)	$\left[\frac{K_i \beta_{N_0}}{C_{N'}} \right]$ Test (per rad)	$\Delta \left[\frac{K_i \beta_{N_0}}{C_{N'}} \right]$ (Calc.-Test) (per rad)
15	1	3.00	37.0	sharp	-0.172	-0.122	-.060
	2	2.00	26.2	sharp	-0.330	-0.190	-.140
	3	1.33	18.03	sharp	-0.503	-0.404	-.099
	4	1.00	14.0	sharp	-0.675	-0.528	-.147
16	Wing alone	2.31	60.0	sharp	-0.286	-0.320	.034
17	1	0.742	10.5	blunt	-0.866	-1.00	.134
18	a	0.783	10.5	blunt	-0.721	-0.670	-.061
	b(basic)	0.783		blunt	-0.721	-0.710	-.011
	b(R=1.5 in.)	0.808		blunt	-0.678	-0.690	.012
19	d	0.783		blunt	-0.721	-0.800	.079
	Delta wing boost-glide	0.740	12.0	sharp	-0.800	-0.940	.140
20	Rt. triangular pyramid	0.780	10.6	blunt	-0.722	-0.580	-.142
21	Wing alone	2.0	26.6	sharp	-0.330	-0.186	-.144

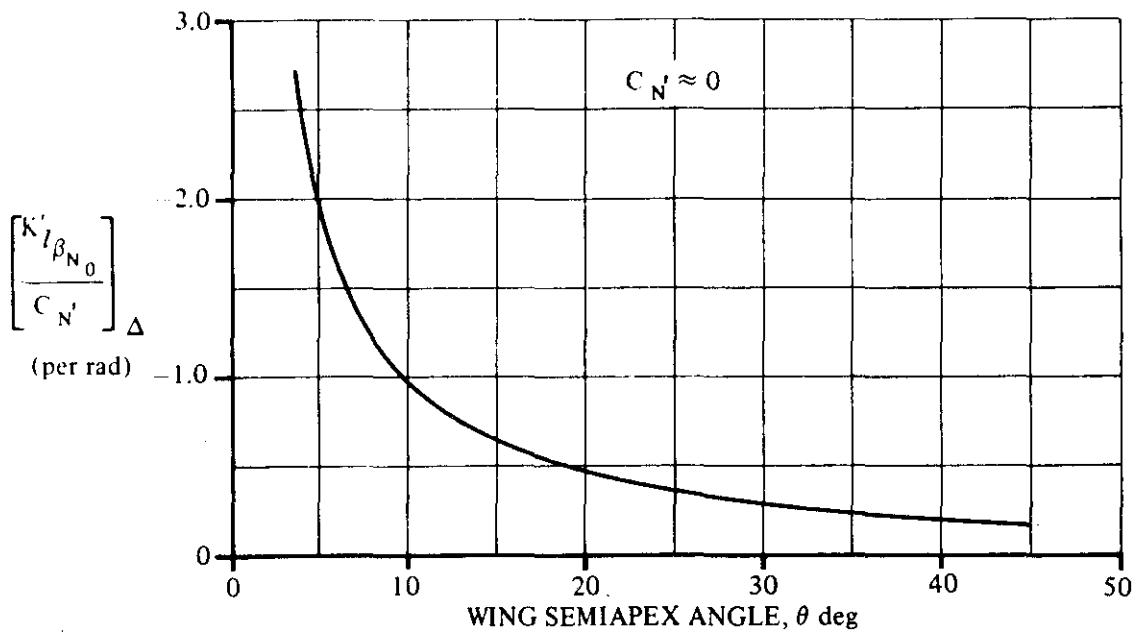


FIGURE 5.5.2.1-8a ROLLING MOMENT DUE TO SIDESLIP
POINTED-NOSED DELTA CONFIGURATIONS

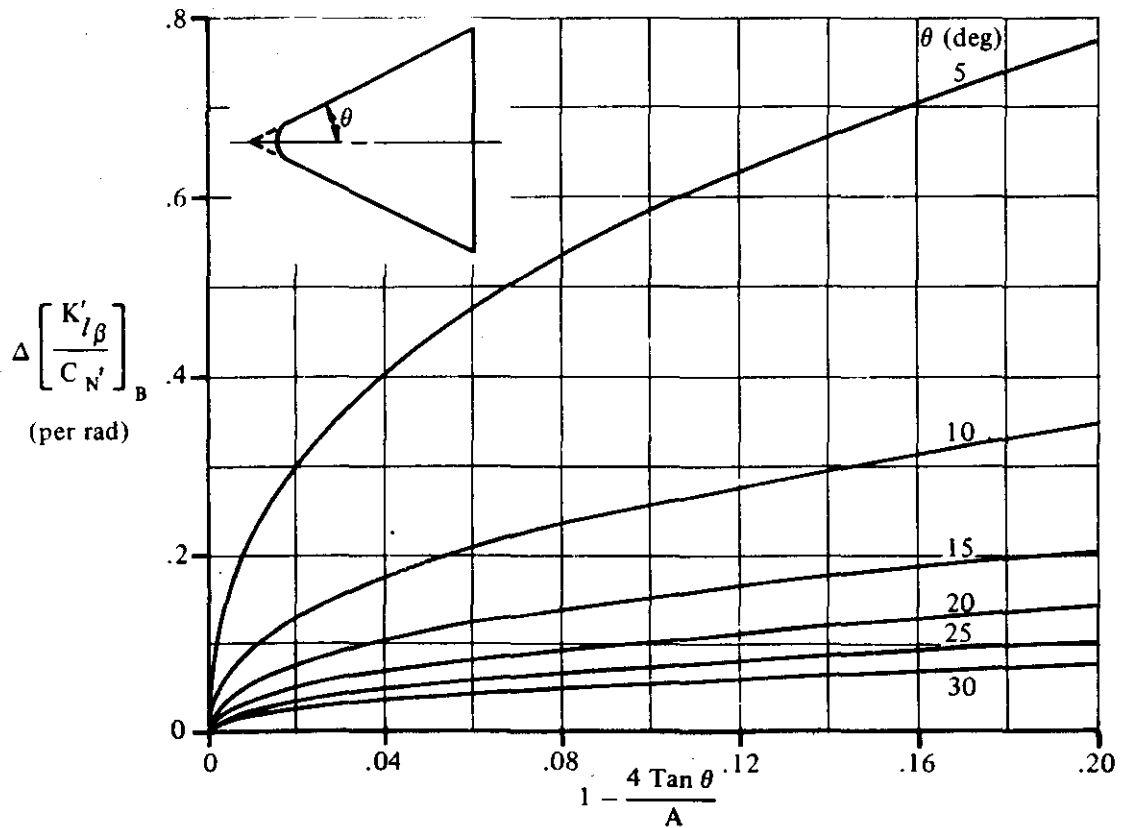


FIGURE 5.5.2.1-8b EFFECTS OF NOSE BLUNTING ON ROLLING MOMENT DUE TO SIDESLIP
DELTA AND BLUNTED DELTA CONFIGURATIONS

5.5.2.2 WING, WING-BODY SIDESLIP-DERIVATIVE $K'_{l\beta}$ VARIATION WITH ANGLE OF ATTACK

A. SUBSONIC

This section presents a method, taken from reference 1, for estimating the sideslip-derivative $K'_{l\beta}$ variation with angle of attack for delta and modified-delta configurations at subsonic speeds.

The variation of $K'_{l\beta}$ with angle of attack for a thin delta wing is based on the conceptual model described briefly in Section 5.5.2.1, and the semiempirical technique used to obtain the variation of normal force with angle of attack is that described in reference 2. It is shown in reference 2 that the longitudinal position of the center of pressure and the distribution of the load over the surface of an unyawed, thin delta wing are both independent of angle of attack. As noted in Section 5.5.2.1, experimental data also show that the longitudinal position of the center of pressure does not change as the wing is sideslipped through small sideslip angles. Therefore, it was concluded that the ratio of the normal-force component that is considered to act at the leading edge to that uniformly distributed over the wing (see discussion in Section 5.5.2.1) does not change, and that the change in $K'_{l\beta}$ with angle of attack results because of the spanwise shift in one or both of these normal-force components as the angle of attack is increased. In accordance with these considerations, the variation of the sideslip derivative $K'_{l\beta}$ with angle of attack is related to the normal-force coefficient by

$$\frac{(K'_{l\beta}/C_N')_{\text{linear}}}{(K'_{l\beta}/C_N')_{\text{nonlinear}}} = \frac{(C_N')_{\text{linear}}}{(C_N')_{\text{nonlinear}}}$$

The technique used to obtain a correlation of normal force in reference 2 (see Section 4.8.1.2) was then applied to determine a reference value for $K'_{l\beta}$ at $\alpha' = 20^\circ$. The correlation parameters used were leading-edge radius and leading-edge angle for thin delta wings with round and sharp leading edges, respectively. It was then assumed that the variation of $K'_{l\beta}/C_N'$ within the angle-of-attack range from 0 to 20° is parabolic. It should be noted that as the leading-edge radius approaches zero, the rolling-moment coefficient with respect to sideslip approaches the same value as for a sharp leading edge. Therefore, a configuration with a small leading-edge radius can be analyzed as one having a sharp leading edge.

As wing thickness is increased, the pressure distribution on the upper and lower surfaces of a sideslipping delta wing at angle of attack become significantly different. A couple will be introduced due to this pressure distribution and a corresponding rolling-moment increment will result. An empirical correlation, taken from reference 1, is presented to account for this thickness effect. This correlation is based on data at $\alpha' = 20^\circ$ only; however, it is applied over the angle-of-attack range from 0 to 20° in the Datcom.

The increment in rolling-moment coefficient with respect to sideslip due to nose blunting is assumed invariant with angle of attack. Therefore, the effect of nose blunting is taken as that presented in Section 5.5.2.1.

The Datcom method is considered valid for sideslip angles between $\pm 10^\circ$ and angles of attack up to 20° .

DATCOM METHOD

The sideslip-derivative $K'_{l\beta}$ variation with angle of attack for a delta or modified-delta configuration at subsonic speeds, based on the product of planform area and span S_b , is obtained from the procedure outlined in the following steps:

- Step 1. Determine the effective leading-edge angle δ_{e1} for sharp leading edges or the effective leading-edge radius $R_{\frac{1}{3} \text{ LE}}$ for round leading edges. These parameters are functions of the configuration geometry in a plane normal to the leading edge at $\frac{1}{3} c_r$ from the nose. The applicable configuration geometry is illustrated on figure 4.8.1.2-11a and 4.8.1.2-11b.

- Step 2. Determine the ratio $\left[\frac{K'_{l\beta N_0}}{C_{N'}} \right]_{\Delta}$ of the sideslip derivative $K'_{l\beta}$ near zero normal force to the normal-force coefficient for a thin, pointed-nose delta wing. This parameter is obtained from figure 5.5.2.1-8a as a function of the wing semiapex angle θ .
- Step 3. Determine the calculated value of $K'_{l\beta}/C_{N'}$ at $\alpha' = 20^\circ$ by

$$\left[\left(\frac{K'_{l\beta}}{C_{N'}} \right)_{\text{calc}} \right]_{20} = \frac{1}{1 + \frac{0.152}{\tan \theta}} \left[\frac{K'_{l\beta N_0}}{C_{N'}} \right]_{\Delta} \quad (\text{per radian}) \quad 5.5.2.2-a$$

where θ is the semiapex angle in degrees and $\left[\frac{K'_{l\beta N_0}}{C_{N'}} \right]_{\Delta}$ is obtained from step 2.

- Step 4. Obtain the empirical correlation factor for the ratio of $K'_{l\beta}$ to normal-force coefficient at $\alpha' = 20^\circ$. This parameter is expressed as $\frac{\left(K'_{l\beta}/C_{N'} \right)_{20}}{\left[\left(K'_{l\beta}/C_{N'} \right)_{\text{calc}} \right]_{20}}$ and is presented as a function of the effective leading-edge radius for configurations with round leading edges in figure 5.5.2.2-12a, and as a function of leading-edge angle for configurations with sharp leading edges in figure 5.5.2.2-12b.

- Step 5. Obtain the empirical correlation factor for the increment in the ratio of $K'_{l\beta}$ to normal-force coefficient due to thickness effects at $\alpha' = 20^\circ$. This parameter is expressed as

$\Delta \frac{\left(K'_{l\beta}/C_{N'} \right)_{20}}{\left[\left(K'_{l\beta}/C_{N'} \right)_{\text{calc}} \right]_{20}}$ and is presented in figure 5.5.2.2-13 as a function of the ratio of the projected side area of the configuration to the planform area S_{BS}/S .

- Step 6. Determine the ratio of the increment in sideslip derivative $K'_{l\beta}$ to the normal-force coefficient due to nose blunting $\Delta \left[\frac{K'_{l\beta}}{C_{N'}} \right]_B$ from figure 5.5.2.1-8b as a function of the configuration semiapex angle θ and the aspect ratio. The semiapex angle is measured as illustrated on figure 5.5.2.1-8b and the aspect ratio is that of the blunt-nose configuration.
- Step 7. Using the terms obtained in steps 2 through 6 determine the variation of the ratio of $K'_{l\beta}/C_{N'}$ with α' by

$$\frac{K'_{l\beta}}{C_{N'}} = \left[\frac{K'_{l\beta N_0}}{C_{N'}} \right]_{\Delta} \left[1 - \left(\frac{\alpha'}{20} \right)^2 \right] + \left(\left(\frac{(K'_{l\beta}/C_{N'})_{20}}{[(K'_{l\beta}/C_{N'})_{\text{calc}}]_{20}} \right) \right. \\ \left. + \Delta \frac{(K'_{l\beta}/C_{N'})_{20}}{[(K'_{l\beta}/C_{N'})_{\text{calc}}]_{20}} \right) \left(\left(\frac{K'_{l\beta}}{C_{N'}} \right)_{\text{calc}} \right)_{20} + \Delta \left[\frac{K'_{l\beta}}{C_{N'}} \right]_B \left(\frac{\alpha'}{20} \right)^2 \quad (\text{per radian})$$

5.5.2.2-b

where α' is in degrees.

- Step 8. Determine the variation of $K'_{l\beta}$ with angle of attack by

$$K'_{l\beta} = \left(\frac{K'_{l\beta}}{C_{N'}} \right) C_{N'} \quad 5.5.2.2-c$$

where $(K'_{l\beta}/C_{N'})$ is from step 7 and $C_{N'}$ is the normal-force coefficient at angle of attack obtained from Section 4.8.1.2.

The variation of the sideslip derivative $K'_{l\beta}$ with angle of attack calculated by this method is compared with test data in table 5.5.2.2-A. The variations of $C_{N'}$ with angle of attack, used to obtain the calculated values of $K'_{l\beta}$ in table 5.5.2.2-A, were calculated by using the method of Section 4.8.1.2.

It should be noted that a considerable amount of scatter was involved in the data correlation used to define the design charts. In the case of sharp-leading-edged configurations it was necessary to estimate the nature of the effect of leading-edge angle on the basis of very few test data. Therefore, the accuracy of the design chart used for sharp leading edges (figure 5.5.2.2-12b) is questionable.

The lift distribution over a lifting delta wing is such that maximum local lifts occur in the area immediately below the cores of the shed vortices (see discussion in Section 5.5.1.2). Since these vortices do not move with the wing as it is sideslipped, the region of high local lift may act on the surface at one sideslip angle while the wing-vortex which produces it may be outboard of the leading edge at

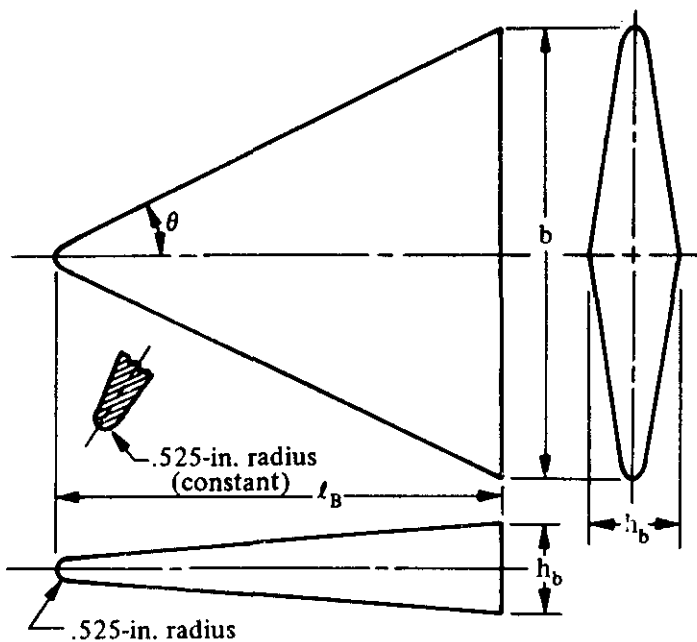
5.5.2.2-3

another. Therefore, nonlinearities in the variation of rolling moment with sideslip may exist with low-aspect-ratio delta planforms. The available data are not sufficient to allow isolation of this effect. However, it should be realized that a constant value of $K'_{l\beta}$ valid for $\beta = \pm 10^\circ$ may not be a useful representation of the physical phenomena involved.

Sample Problems

1. Round Leading Edge

Given: A delta wing model of reference 6 designated D-6. This is the configuration of sample problem 1 of Section 4.8.1.2.



$$A = 1.868$$

$$b = 22.116 \text{ in.}$$

$$S = 261.95 \text{ sq in.}$$

$$S_{B_S} = 61.82 \text{ sq in.}$$

$$R_{\frac{1}{3} LE} = 0.525 \text{ in.}$$

$$\theta = 25^\circ$$

$$h_b = 4.32 \text{ in.}$$

The following variation of $C_{N'}$ with α' from sample problem 1 of Section 4.8.1.2:

α'	0	5°	10°	15°	20°
$C_{N'}$	0	0.2017	0.4122	0.6323	0.8618

Compute:

$$\left[\frac{K'_{l\beta_{N_0}}}{C_{N'}} \right]_\Delta = -0.36 \text{ per rad} \quad (\text{figure 5.5.2.1-8a})$$

$$\left[\left(\frac{K'_I \beta}{C_{N'}} \right)_{\text{calc}} \right]_{20} = \frac{1}{1 + \frac{0.152}{\tan \theta}} \left[\frac{K'_I \beta_{N_0}}{C_{N'}} \right]_{\Delta} \quad (\text{equation 5.5.2.2-a})$$

$$= \frac{1}{1 + \frac{0.152}{\tan 25^\circ}} \quad (-0.36)$$

$$= -0.271 \text{ per rad}$$

$$R_{\frac{1}{3} \text{ LE}} / b = 0.525 / 22.116 = 0.0237$$

$$\frac{\left(K'_I \beta / C_{N'} \right)_{20}}{\left[\left(K'_I \beta / C_{N'} \right)_{\text{calc}} \right]_{20}} = 0.655 \quad (\text{figure 5.5.2.2-12a})$$

$$S_B / S = 61.82 / 261.95 = 0.236$$

$$\Delta \left[\frac{\left(K'_I \beta / C_{N'} \right)_{20}}{\left[\left(K'_I \beta / C_{N'} \right)_{\text{calc}} \right]_{20}} \right] = 0.10 \quad (\text{figure 5.5.2.2-13})$$

$$1 - \frac{4 \tan \theta}{A} = 1 - \frac{4 \tan 25^\circ}{1.868} = 0.0015$$

$$\Delta \left[\frac{K'_I \beta}{C_{N'}} \right]_B = 0.005 \text{ per rad} \quad (\text{figure 5.5.2.1-8b})$$

$$\frac{K'_I \beta}{C_{N'}} = \left[\frac{K'_I \beta_{N_0}}{C_{N'}} \right]_{\Delta} \left[1 - \left(\frac{\alpha'}{20} \right)^2 \right] + \left(\frac{\left(K'_I \beta / C_{N'} \right)_{20}}{\left[\left(K'_I \beta / C_{N'} \right)_{\text{calc}} \right]_{20}} \right.$$

$$+ \Delta \left. \frac{\left(K'_I \beta / C_{N'} \right)_{20}}{\left[\left(K'_I \beta / C_{N'} \right)_{\text{calc}} \right]_{20}} \right) \left[\left(\frac{K'_I \beta}{C_{N'}} \right)_{\text{calc}} \right]_{20}$$

$$+ \Delta \left[\frac{K'_I \beta}{C_{N'}} \right]_B \left(\frac{\alpha'}{20} \right)^2 \quad (\text{equation 5.5.2.2-b})$$

$$\begin{aligned}
 &= (-0.36) \left[1 - \left(\frac{\alpha'}{20} \right)^2 \right] + ((0.655 + 0.10) \{-0.271\} + 0.005) \left(\frac{\alpha'}{20} \right)^2 \\
 &= -0.36 + 0.36 \left(\frac{\alpha'}{20} \right)^2 - 0.200 \left(\frac{\alpha'}{20} \right)^2 \\
 &= -0.36 + 0.160 \left(\frac{\alpha'}{20} \right)^2 \text{ per rad}
 \end{aligned}$$

Solution:

$$K'_{I\beta} = \left(\frac{K'_{I\beta}}{C_N} \right) C_N \quad (\text{equation 5.5.2.2-c})$$

$$= \left[-0.36 + 0.160 \left(\frac{\alpha'}{20} \right)^2 \right] C_N \text{ per rad}$$

①

②

③

④

⑤

⑥

α' (deg)	C_N' (given)	$\alpha'/20$ ① / 20	$0.160 \left(\frac{\alpha'}{20} \right)^2$ $0.160 \cdot ③^2$	$\frac{K'_{I\beta}}{C_N}$ (per rad) -0.36 + ④	$K'_{I\beta}$ (based on Sb) eq. 5.5.2.2-c (per rad) ⑥ ②
0	0	0	0	-0.360	0
5	0.202	0.25	0.010	-0.350	-0.071
10	0.412	0.50	0.040	-0.320	-0.132
15	0.632	0.75	0.090	-0.270	-0.171
20	0.862	1.00	0.160	-0.200	-0.172

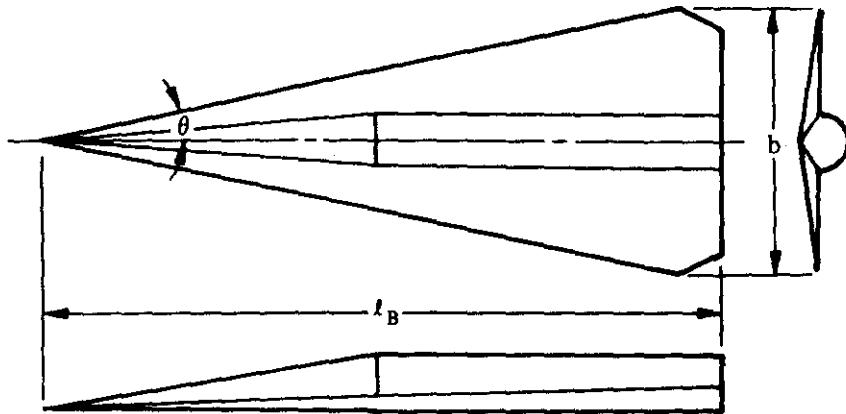
The calculated results are compared with test values from reference 6 in sketch (a) and in table 5.5.2.2-A.

2. Sharp Leading Edge

Given: The hypersonic boost-glide configuration of reference 8 without tip cones and ventrals.

$$A = 0.74 \quad b = 35.40 \text{ in.} \quad S = 11.70 \text{ sq ft} \quad S_{BS} = 3.39 \text{ sq ft}$$

$$\delta_{e\perp} = 10.1^\circ \quad \theta = 12^\circ$$



The following variation of C_N' with α' , calculated by using the method of Section 4.8.1.2:

α'	0	5°	10°	15°	20°
C_N'	0	0.119	0.276	0.471	0.704

Compute:

$$\left[\frac{K'_I \beta_{N_0}}{C_N'} \right]_\Delta = -0.800 \text{ per rad} \quad (\text{figure 5.5.2.1-8a})$$

$$\begin{aligned} \left[\left(\frac{K'_I \beta}{C_N'} \right)_{\text{calc}} \right]_{20} &= \frac{1}{1 + \frac{0.152}{\tan \theta}} \left[\frac{K'_I \beta_{N_0}}{C_N'} \right]_\Delta \quad (\text{equation 5.5.2.2-a}) \\ &= \frac{1}{1 + \frac{0.152}{\tan 12^\circ}} (-0.800) \\ &= -0.466 \text{ per rad} \end{aligned}$$

$$\frac{\left(K'_I \beta / C_N' \right)_{20}}{\left[\left(K'_I \beta / C_N' \right)_{\text{calc}} \right]_{20}} = 0.950 \quad (\text{figure 5.5.2.2-12b})$$

$$S_{B_S} / S = 3.39 / 11.70 = 0.290$$

$$\Delta \frac{\left(K'_I \beta / C_N' \right)_{20}}{\left[\left(K'_I \beta / C_N' \right)_{\text{calc}} \right]_{20}} = 0.12 \quad (\text{figure 5.5.2.2-13})$$

$$\Delta \left[\frac{K'_{l\beta}}{C_{N'}} \right]_B = 0 \text{ (no nose bluntness)}$$

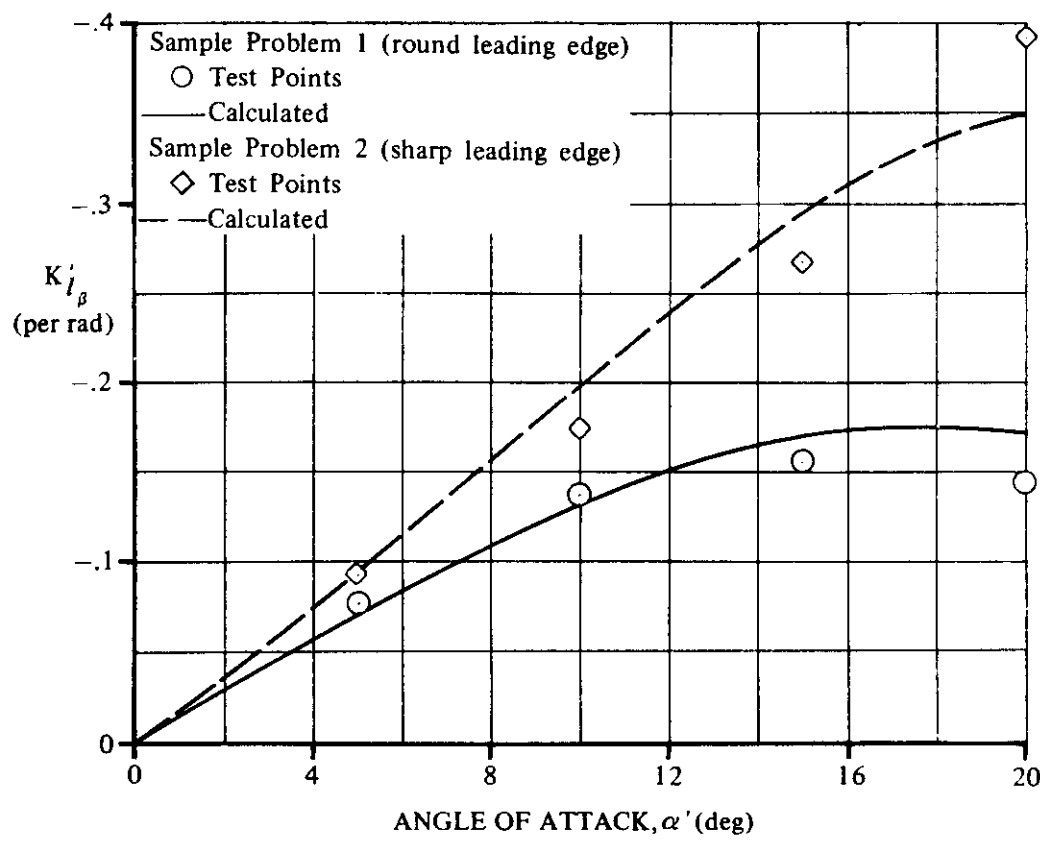
$$\begin{aligned}
 \frac{K'_{l\beta}}{C_{N'}} &= \left[\frac{K'_{l\beta_{N_0}}}{C_{N'}} \right]_\Delta \left[1 - \left(\frac{\alpha'}{20} \right)^2 \right] + \left(\left\{ \frac{(K'_{l\beta}/C_{N'})_{20}}{[(K'_{l\beta}/C_{N'})_{\text{calc}}]_{20}} \right. \right. \\
 &\quad \left. \left. + \Delta \left[\frac{(K'_{l\beta}/C_{N'})_{20}}{(K'_{l\beta}/C_{N'})_{\text{calc}}} \right]_{20} \right\} \left[\left(\frac{K'_{l\beta}}{C_{N'}} \right)_{\text{calc}} \right]_{20} \right. \\
 &\quad \left. + \Delta \left[\frac{K'_{l\beta}}{C_{N'}} \right]_B \right) \left(\frac{\alpha'}{20} \right)^2 \quad (\text{equation 5.5.2.2-b}) \\
 &= (-0.800) \left[1 - \left(\frac{\alpha'}{20} \right)^2 \right] + ((0.950 + 0.12)[-0.466] + 0) \left(\frac{\alpha'}{20} \right)^2 \\
 &= -0.800 + 0.800 \left(\frac{\alpha'}{20} \right)^2 - 0.499 \left(\frac{\alpha'}{20} \right)^2 \\
 &= -0.800 + 0.301 \left(\frac{\alpha'}{20} \right)^2 \text{ per rad}
 \end{aligned}$$

Solution:

$$\begin{aligned}
 K'_{l\beta} &= \left(\frac{K'_{l\beta}}{C_{N'}} \right) C_{N'} \quad (\text{equation 5.5.2.2-c}) \\
 &= \left[-0.800 + 0.301 \left(\frac{\alpha'}{20} \right)^2 \right] C_{N'} \text{ per rad}
 \end{aligned}$$

	(1)	(2)	(3)	(4)	(5)	(6)
α' (deg)	C_N' (given)	$\alpha'/20$ (1) /20	$0.301 \left(\frac{\alpha'}{20}\right)^2$ 0.301 (3) ²	$\frac{K_{I_\beta}'}{C_N'}$ (per rad) -0.800 + (4)	K_{I_β}' (based on Sb) eq. 5.5.2.2-c (per rad) (5) (2)	
0	0	0	0	-0.800	0	
5	0.119	0.25	0.019	-0.781	-0.093	
10	0.276	0.50	0.075	-0.725	-0.200	
15	0.471	0.75	0.169	-0.631	-0.297	
20	0.704	1.00	0.301	-0.499	-0.351	

The calculated results are compared with test values from reference 8 in sketch (a) and in table 5.5.2.2-A.



SKETCH (a)

REFERENCES

1. Seeger, D. B., and Ross, R.: Investigation of the Low-Speed Stability and Control Characteristics of Advanced Flight Vehicles. ASD-TDR-63-671, 1963. (C) Title Unclassified
2. Seeger, D. B., and Meyer, J. E.: An Investigation of the Subsonic Aerodynamic Characteristics and the Landing Flare Maneuver for Hypersonic Re-entry Configurations. ASD-TDR-62-271, 1962. (C) Title Unclassified
3. Mantz, K., and Seeger, D. B.: Tests to Determine the Subsonic Pressures, Forces and Moments Acting on a Hypersonic Re-entry Configuration. ASD-TDR-62-270, 1962. (C) Title Unclassified
4. Mantz, K., Seeger, D. B., and Ross, R.: Tests to Determine Subsonic Pressures, Forces and Moments Acting on a Hypersonic Re-entry Configuration. ASD-TDR-62-270, Supplement 1, 1963. (U)
5. Sipe, O. E., and Seeger, D. B.: Tests to Determine Subsonic Aerodynamic Characteristics of Hypersonic Re-entry Configurations. ASD-TR-61-485, 1961. (C) Title Unclassified
6. Mantz, K., Seeger, D. B., and Ross, R.: Tests to Determine Subsonic Aerodynamic Characteristics of Hypersonic Re-entry Configurations. ASD-TR-61-485, Supplement 1, 1963. (U)
7. Ware, G. M.: Low-Subsonic-Speed Static Stability of Right-Triangular-Pyramid and Half-Cone Lifting Re-entry Configurations. NASA TN D-646, 1961. (U)
8. Paulson, J. W., and Shanks, R. E.: Investigation of Low-Subsonic Flight Characteristics of a Model of a Hypersonic Boost-Glide Configuration Having a 78° Delta Wing. NASA TN D-894, 1961. (U)
9. Edwards, G. G., and Savage, H. F.: The Subsonic Aerodynamic Characteristics of Some Blunt Delta Configurations with 75° Sweepback. NASA TM X-581, 1961. (C) Title Unclassified
10. McDevitt, J. B., and Rakich, J. V.: The Aerodynamic Characteristics of Several Thick Delta Wings at Mach Numbers to 6 and Angles of Attack to 50°. NASA TM X-162, 1960. (C) Title Unclassified

TABLE 5.5.2.2-A

SUBSONIC ROLLING MOMENT WITH RESPECT TO SIDESLIP — VARIATION WITH ANGLE OF ATTACK

DELTA PLANFORM CONFIGURATIONS

DATA SUMMARY

Ref.	Configuration	A	θ (deg)	$\frac{S_B}{S}$	Leading Edge	α' (deg)	$K'_{I\beta}$ Calc. (per rad)	$K'_{I\beta}$ Test (per rad)	$\Delta K'_{I\beta}$ Calc.-Test (per rad)
4	D50	1.076	15	0.386	Round $R_1 = 2.10$ in. —LE 3	0 5 10 15 20	0 -0.076 -0.148 -0.210 -0.257	0 -0.077 -0.138 -0.183 -0.212	0 0.001 -0.010 -0.027 -0.045

TABLE 5.5.2.2-A (CONTD)

Ref.	Configuration	A	θ (deg)	$\frac{s_{BS}}{S}$	Leading Edge	α' (deg)	$K'_{I\beta}$ Calc. (per rad)	$K'_{I\beta}$ Test (per rad)	$\Delta K'_{I\beta}$ Calc.-Test (per rad)
6	D-2	1.076	15	0.349	Sharp $\delta_{e1} = 58^\circ$	0	0	0	0
						5	-0.079	-0.070	-0.009
						10	-0.162	-0.148	-0.014
						15	-0.185	-0.210	0.025
						20	-0.118	-0.274	0.156
	D-6	1.076	15	0.386	Round $R_1 = 1.05$ in. —LE 3	0	0	0	0
						5	-0.076	-0.067	-0.009
						10	-0.147	-0.138	-0.009
						15	-0.210	-0.195	-0.015
						20	-0.257	-0.250	-0.007
7	d	1.868	26	0.236	Round $R_1 = .525$ in. —LE 3	0	0	0	0
						5	-0.071	-0.078	0.007
						10	-0.132	-0.137	0.005
						15	-0.171	-0.155	-0.016
						20	-0.172	-0.143	-0.029
8	Hypersonic-boost-glide without tip cones and ventrals	0.783	10.5	0.518	Round $R_1 = .50$ in. —LE 3	0	0	0	0
						5	-0.086	-0.090	0.004
						10	-0.160	-0.172	0.012
						15	-0.208	-0.246	0.038
						20	-0.173	-0.215	0.042
8	Hypersonic-boost-glide without tip cones and ventrals	0.74	12	0.29	Sharp $\delta_{e1} = 10.1^\circ$	0	0	0	0
						5	-0.093	-0.091	-0.002
						10	-0.200	-0.174	-0.026
						15	-0.297	-0.267	-0.030
						20	-0.361	-0.392	0.041

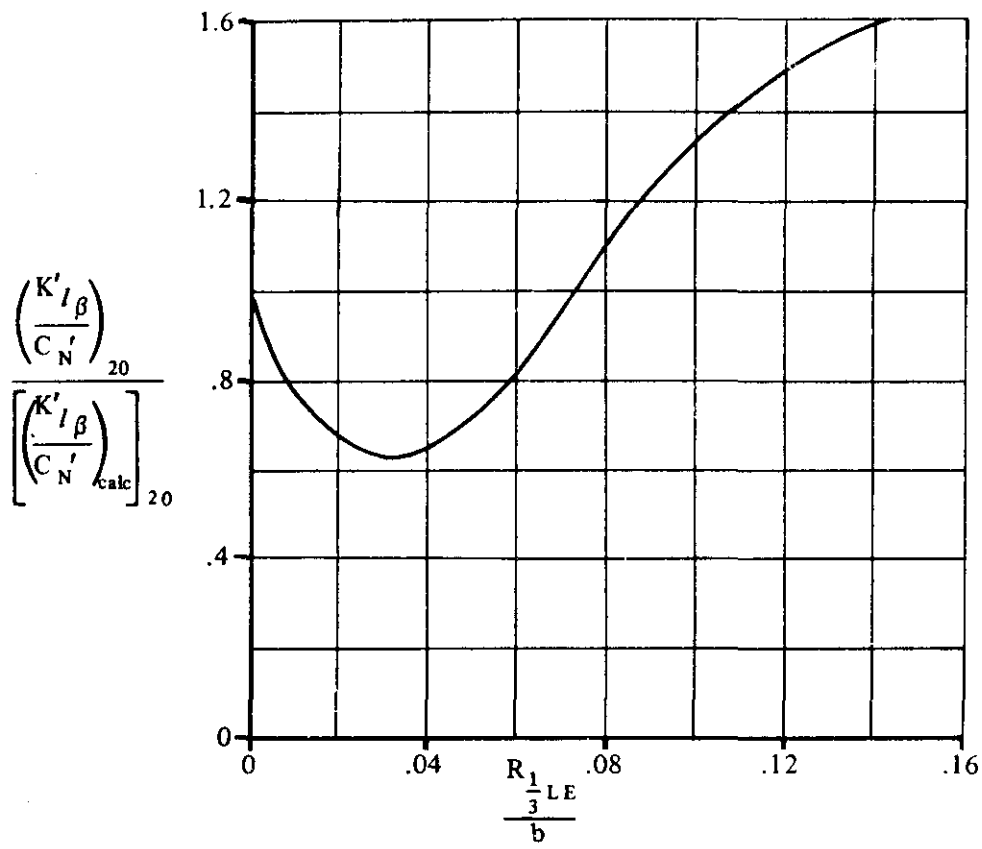


FIGURE 5.5.2.2-12a ROLLING-MOMENT-DERIVATIVE CORRELATION FACTOR AT $\alpha' = 20^\circ$ – DELTA CONFIGURATIONS WITH ROUND LEADING EDGES

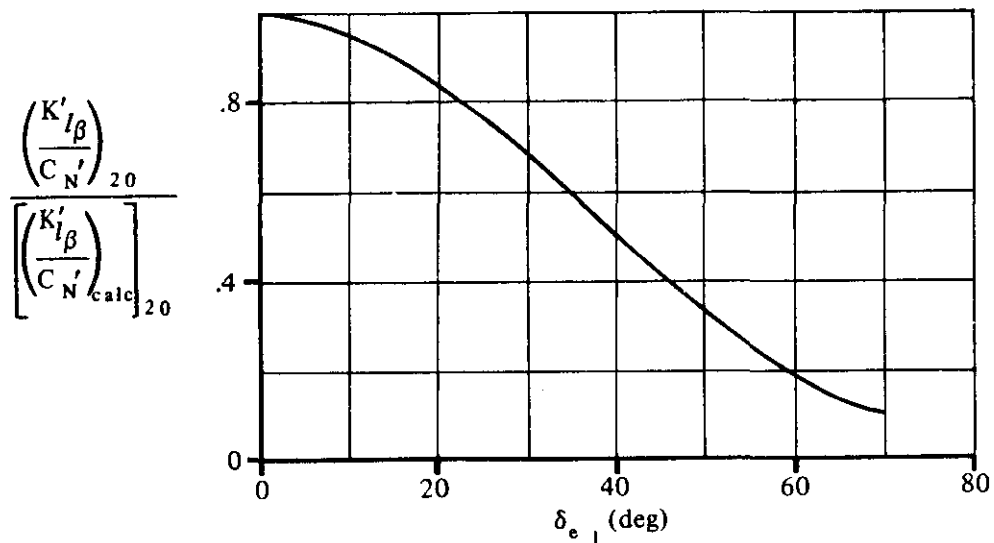


FIGURE 5.5.2.2-12b ROLLING-MOMENT-DERIVATION CORRELATION FACTOR AT $\alpha' = 20^\circ$ – DELTA CONFIGURATIONS WITH SHARP LEADING EDGES

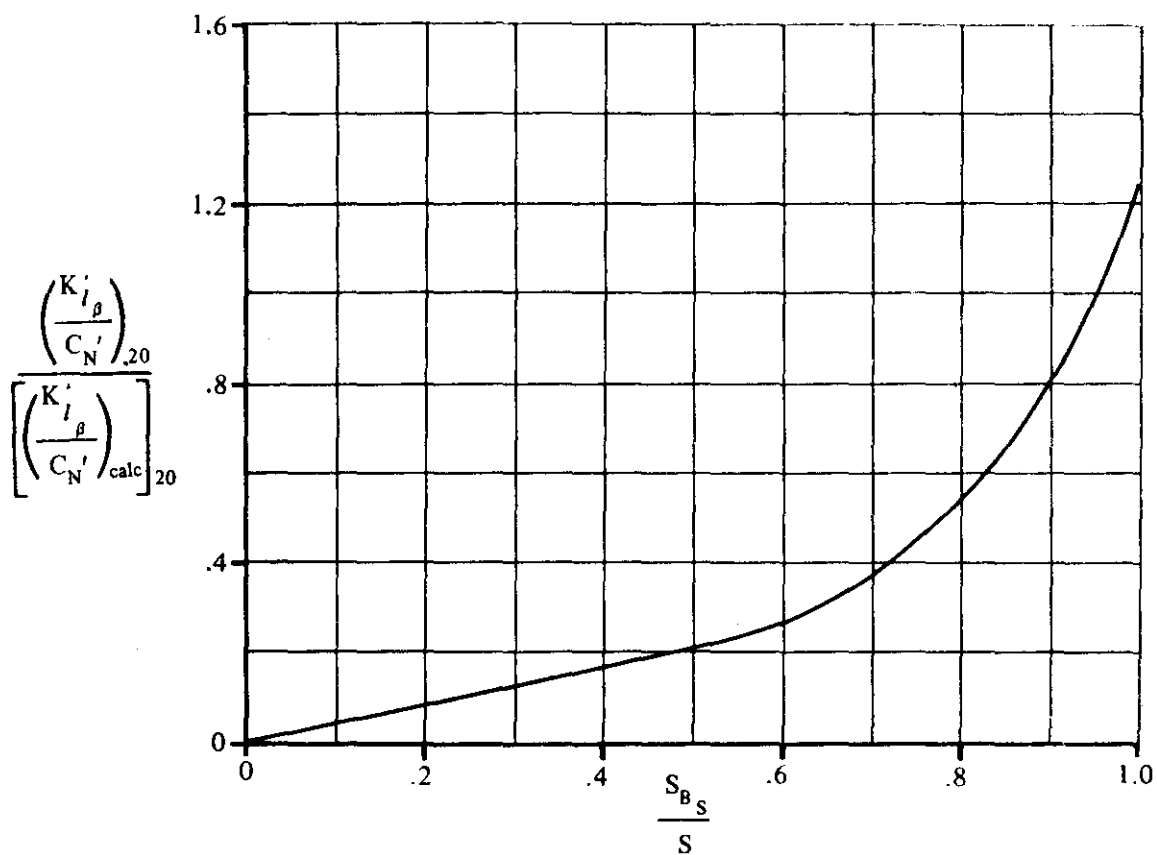


FIGURE 5.5.2.2-13 EFFECTS OF CONFIGURATION THICKNESS ON ROLLING MOMENT DUE TO SLIDESLIP AT $\alpha' = 20^\circ$ - DELTA CONFIGURATIONS

5.5.3 WING, WING-BODY SIDESLIP DERIVATIVE $K'_{n\beta}$

5.5.3.1 WING, WING-BODY SIDESLIP DERIVATIVE $K'_{n\beta}$ AT ZERO NORMAL FORCE

A. SUBSONIC

This section presents a method, taken from reference 1, for estimating $K'_{n\beta N_0}$, the yawing-moment coefficient with respect to sideslip at zero normal force, for delta and modified-delta configurations at subsonic speeds.

The yawing moment due to sideslip is estimated by determining the side force due to sideslip and determining its effective point of application. The side force due to sideslip at zero normal force is estimated by using the method of Section 5.5.1.1.

The nature of the side force, and consequently the location of the center of pressure, is basically different for thin and for thick wings. As noted in Section 5.5.1.1, the side force at zero normal force is assumed to be composed of two parts, side force due to skin friction and side force due to the pressure acting on the configuration. For thin wings the side force is produced primarily by skin friction, and the side-force center of pressure can be related to the wing planform. As the wing thickness is increased, the side force is produced primarily by the difference in pressure distribution between the right and left sides. While the wing planform area would be expected to influence this pressure distribution, the side-area distribution has a major effect. In accordance with these considerations, the skin-friction drag component is assumed to act at the centroid of the planform area and the pressure-drag component at the center of pressure of the side area of the configuration.

An empirical correlation was used to determine the position of the resultant of the side-force components. It was assumed that the center-of-pressure position of the pressure component depends primarily on the shape of the side area and that the influence of other geometric parameters can be neglected. Test data indicated that nose shape has an important influence on this center-of-pressure location, and the final correlation is presented as a function of the ratio of the side area forward of the 20-percent root-chord point (see figure 5.5.3.1-6) to the total side area.

The zero-normal-force sideslip derivative $K'_{n\beta N_0}$ for very thin wings is taken to be equal to the incompressible skin-friction coefficient of the wing, which is taken as $C_f = 0.006$, so that $K'_{n\beta N_0 \text{thin wing}} = -0.006$ per radian, based on planform area. This value is maintained constant for

thicker wings, since the side force due to pressure is much greater than that produced by friction and a more accurate value of it is not required.

DATCOM METHOD

The zero-normal-force sideslip derivative $K'_{n\beta N_0}$ of a delta or modified-delta configuration, based on the product of planform area and span S_b , and taken about an axis at the nose of the configuration, is determined from the procedure outlined in the following steps:

Step 1. From the configuration geometry determine the following:

S_{B_S} the projected side area of the configuration

$(S_{B_S})_{.2c_r}$ the projected side area of the configuration forward of 0.2 c_r

$x_{\text{centroid},w}$ the distance from the nose of the configuration to the centroid location of the wing planform, positive aft of the nose

$x_{\text{centroid},S_{B_S}}$ the distance from the nose of the configuration to the centroid location of the projected side area, positive aft of the nose

Step 2. Determine $K'_{n_{\beta N_0}}$ by

$$K'_{n_{\beta N_0}} = (K_{Y_{\beta N_0}} + 0.006) \frac{(x_{c.p.})_p}{x_{\text{centroid},S_{B_S}}} - 0.006 \frac{x_{\text{centroid},w}}{b} \quad (\text{per radian}) \quad 5.5.3.1-a$$

where

$K_{Y_{\beta N_0}}$ is the side-force coefficient due to sideslip at zero normal force, obtained from Section 5.5.1.1.

$\frac{(x_{c.p.})_p}{x_{\text{centroid},S_{B_S}}}$ is the ratio of the center-of-pressure location of the pressure component of side force to the centroid location of the projected side area.

This parameter is obtained from figure 5.5.3.1-6 as a function of $(S_{B_S})_{.2c_r}/S_{B_S}$.

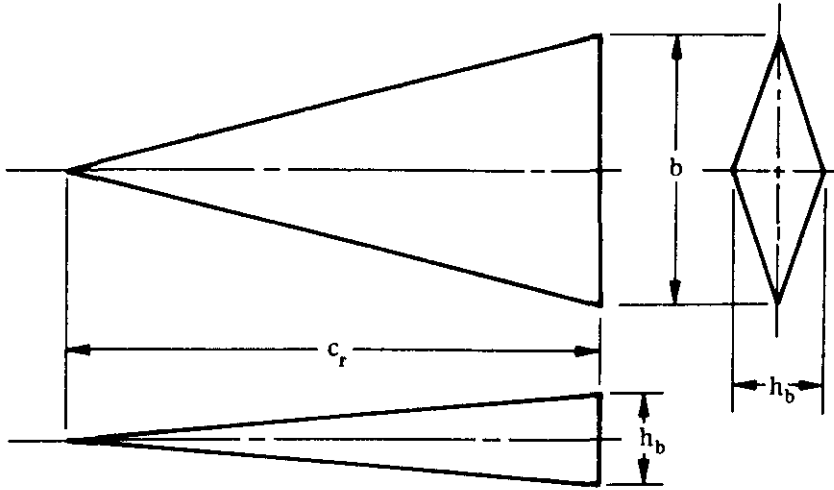
b is the wing span.

A comparison of $K'_{n_{\beta N_0}}$ calculated by using this method with test results is presented as table 5.5.3.1-A. The sideslip derivatives $K_{Y_{\beta N_0}}$, used to obtain the calculated values of $K'_{n_{\beta N_0}}$ in table 5.5.3.1-A, were calculated by using the method of Section 5.5.1.1.

It should be noted that a considerable amount of scatter was involved in the data correlation used to define the center-of-pressure location of the pressure component of side force. For configurations with values of $(S_{B_S})_{.2c_r}/S_{B_S}$ greater than approximately 0.15, the location of $(x_{c.p.})_p$ is not well established.

Sample Problem

Given: A delta-series configuration of reference 6 designated D-2.



$$S = 142.3 \text{ sq in.}$$

$$S_{B_S} = 49.68 \text{ sq in.}$$

$$(S_{B_S})_{.2c_r} = 1.99 \text{ sq in.}$$

$$c_r = 23.0 \text{ in.}$$

$$b = 12.374 \text{ in.}$$

$$h_b = 4.32 \text{ in.}$$

Compute:

$$S_{B_S}/S = 49.68/142.3 = 0.349$$

$$K_{Y_{\beta N_0}} = -0.110 \text{ per rad (figure 5.5.1.1-6)}$$

$$x_{\text{centroid}_W} = 2c_r/3 = 2(23.0)/3 = 15.33 \text{ in.}$$

$$x_{\text{centroid}_{S_{B_S}}} = 2c_r/3 = 15.33 \text{ in.}$$

$$(S_{B_S})_{.2c_r}/S_{B_S} = 1.99/49.68 = 0.040$$

$$\frac{(x_{\text{c.p.}})_p}{x_{\text{centroid}_{S_{B_S}}}} = 1.04 \text{ (figure 5.5.3.1-6)}$$

Solution:

$$K'_{\beta N_0} = (K_{Y_{\beta N_0}} + 0.006) \frac{(x_{\text{c.p.}})_p}{x_{\text{centroid}_{S_{B_S}}}} - 0.006 \frac{x_{\text{centroid}_W}}{b} \quad (\text{equation 5.5.3.1-a})$$

$$\begin{aligned}
 &= (-0.110 + 0.006) (1.04) \frac{15.33}{12.374} - 0.006 \frac{15.33}{12.374} \\
 &= -0.1414 \text{ per rad (based on Sb)}
 \end{aligned}$$

This compares with a test value of -0.1485 per radian from reference 6.

REFERENCES

1. Seeger, D. B., and Ross, R.: Investigation of the Low-Speed Stability and Control Characteristics of Advanced Flight Vehicles. ASD-TDR-63-671, 1963. (C) Title Unclassified
2. Seeger, D. B., and Meyer, J. E.: An Investigation of the Subsonic Aerodynamic Characteristics and the Landing Flare Maneuver for Hypersonic Re-entry Configurations. ASD-TDR-62-271, 1962. (C) Title Unclassified
3. Mantz, K., and Seeger, D. B.: Tests to Determine the Subsonic Pressures, Forces and Moments Acting on a Hypersonic Re-entry Configuration. ASD-TDR-62-270, 1962. (C) Title Unclassified
4. Mantz, K., Seeger, D. B., and Ross, R.: Tests to Determine Subsonic Pressures, Forces and Moments Acting on a Hypersonic Re-entry Configuration. ASD-TDR-62-270, Supplement 1, 1963. (U)
5. Sipe, O. E., and Seeger, D. B.: Tests to Determine Subsonic Aerodynamic Characteristics of Hypersonic Re-entry Configurations. ASD-TR-61-485, 1961. (C) Title Unclassified
6. Mantz, K., Seeger, D. B., and Ross, R.: Tests to Determine Subsonic Aerodynamic Characteristics of Hypersonic Re-entry Configurations. ASD-TR-61-485, Supplement 1, 1963. (U)
7. Graham, D., and Koenig, D. G.: Tests in the Ames 40- by 80-Foot Wind Tunnel of an Airplane Configuration with an Aspect Ratio 2 Triangular Wing and an All-Movable Horizontal Tail — Lateral Characteristics. NACA RM A51L03, 1952. (U)
8. Jaquet, B. M., and Brewer, J. D.: Low-Speed Static-Stability and Rolling Characteristics of Low-Aspect-Ratio Wings of Triangular and Modified Triangular Plan Forms. NACA RM L8L29, 1949. (U)
9. McKinney, M. O., Jr., and Drake, H. M.: Flight Characteristics at Low Speed of Delta-Wing Models. NACA RM L7K07, 1948. (U)
10. Goodman, A., and Thomas, D.: Effects of Wing Position and Fuselage Size on the Low-Speed Static and Rolling Stability Characteristics of a Delta-Wing Model. NACA TR 1224, 1955. (U)
11. Lange/Wacke: Test Report on Three- and Six-Component Measurements on a Series of Tapered Wings of Small Aspect Ratio. (Partial Report: Triangular Wing.) NACA TM 1176, 1948. (U)
12. Whittle, E. F., Jr., and Lovell, J. C.: Full-Scale Investigation of an Equilateral Triangular Wing Having 10-Percent Thick Biconvex Airfoil Sections. NACA RM L8G05, 1948. (U)
13. Edwards, G. G., and Savage, H. F.: The Subsonic Aerodynamic Characteristics of Some Blunt Delta Configurations with 75° Sweepback. NASA TM X-581, 1961. (U)
14. McDevitt, J. B., and Rakich, J. V.: The Aerodynamic Characteristics of Several Thick Delta Wings at Mach Numbers to 6 and Angles of Attack to 50° . NASA TM X-162, 1960. (C) Title Unclassified
15. Keating, R. F. A.: Low-Speed Wind-Tunnel Tests on Sharp-Edged Gothic Wings of Aspect-Ratio 3/4. ARC CP 576, 1961. (U)
16. Olsted, W. B., Mugler, J. P., Jr., and Cahn, M. S.: Static Longitudinal and Lateral Stability Characteristics of a Right Triangular Pyramidal Lifting Re-entry Configuration at Transonic Speeds. NASA TN D-655, 1961. (U)
17. Ware, G. M.: Low-Subsonic-Speed Static Stability of Right-Triangular-Pyramid and Half-Cone Lifting Re-entry Configurations. NASA TN D-846, 1961. (U)
18. Paulson, J. W.: Low-Speed Static Stability and Control Characteristics of a Right Triangular Pyramid Re-entry Configuration. NASA Memo 4-11-59L, 1959. (U)

19. Anderson, A. E.: An Investigation at Low-Speed of a Large-Scale Triangular Wing of Aspect Ratio Two. — I. Characteristics of a Wing Having a Double-Wedge Airfoil Section with Maximum Thickness at 20-Percent Chord. NACA RM A7F06, 1947. (U)

TABLE 5.5.3.1-A
SUBSONIC YAWING MOMENT DUE TO SIDESLIP AT
ZERO NORMAL FORCE
DELTA PLANFORM CONFIGURATIONS
DATA SUMMARY

Ref.	Configuration	A	b (in.)	$\frac{S_{BS}}{S}$	$\frac{(S_{BS})}{S} \cdot 2c_r$	$x_{\text{centroid}} S_{BS}$ (in.)	$x_{\text{centroid}} w$ (in.)	$K'_{n\beta N_0}$ Calc. (per rad)	$K'_{n\beta N_0}$ Test (per rad)	$\Delta K'_{n\beta N_0}$ Calc.-Test (per rad)
4	D-50	1.076	26.26	0.386	0.102	27.86	29.78	-0.164	-0.2407	0.0767
6	D-1	1.075	13.13	0.386	0.102	13.83	14.89	-0.164	-0.109	-0.065
	D-2	1.076	12.37	0.349	0.040	15.33	15.33	-0.141	-0.1485	0.0075
	D-5	1.076	13.13	0.386	0.102	13.83	14.89	-0.164	-0.223	0.069
	D-6	1.868	22.12	0.236	0.102	13.83	15.11	-0.020	0.0138	-0.0338
	WB-1	1.084	12.44	0.282	0.129	11.50	12.55	-0.041	-0.0706	0.0295
	WB-3	1.074	11.10	0.282	0.089	12.31	12.57	-0.069	-0.152	0.093
	WB-4	1.147	14.17	0.293	0.189	10.00	12.11	-0.005	-0.073	0.068
9	1	3.00	34.00	0.046	0.215	10.46	15.09	-0.003	0	-0.003
	4	2.00	27.20	0.060	0.215	10.46	14.72	-0.003	0	-0.003
	6	1.00	17.00	0.060	0.215	10.46	13.81	-0.006	0	-0.006
	8	0.50	27.70	0.070	0.212	13.00	18.47	-0.004	0	-0.004
10	Wing Alone	2.31	36.50	0.046	0.167	14.40	21.07	-0.0033	-0.0114	0.0081
11	1	3.00	59.06	0.108	0.207	16.54	26.24	-0.003	-0.012	0.009
	2	2.00	48.23	0.162	0.207	20.28	32.15	-0.004	-0.0287	0.0247
	3	1.33	39.37	0.244	0.207	24.82	39.37	-0.006	-0.0372	0.0312
	4	1.00	34.09	0.325	0.207	28.65	45.48	-0.008	-0.0344	0.0264
17	a	0.783	21.10	0.536	0.051	35.38	35.38	-0.718	-0.743	0.026
	b(basic)	0.783	21.10	0.491	0.051	35.38	35.38	-0.566	-0.585	0.019
	b(R=1.5 in.)	0.808	21.10	0.500	0.072	31.55	31.55	-0.524	-0.572	0.048
	d	0.783	21.10	0.581	0.051	35.38	35.38	-0.653	-0.709	0.056
18	1	0.780	21.10	0.528	0.051	35.38	35.38	-0.688	-0.615	-0.073
19	Wing Alone	2.00	25(ft)	0.060	0.128	10(ft)	16.67(ft)	-0.003	0	-0.003

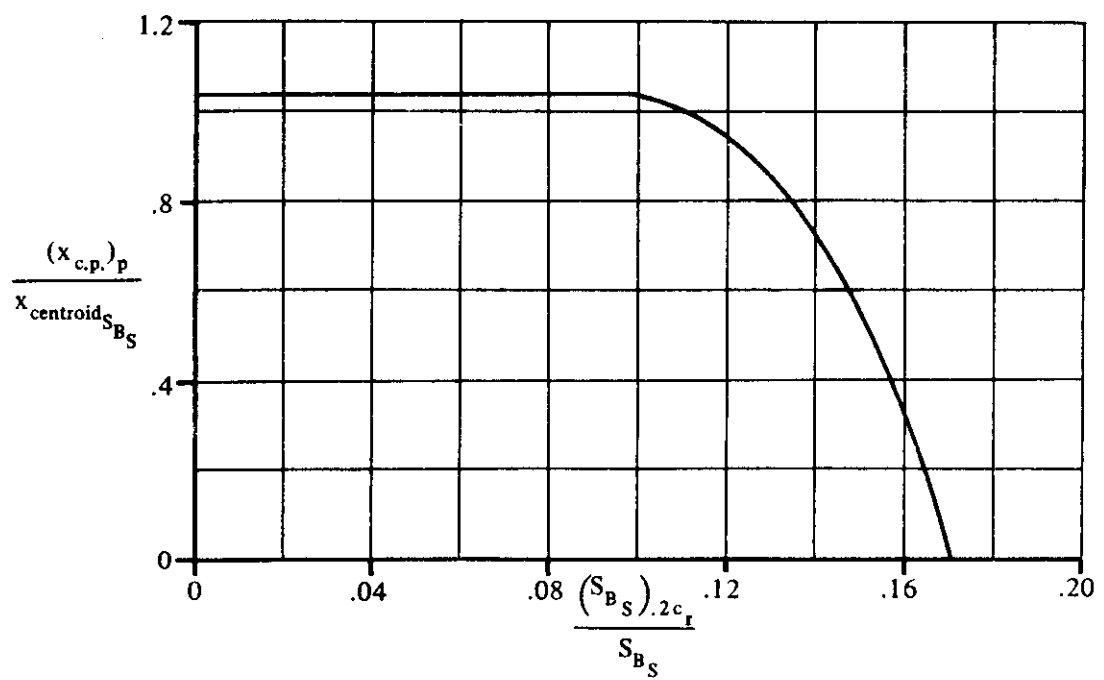
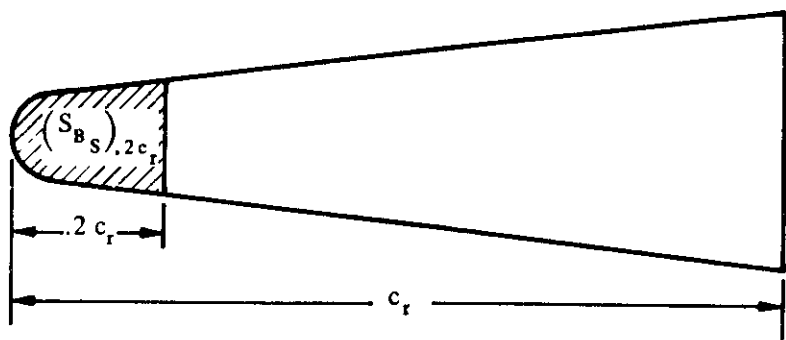


FIGURE 5.5.3.1-6 SIDE-FORCE CENTER OF PRESSURE
DELTA AND MODIFIED DELTA CONFIGURATIONS

5.5.3.2 WING, WING-BODY SIDESLIP-DERIVATIVE $K'_{n\beta}$ VARIATION WITH ANGLE OF ATTACK

A. SUBSONIC

This section presents a method, taken from reference 1, for estimating the sideslip-derivative $K'_{n\beta}$ variation with angle of attack for delta and modified-delta configurations at subsonic speeds.

Although the pressure distribution over a configuration is altered as a result of the lifting process, test data show that side-force center-of-pressure location is not affected appreciably by normal force. Therefore, the change in directional stability is attributed to the change in side force due to sideslip as angle of attack is increased.

Because the location of the side-force center of pressure is considered to be independent of angle of attack, the relationships established in Section 5.5.3.1 for determining the location of the side-force center of pressure at zero normal force are also applicable to this section. Furthermore, the nature of the breakdown of the side force at zero normal force may also be applied at any angle of attack, and the expression for determining the directional stability at angle of attack is the same as that presented in Section 5.5.3.1 for determining $K'_{n\beta}$ at zero normal force.

The Datcom method is considered valid for sideslip angles between $\pm 5^\circ$ and angles of attack from 0 to 20° .

DATCOM METHOD

The variation of the sideslip derivative $K'_{n\beta}$ with angle of attack, based on the product of planform area and span S_B and referred to a moment center at the nose of the configuration, for a delta or modified-delta configuration at subsonic speeds is given by

$$K'_{n\beta} = (K_{Y\beta} + 0.006) \frac{(x_{c.p.})_p}{x_{centroid}_{S_B}} \frac{x_{centroid}_{S_B}}{b} - 0.006 \frac{x_{centroid}_w}{b} \quad (\text{per radian}) \quad 5.5.3.2-a$$

where $K_{Y\beta}$ is the side force due to sideslip at angle of attack, obtained from Section 5.5.1.2, and all the remaining terms are described in Section 5.5.3.1.

A comparison of the variation of $K'_{n\beta}$ with normal-force variation calculated by using this method with test data is presented as table 5.5.3.2-A.

The comments pertaining to nonlinearities in the variation of side force with sideslip in Section 5.5.1.2 also apply to the side-force center-of-pressure location.

Sample Problem

Given: A delta-series model of reference 6 designated D-2. This is the configuration of the sample problem of Section 5.5.3.1.

$$S = 142.3 \text{ sq in.} \quad S_{B_S} = 49.68 \text{ sq in.} \quad (S_{B_S})_{.2c_r} = 1.99 \text{ sq in.}$$

$$c_r = 23.0 \text{ in.} \quad b = 12.374 \text{ in.} \quad \delta_{e\perp} = 58^\circ$$

The following results from the sample problem of Section 5.5.3.1:

$$K_{Y_{\beta N_0}} = -0.110 \text{ per rad} \quad \frac{(x_{c.p.})_p}{x_{\text{centroid}} S_{B_S}} = 1.04$$

$$x_{\text{centroid}} S_{B_S} = x_{\text{centroid}} W = 15.33 \text{ in.} \quad S_{B_S}/S = 0.349$$

Compute:

$$\left[\frac{\Delta K_{Y_\beta}}{(C_N')^2} \right]_{20} = 0.335 \text{ per rad} \quad (\text{figure 5.5.1.2-9})$$

$$K_{Y_\beta} = K_{Y_{\beta N_0}} + \left[\frac{\Delta K_{Y_\beta}}{(C_N')^2} \right]_{20} (C_N')^2 \quad (\text{equation 5.5.1.2-a})$$

$$= -0.110 + (0.335) (C_N')^2$$

①	②	③	④
C_N'	$(C_N')^2$ ① ²	$(0.335)(C_N')^2$ 0.335 ②	K_{Y_β} (based on S) -0.110 + ③
0	0	0	-0.110
0.2	0.04	0.0134	-0.097
0.4	0.16	0.0536	-0.056
0.6	0.36	0.1206	0.011

Solution:

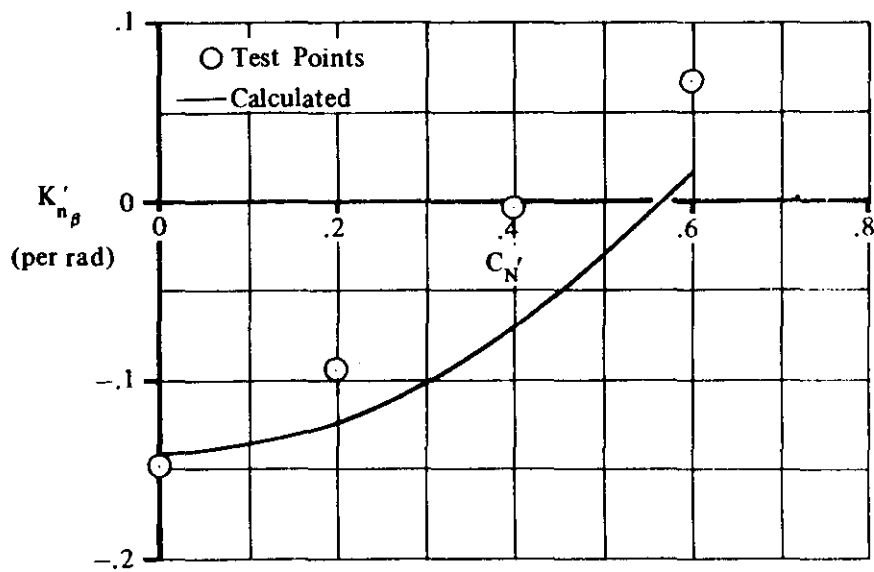
$$K'_{n_\beta} = (K_{Y_\beta} + 0.006) \frac{(x_{c.p.})_p}{x_{\text{centroid}} S_{B_S}} - 0.006 \frac{x_{\text{centroid}} W}{b} \quad (\text{equation 5.5.3.2-a})$$

$$= (K_{Y_\beta} + 0.006)(1.04) \frac{15.33}{12.374} - 0.006 \frac{15.33}{12.374}$$

$$= 1.288 K_{Y_\beta} + 0.0003$$

C_N'	K_{Y_β} (based on Si) (per rad)	$1.288 K_{Y_\beta}$ 1.288 (2)	K'_{n_β} (based on Sb) (per rad) (3) +0.0003
0	-0.110	-0.1417	-0.1414
0.2	-0.097	-0.1249	-0.1246
0.4	-0.056	-0.0721	-0.0718
0.6	0.011	0.0142	0.0145

The calculated results are compared with test values in sketch (a) and in table 5.5.3.2-A.



SKETCH (a)

REFERENCES

1. Seeger, D. B., and Ross, R.: Investigation of the Low-Speed Stability and Control Characteristics of Advanced Flight Vehicles. ASD-TDR-63-671, 1963. (C) Title Unclassified
2. Seeger, D. B., and Meyer, J. E.: An Investigation of the Subsonic Aerodynamic Characteristics and the Landing Flare Maneuver for Hypersonic Re-entry Configurations. ASD-TDR-62-271, 1962. (C) Title Unclassified
3. Mantz, K., and Seeger, D. B.: Tests to Determine the Subsonic Pressures, Forces and Moments Acting on a Hypersonic Re-entry Configuration. ASD-TDR-62-270, 1962. (C) Title Unclassified
4. Mantz, K., Seeger, D. B., and Ross, R.: Tests to Determine Subsonic Pressures, Forces and Moments Acting on a Hypersonic Re-entry Configuration. ASD-TDR-62-270, Supplement 1, 1963. (U)
5. Sipe, O. E., and Seeger, D. B.: Tests to Determine Subsonic Aerodynamic Characteristics of Hypersonic Re-entry Configurations. ASD-TR-61-485, 1961. (C) Title Unclassified
6. Mantz, K., Seeger, D. B., and Ross, R.: Tests to Determine Subsonic Aerodynamic Characteristics of Hypersonic Re-entry Configurations. ASD-TR-61-485, Supplement 1, 1963. (U)
7. Graham, D., and Koenig, D. G.: Tests in the Ames 40- by 80-Foot Wind Tunnel of an Airplane Configuration with an Aspect Ratio 2 Triangular Wing and an All-Movable Horizontal Tail — Lateral Characteristics. NACA RM A51L03, 1952. (U)
8. Jaquet, B. M., and Brewer, J. D.: Low-Speed Static-Stability and Rolling Characteristics of Low-Aspect-Ratio Wings of Triangular and Modified Triangular Plan Forms. NACA RM LBL29, 1949. (U)
9. McKinney, M. O., Jr., and Drake, H. M.: Flight Characteristics at Low Speed of Delta-Wing Models. NACA RM L7K07, 1948. (U)
10. Keeting, R. F. A.: Low-Speed Wind-Tunnel Tests on Sharp-Edged Gothic Wings of Aspect-Ratio 3/4. ARC CP 576, 1961. (U)
11. Goodman, A., and Thomas, D.: Effects of Wing Position and Fuselage Size on the Low-Speed Static and Rolling Stability Characteristics of a Delta-Wing Model. NACA TR 1224, 1955. (U)
12. Whittle, E. F., Jr., and Lovell, J. C.: Full-Scale Investigation of an Equilateral Triangular Wing Having 10-Percent Thick Biconvex Airfoil Sections. NACA RM L8G05, 1948. (U)
13. Olsted, W. B., Mugler, J. P., Jr., and Cahn, M. S.: Static Longitudinal and Lateral Stability Characteristics of a Right Triangular Pyramidal Lifting Re-entry Configuration at Transonic Speeds. NASA TN D-655, 1961. (U)
14. Ware, G. M.: Low-Subsonic-Speed Static Stability of Right-Triangular-Pyramid and Half-Cone Lifting Re-entry Configurations. NASA TN D-646, 1961. (U)
15. Edwards, G. G., and Savage, H. F.: The Subsonic Aerodynamic Characteristics of Some Blunt Delta Configurations with 75° Sweepback. NASA TM X-581, 1961. (U)
16. McDevitt, J. B., and Rakich, J. V.: The Aerodynamic Characteristics of Several Thick Delta Wings at Mach Numbers to 6 and Angles of Attack to 50°. NASA TM X-162, 1960. (C) Title Unclassified

TABLE 5.5.3.2-A
SUBSONIC YAWING MOMENT WITH RESPECT TO SIDESLIP
VARIATION WITH ANGLE OF ATTACK
DELTA PLANFORM CONFIGURATIONS
DATA SUMMARY*

Ref.	Configuration	A	$C_{N'}$	$K'_{n\beta}$ Calc. (per rad)	$K'_{n\beta}$ Test (per rad)	$\Delta K'_{n\beta}$ Calc.-Test (per rad)
4	D-50	1.076	0	-0.164	-0.2407	0.0767
			0.2	-0.164	-0.2196	0.0556
			0.4	-0.164	-0.2035	0.0395
			0.6	-0.164	—	—
6	D-1	1.075	0	-0.164	-0.109	-0.055
			0.2	-0.164	-0.1024	-0.0616
			0.4	-0.164	-0.1257	-0.0384
			0.6	-0.164	-0.1786	0.0146
	D-2	1.076	0	-0.1414	-0.1485	0.0071
			0.2	-0.1246	-0.0947	-0.0299
			0.4	-0.0718	-0.0040	-0.0678
			0.6	0.0145	0.0662	-0.0517
	D-5	1.076	0	-0.164	-0.233	0.069
			0.2	-0.135	-0.214	0.079
			0.4	-0.0489	-0.1963	0.1474
			0.6	0.084	—	—
	D-6	1.868	0	-0.0200	0.0138	-0.0338
			0.2	-0.0224	0.031	-0.0534
			0.4	-0.0309	0.0368	-0.0677
			0.6	-0.0452	0.0279	-0.0731
14	a	0.783	0	-0.718	-0.743	0.025
			0.2	-0.744	-0.937	0.193
			0.4	-0.941	-1.006	0.065
			0.6	-1.220	-1.018	-0.202

TABLE 5.5.3.2-A (CONTD)

Ref.	Configuration	A	C_N'	$K'_{n\beta}$ Calc. (per rad)	$K'_{n\beta}$ Test (per rad)	$\Delta K'_{n\beta}$ Calc.-Test (per rad)
14	b(basic)	0.783	0	-0.586	-0.585	0.019
			0.2	-0.615	-0.760	0.145
			0.4	-0.762	-0.875	0.113
			0.6	-1.006	-0.950	-0.056
			0	-0.524	-0.572	0.048
	b($R=1.5$ in.)	0.808	0.2	-0.568	-0.765	0.197
			0.4	-0.700	-0.912	0.212
			0.6	-0.921	-0.962	0.041

5.6 WING-BODY-TAIL COMBINATIONS IN SIDESLIP

5.6.1 WING-BODY-TAIL SIDESLIP DERIVATIVE $C_{Y\beta}$

5.6.1.1 WING-BODY-TAIL SIDESLIP DERIVATIVE $C_{Y\beta}$ IN THE LINEAR ANGLE-OF-ATTACK RANGE

The information contained in this Section is for estimating the side-force-curve slope $C_{Y\beta}$ of wing-body-tail combinations at low angles of attack. In general, it consists of a synthesis of material presented in other Sections. The method of Section 5.3.1.1 based on the apparent-mass concept for the determination of increments in $C_{Y\beta}$ due to the addition of one panel to an empennage is extended herein to determine the total empennage sideslip derivative $C_{Y\beta}$ at low angles of attack resulting from the addition of all the panels present in the empennage. The methods presented include the mutual interference effects of other vehicle components.

The main contributions to the derivative $C_{Y\beta}$ will come from the fuselage and the vertical stabilizers. The wing contribution is a function of α^2 and can usually be neglected at low angle of attack. A discussion of the various aerodynamic aspects associated with the build-up of vehicle components in relation to side force are discussed in Sections 5.2.1.1 and 5.3.1.1 and are not repeated here.

The methods presented herein are based on the procedure of totaling the coefficient of the wing-body configuration and the incremental coefficient of the total empennage resulting from the addition of all panels present in the empennage.

A. SUBSONIC

Three methods of estimating the subsonic derivative $C_{Y\beta}$ of a complete configuration are presented, differing in their treatment of the incremental coefficient of the total empennage. Methods 1 and 2 treat the mutual interference effects of the wing-body wake and sidewash independently of the body and horizontal tail end-plate effects and lump the total empennage increment into a single parameter. On the other hand, Method 3 utilizes a build-up procedure to determine the total empennage increment wherein the mutual interference effects are lumped into a single effectiveness parameter for each panel in the empennage.

DATCOM METHODS

Method 1

For configurations with a single vertical stabilizer and with horizontal-stabilizer height ranging from positions on the body to the top of the vertical stabilizer or configurations with a single vertical stabilizer and with no horizontal stabilizer the side force due to sideslip is given by

$$C_{Y\beta} = (C_{Y\beta})_{WB} + (\Delta C_{Y\beta})_{VWBH} \quad 5.6.1.1-a$$

where

$(C_{Y\beta})_{WB}$ is obtained from Section 5.2.1.1

$(\Delta C_{Y\beta})_{VWBH}$ is the total empennage increment in $C_{Y\beta}$ obtained from Method 1, paragraph A, Section 5.3.1.1

Method 2

For configurations with twin vertical panels mounted on the tips of a horizontal tail or wing the side force due to sideslip is given by equation 5.6.1.1-a

$$C_{Y\beta} = (C_{Y\beta})_{WB} + (\Delta C_{Y\beta})_{VWBH}$$

where

$(\Delta C_{Y\beta})_{VWBH}$ is the total empennage increment in $C_{Y\beta}$ obtained from Method 2, paragraph A, Section 5.3.1.1

Method 3

The estimation of the total empennage side-force derivative by this method is based on the apparent-mass concept for the determination of increments in $C_{Y\beta}$ due to the addition of one panel to an empennage, presented as Method 3 of paragraph A of Section 5.3.1.1. That method is extended herein to determine the total sideslip derivative $C_{Y\beta}$ resulting from the addition of all panels present in the empennage. The method is limited to configurations in which the horizontal tail is mounted on the body or configurations with no horizontal tail.

The total empennage contribution to $C_{Y\beta}$ is obtained by adding the increments gained by successive additions of the panels in the empennage to the wing-body configuration. The order of build-up should proceed as follows:

1. Determine the increment in $C_{Y\beta}$ due to adding the horizontal stabilizer to the wing-body configuration, $(\Delta C_{Y\beta})_{HWB}$
2. Determine the increment in $C_{Y\beta}$ due to adding the upper vertical stabilizing surface to the combination of wing, body, and horizontal stabilizer, $(\Delta C_{Y\beta})_{VWBH}$
3. Determine the increment in $C_{Y\beta}$ due to adding the lower vertical stabilizing surface to the combination of wing, body, horizontal stabilizer, and upper vertical stabilizer, $(\Delta C_{Y\beta})_{UWBHV}$

The side force due to sideslip for the complete configuration is given by

$$C_{Y\beta} = (C_{Y\beta})_{WB} + \sum_p (\Delta C_{Y\beta})_p \quad 5.6.1.1-b$$

where the subscript p refers to the panels present in the empennage

$(C_{Y\beta})_{WB}$ is obtained from Section 5.2.1.1

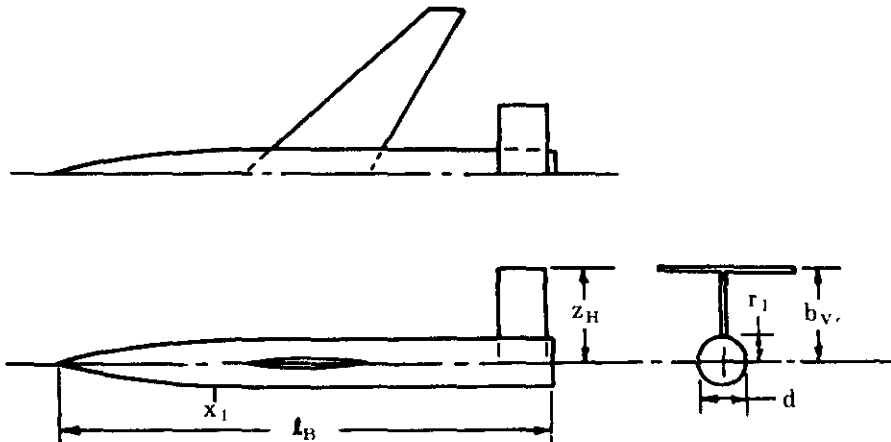
$(\Delta C_{Y\beta})_p$ is the increment in $C_{Y\beta}$ gained by successive additions of the panels in the empennage obtained from Method 3, paragraph A, Section 5.3.1.1

For a wingless configuration, $(\Delta C_{Y\beta})_p$ is based on the vehicle reference area and the contribution of the body to the total derivative can be obtained from Section 4.2.1.1 as $(C_{L\alpha})_B \approx -(C_{L\alpha})_B$, based on the vehicle reference area.

Sample Problems

1. Method 1

Given: A configuration of reference 1 consisting of wing, body, horizontal tail, and vertical tail.



Wing Characteristics

$$A_w = 4.00 \quad S_w = 36.0 \text{ sq in.} \quad \Lambda_{c/4w} = 45^\circ \quad \Gamma = 0 \quad z_w = 0$$

Horizontal Tail Characteristics

$$A_H = 2.78 \quad S_H = 9.0 \text{ sq in.} \quad z_H = -3.30 \text{ in.}$$

Vertical Tail Characteristics

$$A_v = 1.835 \quad S_v = 5.94 \text{ sq in.} \quad A_{c/2v} = 0 \quad b_v = 3.30 \text{ in.} \quad \lambda_v = 1.00$$

NACA 65A006 airfoil

Body Characteristics

$$l_B = 18.25 \text{ in.} \quad x_1 = 5.83 \text{ in.} \quad V_B^{2/3} = 10.4 \text{ sq in.} \quad d = 1.667 \text{ in.}$$

Additional Characteristics

$$M = 0.60 \quad r_1 = 0.8335 \text{ in.} \quad x/c_v = 0.25$$

Compute:

Step 1. Determine the wing-body contribution to $C_{Y\beta}$ using the method of Section 5.2.1.1.

$$K_i = 1.0 \text{ (midwing)}$$

$$f = \frac{l_B}{d} = 10.95$$

$$(k_2 - k_1) = 0.95 \text{ (figure 4.2.1.1-20a)}$$

$$x_1/l_B = 0.319$$

$$x_0/l_B = 0.545 \text{ (figure 4.2.1.1-20b)}$$

$$x_0 = (0.545)(18.25) = 9.95 \text{ in.}$$

$$S_0 = \pi \left(\frac{d}{2} \right)^2 = 2.18 \text{ sq in.}$$

$$\begin{aligned} (C_{Y\beta})_{WB} &= K_i (C_{Y\beta})_B \left(\frac{\text{Body Reference Area}}{S_w} \right) + (\Delta C_{Y\beta}) \Gamma \quad \text{(equation 5.2.1.1-a)} \\ &= K_i \left(\frac{-2(k_2 - k_1) S_0}{V_B^{2/3}} \right) \left(\frac{V_B^{2/3}}{S_w} \right) + (\Delta C_{Y\beta}) \Gamma \\ &= 1.00 \left(\frac{(-2)(0.95)(2.18)}{10.4} \right) \left(\frac{10.4}{36.0} \right) + 0 \\ &= -0.115 \text{ per rad (based on } S_w) \end{aligned}$$

Step 2. Determine the total empennage contribution to $C_{Y\beta}$ using Method 1, Paragraph A, Section 5.3.1.1.

$$(c_{L_a})_v = 6.57 \text{ per rad (Section 4.1.1.2)}$$

$$\kappa = \frac{(c_{L_a})_v}{2\pi} = 1.05 \text{ (ratio of incompressible section lift-curve slope to } 2\pi)$$

$$b_v/2r_1 = 1.98$$

$$k = 0.76 \text{ (figure 5.3.1.1-22d)}$$

$$\frac{(A)_{V(B)}}{A_v} = 1.50 \text{ (figure 5.3.1.1-22a)}$$

$$(A)_{V(B)} = 1.50 (A_v) = 2.75$$

$$S_H/S_v = 1.518$$

$$K_H = 1.06 \text{ (figure 5.3.1.1-22c)}$$

$$z_H/b_V = -1.00$$

$$\frac{(A)_{V(HB)}}{(A)_{V(B)}} = 1.70 \text{ (figure 5.3.1.1-22b)}$$

$$S_V/S_W = 0.165$$

$$z_W/d = 0$$

$$A_{eff} = (A)_{V(B)} \left\{ 1 + K_H \frac{(A)_{V(HB)}}{(A)_{V(B)}} - 1 \right\} \quad (\text{equation 5.3.1.1-a})$$

$$= 2.75 \{ 1 + 1.06 [1.70 - 1] \} = 4.79$$

$$\frac{A_{eff}}{K} [\beta^2 + \tan^2 \Lambda_{c/2_V}]^{1/2} = 3.65$$

$$\frac{(C_{L_a})_V}{A_{eff}} = 1.02 \text{ per rad (figure 4.1.3.2-49)}$$

$$(C_{L_a})_V = 4.88 \text{ per rad}$$

$$\begin{aligned} \left(1 + \frac{\partial \sigma}{\partial \beta}\right) \frac{q_V}{q_\infty} &= 0.724 + 3.06 \frac{S_V/S_W}{1 + \cos \Lambda_{c/4_W}} + 0.4 \frac{z_W}{d} + 0.009 A_W \quad (\text{equation 5.4.1-a}) \\ &= 0.724 + 3.06 \frac{(0.165)}{(1.707)} + 0 + 0.036 \\ &= 1.056 \end{aligned}$$

$$\begin{aligned} (\Delta C_{Y\beta})_{V(WBH)} &= -k (C_{L_a})_V \left(1 + \frac{\partial \sigma}{\partial \beta}\right) \frac{q_V}{q_\infty} \frac{S_V}{S_W} \quad (\text{equation 5.3.1.1-b}) \\ &= -(0.76)(4.88)(1.056)(0.165) \\ &= -0.645 \text{ per rad (based on } S_W) \end{aligned}$$

Solution:

$$\begin{aligned} C_{Y\beta} &= (C_{Y\beta})_{WB} + (\Delta C_{Y\beta})_{V(WBH)} \quad (\text{equation 5.6.1.1-a}) \\ &= -0.115 - 0.645 \\ &= -0.760 \text{ per rad (based on } S_W) \end{aligned}$$

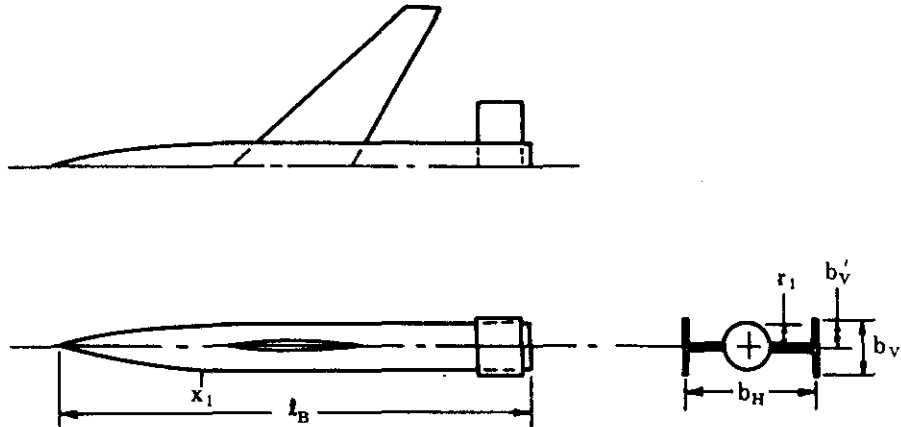
The experimental results (based on S_W) from reference 1, are $(C_{Y\beta})_{WB} = -0.143$ per radian, $(\Delta C_{Y\beta})_{V(WBH)} = -0.716$ per radian, and $C_{Y\beta} = -0.859$ per radian.

2. Method 2

Given: A configuration of reference 1, consisting of wing, body, horizontal tail, and twin vertical tails mounted on the tips of the horizontal tail. The wing and body are identical to those of sample problem 1 and their characteristics are not repeated.

Vertical Tail Characteristics

$$\begin{array}{lll} b_V = 2.00 \text{ in.} & b'_V = 1.00 \text{ in.} & S_V = 3.60 \text{ sq in.} \\ \text{NACA 65A006 airfoil} & & \phi_{TE_V} = 7^\circ \end{array} \quad A_V = 1.11$$



Additional Characteristics

$$r_1 = 0.8335 \text{ in.} \quad b_H = 4.80 \text{ in.} \quad M = 0.60$$

Compute:

Step 1. Determine the wing-body contribution to $C_{Y\beta}$ using the Method of Section 5.3.1.1.

$$(C_{Y\beta})_{WB} = -0.115 \text{ per rad (sample problem 1)}$$

Step 2. Determine the total empennage contribution to $C_{Y\beta}$ using Method 2, paragraph A, Section 5.3.1.1.

$$b'_V/b_V = 0.50$$

$$\frac{A_{eff}}{A} = 1.0 \text{ (figure 5.3.1.1-24a)}$$

$$A_{eff} = 1.11$$

$$(C_{Y\beta})_{V_{eff}} = 1.78 \text{ per rad (figure 5.3.1.1-24b)}$$

$$2r_1/b_V = 0.8335$$

$$\frac{b_H}{t_B} = \frac{4.80}{18.25} = 0.263$$

$$\frac{(C_{Y\beta})_{V(WBH)}}{(C_{Y\beta})_{V_{eff}}} = 0.595 \text{ (figure 5.3.1.1-24c)}$$

$$\begin{aligned} (\Delta C_{Y\beta})_{V(WBH)} &= - \frac{(C_{Y\beta})_{V(WBH)}}{(C_{Y\beta})_{V_{eff}}} (C_{Y\beta})_{V_{eff}} \frac{2S_V}{S_W} \quad \text{(equation 5.3.1.1-c)} \\ &= -(0.595) (1.78) \frac{2(3.60)}{36.0} \\ &= -0.212 \text{ per rad (based on } S_W) \end{aligned}$$

Solution:

$$C_{Y\beta} = (C_{Y\beta})_{WB} + (\Delta C_{Y\beta})_{V(WBH)} \quad \text{(equation 5.6.1.1-a)}$$

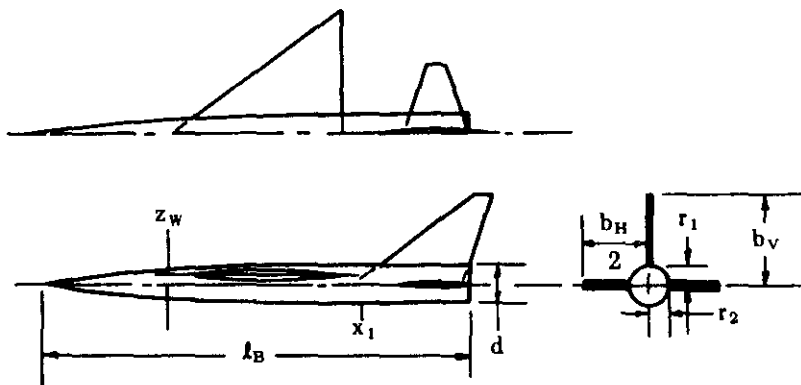
$$= -0.115 - 0.212$$

$$= -0.327 \text{ per rad (based on } S_W)$$

The experimental results (based on S_w) from reference 1 are $(C_{Y\beta})_{WB} = -0.143$ per radian, $(\Delta C_{Y\beta})_{VWBH} = -0.258$ per radian, and $C_{Y\beta} = -0.401$ per radian.

3. Method 3

Given: The configuration of reference 2, consisting of wing, body, horizontal tail, and upper vertical tail.



Wing Characteristics

$$A_w = 3.0 \quad S_w = 576 \text{ sq in.} \quad z_w = -2.08 \text{ in.} \quad \Gamma = 0$$

Horizontal Tail Characteristics

$$A_h = 4.0 \quad b_h/2 = 11.21 \text{ in.} \quad z_h = 0$$

Vertical Tail Characteristics

$$A_v = 1.50 \quad A_{v_e} = 1.43 \quad S_v = 153.7 \text{ sq in.} \quad S_{v_e} = 109.7 \text{ sq in.}$$

$$\Lambda_{av} = 41.9^\circ \quad \lambda_v = 0.16 \quad \lambda_{v_e} = 0.189 \quad b_v = 15.23 \text{ in.}$$

NACA 0003.5-64 airfoil

Body Characteristics

$$l_B = 72.0 \text{ in.} \quad x_1 = 54.0 \text{ in.} \quad V_B^{2/3} = 133.0 \text{ sq in.} \quad d = 6.0 \text{ in.}$$

Additional Characteristics

$$M = 0.25 \quad r_1 = 2.76 \text{ in.} \quad r_2 = 2.76 \text{ in.}$$

Compute:

Step 1. Determine the wing-body contribution to $C_{Y\beta}$ using the method of Section 5.2.1.1.

$$\frac{z_w}{d/2} = \frac{-2.08}{3.0} = -0.694$$

$K_1 = 1.58$ (figure 5.2.1.1-7)

$$f = \frac{l_B}{d} = 12.0$$

$k_2 - k_1 = 0.955$ (figure 4.2.1.1-20a)

$$x_1/l_B = 0.75$$

$$x_0/l_B = 0.765 \text{ (figure 4.2.1.1-20b)}$$

$$x_0 = (0.765)(72.0) = 55.08 \text{ in.}$$

$$S_0 = \pi \left(\frac{d}{2}\right)^2 = 28.28 \text{ sq in.}$$

$$\begin{aligned} (C_{Y\beta})_{WB} &= K_i (C_{Y\beta})_B \left(\frac{\text{Body Reference Area}}{S_w} \right) + (\Delta C_{Y\beta})_\Gamma \quad \text{(equation 5.2.1.1-a)} \\ &= K_i \left(\frac{-2(k_2 - k_1) S_0}{V_B^{2/3}} \right) \left(\frac{V_B^{2/3}}{S_w} \right) + (\Delta C_{Y\beta})_\Gamma \\ &= 1.58 \left(\frac{(-2)(0.955)(28.28)}{133.0} \right) \left(\frac{133.0}{576.0} \right) + 0 \\ &= -0.1480 \text{ per rad (based on } S_w) \end{aligned}$$

Step 2. Determine the total empennage contribution to $C_{Y\beta}$ using Method 3, paragraph A, Section 5.3.1.1 to determine the contributions of individual panels.

$$(c L_a)_v = 6.18 \text{ per rad (Section 4.1.1.2)}$$

$$\kappa = \frac{(c L_a)_v}{2\pi} = 0.984 \text{ (ratio of incompressible section lift-curve slope to } 2\pi)$$

$$2A_{V_e} = 2.86$$

$$\frac{2A_{V_e}}{\kappa} [\beta^2 + \tan^2 \Lambda_{c/2v}]^{1/2} = 3.84$$

$$\frac{(C_{L_a})_v}{2A_{V_e}} = 0.995 \text{ per rad (figure 4.1.3.2-49)}$$

$$(C_{L_a})_v = (0.995)(2A_{V_e}) = 2.85 \text{ per rad (based on } S_{V_e})$$

Determine the increment in $C_{Y\beta}$ due to adding the horizontal tail to the wing-body configuration. In this case the empennage consists of the body and the horizontal tail. The apparent-mass ratio to be found is that due to adding the horizontal tail to the body, $K_{H(B)}$.

$$z_H/r_1 = 0$$

$$K_{H(B)} = 0 \text{ (figure 5.3.1.1-2500)}$$

$$\begin{aligned} (\Delta C_{Y\beta})_{H(WB)} &= K_{H(B)} (C_{Y\beta})_B \frac{S_{B_{Ref}}}{S_w} \quad \text{(equation 5.3.1.1-e)} \\ &= 0 \end{aligned}$$

Determine the increment in $C_{Y\beta}$ due to adding the upper vertical stabilizer to the wing-body-horizontal tail configuration. In this case the empennage consists of body, horizontal tail, and upper vertical stabilizer. The apparent-mass ratio to be found is that due to adding the upper vertical stabilizer to the combination of body and horizontal tail, $K_{V(BH)}$.

$$r_1/r_2 = 1.000; \frac{r_2}{b_H/2} = 0.246; (r_1/b)_U_{\text{existing panel}} = 1.000; (r_1/b)_V_{\text{added panel}} = 0.181$$

By using the above parameters and Table 5.3.1.1-A, $K_{V(BH)}$ can be obtained from figures 5.3.1.1-25b, -25c, and -25d interpolated for a value of $\frac{r_2}{b_H/2} \approx 0.246$.

$$K_{V(BH)} = 1.225$$

$$\begin{aligned} (\Delta C_{Y\beta})_{V(WBH)} &= -K_{V(BH)} (C_{L_a})_V \frac{S_{V_e}}{S_w} \quad (\text{equation 5.3.1.1-d}) \\ &= -(1.225) (2.85) \frac{109.7}{576} \\ &= -0.665 \text{ per rad (based on } S_w) \end{aligned}$$

Solution:

$$\begin{aligned} C_{Y\beta} &= (C_{Y\beta})_{WB} + \sum_p (\Delta C_{Y\beta})_p \quad (\text{equation 5.6.1.1-b}) \\ &= (C_{Y\beta})_{WB} + (\Delta C_{Y\beta})_{H(WB)} + (\Delta C_{Y\beta})_{V(WBH)} \\ &= -0.1480 + 0 - 0.665 \\ &= -0.813 \text{ per rad (based on } S_w) \end{aligned}$$

The experimental results (based on S_w) from reference 2 are $(C_{Y\beta})_{WB} = -0.149$ per radian, $(\Delta C_{Y\beta})_{V(WBH)} = -0.556$ per radian, and $C_{Y\beta} = -0.705$ per radian.

B. TRANSONIC

A brief discussion of the flow phenomena associated with forces generated on a vertical panel at transonic speeds is given in paragraph B of Section 5.3.1.1. The effect of wing-body wake and sidewash, and the mutual interference effects between component combinations at transonic speeds are extremely sensitive to changes in local contour.

At the present time these effects cannot be predicted with accuracy and the vehicle sideslip derivative $C_{Y\beta}$ is usually obtained by wind-tunnel testing or estimated from comparison with similar configurations.

DATCOM METHOD

No method is available in the literature for estimating the vehicle sideslip derivative $C_{Y\beta}$ at transonic speeds and none is presented in the Datcom. Some typical transonic data for this derivative are presented as figure 5.6.1.1-14.

C. SUPERSONIC

The procedure for estimating the supersonic sideslip derivative $C_{Y\beta}$ of a wing-body-tail configuration is essentially the same as that at subsonic speeds. The problem of estimating the contribution of the empennage is complicated by the presence of shock waves. This effect is discussed in paragraph C of Section 5.3.1.1.

DATCOM METHOD

The side force due to sideslip for the complete configuration at supersonic speeds is given by equation 5.6.1.1-b

$$C_{Y\beta} = (C_{Y\beta})_{WB} + \sum_p (\Delta C_{Y\beta})_p$$

where the subscript p refers to panels present in the empennage

$(C_{Y\beta})_{WB}$ is obtained from Section 5.2.1.1

$(\Delta C_{Y\beta})_p$ are the increments in $C_{Y\beta}$ gained by successive additions of the panels in the empennage obtained from paragraph C, Section 5.3.1.1

The order of configuration build-up will generally proceed as outlined for subsonic speeds (Method 3, paragraph A). The one exception to that build-up procedure is the case at supersonic speeds where the vertical panels are stag-

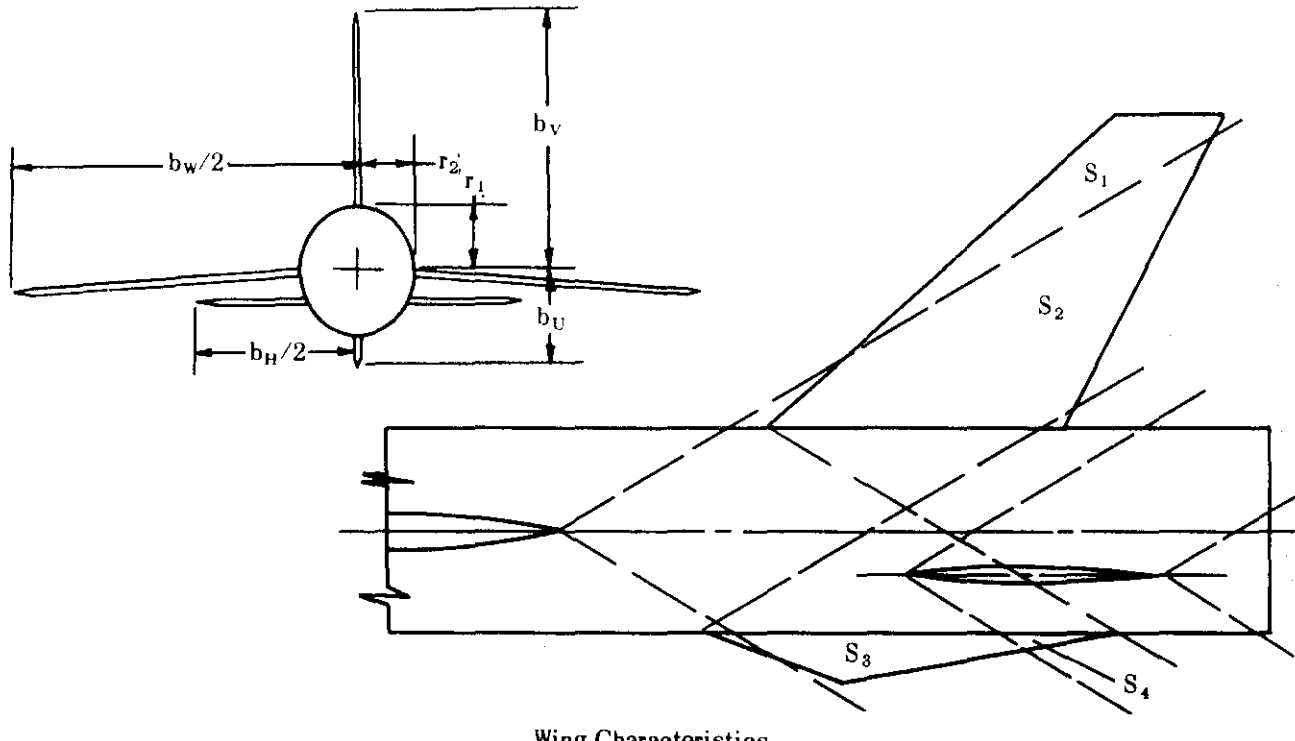
gered along the body so that their leading edges intersect the body at different locations. In this case, the panel whose leading edge intersects the body farthest aft is added first.

This method is limited to configurations in which the horizontal tail is mounted on the body or configurations with no horizontal tail.

For a wingless configuration the remarks following the Datcom methods of paragraph A above are also applicable at supersonic speeds.

Sample Problem

Given: The configuration of reference 3 consisting of wing, body, horizontal tail, upper vertical tail, and lower vertical tail.



$$A_w = 3.18 \quad S_w = 114.5 \text{ sq in.} \quad b_w = 19.08 \text{ in.} \quad z_w = 0 \quad \Gamma = -3.5^\circ$$

Horizontal Tail Characteristics

$$A_h = 3.06 \quad b_h = 9.12 \text{ in.} \quad z_h = 0.84 \text{ in.}$$

Vertical Tail Characteristics

$$A_{v_e} = 1.48 \quad S_{v_e} = 19.20 \text{ sq in.} \quad \Lambda_{LE_V} = 49.2^\circ \quad b_v = 7.08 \text{ in.} \quad \lambda_{v_e} = 0.392$$

Ventral Tail Characteristics

$$A_{U_e} = 0.2025 \quad S_{U_e} = 3.24 \text{ sq in.} \quad \Lambda_{LE_U} = 70.2^\circ \quad b_U = 2.56 \text{ in.} \quad \lambda_U = 0$$

Additional Characteristics

$$M = 2.01 \quad \mu = \sin^{-1} 1/M = 29.8^\circ \quad r_1 = 1.75 \text{ in.} \quad r_2 = 1.496 \text{ in.}$$

$$r_1/r_2 = 1.170 \quad S_1 = 4.63 \text{ sq in.} \quad S_2 = 14.56 \text{ sq in.} \quad S_3 = 2.74 \text{ sq in.}$$

$$S_4 = 0.50 \text{ sq in.} \quad \frac{S_{act}}{S_{ext}} = 0.875$$

Compute:

Step 1. Determine the wing-body contribution to $C_{Y\beta}$.

The Datcom does not present methods at supersonic speeds that will predict the side-force characteristics of the wing-body configuration of this sample problem. In such cases it is suggested that test results of a similar configuration be used, if available, and corrected for the difference in relative size of the fuselage and wing for the two configurations. If the vertical location of the wing on the fuselage is not similar, a correction for wing-fuselage interference must also be made.*

An experimental result for $(C_{Y\beta})_{WB}$ is not available for this configuration. Use is made of the experimental result for $(C_{Y\beta})_{WBH}$. However, the increment due to adding the horizontal tail to the wing-body configuration will be computed for the sake of completeness.

$$(C_{Y\beta})_{WBH} = -0.315 \text{ per rad (based on } S_w)$$

Step 2. Determine the total empennage contribution to $C_{Y\beta}$ using the method of paragraph C, Section 5.3.1.1 to determine the contributions of individual panels.

Upper Vertical Panel

$$2A_{V_e} \tan \Lambda_{LE_V} = 3.42$$

$$\frac{\tan \Lambda_{LE_V}}{\beta} = \frac{1.1585}{1.744} = 0.664$$

$$\beta(C_{N_a})_V = 4.10 \text{ per rad}$$

(figures 4.1.3.2-56c,-56d, -56e interpolated

for $\lambda_{V_e} = 0.392$

$$(C_{N_a})_V = 2.35 \text{ per rad (based on } S_{V_e})$$

Lower Vertical Panel

$$2A_{U_e} \tan \Lambda_{LE_U} = 1.125$$

$$\frac{\beta}{\tan \Lambda_{LE_U}} = 0.628$$

$$\tan \Lambda_{LE_U} (C_{N_a})_U = 1.73 \text{ per rad (figure 4.1.3.2-56a)}$$

$$(C_{N_a})_U = 0.622 \text{ per rad (based on } S_{U_e})$$

Determine the increment in $C_{Y\beta}$ due to adding the horizontal tail to the wing-body configuration. In this case the empennage consists of the body and the horizontal tail. The apparent-mass ratio to be found is that due to adding the horizontal tail to the body, K_{HB} .

$$\left(\frac{z_H}{r_1}\right) = \frac{0.84}{1.75} = 0.480; \left(\frac{r_2}{b_H/2}\right) = \frac{1.496}{4.56} = 0.328$$

From figure 5.3.1.1-2500, values of K_{HB} are obtained for $\left(\frac{z_H}{r_1}\right) = 1.0, 0, -1.0$ at $\left(\frac{r_2}{b_H/2}\right) = 0.328$

Since K charts are not presented for the case of a horizontal surface added to an elliptical body the body is considered circular and an interpolation is performed to obtain

$$K_{HB} \text{ at } \left(\frac{z_H}{r_1}\right) = 0.480^{**}$$

$$K_{HB} = 0.130$$

The side-force-curve slope of the body is given by slender-body theory. $(C_{Y\beta})_B = -2 \text{ per rad (based on } S_B)$

$$(\Delta C_{Y\beta})_{HBW} = K_{HB} (C_{Y\beta})_B \frac{S_{BR_{ref}}}{S_w} \frac{S_{act}}{S_{ext}} \quad (\text{equation 5.3.1.1-g})$$

$$= (0.130) (-2) \left(\frac{\pi r_1 r_2}{114.5}\right) (0.875)$$

*See reference 5 for discussion of design corrections.

**See Method 3, paragraph A, Section 5.3.1.1 for interpolation procedure.

$$= (0.130) (-2) \left[\frac{(\pi)(1.75)(1.496)}{114.5} \right] (0.875)$$

= -0.0163 per rad (based on S_w)

Determine the increment in $C_{Y\beta}$ due to adding the upper vertical stabilizer to the wing-body-horizontal stabilizer combination. The empennage in this case consists of the body, horizontal tail, and upper vertical stabilizer. The apparent-mass ratio to be found is that due to adding the upper vertical stabilizer to the body and horizontal tail, $K'_{V(HB)}$.

In the configuration sketch part of the upper vertical panel S_1 senses only the wing-body combination, while S_2 senses only the body. Therefore, the effective apparent-mass ratio is given by

$$K'_{V(HB)} = K_{V(WB)} \frac{S_1}{S_{V_e}} + K_{V(B)} \frac{S_2}{S_{V_e}}$$

Determine $K_{V(WB)}$:

$$\left(\frac{r_1}{r_2} \right) = 1.170; \left(\frac{r_2}{b_w/2} \right) = 0.157; \left(\frac{r_1}{b} \right)_v^{\text{added panel}} = 0.247; \left(\frac{r_1}{b} \right)_U^{\text{existing panel}} = 1.000$$

By using the above parameters and table 5.3.1.1-A it is seen that $K_{V(WB)}$ can be obtained from figures 5.3.1.1-25b, -25c, -25e, and 5.3.1.1-25x, -25y, -25z, and 5.3.1.1-25dd, -25ee, -25ff, interpolated for

$$\frac{r_2}{b_w/2} = 0.157 \text{ and } r_1/r_2 = 1.170.$$

$$K_{V(WB)} = 1.49$$

Determine $K_{V(B)}$:

$$\left(\frac{r_1}{r_2} \right) = 1.170; \left(\frac{r_1}{b} \right)_v^{\text{added panel}} = 0.247; \left(\frac{r_1}{b} \right)_U^{\text{existing panel}} = 1.000$$

By using the above parameters and table 5.3.1.1-A it is seen that $K_{V(B)}$ can be obtained from figures 5.3.1.1-25a, -25w, and -25cc, interpolated for $r_1/r_2 = 1.170$

$$K_{V(B)} = 1.27$$

$$K'_{V(HB)} = (1.49) \left(\frac{4.63}{19.20} \right) + (1.27) \left(\frac{14.57}{19.20} \right) = 1.32$$

$$(\Delta C_{Y\beta})_{V(WBH)} = -K'_{V(HB)} (C_{N_a})_V \frac{S_{V_e}}{S_w} \quad (\text{equation 5.3.1.1-f})$$

$$= -(1.32) (2.35) \frac{19.20}{114.5}$$

= -0.520 per rad (based on S_w)

Determine the increment in $C_{Y\beta}$ due to adding the lower vertical stabilizer to the wing-body-horizontal stabilizer-upper vertical stabilizer combination. The empennage in this case consists of body, horizontal tail, upper vertical stabilizer, and lower vertical stabilizer. The apparent-mass ratio to be found is that due to adding the lower vertical stabilizer to the combination of body, horizontal tail, and upper vertical stabilizer, $K'_{U(BHV)}$.

In the configuration sketch part of the lower vertical stabilizer S_3 senses only the body, while S_4 senses both the body and horizontal tail. Therefore, the effective apparent-mass ratio is given by

$$K'_{U(BHV)} = K_{U(B)} \frac{S_3}{S_{U_e}} + K_{U(BH)} \frac{S_4}{S_{U_e}}$$

Determine $K_{U(B)}$:

$$\left(\frac{r_1}{r_2}\right) = 1.170; \left(\frac{r_1}{b}\right)_U_{\text{added panel}} = 0.685; \left(\frac{r_1}{b}\right)_V_{\text{existing panel}} = 1.000$$

By using the above parameters and table 5.3.1.1-A it is seen that $K_{U(B)}$ can be obtained from figures 5.3.1.1-25a, -25w, and -25cc, interpolated for $r_1/r_2 = 1.170$.

$$K_{U(B)} = 3.0$$

Determine $K_{U(BH)}$:

$$\left(\frac{r_1}{r_2}\right) = 1.170; \left(\frac{r_1}{b}\right)_U_{\text{added panel}} = 0.685; \left(\frac{r_1}{b}\right)_V_{\text{existing panel}} = 1.000; \left(\frac{r_2}{b_H/2}\right) = 0.328; \left(\frac{z_H}{r_1}\right) = 0.480$$

Since the horizontal tail is located below the body centerline and the body is elliptical, we have a horizontal tail-body combination not covered by the K charts of Section 5.3.1.1. To handle this case, either the body has to be considered circular and an interpolation made for horizontal tail height, or the horizontal tail has to be assumed to be located at the mid-position and an interpolation made between r_1/r_2 ratios. A comparison between figures 5.3.1.1-25d, -25z, and 25ff shows that a small variation in cross section has a significant effect on the apparent-mass ratio in the region of $(r_1/b)_U = 0.685$. Therefore, an interpolation for body shape will be made rather than for horizontal tail height.

From figures 5.3.1.1-25c, -25d, -25e and 5.3.1.1-25y, -25z, -25aa and 5.3.1.1-25ee, -25ff, -25gg obtain

$K_{U(BH)}$ interpolated for $\frac{r_2}{b_H/2} = 0.328$. An interpolation between those values of $K_{U(BH)}$ gives, for $(r_1/r_2) = 1.170$

$$K_{U(BH)} = 3.04$$

$$K'_{U(BHV)} = (3.0)\left(\frac{2.74}{3.24}\right) + (3.04)\left(\frac{0.50}{3.24}\right)$$

$$= 3.01$$

$$\begin{aligned} (\Delta C_{Y\beta})_{U(BHV)} &= -K'_{U(BHV)} (C_{N\alpha})_U \frac{S_{U_e}}{S_w} \quad \text{(equation 5.3.1.1-f)} \\ &= -(3.01)(0.622) \frac{3.24}{114.5} \\ &= -0.053 \text{ per rad (based on } S_w) \end{aligned}$$

Solution:

$$C_{Y\beta} = (C_{Y\beta})_{WB} + \sum_p (\Delta C_{Y\beta})_p \quad \text{(equation 5.6.1.1-b)}$$

$$= (C_{Y\beta})_{WB} + (\Delta C_{Y\beta})_{H(WB)} + (\Delta C_{Y\beta})_{V(WB)} + (\Delta C_{Y\beta})_{U(WBHV)}$$

For this sample problem use is made of the test result for $(C_{Y\beta})_{WBH}$, so

$$C_{Y\beta} = (C_{Y\beta})_{WBH} + (\Delta C_{Y\beta})_{V(WBHV)} + (\Delta C_{Y\beta})_{U(WBHV)}$$

$$= (-0.315) + (-0.520) + (-0.053)$$

$$= -0.888 \text{ per rad (based on } S_w)$$

The experimental result from reference 3 is $C_{Y\beta} = -0.888$ per radian (based on S_w).

REFERENCES

1. Sleeman, W. C., Jr.: An Experimental Study at High Subsonic Speeds of Several Tail Configurations on a Model Having a 45° Sweptback Wing. NACA RM L57C08, 1957. (U)
2. Savage, H. F., and Tinling, B. E.: The Subsonic Static Aerodynamic Characteristics of an Airplane Model Having a Triangular Wing of Aspect Ratio 3. II - Lateral and Directional Characteristics. NACA TN 4042, 1957. (U)
3. Spearman, M. L., Robinson, R. B., and Driver, C.: The Effects of the Addition of Small Fuselage-Mounted Fins on the Static Directional Stability Characteristics of a Model of a 45° Sweptwing Airplane at Angles of Attack up to 15.3° at a Mach Number of 2.01. NACA RM L56D16a, 1956. (U)
4. Goodwin, F. K., and Kaattari, G. E.: Estimation of Directional Stability Derivatives at Small Angles and Subsonic and Supersonic Speeds. NASA Memo 12-2-58A, 1958. (U)
5. Campbell, J. P., and McKinney, M. O.: Summary of Methods for Calculating Dynamic Lateral Stability and Response and for Estimating Lateral Stability Derivatives. NACA TR 1098, 1952. (U)

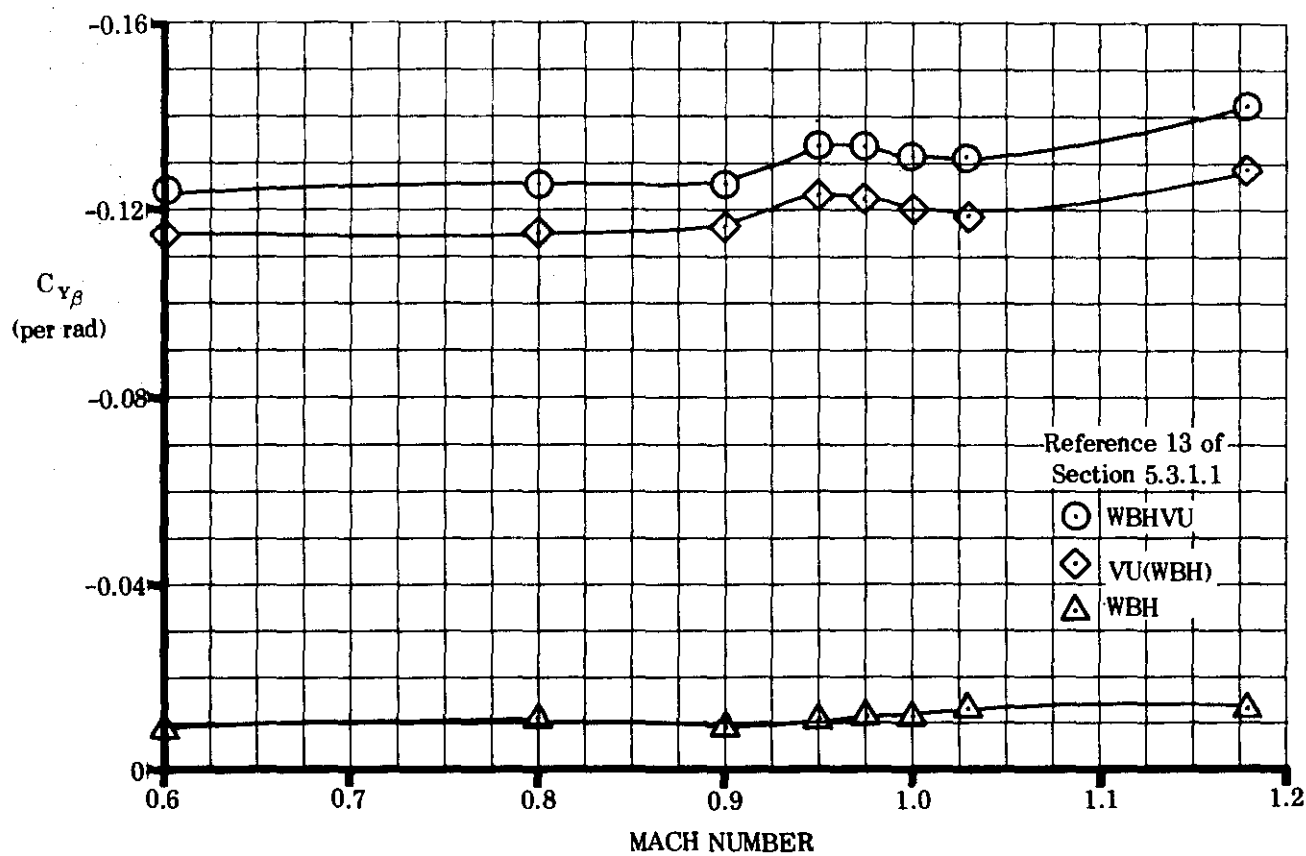
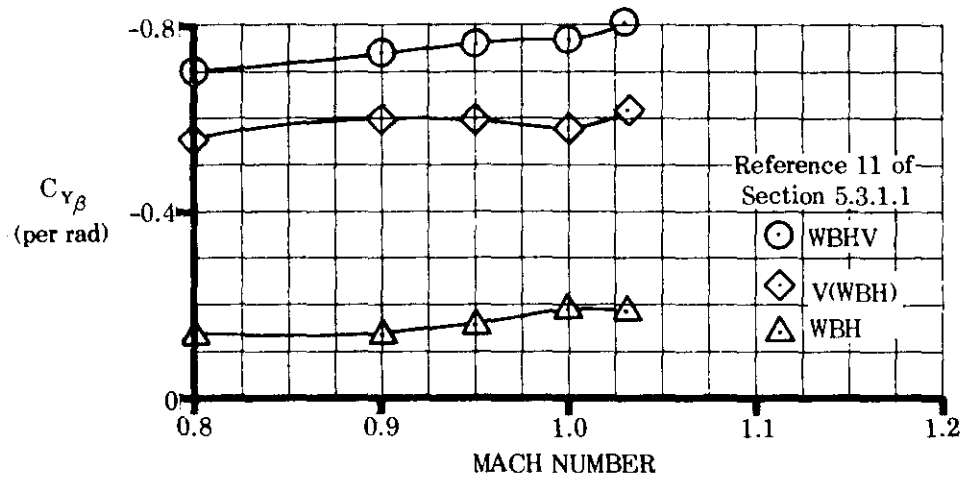


FIGURE 5.6.1.1-14 TYPICAL TRANSONIC DATA

5.6.1.2 WING-BODY-TAIL SIDE-FORCE COEFFICIENT C_y AT ANGLE OF ATTACK

The wing-body-tail side force developed at combined angles is nonlinear with respect to both sideslip and angle of attack for the reasons cited in the introductory remarks of Sections 5.2.1.2 and 5.3.1.2, and as in those Sections, to obtain $C_{y\beta}$, it is recommended that C_y be calculated at several angles of attack for a small sideslip angle ($\beta \leq 4^\circ$). Then at each angle of attack the side force is assumed linear with sideslip for small values of β so that

$$C_{y\beta} = \frac{C_y}{\beta}.$$

A. SUBSONIC

No method is presently available for determining the wing-body-tail side force at large angles of attack and subsonic speeds. The method presented herein is restricted to first-order approximations at relatively low angles of attack.

DATCOM METHOD

It is recommended that the method of paragraph A of Section 5.6.1.1 be used, with consideration given to the angle-of attack restriction presented in figure 5.1.1.1-4.

B. TRANSONIC

The comments appearing in paragraph B of Section 5.6.1.1 are equally appropriate here.

DATCOM METHOD

No method is available for estimating this coefficient and none is presented in the Datcom.

C. SUPERSONIC

The analysis of wing-body-tail configurations at combined angles is taken from reference 1 and is accomplished through a combination of the methods of Sections 5.2.1.2 and 5.3.1.2. Therefore, the discussions in paragraph C of those Sections apply to this Section as well. Note in Section 5.3.1.2 that the method is limited to configurations with circular bodies, and to the analysis of horizontal tail effects only when that surface is body-mounted.

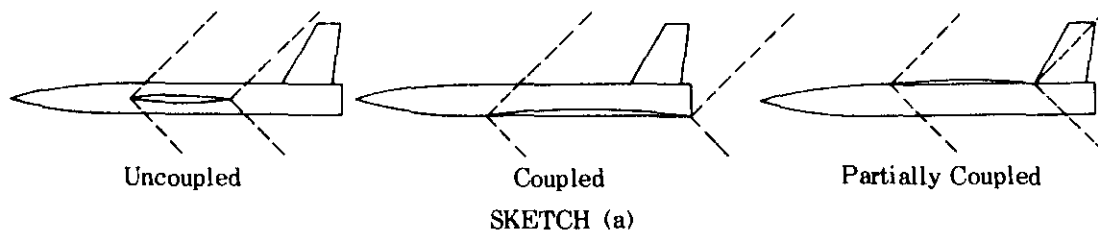
In addition to the phenomena previously discussed, three types of interference exist between the wing and tail surfaces. If the vertical tail panels are in the wing-flow field, mutual interaction occurs in the same way as that between horizontal and vertical tail panels. This effect is taken into account through the apparent-mass factor concept. Secondly, there is interference due to the wing-flow field which alters the local dynamic pressure and Mach number acting on the vertical tail surfaces. This is a nonlinear effect of angle of attack and is taken into account by a tail effectiveness parameter η_w based on two-dimensional shock-expansion theory. Wing-vertical tail interference also results from the effect of the wing-flow field on the body vortices. The positions and strengths of the body vortices are both influenced by the wing. The wing-flow field cuts off the body feeding vortex sheet along the length of the exposed wing root chord and the body vortex path is curved as it passes through the wing-flow field. The effect of the wing is taken into account herein by an approximation to the method of reference 2. It is assumed that both vortex strengths and positions are those about a body alone, foreshortened by the length of the exposed wing root chord. This assumption satisfactorily accounts for the effect of the wing-flow field on vortex strength but neglects the effect of the wing-flow field in altering the path of the vortices; however, the error introduced at small angles of sideslip is negligible.

Two methods are discussed in reference 2 for approximating the effect of the wing-flow field on the body vortex positions. One method is based on two-dimensional shock-expansion theory which precludes accurate prediction of lateral vortex positions and also restricts the results to configurations with slender wing panels. A second method applicable to slender configurations is suggested in which the calculation of the vortex paths with the wing panels

present can be made by using slender-body theory and proceeding step by step. However, the practical calculation of the paths with any degree of accuracy requires the use of automatic computing methods.

Sections 5.2.1.2 and 5.3.1.2 have considered separately wing-body and tail-body configurations. Wing-body-tail configurations may be classified as either uncoupled, coupled, or partially coupled, depending on the physical relationship between the wing-flow field and the tail. The three classes of configurations are illustrated in sketch (a). For the uncoupled configurations a body section separates the wing from the empennage so that the wing-flow field does not directly impinge on the tail surfaces. For the coupled configuration the tail surfaces are totally enveloped in the wing-flow field. Partially coupled configurations have partial coupling between the wing-flow field and the tail. The primary difference between the three classes of configurations in so far as the present theory is concerned is that the shock-expansion effects of the wing on the tail are neglected when dealing with uncoupled configurations.

The wing-flow field at angle of attack and supersonic speeds is defined by the method outlined in Section 5.3.1.2 for determining the horizontal tail-flow field at angle of attack and supersonic speeds.



DATCOM METHOD

The method for determining the wing-body-tail side-force coefficient at combined angles is given by

$$C_{Y_{WBHVU}} = C_{Y_{WB}} + C_{Y_{HVU(WB)}} \quad 5.6.1.2-a$$

where

$C_{Y_{WB}}$ is the wing-body contribution obtained from equation 5.2.1.2-a

$C_{Y_{HVU(WB)}}$ is the empennage contribution obtained from equation 5.6.1.2-b

The contribution of the empennage is given by

$$C_{Y_{HVU(WB)}} = C_{Y_{H(B)}} + C_{Y_{V(\eta)}} + C_{Y_{U(\eta)}} \quad 5.6.1.2-b$$

where

$C_{Y_{H(B)}}$ is the horizontal tail contribution obtained from equation 5.3.1.2-b

$C_{Y_{V(\eta)}}$ is the vertical tail contribution obtained from equation 5.6.1.2-c

$C_{Y_{U(\eta)}}$ is the ventral fin contribution obtained from equation 5.6.1.2-d

The order in which the tail panels should be added to the wing-body configuration for analysis purposes parallels that prescribed in Section 5.3.1.2 for a tail-body configuration.

The contribution of the vertical tail is given by

$$C_{Y_{V(\eta)}} = C_{Y_{V(K,\phi)}} + C_{Y_{V(\Gamma_B)}} \quad 5.6.1.2-c$$

for uncoupled configurations, and by

$$C_{Y_{V(\eta)}} = [C_{Y_{V(K,\phi)}} + C_{Y_{V(\Gamma_B)}}] \eta_{wv} \quad 5.6.1.2-c$$

for coupled or partially coupled configurations;

where

- $C_{YV(\alpha, \beta)}$ accounts for α and β cross-coupling and any mutual interaction between the vertical tail and other surfaces in the empennage and is given by equation 5.3.1.2-d. In addition, any impingement of the wing-flow field on the vertical tail must be considered in determining the effective apparent-mass factor K'_V . The method for defining the wing flow field is the same as for the horizontal tail, and is given step-by-step in paragraph C, Section 5.3.1.2. Note that the upper trailing edge is marked by a shock wave rather than a Mach line.
- $C_{YV(\Gamma_B)}$ accounts for the effect of body vortices on the vertical stabilizer, and includes influence of the wing on the vortex strength. The wing effect is approximated by foreshortening the body length by the exposed wing root chord c_{r_e} when finding vortex strength and position from figures 4.3.1.3-13b, 4.3.1.3-14, and 4.3.1.3-15. That is, the figures are entered with $\frac{\alpha'(x - x_s - c_{r_e})}{r}$, rather than $\frac{\alpha(x - x_s)}{r}$. * The results are then applied to equations 5.3.1.2-f and 5.3.1.2-e to obtain $C_{YV(\Gamma_B)}$. **
- η_{w_V} is the tail effectiveness parameter of the upper vertical stabilizer obtained from figure 5.6.1.2-9 as a function of angle of attack and Mach number. These charts take into account the changes in dynamic pressure and Mach number at the tail by direct application of two-dimensional shock-expansion theory. Any effects of wing-body interference or wing section in distorting the shock-expansion field are neglected.

For a specified initial Mach number there is a maximum value of the angle of attack for which there exists an oblique shock solution. Or, conversely, for a specified angle of attack there is a minimum initial Mach number for which there is an oblique shock solution. The relation between Mach number and angle of attack below which no solutions for η_w may be obtained is indicated in sketch (a) of Section 5.3.1.2.

The procedure for using these charts is

- Step 1: Draw on transparent paper the relative positions of the wing exposed root chord and the vertical surfaces. Choose the scale so that the exposed chord length coincides with that shown in figure 5.6.1.2-9 .
- Step 2: Overlay the drawing on the figure to locate the tail in the proper influence zone.
- Step 3: The vertical tail is divided into several areas. The average value of η_{w_V} in each area is multiplied by the ratio of its area to S_{V_e} .
- Step 4: Sum the weighted values of η_{w_V} to obtain the total tail effectiveness parameter η_{w_V} .
- Step 5: Interpolation for angle of attack and/or Mach number may be necessary. If so, a three-point interpolation for α should be made using weighted values of η_{w_V} . Two points are sufficient for Mach number interpolation.

The contribution of the ventral fin is given by

$$C_{YU(\eta)} = C_{Y_U} \quad 5.6.1.2-d$$

for uncoupled configurations, and by

$$C_{YU(\eta)} = C_{Y_U} \eta_{w_U} \quad 5.6.1.2-d'$$

for coupled or partially coupled configurations;

* If x_s indicates vortex separation aft of the exposed wing root-chord leading edge, then only that portion of c_{r_e} aft of the indicated separation point is subtracted.

** The vortex positions given by equation 5.3.1.2-f are the positions at a given longitudinal station about the body alone foreshortened by c_{r_e} and do not include the effects of the wing-flow field in altering the paths of the vortices.

where

C_{Y_V} accounts for α and β cross-coupling and any mutual interaction between the vertical tail and other surfaces in the empennage, and is given by equation 5.3.1.2-g. In addition, any impingement of the wing flow field on the ventral tail must be considered in determining the effective apparent-mass factor K'_U .

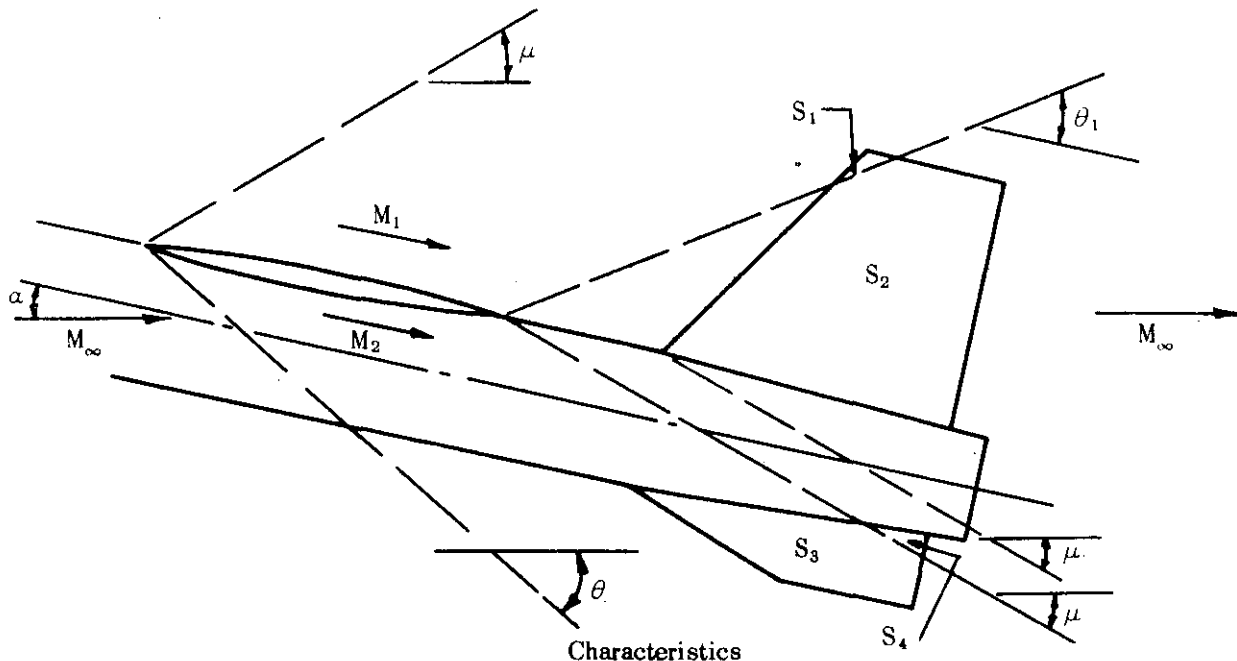
γ_{w_U} is the tail effectiveness parameter of the ventral fin and is obtained from figure 5.6.1.2-9 by following the steps describing the determination of η_{w_V} .

As noted in paragraph C of Section 5.3.1.2, the body vortices do not affect the ventral fin.

Values for the incremental coefficient resulting from the addition of vertical tails to wing-body configurations, calculated using the Datcom method, are compared with experimental results in figure 5.6.1.2-8. The correlation between experiment and estimate is relatively good at $\beta = 5.1^\circ$ and poor at $\beta = 10^\circ$. The poor correlation at $\beta = 10^\circ$ can be attributed to the assumption that the body vortex positions are those about a body foreshortened by the length of the exposed wing root chord. This assumption neglects the effects of the wing-flow field on the body vortex positions and poor correlation can be expected at higher sideslip angles where viscous lateral cross-flow effects become important.

Sample Problem

Given: Configuration of sample problem, paragraph C, Sections 5.2.1.2 (with slight boattail) and 5.3.1.2. There is no horizontal tail on this configuration. Some of the characteristics are repeated. Find the side-force coefficient developed by the wing-body-tail combination at $\alpha = 12^\circ$, $\beta = 4^\circ$, and $M = 2.01$.



$$\frac{r_1}{b_V} = 0.200 \quad \frac{r_1}{b_U} = 0.492, \quad \Lambda_{LE_V} = 32.5^\circ \quad \Lambda_{LE_U} = 70^\circ \quad S_w = 144.0 \text{ sq in.}$$

$$b_w = 24.0 \text{ in.} \quad c_{r_e} = 8.90 \text{ in.}$$

$$S_{V_e} = 31.6 \text{ sq in.} \quad S_{U_e} = 8.54 \text{ sq in.} \quad S_1 = 0.40 \text{ sq in.} \quad S_2 = 31.2 \text{ sq in.} \quad S_3 \approx S_{U_e} = 8.54 \text{ sq in.}$$

$x = 32.8$ in. (x measured from nose to 50-percent-chord point of MAC of exposed vertical panel)

$C_{Y_{WB}} = -0.400$ (sample problem, paragraph C, Section 5.2.1.2)

$C_{Y_{HB}} = 0$ (no horizontal tail on this configuration)

At positive angle of attack, vertical-tail exposed root-chord leading edge is aft of ventral-fin exposed root-chord leading edge.

Ventral fin is not influenced by presence of upper vertical tail at this angle of attack and Mach number.
Configuration is partially coupled at this angle of attack and Mach number.

Compute:

Determine the vertical tail contribution $C_{Y_{V(\eta)}}$

$$K'_V = 1.13 \text{ (method of paragraph C, Section 5.3.1.1 with } S_1 = 0.40 \text{ sq in. and } S_2 = 31.2 \text{ sq in.)}$$

$$K_{\phi_V} = 0.687 \text{ figure 5.3.1.2-12 at } (r_1/b)_V = 0.200$$

$$(C_{N_a})_V = 2.12 \text{ per rad (based on } S_{V_e}) \text{ (sample problem, paragraph C, Section 5.3.1.2)}$$

$$C_{Y_{V(K,\phi)}} = [K'_V - K_{\phi_V} \alpha \tan \Lambda_{LE_V}] (-C_{N_a})_V \beta \frac{S_{V_e}}{S_w} \quad (\text{equation 5.3.1.2-d})$$

$$= [1.13 - (0.687)(0.209) \tan 32.5^\circ] (-2.12) (0.070) \left(\frac{31.6}{144.0} \right)$$

$$\approx -0.0339 \text{ (based on } S_w)$$

For the purpose of finding vortex characteristics:

$$\frac{x_s}{r} = 10.6 \text{ (figure 4.3.1.3-13a at } \alpha' = 12.65^\circ)$$

Vortex separation is forward of exposed wing root-chord leading edge.

$$\frac{\alpha'(x - x_s - c_{re})}{r} = 0.221 \left(\frac{32.8}{1.50} - 10.6 - \frac{8.90}{1.50} \right) = 1.180$$

$$\left. \begin{aligned} \frac{y_0}{r} &= 0.63 \text{ (figure 4.3.1.3-14)} \\ \frac{z_0}{r} &= 1.25 \text{ (figure 4.3.1.3-13b)} \\ \frac{\Gamma_B}{2\pi\alpha' V r} &= 0.62 \text{ (figure 4.3.1.3-15)} \end{aligned} \right\} \text{ at } \frac{\alpha'(x - x_s - c_{re})}{r}$$

$$\phi = 18.4^\circ \text{ (sample problem, paragraph C, Section 5.3.1.2)}$$

then the positions of the body vortices at the vertical tail (neglecting the effect of the wing-flow field in altering the paths of the vortices) are:

$$\frac{z_{v1}}{b_v} = \frac{r}{b_v} \left[\frac{z_0}{r} \cos \phi + \frac{y_0}{r} \sin \phi \right] \quad (\text{equation 5.3.1.2-f})$$

$$= \frac{1.50}{7.48} [1.25 \cos 18.4^\circ + 0.63 \sin 18.4^\circ] = 0.278$$

$$\frac{y_{v1}}{b_v} = \frac{r}{b_v} \left[\frac{z_0}{r} \sin \phi - \frac{y_0}{r} \cos \phi \right] \quad (\text{equation 5.3.1.2-f})$$

$$= \frac{1.50}{7.48} [1.25 \sin 18.4^\circ - 0.63 \cos 18.4^\circ] = -0.0408$$

$$\frac{z_{v2}}{b_v} = \frac{r}{b_v} \left[\frac{z_0}{r} \cos \phi - \frac{y_0}{r} \sin \phi \right] \quad (\text{equation 5.3.1.2-f})$$

$$= \frac{1.50}{7.48} [1.25 \cos 18.4^\circ - 0.63 \sin 18.4^\circ] = 0.198$$

$$\frac{y_{v2}}{b_v} = \frac{r}{b_v} \left[\frac{z_0}{r} \sin \phi + \frac{y_0}{r} \cos \phi \right] \quad (\text{equation 5.3.1.2-f})$$

$$= \frac{1.50}{7.48} [1.25 \sin 18.4^\circ + 0.63 \cos 18.4^\circ] = 0.199$$

$$\begin{aligned} i_{v1} &= -0.9 \\ i_{v2} &= -0.6 \end{aligned} \quad \left. \right\} \quad (\text{figure 5.3.1.2-13a})$$

$$\Delta i_v = i_{v1} - i_{v2} = (-0.9) - (-0.6) = -0.3$$

$$C_{Y_{V(\Gamma_B)}} = \Delta i_v \left[\frac{\Gamma_B}{2\pi \alpha' V r} \right] \left[\frac{(-C_{N_a})_v \alpha' S_{U_e}}{\left(\frac{b_v}{r} - 1 \right) S_w} \right] \quad (\text{equation 5.3.1.2-e})$$

$$= (-0.3) (0.62) \left[\frac{(-2.12)(0.221)(31.6)}{\left(\frac{7.48}{1.5} - 1 \right) (144.0)} \right]$$

$$= 0.00478 \text{ (based on } S_w)$$

Determine tail effectiveness parameter η_{w_v}

By interpolation using figures 5.6.1.2-9g, -9h, and -9i, obtain $\eta_{w_v} = 0.98$ (see steps 1 through 5, page 5.6.1.2-3)

$$\begin{aligned} C_{Y_{V(\eta)}} &= [C_{Y_{V(\kappa, \phi)}} + C_{Y_{V(\Gamma_B)}}] \eta_{w_v} \quad (\text{equation 5.6.1.2-c'}) \\ &= [(-0.0339) + (0.00478)] (0.98) \\ &= -0.0285 \text{ (based on } S_w) \end{aligned}$$

Determine the ventral fin contribution $C_{Y_{U(\eta)}}$

$$K'_U = 3.15 \text{ (method of paragraph C, Section 5.3.1.1 with } S_3 \approx S_{U_e} = 8.54 \text{ sq in.})$$

$$K_{\phi_U} = 0.535 \text{ (figure 5.3.1.2-12 at } (r_1/b)_U = 0.492)$$

$$C_{N_a}_U = 1.09 \text{ per rad (based on } S_{U_e}) \text{ (sample problem, paragraph C, Section 5.3.1.2)}$$

$$\begin{aligned} C_{Y_U} = C_{Y_{U(\kappa, \phi)}} &= [K'_U + K_{\phi_U} \alpha \tan \Lambda_{LE_U}] (-C_{N_a})_U \beta \frac{S_{U_e}}{S_w} \quad (\text{equation 5.3.1.2-g}) \\ &= [3.15 + (0.535)(0.209) \tan 70^\circ] (-1.09)(0.070) \left(\frac{8.54}{144.0} \right) \\ &= -0.0156 \text{ (based on } S_w) \end{aligned}$$

Determine the tail effectiveness parameter η_{w_U}

By interpolation using figures 5.6.1.2-9g, -9h, and -9i, obtain $\eta_{w_U} = 1.20$ (see steps 1 through 5, page 5.6.1.2-3)

$$\begin{aligned} C_{Y_{U(\eta)}} &= C_{Y_U} \eta_{w_U} && \text{(equation 5.6.1.2-d')} \\ &= (-0.0156) (1.20) \\ &= -0.0187 \text{ (based on } S_w) \end{aligned}$$

Determine total empennage contribution

$$\begin{aligned} C_{Y_{HVU(WB)}} &= C_{Y_{H(B)}} + C_{Y_{V(\eta)}} + C_{Y_{U(\eta)}} && \text{(equation 5.6.1.2-b)} \\ &= 0 + (-0.0285) + (-0.0187) \\ &= -0.0472 \text{ (based on } S_w) \end{aligned}$$

Solution:

$$\begin{aligned} C_{Y_{WBHVU}} &= C_{Y_{WB}} + C_{Y_{HVU(WB)}} && \text{(equation 5.6.1.2-a)} \\ &= (-0.0400) + (-0.0472) \\ &= -0.0872 \text{ (based on } S_w) \end{aligned}$$

This compares with an experimental value (based on S_w) of $C_{Y_{WBHVU}} = -0.096$ from reference 3.

REFERENCES

1. Kaattari, G. E.: Estimation of Directional Stability Derivatives at Moderate Angles and Supersonic Speeds. NACA Memo 12-1-58A, 1959. (U)
2. Nielsen, J. N.: The Effect of Body Vortices and the Wing Shock-Expansion Field on the Pitch-Up Characteristics of Supersonic Airplanes. NACA RM A57L28, 1958. (C) Title Unclassified.
3. Spearman, L. M., Driver, C., and Hughes, W. C.: Investigation of Aerodynamic Characteristics in Pitch and Sideslip of a 45° Sweptback-Wing Airplane Model with Various Vertical Locations of Wing and Horizontal Tail. NACA RM L54L06, 1955. (U)

- - - DATCOM METHOD
 ○ EXPERIMENT

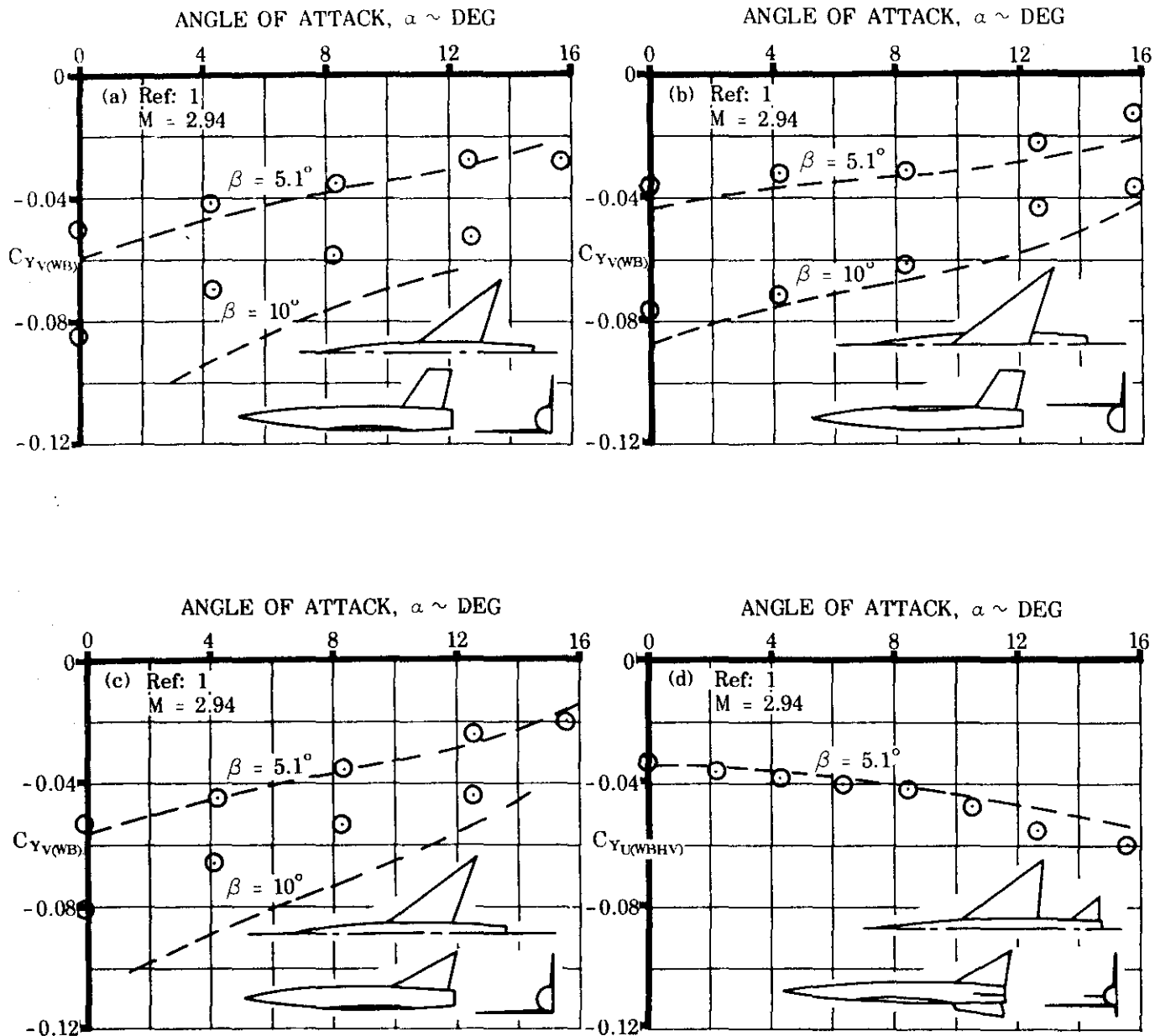


FIGURE 5.6.1.2-8 COMPARISON OF EXPERIMENTAL AND CALCULATED SIDE-FORCE COEFFICIENT INCREMENTS DUE TO ADDING A VERTICAL TAIL TO A WING-BODY

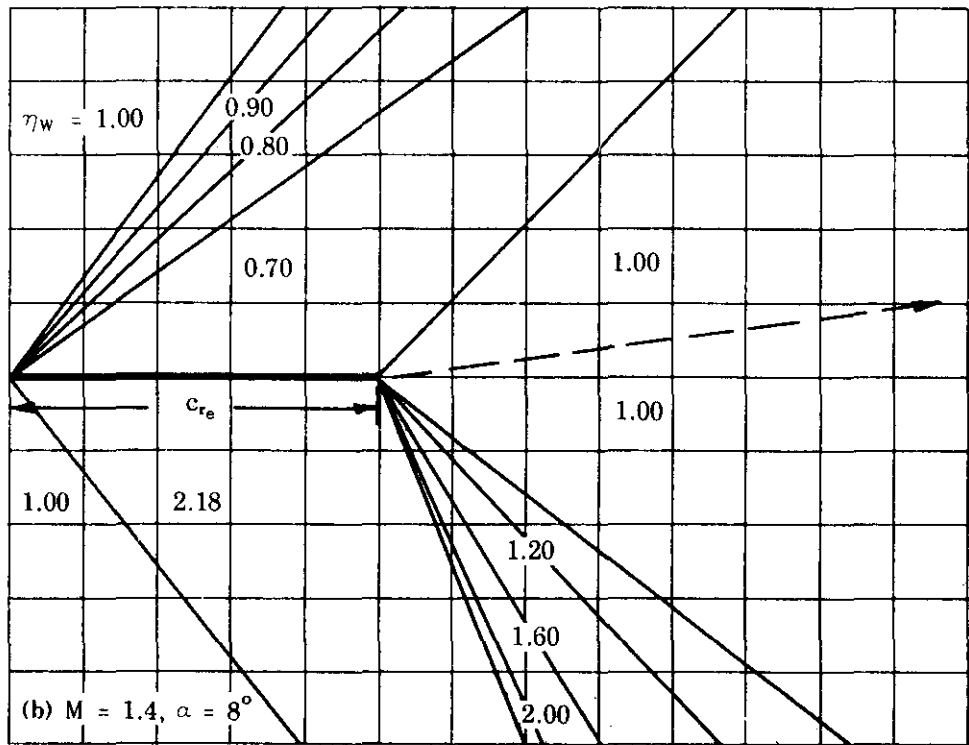
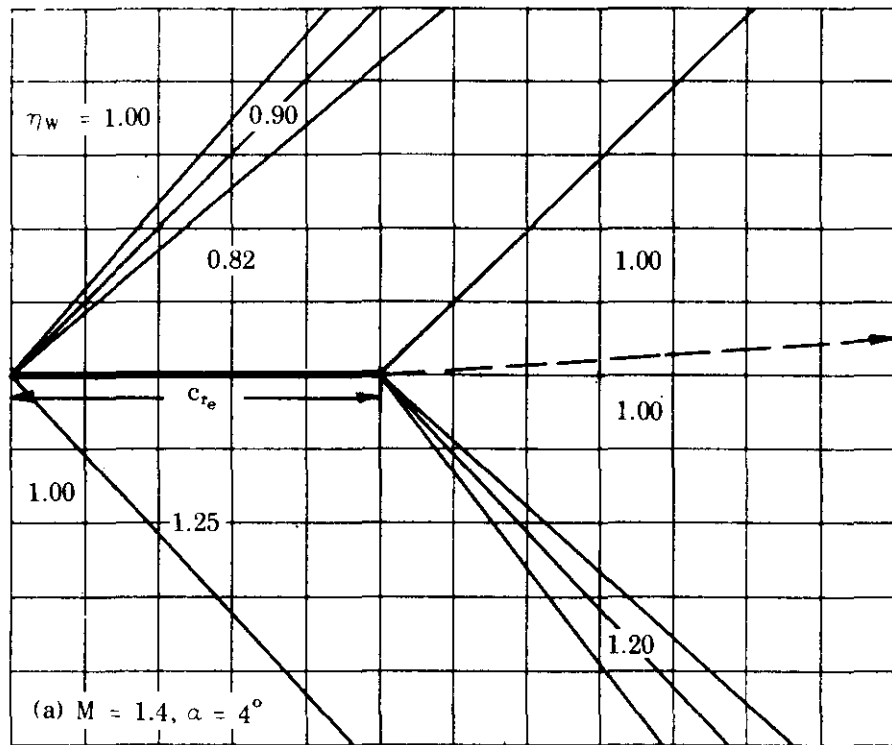


FIGURE 5.6.1.2-9 TAIL EFFECTIVENESS PARAMETER

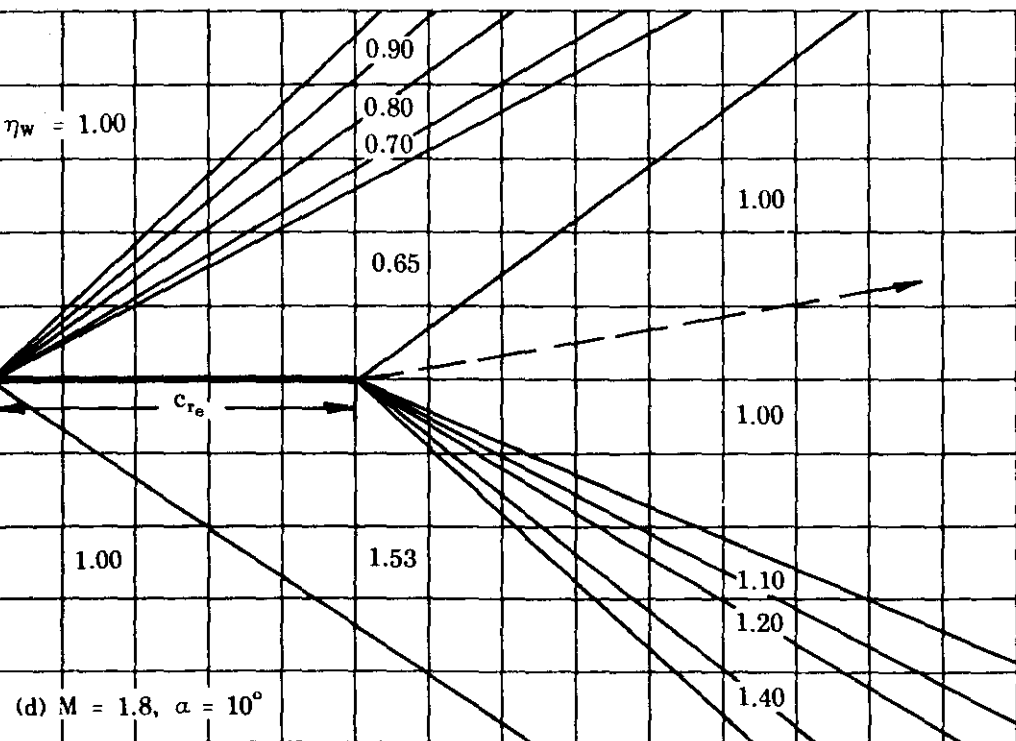
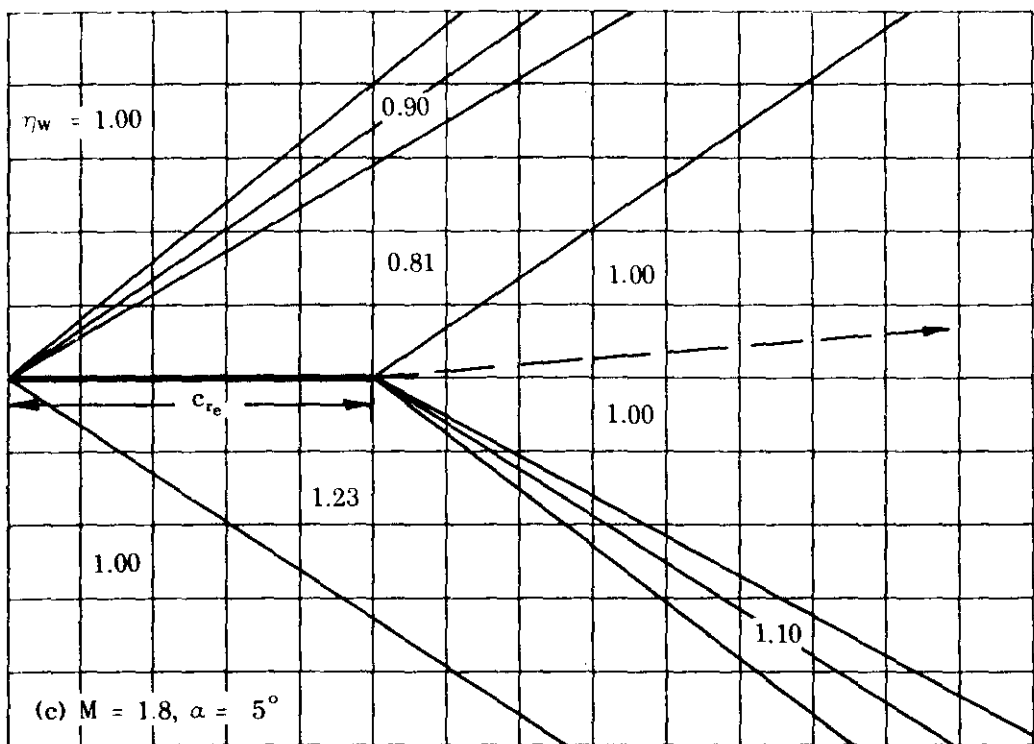


FIGURE 5.6.1.2-9 TAIL EFFECTIVENESS PARAMETER (contd)

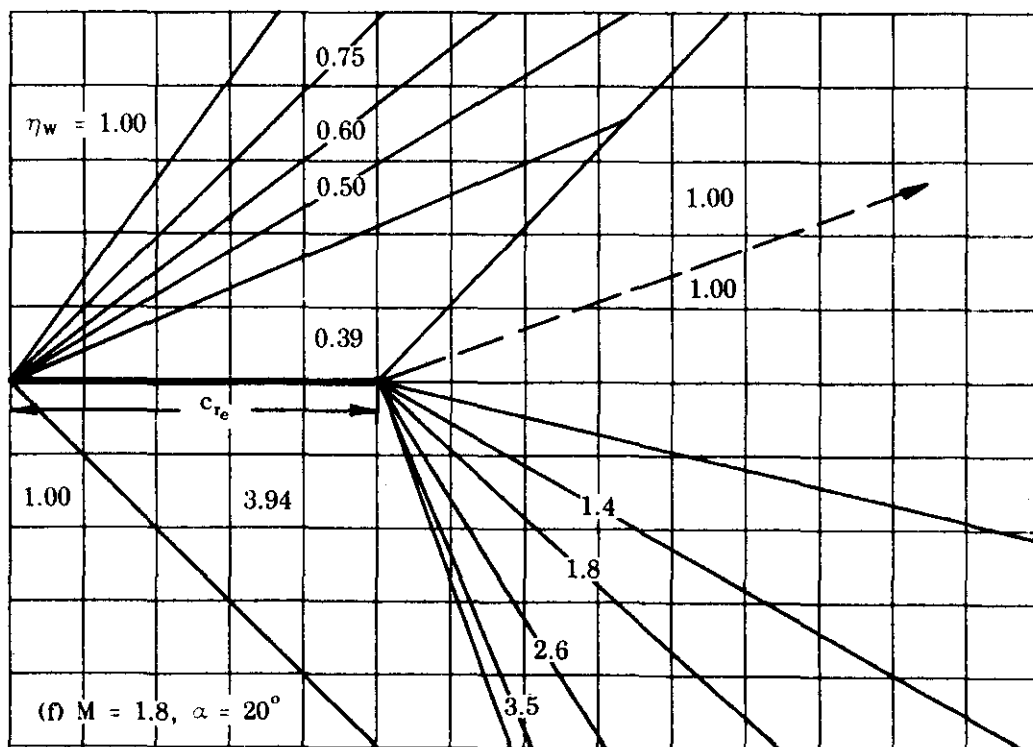
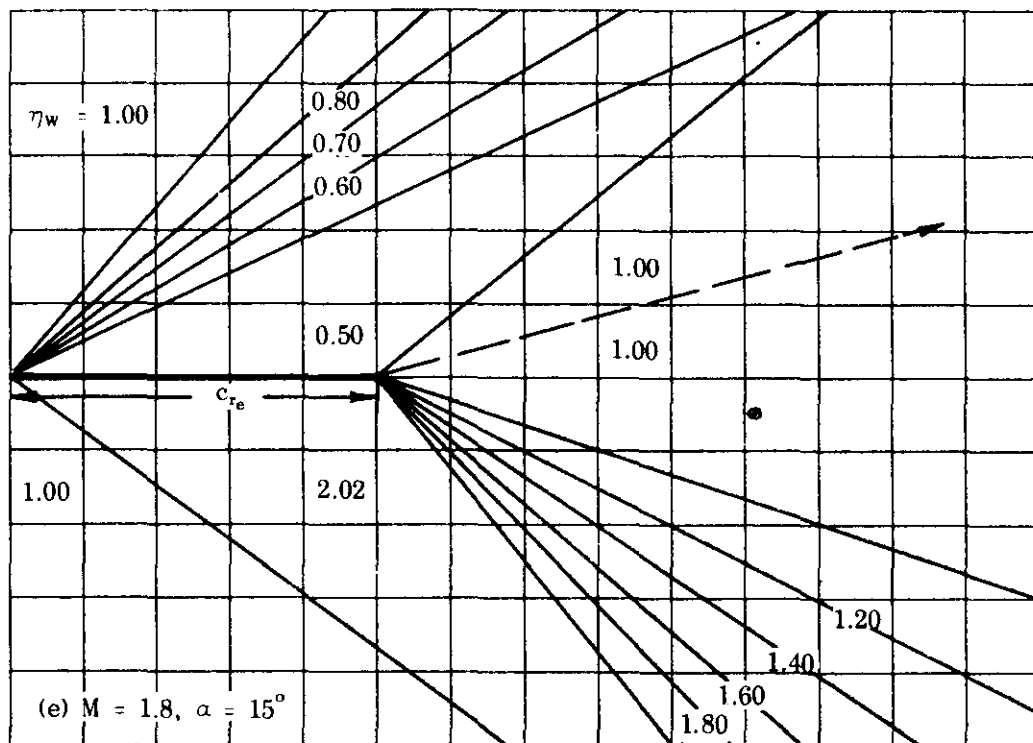


FIGURE 5.6.1.2-9 TAIL EFFECTIVENESS PARAMETER (contd)

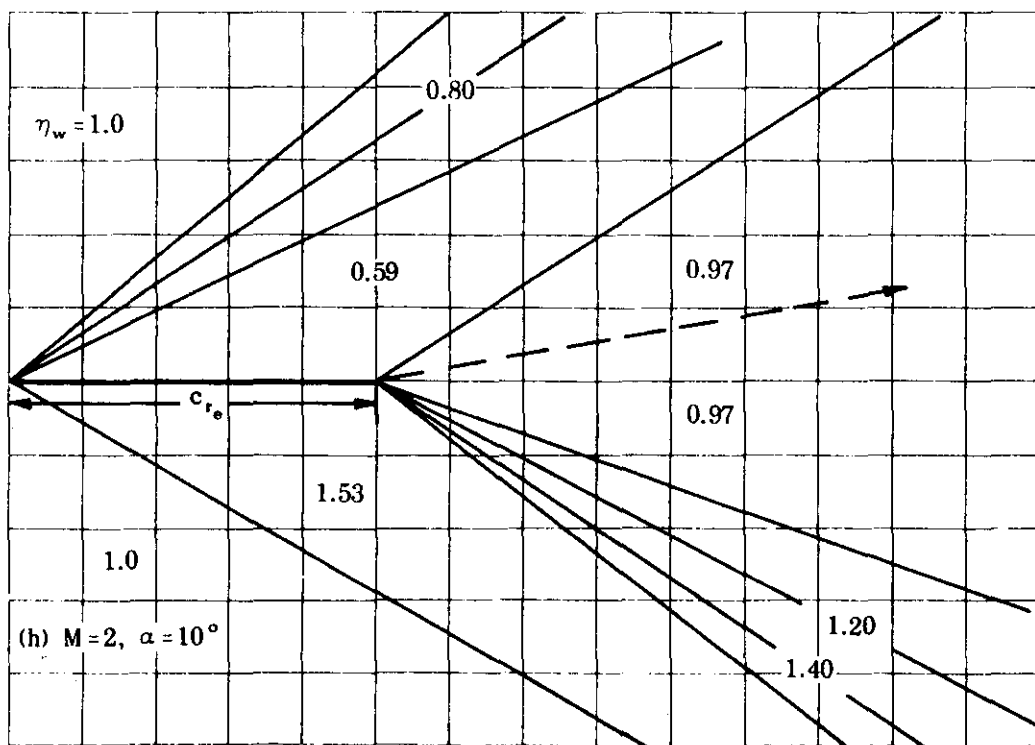
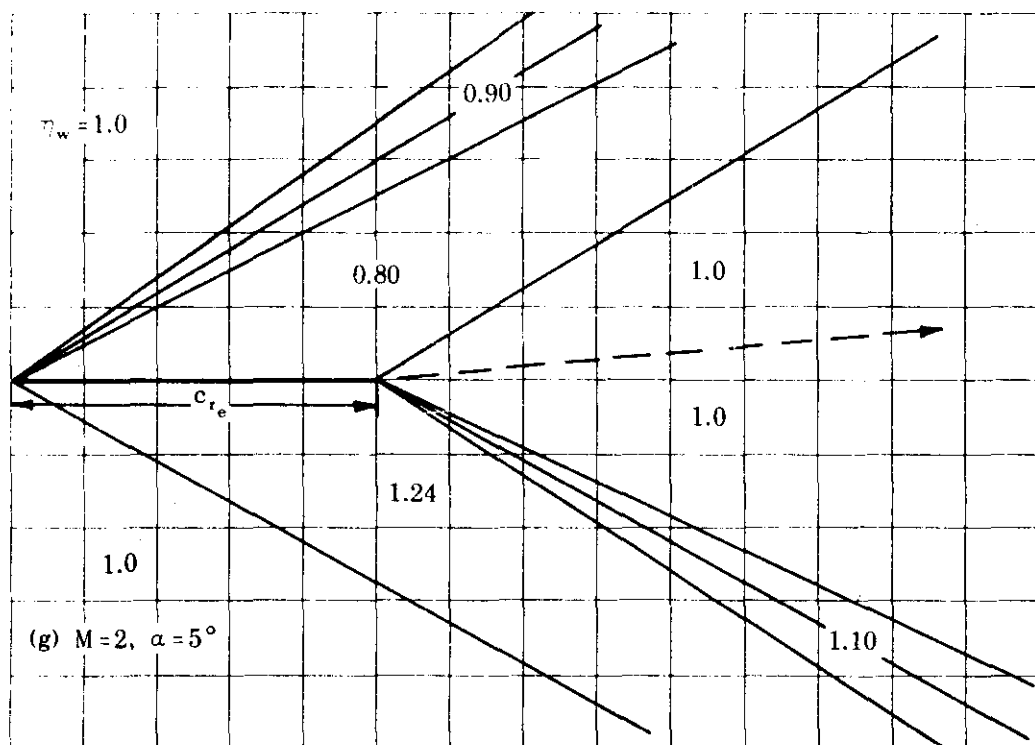
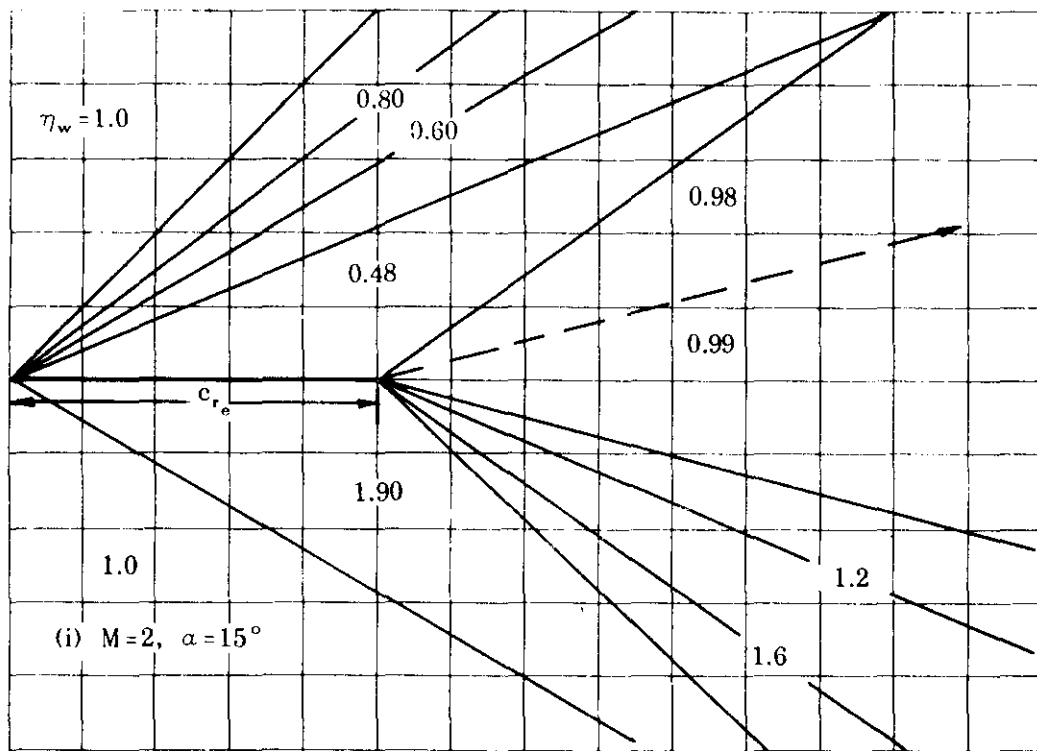


FIGURE 5.6.1.2-9 TAIL EFFECTIVENESS PARAMETER (contd)



(i) $M = 2, \alpha = 15^\circ$

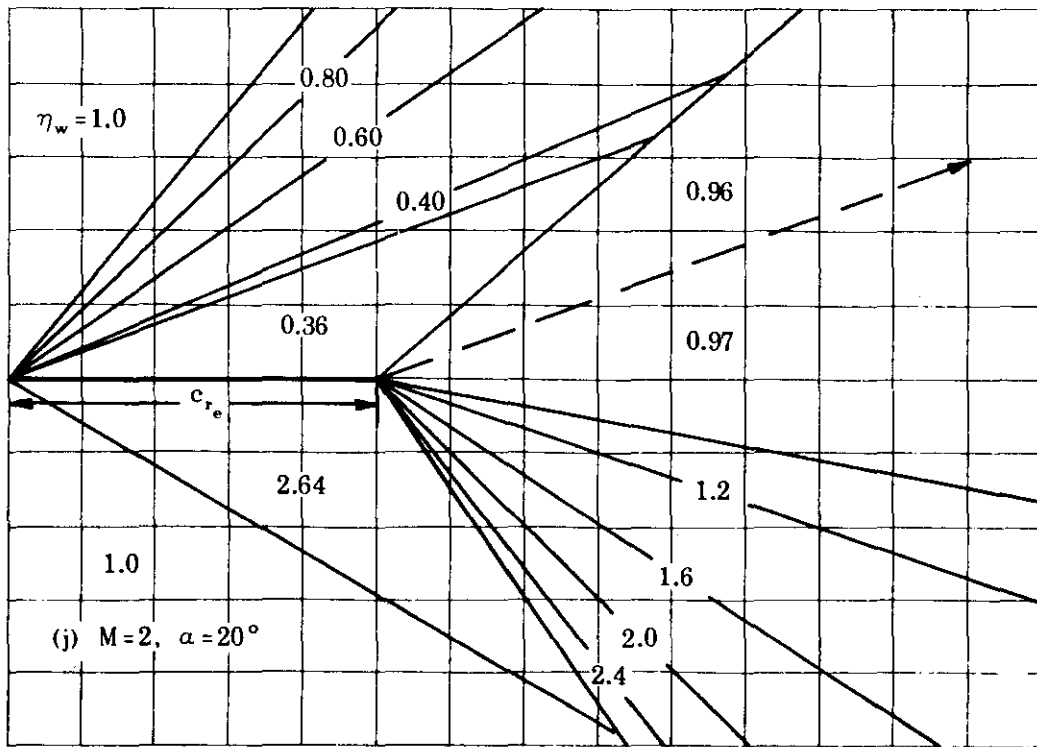


FIGURE 5.6.1.2-9 TAIL EFFECTIVENESS PARAMETER (contd)

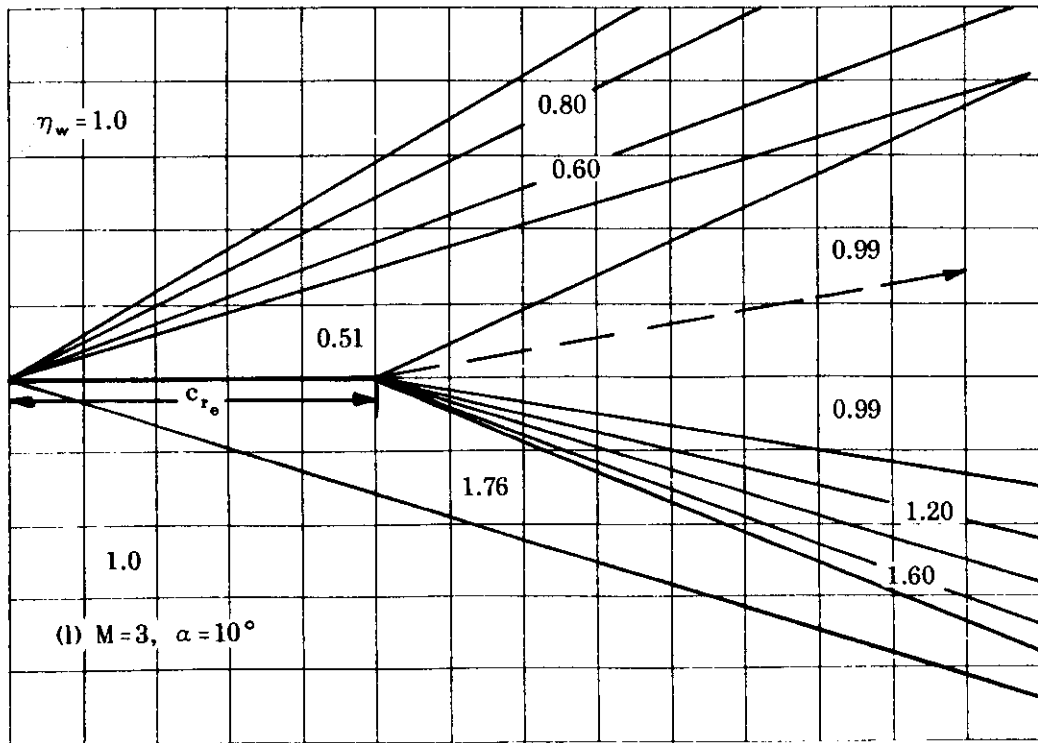
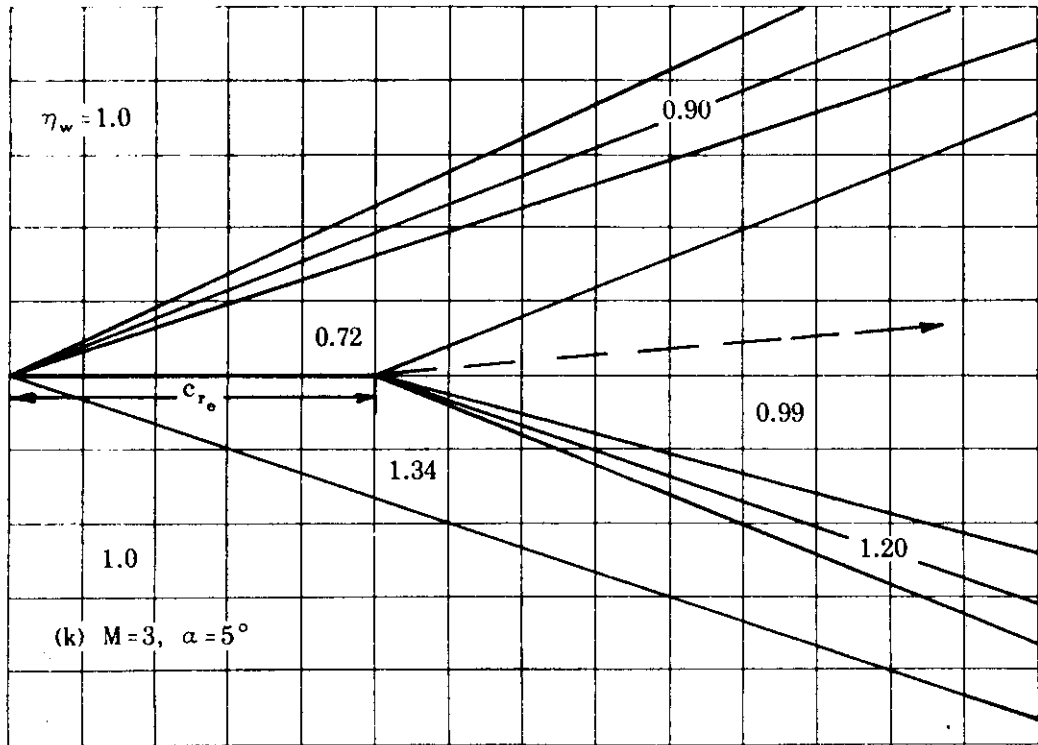


FIGURE 5.6.1.2-9 TAIL EFFECTIVENESS PARAMETER (contd)

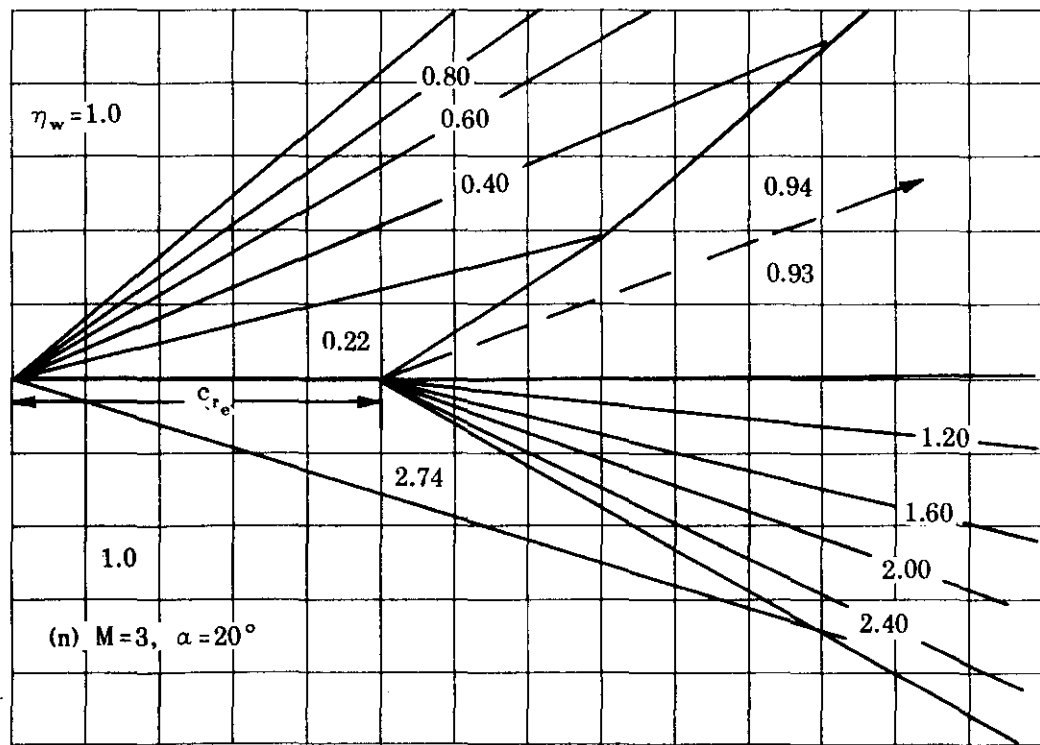
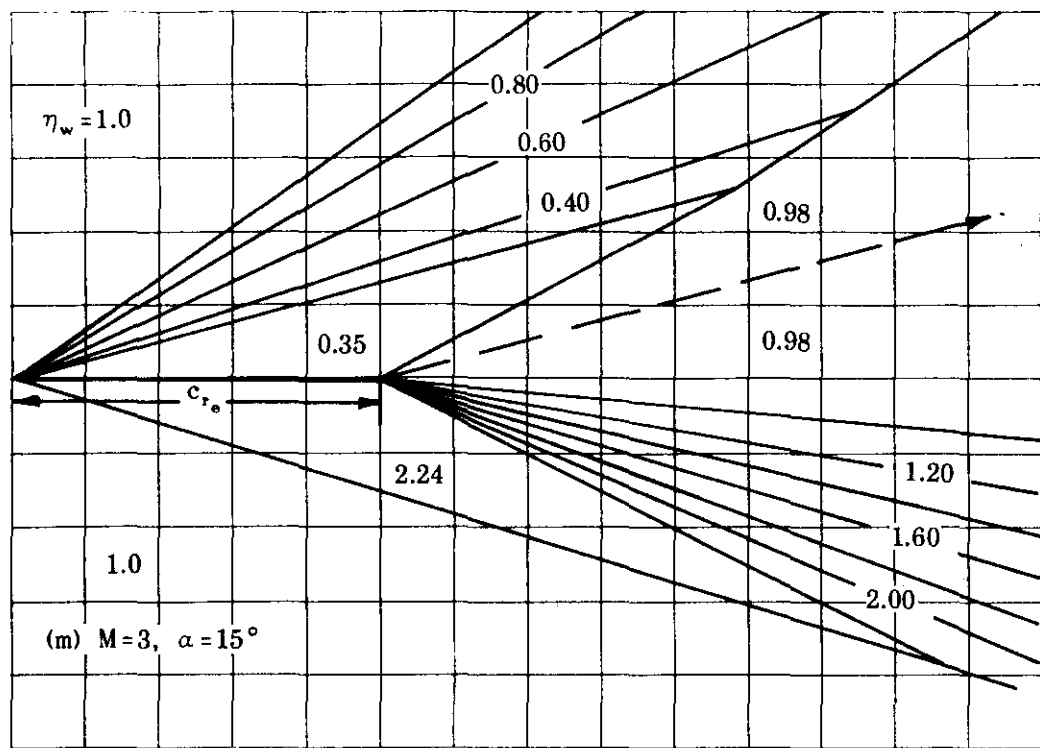


FIGURE 5.6.1.2-9 TAIL EFFECTIVENESS PARAMETER (contd)

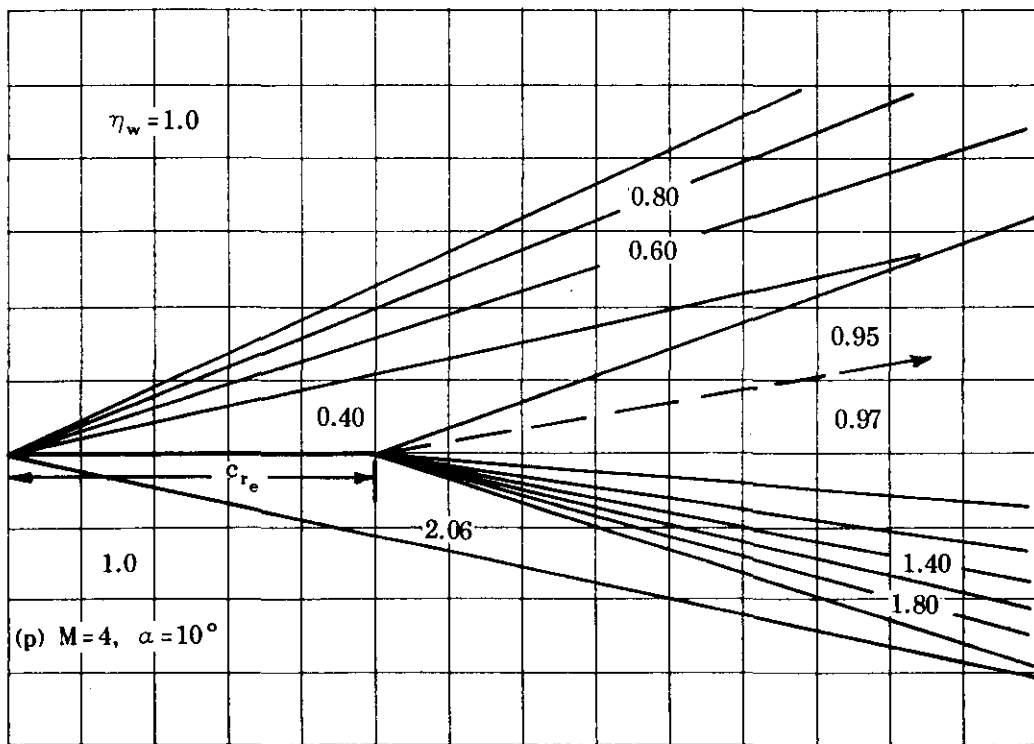
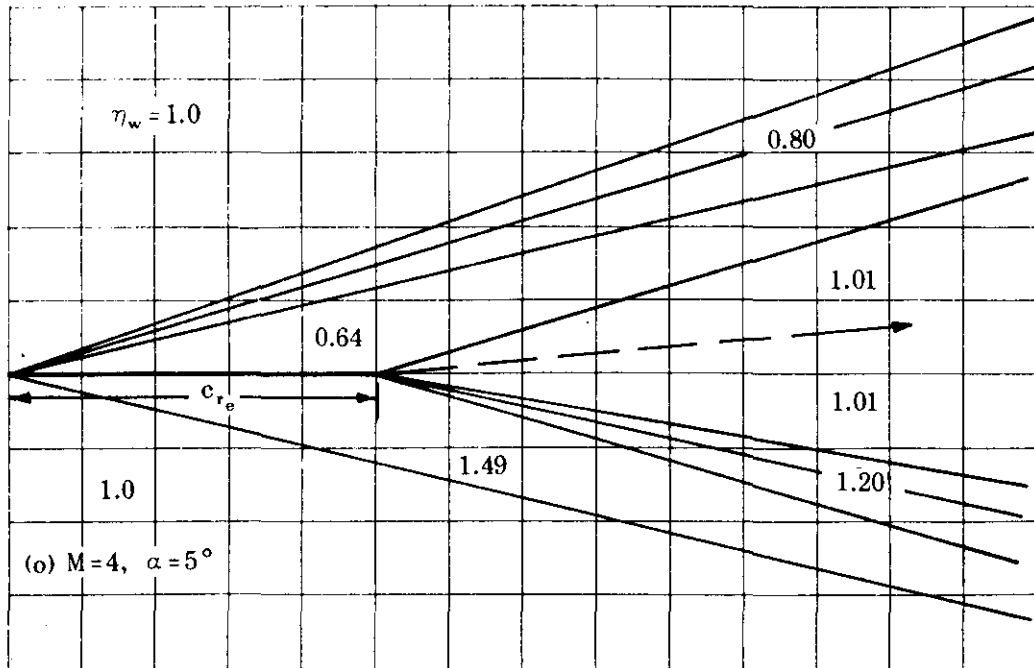


FIGURE 5.6.1.2-9 TAIL EFFECTIVENESS PARAMETER (contd)

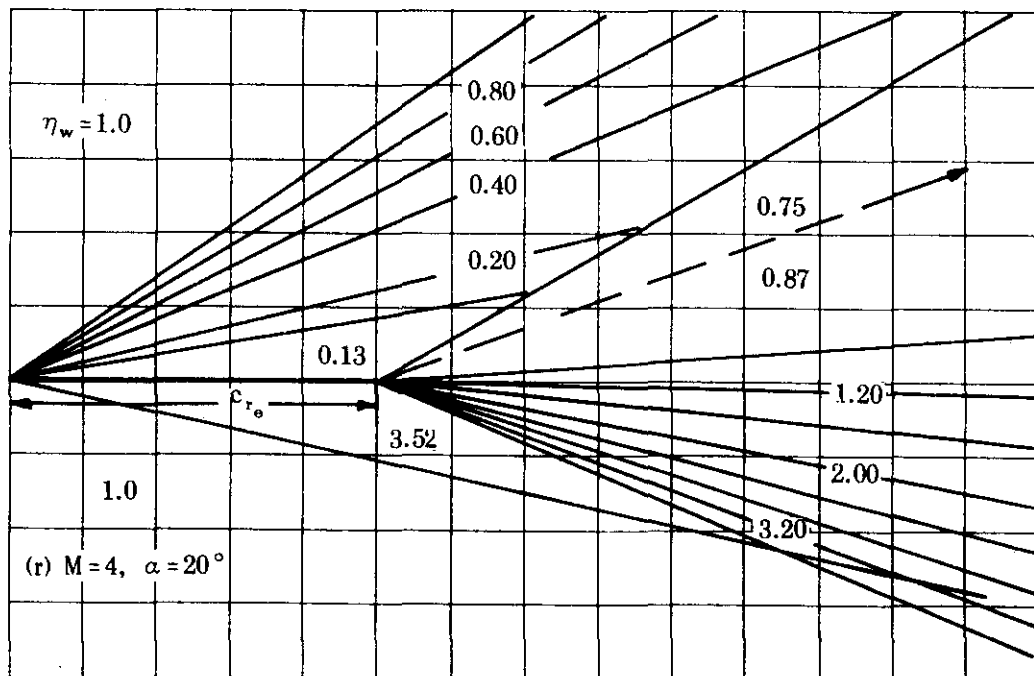
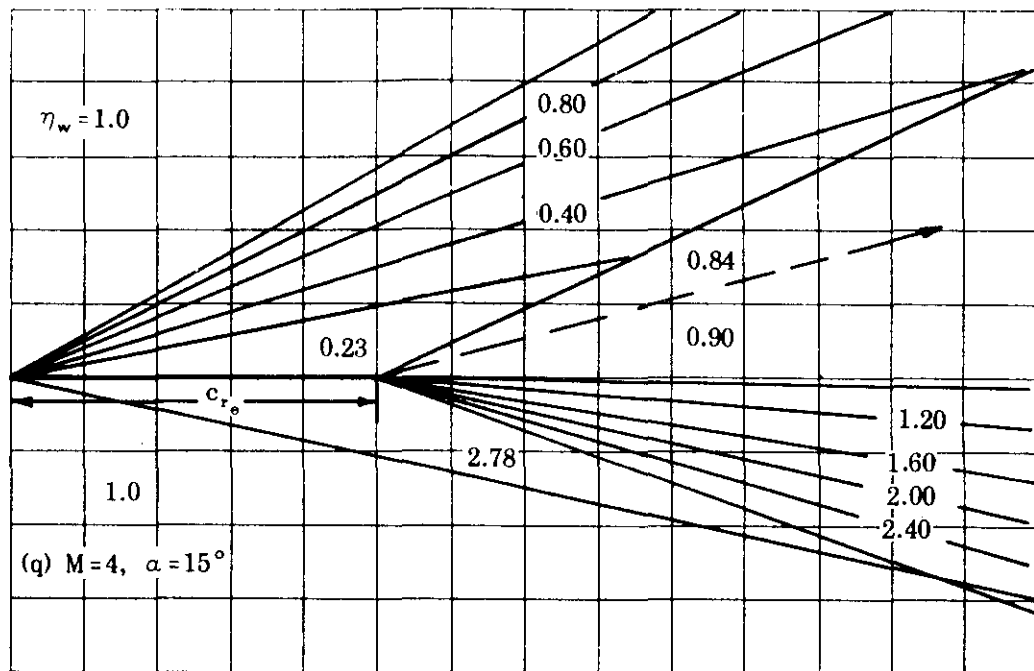


FIGURE 5.6.1.2-9 TAIL EFFECTIVENESS PARAMETER (contd)

5.6.2 WING-BODY-TAIL SIDESLIP DERIVATIVE C_{I_β}

5.6.2.1 WING-BODY-TAIL SIDESLIP DERIVATIVE C_{I_β} IN THE LINEAR ANGLE-OF-ATTACK RANGE

The information contained in this section is for estimating the rolling moment due to sideslip C_{I_β} of wing-body-tail configurations at low angles of attack. In general, it consists of a synthesis of material presented in other sections. Discussions of the various aerodynamic aspects of vehicle components and component combinations in sideslip are presented in other sections and are not repeated here.

The effect of a horizontal tail is more important in estimating C_{I_β} than C_{Y_β} and C_{n_β} , since the tail itself contributes to C_{I_β} in addition to affecting the vertical-panel contribution. The effect of the horizontal tail on the vertical-panel contribution and a discussion regarding the effects of the induced pressure field on the horizontal tail that is generated by the vertical panel are discussed in the introduction to Section 5.3.2.1 and are not repeated here.

For most configurations at subsonic speeds the horizontal-tail contribution is usually very small, and reasonable results can be obtained when it is neglected. However, for configurations employing a large horizontal tail with either significant twist and/or dihedral, the contribution may be worthy of consideration. For such a configuration the contribution of the horizontal tail may be estimated by using the method of Section 5.1.2.1; i.e., by treating the horizontal tail as an isolated wing. (Caution should be exercised to make certain the horizontal-tail contribution to C_{I_β} is converted to the same reference area and length $S_W b_W$ as the wing-body contribution, before adding them together.) However, since the horizontal-tail contribution is very small for most configurations in the subsonic speed regime, the method presented here neglects its contribution.

At transonic and supersonic speeds the horizontal-tail contribution should not be neglected. At transonic speeds the pressure field of the entire horizontal surface is affected by the presence of the vertical panel; while at supersonic speeds the effects are restricted to regions on the horizontal surface within boundaries defined by the shock-wave pattern of the vertical tail. Because of the complexity of the problem, no method is presented at transonic speeds. The method presented at supersonic speeds does not include the contribution of a horizontal tail; however, the effect of the horizontal tail on the vertical-tail contribution is accounted for as in Section 5.3.2.1.

The methods presented are similar to those of Section 5.6.1.1, in that the derivative of the configuration is given as the sum of the contributions of the wing-body combination and the empennage combination. The method of estimating the empennage contribution to C_{I_β} is similar to that for estimating the empennage contribution to C_{n_β} in Section 5.6.3.1. That is, the side-force contributions of the panels of the empennage are multiplied by an appropriate moment arm to obtain their individual contributions to the derivative C_{I_β} .

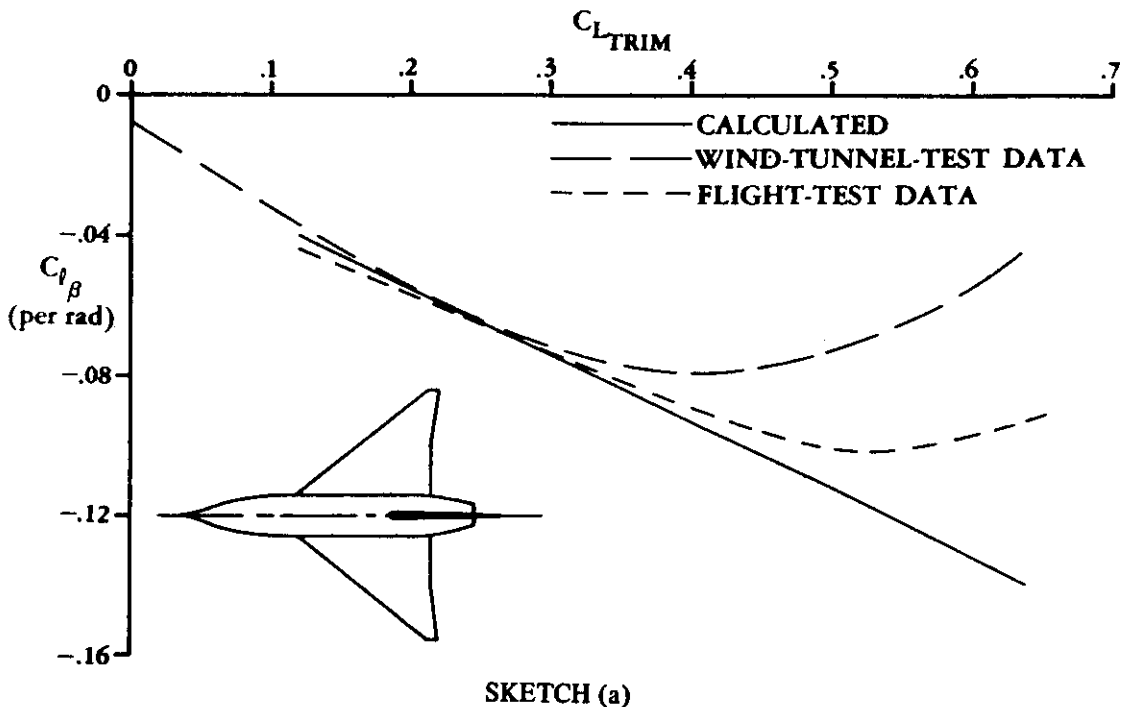
A. SUBSONIC

The method of estimating the subsonic values of the empennage contribution to the derivative C_{I_β} is based on the values of C_{Y_β} estimated by the methods of Paragraph A of Section 5.3.1.1. If the apparent-mass-concept method (Method 3, Paragraph A, Section 5.3.1.1) is used, the build-up

procedure outlined in Method 3 of Paragraph A of Section 5.6.1.1 must be applied in determining the individual side-force derivatives, with one exception. That is, the horizontal-tail increment is not to be expressed explicitly as a contributing term in the total empennage contribution; however, the effect of the presence of the horizontal tail must be considered in computing the contributions of the vertical panels.

For most configurations, the presence of flaps at a given lift coefficient causes $C_{l\beta}$ to become a larger negative value (see References 1 through 7). The exceptions to this are a few cases at low lift coefficients where $C_{l\beta}$ becomes a lower negative value (References 8, 9, and 10). However, the incremental changes in $C_{l\beta}$ vary dramatically with variations in lift coefficient for different configurations. This variation in the incremental change in $C_{l\beta}$ with flaps extended prevents the formulation of a hand procedure to estimate the flap effects on $C_{l\beta}$.

Comparison of the subsonic method presented here with available flight-test data (References 11 through 15) supplements the substantiation of the method based on wind-tunnel data that is presented in Sections 5.2.2.1 and 5.3.2.1. A typical comparison of flight-test data (Reference 11) with the predicted variation of $C_{l\beta}$ as a function of $C_{L_{\text{TRIM}}}$ is shown in Sketch (a).



As implied in the introduction to this section, the Datcom method at subsonic speeds is applicable to a configuration with a horizontal tail in the empennage.

DATCOM METHOD

The rolling moment (about the longitudinal stability axis) due to sideslip of a wing-body-tail configuration, referred to an arbitrary moment center and based on wing area and wing span, is given by

$$C_{I_\beta} = (C_{I_\beta})_{WB} + \sum_p \left\{ (\Delta C_{Y_\beta})_p \left[\frac{z_p \cos \alpha - l_p \sin \alpha}{b_w} \right] \right\} \quad 5.6.2.1-a$$

where

p is the subscript referring to the vertical panels present in the empennage (either an upper vertical stabilizer V or a lower vertical stabilizer U).

$(C_{I_\beta})_{WB}$ is the contribution of the wing-body configuration to the total rolling moment due to sideslip, obtained from Paragraph A, Section 5.2.2.1.

$(\Delta C_{Y_\beta})_p$ is the side force due to sideslip of the added vertical panel determined as follows:

For configurations with the horizontal panel mounted on the body or for configurations with no horizontal panel, use Method 1 or Method 3, Paragraph A, Section 5.3.1.1. If Method 1 of Paragraph A of Section 5.3.1.1 is used, the total empennage increment is given by a single term. If Method 3 of Paragraph A of Section 5.3.1.1 is used, the build-up procedure outlined in Method 3 of Paragraph A of Section 5.6.1.1 must be applied to determine the individual increment of each added vertical panel*.

For configurations with a horizontal panel mounted on the vertical panel, use Method 1, Paragraph A, Section 5.3.1.1. The total empennage increment is given by a single term.

For configurations with twin vertical panels mounted on the tips of a horizontal panel, use Method 2, Paragraph A, Section 5.3.1.1. The total empennage increment is given by a single term.

z_p is the distance measured normal to the longitudinal body axis between the moment reference center and the MAC of the vertical panel, positive for the panel above the body.

l_p is the distance parallel to the longitudinal body axis between the vehicle moment center and the quarter-chord point of the MAC of the vertical panel, positive for the panel aft of the vehicle moment center.**

b_w is the span of the wing.

All geometry used in determining the moment arms for the above method is based on the vertical panel extended to the body center line.

*See remarks of Paragraph A above, regarding horizontal-panel effects when using Method 3 of Paragraph A of Section 5.3.1.1.

**The aerodynamic center of the vertical panel could be used, but the inaccuracies of the basic method do not warrant this degree of refinement.

For a wingless configuration, b_w is replaced by the vehicle reference length, $(\Delta C_{Y_\beta})_p$ is based on the vehicle reference area, and the contribution of the body alone to the total derivative may be ignored.

Sample Problems

- Given: A configuration of Reference 16 consisting of a wing, body, horizontal tail, and vertical tail. This is the same configuration as that of Sample Problem 1, Paragraph A, Section 5.6.1.1. Some of the characteristics are repeated.

Wing Characteristics:

$$A_w = 4.0 \quad S_w = 36.0 \text{ sq in.} \quad b_w = 12.0 \text{ in.} \quad \lambda_w = 0.30$$

$$\Lambda_{c/2_w} = 40.9^\circ \quad \Gamma = 0 \quad z_w = 0 \text{ (midwing)}$$

Additional Characteristics:

$$M = 0.60 \quad l_v = 6.035 \text{ in.} \quad z_v = 1.65 \text{ in.} \quad l_f = 14.3 \text{ in.}$$

C_L	$\alpha \text{ (deg) (test)}$
0	0
0.1	1.55
0.2	3.20
0.3	4.65

Compute:

$$\frac{l_f}{b_w} = 1.192$$

$$\left(\frac{C_{I_\beta}}{C_L} \right)_{\Lambda_{c/2_w}} = -0.0035 \text{ per deg} \quad (\text{Figure 5.1.2.1-27})$$

$$\cos \Lambda_{c/2_w} = 0.755$$

$$M \cos \Lambda_{c/2_w} = 0.453$$

$$\frac{A_w}{\cos \Lambda_{c/2_w}} = 5.30$$

$$K_{M_A} = 1.035 \quad (\text{Figure 5.1.2.1-28a})$$

$$K_f = 0.91 \quad (\text{Figure 5.2.2.1-26})$$

$$\left(\frac{C_{I_\beta}}{C_L} \right)_A = -0.001 \quad (\text{Figure 5.1.2.1-28b})$$

$$\begin{aligned} \left(C_{I_\beta} \right)_{WB} &= C_L \left[\left(\frac{C_{I_\beta}}{C_L} \right)_{A_{c/2_W}} K_{M_A} K_f + \left(\frac{C_{I_\beta}}{C_L} \right)_A \right] \text{ per deg} \quad (\text{Equation 5.2.2.1-c}) \\ &= C_L [(-0.0035)(1.035)(0.91) + (-0.001)] \\ &= -0.0043 C_L \text{ per deg} \end{aligned}$$

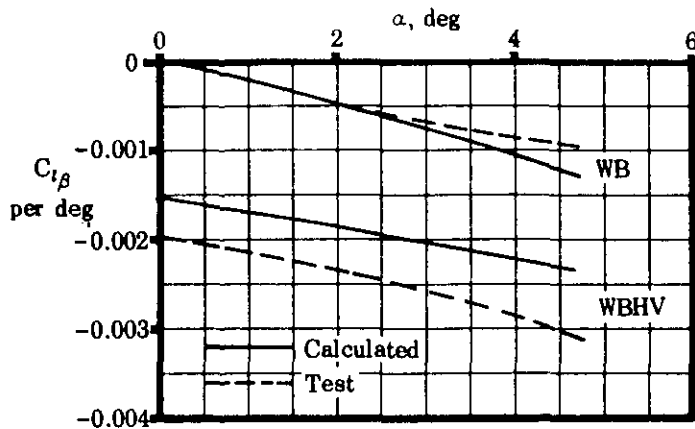
$$\begin{aligned} \left(\Delta C_{Y_\beta} \right)_{V(WBH)} &= -0.645 \text{ per rad} \quad (\text{Sample Problem 1, Paragraph A, Section 5.6.1.1}) \\ &= -0.01125 \text{ per deg (based on } S_W) \end{aligned}$$

Solution:

$$\begin{aligned} C_{I_\beta} &= \left(C_{I_\beta} \right)_{WB} + \sum_p \left\{ \left(\Delta C_{Y_\beta} \right)_p \left[\frac{z_p \cos \alpha - l_p \sin \alpha}{b_W} \right] \right\} \quad (\text{Equation 5.6.2.1-a}) \\ &= \left(C_{I_\beta} \right)_{WB} + \left(\Delta C_{Y_\beta} \right)_{V(WBH)} \left[\frac{z_V \cos \alpha - l_V \sin \alpha}{b_W} \right] \\ &= -0.0043 C_L + (-0.01125) \left(\frac{1.65 \cos \alpha - 6.035 \sin \alpha}{12.0} \right) \text{ per deg (based on } S_W b_W) \end{aligned}$$

(1)	(2)	(3)	(4)	(5)	(6)	(7)	(8)
C_L	α (deg)	$(C_{I_\beta})_{WB}$ (per deg)	$z_V \cos \alpha$ (in.)	$l_V \sin \alpha$ (in.)	$\frac{z_V \cos \alpha - l_V \sin \alpha}{b_W}$ $[(4) - (5)]/12.0$	$(C_{I_\beta})_{V(WBH)}$ (per deg)	C_{I_β} (per deg)
0	0	0	1.660	0	0.1375	-0.00155	-0.00155
0.1	1.55	-0.00043	1.649	0.163	0.1235	-0.00139	-0.00182
0.2	3.20	-0.00086	1.647	0.337	0.1090	-0.00123	-0.00209
0.3	4.66	-0.00129	1.644	0.490	0.0962	-0.00108	-0.00237

These results are compared with experimental results from Reference 16 in Sketch (b).



SKETCH (b)

2. Given: The configuration of Reference 17 consisting of a wing, body, horizontal tail, and vertical tail. This is the same configuration as that of Sample Problem 3, Paragraph A, Section 5.6.1.1. Some of the characteristics are repeated.

Wing Characteristics:

$$A_w = 3.0 \quad S_w = 576 \text{ sq in.} \quad b_w = 41.56 \text{ in.} \quad \lambda_w = 0$$

$$\Lambda_{c/2w} = 33.6^\circ \quad \Gamma = 0 \quad z_w = -2.08 \text{ in.}$$

Additional Characteristics:

$$M = 0.25 \quad l_v = 24.89 \text{ in.} \quad z_v = 5.78 \text{ in.} \quad l_f = 51.13 \text{ in.}$$

$$d = 6.0 \text{ in.} \quad h = 6.0 \text{ in.}$$

c_L	α (deg) (test)
0	0
0.1	2.0
0.2	4.0
0.3	5.7

Compute:

$$\frac{l_f}{b_w} = 1.23$$

$$\left(\frac{C_{I_\beta}}{C_L} \right)_{\Lambda_{c/2} w} = -0.0027 \text{ per deg} \quad (\text{Figure 5.1.2.1-27c})$$

$$\cos \Lambda_{c/2} w = 0.8329$$

$$M \cos \Lambda_{c/2} w = 0.2082$$

$$\frac{A}{\cos \Lambda_{c/2} w} = 3.60$$

$$K_M A = 1.000 \quad (\text{Figure 5.1.2.1-28a})$$

$$K_f = 1.000 \quad (\text{Figure 5.2.2.1-26})$$

$$\left(\frac{C_{I_\beta}}{C_L} \right)_A = -0.001 \quad (\text{Figure 5.1.2.1-28b})$$

$$\left(\Delta C_{I_\beta} \right)_{z_w} = \frac{1.2 \sqrt{A}}{57.3} \frac{z_w}{b} \left(\frac{2d}{b} \right) \text{ per deg} \quad (\text{Equation 5.2.2.1-c})$$

$$= \frac{(1.2)(1.732)}{57.3} \left(\frac{-2.08}{41.56} \right) (0.2885)$$

$$= -0.000524 \text{ per deg}$$

$$\left(C_{I_\beta} \right)_{WB} = C_L \left[\left(\frac{C_{I_\beta}}{C_L} \right)_{\Lambda_{c/2} w} K_M A K_f + \left(\frac{C_{I_\beta}}{C_L} \right)_A \right] + \left(\Delta C_{I_\beta} \right)_{z_w} \text{ per deg} \quad (\text{Equation 5.2.2.1-c})$$

$$= C_L [(-0.0027)(1.00)(1.00) + (-0.001)] + (-0.00052)$$

$$= -0.0037 C_L - 0.00052$$

$$\left(\Delta C_{Y_\beta} \right)_{V(WB)} = 0.665 \text{ per rad} \quad (\text{Sample Problem 3, Paragraph A, Section 5.6.1.1})$$

$$= -0.0116 \text{ per deg} \quad (\text{based on } S_w)$$

Solution:

$$C_{I_\beta} = (C_{I_\beta})_{WB} + \sum_p \left\{ (\Delta C_{Y_\beta})_p \left[\frac{z_p \cos \alpha - l_p \sin \alpha}{b_w} \right] \right\} \quad (\text{Equation 5.6.2.1-a})$$

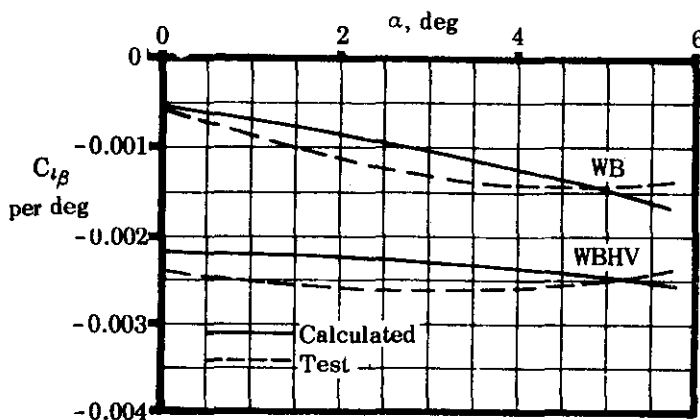
$$= (C_{I_\beta})_{WB} + (\Delta C_{Y_\beta})_{V(WBH)} \left[\frac{z_V \cos \alpha - l_V \sin \alpha}{b_w} \right]$$

$$= -0.0037 C_L - 0.00052 + (-0.0116) \left(\frac{5.78 \cos \alpha - 24.89 \sin \alpha}{41.56} \right)$$

per deg (based on $S_w b_w$)

	(1)	(2)	(3)	(4)	(5)	(6)	(7)	(8)
C_L	α (deg)	$(C_{I_\beta})_{WB}$ (per deg)	$z_V \cos \alpha$ (in.)	$l_V \sin \alpha$ (in.)	$\frac{z_V \cos \alpha - l_V \sin \alpha}{b_w}$	$(C_{I_\beta})_{V(WBH)}$ (per deg)	C_{I_β} (per deg)	
		-0.0037 -0.00052						
0	0	-0.00052	5.780	0	0.1390	-0.00161	-0.00213	
0.1	2.0	-0.00089	5.777	0.870	0.1180	-0.00137	-0.00226	
0.2	4.0	-0.00126	5.766	1.740	0.0969	-0.00112	-0.00238	
0.3	5.7	-0.00163	5.752	2.475	0.0790	-0.00092	-0.00255	

These results are compared with experimental results from Reference 17 in Sketch (c).



SKETCH (c)

B. TRANSONIC

A brief discussion of the flow phenomena associated with the forces generated on vertical panels at transonic speeds is given in Paragraph B of Section 5.3.1.1. At the present time there are no methods available to predict the effect of wing-body wake and sidewash or the mutual interference effects between vehicle components on the sideslip characteristics at transonic speeds. In addition, the effects of the impingement of the pressure field generated by the vertical panel on the horizontal-tail surface are difficult to evaluate.

DATCOM METHOD

No explicit method is available in the literature for estimating the vehicle sideslip derivative C_{I_β} at transonic speeds and none is presented in the Datcom. Some typical transonic data for this derivative are presented as Figure 5.6.2.1-15.

C. SUPERSONIC

The procedure for estimating the supersonic sideslip derivative C_{I_β} is essentially the same as that at subsonic speeds. That is, the rolling-moment contributions of vertical panels are based on the sideslip derivative C_{Y_β} . The problem of estimating the forces generated on vertical panels is complicated by the presence of shock waves. This effect is discussed in Paragraph C of Section 5.3.1.1.

As stated in the introduction to this section, no method is available for determining the horizontal-tail contribution to the derivative C_{I_β} . However, the effect of the horizontal tail on the vertical-tail contribution is accounted for by proper use of the apparent-mass factor (K) charts in determining the vertical-panel side force.

DATCOM METHOD

The rolling moment (about the longitudinal stability axis) due to sideslip of a wing-body-vertical-tail configuration, referred to an arbitrary moment center and based on wing area and wing span, is given by Equation 5.6.2.1-a:

$$C_{I_\beta} = (C_{I_\beta})_{WB} + \sum_p \left\{ (\Delta C_{Y_\beta})_p \left[\frac{z_p \cos \alpha - l_p \sin \alpha}{b_w} \right] \right\}$$

where C_{I_β} , $(C_{I_\beta})_{WB}$, z_p , and b_w are defined in Paragraph A above, and

$(\Delta C_{Y_\beta})_p$ is the side force due to sideslip of an added vertical panel from Paragraph C of Section 5.3.1.1. The build-up procedure outlined in Paragraph C of Section 5.6.1.1 (neglecting the contribution of a horizontal tail) must be applied in determining the individual increment of each added panel. The effect of the presence of a horizontal tail must be considered in computing the contributions of the vertical panels.

l_p

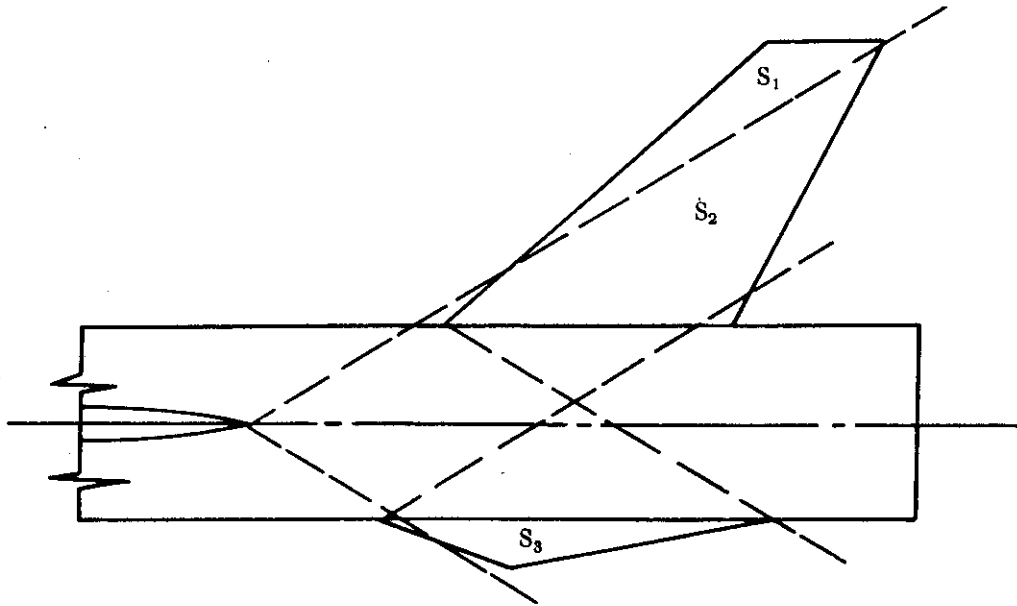
is the distance parallel to the longitudinal body axis between the moment reference center and the 50-percent chord of the MAC of the added vertical panel, positive for panel aft of the vehicle moment center.*

All geometry used in determining the moment arms of the vertical panels is based on the exposed panel.

For a wingless configuration the remarks following the Datcom methods of Paragraph A above are also applicable at supersonic speeds.

Sample Problem

Given: The configuration of Reference 18 consisting of a wing, body, upper vertical tail, and lower vertical tail. This is the same configuration as that of the sample problem of Paragraph C, Section 5.6.1.1 with the horizontal tail removed. Some characteristics are repeated.



Wing Characteristics:

$$A_w = 3.18 \quad S_w = 114.5 \text{ sq in.} \quad z_w = 0 \quad \Gamma = -3.5^\circ$$

$$\lambda_w = 0.468 \quad \Lambda_{LE_w} = 48.08^\circ \quad \text{No twist} \quad b_w = 19.08 \text{ in.}$$

Vertical-Tail Characteristics:

$$A_{V_e} = 1.48 \quad S_{V_e} = 19.20 \text{ sq in.} \quad \Lambda_{LE_V} = 49.2^\circ \quad b_V = 7.08 \text{ in.}$$

*See footnote at bottom of Page 5.6.2.1-3.

$$\lambda_{V_e} = 0.392$$

Ventral-Tail Characteristics:

$$A_{U_e} = 0.2025 \quad S_{U_e} = 3.24 \text{ sq in.} \quad \Lambda_{LE_U} = 70.2^\circ \quad b_U = 2.56 \text{ in.}$$

$$\lambda_{U_e} = 0$$

Additional Characteristics:

$$M = 2.01 \quad \mu = \sin^{-1}(1/M) = 29.8^\circ \quad r_1 = 1.75 \text{ in.}$$

$$r_2 = 1.496 \text{ in.} \quad r_1/r_2 = 1.170 \quad S_1 = 4.63 \text{ sq in.}$$

$$S_2 = 14.56 \text{ sq in.} \quad S_3 = S_{U_e} = 3.24 \text{ sq in.} \quad d/b_w = 0.157$$

$$\ell_V = 10.65 \text{ in.} \quad z_V = 4.05 \text{ in.} \quad \ell_U = 8.40 \text{ in.} \quad z_U = -2.05 \text{ in.}$$

$$C_N = 0.10, \alpha = 2.20^\circ \text{ (test)}$$

Compute:

Step 1. Determine the wing-body contribution $(C_l)_\text{WB}$

$$\sqrt{M^2 - 1} = 1.744$$

$$\Lambda_{LE_W} = 0.84 \text{ rad; } 1 + \Lambda_{LE_W} = 1.84; 1 + \frac{\Lambda_{LE_W}}{2} = 1.42$$

$$1 + \lambda_w (1 + \Lambda_{LE_W}) = 1.860$$

$$\frac{\tan \Lambda_{LE_W}}{\sqrt{M^2 - 1}} = 0.639$$

$$\frac{M^2 \cos^2 \Lambda_{LE_W}}{A} = \frac{(4.04)(0.445)}{3.18} = 0.565$$

$$\left(\frac{\tan \Lambda_{LE_W}}{4} \right)^{4/3} = (0.2785)^{4/3} = 0.182$$

Dihedral effect

$$A_w \sqrt{M^2 - 1} = 5.55; \sqrt{M^2 - 1} \cot \Lambda_{LE_w} = 1.57$$

$$C_{I_p} = -0.28 \text{ per rad} \quad (\text{Figure 7.3.2.2-6})$$

$$\left(\frac{1 + 2\lambda}{1 + 3\lambda} \right)_w = 0.805$$

$$\frac{C_{I_\beta}}{\Gamma} = \frac{2}{(57.3)^2} \left(\frac{1 + 2\lambda}{1 + 3\lambda} \right)_w C_{I_p} = -0.000137 \text{ (per deg)}^2 \quad (\text{Equation 5.1.2.1-d})$$

$$\frac{\Delta C_{I_\beta}}{\Gamma} = -0.0005 \sqrt{A_w} \left(\frac{d}{b_w} \right)^2 = -0.000022 \text{ (per deg)}^2 \quad (\text{Equation 5.2.2.1-b})$$

$$\Gamma \left(\frac{C_{I_\beta}}{\Gamma} + \frac{\Delta C_{I_\beta}}{\Gamma} \right) = -0.000159 \Gamma$$

$$(C_{N_a})_w = 0.041 \text{ per deg (based on } S_w) \quad (\text{Section 4.1.3.2})$$

$$(C_{I_\beta})_{WB} = -0.061 C_N (C_{N_a})_w [1 + \lambda (1 + \Lambda_{LE})]_w \left(1 + \frac{\Lambda_{LE}}{2} \right)_w \left(\frac{\tan \Lambda_{LE_w}}{\sqrt{M^2 - 1}} \right)$$

$$\left[\frac{M^2 \cos^2 \Lambda_{LE_w}}{A_w} + \left(\frac{\tan \Lambda_{LE_w}}{4} \right)^{4/3} \right] + \Gamma \left(\frac{C_{I_\beta}}{\Gamma} + \frac{\Delta C_{I_\beta}}{\Gamma} \right)$$

(Equation 5.2.2.1-d)

$$= (-0.061) C_N (0.041) (1.860) (1.420) (0.639) [0.565 + 0.182]$$

$$+ (-3.5) (-0.000159)$$

$$= -0.00315 C_N + 0.000556 \text{ per deg (based on } S_w b_w)$$

Step 2. Determine the empennage contribution

$$(\Delta C_{Y_\beta})_{VB(WB)} = -0.520 \text{ per rad (based on } S_w) \quad (\text{Sample problem of Paragraph C, Section 5.6.1.1})$$

$$= -0.0091 \text{ per deg}$$

The vertical tail in the sample problem of Paragraph C, Section 5.6.1.1 does not "see" the horizontal tail; therefore the increment in C_{Y_β} of the vertical tail in the presence of a wing and body is identical to $(\Delta C_{Y_\beta})_{V(WBH)}$ calculated in Section 5.6.1.1.

Calculate the increment in C_{Y_β} due to adding the lower vertical panel to the wing-body-upper-vertical-panel combination. In the configuration sketch the ventral panel senses only the body. The effective apparent mass ratio is

$$K'_{U(BV)} = K_{U(B)} = 3.0 \quad (\text{Section 5.3.1.1 with } (r_1/r_2) = 1.170, (r_1/b)_U = 0.685, \text{ added panel})$$

$$\text{and } (r_1/b)_V = 1.000 \quad \begin{matrix} \text{existing} \\ \text{panel} \end{matrix}$$

$$(C_{N_\alpha})_U = 0.622 \text{ per rad (based on } S_{U_e}) \quad (\text{Sample problem, Paragraph C, Section 5.6.1.1})$$

$$(\Delta C_{Y_\beta})_{U(WBV)} = -K'_{U(BV)} (C_{N_\alpha})_U \frac{S_{U_e}}{S_W} \quad (\text{Equation 5.3.1.1-f})$$

$$= (-3.0)(0.622) \left(\frac{3.24}{114.5} \right)$$

$$= -0.0527 \text{ per rad (based on } S_W)$$

$$= -0.00092 \text{ per deg}$$

Solution:

$$C_{I_\beta} = (C_{I_\beta})_{WB} + \sum_p \left\{ (\Delta C_{Y_\beta})_p \left[\frac{z_p \cos \alpha - l_p \sin \alpha}{b_W} \right] \right\} \quad (\text{Equation 5.6.2.1-a})$$

$$= (C_{I_\beta})_{WB} + (\Delta C_{Y_\beta})_{V(WB)} \left[\frac{z_V \cos \alpha - l_V \sin \alpha}{b_W} \right]$$

$$+ (\Delta C_{Y_\beta})_{U(WBV)} \left\{ \frac{z_U \cos \alpha - l_U \sin \alpha}{b_W} \right\}$$

$$\begin{aligned}
&= (-0.00315 C_N + 0.000556) + (-0.0091) \left[\frac{4.05 \cos \alpha - 10.65 \sin \alpha}{19.08} \right] \\
&\quad + (-0.00092) \left[\frac{(-2.05) \cos \alpha - 8.40 \sin \alpha}{19.08} \right] \\
&= [-0.00315 (0.1) + 0.000556] + [(-0.00193) \cos 2.2^\circ + 0.00508 \sin 2.2^\circ] \\
&\quad + [0.00010 \cos 2.2^\circ + 0.000405 \sin 2.2^\circ] \\
&= 0.00024 + (-0.00173) + (0.000116) \\
&= -0.001374 \text{ per deg (based on } S_W b_W)
\end{aligned}$$

REFERENCES

1. Purser, P. E., and Spearman, M. L.: Wind-Tunnel Tests at Low Speed of Swept and Yawed Wings Having Various Plan Forms. NACA TN 2445, 1951. (U)
2. Graham, D., and Koenig, D.: Tests in the Ames 40- by 80-Foot Wind Tunnel of an Airplane Configuration with an Aspect Ratio 2 Triangular Wing and an All-Movable Horizontal Tail — Lateral Characteristics. NACA RM A5IL03, 1952. (U)
3. Koenig, D.: Tests in the Ames 40- by 80-Foot Wind Tunnel of an Airplane Configuration with an Aspect Ratio 3 Triangular Wing and an All-Movable Horizontal Tail — Longitudinal and Lateral Characteristics. NACA RM A52L15, 1953. (U)
4. Griner, R. F.: Static Lateral Stability Characteristics of an Airplane Model Having a 47.7° Sweptback Wing of Aspect Ratio 6 and the Contribution of Various Model Components at a Reynolds Number of 4.45×10^6 . NACA RM L53G09, 1953. (U)
5. Letko, W., and Goodman, A.: Preliminary Wind-Tunnel Investigation at Low Speed of Stability and Control Characteristics of Sweptback Wings. NACA TN 1046, 1946. (U)
6. Fink, M. P., and Freeman, D. C., Jr.: Full-Scale Wind-Tunnel Investigation of Static Longitudinal and Lateral Characteristics of a Light Twin-Engine Airplane. NACA TN D-4983, 1969. (U)
7. Fink, M. P., and Freeman, D. C., Jr.: Full-Scale Wind-Tunnel Investigation of the Static Longitudinal and Lateral Characteristics of a Light Single-Engine Airplane. NACA TN D-5700, 1970. (U)
8. Franks, R. W.: Tests in the Ames 40- by 80-Foot Wind Tunnel of an Airplane Model with an Aspect Ratio 4 Triangular Wing and an All-Movable Horizontal Tail — High-Lift Devices and Lateral Controls. NACA RM A52K13, 1953. (U)
9. Lockwood, V. E., and Watson, J. M.: Stability and Control Characteristics at Low Speed of an Airplane Model Having a 38.7° Sweptback Wing with Aspect Ratio 4.51, Taper Ratio 0.54, and Conventional Tail Surfaces. NACA TN 1742, 1948. (U)
10. Nealey, R. H., and Conner, D. W.: Aerodynamic Characteristics of a 42° Swept-Back Wing with Aspect Ratio 4 and 64-112 Airfoil Sections at Reynolds Numbers from 1,700,000 to 9,500,000. NACA RM L7D14, 1947. (U)
11. Perry, D. H., Morrell, J. C., and Port, W. G. A.: Low Speed Flight Tests on a Tailless Delta Wing Aircraft (Avro 707B). Part 3 — Lateral Stability and Control. ARC CP 1106, 1970. (U)
12. Brown, S. C., and Holloman, E. C.: Experimental and Predicted Lateral-Directional Dynamic-Response Characteristics of a Large Flexible 35° Swept-Wing Airplane at an Altitude of 35,000 Feet. NACA TN 3874, 1956. (U)
13. Wolowicz, C. H., and Redless, H. A.: Effects of Jet Exhausts on Flight-Determined Longitudinal and Lateral Dynamic Stability Characteristics of the Douglas D-568-II Research Airplane. NACA RM H57G09, 1957. (U)
14. DC-8 Unpublished Data. (U)

15. DC-9 Unpublished Dets. (U)
16. Sleeman, W. C., Jr.: An Experimental Study at High Subsonic Speeds of Several Tail Configurations on a Model Having a 45° Sweptback Wing. NACA RM L57C08, 1957. (U)
17. Savage, H. F., and Tinling, B. E.: The Subsonic Static Aerodynamic Characteristics of an Airplane Model Having a Triangular Wing of Aspect Ratio 3. II - Lateral and Directional Characteristics. NACA TN 4042, 1957. (U)
18. Spearman, M. L., Robinson, R. B., and Driver, C.: The Effects of the Addition of Small Fuselage-Mounted Fins on the Static Directional Stability Characteristics of a Model of a 45° Sweptback Wing Airplane at Angles of Attack up to 15.3° at a Mach Number of 2.01. NACA RM L56D16a, 1956. (U)

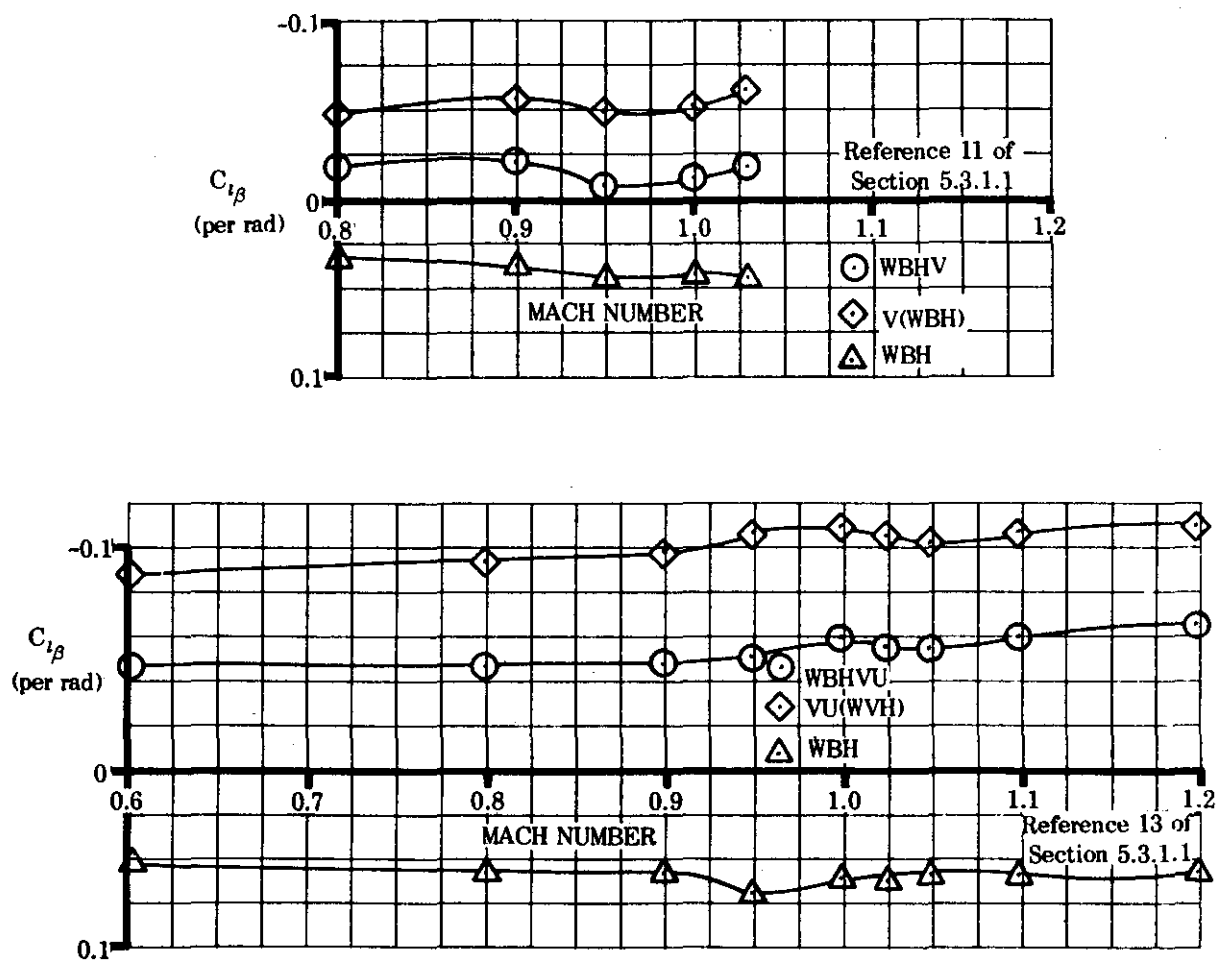


FIGURE 5.6.2.1-15 TYPICAL TRANSONIC DATA

5.6.3 WING-BODY-TAIL SIDESLIP DERIVATIVE $C_{n\beta}$

5.6.3.1 WING-BODY-TAIL SIDESLIP DERIVATIVE $C_{n\beta}$ IN THE LINEAR ANGLE-OF-ATTACK RANGE

The information contained in this Section is for estimating the yawing moment due to sideslip $C_{n\beta}$ of wing-body-tail combinations at low angles of attack. In general, it consists of a synthesis of material presented in other Sections. Discussion of the various aerodynamic aspects of vehicle components in sideslip is given in other Sections of the Datcom and is not repeated here.

The methods presented are based on the procedure of totaling the wing-body contribution and the total empennage increment as was done in Section 5.6.1.1 for the determination of side force due to sideslip for a complete configuration. The yawing moment of the complete empennage is determined by applying the appropriate moment arm to each of the incremental values of side force which make up the total, as determined in Section 5.6.1.1.

A. SUBSONIC

The methods of estimating the subsonic values of the empennage contribution to the derivative $C_{n\beta}$ are based on the values of $C_{Y\beta}$ estimated by the methods of paragraph A of Section 5.3.1.1. If the apparent-mass-concept method (Method 3, paragraph A, Section 5.3.1.1) is used, the build-up procedure outlined in Method 3 of paragraph A of Section 5.6.1.1 must be applied in determining the individual panel side-force derivatives.

Two methods of determining the moment arm through which the empennage panel side force acts at subsonic speeds are presented in Section 5.3.3.1. The moment arm can be taken as (a) the distance parallel to the longitudinal axis between the vehicle moment center and the quarter-chord point of the mean aerodynamic chord of the added panel or (b) the distance parallel to the longitudinal axis between the vehicle moment center and the aerodynamic center of the added panel. For most cases the simplified approximation (a) is used. However, for short coupled configurations where the tail length distance is relatively short and the size of the added panel large the refined approximation (b) is recommended.

DATCOM METHODS

Method 1

Simplified Method

The yawing moment due to sideslip of a wing-body-tail configuration, referred to an arbitrary moment center and based on the wing area and wing span, is given by

$$C_{n\beta} = (C_{n\beta})_{WB} + \sum_p \left[-(\Delta C_{Y\beta})_p \frac{l_p}{b_w} \right] \quad 5.6.3.1-a$$

where the subscript p refers to panels present in the empennage

$(C_{n\beta})_{WB}$ is the contribution of the wing-body combination to the total yawing moment due to sideslip, obtained from Section 5.2.3.1

$(\Delta C_{Y\beta})_p$ is the side force due to sideslip of the added panel determined as follows

For configurations with the horizontal panel mounted on the body, or for configurations with no horizontal panel use Method 1 or Method 3, paragraph A, Section 5.3.1.1. If Method 1 of paragraph A of Section 5.3.1.1 is used, the total empennage increment is given by a single term. If Method 3 of paragraph A of Section 5.3.1.1 is used, the build-up procedure outlined in Method 3 of paragraph A of Section 5.6.1.1 must be applied to determine the individual increment of each added panel.

For configurations with a horizontal panel mounted on the vertical panel, use Method 1, paragraph A, Section 5.3.1.1. The total empennage increment is given by a single term.

For configurations with twin vertical panels mounted on the tips of a horizontal panel use Method 2, paragraph A, Section 5.3.1.1. The total empennage increment is given by a single term.

- l_p is the distance parallel to the longitudinal axis between the vehicle moment center and the quarter-chord point of the MAC of the added panel, positive for the panel aft of the vehicle moment center
 b_w is the span of the wing

Method 2

Refined Method

In this case the sideslip derivative $C_{n\beta}$, referred to an arbitrary moment center and based on wing area and wing span, is given by

$$C_{n\beta} = (C_{n\beta})_{WB} + \sum_p \left[-(\Delta C_{Y\beta})_p \left(\frac{l_p + (x_{a.c.})_p}{b_w} \right) \right] \quad 5.6.3.1-b$$

where $(C_{n\beta})_{WB}$, $(\Delta C_{Y\beta})_p$, l_p , and b_w are defined in Method 1 above, and

$(x_{a.c.})_p$ is the distance parallel to the longitudinal axis between the quarter-chord point of the MAC of the added panel and the aerodynamic center of the added panel obtained from paragraph A of Section 4.1.4.2, positive for the a.c. behind the quarter-chord point of the MAC. (In determining the vertical panel a.c. use the aspect ratio of the panel mounted on an infinite reflection plane).

All geometry used in determining the moment arms for the above methods is based on the panel extended to the body centerline.

For a wingless configuration, b_w is replaced by the vehicle reference length, $(\Delta C_{Y\beta})_p$ is based on the vehicle reference area, and the contribution of the body to the total derivative can be obtained from Section 4.2.2.1 as $(C_{n\beta})_B = -(C_{m\alpha})_B$, based on the vehicle reference area.

Sample Problems

1. Method 1

Given: A wing-body-horizontal tail-vertical tail configuration of reference 1. This is the same configuration as that of sample problem 1, paragraph A, Section 5.6.1.1. Some of the characteristics are repeated.

Wing Characteristics

$$S_w = 36.0 \text{ sq in.} \quad b_w = 12.0 \text{ in.}$$

Body Characteristics

$$l_B = 18.25 \text{ in.} \quad x_m = 10.42 \text{ in.} \quad S_{BS} = 25.6 \text{ sq in.} \quad h_1/h_2 = 0.950$$

$$h/w = 1.000$$

Additional Characteristics

$$M = 0.60 \quad R_l = 7.43 \times 10^6 \text{ (based on } l_B) \quad l_v = 6.035 \text{ in.}$$

Compute:

$$\frac{x_m}{l_B} = 0.572$$

$$\left(\frac{h_1}{h_2} \right)^{1/2} = 0.975$$

$$\frac{l_B^2}{S_{BS}} = 13.00$$

Using the above computed parameters and the Reynolds number obtain K_N from figure 5.2.3.1-5

$$K_N = 0.0014$$

$$(C_{n\beta})_{WB} = -K_N \frac{S_{BS}}{S_w} \frac{l_B}{b_w} \text{ per deg} \quad (\text{equation 5.2.3.1-a})$$

$$= -(0.0014) \left(\frac{25.6}{36.3} \right) \left(\frac{18.25}{12.0} \right)$$

$$= -0.00151 \text{ per deg (based on } S_w b_w)$$

$$= -0.0865 \text{ per rad (based on } S_w b_w)$$

$$(\Delta C_{Y\beta})_{V(WBH)} = -0.645 \text{ per rad (based on } S_w) \text{ (sample problem 1, paragraph A, Section 5.6.1.1)}$$

Solution:

$$C_{n\beta} = (C_{n\beta})_{WB} + \sum_p \left[-(\Delta C_{Y\beta})_p \frac{l_p}{b_w} \right] \quad (\text{equation 5.6.3.1-a})$$

$$= (C_{n\beta})_{WB} + \left[-(\Delta C_{Y\beta})_{V(WBH)} \frac{l_v}{b_w} \right]$$

$$= -0.0865 + \left[-(-0.645) \left(\frac{6.035}{12.0} \right) \right]$$

$$= -0.0865 + 0.324$$

$$= 0.2375 \text{ per rad (based on } S_w b_w)$$

The experimental results (based on $S_w b_w$) from reference 1 are $(C_{n\beta})_{WB} = -0.063$ per radian, $(\Delta C_{n\beta})_{V(WBH)} = 0.350$ per radian, and $C_{n\beta} = 0.286$ per radian.

2. Method 1

Given: The wing-body-horizontal tail-vertical tail configuration of reference 2. This is the same configuration as that of sample problem 3, paragraph A, Section 5.6.1.1. Some characteristics are repeated.

Wing Characteristics

$$S_w = 576 \text{ sq in.}$$

$$b_w = 41.56 \text{ in.}$$

Body Characteristics

$$l_B = 72.0 \text{ in.}$$

$$x_m = 39.60 \text{ in.}$$

$$S_{BS} = 349.9 \text{ sq in.}$$

$$h_1/h_2 = 0.730$$

$$h/w = 1.000$$

Additional Characteristics

$$M = 0.25$$

$$R_f = 9.73 \times 10^6 \text{ (based on } l_B)$$

$$l_v = 24.89 \text{ in.}$$

$$l_H = 26.2 \text{ in.}$$

$$\alpha = 0$$

Compute:

$$\frac{x_m}{l_B} = 0.550$$

$$\left(\frac{h_1}{h_2} \right)^{\frac{1}{2}} = 0.854$$

$$\frac{l_B^2}{S_{BS}} = 14.80$$

Using the parameters computed above and the Reynolds number obtain K_N from figure 5.2.3.1-5

$$K_N = 0.0013$$

$$\begin{aligned} (C_{n\beta})_{WB} &= -K_N \frac{S_{BS}}{S_w} \frac{l_B}{b_w} \text{ per deg} \quad (\text{equation 5.2.3.1-a}) \\ &= -(0.0013) \left(\frac{349.9}{576.0} \right) \left(\frac{72.0}{41.56} \right) \\ &= -0.001365 \text{ per deg (based on } S_w b_w) \\ &= -0.0782 \text{ per rad (based on } S_w b_w) \end{aligned}$$

From sample problem 3, paragraph A, Section 5.6.1.1

$$(\Delta C_{Y\beta})_{H(WB)} = 0$$

$$(\Delta C_{Y\beta})_{V(WBH)} = -0.665 \text{ per rad (based on } S_w)$$

Solution:

$$\begin{aligned} C_{n\beta} &= (C_{n\beta})_{WB} + \sum_p \left[-(\Delta C_{Y\beta})_p \frac{l_p}{b_w} \right] \quad (\text{equation 5.6.3.1-a}) \\ &= (C_{n\beta})_{WB} + \left[-(\Delta C_{Y\beta})_{H(WB)} \frac{l_H}{b_w} \right] + \left[-(\Delta C_{Y\beta})_{V(WBH)} \frac{l_V}{b_w} \right] \\ &= -0.0782 + 0 + \left[-(-0.665) \left(\frac{24.89}{41.56} \right) \right] \\ &= -0.0782 + 0.398 \\ &= 0.3198 \text{ per rad (based on } S_w b_w) \end{aligned}$$

The experimental results (based on $S_w b_w$) from reference 2 are $(C_{n\beta})_{WB} = -0.057$ per radian, $(\Delta C_{n\beta})_{V(WBH)} = 0.409$ per radian, and $C_{n\beta} = 0.352$ per radian.

B. TRANSONIC

A brief discussion of the flow phenomena associated with forces generated on vertical panels at transonic speeds is given in paragraph B of Section 5.3.1.1. At the present time there are no methods available to predict the effect of wing-body wake and sidewash or the mutual interference effects between vehicle components on the sideslip characteristics at transonic speeds.

DATCOM METHOD

No explicit method is available for estimating the vehicle sideslip derivative $C_{n\beta}$ at transonic speeds and none is presented in the Datcom. Some typical transonic data for this derivative are presented as figure 5.6.3.1-8.

C. SUPERSONIC

The procedure for estimating the supersonic sideslip derivative $C_{n\beta}$ of a wing-body-tail configuration is essentially the same as that at subsonic speeds. The problem of estimating the forces generated on vertical panels is complicated by the presence of shock waves. This effect is discussed in paragraph C of Section 5.3.1.1.

The moment arm through which an added vertical panel acts can be taken as (a) the distance parallel to the longitudinal axis between the vehicle moment center and the 50-percent-chord point of the mean aerodynamic chord of the added vertical panel or (b) the distance parallel to the longitudinal axis between the vehicle moment center and

the aerodynamic center of the added vertical panel. For short-coupled configurations with a large vertical panel the latter approach is recommended. At supersonic speeds the centroid of area of the region of interference approximates the center of pressure in the case of the increment gained by adding a horizontal surface.

This method is limited to configurations in which the horizontal tail is mounted on the body or configurations with no horizontal tail.

DATCOM METHODS

Method 1

Simplified Method

The yawing moment due to sideslip of a wing-body-tail configuration, referred to an arbitrary moment center and based on wing area and wing span, is given by equation 5.6.3.1-a

$$C_{n\beta} = (C_{n\beta})_{WB} + \sum_p \left[-(\Delta C_{Y\beta})_p \frac{l_p}{b_w} \right]$$

where $(C_{n\beta})_{WB}$ is defined in paragraph A above, and

$(\Delta C_{Y\beta})_p$ is the side force due to sideslip of an added panel obtained from paragraph C, Section 5.3.1.1. The build-up procedure outlined in paragraph C of Section 5.6.1.1 must be applied in determining the individual increment of each added panel.

l_p is the distance parallel to the longitudinal axis between the vehicle moment center and the 50-percent-chord point of the MAC of an added vertical panel, positive for the vertical panel aft of the vehicle moment center. In the case of the increment gained by adding a horizontal panel, l_p is the distance parallel to the longitudinal axis between the vehicle moment center and the centroid of the area of the region of interference, positive for the horizontal panel aft of the vehicle moment center.

Method 2

Refined Method

In this case the sideslip derivative $C_{n\beta}$, referred to an arbitrary moment center and based on wing area and wing span, is given by equation 5.6.3.1-b

$$C_{n\beta} = (C_{n\beta})_{WB} + \sum_p \left[-(\Delta C_{Y\beta})_p \left(\frac{l_p + (x_{a.c.})_p}{b_w} \right) \right]$$

where $(C_{n\beta})_{WB}$, $(\Delta C_{Y\beta})_p$, and l_p are defined in Method 1 above, and

$(x_{a.c.})_p$ is the distance parallel to the longitudinal axis between the 50-percent-chord point of the MAC of an added vertical panel and the aerodynamic center of the added panel obtained from paragraph C of Section 4.1.4.2, positive for the a.c. behind the 50-percent-chord point. (In determining the vertical panel a.c. use the aspect ratio of the isolated panel mounted on an infinite reflection plane.)

In the case of the increment gained by adding a horizontal panel, the moment arm is treated as in Method 1 above.

All geometry used in determining the moment arms of the vertical panels in the above methods is based on the exposed panel.

For a wingless configuration the remarks following the Datcom methods of paragraph A above are also applicable at supersonic speeds.

Sample Problem

Method 1

Given: The wing-body-horizontal tail-upper vertical tail-lower vertical tail configuration of reference 3. This is the same configuration as that of the sample problem of paragraph C, Section 5.6.1.1. Some characteristics are repeated..

Wing Characteristics

$$S_w = 114.5 \text{ sq in.} \quad b_w = 19.08 \text{ in.}$$

Body Characteristics

$$l_B = 32.88 \text{ in.} \quad x_m = 18.00 \text{ in.} \quad S_{BS} = 92.24 \text{ sq in.} \quad h_1/h_2 = 1.1175$$

$$h/w = 1.340$$

Additional Characteristics

$$M = 2.01 \quad R_f = 3.38 \times 10^6 \text{ (based on } l_B) \quad \alpha = 0$$

$$l_v = 10.65 \text{ in.} \quad l_u = 8.40 \text{ in.} \quad l_h = 11.45 \text{ in. (c.g. to centroid of region of interference)}$$

Compute:

$$\frac{x_m}{l_B} = 0.548$$

$$\left(\frac{h_1}{h_2}\right)^{\frac{1}{2}} = 1.058$$

$$\frac{l_B^2}{S_{BS}} = 11.72$$

Using the parameters computed above and the Reynolds number obtain K_N from figure 5.2.3.1-5

$$K_N = 0.0017$$

$$(C_{n\beta})_{WB} = -K_N \frac{S_{BS}}{S_w} \frac{l_B}{b_w} \text{ per deg} \quad (\text{equation 5.2.3.1-a})$$

$$= -(0.0017) \left(\frac{92.24}{114.5} \right) \left(\frac{32.88}{19.08} \right)$$

$$= -0.00236 \text{ per deg (based on } S_w b_w)$$

$$= -0.135 \text{ per rad (based on } S_w b_w)$$

$$\left. \begin{aligned} (\Delta C_{Y\beta})_{H(WB)} &= -0.0163 \text{ per rad (based on } S_w) \\ (\Delta C_{Y\beta})_{V(WBH)} &= -0.520 \text{ per rad (based on } S_w) \\ (\Delta C_{Y\beta})_{U(WBHV)} &= -0.053 \text{ per rad (based on } S_w) \end{aligned} \right\} \quad (\text{sample problem, paragraph C, Section 5.6.1.1.})$$

Solution:

$$C_{n\beta} = (C_{n\beta})_{WB} + \sum_p \left[-(\Delta C_{Y\beta})_p \frac{l_p}{b_w} \right] \quad (\text{equation 5.6.3.1-a})$$

$$= (C_{n\beta})_{WB} + \left[-(\Delta C_{Y\beta})_{H(WB)} \frac{l_h}{b_w} \right] + \left[-(\Delta C_{Y\beta})_{V(WBH)} \frac{l_v}{b_w} \right] + \left[-(\Delta C_{Y\beta})_{U(WBHV)} \frac{l_u}{b_w} \right]$$

$$\begin{aligned}
 &= -0.135 + \left[-(0.0163) \left(\frac{11.45}{19.08} \right) \right] + \left[-(-0.520) \left(\frac{10.65}{19.08} \right) + \left[-(0.053) \left(\frac{8.40}{19.08} \right) \right] \right] \\
 &\approx -0.135 + 0.0098 + 0.290 + 0.0233 \\
 &\approx 0.1881 \text{ per rad (based on } S_{wbw})
 \end{aligned}$$

The experimental results from reference 3 (based on S_{wbw}) are $(C_{n\beta})_{WBH} = -0.169$ per radian, $(\Delta C_{n\beta})_{WBH} = 0.338$ per radian, $(\Delta C_{n\beta})_{U(WBH)} = 0.0286$ per radian, and $C_{n\beta} = 0.1975$ per radian.

REFERENCES

1. Sleeman, W. C., Jr.: An Experimental Study at High Subsonic Speeds of Several Tail Configurations on a Model Having a 45° Sweptback Wing. NACA RM L57C08, 1957. (U)
2. Savage, H. F., and Tinling, B. E.: The Subsonic Static Aerodynamic Characteristics of an Airplane Model Having a Triangular Wing of Aspect Ratio 3. II - Lateral and Directional Characteristics. NACA TN 4042, 1957. (U)
3. Spearman, M. L., Robinson, R. B., and Driver, C.: The Effects of the Addition of Small Fuselage-Mounted Fins on the Static Directional Stability Characteristics of a Model of a 45° Sweptback Wing Airplane at Angles of Attack up to 15.3° at a Mach Number of 2.01. NACA RM L56D16a, 1956. (U)

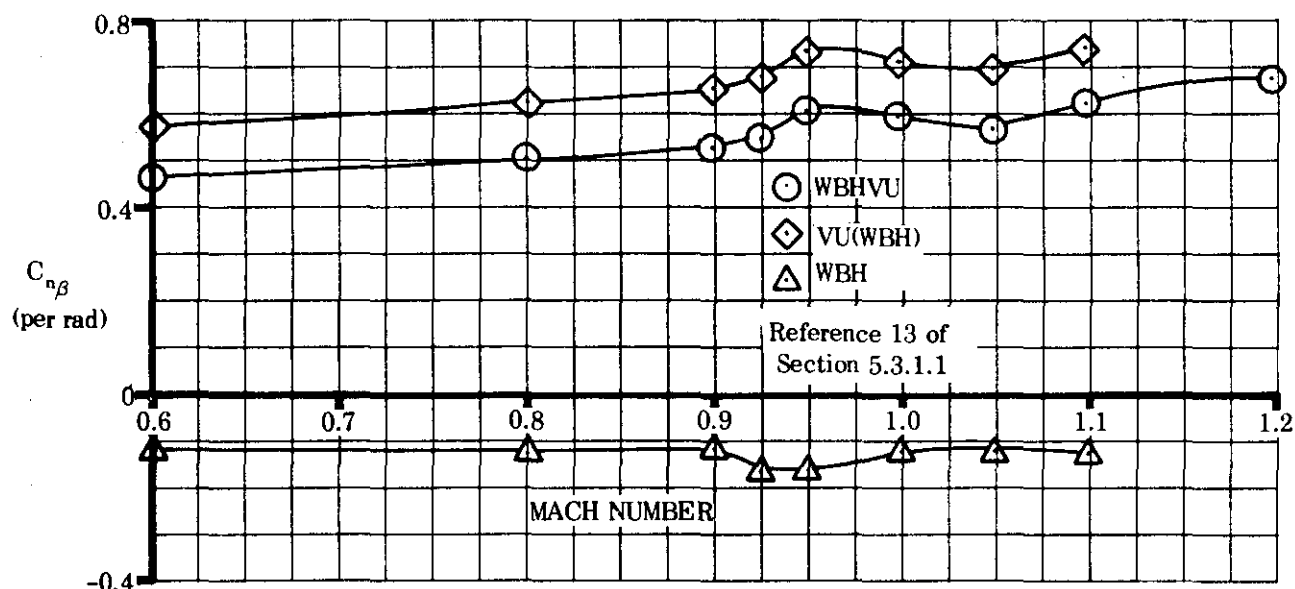
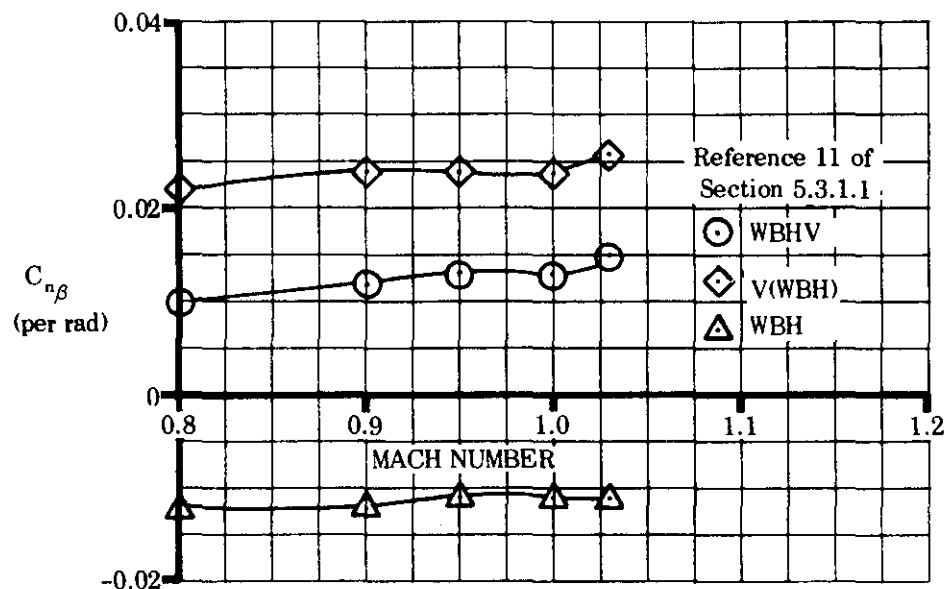


FIGURE 5.6.3.1-8 TYPICAL TRANSONIC DATA

5.6.3.2 WING-BODY-TAIL YAWING-MOMENT COEFFICIENT C_n AT ANGLE OF ATTACK

The wing-body-tail yawing moment developed at combined angles is nonlinear with respect to both sideslip and angle of attack for the reasons cited in the introductory remarks of Sections 5.2.1.2 and 5.3.1.2. To obtain the derivative $C_{n\beta}$ it is recommended that C_n be calculated at several angles of attack for a small sideslip angle ($\beta < 4^\circ$). Then at each angle of attack the yawing moment is assumed linear with sideslip for small values of β so that

$$C_{n\beta} \approx \frac{C_n}{\beta}$$

A. SUBSONIC

No method is presently available for determining the wing-body-tail yawing moment at large angles of attack and subsonic speeds. The method presented herein is restricted to first-order approximations at relatively low angles of attack.

DATCOM METHOD

It is recommended that the method of Section 5.6.3.1 be used in the linear-lift angle-of-attack range.

B. TRANSONIC

The comments appearing in Paragraph B of Section 5.6.1.1 are equally appropriate here.

DATCOM METHOD

No method is available for estimating this coefficient and none is presented in the Datcom.

C. SUPERSONIC

The discussion of Paragraph C in Section 5.6.1.2 applies here also and will not be repeated.

DATCOM METHOD

The method for estimating the wing-body-tail yawing moment at combined angles is basically that of Section 5.6.1.2. The yawing-moment coefficient is obtained simply by applying the proper moment arms to the various side-force coefficients calculated in that section. The restrictions noted in Section 5.6.1.2 also apply here.

The wing-body yawing-moment coefficient is given by

$$(C_n)_{WBHVU} = (C_n)_{WB} + (C_n)_{HVU(WB)} \quad 5.6.3.2-a$$

where

$$(C_n)_{WB}$$

is the wing-body contribution obtained from Equation 5.2.3.2-a

$(C_n)_{HVU(WB)}$ is the empennage contribution obtained from Equation 5.6.3.2-b.

The contribution of the empennage is given by

$$(C_n)_{HVU(WB)} = -\frac{\ell_H \cos \alpha + z_H \sin \alpha}{b_W} (C_Y)_{H(B)} - \frac{\ell_V \cos \alpha + z_V \sin \alpha}{b_W} (C_Y)_{V(\eta)} \\ - \frac{\ell_U \cos \alpha + z_U \sin \alpha}{b_W} (C_Y)_{U(\eta)} \quad 5.6.3.2-b$$

where

$(C_Y)_{H(B)}$ is from Equation 5.3.1.2-b.

$(C_Y)_{V(\eta)}$ is from Equation 5.6.1.2-c.

$(C_Y)_{U(\eta)}$ is from Equation 5.6.1.2-d.

$\left. \begin{matrix} \ell_H \\ z_H \\ \ell_V \\ z_V \\ \ell_U \\ z_U \end{matrix} \right\}$

are defined under Equation 5.3.3.2-a.

Values for the incremental coefficient resulting from the addition of vertical tails to wing-body configurations, calculated using the Datcom method, are compared with experimental results in Figure 5.6.3.2-4. The assessment of the correlation parallels that of the incremental side-force coefficient, and the comments appearing in Section 5.6.1.2 are equally applicable here.

Sample Problem

Given: Configuration of Sample Problem, Paragraph C, Sections 5.2.3.2 (with slight boattail) and 5.6.1.2. There is no horizontail tail on this configuration. Some of the characteristics are repeated. Find the yawing-moment coefficient developed by the wing-body-tail configuration at $\alpha = 12^\circ$, $\beta = 4^\circ$, and $M = 2.01$.

Characteristics:

$$\ell_V = 12.0 \text{ in.} \quad z_V = 4.15 \text{ in.} \quad \ell_U = 12.0 \text{ in.} \quad z_U = -2.15 \text{ in.} \quad b_W = 24.0 \text{ in.}$$

$$(C_n)_{WB} = -0.00695 \text{ (Sample Problem, Paragraph C, Section 5.2.3.2)}$$

$$(C_Y)_{H(B)} = 0 \text{ (no horizontal tail on this configuration)}$$

$$\left. \begin{aligned} (C_Y)_{V(\eta)} &= -0.0285 \\ (C_Y)_{U(\eta)} &= -0.0187 \end{aligned} \right\} \text{ (Sample Problem, Paragraph C, Section 5.6.1.2)}$$

Compute:

$$\begin{aligned} (C_n)_{HVU(WB)} &= -\frac{\ell_H \cos \alpha + z_H \sin \alpha}{b_W} (C_Y)_{H(B)} - \frac{\ell_V \cos \alpha + z_V \sin \alpha}{b_W} (C_Y)_{V(\eta)} \\ &\quad - \frac{\ell_U \cos \alpha + z_U \sin \alpha}{b_W} (C_Y)_{U(\eta)} \quad (\text{Equation 5.6.3.2-b}) \\ &= 0 - \frac{(12.0) \cos 12^\circ + (4.15) \sin 12^\circ}{24.0} (-0.0285) \\ &\quad - \frac{(12.0) \cos 12^\circ + (-2.15) \sin 12^\circ}{24.0} (-0.0187) \\ &= 0.0238 \text{ (based on } S_W b_W) \end{aligned}$$

Solution:

$$\begin{aligned} (C_n)_{WBHVU} &= (C_n)_{WB} + (C_n)_{HVU(WB)} \quad (\text{Equation 5.6.3.2-a}) \\ &= -0.00695 + 0.0238 \\ &= 0.01685 \text{ (based on } S_W b_W) \end{aligned}$$

This compares with an experimental value (based on $S_W b_W$) of $(C_n)_{WBHVU} = 0.0175$ from Reference 2.

REFERENCES

1. Kattawi, G. E.: Estimation of Directional Stability Derivatives at Moderate Angles and Supersonic Speeds. NASA Memo 12-1-58A, 1960. (U)
2. Spearman, L. M., Driver, C., and Hughes, W. C.: Investigation of Aerodynamic Characteristics in Pitch and Sideslip of a 45° Sweptback-Wing Airplane Model with Various Vertical Locations of Wing and Horizontal Tail - Basic-Data Presentation, $M = 2.01$. NACA RM L54L06, 1958. (U)

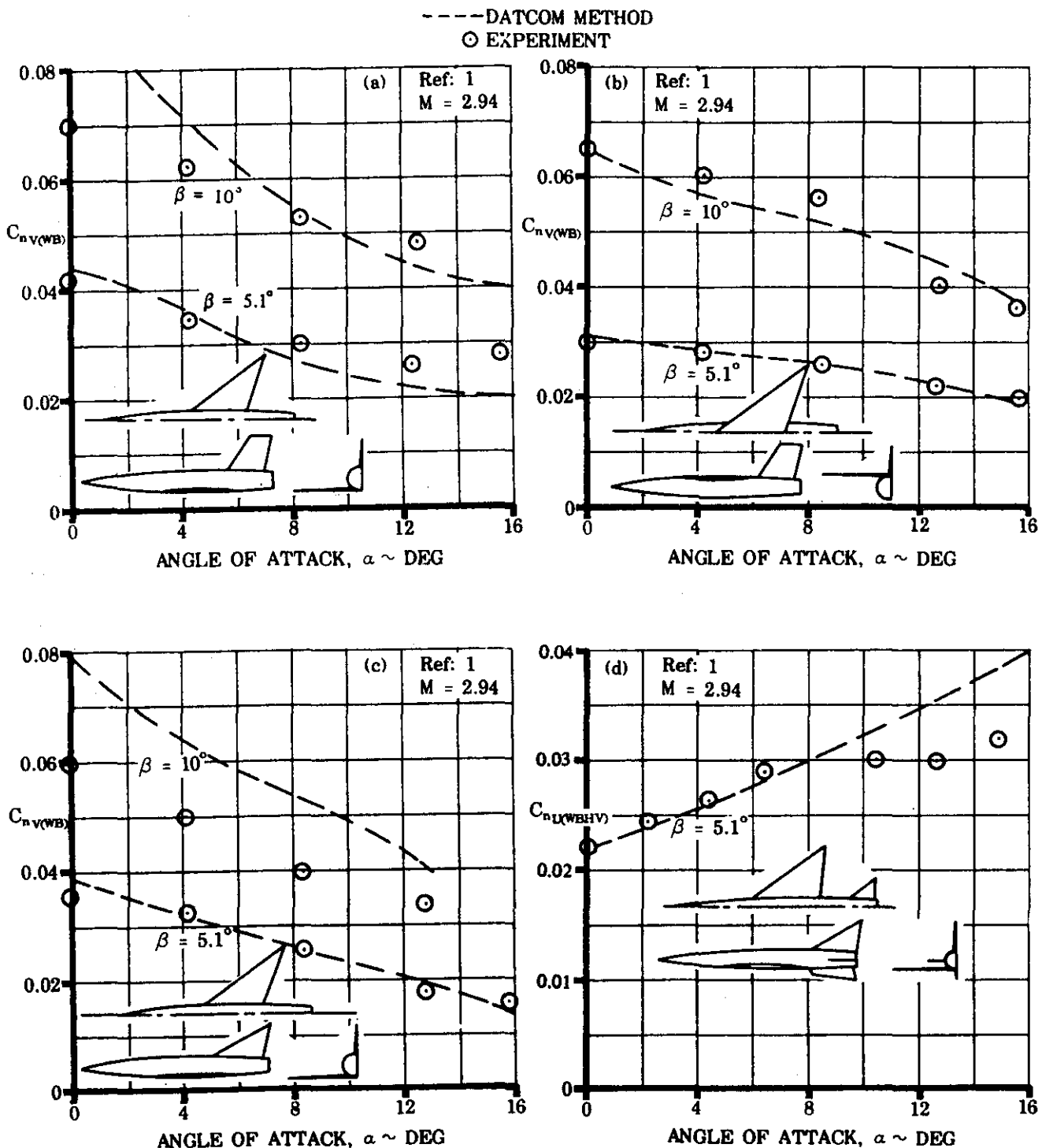


FIGURE 5.6.3.2-4 COMPARISON OF EXPERIMENTAL AND CALCULATED YAWING-MOMENT COEFFICIENT INCREMENTS DUE TO ADDING A VERTICAL TAIL TO A WING-BODY